MECHANISTIC INVESTIGATION ON SOLAR LIGHT INITIATED DESTRUCTION OF INDICATOR BACTERIA

by

Ezgi Lale

B.Sc. in Biology, İstanbul University, 2014

Submitted to the Institute of Environmental Sciences

in partial fulfillment of the requirements for the degree of

Master of Science

in

Environmental Sciences

Boğaziçi University

2021

MECHANISTIC INVESTIGATION ON SOLAR LIGHT INITIATED DESTRUCTION OF INDICATOR BACTERIA

APPROVED BY:

Prof. Dr. Miray Bekbölet Thesis Advisor	...…….
Dr. Ceyda S. Uyguner Demirel Thesis Co-Advisor	……..
Prof. Dr. Ayşen Erdinçler	....……...
Prof. Dr. Bahar İnce	...……
Prof. Dr. Tuğba Ölmez Hancı	……..

DATE OF APPROVAL: 08/09/2021

Dedicated to Lale İpek Lale and Nihat Lale,

to the memory of Ahmet Kara…

ACKNOWLEDGEMENTS

I would like to express my gratitude and respects to my thesis advisor Prof. Dr. Miray Bekbölet for her guidance, support, and supervision throughout this study. Also, I would like to thank my co-advisor Dr. Ceyda Senem Uyguner Demirel for took the lead to my participation in Bekbölet working group.

I would also like to acknowledge my thesis jury committee, Prof. Dr. Ayşen Erdinçler, Prof. Dr. Bahar İnce, and Prof. Dr. Tuğba Ölmez Hancı for spending their valuable time on evaluating this study.

Special thanks are also given to Dr. Ayşe Tomruk, Dr. Nazmiye Cemre Birben, Dr. Nazlı Türkten, and Filiz Ayılmaz for their guidance and help in the laboratory.

I am also indebted sincere thanks to my clarinet teacher Ahmet Kara who had trained me more than 19 years and passed away last year due to Covid-19, and my chorus master Gökçen Koray who I had worked with over 16 years. I am very thankful for their guidance, encouragement, and support which contributed a lot on my personality. It was a great honor to be able to work with them.

Finally, I would like to deeply appreciate my beloved parents, Lale İpek Lale and Nihat Lale for their endless support, encouragement, patience, devotion, and love during all my journeys in my life which made me who I am today. I am very grateful to have you and letting me follow the paths I choose from the start.

ABSTRACT

MECHANISTIC INVESTIGATION ON SOLAR LIGHT INITIATED DESTRUCTION OF INDICATOR BACTERIA

Due to the increasing shortage of clean drinking water around the world, some point of use disinfection techniques has been improved to obtain purified drinking water from pathogen microorganisms. Water disinfection using natural or artificial sunlight has been widely studied for the inactivation of microorganisms. Pathogens can be destructed with the synergistic effects of the solar light and thermal heat. Recently, application of solar photocatalysis has gained attraction for the effective inactivation of microorganisms. In this study, solar light initiated destruction of bacteria typically *Escherichia coli* as the model indicator organism and characterization of the released organic matter were evaluated in the presence/absence of photocatalysts, namely TiO_2 and its second generation type Fe-doped TiO_2. Via destruction of cell membrane, contents of released proteins, carbohydrates and potassium were determined. Solar photolytic/photocatalytic inactivation of *E. coli* was conducted in the presence/absence of water matrix that provides the ionic characteristics of natural waters and in the presence/absence of humic acid that is a dissolved organic matter analogue in natural waters, hence the degradation of humic acid by solar light initiated processes in the presence of *E. coli* was also investigated. Characterization of organic matter in respect of *E. coli* inactivation was evaluated by specified and specific ultraviolet-visible and fluorescence parameters, dissolved organic carbon contents, and excitation emission matrix fluorescence contour plots. *E. coli* inactivation was followed by bacteria reduction kinetic parameters, and detection of organic (protein and carbohydrate) and inorganic (K^+ ion leakage) contents under specified conditions in relation with the spectroscopic parameters.

ÖZET

İNDİKATÖR BAKTERİNİN GÜNEŞ IŞIĞI İLE BAŞLATILAN TAHRİBİNİN MEKANİK İNCELENMESİ

Dünya genelinde artan temiz içme suyu kıtlığı nedeniyle patojen mikroorganizmalardan arındırılmış içme suyu elde etmek için bazı dezenfeksiyon teknikleri geliştirilmiştir. Mikroorganizmaların inaktivasyonu için, doğal veya yapay güneş ışığı kullanılarak suyun dezenfekte edilmesi konusu detaylı olarak çalışılmıştır. Patojenler güneş ışığı ve termal ısının sinerjistik etkisiyle parçalanabilmektedir. Son zamanlarda, mikroorganizmaların etkin bir şekilde inaktivasyonu için solar fotokatalizin uygulanması önem kazanmıştır. Bu çalışmada, model indikatör organizma olarak kullanılan *Escheriscia coli*'nin güneş ışığı ile başlatılan tahribi ve ortama salınan organik maddenin karakterizasyonu fotokatalist olarak titanyum dioksit ve onun ikinci nesil çeşidi Fe-yüklü titanyum dioksitin varlığında ve yokluğunda değerlendirilmiştir. Hücre duvarının tahrip edilmesi sırasında ortama salınan protein, karbonhidrat, ve potasyum miktarları tayin edilmiştir. *E. coli*'nin solar fotolitik/fotokatalitik inaktivasyonu doğal su kaynaklarının iyon karakteristiklerini sağlayan su ortamının varlığında ve yokluğunda, ve doğal su kaynaklarında çözünmüş organik madde analoğu olan hümik asidin varlığında ve yokluğunda yürütülmüş, böylece *E. coli* varlığında hümik asidin güneş ışığı ile başlatılan degredasyon prosesi de incelenmiştir. *E. coli* inaktivasyonuyla bağlantılı olarak organik madde karakterizasyonu spesifik ultraviyole-görünür bölge ve floresans parametreleri, çözünmüş organik karbon içerikleri ve eksitasyon emisyon matrisi floresans kontür çizimleri ile değerlendirilmiştir. *E. coli* inaktivasyonu, bakteri azalım kinetik parametreleri, ve spektroskopik parametrelerle bağlantılı olarak organik (protein ve karbonhidrat) ve inorganik (K^+ iyonu sızıntısı) içerik tayinleri ile açıklanmıştır.

TABLE OF CONTENTS

ACKNOWLEDGEMENTS……iii
ABSTRACT……iv
ÖZET……v
TABLE OF CONTENTS……vi
LIST OF FIGURES……...xiv
LIST OF TABLES……xxxvi
LIST OF SYMBOLS/ABBREVIATIONS……..xliii
1. INTRODUCTION……... 1
2. LITERATURE REVIEW……3
2.1. Solar Disinfection of Water……..3
2.2. Mechanism of Solar Disinfection……3
2.3. Heterogenous Photocatalysis for the Enhancement of Solar Efficiency……...5
2.3.1. Photocatalytic Oxidation Processes……...6
2.3.2. Bare and Visible Light Activated Doped TiO_2 Species……..6
2.4. Indicator Organism: *Escherichia coli*……...8
2.4.1. *E. coli* Motility……10
2.4.2. Surface Properties and Point of Zero Charge of *E. coli*……11
2.4.3. *E. coli* Inactivation Mechanism During Solar Light Initiated Photocatalytic Processes……12
2.4.3.1. Effect of reactive oxygen species on solar light initiated photocatalytic bacteria destruction……...12
2.4.3.2. Cellular targets of reactive oxygen species……14
Bacterial capsule as extracellular polymeric substances……...14
Cell wall and cell membrane……14
Enzymes……...17
Proteins and DNA……17
2.4.3.3. Detection of bacteria inactivation and mineralization……18
2.5. Water Matrix……..18
2.5.1. Effects of Water Matrix Components on Solar Light Initiated Photocatalytic Processes……18
2.5.1.1. Effect of chloride……...19
2.5.1.2. Effect of nitrate……..19

2.5.1.3. Effect of sulfate……20
2.5.1.4. Effect of phosphate……21
2.5.1.5. Effect of bicarbonate……21
2.5.1.6. Effect of monovalent cations……21
2.5.1.7. Effect of divalent cations……...22
2.6. Natural Organic Matter……...23
2.6.1. Humic Substances and Humic Acid……24
2.6.2. Photochemistry of Humic Substances in Natural Water Systems……28
3. MATERIALS AND METHODS……...34
3.1. Materials……34
3.1.1. Preparation of *E. coli* Suspension……34
3.1.2. Luria Bertani Broth……..34
3.1.3. CHROMagar™ ECC……...34
3.1.4. Isotonic Solution……34
3.1.5. Water Matrix Solution……35
3.1.6. Humic Acid Solution……...35
3.1.7. Photocatalyst Specimens……35
3.2. Methods……..36
3.2.1. Experimental Set-Up……...36
3.2.2. Experimental Procedure……..36
3.2.3. Analytical Methods……37
3.2.3.1. *E. coli* enumeration……37
3.2.3.2. Total protein determination……...39
Procedure……..39
The Lowry Reagent……...39
Solution A (alkaline solution)……...40
Solution B……40
Solution C……40
The Folin-Ciocalteu reagent, 1N……...40
3.2.3.3. Total carbohydrate determination……..40
Procedure……..41
5 % Phenol solution……...41
3.2.3.4. K^+ leakage determination……..41
3.2.3.5. Endotoxin determination……...41
3.2.3.6. UV-vis spectroscopic measurements……42

3.2.3.7. Fluorescence spectroscopic measurements……...43
3.2.3.8. Non-purgeable organic carbon measurements……...43
4. RESULTS AND DISCUSSION……44
4.1. Solar Photolytic Inactivation of *E. coli*……...45
4.1.1. Solar Photolytic *E. coli* Inactivation Under Specified Reaction Conditions, Reductions and Kinetics……..…45
4.1.2. Organic Matter Formation and Removal Upon Solar Photolytic Treatment of *E. coli* in IsoT Solution……....48
4.1.3. Mechanistic Evaluation of *E. coli* Inactivation Upon Solar Photolytic Treatment in IsoT Solution……...……..53
4.1.4. Organic Matter Formation and Removal Upon Solar Photolytic Treatment of *E. coli* in WM solution…….……...55
4.1.5. Mechanistic Evaluation of *E. coli* Inactivation Upon Solar Photolytic Treatment in WM Solution……...……..60
4.1.6. Organic Matter Formation and Removal Upon Solar Photolytic Treatment of *E. coli* in HA solution…….……61
4.1.7. Mechanistic Evaluation of *E. coli* Inactivation Upon Solar Photolytic Treatment in HA Solution……...……66
4.1.8. Organic Matter Formation and Removal Upon Solar Photolytic Treatment of *E. coli* in "HA and WM" solution…….……...67
4.1.9. Mechanistic Evaluation of *E. coli* Inactivation Upon Solar Photolytic Treatment in "HA and WM" Solution……...……..72
4.1.10. Comparative Evaluation of Different Experimental Matrixes on Solar Photolytic Inactivation Mechanism of *E. coli*……..……73
4.2. Solar Photocatalytic Inactivation of *E. coli*……77
4.2.1. TiO_2 Solar Photocatalytic Inactivation of *E. coli*……77
4.2.1.1. TiO_2 solar photocatalytic *E. coli* inactivation under specified reaction conditions, reductions, and kinetics……77
4.2.1.2. Organic matter formation and removal upon TiO_2 solar photocatalytic treatment of *E. coli* in IsoT solution……..79
4.2.1.3. Mechanistic evaluation of *E. coli* inactivation upon TiO_2 solar photocatalytic treatment in IsoT solution…….……84
4.2.1.4. Organic matter formation and removal upon TiO_2 solar photocatalytic treatment of *E. coli* in WM solution……..85
4.2.1.5. Mechanistic evaluation of *E. coli* inactivation upon TiO_2 solar

photocatalytic treatment in WM solution……..…….90
4.2.1.6. Organic matter formation and removal upon TiO_2 solar photocatalytic treatment of *E. coli* in HA solution…….91
4.2.1.7. Mechanistic evaluation of *E. coli* inactivation upon TiO_2 solar photocatalytic treatment in HA solution…….……97
4.2.1.8. Organic matter formation and removal upon TiO_2 solar photocatalytic treatment of *E. coli* in "HA and WM" solution……...98
4.2.1.9. Mechanistic evaluation of *E. coli* inactivation upon TiO_2 solar photocatalytic treatment in "HA and WM" solution……103
4.2.1.10. Comparative evaluation of different experimental matrixes on TiO_2 solar photocatalytic inactivation mechanism of *E. coli*……...…...104
4.2.2. SynTiO_2 Solar Photocatalytic Inactivation of *E. coli*……..108
4.2.2.1. SynTiO_2 solar photocatalytic *E. coli* inactivation under specified reaction conditions, reductions, and kinetics……...……108
4.2.2.2. Organic matter formation and removal upon SynTiO_2 solar photocatalytic treatment of *E. coli* in IsoT solution…….……110
4.2.2.3. Mechanistic evaluation of *E. coli* inactivation upon SynTiO_2 solar photocatalytic treatment in IsoT solution…….114
4.2.2.4. Organic matter formation and removal upon SynTiO_2 solar photocatalytic treatment of *E. coli* in WM solution…….……115
4.2.2.5. Mechanistic evaluation of *E. coli* inactivation upon SynTiO_2 solar photocatalytic treatment in WM solution…….120
4.2.2.6. Organic matter formation and removal upon SynTiO_2 solar photocatalytic treatment of *E. coli* in HA solution…….……...121
4.2.2.7. Mechanistic evaluation of *E. coli* inactivation upon SynTiO_2 solar photocatalytic treatment in HA solution……...126
4.2.2.8. Organic matter formation and removal upon SynTiO_2 solar photocatalytic treatment of *E. coli* in "HA and WM" solution…….127
4.2.2.9. Mechanistic evaluation of *E. coli* inactivation upon SynTiO_2 solar photocatalytic treatment in "HA and WM" solution……132
4.2.2.10. Comparative evaluation of different experimental matrixes on SynTiO_2 solar photocatalytic inactivation mechanism of *E. coli*……....133
4.2.3. 0.25% Fe-TiO_2 Solar Photocatalytic Inactivation of *E. coli*……136
4.2.3.1. 0.25% Fe-TiO_2 solar photocatalytic *E. coli* inactivation under specified reaction conditions, reductions, and kinetics……136

4.2.3.2. Organic matter formation and removal upon 0.25% Fe-TiO_2 solar photocatalytic treatment of *E. coli* in IsoT solution……..138
4.2.3.3. Mechanistic evaluation of *E. coli* inactivation upon 0.25% Fe-TiO_2 solar photocatalytic treatment in IsoT solution……....143
4.2.3.4. Organic matter formation and removal upon 0.25% Fe-TiO_2 solar photocatalytic treatment of *E. coli* in WM solution……..144
4.2.3.5. Mechanistic evaluation of *E. coli* inactivation upon 0.25% Fe-TiO_2 solar photocatalytic treatment in WM solution……..……149
4.2.3.6. Organic matter formation and removal upon 0.25% Fe-TiO_2 solar photocatalytic treatment of *E. coli* in HA solution……150
4.2.3.7. Mechanistic evaluation of *E. coli* inactivation upon 0.25% Fe-TiO_2 solar photocatalytic treatment in HA solution……..……...155
4.2.3.8. Organic matter formation and removal upon 0.25% Fe-TiO_2 solar photocatalytic treatment of *E. coli* in "HA and WM" solution…….156
4.2.3.9. Mechanistic evaluation of *E. coli* inactivation upon 0.25% Fe-TiO_2 solar photocatalytic treatment in "HA and WM" solution……161
4.2.3.10. Comparative evaluation of different experimental matrixes on 0.25% Fe-TiO_2 solar photocatalytic inactivation mechanism of *E. coli*.....162
4.2.4. 0.50% Fe-TiO_2 Solar Photocatalytic Inactivation of *E. coli*……165
4.2.4.1. 0.50% Fe-TiO_2 solar photocatalytic *E. coli* inactivation under specified reaction conditions, reductions, and kinetics……165
4.2.4.2. Organic matter formation and removal upon 0.50% Fe-TiO_2 solar photocatalytic treatment of *E. coli* in IsoT solution……..167
4.2.4.3. Mechanistic evaluation of *E. coli* inactivation upon 0.50% Fe-TiO_2 solar photocatalytic treatment in IsoT solution……...….172
4.2.4.4. Organic matter formation and removal upon 0.50% Fe-TiO_2 solar photocatalytic treatment of *E. coli* in WM solution……..173
4.2.4.5. Mechanistic evaluation of *E. coli* inactivation upon 0.50% Fe-TiO_2 solar photocatalytic treatment in WM solution……..……177
4.2.4.6. Organic matter formation and removal upon 0.50% Fe-TiO_2 solar photocatalytic treatment of *E. coli* in HA solution……178
4.2.4.7. Mechanistic evaluation of *E. coli* inactivation upon 0.50% Fe-TiO_2 solar photocatalytic treatment in HA solution……..……...183
4.2.4.8. Organic matter formation and removal upon 0.50% Fe-TiO_2 solar photocatalytic treatment of *E. coli* in "HA and WM" solution…….184

4.2.4.9. Mechanistic evaluation of *E. coli* inactivation upon 0.50% Fe-TiO_2 solar photocatalytic treatment in "HA and WM" solution……189
4.2.4.10. Comparative evaluation of different experimental matrixes on 0.50% Fe-TiO_2 solar photocatalytic inactivation mechanism of *E. coli*….190
4.2.5. 0.25% Fe-SynTiO_2 Solar Photocatalytic Inactivation of *E. coli*……...…..193
4.2.5.1. 0.25% Fe-SynTiO_2 solar photocatalytic *E. coli* inactivation under specified reaction conditions, reductions, and kinetics…….……193
4.2.5.2. Organic matter formation and removal upon 0.25% Fe-SynTiO_2 solar photocatalytic treatment of *E. coli* in IsoT solution……..195
4.2.5.3. Mechanistic evaluation of *E. coli* inactivation upon 0.25% Fe-SynTiO_2 solar photocatalytic treatment in IsoT solution……...…….200
4.2.5.4. Organic matter formation and removal upon 0.25% Fe-SynTiO_2 solar photocatalytic treatment of *E. coli* in WM solution……..201
4.2.5.5. Mechanistic evaluation of *E. coli* inactivation upon 0.25% Fe-SynTiO_2 solar photocatalytic treatment in WM solution……...…….206
4.2.5.6. Organic matter formation and removal upon 0.25% Fe-SynTiO_2 solar photocatalytic treatment of *E. coli* in HA solution……207
4.2.5.7. Mechanistic evaluation of *E. coli* inactivation upon 0.25% Fe-SynTiO_2 solar photocatalytic treatment in HA solution……...……...212
4.2.5.8. Organic matter formation and removal upon 0.25% Fe-SynTiO_2 solar photocatalytic treatment of *E. coli* in "HA and WM" solution…….213
4.2.5.9. Mechanistic evaluation of *E. coli* inactivation upon 0.25% Fe-SynTiO_2 solar photocatalytic treatment in "HA and WM" solution……218
4.2.5.10. Comparative evaluation of different experimental matrixes on 0.25% Fe-SynTiO_2 solar photocatalytic inactivation mechanism of *E. coli*……..……219
4.2.6. 0.50% Fe-SynTiO_2 Solar Photocatalytic Inactivation of *E. coli*……...……..222
4.2.6.1. 0.50% Fe-SynTiO_2 solar photocatalytic *E. coli* inactivation under specified reaction conditions, reductions, and kinetics…….……222
4.2.6.2. Organic matter formation and removal upon 0.50% Fe-SynTiO_2 solar photocatalytic treatment of *E. coli* in IsoT solution……..224
4.2.6.3. Mechanistic evaluation of *E. coli* inactivation upon 0.50% Fe-SynTiO_2 solar photocatalytic treatment in IsoT solution……...…….228
4.2.6.4. Organic matter formation and removal upon 0.50% Fe-SynTiO_2 solar photocatalytic treatment of *E. coli* in WM solution……..229

4.2.6.5. Mechanistic evaluation of *E. coli* inactivation upon 0.50% Fe-SynTiO$_2$ solar photocatalytic treatment in WM solution……..…….233
4.2.6.6. Organic matter formation and removal upon 0.50% Fe-SynTiO$_2$ solar photocatalytic treatment of *E. coli* in HA solution……234
4.2.6.7. Mechanistic evaluation of *E. coli* inactivation upon 0.50% Fe-SynTiO$_2$ solar photocatalytic treatment in HA solution……..……...238
4.2.6.8. Organic matter formation and removal upon 0.50% Fe-SynTiO$_2$ solar photocatalytic treatment of *E. coli* in "HA and WM" solution…….239
4.2.6.9. Mechanistic evaluation of *E. coli* inactivation upon 0.50% Fe-SynTiO$_2$ solar photocatalytic treatment in "HA and WM" solution……244
4.2.6.10. Comparative evaluation of different experimental matrixes on 0.50% Fe-SynTiO$_2$ solar photocatalytic inactivation mechanism of *E. coli*…….……245
4.3. Comparative Evaluation of *E. coli* Inactivation Upon Use of Photocatalyst Specimens……249
4.3.1. Comparative Efficiency Evaluation of Different Photocatalyst Specimens on *E. coli* Inactivation in IsoT Solution.……249
4.3.1.1. Comparative mechanistic evaluation of *E. coli* inactivation in IsoT solution upon solar photocatalytic treatment with undoped and Fe-doped TiO$_2$ specimens……...251
4.3.2. Comparative Efficiency Evaluation of Different Photocatalyst Specimens on *E. coli* Inactivation in WM Solution…….……252
4.3.2.1. Comparative mechanistic evaluation of *E. coli* inactivation in WM solution upon solar photocatalytic treatment with undoped and Fe-doped TiO$_2$ specimens……...254
4.3.3. Comparative Efficiency Evaluation of Different Photocatalyst Specimens on *E. coli* Inactivation in HA Solution…….……..256
4.3.3.1. Comparative mechanistic evaluation of *E. coli* inactivation in HA solution upon solar photocatalytic treatment with undoped and Fe-doped TiO$_2$ specimens……...258
4.3.4. Comparative Efficiency Evaluation of Different Photocatalyst Specimens on *E. coli* Inactivation in "HA and WM" Solution…….……260
4.3.4.1. Comparative mechanistic evaluation of *E. coli* inactivation in "HA and WM" solution upon solar photocatalytic treatment with undoped and Fe-doped TiO$_2$ specimens……..……...262

4.4. Endotoxin Release Upon Solar Photolytic and Photocatalytic Inactivation of *E. coli* in Various Aqueous Solutions……..264
5. CONCLUSION……266
REFERENCES……268
APPENDIX A: COMPOSITION OF WATER MATRIX SOLUTION……...298
APPENDIX B: SPECTROSCOPIC CHARACTERIZATION OF 100 kDa HUMIC ACID SOLUTION……299
APPENDIX C: CHARACTERIZATION OF PHOTOCATALYST SPECIMENS……301
APPENDIX D: CALIBRATION CURVE OF BOVINE SERUM ALBUMIN STANDARD……303
APPENDIX E: CALIBRATION CURVE OF GLUCOSE STANDARD……304

LIST OF FIGURES

Figure 2.1. Proposed schematic process of cell destruction……..4

Figure 2.2. a. Formation of surface hydroxylated species of TiO_2 according to pH;
b. pH dependent electrostatic interactions on TiO_2 surface……7

Figure 2.3. The general structure of a prokaryotic organism. Red-labeled structures
are found in all bacteria species, while black-labeled ones are not……....9

Figure 2.4. a. CCW, CW flagella rotations and movement of *E. coli*; b. Run and tumble
movements of a bacterium. Blue arrows indicate the flagellar rotation direction and
gray arrows indicate the movement direction; c. Random walk pattern of bacteria……..10

Figure 2.5. Transmission electron microscopy (TEM) image of *E. coli* with TiO_2 particles
attached on it……...12

Figure 2.6. Possible mechanism of photocatalytic disinfection of bacteria……13

Figure 2.7. a. Structural membrane composition and possible photocatalytic disinfection
mechanism; b. Lipid peroxidation and membrane leakage process in
Gram-negative bacteria e.g. *E. coli*……..13

Figure 2.8. Cell wall and cell membrane structure of Gram-negative bacteria……...14

Figure 2.9. Schematic diagram of ROS utilized lipid peroxidation reaction……...15

Figure 2.10. Venn diagram of various NOM forms found in natural waters.
TOM or NOM, TOC, DOM, DOC, POC, DON, DOP
and humic and non-humic materials are represented……..23

Figure 2.11. Organic matter mass (Da) and size (μm) distribution diagram of NOM species
and organisms in natural waters. Molecular weight (MW), humic acid (HAc),
fulvic acid (FAc), hydrocarbons (HC), carbohydrates (CHO), fatty acids (FA),

amino acid (AA)…….24

Figure 2.12. Conceptual model of polydisperse HSs……..25

Figure 2.13. The postulated relation of HSs……25

Figure 2.14. a. Conformational changes of HA molecules through alkaline to acidic pH; A. Charge repulsion at alkaline pH, B. Intramolecular aggregation at decreasing pH, C. Intermolecular aggregation at decreasing pH, D. Precipitation at acidic pH; b. Tail, loop, and train formations of a HA polymer chain adsorbed on the surface..…..26

Figure 2.15. a. Hypothetical structure of HA; b. Functional groups and their range of pK_a values present in HA; c. Theoretical structure of HA; d. Proposed three-dimensional structure of HA…….27

Figure 2.16. a. UV-vis absorption spectra; b. emission scan; and c. synchronous scan fluorescence spectra of IHSS soil HA (SHA), IHSS HA, IHSS FA, Aldrich HA (AHA), Roth HA (RHA), and Nordic HA (NHA)……..28

Figure 2.17. Representative functional groups and building blocks of HSs……29

Figure 2.18. Diagram of EEM fluorescence contour plot regions……...33

Figure 3.1. Solar simulator Atlas-Suntest CPS+ and reaction vessel.……36

Figure 3.2. *E. coli* cultured CHROMagar™ ECC plates. Top Left: 10^{-2} dilution from initial *E. coli* solution, inoculation volume: 10 μL. Top Right: 10^{-5} dilution from *E. coli* suspension, inoculation volume: 5 μL. Middle Left: 10^{-3} dilution from initial *E. coli* solution, inoculation volume: 20 μL. Middle Right: 10^{-3} dilution from t=0 *E. coli* solution, inoculation volume: 10 μL. Bottom Left: 10^{-2} dilution from t=0 *E. coli* solution, inoculation volume: 10 μL. Bottom Right: 10^{-2} dilution from t_{irr}=30 min *E. coli* solution, inoculation volume: 50 μL……..38

Figure 3.3. Schematic reaction of phenol-sulfuric acid method……..40

Figure 4.1. Irradiation time dependent *E. coli* inactivation upon solar photolytic treatment in different solution matrixes……...46

Figure 4.2. UV-vis absorption spectra of organic matter: Irradiation time dependent *E. coli* inactivation in IsoT solution upon solar photolytic treatment……...48

Figure 4.3. Synchronous scan fluorescence spectra of organic matter: Irradiation time dependent *E. coli* inactivation in IsoT solution upon solar photolytic treatment……..49

Figure 4.4. Specified UV-vis and fluroscence parameters of organic matter: Irradiation time dependent *E. coli* inactivation in IsoT solution upon solar photolytic treatment……..50

Figure 4.5. Specific UV-vis and fluroscence parameters of organic matter: Irradiation time dependent *E. coli* inactivation in IsoT upon solar photolytic treatment……51

Figure 4.6. EEM fluorescence contour plots of organic matter: Irradiation time dependent *E. coli* inactivation in IsoT solution upon solar photolytic treatment……52

Figure 4.7. UV-vis absorption spectra of organic matter: Irradiation time dependent *E. coli* inactivation in WM solution upon solar photolytic treatment……55

Figure 4.8. Synchronous scan fluorescence spectra of organic matter: Irradiation time dependent *E. coli* inactivation in WM solution upon solar photolytic treatment……56

Figure 4.9. Specified UV-vis and fluroscence parameters of organic matter: Irradiation time dependent *E. coli* inactivation in WM solution upon solar photolytic treatment…….57

Figure 4.10. Specific UV-vis and fluroscence parameters of organic matter: Irradiation time dependent *E. coli* inactivation in WM solution upon solar photolytic treatment……57

Figure 4.11. EEM fluorescence contour plots of organic matter: Irradiation time dependent *E. coli* inactivation in WM solution upon solar photolytic treatment……..59

Figure 4.12. UV-vis absorption spectra of organic matter: Irradiation time dependent *E. coli* inactivation in HA solution upon solar photolytic treatment……..61

Figure 4.13. Synchronous scan fluorescence spectra of organic matter: Irradiation time dependent *E. coli* inactivation in HA solution upon solar photolytic treatment……..62

Figure 4.14. Specified UV-vis and fluroscence parameters of organic matter: Irradiation time dependent *E. coli* inactivation in HA solution upon solar photolytic treatment…….62

Figure 4.15. Specific UV-vis and fluroscence parameters of organic matter: Irradiation time dependent *E. coli* inactivation in HA solution upon solar photolytic treatment…….63

Figure 4.16. EEM fluorescence contour plots of organic matter: Irradiation time dependent *E. coli* inactivation in HA solution upon solar photolytic treatment……...65

Figure 4.17. UV-vis absorption spectra of organic matter. Irradiation time dependent *E. coli* inactivation in "HA and WM" solution upon solar photolytic treatment…….67

Figure 4.18. Synchronous scan fluorescence spectra of organic matter: Irradiation time dependent *E. coli* inactivation in "HA and WM" solution upon solar photolytic treatment……...…….68

Figure 4.19. Specified UV-vis and fluroscence parameters of organic matter: Irradiation time dependent *E. coli* inactivation in "HA and WM" solution upon solar photolytic treatment……...69

Figure 4.20. Specific UV-vis and fluroscence parameters of organic matter: Irradiation time dependent *E. coli* inactivation in "HA and WM" solution upon solar photolytic treatment……...70

Figure 4.21. EEM fluorescence contour plots of organic matter: Irradiation time dependent *E. coli* inactivation in "HA and WM" solution upon solar photolytic treatment……....71

Figure 4.22. Initial and t_{irr}=60 min total K, protein, and carbohydrate contents, and bacteria enumeration results of *E. coli* inactivation upon solar photolytic treatment in various aqueous matrixes.……..73

Figure 4.23. Released protein and carbohydrate contents, and bacteria LRV of *E. coli*

inactivation upon solar photolytic treatment in various aqueous matrixes……74

Figure 4.24. Initial and t_{irr}=60 min protein and carbohydrate contents, $FI_{sync280}$, UV_{280}, NPOC, and bacteria enumeration results upon solar photolytic treatment of *E. coli* in various aqueous matrixes.……...…….....76

Figure 4.25. Irradiation time dependent *E. coli* inactivation upon TiO_2 solar photocatalytic treatment in various solution matrixes……...77

Figure 4.26. UV-vis absorption spectra of organic matter: Irradiation time dependent *E. coli* inactivation in IsoT solution upon TiO_2 solar photocatalytic treatment……..80

Figure 4.27. Synchronous scan fluorescence spectra of organic matter: Irradiation time dependent *E. coli* inactivation in IsoT solution upon TiO_2 solar photocatalytic treatment……...80

Figure 4.28. Specified UV-vis and fluroscence parameters of organic matter: Irradiation time dependent *E. coli* inactivation in IsoT solution upon TiO_2 solar photocatalytic treatment……...81

Figure 4.29. Specific UV-vis and fluroscence parameters of organic matter: Irradiation time dependent *E. coli* inactivation in IsoT solution upon TiO_2 solar photocatalytic treatment……...81

Figure 4.30. EEM fluorescence contour plots of organic matter: Irradiation time dependent *E. coli* inactivation in IsoT solution upon TiO_2 solar photocatalytic treatment……..83

Figure 4.31. UV-vis absorption spectra of organic matter: Irradiation time dependent *E. coli* inactivation in WM solution upon TiO_2 solar photocatalytic treatment……...85

Figure 4.32. Synchronous scan fluorescence spectra of organic matter: Irradiation time dependent *E. coli* inactivation in WM solution upon TiO_2 solar photocatalytic treatment……86

Figure 4.33. Specified UV-vis and fluroscence parameters of organic matter: Irradiation time

dependent *E. coli* inactivation in WM solution upon TiO_2 solar photocatalytic treatment……86

Figure 4.34. Specific UV-vis and fluroscence parameters of organic matter: Irradiation time dependent *E. coli* inactivation in WM solution upon TiO_2 solar photocatalytic treatment……87

Figure 4.35. EEM fluorescence contour plots of organic matter: Irradiation time dependent *E. coli* inactivation in WM solution upon TiO_2 solar photocatalytic treatment……...89

Figure 4.36. UV-vis absorption spectra of organic matter: Irradiation time dependent *E. coli* inactivation in HA solution upon TiO_2 solar photocatalytic treatment……91

Figure 4.37. Synchronous scan fluorescence spectra of organic matter: Irradiation time dependent *E. coli* inactivation in HA solution upon TiO_2 solar photocatalytic treatment……...92

Figure 4.38. Specified UV-vis and fluroscence parameters of organic matter: Irradiation time dependent *E. coli* inactivation in HA solution upon TiO_2 solar photocatalytic treatment……93

Figure 4.39. Specific UV-vis and fluroscence parameters of organic matter: Irradiation time dependent *E. coli* inactivation in HA solution upon TiO_2 solar photocatalytic treatment……94

Figure 4.40. EEM fluorescence contour plots of organic matter. Irradiation time dependent *E. coli* inactivation in HA solution upon TiO_2 solar photocatalytic treatment……96

Figure 4.41. UV-vis absorption spectra of organic matter: Irradiation time dependent *E. coli* inactivation in "HA and WM" solution upon TiO_2 solar photocatalytic treatment…….98

Figure 4.42. Synchronous scan fluorescence spectra of organic matter: Irradiation time dependent *E. coli* inactivation in "HA and WM" solution upon TiO_2 solar photocatalytic treatment…….99

Figure 4.43. Specified UV-vis and fluroscence parameters of organic matter: Irradiation time dependent *E. coli* inactivation in "HA and WM" solution upon TiO_2 solar photocatalytic treatment……...100

Figure 4.44. Specific UV-vis and fluroscence parameters of organic matter: Irradiation time dependent *E. coli* inactivation in "HA and WM" solution upon TiO_2 solar photocatalytic treatment…….…..101

Figure 4.45. EEM fluorescence contour plots of organic matter: Irradiation time dependent *E. coli* inactivation in "HA and WM" solution upon TiO_2 solar photocatalytic treatment……..102

Figure 4.46. Initial, t=0, and t_{irr}=60 min total K, protein, carbohydrate content, and bacteria enumeration results of *E. coli* inactivation upon TiO_2 solar photocatalytic treatment in various aqueous matrixes…….105

Figure 4.47. Released (Left) and degraded (Right) protein and carbohydrate contents, and bacteria LRV of *E. coli* inactivation upon TiO_2 solar photocatalytic treatment in various aqueous matrixes……106

Figure 4.48. Initial, t=0, and t_{irr}=60 min protein and carbohydrate contents, $FI_{sync280}$, UV_{280}, NPOC, and bacteria enumeration results of TiO_2 solar photocatalytic treatment of *E. coli* in various aqueous matrixes……..107

Figure 4.49. Irradiation time dependent *E. coli* inactivation upon $SynTiO_2$ solar photocatalytic treatment in various solution matrixes…….…….108

Figure 4.50. UV-vis absorption spectra of organic matter: Irradiation time dependent *E. coli* inactivation in IsoT solution upon $SynTiO_2$ solar photocatalytic treatment……110

Figure 4.51. Synchronous scan fluorescence spectra of organic matter: Irradiation time dependent *E. coli* inactivation in IsoT solution upon $SynTiO_2$ solar photocatalytic treatment……...111

Figure 4.52. Specified UV-vis and fluroscence parameters of organic matter: Irradiation

time dependent *E. coli* inactivation in IsoT solution upon $SynTiO_2$ solar photocatalytic treatment……..……..111

Figure 4.53. Specific UV-vis and fluroscence parameters of organic matter: Irradiation time dependent *E. coli* inactivation in IsoT solution upon $SynTiO_2$ solar photocatalytic treatment…….……..112

Figure 4.54. EEM fluorescence contour plots of organic matter: Irradiation time dependent *E. coli* inactivation in IsoT solution upon $SynTiO_2$ solar photocatalytic treatment…….……..113

Figure 4.55. UV-vis absorption spectra of organic matter: Irradiation time dependent *E. coli* inactivation in WM solution upon $SynTiO_2$ solar photocatalytic treatment…….115

Figure 4.56. Synchronous scan fluorescence spectra of organic matter: Irradiation time dependent *E. coli* inactivation in WM solution upon $SynTiO_2$ solar photocatalytic treatment……...116

Figure 4.57. Specified UV-vis and fluroscence parameters of organic matter: Irradiation time dependent *E. coli* inactivation in WM solution upon $SynTiO_2$ solar photocatalytic treatment…….……..117

Figure 4.58. Specific UV-vis and fluroscence parameters of organic matter: Irradiation time dependent *E. coli* inactivation in WM solution upon $SynTiO_2$ solar photocatalytic treatment……...117

Figure 4.59. EEM fluorescence contour plots of organic matter: Irradiation time dependent *E. coli* inactivation in WM solution upon $SynTiO_2$ solar photocatalytic treatment……...…119

Figure 4.60. UV-vis absorption spectra of organic matter: Irradiation time dependent *E. coli* inactivation in HA solution upon $SynTiO_2$ solar photocatalytic treatment……...121

Figure 4.61. Synchronous scan fluorescence spectra of organic matter: Irradiation time dependent *E. coli* inactivation in HA solution upon $SynTiO_2$ solar

photocatalytic treatment……...121

Figure 4.62. Specified UV-vis and fluroscence parameters of organic matter: Irradiation time dependent *E. coli* inactivation in HA solution upon $SynTiO_2$ solar photocatalytic treatment……...122

Figure 4.63. Specific UV-vis and fluroscence parameters of organic matter: Irradiation time dependent *E. coli* inactivation in HA solution upon $SynTiO_2$ solar photocatalytic treatment……...123

Figure 4.64. EEM fluorescence contour plots of organic matter: Irradiation time dependent *E. coli* inactivation in HA solution upon $SynTiO_2$ solar photocatalytic treatment……...125

Figure 4.65. UV-vis absorption spectra of organic matter: Irradiation time dependent *E. coli* inactivation in "HA and WM" solution upon $SynTiO_2$ solar photocatalytic treatment……...127

Figure 4.66. Synchronous scan fluorescence spectra of organic matter: Irradiation time dependent *E. coli* inactivation in "HA and WM" solution upon $SynTiO_2$ solar photocatalytic treatment……...128

Figure 4.67. Specified UV-vis and fluroscence parameters of organic matter: Irradiation time dependent *E. coli* inactivation in "HA and WM" solution upon $SynTiO_2$ solar photocatalytic treatment…….....129

Figure 4.68. Specific UV-vis and fluroscence parameters of organic matter: Irradiation time dependent *E. coli* inactivation in "HA and WM" solution upon $SynTiO_2$ solar photocatalytic treatment…….…….130

Figure 4.69. EEM fluorescence contour plots of organic matter: Irradiation time dependent *E. coli* inactivation in "HA and WM" solution upon $SynTiO_2$ solar photocatalytic treatment…….……..131

Figure 4.70. Initial, t=0, and t_{irr}=60 min total K, protein, and carbohydrate contents, and

bacteria enumeration results of *E. coli* inactivation upon $SynTiO_2$ solar photocatalytic treatment in various aqueous matrixes……..133

Figure 4.71. Released protein and carbohydrate contents, and bacteria LRV of *E. coli* inactivation upon $SynTiO_2$ solar photocatalytic treatment in various aqueous matrixes……...……..134

Figure 4.72. Initial, t=0, and t_{irr}=60 min protein and carbohydrate contents, $FI_{sync280}$, UV_{280}, NPOC, and bacteria enumeration results of $SynTiO_2$ solar photocatalytic treatment of *E. coli* in various aqueous matrixes……..135

Figure 4.73. Irradiation time dependent *E. coli* inactivation upon 0.25% Fe-TiO_2 solar photocatalytic treatment in various solution matrixes……..……136

Figure 4.74. UV-vis absorption spectra of organic matter: Irradiation time dependent *E. coli* inactivation in IsoT solution upon 0.25% Fe-TiO_2 solar photocatalytic treatment……..139

Figure 4.75. Synchronous scan fluorescence spectra of organic matter: Irradiation time dependent *E. coli* inactivation in IsoT solution upon 0.25% Fe-TiO_2 solar photocatalytic treatment……...139

Figure 4.76. Specified UV-vis and fluroscence parameters of organic matter: Irradiation time dependent *E. coli* inactivation in IsoT solution upon 0.25% Fe-TiO_2 solar photocatalytic treatment……...140

Figure 4.77. Specific UV-vis and fluroscence parameters of organic matter: Irradiation time dependent *E. coli* inactivation in IsoT solution upon 0.25% Fe-TiO_2 solar photocatalytic treatment……...140

Figure 4.78. EEM fluorescence contour plots of organic matter: Irradiation time dependent *E. coli* inactivation in IsoT solution upon 0.25% Fe-TiO_2 solar photocatalytic treatment……..…142

Figure 4.79. UV-vis absorption spectra of organic matter: Irradiation time dependent

E. coli inactivation in WM solution upon 0.25% Fe-TiO_2 solar photocatalytic treatment……..144

Figure 4.80. Synchronous scan fluorescence spectra of organic matter: Irradiation time dependent *E. coli* inactivation in WM solution upon 0.25% Fe-TiO_2 solar photocatalytic treatment……..145

Figure 4.81. Specified UV-vis and fluroscence parameters of organic matter: Irradiation time dependent *E. coli* inactivation in WM solution upon 0.25% Fe-TiO_2 solar photocatalytic treatment……...145

Figure 4.82. Specific UV-vis and fluroscence parameters of organic matter: Irradiation time dependent *E. coli* inactivation in WM solution upon 0.25% Fe-TiO_2 solar photocatalytic treatment……..146

Figure 4.83. EEM fluorescence contour plots of organic matter: Irradiation time dependent *E. coli* inactivation in WM solution upon 0.25% Fe-TiO_2 solar photocatalytic treatment……..148

Figure 4.84. UV-vis absorption spectra of organic matter: Irradiation time dependent *E. coli* inactivation in HA solution upon 0.25% Fe-TiO_2 solar photocatalytic treatment…….150

Figure 4.85. Synchronous scan fluorescence spectra of organic matter: Irradiation time dependent *E. coli* inactivation in HA solution upon 0.25% Fe-TiO_2 solar photocatalytic treatment……...151

Figure 4.86. Specified UV-vis and fluroscence parameters of organic matter: Irradiation time dependent *E. coli* inactivation in HA solution upon 0.25% Fe-TiO_2 solar photocatalytic treatment……...152

Figure 4.87. Specific UV-vis and fluroscence parameters of organic matter: Irradiation time dependent *E. coli* inactivation in HA solution upon 0.25% Fe-TiO_2 solar photocatalytic treatment……...152

Figure 4.88. EEM fluorescence contour plots of organic matter: Irradiation time dependent *E. coli* inactivation in HA solution upon 0.25% Fe-TiO_2 solar photocatalytic treatment……..154

Figure 4.89. UV-vis absorption spectra of organic matter: Irradiation time dependent *E. coli* inactivation in "HA and WM" solution upon 0.25% Fe-TiO_2 solar photocatalytic treatment……..156

Figure 4.90. Synchronous scan fluorescence spectra of organic matter: Irradiation time dependent *E. coli* inactivation in "HA and WM" solution upon 0.25% Fe-TiO_2 solar photocatalytic treatment……..157

Figure 4.91. Specified UV-vis and fluroscence parameters of organic matter: Irradiation time dependent *E. coli* inactivation in "HA and WM" solution upon 0.25% Fe-TiO_2 solar photocatalytic treatment……..158

Figure 4.92. Specific UV-vis and fluroscence parameters of organic matter: Irradiation time dependent *E. coli* inactivation in "HA and WM" solution upon 0.25% Fe-TiO_2 solar photocatalytic treatment……..158

Figure 4.93. EEM fluorescence contour plots of organic matter: Irradiation time dependent *E. coli* inactivation in "HA and WM" solution upon 0.25% Fe-TiO_2 solar photocatalytic treatment……...160

Figure 4.94. Initial, t=0, and t_{irr}=60 min total K, protein, and carbohydrate contents, and bacteria enumeration results of *E. coli* inactivation upon 0.25% Fe-TiO_2 solar photocatalytic treatment in various aqueous matrixes……..162

Figure 4.95. Released protein and carbohydrate contents, and bacteria LRV of *E. coli* inactivation upon 0.25% Fe-TiO_2 solar photocatalytic treatment in various aqueous matrixes……...…..163

Figure 4.96. Initial, t=0, and t_{irr}=60 min protein and carbohydrate contents, $FI_{sync280}$, UV_{280}, NPOC, and bacteria enumeration results of 0.25% Fe-TiO_2 solar photocatalytic treatment of *E. coli* in various aqueous matrixes……..164

Figure 4.97. Irradiation time dependent *E. coli* inactivation upon 0.50% Fe-TiO_2 solar photocatalytic treatment in various solution matrixes……..165

Figure 4.98. UV-vis absorption spectra of organic matter: Irradiation time dependent *E. coli* inactivation in IsoT solution upon 0.50% Fe-TiO_2 solar photocatalytic treatment……..167

Figure 4.99. Synchronous scan fluorescence spectra of organic matter: Irradiation time dependent *E. coli* inactivation in IsoT solution upon 0.50% Fe-TiO_2 solar photocatalytic treatment……...168

Figure 4.100. Specified UV-vis and fluroscence parameters of organic matter: Irradiation time dependent *E. coli* inactivation in IsoT solution upon 0.50% Fe-TiO_2 solar photocatalytic treatment……169

Figure 4.101. Specific UV-vis and fluroscence parameters of organic matter: Irradiation time dependent *E. coli* inactivation in IsoT solution upon 0.50% Fe-TiO_2 solar photocatalytic treatment……169

Figure 4.102. EEM fluorescence contour plots of organic matter: Irradiation time dependent *E. coli* inactivation in IsoT solution upon 0.50% Fe-TiO_2 solar photocatalytic treatment……171

Figure 4.103. UV-vis absorption spectra of organic matter: Irradiation time dependent *E. coli* inactivation in WM solution upon 0.50% Fe-TiO_2 solar photocatalytic treatment……173

Figure 4.104. Synchronous scan fluorescence spectra of organic matter: Irradiation time dependent *E. coli* inactivation in WM solution upon 0.50% Fe-TiO_2 solar photocatalytic treatment……174

Figure 4.105. Specified UV-vis and fluroscence parameters of organic matter: Irradiation time dependent *E. coli* inactivation in WM solution upon 0.50% Fe-TiO_2 solar photocatalytic treatment……174

Figure 4.106. Specific UV-vis and fluroscence parameters of organic matter: Irradiation time dependent *E. coli* inactivation in WM solution upon 0.50% Fe-TiO_2 solar photocatalytic treatment……175

Figure 4.107. EEM fluorescence contour plots of organic matter: Irradiation time dependent *E. coli* inactivation in WM solution upon 0.50% Fe-TiO_2 solar photocatalytic treatment……176

Figure 4.108. UV-vis absorption spectra of organic matter: Irradiation time dependent *E. coli* inactivation in HA solution upon 0.50% Fe-TiO_2 solar photocatalytic treatment……178

Figure 4.109. Synchronous scan fluorescence spectra of organic matter: Irradiation time dependent *E. coli* inactivation in HA solution upon 0.50% Fe-TiO_2 solar photocatalytic treatment……179

Figure 4.110. Specified UV-vis and fluroscence parameters of organic matter: Irradiation time dependent *E. coli* inactivation in HA solution upon 0.50% Fe-TiO_2 solar photocatalytic treatment……...180

Figure 4.111. Specific UV-vis and fluroscence parameters of organic matter: Irradiation time dependent *E. coli* inactivation in HA solution upon 0.50% Fe-TiO_2 solar photocatalytic treatment……180

Figure 4.112. EEM fluorescence contour plots of organic matter: Irradiation time dependent *E. coli* inactivation in HA solution upon 0.50% Fe-TiO_2 solar photocatalytic treatment……182

Figure 4.113. UV-vis absorption spectra of organic matter: Irradiation time dependent *E. coli* inactivation in “HA and WM” solution upon 0.50% Fe-TiO_2 solar photocatalytic treatment……184

Figure 4.114. Synchronous scan fluorescence spectra of organic matter: Irradiation time dependent *E. coli* inactivation in “HA and WM” solution upon 0.50% Fe-TiO_2 solar photocatalytic treatment……185

Figure 4.115. Specified UV-vis and fluroscence parameters of organic matter: Irradiation time dependent *E. coli* inactivation in "HA and WM" solution upon 0.50% Fe-TiO_2 solar photocatalytic treatment……186

Figure 4.116. Specific UV-vis and fluroscence parameters of organic matter: Irradiation time dependent *E. coli* inactivation in "HA and WM" solution upon 0.50% Fe-TiO_2 solar photocatalytic treatment…….……...186

Figure 4.117. EEM fluorescence contour plots of organic matter: Irradiation time dependent *E. coli* inactivation in "HA and WM" solution upon 0.50% Fe-TiO_2 solar photocatalytic treatment…….188

Figure 4.118. Initial, t=0, and t_{irr}=60 min total K, protein, and carbohydrate contents, and bacteria enumeration results of *E. coli* inactivation upon 0.50% Fe-TiO_2 solar photocatalytic treatment in various aqueous matrixes……...190

Figure 4.119. Released protein and carbohydrate contents, and bacteria LRV of *E. coli* inactivation upon 0.50% Fe-TiO_2 solar photocatalytic treatment in various aqueous matrixes……...……191

Figure 4.120. Initial, t=0, and t_{irr}=60 min protein and carbohydrate contents, $FI_{sync280}$, UV_{280}, NPOC and bacteria enumeration results of 0.50% Fe-TiO_2 solar photocatalytic treatment of *E. coli* in various aqueous matrixes……192

Figure 4.121. Irradiation time dependent *E. coli* inactivation upon 0.25% Fe-SynTiO_2 solar photocatalytic treatment in various solution matrixes……193

Figure 4.122. UV-vis absorption spectra of organic matter: Irradiation time dependent *E. coli* inactivation in IsoT solution upon 0.25% Fe-SynTiO_2 solar photocatalytic treatment……195

Figure 4.123. Synchronous scan fluorescence spectra of organic matter: Irradiation time dependent *E. coli* inactivation in IsoT solution upon 0.25% Fe-SynTiO_2 solar photocatalytic treatment……196

Figure 4.124. Specified UV-vis and fluroscence parameters of organic matter: Irradiation time dependent *E. coli* inactivation in IsoT solution upon 0.25% Fe-SynTiO$_2$ solar photocatalytic treatment……...196

Figure 4.125. Specific UV-vis and fluroscence parameters of organic matter: Irradiation time dependent *E. coli* inactivation in IsoT solution upon 0.25% Fe-SynTiO$_2$ solar photocatalytic treatment……...197

Figure 4.126. EEM fluorescence contour plots of organic matter: Irradiation time dependent *E. coli* inactivation in IsoT solution upon 0.25% Fe-SynTiO$_2$ solar photocatalytic treatment……199

Figure 4.127. UV-vis absorption spectra of organic matter: Irradiation time dependent *E. coli* inactivation in WM solution upon 0.25% Fe-SynTiO$_2$ solar photocatalytic treatment…….201

Figure 4.128. Synchronous scan fluorescence spectra of organic matter: Irradiation time dependent *E. coli* inactivation in WM solution upon 0.25% Fe-SynTiO$_2$ solar photocatalytic treatment……202

Figure 4.129. Specified UV-vis and fluroscence parameters of organic matter: Irradiation time dependent *E. coli* inactivation in WM solution upon 0.25% Fe-SynTiO$_2$ solar photocatalytic treatment……202

Figure 4.130. Specific UV-vis and fluroscence parameters of organic matter: Irradiation time dependent *E. coli* inactivation in WM solution upon 0.25% Fe-SynTiO$_2$ solar photocatalytic treatment……...203

Figure 4.131. EEM fluorescence contour plots of organic matter: Irradiation time dependent *E. coli* inactivation in WM solution upon 0.25% Fe-SynTiO$_2$ solar photocatalytic treatment……205

Figure 4.132. UV-vis absorption spectra of organic matter: Irradiation time dependent *E. coli* inactivation in HA solution upon 0.25% Fe-SynTiO$_2$ solar photocatalytic treatment…….207

Figure 4.133. Synchronous scan fluorescence spectra of organic matter: Irradiation time dependent *E. coli* inactivation in HA solution upon 0.25% Fe-SynTiO$_2$ solar photocatalytic treatment……208

Figure 4.134. Specified UV-vis and fluroscence parameters of organic matter: Irradiation time dependent *E. coli* inactivation in HA solution upon 0.25% Fe-SynTiO$_2$ solar photocatalytic treatment……208

Figure 4.135. Specific UV-vis and fluroscence parameters of organic matter: Irradiation time dependent *E. coli* inactivation in HA solution upon 0.25% Fe-SynTiO$_2$ solar photocatalytic treatment……209

Figure 4.136. EEM fluorescence contour plots of organic matter: Irradiation time dependent *E. coli* inactivation in HA solution upon 0.25% Fe-SynTiO$_2$ solar photocatalytic treatment……211

Figure 4.137. UV-vis absorption spectra of organic matter: Irradiation time dependent *E. coli* inactivation in "HA and WM" solution upon 0.25% Fe-SynTiO$_2$ solar photocatalytic treatment……213

Figure 4.138. Synchronous scan fluorescence spectra of organic matter: Irradiation time dependent *E. coli* inactivation in "HA and WM" solution upon 0.25% Fe-SynTiO$_2$ solar photocatalytic treatment……214

Figure 4.139. Specified UV-vis and fluroscence parameters of organic matter: Irradiation time dependent *E. coli* inactivation in "HA and WM" solution upon 0.25% Fe-SynTiO$_2$ solar photocatalytic treatment……215

Figure 4.140. Specific UV-vis and fluroscence parameters of organic matter: Irradiation time dependent *E. coli* inactivation in "HA and WM" solution upon 0.25% Fe-SynTiO$_2$ solar photocatalytic treatment……216

Figure 4.141. EEM fluorescence contour plots of organic matter: Irradiation time dependent *E. coli* inactivation in "HA and WM" solution upon 0.25% Fe-SynTiO$_2$ solar photocatalytic treatment……217

Figure 4.142. Initial, t=0, and t_{irr}=60 min total K, protein, and carbohydrate contents and bacteria enumeration results of *E. coli* inactivation upon 0.25% Fe-SynTiO$_2$ solar photocatalytic treatment in various aqueous matrixes……...219

Figure 4.143. Released protein and carbohydrate contents, and bacteria LRV of *E. coli* inactivation upon 0.25% Fe-SynTiO$_2$ solar photocatalytic treatment in various aqueous matrixes……...220

Figure 4.144. Initial, t=0, and t_{irr}=60 min protein and carbohydrate contents, $FI_{sync280}$, UV_{280}, NPOC, and bacteria enumeration results of 0.25% Fe-SynTiO$_2$ solar photocatalytic treatment of *E. coli* in various aqueous matrixes…….221

Figure 4.145. Irradiation time dependent *E. coli* inactivation upon 0.50% Fe-SynTiO$_2$ solar photocatalytic treatment in various solution matrixes……222

Figure 4.146. UV-vis absorption spectra of organic matter: Irradiation time dependent *E. coli* inactivation in IsoT solution upon 0.50% Fe-SynTiO$_2$ solar photocatalytic treatment…….224

Figure 4.147. Synchronous scan fluorescence spectra of organic matter: Irradiation time dependent *E. coli* inactivation in IsoT solution upon 0.50% Fe-SynTiO$_2$ solar photocatalytic treatment……225

Figure 4.148. Specified UV-vis and fluroscence parameters of organic matter: Irradiation time dependent *E. coli* inactivation in IsoT solution upon 0.50% Fe-SynTiO$_2$ solar photocatalytic treatment……..…..225

Figure 4.149. Specific UV-vis and fluroscence parameters of organic matter: Irradiation time dependent *E. coli* inactivation in IsoT solution upon 0.50% Fe-SynTiO$_2$ solar photocatalytic treatment……226

Figure 4.150. EEM fluorescence contour plots of organic matter: Irradiation time dependent *E. coli* inactivation in IsoT solution upon 0.50% Fe-SynTiO$_2$ solar photocatalytic treatment……227

Figure 4.151. UV-vis absorption spectra of organic matter: Irradiation time dependent *E. coli* inactivation in WM solution upon 0.50% Fe-SynTiO$_2$ solar photocatalytic treatment……229

Figure 4.152. Synchronous scan fluorescence spectra of organic matter: Irradiation time dependent *E. coli* inactivation in WM solution upon 0.50% Fe-SynTiO$_2$ solar photocatalytic treatment……230

Figure 4.153. Specified UV-vis and fluroscence parameters of organic matter: Irradiation time dependent *E. coli* inactivation in WM solution upon 0.50% Fe-SynTiO$_2$ solar photocatalytic treatment……230

Figure 4.154. Specific UV-vis and fluroscence parameters of organic matter: Irradiation time dependent *E. coli* inactivation in WM solution upon 0.50% Fe-SynTiO$_2$ solar photocatalytic treatment……231

Figure 4.155. EEM fluorescence contour plots of organic matter: Irradiation time dependent *E. coli* inactivation in WM solution upon 0.50% Fe-SynTiO$_2$ solar photocatalytic treatment……232

Figure 4.156. UV-vis absorption spectra of organic matter: Irradiation time dependent *E. coli* inactivation in HA solution upon 0.50% Fe-SynTiO$_2$ solar photocatalytic treatment……234

Figure 4.157. Synchronous scan fluorescence spectra of organic matter: Irradiation time dependent *E. coli* inactivation in HA solution upon 0.50% Fe-SynTiO$_2$ solar photocatalytic treatment……235

Figure 4.158. Specified UV-vis and fluroscence parameters of organic matter: Irradiation time dependent *E. coli* inactivation in HA solution upon 0.50% Fe-SynTiO$_2$ solar photocatalytic treatment……236

Figure 4.159. Specific UV-vis and fluroscence parameters of organic matter: Irradiation time dependent *E. coli* inactivation in HA solution upon 0.50% Fe-SynTiO$_2$ solar photocatalytic treatment……236

Figure 4.160. EEM fluorescence contour plots of organic matter: Irradiation time dependent *E. coli* inactivation in HA solution upon 0.50% Fe-SynTiO$_2$ solar photocatalytic treatment……238

Figure 4.161. UV-vis absorption spectra of organic matter: Irradiation time dependent *E. coli* inactivation in "HA and WM" solution upon 0.50% Fe-SynTiO$_2$ solar photocatalytic treatment……240

Figure 4.162. Synchronous scan fluorescence spectra of organic matter: Irradiation time dependent *E. coli* inactivation in "HA and WM" solution upon 0.50% Fe-SynTiO$_2$ solar photocatalytic treatment……240

Figure 4.163. Specified UV-vis and fluroscence parameters of organic matter: Irradiation time dependent *E. coli* inactivation in "HA and WM" solution upon 0.50% Fe-SynTiO$_2$ solar photocatalytic treatment……241

Figure 4.164. Specific UV-vis and fluroscence parameters of organic matter: Irradiation time dependent *E. coli* inactivation in "HA and WM" solution upon 0.50% Fe-SynTiO$_2$ solar photocatalytic treatment……242

Figure 4.165. EEM fluorescence contour plots of organic matter: Irradiation time dependent *E. coli* inactivation in "HA and WM" solution upon 0.50% Fe-SynTiO$_2$ solar photocatalytic treatment……244

Figure 4.166. Initial, t=0, and t_{irr}=60 min total K, protein, and carbohydrate contents and bacteria enumeration results of *E. coli* inactivation upon 0.50% Fe-SynTiO$_2$ solar photocatalytic treatment in various aqueous matrixes……246

Figure 4.167. Released protein and carbohydrate contents, and bacteria LRV of *E. coli* inactivation upon 0.50% Fe-SynTiO$_2$ solar photocatalytic treatment in various aqueous matrixes……247

Figure 4.168. Initial, t=0, and t_{irr}=60 min protein and carbohydrate contents, $FI_{sync280}$, UV_{280}, NPOC, and bacteria enumeration results of 0.50% Fe-SynTiO$_2$ solar photocatalytic treatment of *E. coli* in various aqueous matrixes……248

Figure 4.169. Irradiation time dependent *E. coli* inactivation in IsoT solution upon solar photocatalytic treatments performed in the presence of undoped and Fe-doped TiO_2 specimens……..249

Figure 4.170. Initial, t=0, and t_{irr}=60 min total K, protein, and carbohydrate contents of *E. coli* inactivation in IsoT solution upon solar photocatalytic treatments performed in the presence of bare and Fe-doped TiO_2 specimens……..251

Figure 4.171. Irradiation time dependent *E. coli* inactivation in WM solution upon solar photocatalytic treatments performed in the presence of undoped and Fe-doped TiO_2 specimens……..253

Figure 4.172. Initial, t=0, and t_{irr}=60 min total K, protein, and carbohydrate contents of *E. coli* inactivation in WM solution upon solar photocatalytic treatments performed in the presence of bare and Fe-doped TiO_2 specimens……..255

Figure 4.173. Irradiation time dependent *E. coli* inactivation in HA solution upon solar photocatalytic treatments performed in the presence of undoped and Fe-doped TiO_2 specimens……..257

Figure 4.174. Initial, t=0, and t_{irr}=60 min total K, protein, and carbohydrate contents of *E. coli* inactivation in HA solution upon solar photocatalytic treatments performed in the presence of bare and Fe-doped TiO_2 specimens……..259

Figure 4.175. Irradiation time dependent *E. coli* inactivation in "HA and WM" solution upon solar photocatalytic treatments performed in the presence of undoped and Fe-doped TiO_2 specimens……..……..261

Figure 4.176. Initial, t=0, and t_{irr}=60 min total K, protein, and carbohydrate contents of *E. coli* inactivation in "HA and WM" solution upon solar photocatalytic treatments performed in the presence of bare and Fe-doped TiO_2 specimens…….263

Figure 4.177. Schematic diagram of LPS structure and positioning on Gram-negative bacteria cell wall……..……..265

Figure B.1. UV-vis absorption spectra of 100 kDa HA solution……...299

Figure B.2. Synchronous scan fluorescence spectra of 100 kDa HA solution……...299

Figure B.3. EEM fluorescence contour plot of 100 kDa HA solution……...300

Figure C.1. X-Ray Diffraction (XRD) diffractograms of undoped and Fe-doped photocatalyst specimens: a. TiO_2, b. 0.25% Fe-TiO_2, c. 0.50% Fe-TiO_2, d. SynTiO_2, e. 0.25% Fe-SynTiO_2, f. 0.50% Fe-SynTiO_2…….301

Figure C.2. SEM micrographs and Energy-Dispersive X-Ray (EDX) spectra of undoped and Fe-doped photocatalyst specimens: a. TiO_2, b. 0.25% Fe-TiO_2, c. SynTiO_2, d. 0.50% Fe-SynTiO_2…….302

Figure D.1. Calibration curve of bovine serum albumin **(**BSA) standard…….303

Figure E.1. Calibration curve of glucose standard……304

LIST OF TABLES

Table 4.1. Bacteria LRV in terms of percentage reduction……45

Table 4.2. Solar photolytic treatment of *E. coli*: Inactivation parameters……..……47

Table 4.3. Characteristic properties of organic matter present in solar photolytic treatment of *E. coli* in IsoT solution……..51

Table 4.4. Total K, protein, and carbohydrate contents of time dependent *E. coli* inactivation in IsoT solution upon solar photolytic treatment……53

Table 4.5. Characteristic properties of organic matter present in solar photolytic treatment of *E. coli* in WM solution……..58

Table 4.6. Total K, protein, and carbohydrate contents of time dependent *E. coli* inactivation in WM solution upon solar photolytic treatment……60

Table 4.7. Characteristic properties of organic matter present in solar photolytic treatment of *E. coli* in HA solution……64

Table 4.8. Total K, protein, and carbohydrate contents of time dependent *E. coli* inactivation in HA solution upon solar photolytic treatment……66

Table 4.9. Characteristic properties of organic matter present in solar photolytic treatment of *E. coli* in "HA and WM" solution……..70

Table 4.10. Total K, protein, and carbohydrate contents of time dependent *E. coli* inactivation in "HA and WM" solution upon solar photolytic treatment……72

Table 4.11. TiO_2 solar photocatalytic treatment of *E. coli*: Inactivation parameters……...78

Table 4.12. Characteristic properties of organic matter present in TiO_2 solar photocatalytic treatment of *E. coli* in IsoT solution……82

Table 4.13. Total K, protein, and carbohydrate contents of time dependent *E. coli* inactivation in IsoT solution upon TiO_2 solar photocatalytic treatment……...84

Table 4.14. Characteristic properties of organic matter present in TiO_2 solar photocatalytic treatment of *E. coli* in WM solution…….88

Table 4.15. Total K, protein, and carbohydrate contents of time dependent *E. coli* inactivation in WM solution upon TiO_2 solar photocatalytic treatment……...90

Table 4.16. Characteristic properties of organic matter present in TiO_2 solar photocatalytic treatment of *E. coli* in HA solution……...94

Table 4.17. Total K, protein, and carbohydrate content of time dependent *E. coli* inactivation in HA solution upon TiO_2 solar photocatalytic treatment……97

Table 4.18. Characteristic properties of organic matter present in TiO_2 solar photocatalytic treatment of *E. coli* in "HA and WM" solution……..101

Table 4.19. Total K, protein, and carbohydrate contents of time dependent *E. coli* inactivation in "HA and WM" solution upon TiO_2 solar photocatalytic treatment…….…..103

Table 4.20. SynTiO_2 solar photocatalytic treatment of *E. coli*: Inactivation parameters……...109

Table 4.21. Characteristic properties of organic matter present in SynTiO_2 solar photolytic treatment of *E. coli* in IsoT solution…….112

Table 4.22. Total K, protein, and carbohydrate contents of time dependent *E. coli* inactivation in IsoT solution upon SynTiO_2 solar photocatalytic treatment……..114

Table 4.23. Characteristic properties of organic matter present in SynTiO_2 solar photolytic treatment of *E. coli* in WM solution…….118

Table 4.24. Total K, protein, and carbohydrate contents of time dependent *E. coli* inactivation in WM solution upon SynTiO_2 solar photocatalytic treatment……..120

Table 4.25. Characteristic properties of organic matter present in $SynTiO_2$ solar photolytic treatment of *E. coli* in HA solution……..124

Table 4.26. Total K, protein, and carbohydrate content of time dependent *E. coli* inactivation in HA solution upon $SynTiO_2$ solar photocatalytic treatment……126

Table 4.27. Characteristic properties of organic matter present in $SynTiO_2$ solar photolytic treatment of *E. coli* in "HA and WM" solution……130

Table 4.28. Total K, protein, and carbohydrate content of time dependent *E. coli* inactivation in "HA and WM" solution upon $SynTiO_2$ solar photocatalytic treatment…….132

Table 4.29. 0.25% Fe-TiO_2 solar photocatalytic treatment of *E. coli*: Inactivation parameters…….137

Table 4.30. Characteristic properties of organic matter present in 0.25% Fe-TiO_2 solar photocatalytic treatment of *E. coli* in IsoT solution……..141

Table 4.31. Total K, protein, and carbohydrate contents of time dependent *E. coli* inactivation in IsoT solution upon 0.25% Fe-TiO_2 solar photocatalytic treatment……143

Table 4.32. Characteristic properties of organic matter present in 0.25% Fe-TiO_2 solar photolytic treatment of *E. coli* in WM solution…….147

Table 4.33. Total K, protein, and carbohydrate content of time dependent *E. coli* inactivation in WM upon 0.25% Fe-TiO_2 solar photocatalytic treatment…….149

Table 4.34. Characteristic properties of organic matter present in 0.25% Fe-TiO_2 solar photolytic treatment of *E. coli* in HA solution……..153

Table 4.35. Total K, protein, and carbohydrate content of time dependent *E. coli* inactivation in HA solution upon 0.25% Fe-TiO_2 solar photocatalytic treatment…….155

Table 4.36. Characteristic properties of organic matter present in 0.25% Fe-TiO_2 solar photolytic treatment of *E. coli* in "HA and WM" solution……159

Table 4.37. Total K, protein, and carbohydrate content of time dependent *E. coli* inactivation in "HA and WM" solution upon 0.25% Fe-TiO_2 solar photocatalytic treatment……...161

Table 4.38. 0.50% Fe-TiO_2 solar photocatalytic treatment of *E. coli*: Inactivation parameters…….166

Table 4.39. Characteristic properties of organic matter present in 0.50% Fe-TiO_2 solar photolytic treatment of *E. coli* in IsoT solution…….170

Table 4.40. Total K, protein, and carbohydrate contents of time dependent *E. coli* inactivation in IsoT solution upon 0.50% Fe-TiO_2 solar photocatalytic treatment……172

Table 4.41. Characteristic properties of organic matter present in 0.50% Fe-TiO_2 solar photolytic treatment of *E. coli* in WM solution…….175

Table 4.42. Total K, protein, and carbohydrate content of time dependent *E. coli* inactivation in WM solution upon 0.50% Fe-TiO_2 solar photocatalytic treatment……177

Table 4.43. Characteristic properties of organic matter present in 0.50% Fe-TiO_2 solar photolytic treatment of *E. coli* in HA solution……..181

Table 4.44. Total K, protein, and carbohydrate contents of time dependent *E. coli* inactivation in HA solution upon 0.50% Fe-TiO_2 solar photocatalytic treatment…….183

Table 4.45. Characteristic properties of organic matter present in 0.50% Fe-TiO_2 solar photolytic treatment of *E. coli* in "HA and WM" solution……187

Table 4.46. Total K, protein, and carbohydrate contents of time dependent *E. coli* inactivation in "HA and WM" solution upon 0.50% Fe-TiO_2 solar photocatalytic treatment……...189

Table 4.47. 0.25% Fe-SynTiO_2 solar photocatalytic treatment of *E. coli*: Inactivation parameters…….194

Table 4.48. Characteristic properties of organic matter present in 0.25% Fe-SynTiO_2 solar photolytic treatment of *E. coli* in IsoT solution…….198

Table 4.49. Total K, protein, and carbohydrate contents of time dependent *E. coli* inactivation in IsoT solution upon 0.25% Fe-SynTiO$_2$ solar photocatalytic treatment……..200

Table 4.50. Characteristic properties of organic matter present in 0.25% Fe-SynTiO$_2$ solar photolytic treatment of *E. coli* in WM solution…….204

Table 4.51. Total K, protein, and carbohydrate contents of time dependent *E. coli* inactivation in WM solution upon 0.25% Fe-SynTiO$_2$ solar photocatalytic treatment……..206

Table 4.52. Characteristic properties of organic matter present in 0.25% Fe-SynTiO$_2$ solar photolytic treatment of *E. coli* in HA solution……..210

Table 4.53. Total K, protein, and carbohydrate contents of time dependent *E. coli* inactivation in HA solution upon 0.25% Fe-SynTiO$_2$ solar photocatalytic treatment……...212

Table 4.54. Characteristic properties of organic matter present in 0.25% Fe-SynTiO$_2$ solar photolytic treatment of *E. coli* in "HA and WM" solution……216

Table 4.55. Total K, protein, and carbohydrate contents of time dependent *E. coli* inactivation in "HA and WM" solution upon 0.25% Fe-SynTiO$_2$ solar photocatalytic treatment……....218

Table 4.56. 0.50% Fe-SynTiO$_2$ solar photocatalytic treatment of *E. coli*: Inactivation parameters…….223

Table 4.57. Characteristic properties of organic matter present in 0.50% Fe-SynTiO$_2$ solar photocatalytic treatment of *E. coli* in IsoT solution……..226

Table 4.58. Total K, protein, and carbohydrate contents of time dependent *E. coli* inactivation in IsoT solution upon 0.50% Fe-SynTiO$_2$ solar photocatalytic treatment……..228

Table 4.59. Characteristic properties of organic matter present in 0.50% Fe-SynTiO$_2$ solar photocatalytic treatment of *E. coli* in WM solution……..231

Table 4.60. Total K, protein, and carbohydrate contents of time dependent *E. coli* inactivation

in WM solution upon 0.50% Fe-SynTiO_2 solar photocatalytic treatment……..233

Table 4.61. Characteristic properties of organic matter present in 0.50% Fe-SynTiO_2 solar photocatalytic treatment of *E. coli* in HA solution……237

Table 4.62. Total K, protein, and carbohydrate contents of time dependent *E. coli* inactivation in HA solution upon 0.50% Fe-SynTiO_2 solar photocatalytic treatment……...239

Table 4.63. Characteristic properties of organic matter present in 0.50% Fe-SynTiO_2 solar photocatalytic treatment of *E. coli* in "HA and WM" solution……..243

Table 4.64. Total K, protein, and carbohydrate content of time dependent *E. coli* inactivation in "HA and WM" solution upon 0.50% Fe-SynTiO_2 solar photocatalytic treatment……..……..245

Table 4.65. Solar photocatalytic treatment of *E. coli* in IsoT solution performed in the presence of undoped and Fe-doped TiO_2 specimens: Inactivation parameters…….249

Table 4.66. Solar photocatalytic treatment of *E. coli* in WM solution performed in the presence of undoped and Fe-doped TiO_2 specimens: Inactivation parameters…….253

Table 4.67. Solar photocatalytic treatment of *E. coli* in HA solution performed in the presence of undoped and Fe-doped TiO_2 specimens: Inactivation parameters…….257

Table 4.68. Solar photocatalytic treatment of *E. coli* in "HA and WM" solution performed in the presence of undoped and Fe-doped TiO_2 specimens: Inactivation parameters…….261

Table A.1. Composition of WM solution…….298

Table B.1. Specified and specific UV-vis and fluorescence spectroscopic properties and NPOC of 100 kDa HA solution……..299

Table C.1. Crystallite particle sizes, absorption wavelengths and band-gap energies (E_{bg}) of undoped and Fe-doped TiO_2 specimens…….301

Table C.2. BET surface areas of photocatalyst specimens……301

LIST OF SYMBOLS / ABBREVIATIONS

Symbol	Explanation	Unit
°C	Celsius	
Ca^{2+}	Calcium ion	
Cl^-	Chloride ion	
$Cl^{\bullet}$	Chlorine radical	
Cl_2	Molecular chlorine	
$Cl_2^{\bullet-}$	Dichloride radical anion	
cm	Centimeter	
CO_3^{2-}	Carbonate ion	
$CO_3^{\bullet-}$	Carbonate radical	
COOH	Carboxyl group	
^{1}DOM	Singlet DOM	
^{3}DOM	Triplet DOM	
Da	Daltons	
E_{bg}	Band-gap energy	eV
e^-	Electron	
e^-_{CB}	Photogenerated electron	
Fe^{2+}	Iron (II) ion	
Fe^{3+}	Iron (III) ion	
FI_{sync}	Fluorescence intensity in synchronous scan mode	A.U.
$FI_{sync280}$	Fluorescence intensity in synchronous scan mode at λ_{emis}=280 nm	A.U.
$FI_{sync470}$	Fluorescence intensity in synchronous scan mode at λ_{emis}=470 nm	A.U.
g	Gram	
h	Planck's constant, $6.63x10^{-34}$ m^2 kg/s	
h^+	Positive holes	
h^+_{VB}	Photogenerated hole	
H^+	Hydrogen ion	

H_2O	Water	
H_2O_2	Hydrogen peroxide	
$H_2PO_4^-$	Dihydrogen phosphate ion	
$H_2PO_4^{\bullet}$	Dihydrogen phosphate radical	
H_2SO_4	Sulfuric acid	
HCO_3^-	Bicarbonate ion	
$HCO_3^{\bullet}$	Bicarbonate radical	
HSO_4^-	Hydrogen sulfate ion	
$HO^{\bullet}$	Hydroxyl radical	
$HO_2^{\bullet}$	Hydroperoxyl radical	
I_o	Incident photon flux	W/m^2
K^+	Potassium ion	
kDa	Kilodalton	
λ	Wavelength	nm
$\Delta\lambda$	Bandwidth	nm
λ_{emis}	Emission wavelength	nm
λ_{exc}	Excitation wavelength	nm
λ_{max}	Maximum wavelength	nm
L	Liter	
Mg^{2+}	Magnesium ion	
m	Meter	
µL	Microliter	
µm	Micrometer	
µM	Micromolar	
mg	Milligram	
mL	Milliliter	
ν	Frequency of the light	s^{-1}
N	Normality	
Na^+	Sodium ion	
NaCl	Sodium chloride	
nm	Nanometer	
$NO^{\bullet}$	Nitric oxide radical	
NO_2^-	Nitrite ion	
$NO_2^{\bullet}$	Nitrogen dioxide radical	
$NO_2^{\bullet-}$	Nitrite radical anion	

NO_3^-	Nitrate ion	
$NO_3^{\bullet-}$	Nitrate radical ion	
N_o	Initial *E. coli* cell count	CFU/mL
N_{60}	*E. coli* cell count at irradiation time of 60 min	CFU/mL
$^{\bullet}ox$	Oxidizing radical species	
$^1O_2$	Singlet oxygen	
$^3O_2$	Triplet oxygen	
$O^{\bullet-}$	Oxide radical anion	
O_2	Oxygen	
O_3	Ozone	
O (^3P)	Atomic oxygen	
$O_2^{\bullet-}$	Superoxide radical anion	
OH^-	Hydroxyl ion	
pK_a	p function of acid dissociation constant	
%	Percentage	
pH	Power of hydrogen	
pH_{zpc}	Point of zero charge	
PO_4^{3-}	Phosphate ion	
R	First order rate	CFU/mL min
SFI_{sync}	Specific Fluorescence Intensity in synchronous scan mode	
$SFI_{sync280}$	Specific fluorescence intensity in synchronous scan mode at λ_{emis}=280 nm	
$SFI_{sync470}$	Specific fluorescence intensity in synchronous scan mode at λ_{emis}=470 nm	
SO_4^{2-}	Sulfate ion	
$SO_4^{\bullet-}$	Sulfate radical	
t	Irradiation time	min
$t_{1/2}$	Half-life	min
TiO_2	Titanium dioxide	
t_{irr}	Irradiation period	min
W	Watt	

Abbreviation	Explanation	
AOPs	Advanced Oxidation Processes	
ATCC	American Type Culture Collection	
ATP	Adenosine triphosphate	
ATPase	Adenosine triphosphatase	
BET	Brunauer-Emmett-Teller	
CAT	Catalase	
CB	Conduction Band	
CW	Clockwise	
CCW	Counterclockwise	
CFU	Colony Forming Unit	
$Color_{436}$	Absorbance at 436 nm	
DBPs	Disinfection by-products	
DNA	Deoxyribonucleic acid	
DOM	Dissolved Organic Matter	
DOC	Dissolved Organic Carbon	mg/L
DON	Dissolved Organic Nitrogen	
DOP	Dissolved Organic Phosphorus	
E. coli	*Escherichia coli*	CFU/mL
EDX	Energy-Dispersive X-Ray spectroscopy	
EEM	Excitation Emission Matrix	
EPS	Extracellular Polymeric Substances	
EU	Endotoxin Unit	
FA	Fulvic Acid	
FAAS	Flame Atomic Absorption Spectroscopy	
FI	Fluorescence Index	
HA	Humic Acid	
HSs	Humic Substances	
IC	Ion Chromatography	
IEP	Isoelectric point	
IHSS	International Humic Substance Society	
IsoT	Isotonic solution	
L. acidophilus	*Lactobacillus acidophilus*	
LAL	Limulus Amebocyte Lysate	
LB	Luria Bertani	

LPS	Lipopolysaccharide	
LRV	Logarithmic Reduction Value	%
MDA	Malonaldehyde	
min	Minute	
MW	Molecular Weight	
NADH	Nicotinamide adenine dinucleotide	
NADPH	Nicotinamide adenine dinucleotide phosphate	
NP	Nanoparticle	
NPOC	Non-Purgeable Organic Carbon	mg Org C/L
NOM	Natural Organic Matter	
POM	Particulate Organic Matter	
ROS	Reactive Oxygen Species	
S. cerevisiae	*Saccharomyces cerevisiae*	
$SCoA_{436}$	Specific Color Absorbance at 436 nm	L/m mg
SEM	Scanning Electron Microscopy	
SFI	Specific Fluorescence Intensity	
SOD	Superoxide dismutase	
SODIS	Solar water disinfection	
S. typhimurium	*Salmonella typhimurium*	
$SUVA_{254}$	Specific UV Absorbance at 254 nm	L/m mg
$SUVA_{280}$	Specific UV Absorbance at 280 nm	L/m mg
$SUVA_{365}$	Specific UV Absorbance at 365 nm	L/m mg
$SynTiO_2$	Synthesized TiO_2	
TEM	Transmission Electron Microscopy	
TOC	Total Organic Carbon	
TOM	Total Organic Matter	
UV	Ultraviolet	
UV-A	Ultraviolet A	
UV-B	Ultraviolet B	
UV-C	Ultraviolet C	
UV_{254}	Absorbance at 254 nm	
UV_{280}	Absorbance at 280 nm	
UV_{365}	Absorbance at 365 nm	
UV-DRS	Ultraviolet Diffuse Reflectance Spectroscopy	
UV-vis	Ultraviolet-visible	

VB	Valence Band
VLA	Visible Light Activated
WM	Water Matrix
XRD	X-Ray Diffraction

1. INTRODUCTION

With climate change and increased global population, many people will suffer from lack of clean freshwater which is one of the biggest problems throughout the world. The challenges with water are expected to go worse in following years due to globally occurring water scarcity (Montgomery and Elimelech, 2007). According to UNICEF, 38 % of the world's population, suffered from lack of proper sanitation facilities whereas almost one billion people continue to use unsafe drinking water sources. Especially, in Sub-Saharan Africa, 42 % of people still use unimproved water sources (UNICEF, 2009). No access to good quality drinking water causes a high risk of waterborne diseases like diarrhea, cholera, typhoid fever, hepatitis A, amoebic and bacillary dysentery, and others (WHO, 1999).

Due to the absence of clean drinking water around the world, disinfection of water by the application of different treatment methods has been widely investigated (Helali et al., 2014). Water disinfection is traditionally achieved by using chlorination and ozonation processes. However, the usage of chlorine leads to the formation of disinfection byproducts (DBPs) that have adverse effects on human health and environment by reacting with dissolved organic matter (DOM) in water (Nieuwenhuijsen et al., 2000). Ozonation also causes the formation of organic DBPs like aldehydes, carboxylic acids, ketones and bromates (Huang et al., 2005). However, ozonation process requires more complex technologies than chlorination (Sichel et al, 2007). On the other hand, water disinfection using natural and/or artificial sunlight have been widely studied for the inactivation of a wide range of microorganisms (Busse et al., 2019; Carratala et al., 2016; Mattle et al., 2015; Vivar et al., 2017). Solar water disinfection (SODIS), which is a simple, inexpensive method for the household water treatment, relies on the combined effect of ultraviolet (UV) radiation and thermal heating of solar light. Since 1980s, studies have been conducted to investigate the mechanism of solar disinfection and to develop new technologies to make this technique faster and safer (McGuigan et al., 2012). Literature suggests that SODIS in natural water is in reality an in-situ generated photocatalytic process promoted by solar light (Pulgarin, 2015).

The usage of TiO_2-UV bactericidal activity to decontaminate water was first demonstrated by Matsunaga and colleagues (Matsunaga et al., 1985). Since then, photocatalytic disinfection of microorganisms gained an increasing interest and many review papers are available in literature covering background information as well as recent developments in the field (Bekbolet, 2007; Byrne

et al., 2015; Gupta and Modak, 2020; Helali et al., 2014; Reddy et al., 2017; Uyguner-Demirel et al., 2017, 2018; Vale et al., 2016; Wang et al., 2015).

Solar photocatalytic disinfection studies of *E. coli* as the indicator microorganism in the presence/absence of DOM using bare TiO_2 and visible light activated (VLA) doped TiO_2 (*i.e.*, N-doped, Fe-doped, Se-doped, and Se-N co-doped TiO_2) has been carried out so far by Bekbolet and collegues (Bekbolet and Araz, 1996; Bekbolet, 1997, 2007; Birben et al., 2017a, 2017b, 2021b).

Complimentary to previous research, the main objective of the present study is to evaluate and propose heterogeneous photocatalysis using bare and Fe-doped TiO_2 under solar light for destruction of indicator bacteria. Considering its extensive use in literature and for comparison purposes, the pure cultures of the fecal indicator bacterium *E. coli* were used in photolytic and photocatalytic disinfection studies. Inactivation of *E. coli* was considered under identical solar irradiation conditions. Considering the real case in aquatic systems, effect of DOM on solar light initiated *E. coli* inactivation was evaluated with the use of humic acid (HA) as a DOM analogue in natural waters. Besides ultraviolet-visible (UV-vis) and fluorescence spectroscopic analysis to characterize DOM under photo-initiated reaction conditions, destruction of *E. coli* was followed by released cell components like proteins, carbohydrates, and total potassium content. Further evaluation of released cytoplasmic organic content was followed by the occurrence of fluorophores of microbial by-products and protein-like fluorophores as presented in excitation emission matrix (EEM) contour plots. Moreover, absence or presence of endotoxin was also investigated.

2. LITERATURE REVIEW

2.1. Solar Disinfection of Water

The usage of sunlight for water purification is one of the oldest methods, communities from the Indian sub-continent placed their drinking water in open trays to be "blessed" by the sun nearly 2000 years ago. The first systematic study about the bactericidal effect of sunlight was investigated by Downes and Blunt in 1877. They showed that short wavelength solar radiation has the greatest antimicrobial effect (Downes and Blunt, 1877a, 1877b, 1878). After a century, Acra and colleagues suggested the practical application of sunlight for the disinfection of oral rehydration solutions and drinking water and this process was generally named as solar disinfection (Acra et al., 1980, 1984, 1989). Also, they contemplated that the solar disinfection can be used as an alternative, inexpensive, sustainable and simple water treatment method by people who had no access to other water treatment systems. After these findings, bacterial inactivation potential of solar disinfection namely SODIS has been investigated in detail by several groups (Conroy et al., 1996; Joyce et al., 1992, 1996; Kehoe et al., 2001; Lawand et al., 1988; McGuigan et al., 1998, 1999; Reed, 1997; Sommer et al., 1997; Wegelin et al; 1994; Wegelin and Sommer, 1998).

2.2. Mechanism of Solar Disinfection

The solar irradiance incident on the Earth's outer atmosphere is almost around 1360 W/m^2. However, received irradiance at the ground level on a horizontal surface of the equator in summer is 1120 W/m^2. This decrease is caused from the absorption of the irradiance by the water vapor, carbon dioxide, oxygen, ozone and pollutants in the atmosphere (McGuigan et al., 2012). Solar light contains infrared radiation, visible light and ultraviolet radiation. Visible light and infrared light make up approximately 95 % and UV light generates 5 % of the solar light that reaches the Earth's atmosphere. The wavelength ranges of UV light are: 400 to 315 nm for UV-A; 315 to 280 nm for UV-B and 280 to 100 nm for UV-C light (IARC, 2012).

Natural waters can contain a variety of microorganisms such as bacteria, viruses, fungi, protozoa, and algae. The removal or inactivation of pathogenic bacteria in drinking water has high importance to prevent the transmission of waterborne diseases. Due to difficulty and cost of individual detection of pathogenic microorganisms, particular indicator organisms are used to test drinking water safety (Bekbolet, 2007; Tortora et al., 2018). Coliform bacteria were first used as indicator organisms by

Phelps (1909). Moreover, *E. coli*, which is a fecal coliform bacterium, has been widely used as an indicator organism to detect drinking water contamination. Bacteria destruction in solar disinfection process could be formed in two main ways as direct and indirect damage. When genetic material of the organism, namely deoxyribonucleic acid (DNA), is irradiated by UV light, especially UV-B, direct damage of DNA occurs (Halliwell and Gutteridge, 1989). Although UV-A irradiation is not as effective as UV-B to directly damage DNA, it plays an important role on the inactivation of bacteria by causing indirect damage. Indirect damage occurs by the absorption of UV wavelengths via photosensitizers. When photosensitizers are excited, they lead to the formation of reactive oxygen species (ROS) in water such as singlet oxygen, superoxide, hydrogen peroxide, and hydroxyl radical (Cooper et al., 1988a; Foyer et al., 1994).

Photosensitizers could be endogenous (internal) ones such as porphyrins, flavins, quinones, nicotinamide adenine dinucleotide/nicotinamide adenine dinucleotide phosphate (NADH/NADPH), cytochromes, photosynthetic pigments etc. (Curtis et al., 1992; Eisenstark, 1987; Foyer et al., 1994; Jagger, 1981; Sammatro and Tuveson, 1987; Tuveson and Sammartano, 1986) and exogenous (external) ones which are present in surface waters like humic compounds and chlorophylls (Blough and Zepp, 1995; Cooper et al., 1988b; Voelker et al., 1997). ROS generated by solar irradiation react with the cell membrane, membrane lipids, proteins and DNA and cause inactivation of the cell (Figure 2.1) (Bose and Chatterjee, 1995; Futsaether et al., 1995; Gourmelon et al., 1994). When ROS are formed, they cause a series of oxidation reactions as of polyunsaturated fatty acids in lipids, amino acids in proteins and oxidative damage to DNA (Reed et al., 2000). This DNA damage can occur via the strand breakage, which is fatal for the microorganism, and base changes, which can cause some mutagenic effects like blockage of replication (McGuigan et al, 2012).

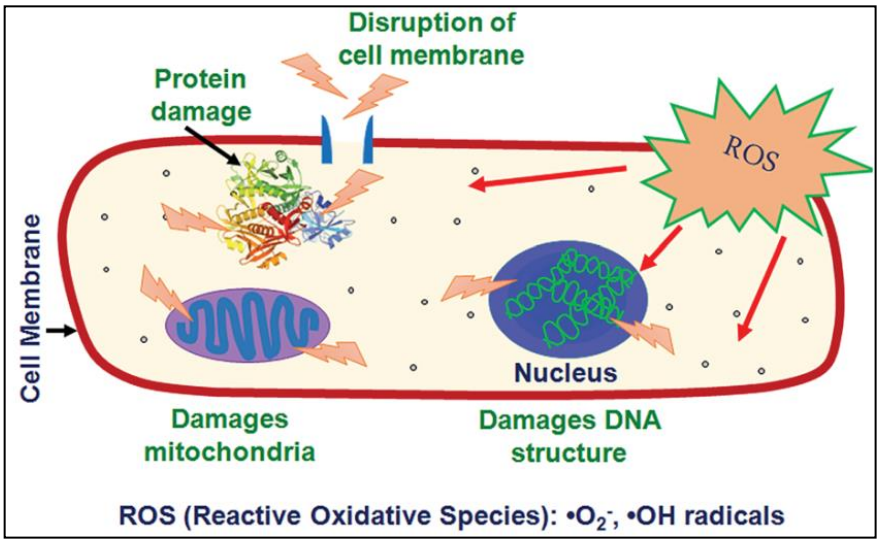

Figure 2.1. Proposed schematic process of cell destruction (Adhikari et al., 2015).

Other than the effect of UV light, increased temperature also plays an important role in SODIS. The temperature of the water increases to a point that bacteria are inactivated by the absorption of solar light, especially the solar infrared radiation and this thermal inactivation process is named as solar pasteurization (Wegelin and Sommer, 1998). In addition, when the bactericidal effect of UV light combines with thermal inactivation process, a synergistic effect has been observed at the water temperature exceeding 45°C (McGuigan et al., 1998). Researchers suggested that increased water temperatures occurring in the solar pasteurization process inhibits DNA repair mechanisms, therefore, synergistic effect can be more effective (McGuigan et al., 1998).

The main disadvantage of photoinactivation is attributed to microbial regrowth and not being effective in case of bacterial strains such as Gram-negative *S. typhimurium.* Therefore, research was directed to the application of photocatalysis as an alternative.

2.3. Heterogeneous Photocatalysis for the Enhancement of Solar Disinfection Efficiency

Advanced oxidation processes (AOPs) were established by Glaze and colleagues and defined as treatment processes which form hydroxyl radicals ($HO^{\bullet}$) in sufficient quantity to oxidize organic pollutants and microorganisms in water (Glaze et al., 1987). In general, AOPs could be classified in two major groups as homogeneous and heterogeneous AOPs. In homogeneous systems such as photo-Fenton, O_3, O_3/UV, O_3/H_2O_2, H_2O_2/UV, reaction takes part in liquid phase however in heterogenous systems like TiO_2/O_2/UV and TiO_2/H_2O_2/UV, catalysts are not dissolved in liquid, and reaction occurs in liquid-solid phase (Buthiyappan et al., 2016; Mansilla et al., 1997; Centi and Perathoner, 2005; Uyguner and Bekbolet, 2007). In the last few decades, main interest has been directed to heterogeneous photocatalysis which is a promising AOP in various photochemical applications consisting of water splitting, degradation of organic compounds, reduction of CO_2 and water disinfection (Carey et al., 1976; Fujishima and Honda, 1972; Frank and Bard, 1977; Matsunaga, 1985; Matsunaga et al., 1985).

According to IUPAC, photocatalysis is defined as the change in the rate of a chemical reaction or its initiation under the action of UV, visible or infrared radiation in the presence of a photocatalyst which absorbs light and also involves in the chemical transformation of the reaction partners (IUPAC, 2004). One of the earliest studies about TiO_2 and UV light's bactericidal activity was demonstrated in 1985 by Matsunaga and colleagues to inactivate *E. coli*, *L. acidophilus* and *S. cerevisiae* cells covering also a mechanistic explanation (Matsunaga et al., 1985). TiO_2 is the most widely used

semiconductor for water treatment processes since its excitation by wavelengths shorter than 390 nm (UV-A) generates ROS, especially $HO^{\bullet}$ (Harper et al., 2001; Ollis et al., 1991).

2.3.1. Photocatalytic Oxidation Processes

When a semiconductor like TiO_2 is irradiated by a suitable wavelength, the photocatalytic oxidation processes occur. Throughout the irradiation of TiO_2, the electrons (e^-) are excited into the conduction band (CB) which leaves a hole (h^+) in the valence band (VB) of TiO_2. The charge carriers (e^-/h^+ pairs) migrate to the surface/interface of TiO_2 and take part in redox reactions to form highly active ROS like $HO^{\bullet}$, superoxide radical anion ($O_2^{\bullet-}$), hydroperoxyl radical ($HO_2^{\bullet}$) and hydrogen peroxide (H_2O_2) (Equations 2.1-2.8) (Rengifo-Herrera et al., 2013).

$$TiO_2 + h\nu \rightarrow TiO_2\,(e^-_{CB} + h^+_{VB}) \quad (2.1)$$

$$TiO_2\,(h^+_{VB}) + H_2O_{ads} \rightarrow TiO_2 + HO^{\bullet}_{ads} + H^+ \quad (2.2)$$

$$TiO_2\,(h^+_{VB}) + OH^-_{ads} \rightarrow TiO_2 + HO^{\bullet} \quad (2.3)$$

$$TiO_2\,(e^-_{CB}) + O_2 \rightarrow TiO_2 + O_2^{\bullet-} \quad (2.4)$$

$$O_2^{\bullet-} + H^+ \leftrightarrow HO_2^{\bullet} \qquad pK_a=4.8 \quad (2.5)$$

$$HO_2^{\bullet} + O_2^{\bullet-} + H^+ \rightarrow H_2O_2 + O_2 \quad (2.6)$$

$$2HO_2^{\bullet} \rightarrow H_2O_2 + O_2 \quad (2.7)$$

$$TiO_2\,(e^-_{CB}) + H_2O_2 \rightarrow TiO_2 + OH^- + HO^{\bullet} \quad (2.8)$$

2.3.2. Bare and Visible Light Activated Doped TiO_2 Species

TiO_2 P-25 (Evonik) which is one of the most widely used photocatalyst, mainly contains free nanoparticle (NP) with single anatase (80 %) and rutile (20 %) crystal structure (Jiang et al., 2017). Although both of them are equally detrimental to bacteria (Simon-Deckers et al., 2009), anatase crystal phase shows stronger photocatalytic properties in comparison to rutile phase (Joost et al., 2015). Isoelectric point (IEP) or point of zero charge (pH_{zpc}) of TiO_2 equals to pH=6.25 (Birben et al., 2015). Its pH dependent positively and negatively charged surface-active sites are shown in Figure 2.2. Surface groups of a metal oxide like semiconductor TiO_2 express amphoteric properties and the surface acid-base equilibria at 25°C can be displayed by the following equations (Equations 2.9 and 2.10) (Kormann et al., 1991).

$$TiOH_2^+ \leftrightarrow TiOH + H^+ \qquad pK_{a1} = 2.4 \quad (2.9)$$

$$TiOH \leftrightarrow TiO^- + H^+ \qquad pK_{a2} = 8.0 \quad (2.10)$$

a.

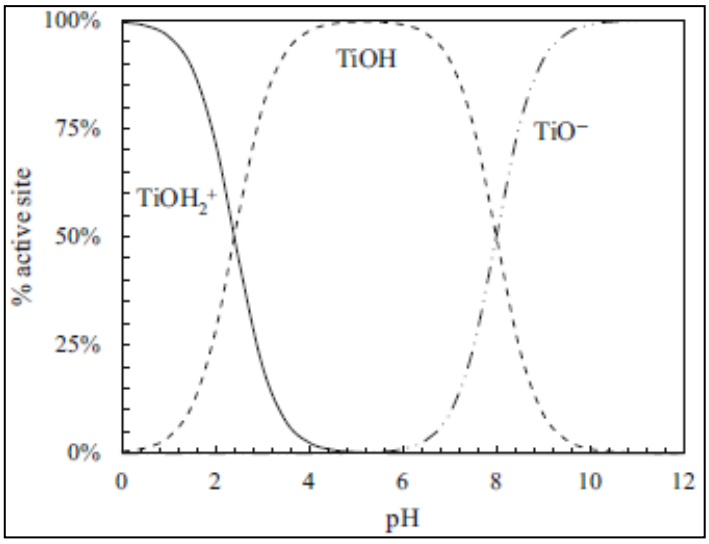

b.

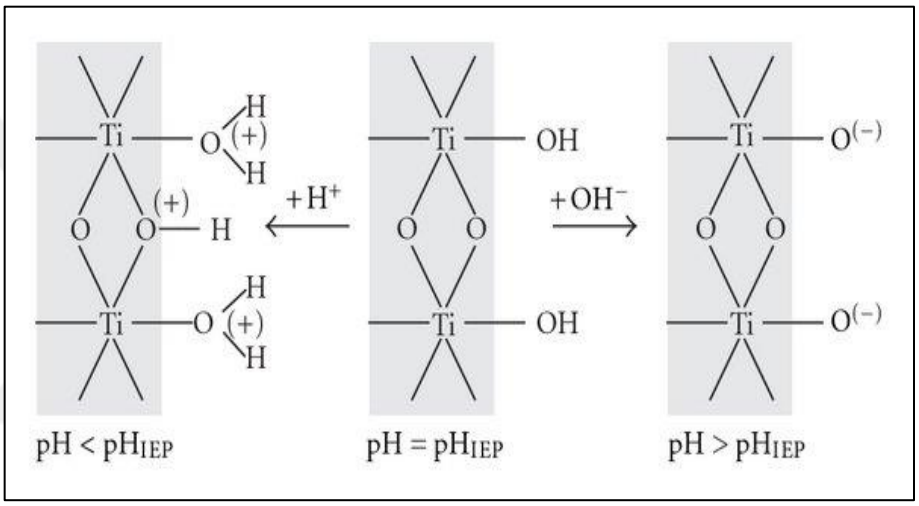

Figure 2.2. a. Formation of surface hydroxylated species of TiO_2 according to pH (Dalrymple and Goswami, 2017); b. pH dependent electrostatic interactions on TiO_2 surface (Beranek, 2011).

Bare TiO_2 has a wide band-gap energy, as electromagnetic band-gap (E_{bg}) = 3.2 eV, that cause some drawbacks on photocatalytic process such as; restriction of light absorption to only UV region which is approximately 5 % of solar spectrum, rapid charge recombination between electron hole pairs and low surface coverage of photocatalyst particles causing slower degradation rates of organic compounds (Kılıc and Cinar, 2009). The effectiveness of bare TiO_2 can be increased by doping it with metal elements or metallic salts such as iron, silver, copper, tungsten and ruthenium (Dobosz and Sobczyński, 2003; Fung et al., 2003; Koli et al., 2016; Lettmann et al., 2001; Li et al., 2001; Sangchay and Ubonchonlakat, 2015; Sun et al., 2003; Yu et al., 2003) or non-metals like sulphur (Yu et al., 2005) or by coating the surface of TiO_2 with photosensitizing dyes (Cho et al., 2001; Lobedank et al., 1997). TiO_2 doping process forms VLA TiO_2 by shifting the light absorption range of bare TiO_2 from UV to visible light. Doped photocatalyst specimens could be used to improve solar light harvesting in TiO_2 photocatalytic process and improve the photocatalytic activity. Doping TiO_2 with

a transition metal like Fe increases the activity of TiO_2 with two main ways; *i.* shifting light absorption to the visible light by narrowing the band-gap and creating additional electronic states within TiO_2 band-gap which could be induced by lower energy light, and *ii.* increased $HO^{\bullet}$ formation by reducing electron hole pair recombination speed (Yalcin et al., 2010). Fe and Se-doped TiO_2 specimens were studied in detail by Bekbolet and colleagues (Birben et al., 2015, 2017a, 2017b). Fe-doped TiO_2 specimens were prepared by using TiO_2 P-25 and TiO_2 Hombikat UV-100 by wet impregnation method. Humic acid sample was selected as a specific molecular size fraction as < 100 kDa. Following treatment, humic molecular size fractions were further characterized by UV-vis and advanced fluorescence techniques such as EEM. Furthermore, VLA TiO_2 specimens were selected as Se-doped and Se-N co-doped TiO_2. Solar photocatalytic inactivation of *E. coli* was investigated in the presence and absence of humic matter. Besides photocatalytic inactivation kinetics, organic matter degradation was also followed and characterized by UV-vis and EEM (Bekbolet, 1997, 2020; Bekbolet and Araz, 1996; Bekbolet and Sen-Kavurmaci, 2015; Bekbolet and Turkten, 2020; Birben et al., 2015, 2017a, 2017b; Uyguner-Demirel and Bekbolet, 2011; Sen-Kavurmaci and Bekbolet, 2014).

2.4. Indicator Organism: *Escherichia coli*

As the main indicator organism, *E. coli* is a prokaryotic, single-celled organism lacking a distinct nucleus and membrane enclosed organelles (Figure 2.3).

Taxonomy of *E. coli*:
Domain: Bacteria
Phylum: Proteobacteria
Class: Gammaproteobacteria
Order: Enterobacteriales
Family: Enterobacteriaceae
Genus: *Escherichia*
Species: *Escherichia coli*

Belonging to the main domain of Bacteria and phylum Proteobacteria *E. coli* is from Enterobacteriaceae or enteric family which includes facultative anaerobe microorganisms. As a member of *Escherichia* genus, rod shaped *E. coli* is recognized as Gram-negative bacteria. Motile forms of Enterobacteriaceae have peritrichous multi-flagella like *E. coli* (Hogg, 2005; Tortora et al., 2018). It is a neutrophilic bacterium maintaining its growth between almost at neutral conditions as pH: 6-8 (Ingraham, 1999).

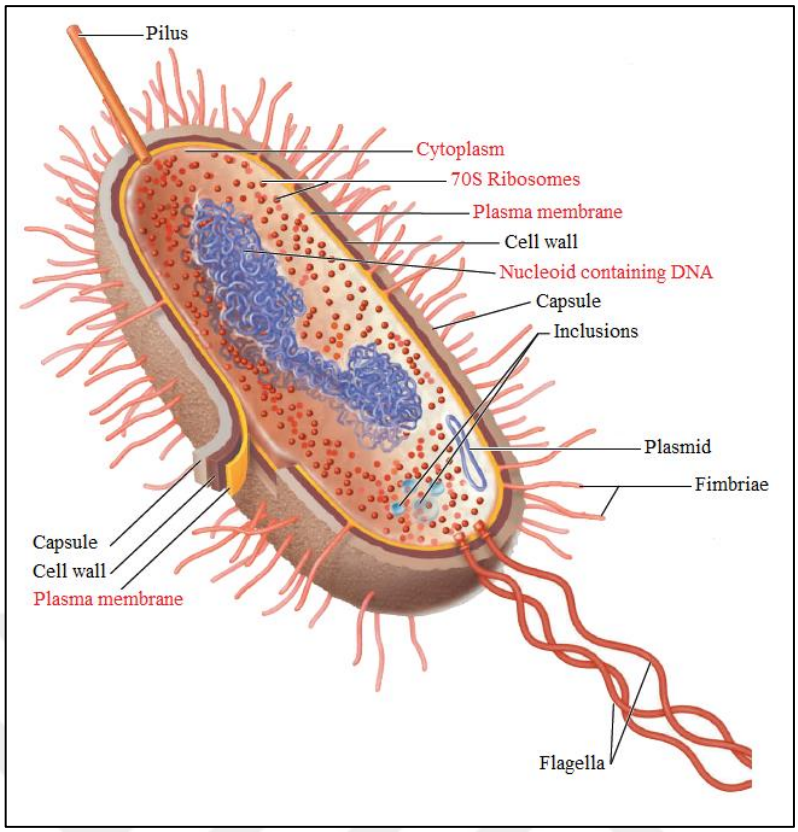

Figure 2.3. The general structure of a prokaryotic organism. Red-labeled structures are found in all bacteria species, while black-labeled ones are not (Tortora et al., 2018).

Approximately 70 % of an *E. coli* cell is made up of water. Remaining part of the bacterium biomass proportions are protein, 50-60 %; RNA, 13-25 %; polysaccharide, 9-17 %; lipid, 8-9 %; and DNA, 2-4 % per gram dry weight (Sucher et al., 2012). Cells are 1.0-2.0 μm long and 0.5 to 1.0 μm in diameter; and volume and surface area of an *E. coli* is nearly 1.0 μm^3 and 6.0 μm^2, respectively (Phillips et al., 2013). C, O, H, N, S, P, K, Mg, Ca, Na, Cl and Fe are the macronutrients that *E. coli* needs to maintain its growth (Dworkin et al., 2006). Also, *E. coli* can be represented with a chemical formula of $CH_{1.74}O_{0.34}N_{0.22}$ (Duboc et al., 1999). It is an important pathogen founding in soil, plants, animal respiratory and intestinal tracts. The presence of *E. coli* in water and food indicates fecal contamination. Due to its high numbered permanent presence in human feces, ability of survival in water and simple detectability, it is known as an indicator organism. The usual indicator organisms are coliform bacteria defined as Gram-negative, aerobic or facultative anaerobic, non-endospore forming, rod-shaped bacteria that ferment lactose to form gas in 48 hours after being placed in lactose broth at 35 °C. *E. coli* is the dominant fecal coliform bacteria because it generates a large portion of human intestinal population. *E. coli* is normally not disease causing, although some strains of it can cause gastroenteritis, traveler's diarrhea, in developing countries infant diarrhea and urinary tract infections. The best-known and most infectious type of *E. coli* is serotype O157:H7 (Tortora et al., 2018).

2.4.1. *E. coli* Motility

Most of the bacteria can actively move in liquid media by itself and this movement is called as motility. Flagellar motility requires energy to rotate flagellum from the basal body and this motion could be provided by one or more flagella. Bacteria can modify the speed of the movement and change the rotation direction of the flagella (Singleton, 1997; Tortora et al., 2018). *E. coli* has about 10 flagella arising from different points of the cell surface and this type of positioning of flagella is called as peritrichous (Hogg, 2005; Wilson et al., 2002). Peritrichous flagella of *E. coli* rotate independently from each other (Macnab and Han, 1983). Most of the time (95 %) each flagellum rotates counterclockwise (CCW) and rest of the time clockwise (CW). When most of the flagella rotate CCW, they pile up in a helical bundle at one end of the cell and bacterium moves toward one direction, the movement is called as "run" or "swim" movement. Run movements are periodically interrupted about one per second by directionless "tumbles". Changed direction of flagellar rotation causes tumbles; it occurs randomly (Figures 2.4a and 2.4b). Flagellar rotation determines the type of the movement (Singleton, 1997; Tortora et al., 2018). Consecutive running and tumbling movements cause the formation of a three dimensional "random walk" similar to Brownian motion of electrons. (Figure 2.4c) (Singleton, 1997; Macnab, 1979).

a.

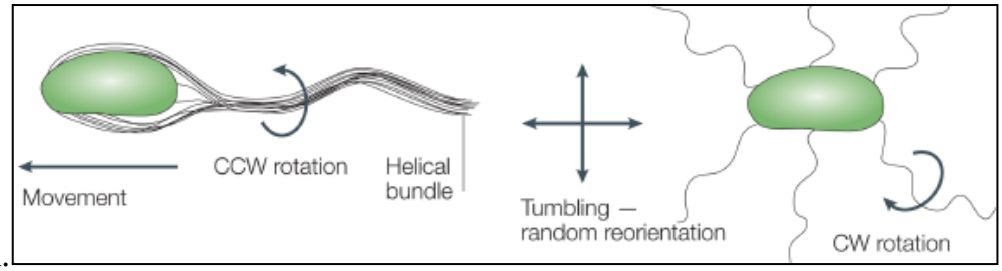

b.

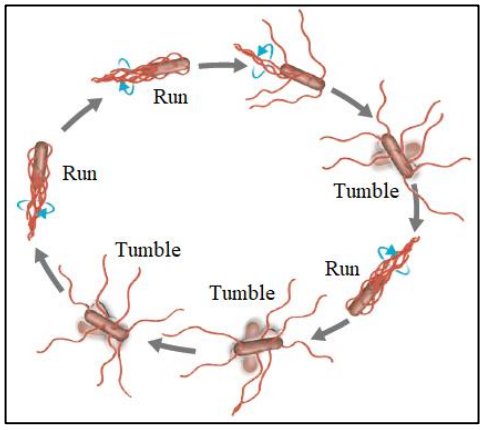

c.



Figure 2.4. a. CCW, CW flagella rotations and movement of *E. coli* (Butler and Camilli, 2005). b. Run and tumble movements of a bacterium. Blue arrows indicate the flagellar rotation direction and gray arrows indicate the movement direction (Tortora et al., 2018). c. Random walk pattern of bacteria (Phillips et al., 2013).

Growth of flagella occurs from the distal tip by polymerization of protein molecules (Rosenbaum and Child, 1967). Naturally or mechanically displaced flagella can regenerate themselves (Levy, 1974). Furthermore, researchers showed that flagellar assembly of bacteria did not detach with the effect of photocatalytic disinfection process. However, after recurrent photocatalytic treatment, genes taking place in the expression of flagellar assembly are downregulated (Zhang et al., 2019). Therefore, it can be concluded that the protein content of the experiment solution could not increase due to separation of flagella.

2.4.2. Surface Properties and Point of Zero Charge of *E. coli*

Bacterial cells have a net negative charge under the influence of surface components (Corpe, 1970). Dissociation of the charged functional groups founding in the cell wall causes this electronegative characteristic. Neihof and Echols showed that carboxyl groups on the surface of *E. coli* cells are the source of electronegativity (Neihof and Echols, 1973). These carboxylic groups of peptidoglycans are located on the D-glumatic acid, meso-diaminopimelic acid and terminal D-alanine residues of the peptide groups. Due to the presence of the electronegative groups, the cell surface of the bacteria is negatively charged at neutral pH. Furthermore, the presence of amino groups in the peptidoglycan layer and counter-ions from the environment neutralize the negative charges and prevent shreding of the cell wall due to electrostatic repulsion of the negative charges (Thwaites and Mendelson, 1991).

With regard to basic definition of zeta potential as the electric charge at the shear plane, is generally used as a surrogate parameter to explain surface charge of bacteria cells. Proteins and metabolites which are present in the growth medium can be adsorbed to the bacteria cell surface via various electrostatic interactions as well as by *van der Waals* attractions and London forces. These absorbed structures can form layers on the cell wall. Therefore, the bacteria cell wall contains both the cell wall charge and the effect of the formed layer. It was reported that pH_{zpc} of *E. coli* (1.5-3) grown in different growth mediums like Luria Bertani (LB) Lennox, LB Lennox with 2 mg/L glucose and buffered LB Lennox demonstrated similar values with each other (Ng, 2018). Additionally, research investigating the effect of different wash buffers (such as 0.154M NaCl, 0.001M KCl, and 0.1M $NaNO_3$) on pH_{zpc} of *E. coli* showed that there was no significant effect of the buffers against the pH_{zpc} of the cell surface (Ng and Ting, 2017). The attained results significantly indicated that neither different growth media nor wash buffers substantially exert an effect on the pH_{zpc} of *E. coli* in aqueous medium. Therefore, under almost neutral conditions ($pH \approx 6\text{-}7$), *E. coli* cell surface would be regarded as negatively charged.

2.4.3. *E. coli* Inactivation Mechanism During Solar Light Initiated Photocatalytic Processes

In photocatalytic inactivation processes in situ generated ROSs attack bacteria cell components, starting with the cell capsule. When ROSs attack the cell capsule, damage lipid contents of the cell membrane and cause increased membrane permeability resulting in the leakage of K^+, proteins and DNA of the bacteria. Increased ROSs concentration at the periphery and inside the cell could cause inactivation of enzymes and give oxidative damage to DNA and proteins (An et al., 2017).

During exposure of stress like osmotic, heat, or oxidative, bacteria cells may continue their metabolic activities but stop growing. As a consequence of these type of stress factors, bacteria cells start to produce excessive amount of free radicals that could be lethal for the cell and this process is called as "suicide response" (Overman, 2006). Bacteria in exponential phase are more sensitive to suicide response than stationary phase (Aldsworth et al., 1999).

2.4.3.1. Effect of reactive oxygen species on solar light initiated photocatalytic bacteria destruction.
ROS not only destroy the chemical contaminants in water but also cause fatal damage to bacteria via oxidation of cellular components, membrane leakage of the cell wall, etc. (Blake et al., 1999; Cabiscol et al., 2000; Reddy et al., 2016). Hydroxyl radicals are very active and primarily responsible for the disinfection of bacteria (Fujishima et al., 2000; Reddy et al., 2017). The oxidative effects of TiO_2 on bacteria occur via direct contact of bacteria with the catalyst (Figure 2.5), therefore the first damage of bacteria occurs at the outer membrane (Figures 2.6 and 2.7a) (Stage A) (Reddy et al., 2017; Sunada et al., 2003). After the first damage on the outer membrane, the fatal damage can occur by the destruction of DNA (Stage B) (McGuigan et al., 2012; Reddy et al., 2017). It was also demonstrated that cell wall damages take place prior to cytoplasmic membrane damage.

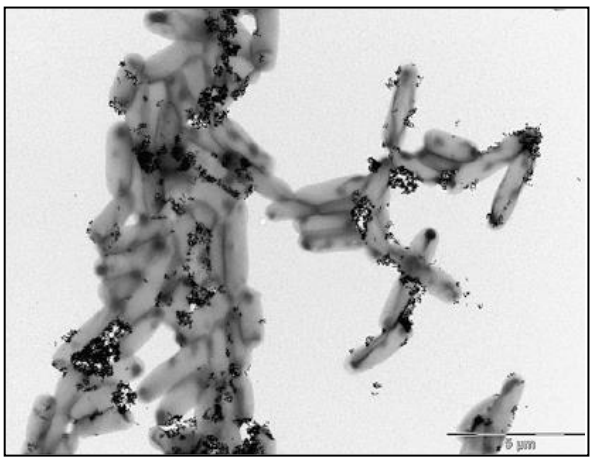

Figure 2.5. Transmission electron microscopy (TEM) image of *E. coli* with TiO_2 particles attached on it (Dalrymple and Goswami, 2017).

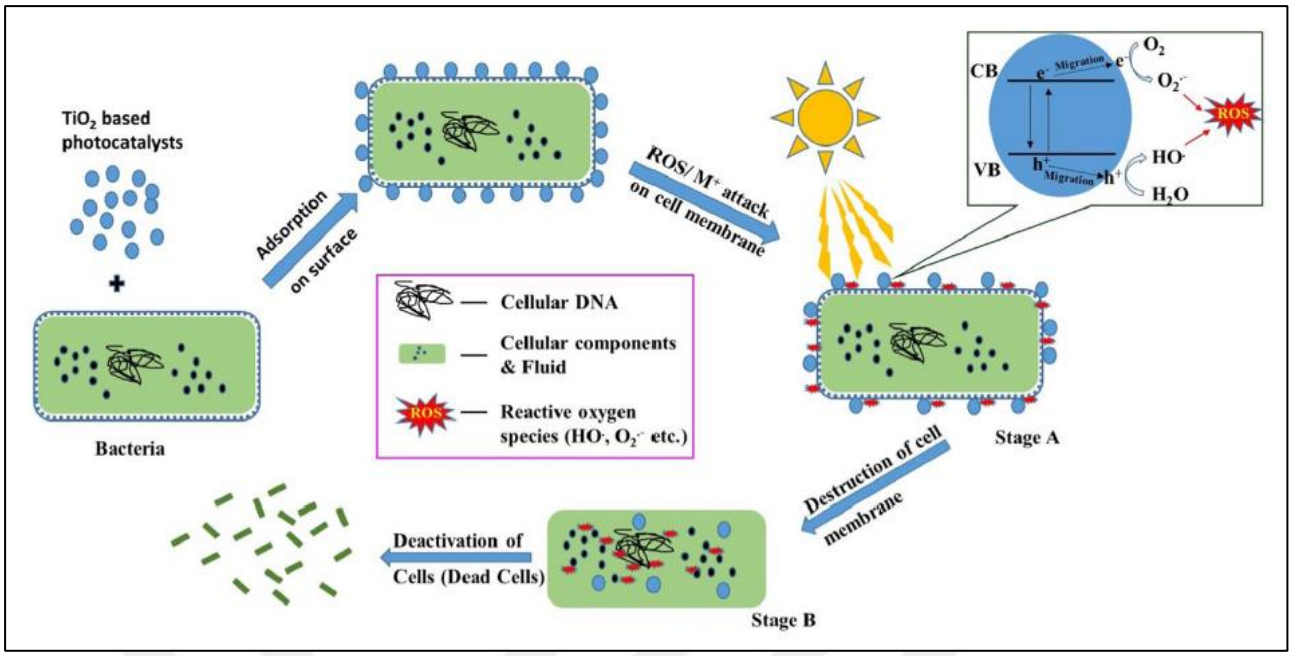

Figure 2.6. Possible mechanism of photocatalytic disinfection of bacteria (Reddy et al., 2017).

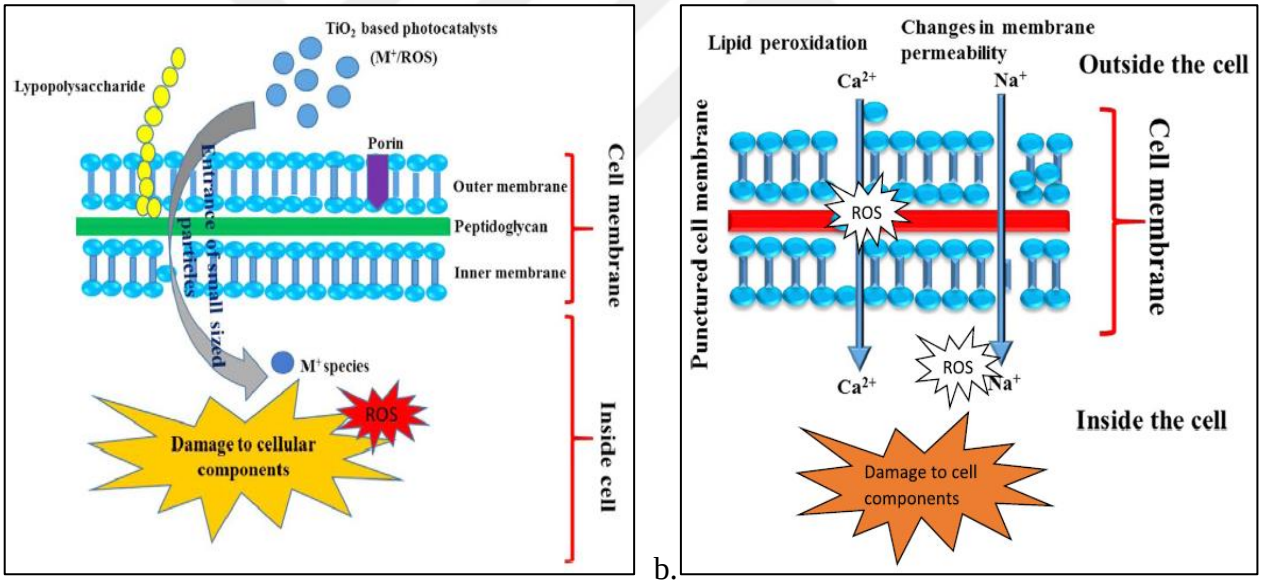

a. b.

Figure 2.7. a. Structural membrane composition and possible photocatalytic disinfection mechanism, b. Lipid peroxidation and membrane leakage process in Gram-negative bacteria e.g. *E. coli* (Reddy et al., 2017).

The bactericidal inactivation processes generally occur in following stages; *i.* Cytoplasmic membrane destruction, *ii.* Increase in cell permeability, *iii.* Release of intracellular components, *iv.* Loss of viability, *v.* Distortion of cellular surface, *vi.* Change in overall shape and size. Increase in cell membrane permeability (Figure 2.7b) could be related to the increase in the release of protein, carbohydrate, and K^+ (Carré et al., 2014; Ren et al., 2009). Loss of viability could be related to the photooxidation of co-enzyme A and it causes the inhibition of respiration (Reddy et al., 2017).

2.4.3.2. Cellular targets of reactive oxygen species.

Bacterial capsule as extracellular polymeric substances. Extracellular polymeric substances (EPS) or glycocalyx are produced and secreted by bacteria which are composed of polysaccharides and polypeptides (Decho, 2011). EPS are located outside of the cell wall and help bacteria to maintain moisture, store nutrients, and attach to surfaces and EPS attached tightly on the cell wall is called capsule (Eboigbodin and Biggs, 2008; Tortora et al., 2018). EPS provide contact between bacteria and photocatalyst and protect the cell from ROS attack (Hessler et al., 2012). Researchers showed that bacteria without capsule are more sensitive to photocatalytic inactivation than the capsulated ones (Liu et al., 2007). Also, bacteria that have direct contact with TiO_2 have high sensitivity to photocatalytic inactivation. When bacteria–TiO_2 direct contact is inhibited, the amount of EPS increases which can result in higher resistance capacity to treatment (Huang et al, 2015).

Cell wall and cell membrane. Bacteria cell envelope consists of plasma/cell membrane and cell wall (Figure 2.8). Cell envelope provides stable inner conditions to the cell and prevent unwanted materials from entering the cell.

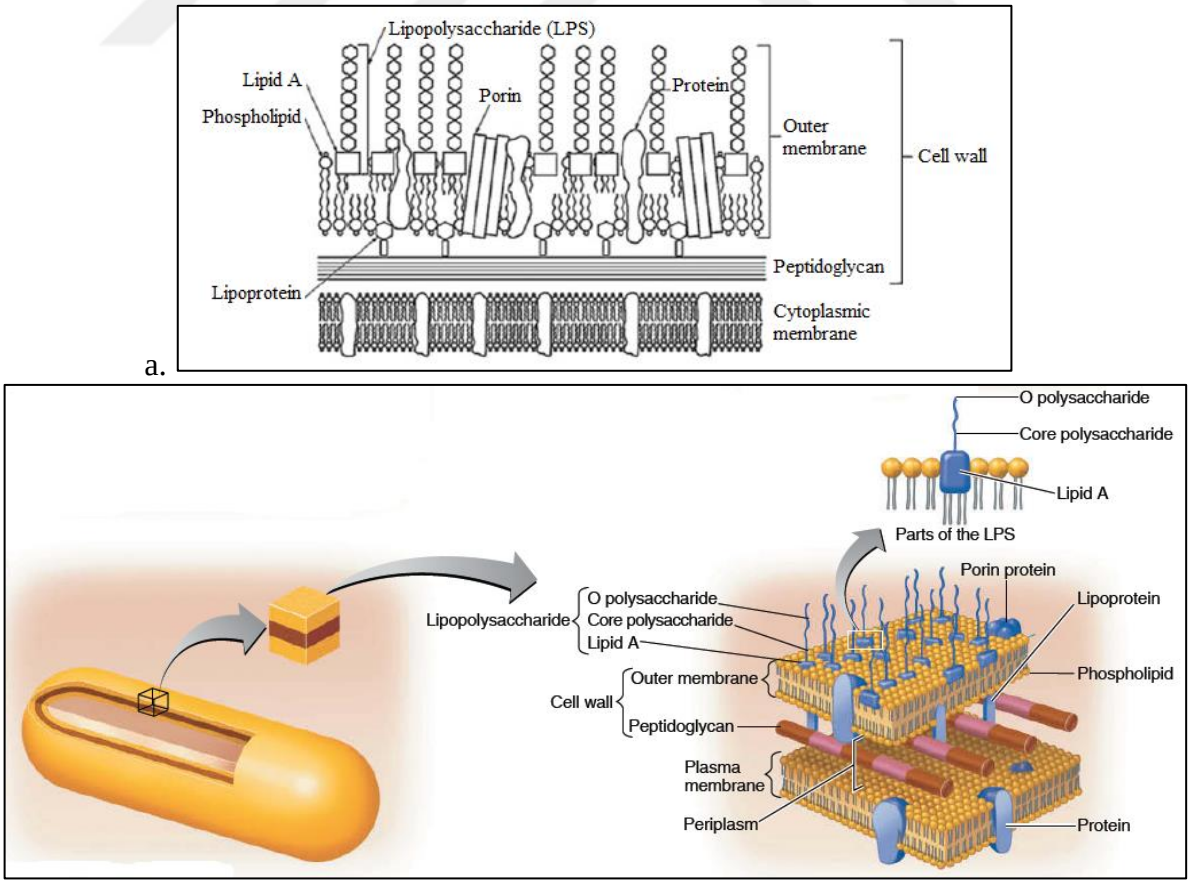

Figure 2.8. Cell wall and cytoplasmic membrane structure of Gram-negative bacteria (a. Madigan and Martinko, 2006; b. Tortora et al., 2018).

Unlike Gram-positive bacteria, cell wall of Gram-negative bacteria has a thinner peptidoglycan layer and an outer membrane outside this peptidoglycan layer (An et al., 2017; Dalrymple et al., 2010; Tortora et al., 2018). Peptidoglycan layer composed of peptide cross-linked polysaccharide in Gram-negative bacteria generates 10 % of the cell wall (1-2 nm). It provides the shape and internal pressure of the cell and allows passage of particles of 2 nm size through due to its porous structure (Dalrymple and Goswami, 2017; Demchick and Koch, 2006). Outer membrane of Gram-negative bacteria includes lipopolysaccharides (LPS), lipoproteins and phospholipids in its structure. LPS consists of three components as; O polysaccharide, core polysaccharide, and lipid A which released from cell wall after bacteria death and functions as an endotoxin. Moreover, outer membrane has porin proteins allowing to enter some nutrients into the cell, such as disaccharides, peptides, amino acids, nucleotides, vitamin B_{12}, and iron (Tortora et al., 2018).

Bacterial envelope damage may form as a result of lipid peroxidation process induced by the oxidative stress (Figure 2.9) (Dalrymple et al., 2010, Singh et al., 2013). ROS attack to unsaturated lipids and start a chain reaction. Phospholipids constitute most part of the outer membrane in *E. coli* and due to their amplitude and convenience to oxidation they are the first targets to $HO^{\bullet}$ attacks (Dalrymple and Goswami, 2017).

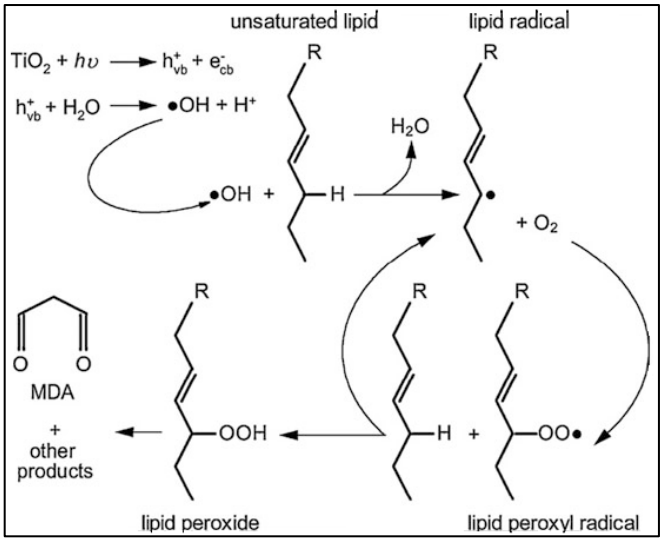

Figure 2.9. Schematic diagram of ROS utilized lipid peroxidation reaction (Dalrymple et al., 2011).

Lipid peroxidation occurs in three steps. The first step is initiation, $HO^{\bullet}$ takes a H atom from an unsaturated fatty acid and forms a lipid radical. The second step is propagation, the carbon centered lipid radical reacts with an oxygen and generates a lipid peroxyl radical, and then newly formed radical takes one H atom from another unsaturated fatty acid that forms a lipid peroxide molecule and leaves another lipid radical. Generated lipid peroxide degrades into malonaldehyde (MDA) that is

usually used as an indicator of lipid peroxidation. The third step is termination that occurs by the formation of neutral products from two radicals. Because lipid peroxidation is a chain reaction, termination reaction can end far from the first unsaturated fatty acid in the initiation reaction (Dalrymple and Goswami, 2017; Sun et al., 2017).

As a result of bacterial damage, leakage of intracellular components like K^+ could be detected. The main functions of K^+ in bacteria are to sustain membrane potential, osmotic pressure and to conduct signals. Some enzymes those take part in protein synthesis require potassium, as well. In unharmed cells, high intracellular K^+ concentration is provided with Na^+-K^+ pumps to maintain turgor pressure of the cell (Wang and O'Doherty, 2012). The leakage of intracellular components indicates that bacterial cell wall has been damaged and cell membrane permeability has increased. Moreover, relative permeability of membranes are 10 times higher to K^+ than Na^+ (Brock et al., 2000). Other than K^+ leakage, endotoxin (an outer membrane component of *E. coli*, Lipid A) release is another sign of the outer membrane damage in *E. coli*. Lu and colleagues reported that ~5 nm TiO_2 particles penetrate *E. coli* cell only after 20 min of photocatalytic treatment and this finding supports that the destruction of cell wall and leakage of macromolecules from the cell occurs during the treatment (Lu et al., 2003). In addition, it has been reported that in the presence of TiO_2, K^+ leakage starts immediately after illumination and K^+ concentration shows an increase up to a stable point. Researchers' findings show a consistency between K^+ leakage and the loss of cell viability (Saito et al., 1992).

During the photocatalytic inactivation process bacterial envelop is damaged and cell membrane permeability is increased. It could also be associated with the disruption of membrane-associated proteins. Researchers found that, respiratory chain membrane proteins and the adenosine triphosphatase (ATPase), which play a crucial role to transform energy into adenosine triphosphate (ATP), were inactivated rapidly and caused inadequate energy to maintain membrane unity (Bosshard et al., 2010a).

Research showed that respiration rate decrease occurs faster than bacteria inactivation (Sun et al., 2017). Damaged membrane proteins participating in bacterial respiratory chain causes a decreased respiration rate, this generates harm but does not inactivate bacteria directly, it can be due to the fermentation ability of *E. coli* (Clark, 1989). ATP generation capability of bacteria decreases through photocatalysis and results in the complete loss of ATP synthesis. Without ATP synthesis, bacteria cannot repair the damaged cell membrane, cannot sustain Na^+-K^+ pump activity and membrane potential. In addition, the absence of ATP causes K^+ leakage from the cytoplasm (Sun et al., 2014;

Bosshard et al., 2009). According to the findings of researchers, it can be concluded that direct cause of bacteria inactivation is due to the loss of ATP synthesis ability instead of damaged membrane structure and decreased respiration (Sun et al., 2017).

Enzymes. Upon photocatalysis, intracellular ROS like H_2O_2 and $O_2^{\bullet -}$ which can be named as secondary oxidants are generated. Inside the cell, H_2O_2 and $O_2^{\bullet -}$ can produce reactive $HO^{\bullet}$ by a Fenton reaction including free iron (Equations 2.11 and 2.12) (An et al., 2017). *E. coli* contains almost 20 μM of iron for Fenton reactions (Park and Imlay, 2003). $O_2^{\bullet -}$ is continuously created as a by-product upon aerobic respiration (Tortora et al., 2018).

$$Fe^{2+} + H_2O_2 \rightarrow Fe^{3+} + HO^{\bullet} + OH^{-} \quad (2.11)$$

$$O_2^{\bullet -} + H_2O_2 \rightarrow HO^{\bullet} + OH^{-} + O_2 \quad (2.12)$$

Photocatalytic treatment processes and increased inner ROS generate oxidative stress to the cell and bacteria produce some anti-oxidative enzymes against this stress. Superoxide dismutase (SOD) and catalase (CAT) are the main enzymes. SOD catalyzes the conversion and detoxification of $O_2^{\bullet -}$ by converting to H_2O_2 and O_2, afterwards CAT carries out the decomposition of H_2O_2 to harmless H_2O and O_2 (Sun et al., 2017; Chiang and Schellhorn, 2012). Upon photocatalytic inactivation, SOD and CAT levels decrease and as a result of this, intracellular ROS formation increases. The inactivation of these enzymes causes the accumulation of both intracellular and extracellular ROS and accelerates the inactivation rate of the system (An et al., 2017). Moreover, lesion repairing process of DNA after oxidative damage could be achieved by the action of specific enzymes and proteins (Cabiscol et al., 2000).

Proteins and DNA. Researchers detected leakage of intracellular substances like protein and nucleic acids by using scanning electron microscopy (SEM) images after photoelectrocatalytic treatment (Sun et al., 2014). Carré and colleagues showed that after photocatalytic treatment of *E. coli*, bacteria lost membrane associated proteins (Carré et al., 2014). Furthermore, intracellular ROS can lead to the oxidation of proteins which produces carbonyl groups (Dalle-Donne et al., 2003). After solar disinfection process, bacterial proteins can be aggregated by the attack of ROS and this aggregation occurs due to the oxidation of proteins (Bosshard et al, 2010b).

DNA is a more sensitive macromolecule to the oxidative stress than others; therefore, the damage or loss of bacterial DNA is a fatal factor for inactivation. This DNA damage can occur via base losses, breakage of one strand or double strand of the DNA (Hidaka et al., 1997).

2.4.3.3. Detection of bacteria inactivation and mineralization. During photocatalysis and as a result of oxidative degradation, leakage of cytoplasmic components of bacteria to the solution matrix would be expected to occur and leaked cytoplasmic substances would also be subjected to direct interaction with extracellular ROS. Therefore, leaked cytoplasmic components can be oxidized, segmented, or go for complete mineralization upon exposure to ROS attack (Suryo et al., 2012; Hirakawa et al., 2004).

Leung and colleagues examined dissolved organic carbon (DOC) content of the reaction medium after photocatalytic treatment and detected an increase reaching a peak and then a decreasing trend following the experiment. These findings showed that the released bacterial components can be degraded within extended irradiation periods, even complete mineralization of total DOC content can be expected (Leung et al., 2008). Consequently, from a general perspective, it can be expected that bacterial inactivation could also be followed via DOC variations in the reaction medium along with cell enumeration.

2.5. Water Matrix

Natural aquatic systems contain natural organic matter (NOM), microorganisms, anions, cations and pollutants giving chemical, physical and biological characteristics to water. In this study, organic materials like NOM and microorganisms and a water matrix (WM) comprised of inorganic materials as common anions (Cl^-, NO_3^-, SO_4^{2-}, PO_4^{3-}, HCO_3^-/CO_3^{2-}) and cations (Na^+, K^+, Ca^{2+}, Mg^{2+}) were used to simulate natural water conditions.

2.5.1. Effect of Water Matrix Components on Solar Light Initiated Photocatalytic Processes

In photocatalytic degradation processes, the solution matrix is very important since the adsorptive effect of the components can inhibit or alter the reaction rate of the process. The competition and retardation effects of different types of NOM, photocatalysts, metal ions, common anions and cations and inhibitory effects of alkalinity on TiO_2 photocatalysis process have been investigated to understand the limitations of the photocatalytic system (Bekbolet, 1997; Bekbolet and Balcioglu, 1996; Bekbolet et al., 1998; Gonenc and Bekbolet, 2001; Uyguner and Bekbolet, 2007, 2009; Uyguner-Demirel and Bekbolet, 2011).

Related to pH_{zpc} values of the particles and the pH of the solution, surface of the particles gains negative or positive charges. The presence of common anions and cations could hinder or improve

the generation of electrostatic attractions between organic matter, bacteria and photocatalyst surfaces. Uyguner and Bekbolet reported that the presence of common anions could lead the shrinkage of HA volume and shape however the presence of divalent, trivalent cations could cause enhanced intermolecular attractions and could end up with coagulation or precipitation (Uyguner and Bekbolet, 2009).

2.5.1.1. Effect of chloride. The presence of chloride ions (Cl^-) causes decreased oxidation rates in the system since they are adsorbed by the catalyst. Chloride ions could block the photocatalyst's active surface sites thus the catalyst could be deactivated against organic molecules (Abdullah et al., 1990; Bekbolet et al., 1998). This can also occur by the scavenging effect of chloride. Chloride ions decrease the oxidation rate by scavenging oxidizing radical species ($^{\bullet}ox$) (Equation 2.13) (Abdullah et al., 1990; Matthews, 1988). Moreover, Cl^- may react with the $HO^{\bullet}$ as given in the following reactions (Equations 2.14-2.16) (Grigor'ev et al., 1987; Jayson et al., 1973).

$$^{\bullet}ox + Cl^- \rightarrow Cl^{\bullet} + ox^- \quad (2.13)$$

$$HO^{\bullet} + Cl^- \rightarrow ClOH^{\bullet -} \quad (2.14)$$

$$ClOH^{\bullet -} \rightarrow HO^{\bullet} + Cl^- \quad (2.15)$$

$$ClOH^{\bullet -} + H^+ \rightarrow Cl^{\bullet} + H_2O \quad (2.16)$$

Also, some competitive reactions could form chloride ion and photogenerated holes, h^+_{VB} / electrons, e^-_{CB} and NOM species (Equations 2.17-2.19) (Uyguner and Bekbolet, 2009). Formed dichloride radical anion ($Cl_2^{\bullet -}$) is less reactive than chlorine radical ($Cl^{\bullet}$), however, reactive for both bacteria and organic matter (Alegre et al., 2000; Rincón and Pulgarin, 2004). Re-combination of both two previously generated $Cl^{\bullet}$ (Equation 2.20) and $Cl_2^{\bullet -}$ (Equation 2.21) form molecular chlorine (Cl_2) in water. These reactions can enhance the inactivation rate due to disinfectant effect of chlorine (Rincón and Pulgarin, 2004).

$$Cl^- + h^+_{VB} \rightarrow Cl^{\bullet} \quad (2.17)$$

$$Cl^- + e^-_{CB} \rightarrow Cl^- \quad (2.18)$$

$$Cl^{\bullet} + Cl^- \rightarrow Cl_2^{\bullet -} \quad (2.19)$$

$$Cl^{\bullet} + Cl^{\bullet} \rightarrow Cl_2 \quad (2.20)$$

$$Cl_2^{\bullet -} + Cl_2^{\bullet -} \rightarrow Cl_2 + 2Cl^- \quad (2.21)$$

2.5.1.2. Effect of nitrate. Nitrate ions (NO_3^-) could block the active sites of the photocatalysts partially thus its inhibitory effect is less than Cl^-. (Abdullah et al., 1990). On the other hand, NO_3^-

ions have reactivity in natural water. As they are irradiated (λ=320 nm), $HO^{\bullet}$ form thus they could enhance the degradation rate of organic compounds. Nitrate and nitrite (NO_2^-) give the following reaction in water (Equations 2.22-2.30) (Bekbolet et al., 1998; Uyguner and Bekbolet, 2009; Vione et al., 2014; Zafiriou and True, 1979a, 1979b).

$$NO_3^- + h\nu \rightarrow NO_3^{\bullet -} \rightarrow NO_2^- + O\ (^3P) \quad (2.22)$$

$$NO_3^- + h\nu \rightarrow NO_2^{\bullet} + O^{\bullet -} \quad (2.23)$$

$$O^{\bullet -} + H_2O \rightarrow HO^{\bullet} + OH^- \quad (2.24)$$

$$NO_3^- + H_2O + h\nu \rightarrow NO_2 + HO^{\bullet} + OH^- \quad (2.25)$$

$$NO_3^- + H^+ + h\nu \rightarrow NO_2^{\bullet} + HO^{\bullet} \quad (2.26)$$

$$NO_2^- + h\nu \rightarrow NO_2^{\bullet -} \rightarrow NO^{\bullet} + O^{\bullet -} \quad (2.27)$$

$$O^{\bullet -} + H^+ \rightarrow HO^{\bullet} \quad (2.28)$$

$$NO_2^- + H_2O + h\nu \rightarrow NO^{\bullet} + HO^{\bullet} + OH^- \quad (2.29)$$

$$NO_2^- + H^+ + h\nu \rightarrow NO^{\bullet} + HO^{\bullet} \quad (2.30)$$

$HO^{\bullet}$ formed in natural waters mainly give rections with HAs. This non-selective aqueous $HO^{\bullet}$ can seperate H atoms from organic molecules or add to C=C double bond or accept an electron (Hoigné, 1990). NO_3^- have ability to photolyze under sunlight conditions to form $HO^{\bullet}$ in natural water bodies; therefore, oxidation of humic substances (HSs) in sunlit natural surface waters could be induced in the presence of NO_3^- (Kotzias et al., 1982; Zafiriou, 1974).

2.5.1.3. Effect of sulfate. Sulfate ions (SO_4^{2-}) could directly be adsorbed on positively charged TiO_2 surface sites and deactivate some portion of the photocatalyst. This deactivation can cause retardation in the oxidation rates of organic molecules. Moreover, SO_4^{2-} could bind with the positive holes (h^+) and form sulfate radicals ($SO_4^{\bullet -}$) if all oxidizing sites of the surface are available for adsorption (Equation 2.31) (Abdullah et al., 1990).

$$h^+ + SO_4^{2-} \rightarrow SO_4^{\bullet -} \quad (2.31)$$

Also, $HO^{\bullet}$ radicals could react with SO_4^{2-} species to give $SO_4^{\bullet -}$ (Equations 2.32 and 2.33) (Matthews at al., 1972; Uyguner and Bekbolet, 2009). With the effect of these reactions, oxidation rate of the organic molecules could be enhanced.

$$HO^{\bullet} + HSO_4^- \rightarrow H_2O + SO_4^{\bullet -} \quad (2.32)$$

$$HO^{\bullet} + SO_4^{2-} \rightarrow H_2O + SO_4^{\bullet -} \quad (2.33)$$

2.5.1.4. Effect of phosphate. Phosphate ions ($H_2PO_4^-$) react like SO_4^{2-} anions by adsorbing on the surface active sites of the photocatalyst and decrease the rate of oxidation (Abdullah et al., 1990; Uyguner and Bekbolet, 2009). Phosphate ions could react similarly with sulfate ions by binding with the positive holes and form dihydrogen phosphate radicals ($H_2PO_4^{\bullet}$) (Equation 2.34) (Abdullah et al., 1990). Formed $H_2PO_4^{\bullet}$ is not reactive as $HO^{\bullet}$ (Rincón and Pulgarin, 2004).

$$h^+ + H_2PO_4^- \rightarrow H_2PO_4^{\bullet} \quad (2.34)$$

Moreover, $H_2PO_4^-$ anion actions like a screen by absorbing UV radiation and this low amount of photo absorption could reduce the light reaching bacteria in the solution and provide some light protection to bacteria (Rincón and Pulgarin, 2004).

2.5.1.5. Effect of bicarbonate. Bicarbonate ions (HCO_3^-) behave as scavengers of h^+ formed on irradiatied TiO_2 surface (Equation 2.35) and decrease the inactivation rate (Abdullah et al., 1990).

$$h^+ + HCO_3^- \rightarrow HCO_3^{\bullet} \quad (2.35)$$

At neutral pH conditions (pH: 6-7), the surface charge of TiO_2 is neutral as well ($pH_{zpc} \approx 6.5$). Under these conditions, HCO_3^- adsorbs on TiO_2 and forms a negatively charged layer on the surface causing less positive surface charge. Due to this change on the surface charge, TiO_2 adsorption on *E. coli* decreases and causes reduced inactivation rates. Moreover, HCO_3^- could demonstrate photo absorption and reduce light penetration into the bacteria solution, resulting in some light protection to bacteria like phosphate ions (Rincón and Pulgarin, 2004).

HCO_3^- could react with $HO^{\bullet}$ radical to produce less reactive carbonate radical ($CO_3^{\bullet -}$) (Equations 2.36 and 2.37) (Chen et al., 1997), its reactions are slower than $HO^{\bullet}$ (Rincón and Pulgarin, 2004).

$$HO^{\bullet} + HCO_3^- \rightarrow CO_3^{\bullet -} + H_2O \quad (2.36)$$
$$HO^{\bullet} + CO_3^{2-} \rightarrow CO_3^{\bullet -} + OH^- \quad (2.37)$$

2.5.1.6. Effect of monovalent cations. The presence of both Na^+ and K^+ as monovalent cations decrease the inactivation rate of bacteria. In addition, researchers reported that inhibitory effect of K^+ is higher than Na^+. Rincón and Pulgarin suggested that the addition of K^+ into the solution containing *E. coli*, compensates K^+ leakage from the cell membrane and cause the retardation of cell damage (Rincón and Pulgarin, 2004).

2.5.1.7. Effect of divalent cations. The presence of divalent cations as Ca^{2+} and Mg^{2+} in low concentrations displayed enhanced DOC removal efficiency in high DOC containing samples. Uyguner and Bekbolet reported that Ca^{2+} has more effectiveness than Mg^{2+} (Uyguner and Bekbolet, 2009).

Rincón and Pulgarin performed a study to elucidate the effect of individual common anions and cations on TiO_2 photocatalytic inactivation of *E. coli* (Rincón and Pulgarin, 2004). It was reported that preliminary experiments conducted in the absence of photocatalyst specimen and sole HCO_3^- showed an enhancement in the inactivation rate of bacteria. However in the presence of SO_4^{2-}, NO_3^-, Cl^- and $H_2PO_4^{2-}$ anions a retardation effect was observed in inactivation rates expressing no significant difference between *E. coli* count in the presence of SO_4^{2-}, NO_3^-, Cl^- and $H_2PO_4^{2-}$ anions. In the presence of TiO_2, anions decrease the inactivation rates in an increasing order as: Cl^-, NO_3^-, SO_4^{2-}, HCO_3^- and HPO_4^{2-}; the effectiveness of HCO_3^- and HPO_4^{2-} was higher than other anions. Besides the effects of individual anions, researchers further studied the removal extends of anions from the system with respect to their dissappearnce from filtered solution via *E. coli* intake and/or adsorption onto TiO_2 surface occurring mainly throuh electrostatic interactions. Only in the presence of TiO_2 and negatively charged anions, removal % of anions by adsorption onto photocatalys surface showed a decreasing order as: $NO_3^- \geq Cl^- > SO_4^{2-} > HPO_4^{2-} > HCO_3^-$. On the other hand in the presence of *E. coli* and anions, removal % of anions followed a decreasing trend as: $HCO_3^- > SO_4^{2-} > Cl^- >> HPO_4^{2-} > NO_3^-$. Conclusively, in the presence of all reactive species as anions, *E. coli*, and TiO_2, anion removal % via both bacteria uptake and adsorption onto TiO_2 showed a decreasing trend as: $HCO_3^- > HPO_4^{2-} > SO_4^{2-} > NO_3^- > Cl^-$. According to removal % of anions, HCO_3^- was the most absorbed anion by *E. coli*, causing enhanced sensitivity to irradiation by changing membrane characteristics of bacteria, and increased bacteria inactivation efficiency (Rincón and Pulgarin, 2004).

Romazzoni and colleagues studied SODIS and photo-Fenton processes in the presence of inorganic ions and suggested that *E. coli* K-12 inactivation in both processes increased with the usage of 10 mg/L HCO_3^- (Romazzoni et al., 2020). This enhancement could be due to formation of $CO_3^{\bullet-}$ radical which has much longer lifetime in aqueous solutions than $HO^{\bullet}$. Addition of 100 mg/L Cl^- provides enhanced disinfection rates in both processes. When researchers used increased concentrations of Cl^-, SODIS showed enhanced results but photo-Fenton process was disrupted. SO_4^{2-} addition in the range of 0-500 mg/L showed no difference in SODIS but led to increased inactivation rates in photo-Fenton process. NO_2^- and NO_3^- usage provide increased inactivation to both processes and the effect of NO_2^- was higher than NO_3^-. Moreover, the addition of NH_4^+ showed an enhancement for photo-Fenton, while had no effect on SODIS (Romazzoni et al., 2020).

2.6. Natural Organic Matter

NOM can be defined as all the organic matter, in both dissolved and particulate form in nature other than living organisms and synthetic materials (Buffle, 1984; Buffle, 1988). Dissolved form of NOM in oceans and in all types of freshwaters is named as dissolved organic matter (DOM) and particulate fraction of NOM is referred to as particulate organic matter (POM) (vanLoon and Duffy, 2000). Various forms of NOM under the concept of total organic matter (TOM) and total organic carbon (TOC) present in natural waters are displayed as a Venn schema in Figure 2.10. Dissolved organic nitrogen (DON) species e.g., proteins, peptides, amino acids and dissolved organic phosphorus (DOP) species e.g., phospholipids and polyphosphates are also considered in general domain of TOM, explicitly in DOM and more specifically as a part of DOC. Non-humic fraction should also be expressed within the dissolved organic matrix.

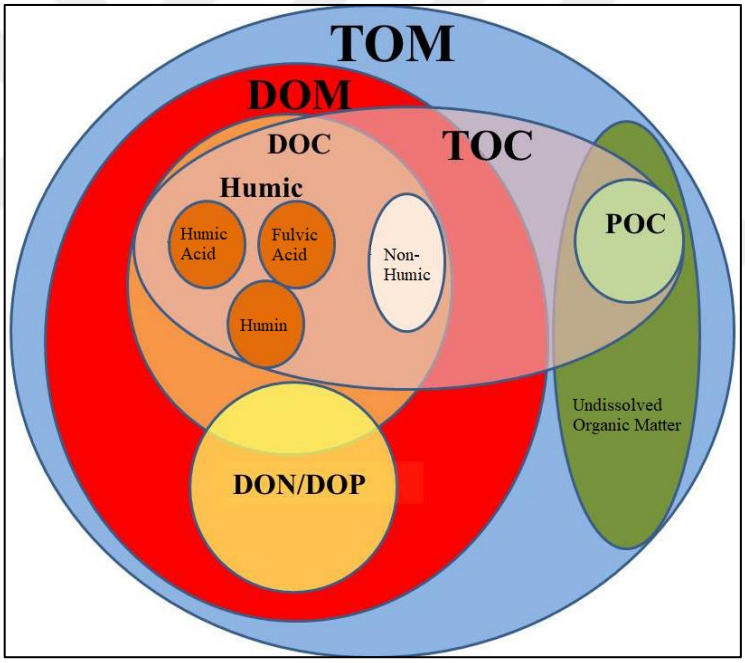

Figure 2.10. Venn diagram of various NOM forms found in natural waters. TOM or NOM, TOC, DOM, DOC, POC, DON, DOP and humic and non-humic materials are represented (Pagano et al., 2014).

DOM is the main carbon-based component that can range in molecular weight from a few hundred to 100,000 daltons (Da), in the colloidal size range (Aiken et al., 1985; Thurman, 1985). A schematic mass (MW, Da) and size (μm) distribution diagram of NOM species and organisms in natural waters is shown in Figure 2.11. Expressing comparatively larger size mostly greater than 1 μm, species like zooplankton, phytoplankton and bacteria could be regarded as POM. The International Humic Substance Society (IHSS) uses natural waters to isolate NOM fractions.

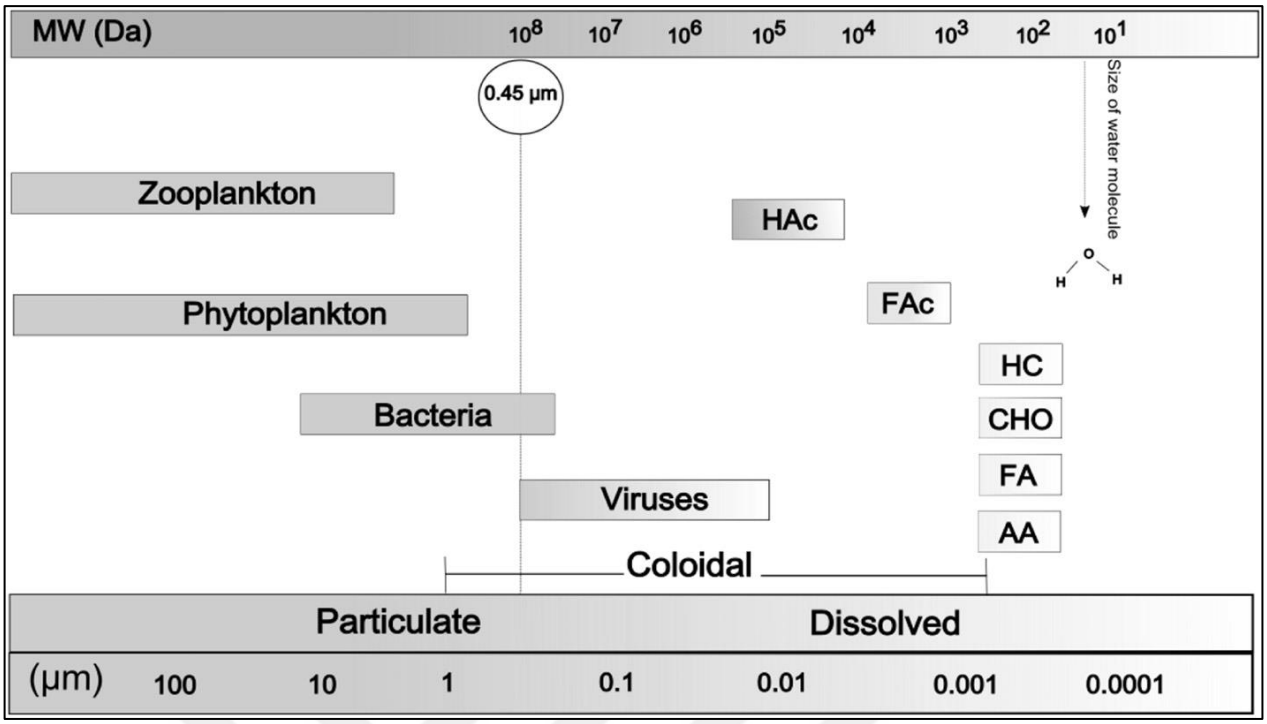

Figure 2.11. Organic matter mass (Da) and size (µm) distribution diagram of NOM species and organisms in natural waters. Molecular weight (MW), humic acid (HAc), fulvic acid (FAc), hydrocarbons (HC), carbohydrates (CHO), fatty acids (FA), amino acid (AA) (Artifon et al., 2019).

NOM contains HSs like HAs and fulvic acids (FAs) and non-humic substances covering proteins, polysaccharides and other various components in its structure (MacCarthy et al., 1990). NOM can originate from two different types of sources as allochthonous and autochthonous. While allochthonous NOM is generated from terrestrial or watershed sources, it indicates the presence of HS, autochthonous NOM arises from algae, bacteria and macrophytes and it mainly indicates the presence of algal derived organic matter. NOM chemistry, composition and amount can change with the source of the organic matter, climate, geology of the field and other cases like algal blooms and runoffs (Leenheer and Croué, 2003).

2.6.1. Humic Substances and Humic Acid

HSs are polyelectrolytic, dark colored organic acids expressing highly complex and heterogeneous chemical nature. From a general perspective, HSs can also be defined as the heteropolycondensed products of carbohydrates, proteins, fatty acids, lignins, tannins and many other compounds based on their origin (Gjessing, 1976). HSs display polydisperse characteristic with respect to their wide range of molecular sizes (Figure 2.12) (Aiken et al., 1985). HSs constitute 60 to 80 % of DOM in natural waters. The elementary composition of most HSs could be represented in the following order as; C: 45-55 %; O: 30-45 %; H: 3-6 %; N: 1-5 %; and S: 0-1 % (Manahan, 1999).

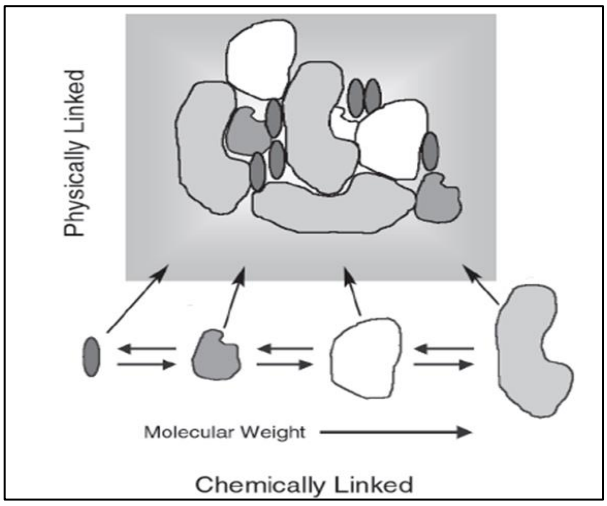

Figure 2.12. Conceptual model of polydisperse HSs (Haberhauer et al., 2000).

HSs can be examined in three different types according to their solubility characteristics (Figure 2.13). HA is not soluble at pH below 2 but soluble at higher pH. FA is soluble at all pH values. And lastly humin is the non-extractable plant residue that is insoluble at any pH (Gaffney et al., 1996).

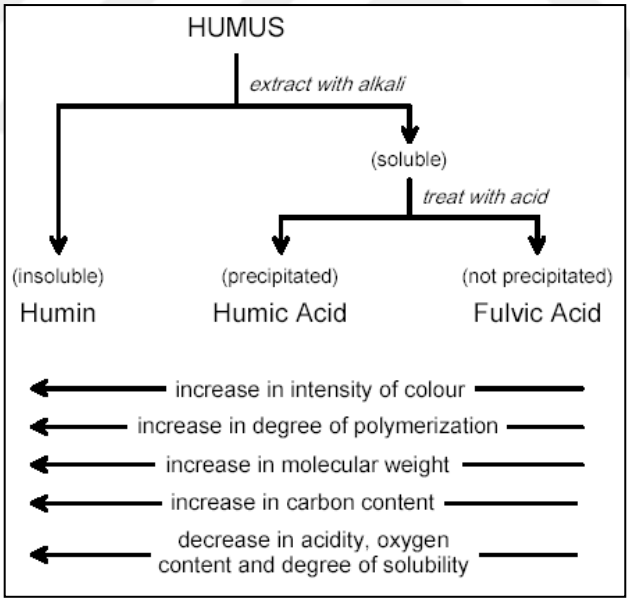

Figure 2.13. The postulated relation of HSs (Uyguner et al., 2007).

The humic content of various soils expressing diverse characteristics display variations in the range of 0 to 10 %. On the other hand, humic content of surface waters is expressed as DOC differing from 0.1 to 50 ppm in dark-water swamps. Whereas, in ocean water DOC changes in the range of 0.5 to 1.2 ppm at the surface, and 0.1 to 10 ppm in deep groundwaters (Choppin and Allard, 1985). Moreover, approximately 10 % of DOC in surface waters is found as suspended matter that can be present in the form of organic or organically coated inorganic particulates e.g., clay minerals and oxide surfaces (Gaffney et al., 1996). HSs generate 60-80 % of DOC and POC in surface waters

(Reuter and Perdue, 1977). As the acid insoluble fraction of HS, elemental content of HA could be expressed in the following order as: C: 60.0 %; O: 34.5 %; H: 4.47 %; N: 0.96 % (Mao et al., 1998).

It is reported that pH_{zpc} of HA can vary in the narrow range of pH: 4-5 due to the presence of functional groups (vanLoon and Duffy, 2000). Therefore, under acidic or alkaline pH conditions, structure of HA can exhibit conformational rearrangements (Figure 2.14). While at low pH conditions, HA shows a compact and coiled structure, however, at high pH values HA has almost linear structure resembling extended polymer configuration. At neutral pH conditions (pH: 6-7) resembling natural water, the surface of HA can be recognized as partially-negatively charged due to the deprotonation of carboxylic functional groups (pH: 3-5). Deprotonation of phenolic functional groups can also increase the number of negatively charged sites on HA in aqueous medium conditions expressing alkaline pH > 8 conditions.

a.

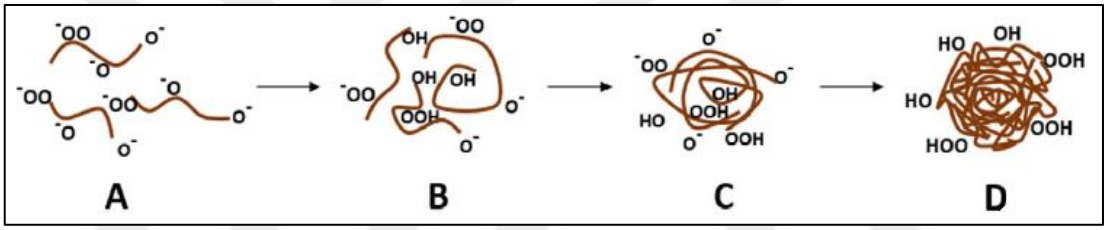

b.

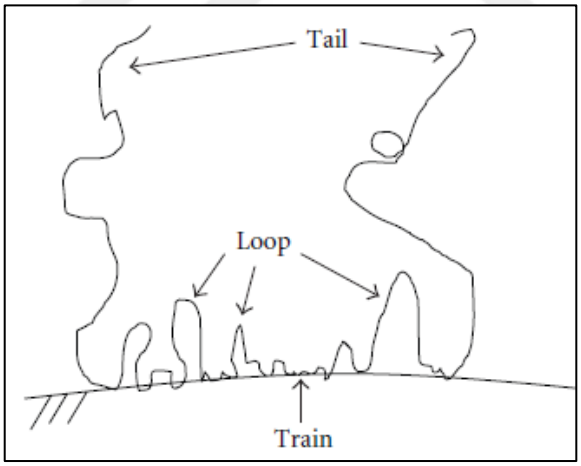

Figure 2.14. a. Conformational changes of HA molecules through alkaline to acidic pH; A. Charge repulsion at alkaline pH, B. Intramolecular aggregation at decreasing pH, C. Intermolecular aggregation at decreasing pH, D. Precipitation at acidic pH (de Melo et al., 2016). b. Tail, loop, and train formations of a HA polymer chain adsorbed on the surface (Adachi et al., 2012).

The hypothetical structure of HA has a hydrophobic aromatic core which is substituted with functional groups like free and bonded phenolic groups, quinine structures, nitrogen and oxygen as bridge units and carboxyl groups (COOH) (Figure 2.15). The hypothetic model contains both

hydrophilic and hydrophobic sites and has an immensely polyelectrolytic feature and some available sites to bind with organic compounds, mineral surfaces, and metal ions (Suffet and MacCarthy, 1989).

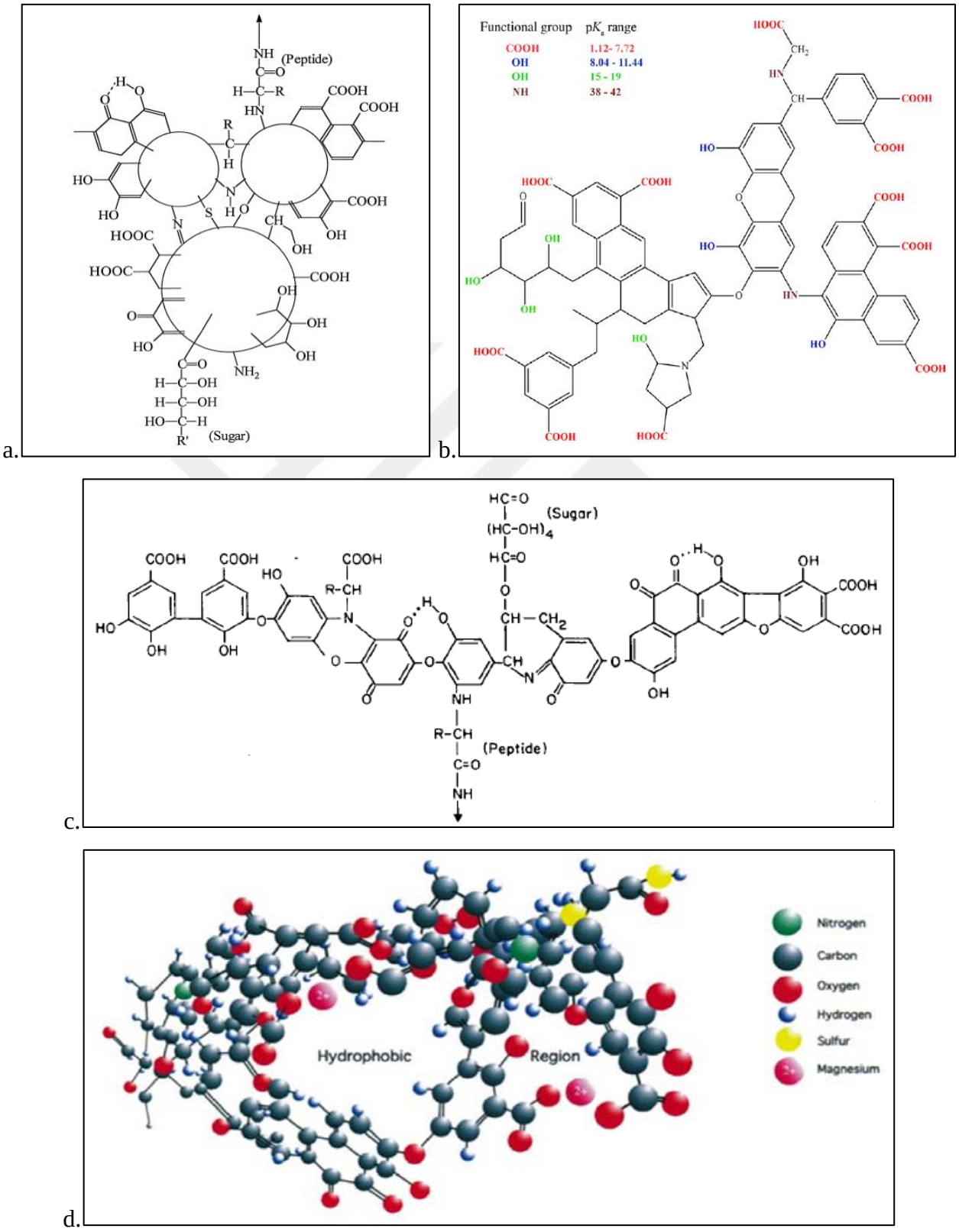

Figure 2.15. a. Hypothetical structure of HA (Fetsch et al., 1998); b. Functional groups and their range of pK_a values present in HA (Nada et al., 2019); c. Theoretical structure of HA (Stevenson, 1982); d. Proposed three-dimensional structure of HA (Engebretson and von Wandruszka, 1994).

2.6.2. Photochemistry of Humic Substances in Natural Water Systems

From a general perspective aquatic photochemistry is mainly dependent upon solar irradiation. Besides various photo-reactions occurring by inorganic species, as the principal component of natural waters, NOM may undergo either direct or indirect photolysis although both of the mechanisms may occur simultaneously.

UV-vis absorption spectra and fluorescence spectral features display the presence of chromophores and fluorophores present in NOM. Although a continuous decreasing absorbance with respect to increasing wavelength is a general trend of HSs, origin and type dependent variations may also be assessed (Figure 2.16) (Uyguner et al., 2007).

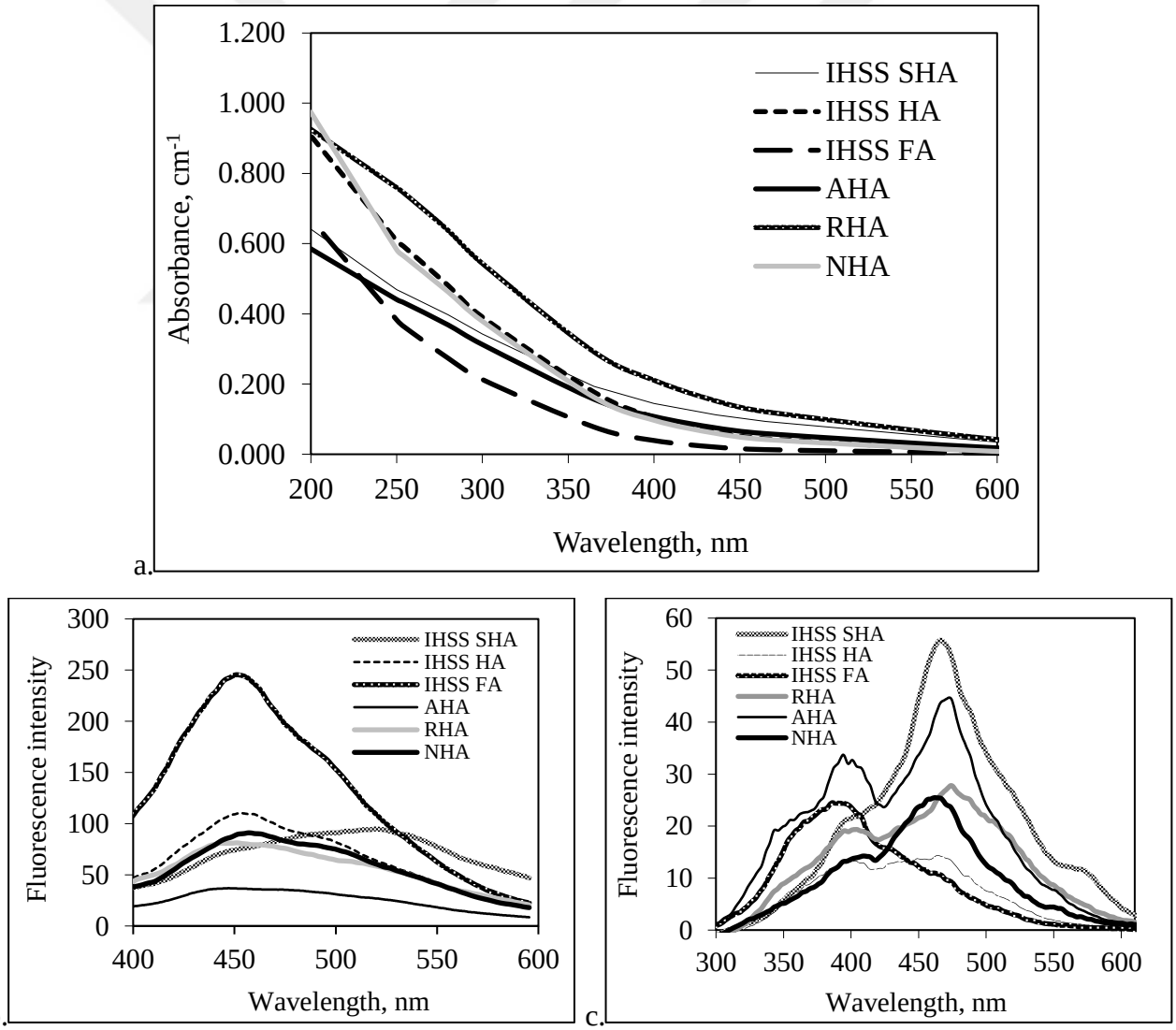

Figure 2.16. a. UV-vis absorption spectra, b. emission scan, and c. synchronous scan fluorescence spectra of IHSS soil HA (SHA), IHSS HA, IHSS FA, Aldrich HA (AHA), Roth HA (RHA), and Nordic HA (NHA) (Uyguner et al., 2007).

The chromophoric centers in numerous compounds that are also considered as building blocks of natural organic matter express quite different absorption and photochemical properties (Figure 2.17) (Vione et al., 2014). Examples of these reactions could simply be photoionization (phenolic groups), photoreduction (quinonoid groups, conjugated systems) and homolysis.

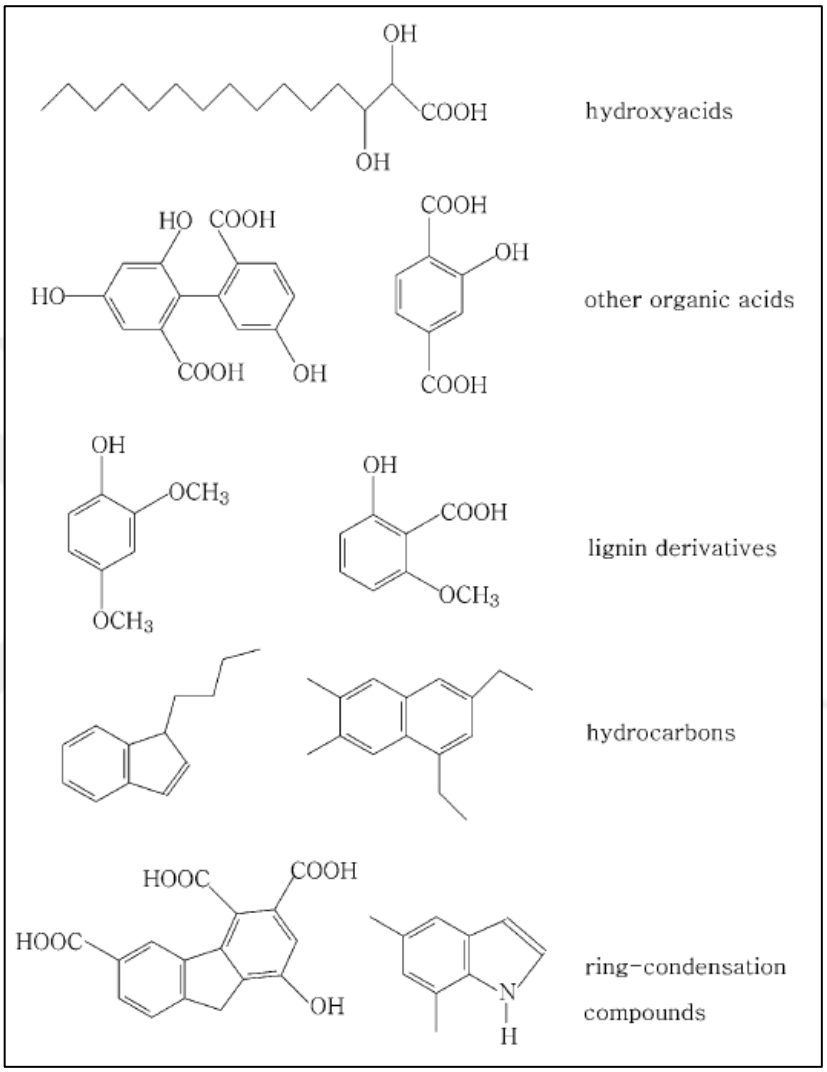

Figure 2.17. Representative functional groups and building blocks of HSs (Vione et al., 2014).

Aquatic NOM can either be originated from terrestrial runoff as allochthonous or directly formed within the system as autochthonous. Therefore, the photosensitizing properties are extensively investigated and generally considered as the same for both allochthonous and/or autochthonous organic matter. Upon light absorption, changes in absorption and fluorescence properties of organic matter may occur via photolysis and irreversible reactions may lead to structural changes in organic matter. During indirect photolysis process, photosensitization process predominates over direct photolysis. HSs are known to be the main photosensitizers in natural waters since HSs are Omni present organic matter expressing ill-defined chemical structure as explained in Section 2.6.1.

In natural waters, HSs are the most important sunlight absorbing substances leading to photosensitized oxygenation reactions (Zepp et al., 1977). Photosensitization can be defined as a process initiating a photochemical reaction using a photosensitizer which is a substance having the ability of absorbing light and transferring the energy to another molecule (Zafiriou et al., 1984). When a photosensitizer is excited by photon energy, fundamental changes in its electron distribution occurs as described by internal homolysis of electron pairs. Electron pair homolysis of a molecule results in formation of excited singlet and triplet states (Schenck, 1963). Photosensitizers may not be consumed during these reactions, they may excite and/or transfer energy to other molecules or simply return to their original states (IUPAC, 2004). The altered molecule by photosensitizer is called as substrate or acceptor. Further reactions could result transformation and even degradation of organic compounds through various pathways such as photochemical, redox and hydrolysis.

Photochemical performances of NOM and its analogs has been widely studied since 1970s (Zepp et al., 1976, 1977; Aguer and Richard, 1993, 1996; Aguer et al., 1999). DOM mainly HSs control photochemical reactions in water systems. The photoinduction of DOM causes the formation of ROS. Probable photochemical reactions of DOM in aqueous media presented below (Equations 2.38-2.49), where the contributors are singlet DOM (^{1}DOM), triplet DOM (^{3}DOM), $e^-_{(aq)}$, $HO^\bullet$, scavenger (R), $O_2^{\bullet-}$, $HO_2^\bullet$, H_2O_2, triplet oxygen ($^3O_2$) and singlet oxygen ($^1O_2$) (Cooper, 1988; Uyguner-Demirel et al., 2017; Zepp et al., 1985). Reactions begin with the absorption of light by the functional groups of DOM which generates the photo-exited ^{1}DOM and ^{3}DOM, and following reactions form ROS.

$$DOM + h\nu \rightarrow {}^1DOM^* \rightarrow {}^3DOM^* \quad (2.38)$$

$${}^1DOM^*_{(aq)} \rightarrow DOM^{\bullet+} + e^-_{(aq)} \quad (2.39)$$

$$DOM^{\bullet+} + O_2/H_2O \rightarrow HO^\bullet + DOM \quad (2.40)$$

$$O_2 + e^-_{(aq)} \rightarrow O_2^{\bullet-} \quad (2.41)$$

$${}^1DOM^*_{(aq)} + R \rightarrow R^\bullet + DOM^\bullet \quad (2.42)$$

$$R^\bullet + DOM^\bullet + O_2/H_2O \rightarrow HO^\bullet + R + DOM \quad (2.43)$$

$${}^3DOM^* + O_2 \rightarrow DOM^\bullet + O_2^{\bullet-} \quad (2.44)$$

$$O_2^{\bullet-} + H^+ \leftrightarrow HO_2^\bullet \qquad pK_a=4.8 \quad (2.5)$$

$$HO_2^\bullet + HO_2^\bullet \rightarrow H_2O_2 + O_2 \quad (2.7)$$

$$HO_2^\bullet + O_2^{\bullet-} + H_2O \rightarrow H_2O_2 + O_2 + OH^- \quad (2.45)$$

$${}^3DOM^* + {}^3O_2 \rightarrow DOM^{\bullet+} + O_2^{\bullet-} \quad (2.46)$$

$${}^3DOM^* + {}^3O_2 \rightarrow {}^1DOM + {}^1O_2 \quad (2.47)$$

$${}^1O_2 + H_2O \rightarrow {}^3O_2 + H_2O \quad (2.48)$$

$${}^1DOM + {}^1O_2 \rightarrow DOM^{\bullet+} + O_2^{\bullet-} \quad (2.49)$$

Indirect photoreactions take place through initial excitation followed by energy transfer leading to formation of various photo-products namely ROS in the presence of dissolved oxygen. These free-radical species could react with various compounds e.g., amino acids (tryptophan) or fatty acids, etc.. If such materials are released from cells, they may be subjected to irradiation directly resulting in complete destruction and forming components of organic debris. Considering heterogeneous and polydisperse nature of HSs, generation of ROS could proceed selectively via light interaction with low molecular or high molecular fractions with respect to their degree of functionality and hydrophobic core (Vione et al., 2014). Since all natural waters contain colloidal matter either as living or non-living in nature, these compounds are also prone to photolysis and/or photo-initiated reactions under sunlit environmental conditions (Scully et al., 2003).

DOM has attracted attention of researchers in recent years due to its influence in water treatment. Especially for disinfection purposes in case that chlorination process is applied, DOM is the major precursor in the formation of DBPs most significantly trihalomethanes (Richardson et al., 2002; 2007). Furthermore, DOM can serve as substrates for the undesirable microbiological growth in pipelines promoting public health concern. Therefore, removal of DOM is considered as the main target of all water treatment facilities. Besides conventional treatment processes (coagulation and flocculation), oxidation based technologies i.e. UV-irradiation, or ozonation are also frequently applied (Parsons, 2004). Photocatalytic degradation of NOM and its representative compounds like HA and FA have been investigated by Bekbolet and colleagues (Bekbolet and Ozkosemen, 1996, Bekbolet et al., 1998; Uyguner and Bekbolet, 2005; Uyguner-Demirel and Bekbolet, 2011). The investigation of photocatalytic degradation of NOM was studied in detail by various reseachers (Espinoza and Frimmel, 2009) and several review papers were published about this subject (Matilainen and Sillanpää, 2010; Uyguner-Demirel et al., 2017).

Throughout the application of solar light initiated photolytic and photocatalytic destruction of bacteria, the release of organic matter can be observed and characterized (Carré et al., 2014; Castro-Alférez et al., 2016; Kiwi and Nadtochenko, 2005). The release of organic matter and DOM can be followed with UV-vis absorption spectra and with the application of specific fluorescence techniques like EEM. UV-vis parameters at 436 nm ($Color_{436}$) and 365 nm (UV_{365}) give information about the presence of color forming moieties and absorbance at 280 nm (UV_{280}) and 254 nm (UV_{254}) present the aromatic fractions (Uyguner and Bekbolet, 2005).

Specific visible ($SCoA_{436}$) and UV absorbance ($SUVA_{365}$, $SUVA_{280}$ and $SUVA_{254}$) values represent DOC normalized color forming and aromatic moieties (Uyguner and Bekbolet, 2005).

$SUVA_{254}$ value can be used to identify water sample's composition in terms of hydrophobicity and hydrophilicity. $SUVA_{254} < 3$ indicates the presence of hydrophilic and aliphatic content however $SUVA_{254} > 4$ represents the existence of hydrophobic and aromatic material (Edzwald et al., 1985).

Fluorescence spectroscopy techniques are quantitative analytical techniques can be used to characterize NOM due to their sensitivity and non-destructive features (Alberts and Takács, 2004; Senesi, 1990). Fluorescence occurs during the excitation of a substance by the absorption of a photon from UV-vis region and emission of light while returning to its ground state, and at specific wavelengths it describes the relation of absorbed and emitted photons (Valeur, 2002). NOM has internal fluorescence characteristics accompanying with changes in the emission maximum wavelength when exiting at different ones. Besides limited distinctiveness of excitation scan spectra and emission scan spectra, synchronous scan fluorescence spectroscopy maintains a constant between excitation and emission wavelengths; therefore, it is a useful tool to indicate differences and similarities between samples (Figure 2.16). Synchronous scan fluorescence spectrum at λ_{emis}=470 nm ($FI_{sync470}$) indicates the presence of HA (Uyguner and Bekbolet, 2005), and at λ_{emis}=280 nm ($FI_{sync280}$) reflects the presence of protein, especially tryptophan in the solution (Reynolds, 2003).

EEM fluorescence spectrophotometry can also be used to characterize different fluorophores in the water sample. In EEM fluorescence contour plots, natural organic matter exhibits fluorescence in excitation wavelength range of λ_{exc} ~200 to 500 nm and emission wavelength range of λ_{emis} ~280 to 600 nm (Baker et al., 2008). When the destruction of bacteria occurs, the presence of aromatic proteins I (λ_{exc} 220-250 nm and λ_{emis} 280-332 nm), aromatic proteins II (λ_{exc} 220-250 nm and λ_{emis} 332-380 nm), microbial by-products (λ_{exc} 250-470 nm and λ_{emis} 280-380 nm), humic-like substances (λ_{exc} 220-470 nm and λ_{emis} 380-580 nm), and fulvic-like substances (λ_{exc} 220-250 nm and λ_{emis} 380-580 nm) can be seen in EEM fluorescence plots (Figure 2.18) (Coble, 1996).

Since intrinsic fluorescence properties reflects information pertaining to structure, conformation, and heterogeneity of organic matter as well as dynamical properties related to intramolecular and intermolecular interactions, a fluorescence-derived index as fluorescence index (FI) is defined as the ratio of the emission intensity at λ_{emis}=450 nm to that at λ_{emis}=500 nm, following the excitation at λ_{exc}=370 nm (Bekbolet and Sen-Kavurmaci, 2015; McKnight et al., 2001). $FI \leq 1.4$ represents the presence of humic fluorophores of organic matter mainly derived from terrestrial sources. On the other hand, $FI \geq 1.9$ indicates the existence of organic material stemming from microbial origin (Sen-Kavurmaci and Bekbolet, 2014). Relating this information to DOM characterization and bacteria cell

destruction probably resulting in release of fluorophoric organic compounds and/or fractions would be crucial in understanding mechanism of microorganism inactivation.

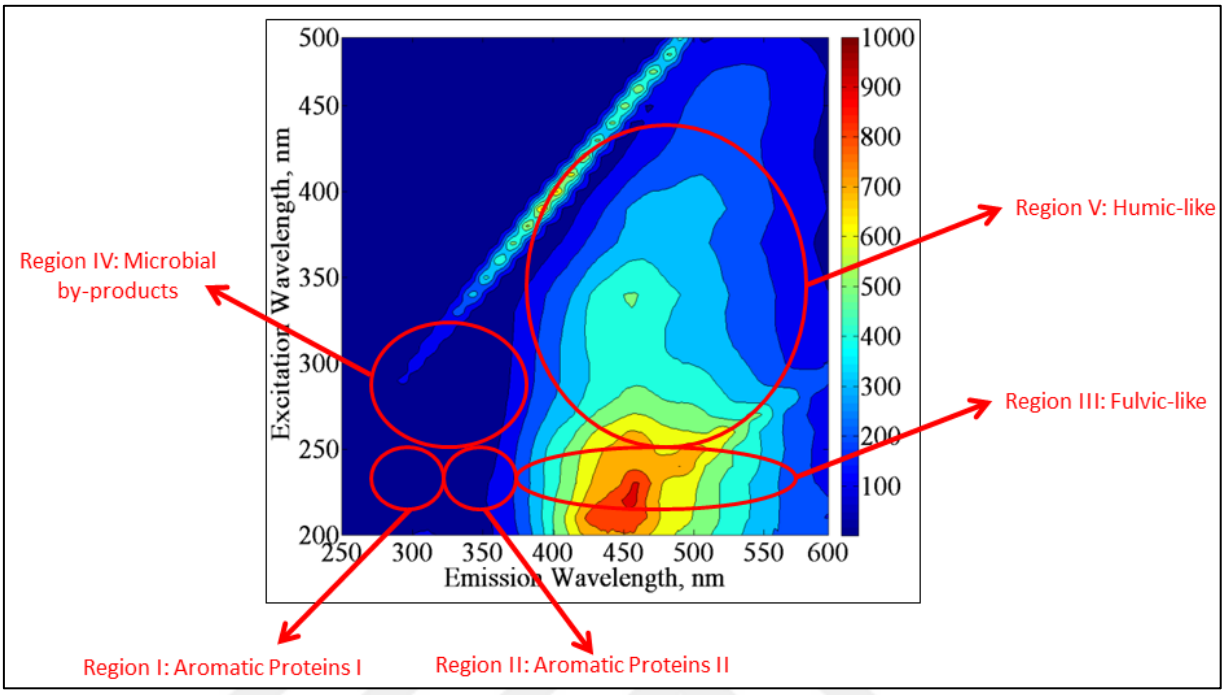

Figure 2.18. Diagram of EEM fluorescence contour plot regions.

Bacteria inactivation by TiO_2 photocatalysis has been studied for elucidation of mechanistic details by many research groups as stated previously in Section 2.4.2. (Bekbolet, 1997; Bekbolet and Araz, 1996; Bekbolet and Tomruk, 1998; Bekbolet, 2007). Birben and colleagues presented that the presence of humic matter expressed a retardation effect on solar photocatalytic inactivation of *E. coli*. Regrowth of *E. coli* could not be assessed under specific experimental conditions. EEM fluorescence contour plots displayed the formation of new fluorophoric regions described as microbial by-products and aromatic proteins. Also, undoped TiO_2 P-25 expressed comparatively slower removal rates in comparison to doped specimens (Birben et al., 2017a).

Besides the already reported studies by Bekbolet and colleagues on *E. coli* photocatalytic inactivation, further interest was directed to use of a VLA photocatalyst such as Fe-doped TiO_2. TiO_2 source was P-25 serving as a base specimen and a novel sol-gel synthesized TiO_2 was also introduced expressing different physico-chemical and morphological properties. It should also be mentioned that the aforementioned VLA Fe-doped TiO_2 specimens were previously utilized for HA degradation under simulated solar light irradiation (Birben et al., 2017b). Therefore, solar light initiated photocatalytic treatment of *E. coli* by using Fe-doped TiO_2 species in various aqueous matrix conditions would bring further insight into bacteria inactivation in natural waters.

3. MATERIALS AND METHODS

3.1. Materials

3.1.1. Preparation of *E. coli* suspension

E. coli K12 strain, ATCC 23716 was used as an indicator bacterium. *E. coli* growth was provided by inoculation of one *E. coli* colony in 25 mL of LB broth. The suspension was incubated at 37°C and shaken at 90 rpm for 16-18 hours. Working *E. coli* solutions (10^{5-8} Colony Forming Unit (CFU)/mL) were prepared in various reaction media which was explained below Sections 3.1.4, 3.1.5, and 3.1.6. Cell samples were taken from *E. coli* suspension during the stationary phase of the bacteria growth. *E. coli* was freshly incubated in LB broth for each experiment set.

3.1.2. Luria Bertani Broth

Aqueous solution of LB broth was prepared by using 2 g tryptone, 1 g yeast extract and 2 g NaCl (Bertani, 1951; Singleton, 1997). LB broth was freshly prepared as a volume of 200 mL when required.

3.1.3. CHROMagar™ ECC

CHROMagar™ ECC, which is a selective solid medium for *E. coli* and other coliforms was used. CHROMagar™ ECC was composed from 15 g/L agar, 8 g/L peptone and yeast extract, 5 g/L NaCl, and 4.8 g/L chromogenic mix, was used as a culture medium (CHROMagar, 2019). It provides easy plate reading by giving different colors to different bacteria. *E. coli* colonies demonstrate blue color while other coliform colonies have mauve color. Other bacteria colonies are either colorless, or growth has been inhibited.

3.1.4. Isotonic Solution

Saline solution designated as isotonic solution (IsoT) is used in the experiments to obtain optimal osmatic pressure condition to bacteria. IsoT as 0.85 % solution was prepared by adding 8.5 g NaCl (Sigma-Aldrich) into 1 L of distilled-deionized water and dissolved using magnetic stirrer to obtain complete dissolution (APHA, AWWA, WPCF, 2012).

3.1.5. Water Matrix Solution

Water matrix referred as WM, containing common anions and cations such as Cl^-, NO_3^-, SO_4^{2-}, $H_2PO_4^-$, HCO_3^-/CO_3^{2-}, Na^+, K^+, Ca^{2+}, and Mg^{2+} was used as a natural surface water analogue and prepared according to the recipe from Smith and colleagues (Smith et al., 2002). Concentrations of anions and cations were verified and presented at Table A.1.

3.1.6. Humic Acid Solution

Commercial humic acid sodium salt as purchased from Aldrich was used as a DOM analogue. Aqueous stock solution of 1000 mg/L HA was prepared by dissolving 1.0 g HA in 1 L of ultrapure water (Millipore Milli-Q plus system, with resistivity of 18.2 MΩ cm at 25°C). Working HA solution's concentration was chosen as 50 mg/L and it was prepared by diluting the stock solution. In order to prepare 100 kDa molecular size fraction of 50 mg/L HA, sequential fractionation as prefiltration through 0.45 μm cellulose acetate membrane filter and subsequent ultrafiltration process using 100 kDa cut-off membrane filter (Amicon 8050 stirred cell unit) was applied. Spectroscopic characterization of 100 kDa HA was presented at Appendix B Section.

3.1.7. Photocatalyst Specimens

A total of six photocatalyst specimens were used as two undoped and four Fe-doped types. TiO_2 P-25 (Evonik) and synthesized TiO_2 ($SynTiO_2$) were used as bare TiO_2 specimens and their 0.25% and 0.50% Fe-doped species, namely as 0.25% Fe-TiO_2, 0.50% Fe-TiO_2, 0.25% Fe-$SynTiO_2$, and 0.50% Fe-$SynTiO_2$, were used as doped types.

TiO_2 P-25 which mainly composed of 80 % anatase and 20 % rutile crystal phases was supplied from Evonik and used as a standard photocatalyst specimen. TiO_2 exhibits surface area of 55 ±5 m^2/g, primary particle size as 30 nm and pH_{zpc} as 6.25. $SynTiO_2$ was prepared by applying a modified sol gel method using titanium (IV) isopropoxide (97 % Aldrich) as the precursor material (Turkten and Cinar, 2017). Fe-doped TiO_2 and $SynTiO_2$ photocatalyst specimens were prepared according to wet impregnation method using $Fe(NO_3)_3 \cdot 9H_2O$ (Merck) as the iron source (Yalcin et al., 2010). Excluding TiO_2 P-25, all of the prepared photocatalyst specimens were calcined at 500ºC for 5 h. Physicochemical and morphological characteristic properties of all six photocatalysts specimens were previously reported and elucidated by crystallographic properties (XRD), band-gap energy (UV-DRS), surface morphology (SEM) and Brunauer-Emmett-Teller (BET) surface area, and presented

in Appendix C Section (Birben et al., 2015, 2017; Turkten, 2016; Turkten and Cinar, 2019; Turkten et al., 2019; Yalcin et al., 2010). Photocatalyst loading was chosen as 0.25 mg/mL and kept constant for all experiments.

3.2. Methods

3.2.1. Experimental Set-Up

Solar light initiated photolytic and photocatalytic inactivation experiments were carried out using an Atlas-Suntest CPS+ solar simulator. The light source is an air-cooled Xenon lamp with a wavelength range of λ=290 nm to 800 nm and light intensity, I_o=250 W/m^2. The solar simulator is equipped with quartz and UV special glass filters to simulate typical outdoor sunlight irradiation. All experiments were carried out by using 150 mL cylindrical Pyrex reaction vessel the diameter and height of which is equal to 7.5 cm and 3.5 cm, respectively (Figure 3.1).



Figure 3.1. Solar simulator Atlas-Suntest CPS+ and reaction vessel.

3.2.2. Experimental Procedure

Photocatalyst concentration was used as 0.25 mg/mL in all solar light initiated photocatalytic disinfection experiments. An ultrasonic water bath was used to obtain a homogenous suspension of the working solution and the photocatalyst prior to the addition of *E. coli*. Sample volumes were kept constant for all experiments as 100 mL. In order to maintain a homogenized sample, all experiments were carried out under constant continuous stirring. Samples were subjected to treatment for specified reaction periods (0, 10, 20, 30, 40 and 60 minutes). Distilled-deionized water was used for volume correction to account for loss due to evaporation (<10 % in 60 min). Following each treatment period,

10 mL of sample was collected for bacteria enumeration processes and the remaining 90 mL sample was filtered through 0.45 μm membrane filters to remove bacteria and TiO_2 specimens from the solution prior to analysis.

3.2.3. Analytical Methods

3.2.3.1. *E. coli* enumeration. After each treatment period, 10 mL composite sample was collected in 15 mL falcon tube. Extreme care was taken to sampling in order to ensure that the sample would be representing the whole reaction medium. Samples were further subjected to *E. coli* enumeration. Sampling was carried out under continuous mixing by pipetting 1 mL sample from 10 different locations of the pyrex reaction vessel. Samples were diluted with 0.85 % NaCl IsoT solution before inoculation. Appropriate sample dilutions (10^{-2} to 10^{-5}) were selected based on irradiation time of each sample. Under prolonged irradiation periods, lower dilutions and high sample volumes were preferred. In the experiments where high *E. coli* concentration is expected, samples were diluted three times and low inoculation volumes were preferred like 10 or 20 μL. In case that the expected *E. coli* concentration would be low, samples were not diluted at all or simply diluted one-fold, and high inoculation volumes were used such as 50 or 100 μL. All experiments were performed as triplicate runs.

E. coli enumeration as CFU/mL was performed by viability test and calculations were made according to following equation presented in Standard Methods (Equation 3.1) (APHA, AWWA, WPCF, 2012).

$$\text{CFU/mL} = \frac{\text{Colonies counted}}{\text{Volume plated (mL)}} \times \text{Dilution Factor} \quad (3.1)$$

Drop plate method was chosen for the *E. coli* enumeration due to its practicability and to allow inoculating sufficient number of parallel cultures (Miles and Misra, 1938; Reed and Reed, 1948). CHROMagar™ ECC was used as a culture medium to provide high color contrast as could be visualized by blue color between *E. coli* and other coliform bacteria colonies having mauve colorization. Petri dish diameter was chosen as 9 cm. An appropriate dilution and volume of sample which inoculated on the medium was chosen according to expected bacteria inactivation rate. Inoculated petri dishes were kept in the incubator at 44ºC for 24 h. Enumeration of *E. coli* colonies were carried out by visual inspection (Figure 3.3).

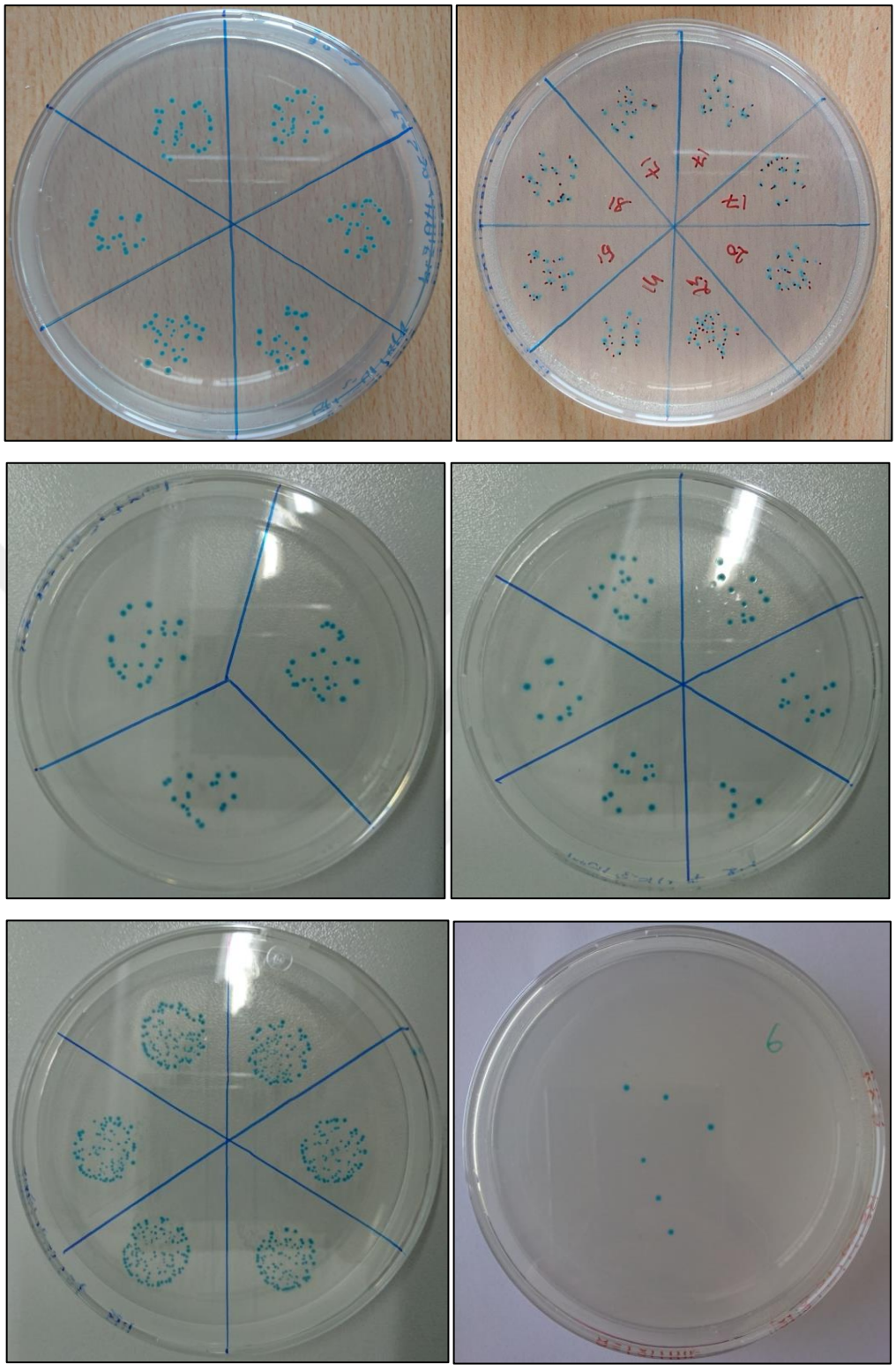

Figure 3.2. *E. coli* cultured CHROMagar^{TM} ECC plates.

Top Left: 10^{-2} dilution from initial *E. coli* solution, inoculation volume: 10 µL.

Top Right: 10^{-5} dilution from *E. coli* suspension, inoculation volume: 5 µL.

Middle Left: 10^{-3} dilution from initial *E. coli* solution, inoculation volume: 20 µL.

Middle Right: 10^{-3} dilution from t=0 *E. coli* solution, inoculation volume: 10 µL.

Bottom Left: 10^{-2} dilution from t=0 *E. coli* solution, inoculation volume: 10 µL.

Bottom Right: 10^{-2} dilution from t_{irr}=30 min *E. coli* solution, inoculation volume: 50 µL.

3.2.3.2. Total protein determination. Lowry method as developed by Lowry and colleagues was chosen as protein determination method (Lowry et al., 1951). It has been the most widely used protein estimation method in molecular biology due to its moderately constant sensitivity, applicability, and suitability for protein concentration in the range of 0.01–1.0 mg/mL.

The method consists of two distinct steps. In the first step, which is based on Biuret reaction, sample treated with the Lowry reagent that contains NaOH-Na_2CO_3-$CuSO_4$-$Na_2C_4H_4O_6$ and peptide bonds in the proteins react with copper under alkaline conditions to form a copper-protein complex. In the second step of the method, copper-protein complex is treated with the phenol reagent developed by Folin and Ciocalteu (Folin and Ciocalteu, 1927). The Folin-Ciocalteu reagent is a phosphotungustic-phosphomolybdic acid solution. The reagent is reduced by the copper-treated proteins to molybdenum blue which can be determined colorimetrically at λ=750 nm.

$$\text{Protein} + Cu^{2+} \xrightarrow{OH^-} \text{Tetradendrate } Cu^{+} \text{ complex} \xrightarrow{\text{Folin-Ciocalteu reagent}} \text{Copper – protein complex}$$

The reaction mainly depends on the tyrosine and tryptophan content of the sample. The main advantage of the method is its sensitivity, but a wide range of substances can interfere with the method, including nitrogen containing buffers, drugs, nucleic acids, glucose, uric acid, guanine, xanthine, aromatic amines, unsaturated aromatic compounds, sulphides, sulphurous acid, H_2O_2, ferrous ions, thymol, sulfosalicylic acid, picric acid (over 0.1 percent), glycine (over 0.5 percent), hydrazine (over 0.5 percent) and ammonium sulphate (over 0.15 percent) (Herbert et al., 1971; Lowry et al., 1951; Sapan et al., 1999; Waterborg, 2002).

Procedure. Samples were taken from the +4°C and brought to room temperature. Then, samples were vortexed, and 3.0 mL of sample was inserted into a 16x100 mm glass tube. Then, 4.2 mL of Lowry reagent was added into the tubes. Tubes were capped and vortexed, then incubated for 20 minutes at room temperature in dark conditions. After 20 minutes of incubation, 0.6 mL of diluted Folin-Ciocalteu Reagent was added into the tubes. Samples were vortexed and incubated for 35 minutes at room temperature in dark conditions. After incubation, molybdenum blue color formed which represented the concentration of reduced Folin-Ciocalteu Reagent measured at λ=750 nm. Bovine Serum Albumin (BSA) was used as a standard and calibration curve was plotted in the range of 0-100 mg/L (Appendix D).

The Lowry Reagent. The Lowry reagent was daily prepared by mixing Solution A, B and C with a volume ratio of 100:1:1 respectively.

Solution A (alkaline solution). 2.8598 g NaOH and 14.3084 g Na_2CO_3 were dissolved in 500 mL of distilled-deionized water.

Solution B. 0.9104 g $CuSO_4$ was dissolved in 100 mL of distilled-deionized water.

Solution C. 2.8530 g $Na_2C_4H_4O_6.2H_2O$ was dissolved in 100 mL of distilled-deionized water.

The Folin-Ciocalteu reagent, 1N. The reagent was prepared prior to use at the last five minutes of the first incubation time by mixing 5 mL of 2N Folin-Ciocalteu's phenol reagent and 5 mL of distilled-deionized water in an amber bottle.

3.2.3.3. Total carbohydrate determination. Phenol-sulfuric acid method was chosen as carbohydrate determination method. It is the most widely used colorimetric carbohydrate determination method. The method can be applied to detect all types of carbohydrates including monosaccharides, disaccharides, oligosaccharides, and polysaccharides (Dubois et al., 1956).

Colorimetric methods for detection of carbohydrates are based on mild oxidizing/reducing properties of monosaccharides. In phenol-sulfuric acid method monosaccharides act as reducing agents (Panagiotopoulos and Sempere, 2005). Addition of H_2SO_4 into phenol solutions containing carbohydrate provides enough heat under highly acidic conditions thus glycosidic bonds of the carbohydrate can completely hydrolyze and the condensation of dehydrated sugars with phenol groups generate a yellow-orange colored aromatic complex which is characteristic for the reaction (Figure 3.4) (Saha and Brewer, 1994; Panagiotopoulos and Sempere, 2005). The color produced is proportional to the amount of carbohydrate and stable for several hours. Absorbance of the solution is measured quantitatively at λ=490 nm to determine sugar concentration. This method is accurate to ±2 % under appropriate conditions (Dubois et al., 1956; An and Smith, 2005).

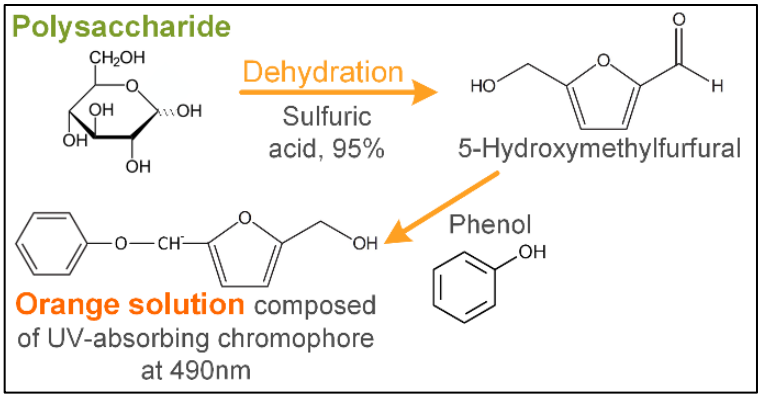

Figure 3.3. Schematic reaction of phenol-sulfuric acid method (Viel et al., 2018).

Despite the wide range of applicability of phenol-sulfuric acid method, broad range of substances can interfere with the reaction including cellulose fibres, other insoluble carbohydrates, NO_3^- and Fe^{3+} and glycoproteins (Dubois et al., 1956; Martens and Frankenberger, 1990; Rao and Pattabiraman, 1989). Moreover, investigators reported that when humic material is treated with H_2SO_4, it gives absorbance in 350-500 nm range and may interfere with the total carbohydrate determination (Sieburth and Jensen, 1969; Meadows and Campbell, 1978). Additionally, a strong acid usage may cause the production of some degradation products which can absorb the light in the same spectral band with carbohydrates, resulting in the overestimation of carbohydrate concentration (Josefsson et al. 1972; Dawson and Liebezeit, 1981). Researchers indicated that color development depends on the order of the reagent addition and sample matrix which could cause low reproducibility in environmental samples (Artem'yev, 1970; Gerchakov and Hatcher, 1972). Moreover, researchers reported that method gives various absorbance values for equal concentrations of different types of sugars, so it is more accurate when it is used for the samples that contain only one type of carbohydrate (Brummer and Cui, 2005; Josefsson et al., 1972).

Procedure. Samples were taken from +4°C and brought to room temperature. Then, samples were vortexed, and 1.0 mL of samples were inserted into 16x100 mm glass tube. Then, 1.0 mL of 5 % of phenol solution and 5 mL of concentrated H_2SO_4 were added rapidly and directly against the liquid surface to achieve good mixing. Samples were kept on stand for 10 minutes, and then they were vortexed and placed into thermoreactor for digestion at 32°C for 25 minutes. After digestion, samples were cooled down and generated yellow-orange color was measured at λ= 490 nm. Glucose was used as a standard and calibration curve was plotted in the range of 0-50 mg/L (Appendix E).

5 % Phenol solution. Phenol was supplied from Merck and 5 g was dissolved in 100 mL of distilled-deionized water.

3.2.3.4. K^+ leakage determination. K^+ leakage from bacterial cells via solar photocatalytic inactivation was determined by applying the flame photometric method outlined as 3500-K B in Standard Methods (Standard Methods for the Examination of Water and Wastewater, 2012). Perkin Elmer AAnalyst 300 Atomic Absorption Spectrometer was used. The method is based on the determination of potassium at λ=766.5 nm and reported as Total K, mg/L. Calibration range was selected as 0-2.0 mg/L and Potassium Inductively Coupled Plasma Certipur® solution (Merck) was used as a standard.

3.2.3.5. Endotoxin determination. Endotoxin detection was carried out using ENDOSAFE® Gel-Clot Limulus Amebocyte Lysate test (LAL). LAL test is based on the usage of LAL clotting protein

derived from horseshoe crab *Limulus polyphemus amebocytes* for the qualitative detection of Gram-negative bacteria endotoxins by gel-clot method (Levin and Bang, 1968). LAL technique can detect as low as 10^{-6} μg/mL of endotoxin (Reinhold and Fine, 1971; Yin et al., 1972). When in-activated endotoxins are used, the test gives negative results. In addition, LAL gives reactions not only with the lipopolysaccharide (LPS) but also free lipid A fractions of LPS (Yin et al., 1972).

Samples were treated by buffered lysate in single test-vials in a thermoreactor at 37ºC for 60 minutes. Presence of endotoxin was detected by the formation of visible clot in test tubes with respect to a selected limiting value as 0.125 (Endotoxin Units) EU/mL. It can be detected with momentary inversion of the test tube up to two minutes after the incubation period (WHO, 2012; Maji and Chatterjee, 2011).

3.2.3.6. UV-vis spectroscopic absorbance measurements. Absorbance recordings were taken in wavelength range of 200-600 nm by employing Perkin Elmer Lambda 35 UV-vis Spectrometer. Perkin Elmer quartz cuvettes with 1.0 cm path-length that were rinsed with distilled-deionized water prior to each analysis. UV-vis absorption spectra of the samples were measured in the indicated wavelength range using distilled-deionized water as a reference. The presence of color forming moieties and aromatic domains were measured by using specified absorbance measurements as wavelength of 436 nm, 365 nm, 280 nm, and 254 nm and designed as $Color_{436}$, UV_{365}, UV_{280}, and UV_{254} respectively. Specified UV-vis parameters were explained as follows:

$Color_{436}$: Absorbance at 436 nm, Color forming moieties
UV_{365} : Absorbance at 365 nm, Organic matter content
UV_{280} : Absorbance at 280 nm, Aromaticity, Organic matter content
UV_{254} : Absorbance at 254 nm, Surrogate parameter for DOC

Specific UV-vis parameters defined as $SCoA_{436}$, $SUVA_{365}$, $SUVA_{280}$ and $SUVA_{254}$ were calculated by normalization of specified UV-vis parameters to DOC (mg/L) according to following equations (Equations 3.2-3.5).

$$SCoA_{436} = Color_{436}/DOC \text{ (L/m mg)} \quad (3.2)$$
$$SUVA_{365} = UV_{365}/DOC \text{ (L/m mg)} \quad (3.3)$$
$$SUVA_{280} = UV_{280}/DOC \text{ (L/m mg)} \quad (3.4)$$
$$SUVA_{254} = UV_{254}/DOC \text{ (L/m mg)} \quad (3.5)$$

3.2.3.7. Fluorescence spectroscopic measurements. Fluorescence spectroscopic measurements in the synchronous scan mode were recorded by using Perkin Elmer LS 55 Luminescence Spectrometer. Luminescence spectrometer is equipped with a 150W Xenon arc lamp and a red sensitive photomultiplier tube. 1.0 cm path-length quartz cuvettes were rinsed with distilled-deionized water before and after each analysis to prevent the presence of any contamination.

Synchronous scan fluorescence data were obtained using a bandwidth of $\Delta\lambda$=18 nm between excitation and emission monochromators and in an emission wavelength range of λ_{emis}=200 nm to 600 nm. Depending on the system characteristics, specified fluorescence intensities detected at λ_{emis}=280 nm and λ_{emis}=470 nm were elucidated and designated as $FI_{sync280}$ and $FI_{sync470}$. Moreover, specific fluorescence intensities $SFI_{sync470}$ and $SFI_{sync280}$ were also calculated by normalization of maximum synchronous scan fluorescence intensities as $FI_{sync280}$ and $FI_{sync470}$ to DOC content of the sample (Equations 3.6 and 3.7).

$$SFI_{sync280} = FI_{sync280}/DOC \quad (3.6)$$

$$SFI_{sync470} = FI_{sync470}/DOC \quad (3.7)$$

FI values were calculated by using the ratio of the emission intensity at λ_{emis}=450 nm to that at λ_{emis}=500 nm, following the excitation at λ_{exc}=370 nm (Equation 3.8).

$$FI = \frac{\text{The emission intensity at } \lambda emis=450 \text{ nm following the excitation at } \lambda exc=370 \text{ nm}}{\text{The emission intensity at } \lambda emis=500 \text{ nm following the excitation at } \lambda exc=370 \text{ nm}} \quad (3.8)$$

EEM fluorescence profiles were obtained by simultaneous incremental changes in both excitation and emission wavelengths. A gradual increase of λ_{exc} from 200 nm to 500 nm and λ_{emis} from 200 nm to 600 nm were recorded. Three-dimensional contour plots were derived from data and modelled using MATLAB R2013a program. Fluorescence trend based selected excitation-emission regional information of EEM fluorescence contour plots were explained in detail in Section 2.4.

3.2.3.8. Non-purgeable organic carbon measurements. Non-purgeable organic carbon (NPOC) (mg Org C/L) contents of the samples were determined by Total Organic Carbon Analyzer Shimadzu TOC-VWP calibrated using potassium hydrogen phthalate with a concentration range of 0-25 mg Org C/L as the standard. NPOC mode sparging inorganic carbon contents prior to organic carbon determination was selected to determine the DOC contents. All NPOC measurements were represented with mg/L for simplicity reasons.

4. RESULTS AND DISCUSSION

In this study, four different aqueous matrix conditions referred to as follows; IsoT solution, WM solution, HA solution, and "HA and WM" solution were used, to investigate their different effects on solar photolytic and photocatalytic inactivation of *E. coli*. IsoT solution was used to obtain optimum osmotic pressure condition to bacteria in the absence of other inorganic and organic content and its results represented the baseline conditions for other matrixes. WM solution was used as a synthetic natural water representative containing common anions and cations and its composition was addressed in Table A.1. HA solution having 100 kDa molecular size fraction was used to introduce NOM in the system and observe the bacteria inactivation in the presence of organic matter. Spectroscopic characterization of 100 kDa HA was presented in Appendix B Section. "HA and WM" solution was prepared as a mixture of WM and HA solutions and used to mimic natural water conditions containing both inorganic and organic matter in the medium.

Solar photocatalytic inactivation treatments were carried out with mainly two types of photocatalyst as undoped and Fe-doped TiO_2 specimens. TiO_2 (Evonik) and $SynTiO_2$ were used as undoped photocatalyst specimens and 0.25% Fe-TiO_2, 0.50% Fe-TiO_2, 0.25% Fe-$SynTiO_2$ and 0.50% Fe-$SynTiO_2$ were used as their Fe-doped versions. Characteristic properties of all six photocatalysts were represented in Appendix C Section.

Solar photolytic and photocatalytic inactivation of *E. coli* could be successfully expressed by first order kinetic model, logarithmic reduction value (LRV) and percentage of reduction. Logarithmic reduction profile of bacteria inactivation indicated that kinetics could well be expressed by first order kinetic model. Calculations were made according to Chick's law equation (Equation 4.1) (Chick, 1908).

$$\text{Rate } (R) = -dN/dt = kN \quad \text{or} \quad \ln(N/N_o) = -kt \quad \text{or} \quad N/N_o = e^{-kt} \tag{4.1}$$

Where,

R: first order rate (CFU/mL min)

N: *E. coli* count, CFU/mL at time t

N_o: initial *E. coli* count, CFU/mL

t: irradiation time, min

k: first order reaction rate constant, min^{-1}

Half-life ($t_{1/2}$, min) was calculated by the following Equation 4.2 as; $t_{1/2}=0.693/k$ (4.2)

LRV of bacteria was calculated according to following equation (Equation 4.3).

$$LRV = \log_{10}(N_o/N_{60}) \quad (4.3)$$

Where,

N_o: initial *E. coli* count, CFU/mL as indicated above

N_{60}: *E. coli* count, CFU/mL at irradiation time of 60 min

LRV could also be expressed as percentage reduction and the respective conversions were given in Table 4.1. (EPA, 1991).

Table 4.1. Bacteria LRV in terms of percentage reduction.

LRV	Reduction, %
0.5	68
1	90
1.5	96.8
2	99
2.5	99.7
3	99.9
4	99.99

As could be visualized in Table 4.1, LRV of 4 indicates 99.99 % bacteria reduction and it could go further as LRV of 5 and 6 expressing reductions as 99.999 and 99.9999 %.

4.1. Solar Photolytic Inactivation of *E. coli*

4.1.1. Solar Photolytic *E. coli* Inactivation Under Specified Reaction Conditions, Reductions and Kinetics

E. coli suspension in IsoT solution (N_o=5.46E+05 CFU/mL) was subjected to solar photolytic treatment. Upon irradiation period of 30 min, *E. coli* count decreased to 5.25E+02 CFU/mL and following further exposure of t_{irr}=60 min, *E. coli* count was reduced almost by half to 2.65E+01 CFU/mL. Under these conditions LRV of *E. coli* was 4.31 and reduction percentage was 99.99 %. In case when *E. coli* suspension in WM solution (N_o=4.61E+05 CFU/mL) was treated for an irradiation period of 30 min, bacteria count reduced to 2.67E+02 CFU/mL. Following light exposure of t_{irr}=60

min, *E. coli* count decreased to 2.30E+01 CFU/mL revealing LRV as 4.30 and reduction as 99.99 %. *E. coli* (N_o=1.09E+06 CFU/mL) suspension was directly prepared in HA solution and exposed to irradiation for a period of 30 min revealing an *E. coli* count of 5.37E+03 CFU/mL. Upon light exposure for a duration of t_{irr}=60 min, *E. coli* cell count further decreased to 2.50E+02 CFU/mL revealing LRV as 3.64 and reduction as 99.9 %. *E. coli* suspension with an initial count of N_o=7.09E+05 CFU/mL was prepared in a solution composed of "HA and WM" components resembling natural waters was further subjected to irradiation for 30 min. Under these conditions, *E. coli* count decreased to 2.98E+04 CFU/mL. Upon light exposure of t_{irr}=60 min, *E. coli* count slightly decreased to 2.63E+03 CFU/mL revealing LRV as 2.43 and reduction as 99 %.

Based on these results, the effect of solution matrix for *E. coli* reduction could be displayed in terms of LRV of *E. coli* in an increasing order as: "HA and WM" < HA < WM < IsoT. Irradiation time dependent *E. coli* inactivation profiles in the presence of different solution matrixes were presented in a comparative manner (Figure 4.1). First order kinetic model parameters of solar photolytic treatment of *E. coli* were also presented in Table 4.2.

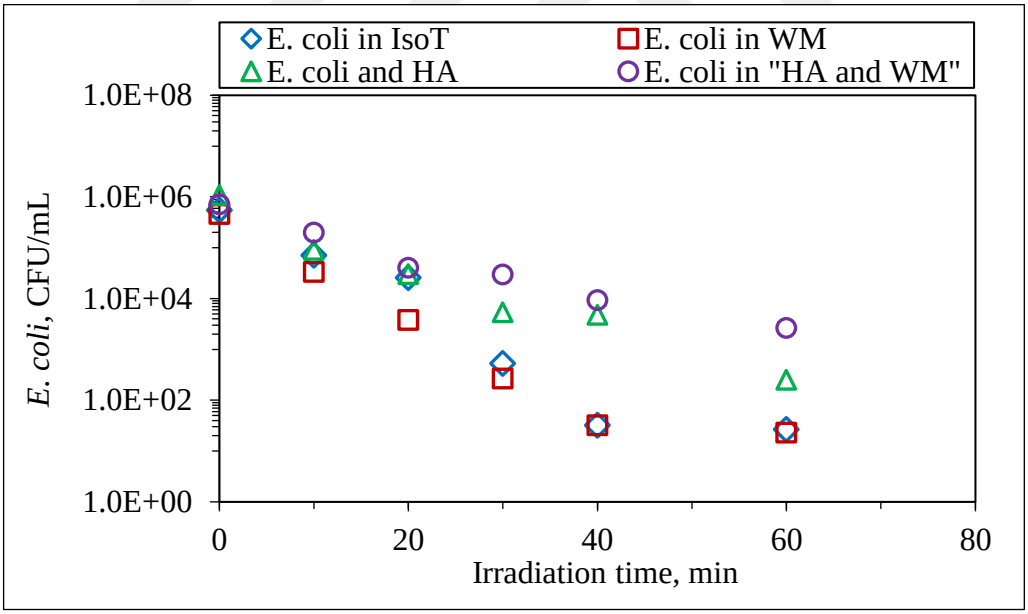

Figure 4.1. Irradiation time dependent *E. coli* inactivation upon solar photolytic treatment in different solution matrixes.

Solar photolytic treatment of *E. coli* in IsoT solution resulted in a rather fast reduction with k=0.184 min^{-1} and half-life as 3.76 min. On the other hand, in the presence of both "HA and WM", reaction rate decreased significantly revealing k=0.0920 min^{-1} and half-life as 7.53 min. The effect of reaction medium could be expressed in terms of inactivation rate constant (k, min^{-1}) in a decreasing order of IsoT > WM > HA > "HA and WM". With respect to the minor differences in initial bacteria

counts, inactivation rates (CFU/mL min) followed a decreasing trend as; 1.42E+05 > 1.00E+05 > 8.02E+04 > 6.52E+04 for HA, IsoT, WM, and "HA and WM", respectively.

Table 4.2. Solar photolytic treatment of *E. coli*: Inactivation parameters.

Matrix	First order kinetic model			LRV	Reduction, %
	k, min^{-1}	$t_{1/2}$, min	R, CFU/mL min		
E. coli in IsoT	0.184	3.76	1.00E+05	4.31	99.99
E. coli in WM	0.174	3.98	8.02E+04	4.30	99.99
E. coli and HA	0.130	5.33	1.42E+05	3.64	99.9
E. coli in "HA and WM"	0.0920	7.53	6.52E+04	2.43	99

Saline solution (0.85 % NaCl) is an isotonic solution with pH=7.36 which provides a stable osmotic pressure on cell membrane of the bacteria and prevents the osmotic lysis of the cell (Tortora et al., 2018). Isotonic solution was chosen as the base experimental medium instead of phosphate buffer solution to prevent the inhibitory effect of phosphate species to the reaction medium upon photocatalysis (Long et al., 2017; Lyon et al., 2005). Even though the presence of this optimal osmotic conditions were assessed, cell counts of *E. coli* in IsoT solution showed high inactivation efficiency than expected. Sichel and colleagues reported that 0.7 log bacteria inactivation was achieved after t_{irr}=90 min of solar photolytic treatment (Sichel et al., 2007). Likewise, Birben and co-workers showed that almost 1 log *E. coli* reduction was attained at t_{irr}=60 min of solar photolytic treatment (Birben et al., 2017a). In this study, *E. coli* in IsoT solution showed 4 log bacteria reduction with the fastest reduction rate among other mediums, this high LRV could be explained with the combined effect of mechanistic stress of stirring and increased internal ROS formation due to light and mechanistic stress factors.

E. coli in WM solution showed almost similar percent reduction with *E. coli* in IsoT suspension. High bacteria reduction could be explained with the presence of common anions and cations as Cl^-, NO_3^-, SO_4^{2-}, PO_4^{3-}, HCO_3^-/CO_3^{2-}, Na^+, K^+, Ca^{2+}, and Mg^{2+} in WM. Nitrate ions are reactive in natural waters, once they are irradiated at λ=320 nm $HO^\bullet$ forms in water (Equations 2.22-2.30). Other anions and cations could react with $HO^\bullet$ and form radical species that may enhance the inactivation rate of bacteria. The effect of individual anions and cations in the photolytic inactivation conditions was reported that only in the presence of HCO_3^- an enhanced inactivation rate of bacteria was achived with ~7 log inactivation at t_{irr}=90 min. It was higher than the inactivation attained in the absence of any anion reaching 7 log bacteria reduction in ~135 min (Rincón and Pulgarin, 2004).

In the presence of HA solution, *E. coli* reduction was 99.9 % after t_{irr}=60 min. This value was lower than IsoT and WM media results (99.99 % for *E. coli* in IsoT solution and WM solution

conditions). Although HA acts like an exogenous photosensitizer (Cooper et al., 1988a), no significant effect was observed for bacteria inactivation. Presence of HA could cause lower bacteria inactivation rates in two ways; high NPOC content of HA solution as 4.78 mg/L and reduced light transmittance to bacteria due to HA. Similar findings were also reported in previous studies (Birben et al., 2017a, 2021b; Cantwell et al., 2008; Maraccini et al., 2016; Uyguner-Demirel et al., 2020).

The addition of WM into HA medium caused a slight retardation effect on bacteria reduction values. At the pH condition of the experimental solution as pH=6, surface charges of both *E. coli* and HA are negative. The cations present in the WM solution could be adsorbed on the surfaces of bacteria and organic matter which can decrease the available surface area giving reaction with ROS formed by anions in the WM. Moreover, photosensitization ability of HA could possibly be reduced by the adsorbed cations onto its surface. The observed retardation effect of reaction medium was also presented by Uyguner-Demirel and colleagues (Birben et al., 2021b; Uyguner-Demirel et al., 2020).

4.1.2. Organic Matter Formation and Removal Upon Solar Photolytic Treatment of *E. coli* in IsoT Solution

UV-vis absorption spectra of emerged organic matter in IsoT matrix in comparison to sole IsoT solution were presented in Figure 4.2. A consistent decreasing trend of UV-vis spectral features was observed under all irradiation periods. Moreover, UV-vis spectra of sole 0.85 % IsoT solution also expressed similar characteristics with the findings of Tong and colleagues (Tong et al., 2020).

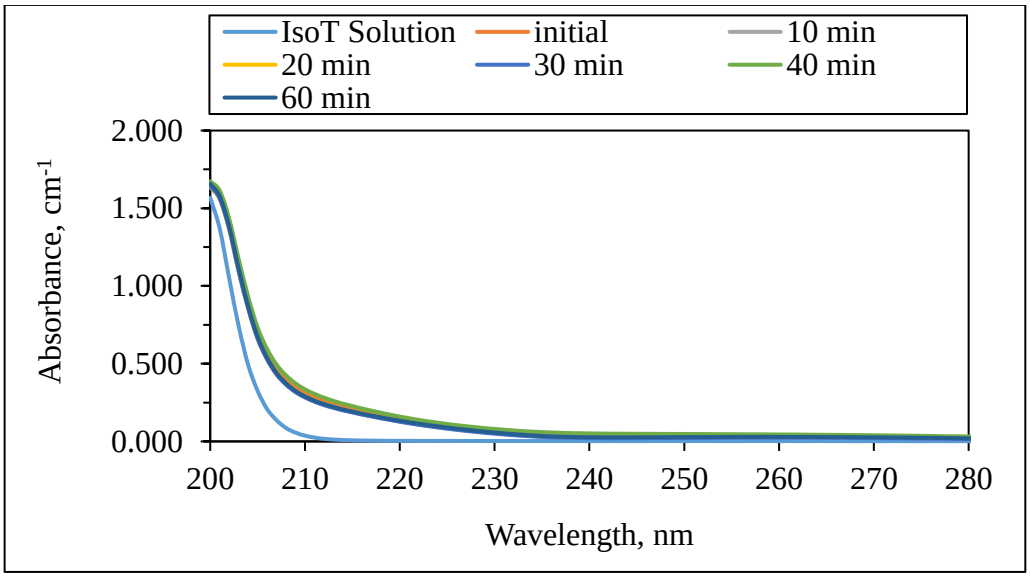

Figure 4.2. UV-vis absorption spectra of organic matter: Irradiation time dependent *E. coli* inactivation in IsoT solution upon solar photolytic treatment.

After addition of *E. coli* into IsoT solution, increased absorbances were recorded between λ=200 nm and 240 nm could be related to presence of organic moieties originating from EPS of bacteria. On the other hand, irradiation time dependent absorbance changes were significantly similar to each other in UV wavelength range of λ=200-240 nm excluding the presence of dense aromatic domains and color forming moieties ($Color_{436}$, UV_{365} and UV_{280}) that should be evident in longer wavelengths.

Synchronous scan fluorescence spectra of emerged organic matter displayed an intense peak at λ_{emis}=280 nm which indicates the presence of proteins, especially tryptophan contents (Reynolds, 2003) in the sample (Figure 4.3). A significant increase of the fluorescence intensities (FI_{sync}) was recorded upon irradiation period of 40 min expressing the formation of fluorophores by cell damage and a decreasing trend was detected at the end of 60 min irradiation period. Accordingly, under initial conditions, $FI_{sync280}$ was 25.1 following an increasing trend up to 20 min, then a sharp decrease followed by a sharp increase to 52.7 upon irradiation period of 40 min at which both UV_{280} and UV_{254} expressed the highest values as 0.0318 and 0.0464, respectively. These results would indicate the release of organics mainly composed of UV-absorbing centers also exhibiting fluorophores. Furthermore, $FI_{sync470}$ displayed quite low presence changing in the range of 0.472-5.79.

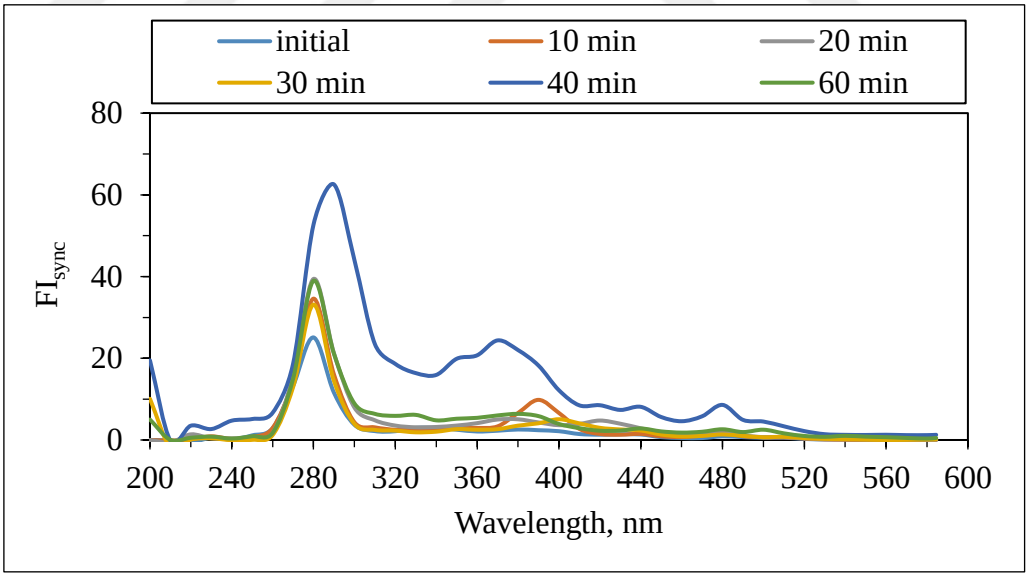

Figure 4.3. Synchronous scan fluorescence spectra of organic matter: Irradiation time dependent *E. coli* inactivation in IsoT solution upon solar photolytic treatment.

Due to the non-existence and possibly subsequent degradation of color forming moieties of the released organic matrix upon irradiation and the usage of IsoT solution, which was also a colorless solution, $Color_{436}$ and UV_{365} values attained upon 30 min irradiation time were very low ≤ 0.0001 that could be regarded as insignificant (Figure 4.4). Under initial conditions, UV_{280} and UV_{254} were

recorded as 0.0238 and 0.0332 respectively. Upon treatment, UV_{280} variations expressed irradiation time dependent inconsistent trend in the range of 0.0149 to 0.0318. The highest UV_{280} was observed upon irradiation period of 40 min at which 62.6 % was removed at the end of t_{irr}=60 min. On the other hand, following a similar trend to UV_{280}, UV_{254} displayed variations 0.0232 to 0.0464. The highest UV-vis parameters were recorded upon irradiation period of 40 min.

From a general view, NPOC expressed variations in the range of 2.35-9.26 mg/L (Figure 4.4). The highest NPOC release was attained upon irradiation period of 30 min. NPOC content increased between initial (2.35 mg/L) and t_{irr}=30 min (9.26 mg/L) due to the release of organics from damaged and/or destructed *E. coli* cells, followed by a sharp decrease at t_{irr}=40 min (3.66 mg/L) and again followed by a decreasing trend during solar photocatalytic treatment.

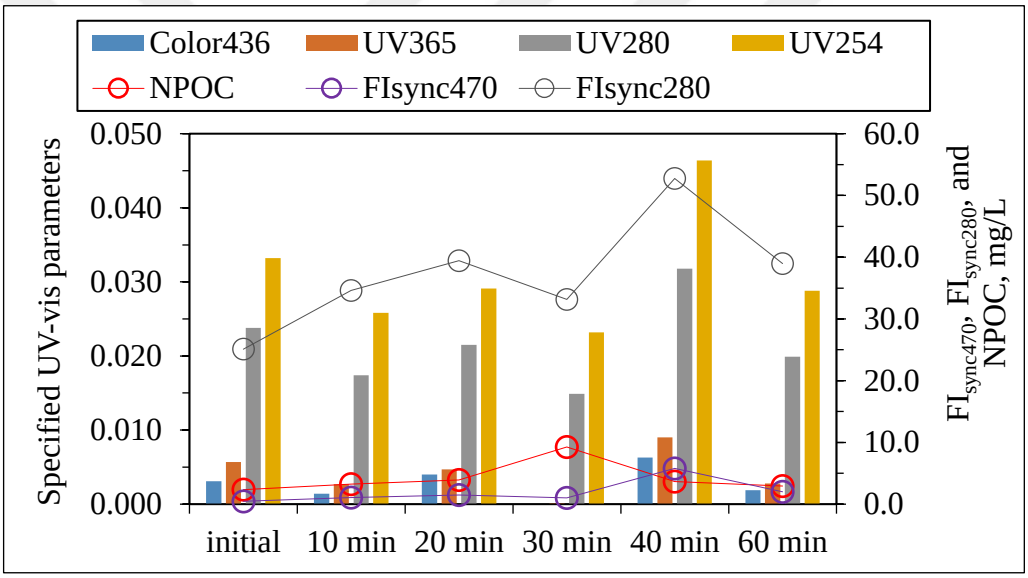

Figure 4.4. Specified UV-vis and fluroscence parameters of organic matter: Irradiation time dependent *E. coli* inactivation in IsoT solution upon solar photolytic treatment.

Based on NPOC contents, $SCoA_{436}$, $SUVA_{365}$, $SUVA_{280}$, $SUVA_{254}$, $SFI_{sync470}$, and $SFI_{sync280}$ parameters were calculated and presented in Figure 4.5. As the most significant parameter, $SUVA_{254}$ displayed variations in the range of 0.251-1.41 L/m mg during photolytic treatment expressing differences in both UV_{254} and NPOC removals. $SUVA_{280}$ was recognized as the second significant specific UV-vis parameter varied in between 0.161 L/m mg and 1.01 L/m mg being the lowest for t_{irr}=30 min and the highest for initial solution. Accordingly, $SCoA_{436}$ expressed changes in between $\leq$ 0.0001 L/m mg and 0.172 L/m mg. Due to almost non-existence of $Color_{436}$ at t_{irr}=30 min, $SCoA_{436}$ could not be calculated. Contrary to very low $SFI_{sync470}$ in the range of 0.108-1.58, predominant $SFI_{sync280}$ expressed variations in the range of 3.58-14.4.

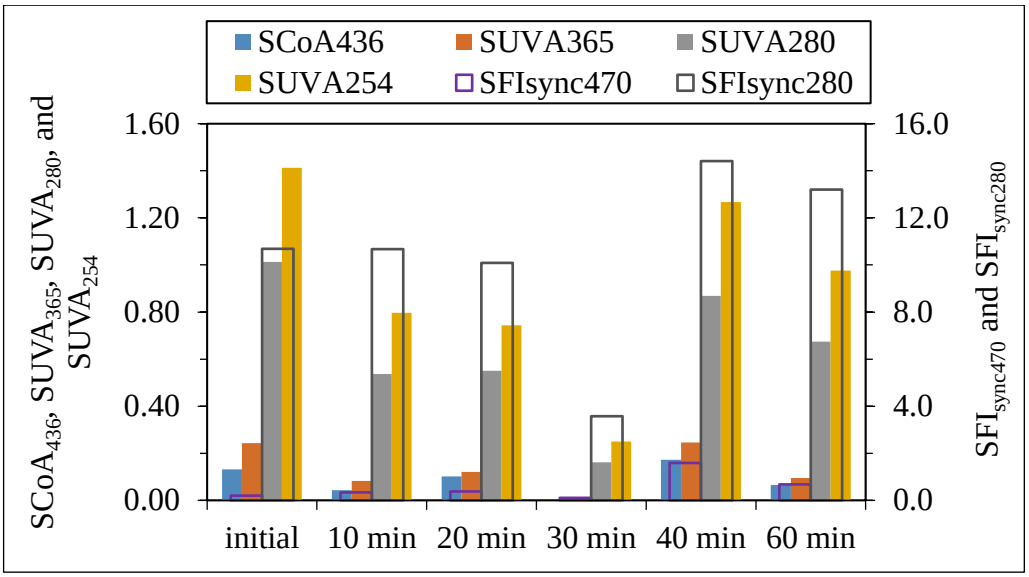

Figure 4.5. Specific UV-vis and fluroscence parameters of organic matter: Irradiation time dependent *E. coli* inactivation in IsoT upon solar photolytic treatment.

Characteristic properties of organic matter under initial condition and upon solar photolytic inactivation of *E. coli* in IsoT solution exposed to irradiation for 60 min were presented in Table 4.3.

Table 4.3. Characteristic properties of organic matter present in solar photolytic treatment of *E. coli* in IsoT solution.

Irradiation time, min	UV-vis Spectroscopic Parameters, cm^{-1}				NPOC, mg/L	$SUVA_{254}$, L/m mg	$FI_{sync280}$	$SFI_{sync280}$	FI
	$Color_{436}$	UV_{365}	UV_{280}	UV_{254}					
Initial	0.0031	0.0057	0.0238	0.0332	2.35	1.41	25.1	10.7	1.44
60 min	0.0019	0.0028	0.0199	0.0288	2.95	0.976	39.0	13.2	2.09

Upon irradiation period of 60 min at which 4.31 log reduction of *E. coli* in IsoT solution was attained (Table 4.2), released organic matter expressed the following UV-vis parameters (cm^{-1}); $Color_{436}$: 0.0019, UV_{365}: 0.0028, UV_{280}: 0.0199, UV_{254}: 0.0288, and NPOC as 2.95 mg/L. Edzwald and colleagues reported that $SUVA_{254} < 3$ indicated the presence of hydrophilic and aliphatic content of the sample (Edzwald et al., 1985). Initial and t_{irr}=60 min $SUVA_{254}$ values were calculated as 1.41 L/m mg and 0.976 L/m mg, respectively, representing that initial and remaining organic matter after t_{irr}=60 min could be considered having hydrophilic and aliphatic character.

$FI_{sync280}$ increased at t_{irr}=60 min due to the released protein content of *E. coli*. $SFI_{sync280}$ displayed slight increase at t_{irr}=60 min in accordance with the increased NPOC due to the released organic material from bacteria. Moreover, $FI_{sync470}$, which represents synchronous fluorescence intensity at λ_{emis}=470 nm and indicates the presence of humic-like fluorophores (Uyguner and Bekbolet, 2005),

were detected under initial and t_{irr}=60 min conditions as 0.472 and 2.02, respectively. Since the treatment was conducted in the absence of any humic material, $FI_{sync470}$ did not show any detectable peak as expected. A slight increase of $FI_{sync470}$ could be due to the released organics from damaged *E. coli* cells expressing complex aromatic structure. Accordingly, $SFI_{sync470}$ of initial and t_{irr}=60 min conditions were calculated as 0.201 and 0.683, respectively. Slightly increased $FI_{sync470}$ and NPOC contents caused an increase in $SFI_{sync470}$ at the end of 60 min irradiation period. From a general perspective, as FI ≥ 1.9 represents the presence of microbially derived organic material, after t_{irr}=60 min, FI was calculated as 2.09 which complies with the previous findings of the researchers (Sen-Kavurmaci and Bekbolet, 2014). Bearing in mind the presence of extracellular organics, the results also implied that upon solar simulated irradiation conditions cell destruction could also be attained over an irradiation period of 60 min at which 99.99 % reduction was attained.

In accordance with the UV-vis absorbance and synchronous scan fluorescence spectroscopic analyses, EEM fluorescence contour plots of organic matter during irradiation time dependent *E. coli* inactivation in IsoT solution under solar photolytic treatment conditions were also followed and illustrated in Figure 4.6. It should be indicated that both emergence and removal mechanisms were prevailing under the specified conditions.

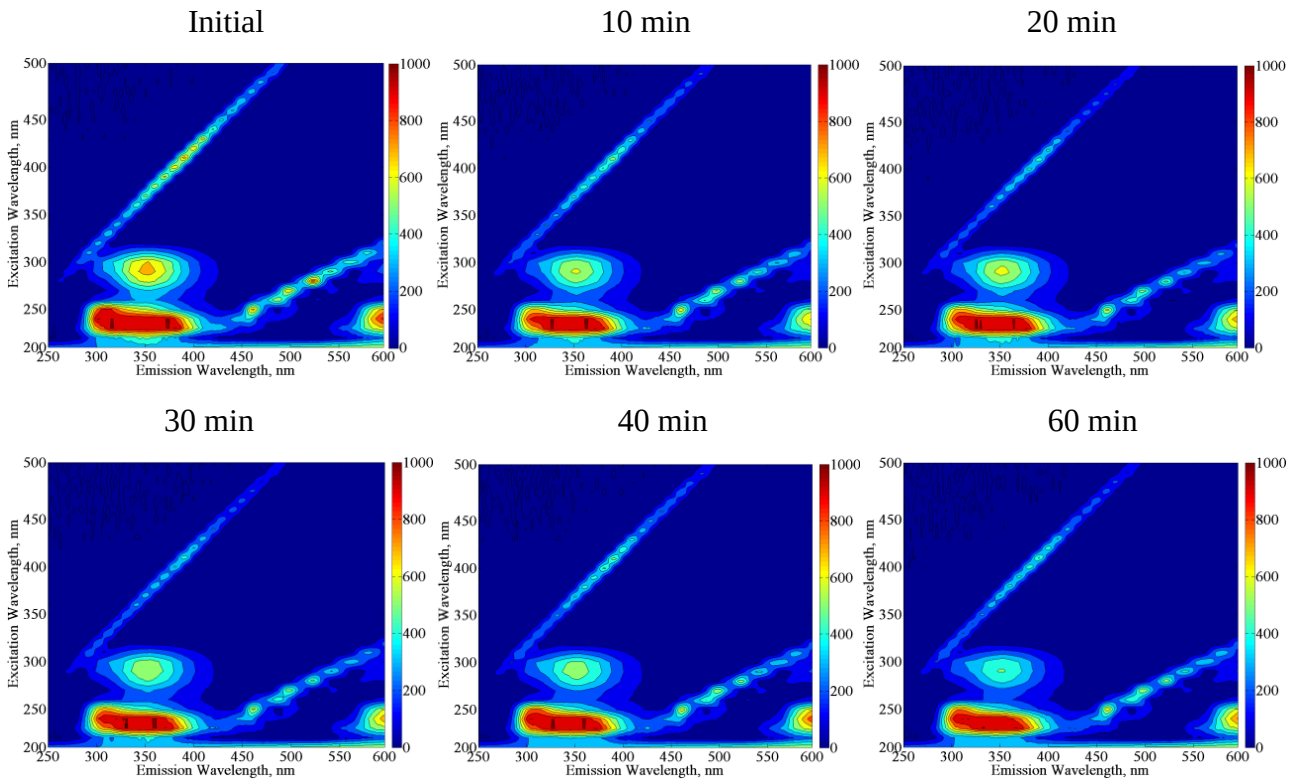

Figure 4.6. EEM fluorescence contour plots of organic matter: Irradiation time dependent *E. coli* inactivation in IsoT solution upon solar photolytic treatment.

EEM fluorescence contour plots displayed the presence of Regions I (λ_{exc} 220-250 nm and λ_{emis} 280-332 nm), II (λ_{exc} 220-250 nm and λ_{emis} 332-380 nm), and IV (λ_{exc} 250-470 nm and λ_{emis} 280-380 nm) expressing that the fluorophores were mainly originated from aromatic proteins and microbial by-products under all irradiation conditions. Throughout the irradiation periods, released microbial by-products and proteins from damaged and destructed *E. coli* cells showed a decreasing trend in accordance with the solar photolytic degradation of released organic matter along with reduction of *E. coli* cells. The observed release of microbial by-products and proteins as a result of photolytic treatment of *E. coli* in IsoT solution was expected in accordance with previous studies of Birben and colleagues (Birben et al., 2017a, 2021b; Uyguner-Demirel et al., 2020). However, removal of these chromophoric groups and fluorophores could not be observed under the specified irradiation conditions most probably due to the inefficiency of the energy provided by simulated solar radiation and resistivity of these groups to degradation.

4.1.3. Mechanistic Evaluation of *E. coli* Inactivation Upon Solar Photolytic Treatment in IsoT Solution

Upon solar irradiation total K, protein, and carbohydrate contents present under initial and t_{irr}=60 min conditions as inactivation products of solar photolytic treatment of *E. coli* in IsoT solution were illustrated in Table 4.4.

Table 4.4. Total K, protein, and carbohydrate contents of time dependent *E. coli* inactivation in IsoT solution upon solar photolytic treatment.

Solar photolytic treatment	*E. coli* in IsoT solution	
	Initial	60 min
Total K, mg/L	0.72	0.85
Protein, mg/L	4.84	6.64
Carbohydrate, mg/L	1.23	11.6

Total K content of sole IsoT solution was detected as 0.042 mg/L however initial solution displayed higher total K which measured as 0.72 mg/L. High total K content of initial solution could be due to the membrane filtration applied prior to total K measurement. In membrane filtration step, reverse osmosis exerts to overcome osmotic pressure. Applied pressure is greater than osmotic pressure of solution to provide effective filtration. When bacteria exposed to increased external osmotic pressure, cell goes to dehydration and release solutes, namely osmolytes, including inorganic ions, mainly K^+ ion, and organic molecules (Wood, 2015). Application of membrane filtration

generating increased osmotic pressure on *E. coli* cell wall could be the cause of K^+ ion release and detected as total K content in initial solution. Therefore, initial total K content (0.72 mg/L) could be regarded as a background concentration for starting solutions following application of membrane filtration, irrespective of the minor differences between initial bacteria counts. After t_{irr}=60 min, total K content showed a slight increase. In regular conditions, K^+ ion transportation in bacteria occurs via K^+ ion channels and transporter proteins present in cytoplasmic membrane as passive transport mechanisms or Na^+-K^+ pumps by active transport; however, after solar photolytic inactivation process, damaged *E. coli* cell wall increases its permeability resulting in enhanced K^+ ion release from the cell (Beagle and Lockless, 2020; Tortora et al., 2018).

Initial protein concentration of *E. coli* in IsoT solution prior to solar photolytic treatment was detected as 4.84 mg/L. Besides the inner protein content of bacteria, other protein containing structures are present on outer membrane of the cell wall as porin proteins, on cytoplasmic membrane as transporter proteins, and outside of the cell wall as flagella, fimbriae, and pili. Fimbriae and pili have different structures and functions than flagella. Fimbriae are shorter, thinner, and straighter than flagella and provide surface adhesion ability to bacteria, also it could be found over the entire surface. Pili are longer than fimbriae and each bacterium contains only one or two pili used in the DNA transfer from one bacterium to another. While flagella contain flagellar proteins like flagellin; fimbriae and pili consist of pilin protein. Moreover, degradative enzymes and transporter proteins are founding in periplasmic space defined as the region between outer membrane and cytoplasmic membrane (Tortora et al., 2018). It could be indicated that, the initial protein content of *E. coli* in IsoT solution could be due to the presence of these protein containing structures present on and outside of the bacterial plasma membrane and cell wall. Furthermore, protein content was also evidenced by EEM fluorescence contour plot under initial conditions prior to irradiation (Figure 4.6). At the end of 60 min irradiation period, protein content showed an increase (4.84-6.64 mg/L) due to release of proteins from damaged *E. coli* cells. Increased protein concentration in solution at t_{irr}=60 min could also be verified by increased $FI_{sync280}$ (Table 4.3).

Initial carbohydrate concentration was detected as 1.23 mg/L. It could be indicated that, the presence of glycocalyx or EPS highly composed of polysaccharides which synthesized inside the bacteria cell and secreted to the external part of the cell wall could be the cause of detected initial carbohydrate concentration. Due to released carbohydrate content from damaged bacteria, and carbohydrate containing cell structures, an increase was observed in carbohydrate concentration via bacteria inactivation upon irradiation period of 60 min as 11.6 mg/L. Increased NPOC contents significantly supported increased protein and carbohydrate contents at t_{irr}=60 min (Table 4.3).

4.1.4. Organic Matter Formation and Removal Upon Solar Photolytic Treatment of *E. coli* in WM Solution

UV-vis absorption spectra of organic matter in WM solution were displayed in Figure 4.7. Sole WM solution displayed a lower trend from initial and solar photolytic treatment samples. Different from IsoT solution conditions, the use of WM solution resulted in different absorbance characteristics wavelength at $\lambda < 250$ nm. Especially between λ=200 nm and 210 nm, a shoulder effect was detected for all solutions originating from the strong absorption spectrum of NO_3^- having its λ_{max} at approximately 200 nm (Krishnan and Guha, 1934; Edwards at el., 2001). Increased absorbances were recorded between λ=200 nm and 240 nm following the addition of *E. coli* into WM solution, which could be revealing the presence of organic moieties originating from bacteria. On the other hand, irradiation time dependent absorbance changes were significantly similar to each other in UV wavelength range of λ=200-260 nm in the predominant absence of aromatic domains and color forming moieties ($Color_{436}$, UV_{365} and UV_{280}) that should be evident in longer wavelengths. UV-vis absorption spectra of organic matter in WM solution displayed a declining trend without any absorption peaks complying UV-vis absorption spectra of humic substance which was represented in Section 2.4. (Figure 2.16a). A slightly increasing trend in between λ=240 nm and 280 nm could be distinguished under all irradiation period conditions, which could be due to released organic aromatic groups from bacteria. The existence of amino acids having aromatic moieties originating from the presence of EPS or inner content of lysed *E. coli* cells could be the cause of detected absorbance variations in the indicated region (Birben et al., 2021a).

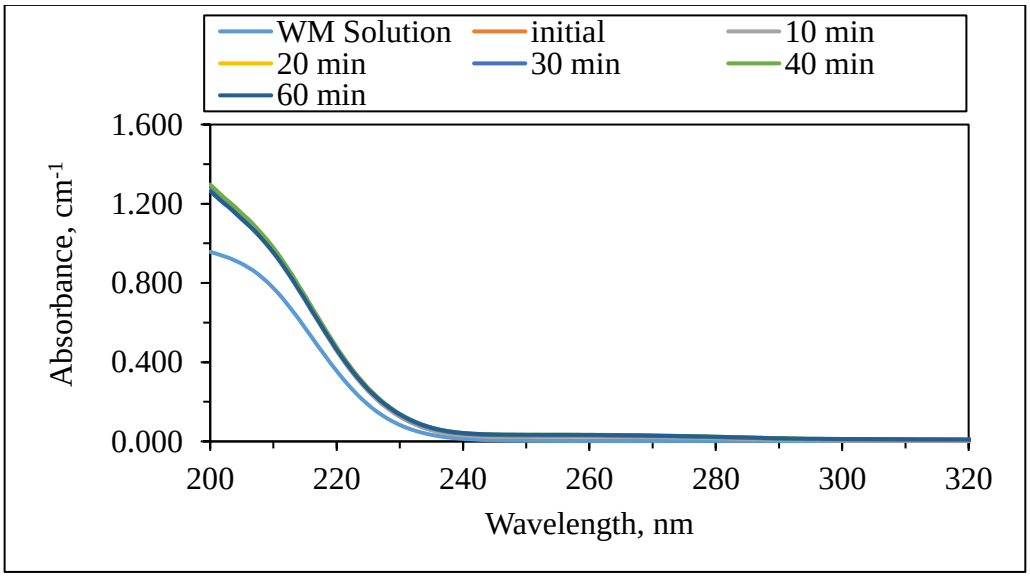

Figure 4.7. UV-vis absorption spectra of organic matter: Irradiation time dependent *E. coli* inactivation in WM solution upon solar photolytic treatment.

Synchronous scan fluorescence spectra of emerged organic matter displayed intense peaks at λ_{emis}=280 nm and λ_{emis}=420 nm (Figure 4.8). A significant increase of FI_{sync} was recorded upon t_{irr}=40 min expressing the formation of fluorophores by cell damage and a decreasing trend was detected at 60 min of irradiation period. Similar emergence and removal of fluorescence intensities between irradiation period of 40 min and 60 min was also recorded for solar photolytic treatment of *E. coli* in IsoT solution (Figure 4.3). Maximum fluorescence intensity after λ_{emis}=300 nm indicates the presence of aromatic hydrocarbons (Dujmov and Sučević, 1990). An intense peak formed at λ_{emis}=420 nm could be originating from released organic content from bacteria. The intensities at λ_{emis}=420 nm displayed variations but decreased at t_{irr}=60 min showing the degradation of aromatic content in the sample. In the absence of HA, $FI_{sync470}$ displayed quite low changes in the range of 0.805-2.46 however predominant $FI_{sync280}$ expressed variations in the range of 10.8-37.9.

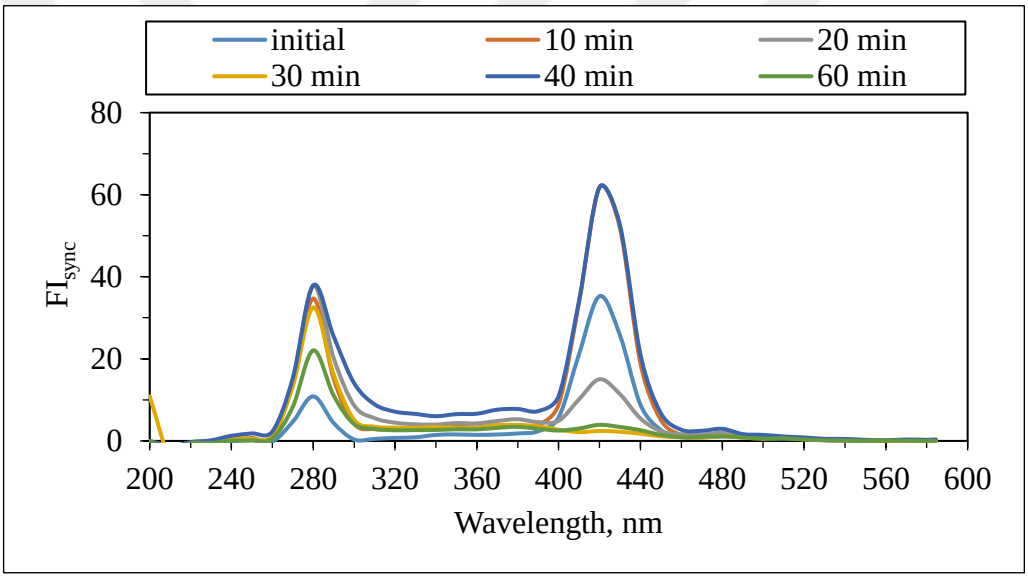

Figure 4.8. Synchronous scan fluorescence spectra of organic matter: Irradiation time dependent *E. coli* inactivation in WM solution upon solar photolytic treatment.

From a general perspective, NPOC expressed variations in the range of 7.82-15.8 mg/L (Figure 4.9). NPOC content displayed a fluctuating trend approximately as 2 mg/L until t_{irr}=20 min (9.29-9.81 mg/L) and increased significantly at t_{irr}=40 min (15.8 mg/L) due to the release of organics from damaged and destructed *E. coli* cells, followed by a sharp decrease after t_{irr}=40 min of solar photolytic treatment (7.82 mg/L). All UV-vis parameters displayed quite low presence however in the absence and subsequent degradation of color forming moieties of the released organic matter, $Color_{436}$ and UV_{365} expressed lower values than UV_{280} and UV_{254}. Highest UV_{280} and UV_{254} were recorded at t_{irr}=40 min as 0.0240 and 0.0338, respectively as could also be considered as similar to t_{irr}=60 min (0.0232 for UV_{280}; 0.0332 for UV_{254}).

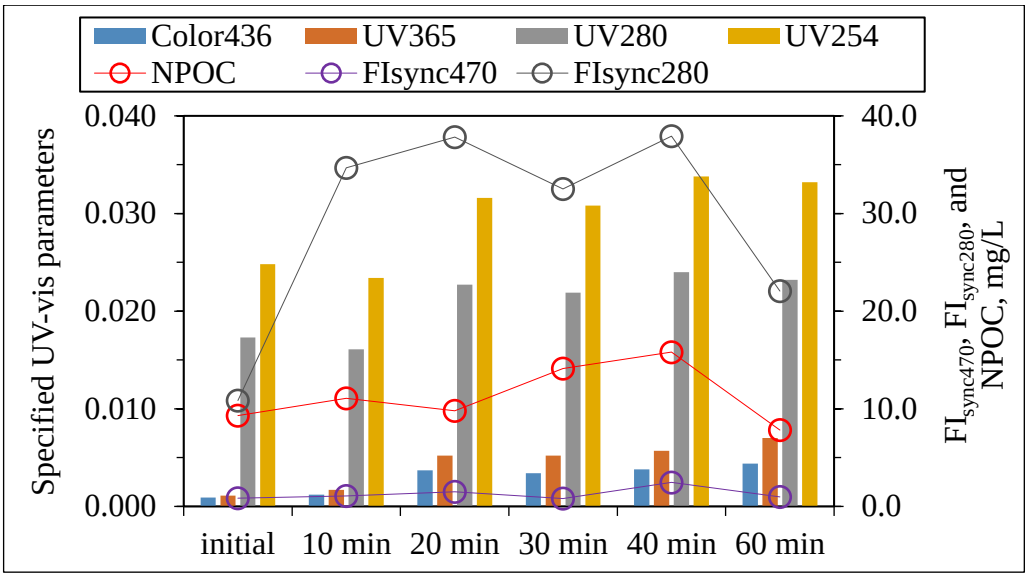

Figure 4.9. Specified UV-vis and fluroscence parameters of organic matter: Irradiation time dependent *E. coli* inactivation in WM solution upon solar photolytic treatment.

Based on NPOC contents, $SCoA_{436}$, $SUVA_{365}$, $SUVA_{280}$, $SUVA_{254}$, $SFI_{sync470}$, and $SFI_{sync280}$ parameters were calculated and presented in Figure 4.10. $SUVA_{254}$ displayed variations in between 0.211-0.425 L/m mg during photolysis expressing differences in both UV_{254} and NPOC removals. The highest $SUVA_{254}$ was calculated for irradiation period of 60 min. As the second significant parameter, $SUVA_{280}$ varied in between 0.145 and 0.297 L/m mg, being the lowest for t_{irr}=10 min and the highest for t_{irr}=60 min conditions. Furthermore, $SFI_{sync470}$ and $SFI_{sync280}$ expressed variations in the range of 0.057-0.156 and 1.17-3.86, respectively. The predominant fluorophoric group was accepted as $SFI_{sync280}$.

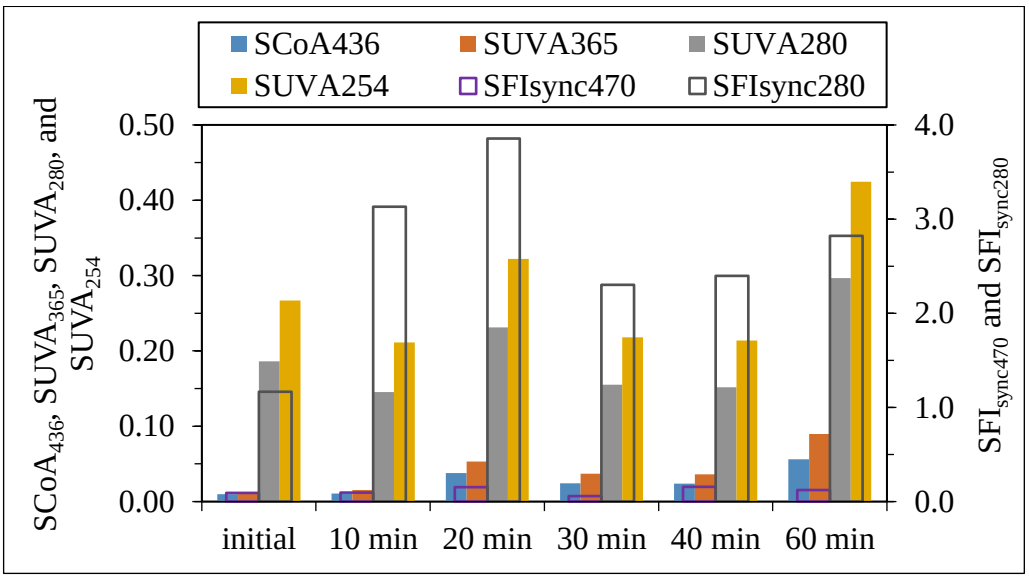

Figure 4.10. Specific UV-vis and fluroscence parameters of organic matter: Irradiation time dependent *E. coli* inactivation in WM solution upon solar photolytic treatment.

Characteristic properties of organic matter under initial condition and upon solar photolytic inactivation of *E. coli* in WM solution exposed to irradiation for 60 min were presented in Table 4.5.

Table 4.5. Characteristic properties of organic matter present in solar photolytic treatment of *E. coli* in WM solution.

Irradiation time, min	UV-vis Spectroscopic Parameters, cm^{-1}				NPOC, mg/L	$SUVA_{254}$, L/m mg	$FI_{sync280}$	$SFI_{sync280}$	FI
	$Color_{436}$	UV_{365}	UV_{280}	UV_{254}					
Initial	0.0009	0.0011	0.0173	0.0248	9.29	0.267	10.9	1.17	1.36
60 min	0.0044	0.0070	0.0232	0.0332	7.82	0.425	22.1	2.82	1.54

Upon irradiation period of 60 min at which 4.30 log reduction of *E. coli* in WM solution was attained (Table 4.2), released organic matter expressed the following UV-vis parameters (cm^{-1}); $Color_{436}$: 0.0044, UV_{365}: 0.0070, UV_{280}: 0.0232, UV_{254}: 0.0332, and NPOC as 7.82 mg/L.

In the absence of HA containing solution matrix, initial and irradiation period of 60 min $SUVA_{254}$ values were calculated as 0.257 L/m mg and 0.425 L/m mg, respectively. Besides the increase of $SUVA_{254}$ at the end of 60 min irradiation period, remaining organic matter could be considered having hydrophilic and aliphatic character (Edzwald et al., 1985).

$FI_{sync280}$ also increased due to released protein content from *E. coli* cells. Relative to increased $FI_{sync280}$ and decreased NPOC content at t_{irr}=60 min, $SFI_{sync280}$ displayed an increase at 60 min of irradiation period. Detected $FI_{sync470}$ were low in the absence of HA as 0.843 and 0.960 for initial and t_{irr}=60 min, respectively. This solar photolytic treatment was conducted in the absence of any humic material, therefore; $FI_{sync470}$ did not exhibit any detectable peak. However, at λ_{emis}=420 nm FI_{sync} data displayed intense peaks for initial, t_{irr}=10 min, 20 min, and 40 min solutions due to released organic content from damaged bacteria cells. Moreover, $SFI_{sync470}$ of initial and t_{irr}=60 min conditions were calculated almost insignificant as 0.0908 and 0.123, respectively. Besides slightly increased $SFI_{sync470}$, it displayed a decrease after t_{irr}=40 min (Figure 4.10) which means that released organic material from bacteria was degraded the end of the irradiation period of 60 min.

FI ≤ 1.4 represents the presence of humic fluorophores originating from the presence of humic matter and FI ≥ 1.9 indicates the existence of microbially derived organic material (Sen-Kavurmaci and Bekbolet, 2014). Although this solar photolytic treatment set was carried out in the absence of HA solution, FI was calculated as 1.54 after irradiation period of 60 min. It could be attributed that after *E. coli* reduction attained as 99.99 % at the end of 60 min irradiation period, released organic

content from damaged bacteria degraded and caused detection of a FI value between humic fluorophores and microbially derived fluorophores.

In a similar manner to the UV-vis absorbance and synchronous scan fluorescence analyses, EEM fluorescence contour plots of organic matter emerged and removed during irradiation time dependent *E. coli* inactivation in WM solution upon solar photolytic treatment were also followed and displayed in Figure 4.11.

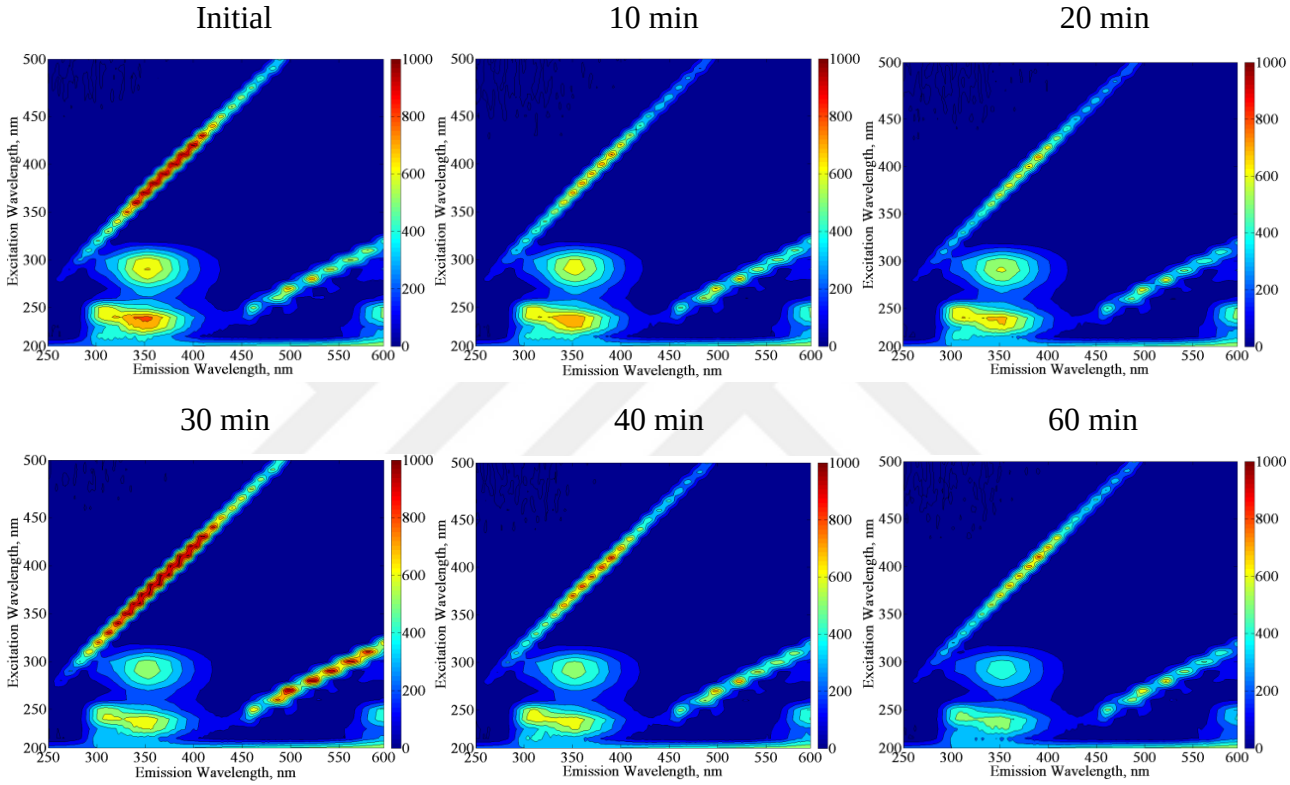

Figure 4.11. EEM fluorescence contour plots of organic matter: Irradiation time dependent *E. coli* inactivation in WM solution upon solar photolytic treatment.

EEM fluorescence contour plots displayed the presence of Regions I, II and IV indicating that the fluorophores were mainly originated from proteins and microbial by-products under all irradiation conditions. Following further irradiation times, released microbial by-products and proteins from *E. coli* cells showed a decreasing trend in accordance with the solar photolytic degradation of organic matter along with reduction of *E. coli*. However, complete removal of these chromophoric groups and fluorophores could not be observed under the specified irradiation conditions most probably due to the inefficiency of the energy provided by simulated solar radiation and resistivity of these groups to degradation. EEM fluorescence contour plots of organics observed under IsoT (Figure 4.6) and WM conditions could be considered as similar excluding regional fluorescence intensities.

4.1.5. Mechanistic Evaluation of *E. coli* Inactivation Upon Solar Photolytic Treatment in WM Solution

Upon irradiation, as inactivation products of *E. coli* cells in WM solution upon solar photolytic treatment, total K, protein, and carbohydrate contents released under initial and t_{irr}=60 min conditions were shown in Table 4.6.

Table 4.6. Total K, protein, and carbohydrate contents of time dependent *E. coli* inactivation in WM solution upon solar photolytic treatment.

Solar photolytic treatment	*E. coli* in WM solution	
	Initial	60 min
Total K, mg/L	3.92	4.08
Protein, mg/L	1.46	7.55
Carbohydrate, mg/L	1.53	14.0

Total K content showed a slight increase at t_{irr}=60 min expressing K^+ ion release from the bacteria cells. Solar photolytic inactivation of *E. coli* in WM solution resulted in a total K content of 4.08 mg/L. Initial total K concentration could be the result of K^+ ion containing components present in WM solution which resulted in a concentration of 3.84 mg/L. Therefore, in the presence of WM, total K content of WM solution could be considered as a baseline concentration. In comparison to the very low total K attained in the presence of IsoT as 0.85 mg/L (Table 4.4) it could be indicated that almost similar amount of K^+ ion was released upon irradiation for 60 min.

Initial protein concentration of *E. coli* in WM solution prior to solar photolytic treatment was lower than the protein content attained in the presence of IsoT solution (4.84 mg/L) as presented in Table 4.4. The reason could be attributed to sole presence of EPS in IsoT solution in the absence of any interfering components like WM solution. Moreover, upon irradiation for 60 min 7.55 mg/L protein release was attained being higher than the protein content released in the presence of IsoT solution (6.64 mg/L) (Table 4.4). In a comparative manner, it could be indicated that both under initial conditions and upon t_{irr}=60 min, carbohydrate contents were higher than *E. coli* treatment in IsoT solution (Table 4.4). Total carbohydrate content was 14.0 mg/L upon irradiation period of 60 min. Based on the attained concentrations, released protein and carbohydrate contents increased due to damaged bacteria cells. It should also be indicated that the WM components could certainly affect the findings occurring through various competing photo-initiated reactions as indicated previously at Equations 2.13-2.37, resulting in diminished effective light irradiation for direct *E. coli* inactivation.

4.1.6. Organic Matter Formation and Removal Upon Solar Photolytic Treatment of *E. coli* in HA Solution

UV-vis absorption and synchronous scan fluorescence spectra of organic matter in solution were presented in Figures 4.12 and 4.13. Irradiation time dependent absorbance changes were significantly similar to each other in UV wavelength range of λ=200-550 nm due to the presence of aromatic domains, UV absorbing centers as well as color forming moieties (all specified UV-vis parameters as $Color_{436}$, UV_{365}, UV_{280} and UV_{254}). On the other hand, sole HA solution representing as HA initial (HA_i) expressed distinctly different trend in wavelength region below λ=230 nm at which ~0.582 absorbance was recorded for all solutions. Upon decreasing wavelength, HA_i expressed lower absorbance values contrary to the increasing trend of released organic matter due to cell destruction. However, obtained UV-vis absorption spectra of HA_i complying with UV-vis absorption spectra of humic substance which was represented in Section 2.4. (Figure 2.16a).

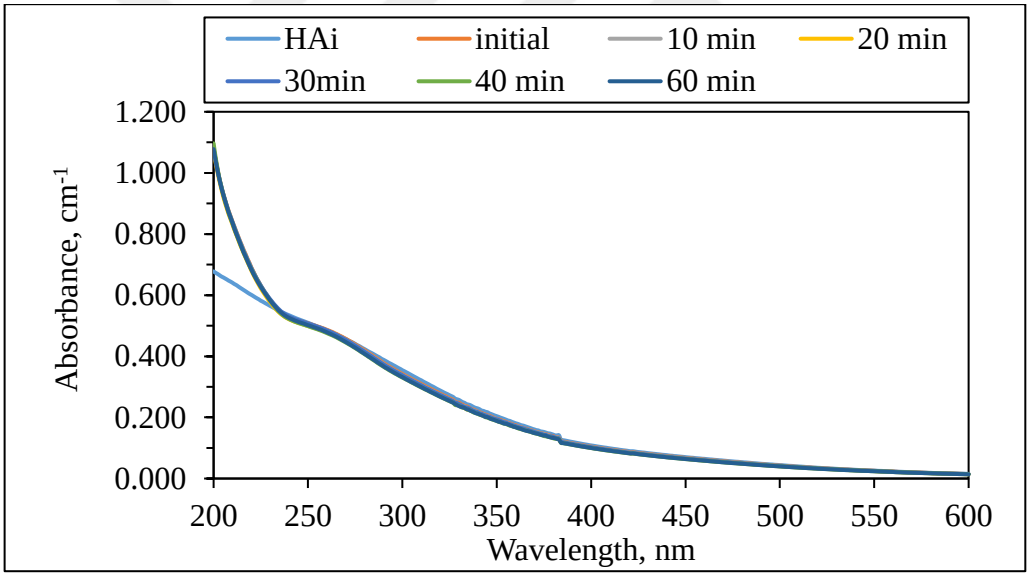

Figure 4.12. UV-vis absorption spectra of organic matter: Irradiation time dependent *E. coli* inactivation in HA solution upon solar photolytic treatment.

Synchronous scan fluorescence spectra of emerged organic matter displayed two intense peaks at λ_{emis}=400 nm and 470 nm, and a minor peak at λ_{emis}=280 nm (Figure 4.13). While peaks at λ_{emis}=280 nm specific to proteins, peaks at λ_{emis}=400 nm and 470 nm are characteristic to HA and in resemblance with the findings of Uyguner and Bekbolet (Reynolds, 2003; Uyguner and Bekbolet, 2005). An irradiation time dependent sequential decreasing order especially in $FI_{sync470}$ was observed throughout light exposure. On the other hand, $FI_{sync470}$ and $FI_{sync280}$ displayed changes in the range of 35.4-58.6 and 6.38-9.60, respectively. In the presence of HA solution, $FI_{sync470}$ accepted as the predominant

fluorophoric group. Moreover, $FI_{sync280}$ value of HA_i could not be detected however after the addition of bacteria into HA solution (initial), $FI_{sync280}$ increased to 7.70 indicating the presence of fluorophores reflecting proteinaceous content in the solution. After irradiation period of 60 min, $FI_{sync280}$ decreased (6.49) due to degradation of released protein content from *E. coli* cells.

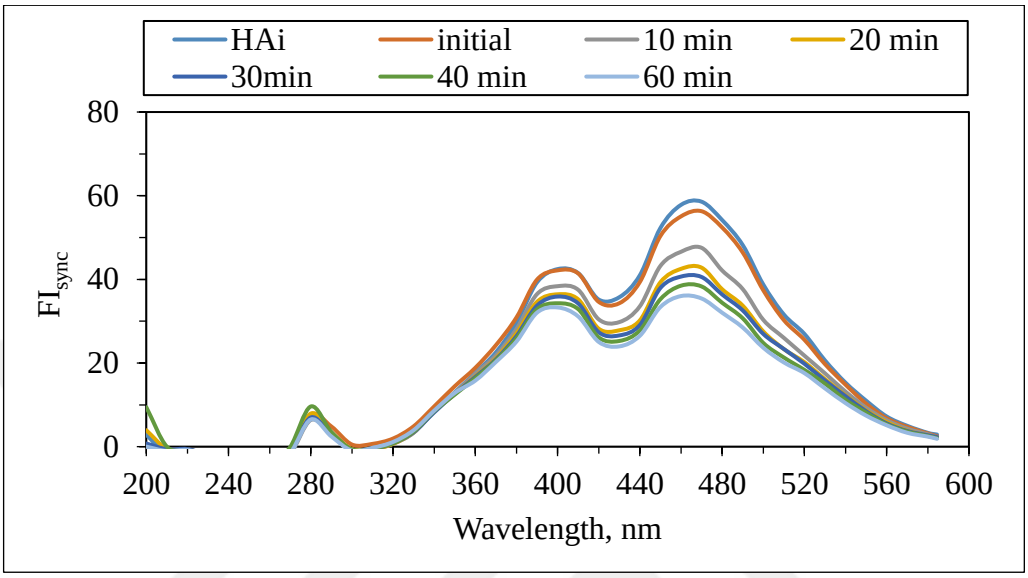

Figure 4.13. Synchronous scan fluorescence spectra of organic matter: Irradiation time dependent *E. coli* inactivation in HA solution upon solar photolytic treatment.

NPOC content increased up to t_{irr}=30 min (4.78-17.3 mg/L) due to the release of the organics from the damaged and destructed *E. coli* cells, followed by a sharp decrease at t_{irr}=40 min (9.95 mg/L) and again followed by an increasing trend during solar photolytic treatment (17.4 mg/L) (Figure 4.14).

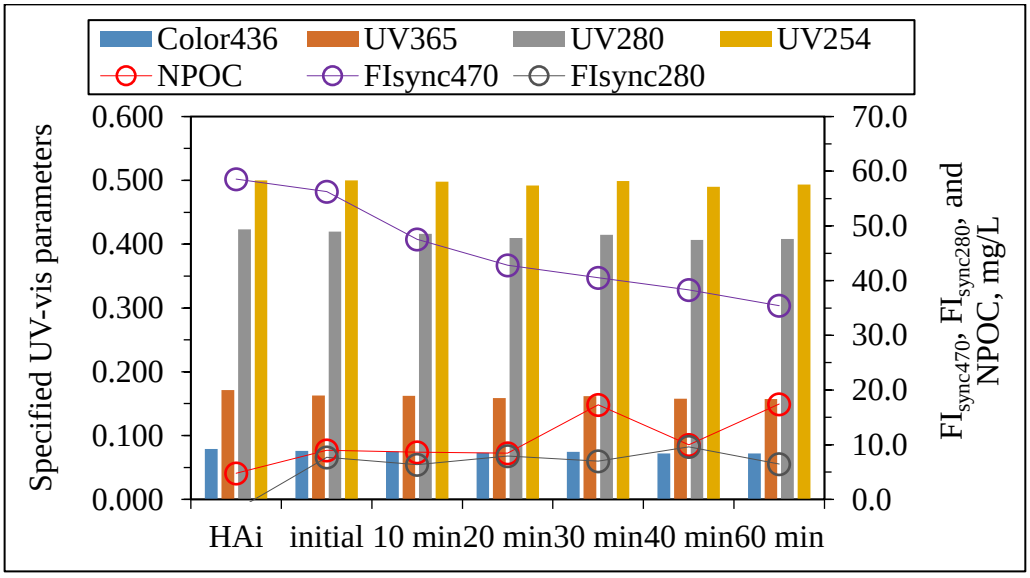

Figure 4.14. Specified UV-vis and fluroscence parameters of organic matter: Irradiation time dependent *E. coli* inactivation in HA solution upon solar photolytic treatment.

All UV-vis parameters expressed high presence relative to treatments conducted in the absence of HA solution (Figures 4.4, 4.9, and 4.14). Especially $Color_{436}$ and UV_{365} displayed evident existence due to presence of colorful HA solution. Similar to previous solar photolytic inactivation treatments of *E. coli* in IsoT and WM solutions (Figures 4.4 and 4.9), the most significant UV-vis parameter was visualized as UV_{254} showing variations in between 0.4917-0.5000. However, specified UV-vis parameters did not express any significant difference between irradiation periods, therefore; it could be indicated that upon solar photolytic treatment, no significant degradation of organic content and color forming moieties was achieved.

Based on NPOC contents, $SCoA_{436}$, $SUVA_{365}$, $SUVA_{280}$, $SUVA_{254}$, $SFI_{sync470}$, and $SFI_{sync280}$ parameters were calculated and presented in Figure 4.15. In contradiction to solar photolytic treatment sets of *E. coli* in IsoT and WM solutions (Figures 4.5 and 4.10) higher SUVA values were calculated in the presence of HA solution. As the most pronounced parameter, $SUVA_{254}$ displayed variations in the range of 2.83-10.5 L/m mg during solar photolysis expressing differences in both UV_{254} and NPOC removals. The highest $SUVA_{254}$ was attained from initial condition.

Furthermore, besides very low $SFI_{sync280}$ in the range of 0.372-0.965, $SFI_{sync470}$ expressed variations in the range of 2.03-12.3. In the presence of HA solution, calculated $SFI_{sync280}$ values were almost insignificant however $SFI_{sync470}$ was accepted as the predominant fluorophoric group due to its remarkable presence in comparison to $SFI_{sync280}$. Moreover, according to insignificant presence of $FI_{sync280}$ related to HA_i, $SFI_{sync280}$ would be irrelevant compared to $SFI_{sync470}$.

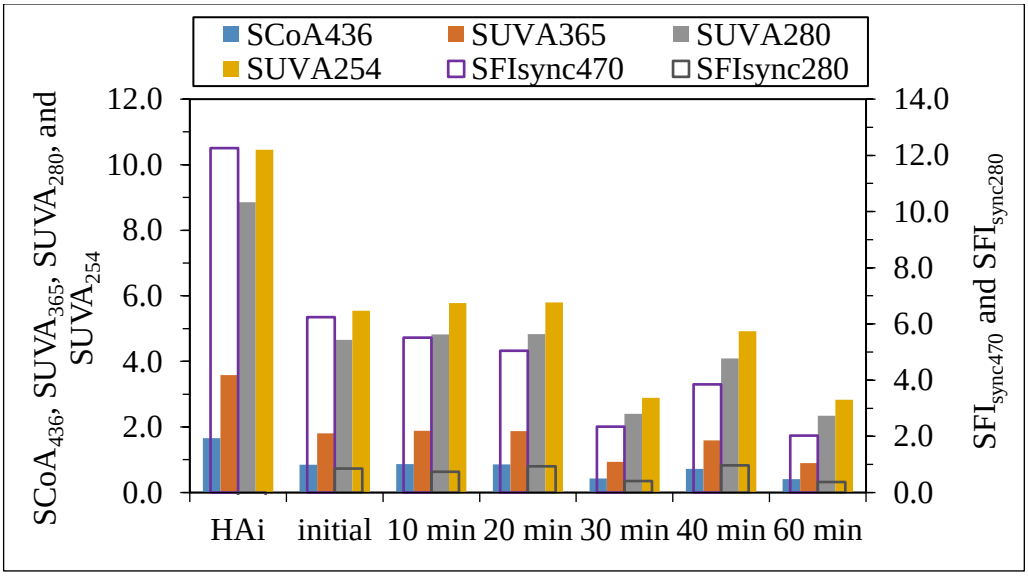

Figure 4.15. Specific UV-vis and fluroscence parameters of organic matter: Irradiation time dependent *E. coli* inactivation in HA solution upon solar photolytic treatment.

Characteristic properties of organic matter under initial condition and upon solar photolytic inactivation of *E. coli* in HA solution exposed to irradiation for 60 min were presented in Table 4.7.

Table 4.7. Characteristic properties of organic matter present in solar photolytic treatment of *E. coli* in HA solution.

Irradiation time, min	UV-vis Spectroscopic Parameters, cm^{-1}				NPOC, mg/L	$SUVA_{254}$, L/m mg	$FI_{sync470}$	$SFI_{sync470}$	FI
	$Color_{436}$	UV_{365}	UV_{280}	UV_{254}					
Initial	0.0761	0.1630	0.4196	0.4997	9.01	5.55	56.3	6.25	1.08
60 min	0.0721	0.1573	0.4079	0.4933	17.4	2.83	35.4	2.03	1.10

Upon 60 min solar photolytic treatment of *E coli* in the presence of HA solution at which 3.64 log *E. coli* reduction was achieved (Table 4.2), released organic matter expressed following UV-vis parameters (cm^{-1}); $Color_{436}$: 0.0721, UV_{365}: 0.1573, UV_{280}: 0.4079, UV_{254}: 0.4933, and NPOC as 17.4 mg/L. After 60 min of irradiation period, NPOC expressed an increase (9.01-17.4 mg/L) due to present humic matter in reaction medium and released cytoplasmic organic content from damaged *E. coli* cells.

$SUVA_{254}$ of initial and t_{irr}=60 min conditions were calculated as 5.55 and 2.83 L/m mg, respectively. $SUVA_{254}$ < 3 indicated the presence of hydrophilic and aliphatic content whereas $SUVA_{254}$ > 4 revealed hydrophobic and aromatic substances in solution (Edzwald et al., 1985). It could be indicated that while initial solution displayed hydrophobic and aromatic features, upon t_{irr}=60 min organic matrix expressed hydrophilic and aliphatic characteristics. Following 60 min of irradiation period, decrease in $SUVA_{254}$ could be related to the degradation of aromatic organics during light exposure.

$FI_{sync470}$ was significantly evident as 56.3 in initial condition due to the presence of HA solution and displayed a decrease to 35.4 at t_{irr}=60 min due to degradation of organics in the reaction medium. Calculated $SFI_{sync470}$ displayed a decrease at the end of 60 min irradiation period (6.25-2.03) in accordance with increased NPOC contents (9.01-17.4 mg/L).

Moreover, $FI_{sync280}$ under initial and t_{irr}=60 min conditions were 7.70 and 6.49, respectively. In the presence of HA solution, quite low $FI_{sync280}$ values were recorded in comparison to IsoT (Table 4.3) and WM solution conditions (Table 4.5); masking effect of HA on protein content could be the cause of low $FI_{sync280}$ values. $SFI_{sync280}$ were 0.855 and 0.372 under initial and t_{irr}=60 min conditions respectively. In contrast to high $SFI_{sync470}$ as being quite low $SFI_{sync280}$ could be considered as

insignificant. However, both $FI_{sync280}$ and $SFI_{sync280}$ displayed a slight decrease at the end of 60 min irradiation period most probably due to the degradation of released proteinaceous matter from *E. coli*.

FI ≤ 1.4 is attributed to presence of humic fluorophores (Sen-Kavurmaci and Bekbolet, 2014). In the presence of HA solution as a reaction medium, FI of initial and t_{irr}=60 min was calculated as 1.08 and 1.10, respectively complying with the findings of researchers.

In a similar manner to the UV-vis absorbance and synchronous scan fluorescence analyses, EEM fluorescence contour plots of organic matter emerged and removed during irradiation time dependent *E. coli* inactivation in HA solution upon solar photolytic treatment were also followed and displayed in Figure 4.16.

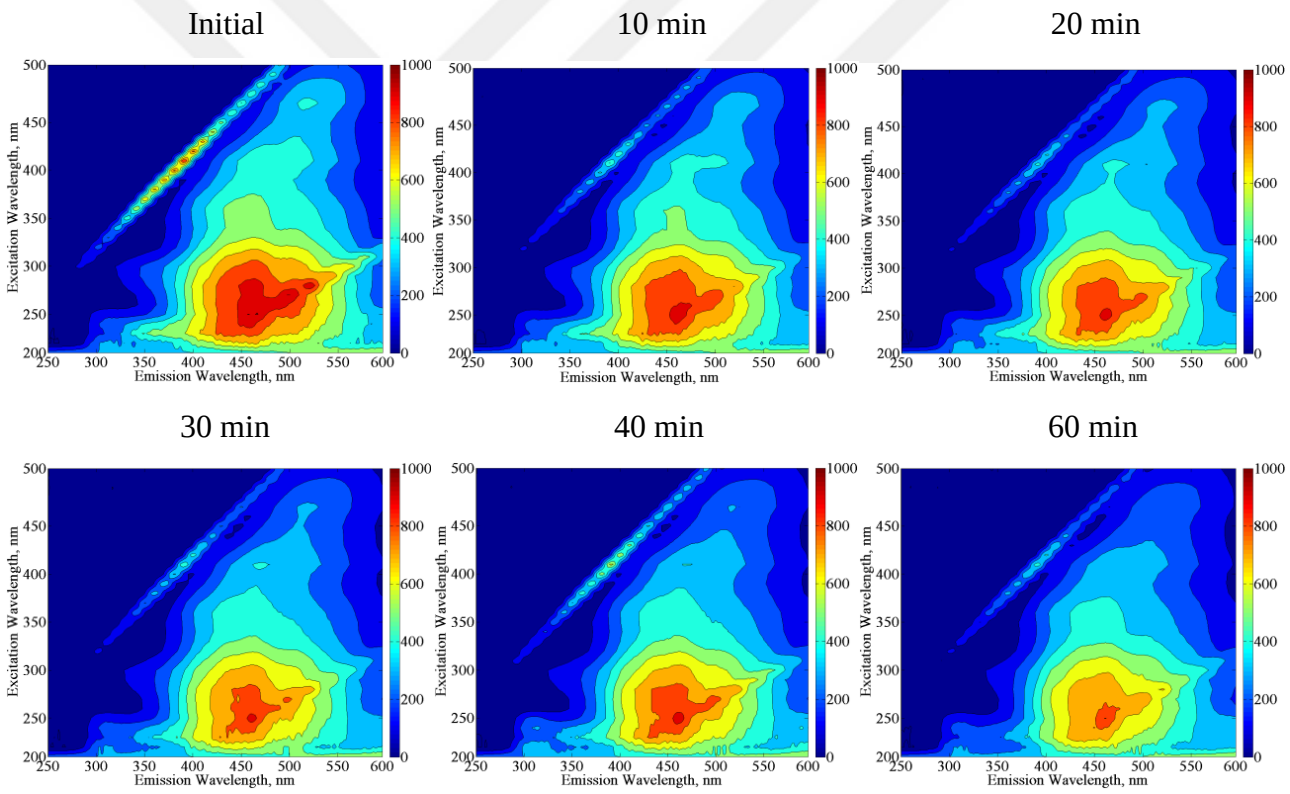

Figure 4.16. EEM fluorescence contour plots of organic matter: Irradiation time dependent *E. coli* inactivation in HA solution upon solar photolytic treatment.

EEM fluorescence contour plots displayed the presence of Regions III (λ_{exc} 220-250 nm and λ_{emis} 380-580 nm), and V (λ_{exc} 220-470 nm and λ_{emis} 380-580 nm) indicating that the fluorophores were mainly originated from fulvic-like and humic-like substances. Presence of HA caused a masking effect over the Region I, II and IV owing to the quenching of fluorophores originating from protein like materials by humic-like materials (Wang et al., 2015). Following further irradiation periods

fulvic-like and humic-like content of the sample showed a decreasing trend in accordance with the solar photolytic degradation of HA and reduction of *E. coli*. In accordance with previous findings of researchers, obtained EEM fluorescence contour plots during solar photolytic traetment of *E. coli* in HA solution displayed an expected degradation trend (Birben et al., 2017a, 2021b; Uyguner-Demirel et al., 2020).

4.1.7. Mechanistic Evaluation of *E. coli* Inactivation Upon Solar Photolytic Treatment in HA Solution

As inactivation products upon solar photolytic treatment of *E. coli* in the presence of HA solution, total K, protein, and carbohydrate contents present under initial and t_{irr}=60 min conditions were presented in Table 4.8.

Table 4.8. Total K, protein, and carbohydrate contents of time dependent *E. coli* inactivation in HA solution upon solar photolytic treatment.

Solar photolytic treatment	*E. coli* and HA	
	Initial	60 min
Total K, mg/L	0.69	0.72
Protein, mg/L	9.70	14.6
Carbohydrate, mg/L	3.25	4.77

In the absence of WM solution, low total K contents were detected similar to *E. coli* in IsoT solution solar photolytic treatment (Table 4.4). Total K content showed a slight increase after 60 min irradiation period, expressing released K^+ ion amount from destructed *E. coli* cells. Besides the reduction of bacteria as 99.9 %, total K content did not show a significant increase at t_{irr}=60 min. The reason could be attributed to possible adsorption of released K^+ ions from bacteria onto negatively charged, ruptured *E. coli* cell wall particles and negatively charged moieties of HA, then consequently eliminated with membrane filtration before total K analysis.

Due to the presence of HA solution, whose protein and carbohydrate concentrations were measured as 9.71 mg/L and 2.63 mg/L, respectively; initial contents of both protein (9.70 mg/L) and carbohydrate (3.25 mg/L) were higher than those achieved by solar photolytic treatment carried out in IsoT (Table 4.4) and WM solutions (Table 4.6). After t_{irr}=60 min, both protein and carbohydrate concentrations displayed an increase (14.6 mg/L for protein; 4.77 mg/L for carbohydrate) due to released protein and carbohydrate contents from damaged and/or destructed *E. coli* cells.

4.1.8. Organic Matter Formation and Removal Upon Solar Photolytic Treatment of *E. coli* in "HA and WM" Solution

Following a similar fashion, UV-vis absorption and synchronous scan fluorescence spectra of organic matter present in "HA and WM" solution were presented in Figures 4.17 and 4.18, respectively. Irradiation time dependent absorbance changes were significantly similar to each other in UV wavelength range of λ=200-550 nm due to the presence of aromatic domains, UV absorbing centers as well as color forming moieties ($Color_{436}$, UV_{365}, UV_{280} and UV_{254}). Main difference could be visualized in between HA_i and "HA and WM" solution. Different from HA_i, HA solution together with WM solution ("HA and WM" solution) displayed a rather different absorbance features at λ < 240 nm with a shoulder between λ=200-210 nm. The reason could be attributed to the presence of NO_3^- in WM solution. Due to strong absorption spectrum of NO_3^-, which having its λ_{max} at approximately 200 nm, solar *E. coli* inactivation conducted in WM solution containing reaction media expressed different absorption trend in comparison to the conditions in the presence of IsoT and HA solution (Krishnan and Guha, 1934; Edwards at el., 2001). Similar UV absorption pattern was also visualized via solar photolytic treatment of *E. coli* in sole WM solution (Figure 4.7). On the other hand, upon irradiation, minor variations could be recorded in wavelength range of 230-500 nm.

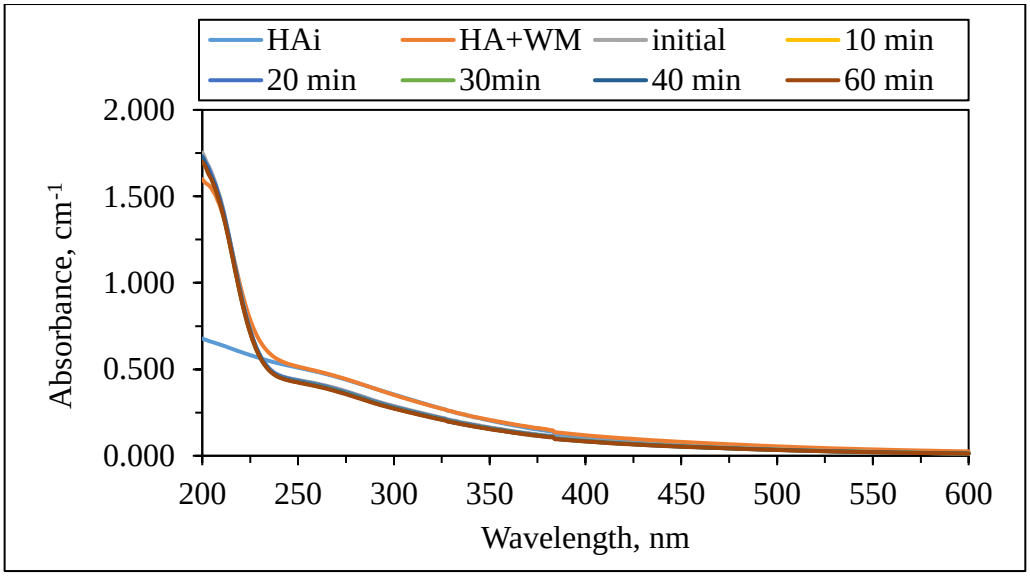

Figure 4.17. UV-vis absorption spectra of organic matter. Irradiation time dependent *E. coli* inactivation in "HA and WM" solution upon solar photolytic treatment.

Synchronous scan fluorescence spectra of emerged organic matter displayed two intense peaks at λ_{emis}=390 nm and 470 nm, and a minor peak at λ_{emis}=280 nm, representing the presence of fluorophores originating from both humic matter and protein content of the solutions (Figure 4.18).

Moreover, both in "HA and WM" solution and after addition of bacteria into the reaction solution (initial), increased fluorescence intensities were observed relative to sole HA_i condition at λ_{emis} < 430 nm. An irradiation time dependent decreasing order in $FI_{sync470}$ data was observed, except a minor increase between t_{irr}=20 min (35.3) and t_{irr}=30 min (36.4) conditions.

In the presence of HA solution, dominant $FI_{sync470}$ displayed changes in the range of 28.4-58.6 however $FI_{sync280}$ showed minor presence with variations in between 4.43-16.3 (Figure 4.19). On the other hand, $FI_{sync280}$ of HA_i solution could not be detected similar to previous HA solution conditions (Figure 4.14).

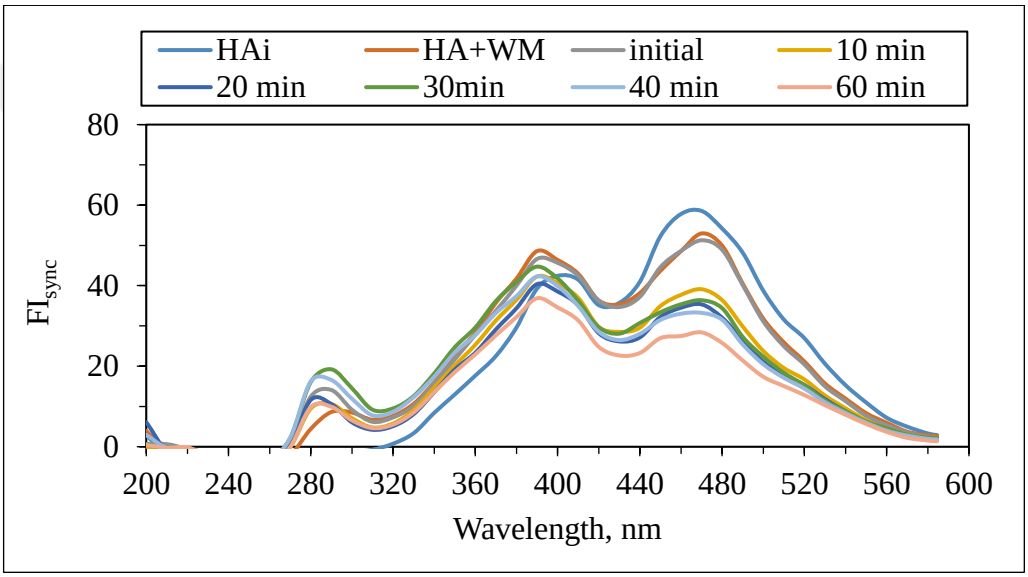

Figure 4.18. Synchronous scan fluorescence spectra of organic matter: Irradiation time dependent *E. coli* inactivation in "HA and WM" solution upon solar photolytic treatment.

In presence of "HA and WM" solution, NPOC expressed changes in between 4.65-7.13 mg/L (Figure 4.19). In accordance with the UV_{254} variations, NPOC content increased up to t_{irr}=10 min (4.65-6.55 mg/L) and slightly decreased upon t_{irr}=20 min (6.40 mg/L). Following further irradiation period of 30 min NPOC significantly increased (7.13 mg/L) and gradually decreased up to t_{irr}=60 min (5.29 mg/L). The highest NPOC release was attained upon irradiation period of 30 min.

Similar to previously presented solar photolysis of *E. coli* inactivation in sole HA solution (Figure 4.14), all UV-vis parameters expressed higher presence than treatments conducted in IsoT and WM solutions (Figures 4.4 and 4.9). As the most significant specified UV-vis parameter, UV_{254} expressed variations in the range of 0.4143-0.5050, being the highest for "HA and WM" solution and the lowest for t_{irr}=60 min condition. UV_{254} values were comparatively higher from UV_{280} as expected

under all conditions. On the other hand, $Color_{436}$ and UV_{365} displayed evident presence due to the use of HA solution as a solution matrix component. However, specified UV-vis parameters did not show any significant difference between initial and t_{irr}=60 min conditions, revealing that there was no significant degradation of organic content and color forming moieties during solar light exposure period of 60 min. Similar findings were also recorded for solar photolytic treatment of *E. coli* in sole HA solution as well (Figure 4.14). In accordance with undetected $FI_{sync280}$ of HA_i solution, $SFI_{sync280}$ could not be calculated either.

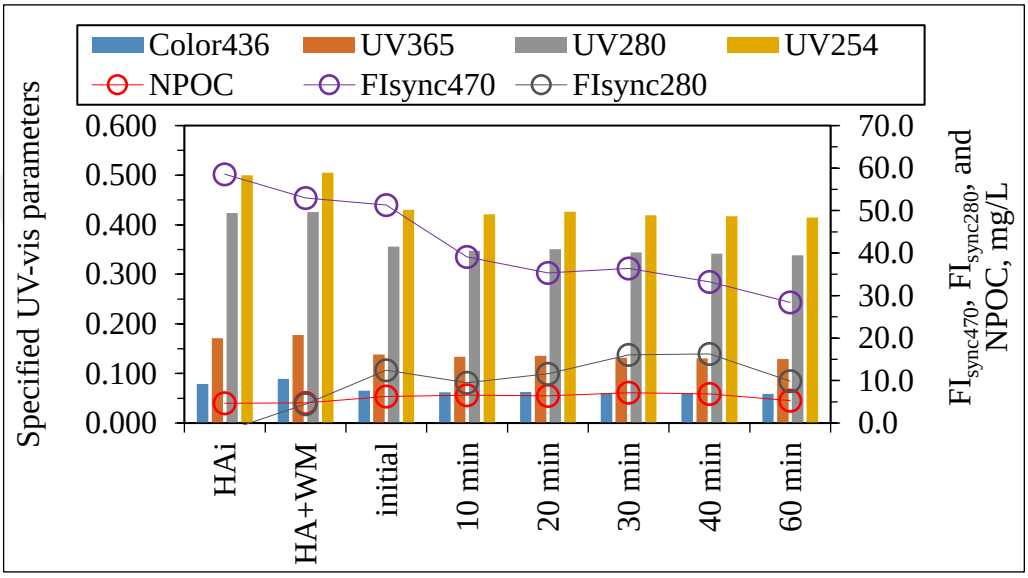

Figure 4.19. Specified UV-vis and fluroscence parameters of organic matter: Irradiation time dependent *E. coli* inactivation in "HA and WM" solution upon solar photolytic treatment.

Based on NPOC contents, $SCoA_{436}$, $SUVA_{365}$, $SUVA_{280}$, $SUVA_{254}$, $SFI_{sync470}$, and $SFI_{sync280}$ parameters were calculated and presented in Figure 4.20. As the most evident parameter, $SUVA_{254}$ displayed variations in between 5.88-10.8 L/m mg during 60 min of solar photolytic treatment, expressing differences in both UV_{254} and NPOC removals. The highest and the lowest $SUVA_{254}$ were recorded for HA_i solution and t_{irr}=30 min condition, respectively. $SUVA_{280}$, which was the second significant specific UV-vis parameter calculated, showed differances in the range of 4.8-9.1 L/m mg. On the other hand, under all conditions, calculated $SCoA_{436}$ and $SUVA_{365}$ were comparatively lower than $SUVA_{280}$ and $SUVA_{254}$ as expected.

Furthermore, contrary to predominant $SFI_{sync470}$ varied in the range of 4.87-12.6, quite low $SFI_{sync280}$ expressed variations in the range of 0.937-2.38. Due to the use of HA solution as an aqueous reaction medium component, calculated $SFI_{sync470}$ values displayed significant presence contrary to $SFI_{sync280}$.

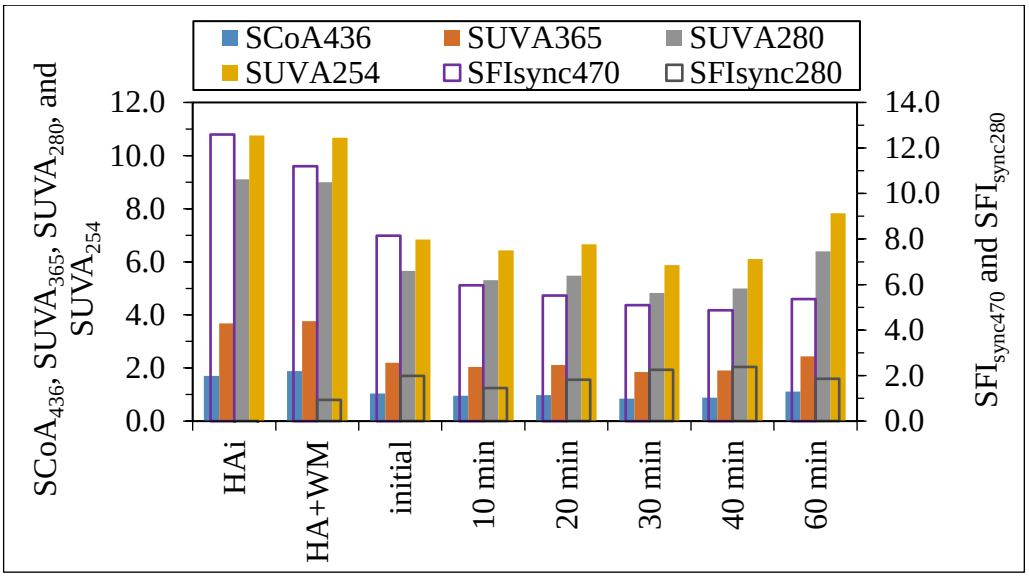

Figure 4.20. Specific UV-vis and fluroscence parameters of organic matter: Irradiation time dependent *E. coli* inactivation in "HA and WM" solution upon solar photolytic treatment.

For comparative evaluation purposes, characteristic properties of organic matter under initial condition and upon solar photolytic inactivation of *E. coli* in "HA and WM" solution for 60 min of solar light exposure were presented in Table 4.9.

Table 4.9. Characteristic properties of organic matter present in solar photolytic treatment of *E. coli* in "HA and WM" solution.

Irradiation time, min	UV-vis Spectroscopic Parameters, cm^{-1}				NPOC, mg/L	$SUVA_{254}$, L/m mg	$FI_{sync470}$	$SFI_{sync470}$	FI
	$Color_{436}$	UV_{365}	UV_{280}	UV_{254}					
Initial	0.0651	0.1385	0.3560	0.4302	6.29	6.84	51.3	8.15	1.18
60 min	0.0591	0.1291	0.3382	0.4143	5.29	7.83	28.4	5.37	1.23

Upon 60 min solar photolytic treatment of *E coli* in the presence of "HA and WM" solution, at which 2.43 log *E. coli* reduction was achieved (Table 4.2), released organic matter expressed the following UV-vis parameters (cm^{-1}); $Color_{436}$: 0.0591, UV_{365}: 0.1291, UV_{280}: 0.3382, UV_{254}: 0.4143, and NPOC as 5.29 mg/L.

$SUVA_{254}$ of initial and t_{irr}=60 min solutions were calculated as 6.84 L/m mg and 7.83 L/m mg, respectively. According to Edzwald and colleagues, $SUVA_{254}$ > 4 indicated the presence of hydrophobic and aromatic substances in solution (Edzwald et al., 1985). Therefore, it could be indicated that throughout the solar irradiation duration of 60 min, no significant degradation of organic content was recorded which could also be supported with data obtained from specified UV-vis measurements (Figure 4.19). Moreover, it could be concluded that when HA solution used with

WM solution, an inhibitory effect could be detected in both *E. coli* reductions and organic matter degradation in comparison to data obtained from solar photolytic inactivation of *E. coli* in sole HA solution (Tables 4.2, 4.7, and 4.9; Figures 4.1, 4.15, and 4.20).

$FI_{sync470}$ displayed significant presence under initial condition due to the existence of HA solution and decreased nearly by half at t_{irr}=60 min via the degradation of organic content in the solution. $SFI_{sync470}$ expressed a decrease upon t_{irr}=60 min. On the other hand, initial and t_{irr}=60 min conditions of $FI_{sync280}$ were recorded as 12.5 and 9.85, respectively. According to $FI_{sync280}$ and NPOC data, $SFI_{sync280}$ of initial and t_{irr}=60 min runs were calculated as 1.98 and 1.86, respectively. Decreased $FI_{sync280}$ at t_{irr}=60 min could possibly be due to degradation of released protein content of *E. coli*. At t_{irr}=60 min, FI was calculated as 1.23 revealing the presence of humic fluorophores which comply with the presence of HA solution as a reaction matrix component. Similar findings were also reported by Birben and colleagues under similar experimental conditions (Birben et al., 2021b).

EEM fluorescence contour plots of organic matter emerged and removed during irradiation time dependent *E. coli* inactivation in "HA and WM" solution during solar photolytic treatment were presented in Figure 4.21.

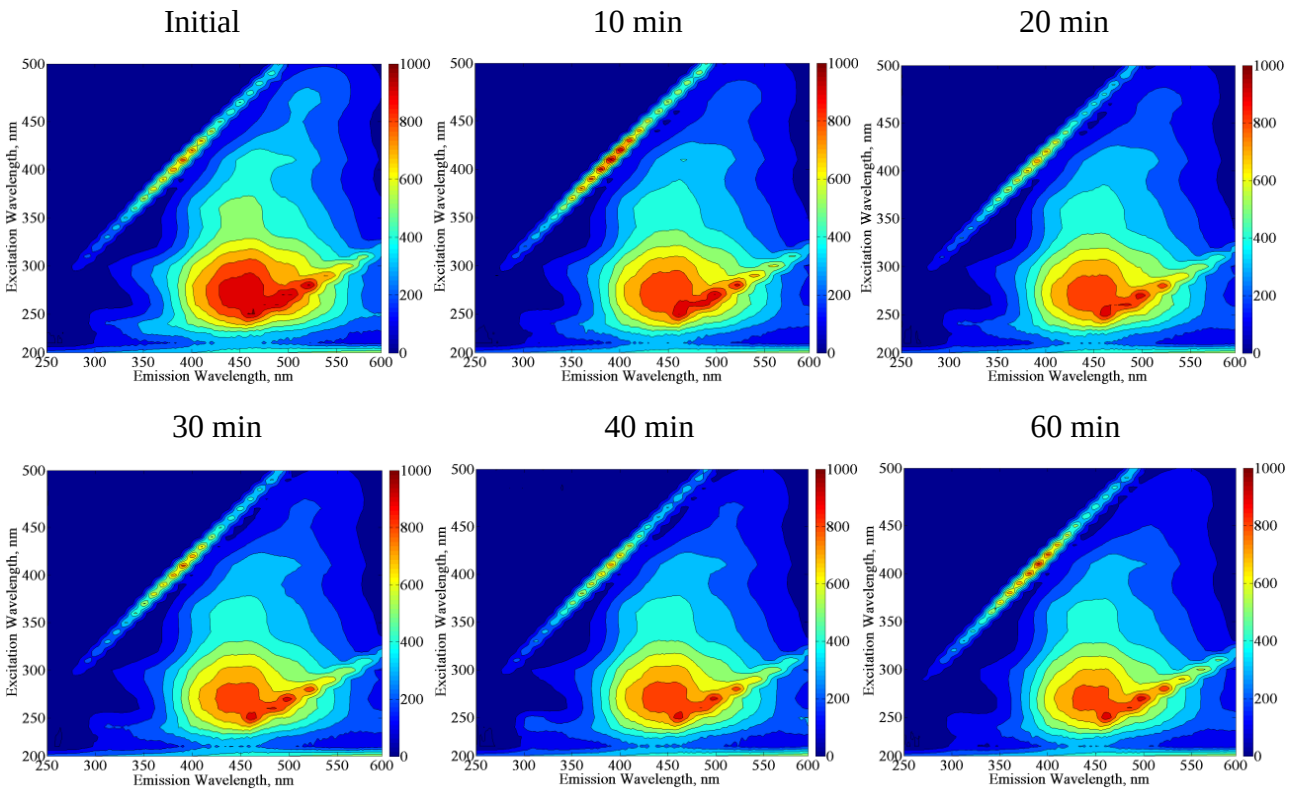

Figure 4.21. EEM fluorescence contour plots of organic matter: Irradiation time dependent *E. coli* inactivation in "HA and WM" solution upon solar photolytic treatment.

EEM fluorescence contour plots expressed the presence of Regions III, and V like *E. coli* inactivation in the presence of HA solution (Figure 4.16). Presence of HA solution caused a masking effect over the Region I, II and IV owing to the quenching of fluorophores originating from protein like materials by humic-like materials (Wang et al., 2015). Following further irradiation periods fulvic-like and humic-like content of the sample showed a decreasing trend in accordance with the solar photolytic degradation of humic matter and reduction of *E. coli*. Similar findings were reported by Uyguner-Demirel and colleagues under similar experimental conditions (Birben et al., 2021b; Uyguner-Demirel et al., 2020).

4.1.9. Mechanistic Evaluation of *E. coli* Inactivation Upon Solar Photolytic Treatment in "HA and WM" Solution

As inactivation products of solar photolytic *E. coli* inactivation in "HA and WM" solution, total K, protein, and carbohydrate contents of initial and t_{irr}=60 min solutions were presented in Table 4.10.

Table 4.10. Total K, protein, and carbohydrate contents of time dependent *E. coli* inactivation in "HA and WM" solution upon solar photolytic treatment.

Solar photolytic treatment	*E. coli* in "HA and WM"	
	Initial	60 min
Total K, mg/L	4.53	4.46
Protein, mg/L	7.57	13.8
Carbohydrate, mg/L	2.63	4.27

Initial total K content was detected as higher than solar photolytic inactivation of *E. coli* in IsoT (0.72 mg/L), WM (3.92 mg/L), and HA (0.69 mg/L) solutions due to the presence of both "HA and WM" as matrix components (Tables 4.4., 4.6, and 4.8). Total K content of sole "HA and WM" solution was detected as 4.15 mg/L, therefore; for solar photolytic treatments conducted in "HA and WM" solution, total K concentration (4.15 mg/L) could be accepted as baseline value of the solution. After t_{irr}=60 min, total K content showed a slight decrease which could be related with low bacteria LRV as 2.43 (Table 4.2). It could be indicated that, excessive amount of K^+ ion in the solution matrix could be used by bacteria to compensate K^+ ion leakage and maintain inner osmotic pressure thus retardation of cell wall damage could be occurred.

Initial protein and carbohydrate concentrations of sole "HA and WM" solution were 9.40 mg/L and 3.78 mg/L, respectively. The reason of high initial protein (7.57 mg/L) and carbohydrate (2.63

mg/L) contents of *E. coli* in complex solution matrix could be attributed to the co-presence of "HA and WM" as solution components. Owing to released cytoplasmic organic matter from bacteria, and EPS present outside of the cell wall, *E. coli* in "HA and WM" solution upon solar photolytic treatment displayed increased protein and carbohydrate contents after irradiation period of 60 min as 13.8 mg/L and 4.27 mg/L, respectively. Besides high protein and carbohydrate contents of initial and solar light exposure duration of 60 min conditions, comparatively higher concentrations were obtained in the case of *E. coli* and sole HA solution exposed to solar photolytic treatment (Table 4.8).

4.1.10. Comparative Evaluation of Different Experimental Matrixes on Solar Photolytic Inactivation Mechanism of *E. coli*

Total K, protein, and carbohydrate concentrations, and bacteria enumeration results of solar photolytic treatment of *E. coli* in different solution matrixes in comparison with initial and t_{irr}=60 min conditions were given in Figure 4.22.

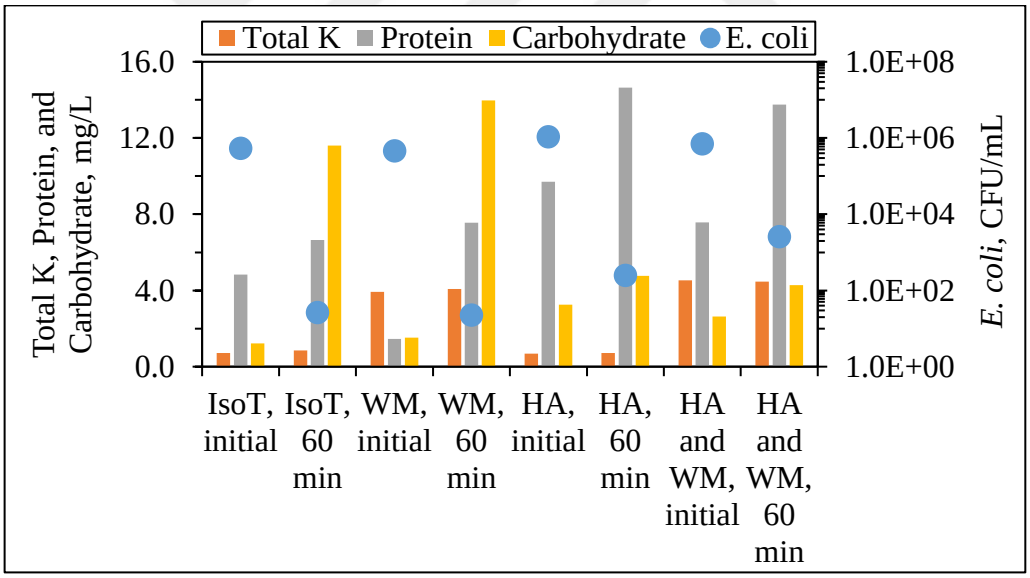

Figure 4.22. Initial and t_{irr}=60 min total K, protein, and carbohydrate contents, and bacteria enumeration results of *E. coli* inactivation upon solar photolytic treatment in various aqueous matrixes.

Total K contents expressed variations in between 0.69-4.53 mg/L being the lowest for initial condition of *E. coli* in HA solution and the highest for initial sample of *E. coli* in "HA and WM" solution matrix. Total K content displayed increased concentrations with the effect of present K^+ ion content in WM solution. Total K concentrations were plotted against bacteria count data in order to detect if there is any correlation between these parameters, initial conditions showed a moderate

correlation, as R^2=0.73, except the presence of IsoT solution, whereas t_{irr}=60 min runs displayed a strong correlation, as R^2=0.99, excluding the presence of WM solution. Solar photolytic treatments carried out with IsoT and WM solutions showed lower protein contents both for initial and t_{irr}=60 min samples, and higher carbohydrate contents at t_{irr}=60 min than sole HA and "HA and WM" solutions.

Covering all conditions, protein contents varied in between 1.46-14.6 mg/L being the lowest for initial sample of *E. coli* in WM solution and the highest for t_{irr}=60 min condition of *E. coli* in HA solution. Similarly, carbohydrate contents varied in between 1.23-14.0 mg/L being the lowest for initial condition of *E. coli* in IsoT solution and the highest for t_{irr}=60 min solution of *E. coli* in WM solution. In the presence of HA solution, increased protein and decreased carbohydrate contents were detected at t_{irr}=60 min (14.6 mg/L protein and 4.77 mg/L carbohydrate for *E. coli* in HA solution; 13.8 mg/L protein and 4.27 mg/L carbohydrate for *E. coli* in "HA and WM" solution), it could be attributed to the formation of HA and protein complexes due to their opposite charges at the pH of the solution (Tan et al., 2008). It could also be indicated that the presence of HA solution was directly proportional to protein content but inversely proportional to carbohydrate content of the solution. Since, *E. coli* cell counts decreased in the presence of sole HA solution to 2.50E+02 CFU/mL and 2.63E+03 CFU/mL for *E. coli* in "HA and WM" solution upon irradiation period of 60 min. Accordingly, "HA and WM" condition affected *E. coli* inactivation more negatively than the presence of sole HA solution.

Released protein and carbohydrate concentrations and bacteria LRV of solar photolytic treatment of *E. coli* in different solution matrixes were given in Figure 4.23.

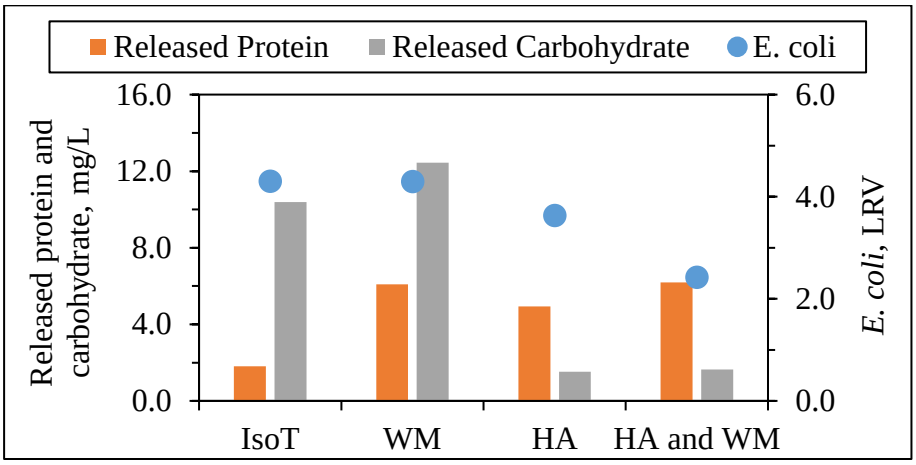

Figure 4.23. Released protein and carbohydrate contents, and bacteria LRV of *E. coli* inactivation upon solar photolytic treatment in various aqueous matrixes.

Released protein and carbohydrate contents were calculated by subtracting initial from concentrations obtained at t_{irr}=60 min condition. Released protein content was detected as the lowest in *E. coli* in IsoT (1.80 mg/L), however it could be due to the degradation of released proteins throughout the 60 min irradiation period. While protein concentrations of the samples were directly proportional to HA contents, released protein concentrations did not display excessive differences in various solution matrixes. However, presence of HA solution showed inverse proportionality to released carbohydrate concentrations. It could be concluded that both carbohydrate concentrations after 60 min of irradiation period (4.77 mg/L for *E. coli* and HA solution; 4.27 mg/L for *E. coli* in "HA and WM" solution) and released carbohydrate concentrations (1.52 mg/L for *E. coli* and HA solution; 1.65 mg/L for *E. coli* in "HA and WM" solution) of the samples were inversely proportional to HA contents. Similar *E. coli* LRV calculated in the presence of IsoT (4.31) and WM (4.30) solutions however solar photolytic treatment conducted with sole HA (3.64) and "HA and WM" (2.43) solutions displayed decreased LRV of *E. coli*. In order to investigate the possible correlation between *E. coli* LRV and released organic content, both released protein and carbohydrate concentrations were plotted against LRV individually. Bacteria LRV and released protein concentration showed a strong correlation as R^2=0.84, except for WM solution, also LRV and released carbohydrate concentration expressed a strong correlation as R^2=0.97, excluding the presence of sole HA solution.

Upon solar photolytic treatment of *E. coli* in different solution matrixes, the attained protein and carbohydrate contents, $FI_{sync280}$, UV_{280} and NPOC under initial and t_{irr}=60 min conditions were given in Figure 4.24. Protein concentrations and UV_{280} displayed an increased trend in the presence of HA solution contrary to, $FI_{sync280}$ showing reverse relation with HA content. Covering all conditions, $FI_{sync280}$ varied in between 6.46-39.0 being the lowest for t_{irr}=60 min sample of *E. coli* in HA solution and the highest for t_{irr}=60 min solution of *E. coli* in IsoT solution. Similarly, UV_{280} data displayed differences in the range of 0.0173-0.420 being the lowest for initial condition of *E. coli* in WM solution and the highest for initial sample of *E. coli* in HA solution. Lower $FI_{sync280}$ values were attained for either sole HA solution and "HA and WM" solution conditions, which could be derived from the masking effect of humic-like fluorophores over protein-like fluorophores due to the quenching of the fluorophores. Masking effect of fluorophores having HA origin over protein like materials were previously detected with EEM fluorescence contour plots (Figures 4.16 and 4.21).

Furthermore, protein concentrations were plotted against $FI_{sync280}$ data to evaluate any correlation between these two protein related parameters. As a result, a strong correlation, as $R^2 > 0.97$, was detected under all conditions except for the presence of sole WM solution.

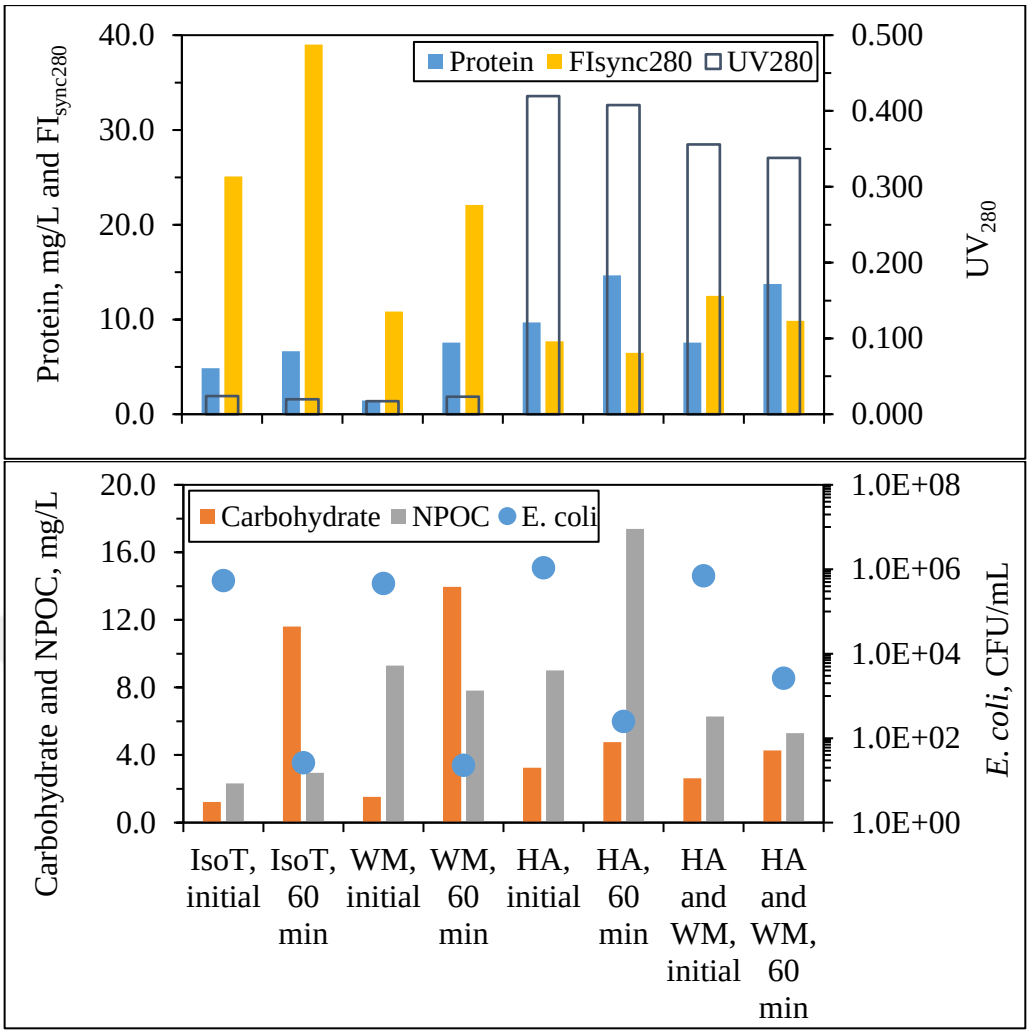

Figure 4.24. Initial and t_{irr}=60 min protein and carbohydrate contents, $FI_{sync280}$, UV_{280}, NPOC and bacteria enumeration results upon solar photolytic treatment of *E. coli* in various aqueous matrixes.

NPOC contents were detected as higher than carbohydrate concentrations under all conditions, except *E. coli* in IsoT and WM solutions at t_{irr}=60 min ones (11.6 mg/L carbohydrate and 2.95 mg/L NPOC for *E. coli* in IsoT solution; 14.0 mg/L carbohydrate and 7.82 mg/L NPOC for *E. coli* in WM solution). The highest NPOC content (17.4 mg/L) was detected in *E. coli* in HA solution after t_{irr}=60 min of treatment. In comparison with sole HA solution, reduced *E. coli* inactivation, carbohydrate concentration and NPOC contents were recorded upon use of both "HA and WM" as solution matrix constituents. Therefore, it could be indicated that in the presence of "HA and WM" solution, solar photolytic process expressed selectivity towards degradation of humic matter rather than bacteria.

Moreover, carbohydrate concentrations were plotted against NPOC contents in order to detect if there is any correlation between these parameters. While initial conditions displayed a strong correlation as R^2=0.99, excluding the presence of sole WM solution, t_{irr}=60 min runs showed a moderate correlation as R^2=0.69, except the presence of "HA and WM" solution.

4.2. Solar Photocatalytic Inactivation of *E. coli*

4.2.1. TiO_2 Solar Photocatalytic Inactivation of *E. coli*

4.2.1.1. TiO_2 solar photocatalytic *E. coli* inactivation under specified reaction conditions, reductions, and kinetics. *E. coli* suspension in IsoT solution (N_o=7.95E+05 CFU/mL) was subjected to TiO_2 solar photocatalysis. Upon irradiation period of 30 min, *E. coli* count decreased to 6.18E+02 CFU/mL. Following further exposure of t_{irr}=60 min, a drastic decrease was attained as < 10 CFU/mL. Under these conditions, LRV was 5.90 and reduction was 99.999 %. *E. coli* suspension in WM solution (N_o=6.41E+05 CFU/mL) treated for an irradiation period of 30 min, expressed a decrease of 2.50E+03 CFU/mL. Following light exposure of t_{irr}=60 min, *E. coli* count declined to 1.33E+02 CFU/mL revealing LRV as 3.73 and reduction as 99.9 %. *E. coli* (N_o=1.39E+06 CFU/mL) suspension was prepared in HA solution and exposed to irradiation for a period of 30 min, *E. coli* count was 5.66E+05 CFU/mL. Upon light exposure of t_{irr}=60 min, *E. coli* count further decreased to 3.85E+04 CFU/mL revealing LRV as 1.45 and reduction as 90 %. *E. coli* (N_o=7.32E+05 CFU/mL) suspension was prepared in a solution composed of "HA and WM" components and was subjected to irradiation for 30 min, *E. coli* count decreased to 1.65E+05 CFU/mL. Upon light exposure of t_{irr}=60 min, *E. coli* count decreased to 5.50E+04 CFU/mL revealing LRV as 1.08 and reduction as 90 %. Irradiation time dependent *E. coli* inactivation profiles in the presence of various solution matrixes were presented in Figure 4.25. First order kinetic model parameters rate constant (k, min^{-1}), half-life ($t_{1/2}$, min), and rate, (R, CFU/mL min) of TiO_2 solar photocatalytic inactivation of *E. coli* were presented in Table 4.11.

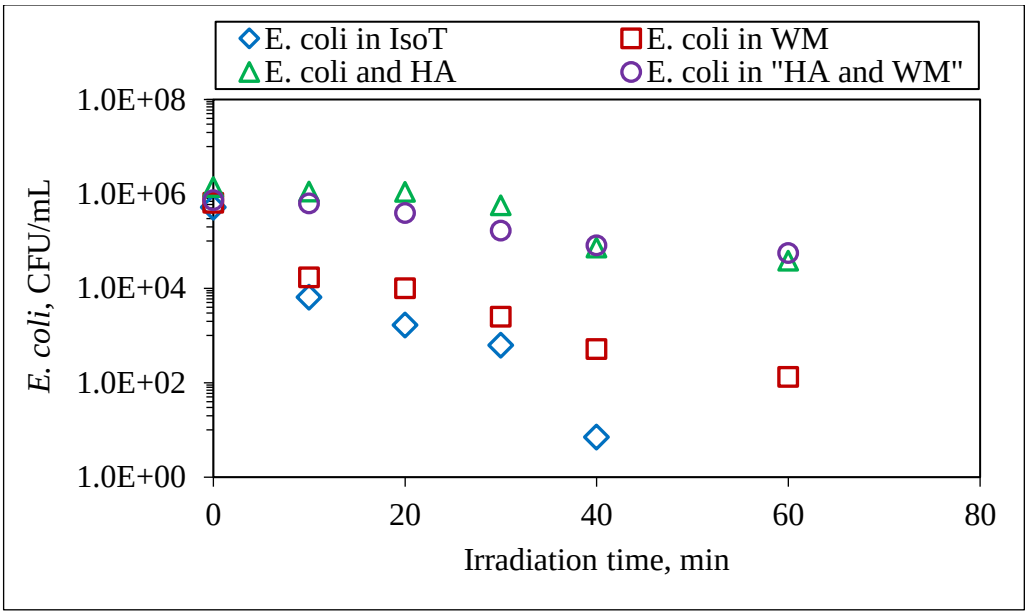

Figure 4.25. Irradiation time dependent *E. coli* inactivation upon TiO_2 solar photocatalytic treatment in various solution matrixes.

Based on these results, the effect of solution matrix could be displayed in terms of LRV of *E. coli* in an increasing order as: "HA and WM" < HA < WM < IsoT. TiO_2 solar photocatalytic treatment of *E. coli* in IsoT solution resulted in a rather fast reduction with k=0.248 min^{-1} and half-life as 2.79 min. In "HA and WM" solution, a reaction rate constant of k=0.0488 min^{-1} and half-life as 14.2 min were attained. The effect of reaction medium could also be expressed in terms of inactivation reaction rate constant (k, min^{-1}) in a decreasing order as; IsoT > WM > HA > "HA and WM". Irrespective of the minor differences in initial bacteria counts, inactivation rates (CFU/mL min) also followed the same trend as; 1.97E+05 > 9.44E+04 > 7.26E+04 > 3.22E+04 for IsoT, WM, HA, and "HA and WM", respectively.

Table 4.11. TiO_2 solar photocatalytic treatment of *E. coli*: Inactivation parameters.

Matrix	First order kinetic model			LRV	Reduction, %
	k, min^{-1}	$t_{1/2}$, min	R, CFU/mL min		
E. coli in IsoT	0.248	2.79	1.97E+05	5.90	99.999
E. coli in WM	0.132	5.25	9.44E+04	3.73	99.9
E. coli and HA	0.0672	10.3	7.26E+04	1.45	90
E. coli in "HA and WM"	0.0488	14.2	3.22E+04	1.08	90

TiO_2 solar photocatalytic treatment of *E. coli* in IsoT solution showed the highest bacteria reduction percentage among other media as 99.999 %. Besides the combined effect of mechanistic stress factors as light and stirring, the addition of TiO_2 into the system provided higher LRV than *E. coli* in IsoT solution under photolytic conditions. The presence of TiO_2 particles caused external ROS formation and increased the detrimental effect of formed internal ROS.

TiO_2 solar photocatalytic treatment of *E. coli* in WM solution displayed comparatively lower percentage reduction than *E. coli* in IsoT solution. Lower bacteria reduction could be explained by the presence of common anions and cations in WM solution. As mentioned before in Section 2.5, WM components as mono and multivalent common anions (Cl^-, NO_3^-, SO_4^{2-}, PO_4^{3-} and HCO_3^-) could be adsorbed onto positively charged surface sites of TiO_2 thereby reduced the inactivation rate by decreased light absorption efficiency. Furthermore, their adsorption could create a negatively charge layer on the photocatalyst which causes the repulsion between TiO_2 and negatively charged *E. coli* (Abdullah et al., 1990; Bekbolet et al., 1998; Gogniat et al., 2006; Rincón and Pulgarin, 2004; Uyguner and Bekbolet, 2009; Uyguner-Demirel et al., 2013). Moreover, these anions could also be removed by *E. coli* intake via passive transport (Rincón and Pulgarin, 2004). Adsorbed anions onto the surface of TiO_2 hinders the surface interaction and reduces bacteria inactivation rate directly. Marugan and colleagues showed that inorganic matter present in the solution could serve as nutrients for the bacteria and help to maintain their survival as well (Marugán et al., 2010).

In the presence of HA, a retardation effect was observed on *E. coli* decline expressed as a reduction of 90 % after 60 min of irradiation time. Decreased *E. coli* inactivation rate could be attributed to the presence of HA acting both as a ROS scavenger and a TiO_2 surface blocker, which could cause TiO_2 aggregation and prevent the contact of *E. coli* and photocatalyst (Birben et al., 2017a; Planchon et al., 2013). Under solution pH=6.5 conditions, HA possessed negatively charged centers due to deprotonation of carboxylic groups, TiO_2 surface was neutral due to the presence of equal number of oppositely charged sites ($pH=pH_{zpc}$) and as always *E. coli* surface was negative. As a consequence of surface interactions prevailing between HA and TiO_2, HA through reconformational changes inhibited the surface-active sites of photocatalyst which resulted in reduced surface interaction between *E. coli* cells and TiO_2 (Birben et al., 2021b). Similar findings were also presented by Marugán and colleagues (Marugán et al., 2008, 2010).

When reaction matrix changed to "HA and WM" solution, the lowest *E. coli* LRV was attained as 1.08. Combined effect of "HA and WM" resulted in decreased *E. coli* inactivation rates. These findings could be attributed to co-presence of HA and WM which played beneficial roles for bacteria as a nutrient source and increased the resistance towards photocatalysis. It could be concluded that TiO_2 expressed selectivity towards organic matrix rather than *E. coli* in matrixes containing HA (Birben et al., 2021b).

4.2.1.2. Organic matter formation and removal upon TiO_2 solar photocatalytic treatment of *E. coli* in IsoT solution. UV-vis absorption and synchronous scan fluorescence spectra of organic matter in solution were illustrated in Figures 4.26 and 4.27. A general trend of a continuously declining absorbance with respect to increasing wavelength was attained under all irradiation periods. Besides significantly similar UV absorbance changes obtained from solar photolytic treatment of *E. coli* in IsoT solution (Figure 4.2), TiO_2 solar photocatalytic treatment of *E. coli* in the same aqueous matrix displayed quite low variations in the wavelength range of λ=205-240 nm excluding the minor presence of dense aromatic domains and color forming moieties ($Color_{436}$, UV_{365} and UV_{280}) (Figure 4.26). The highest absorption was detected between the stated wavelength range at t_{irr}=60 min. A very narrow wavelength region in between λ=210-220 nm revealed the presence of organic moieties with changing absorption upon increasing irradiation periods. On the other hand, absorbances detected at $\lambda < 210$ nm were characteristic to IsoT solution present as an aqueous medium (Tong et al., 2020).

Synchronous scan fluorescence spectra of emerged organic matter displayed a specific intensity peak at λ_{emis}=280 nm (Figure 4.27) followed by a tailing was noticed. FI_{sync} recorded at λ_{emis}=280 nm expressed a consistent irradiation time dependent decreasing order. The reason of the indicated

decrease in FI_{sync} could be related to the degradation of these fluorophores upon irradiation for the specified periods during TiO_2 photocatalysis. Moreover, the presence of fluorophoric groups expressing very minor intensities at λ_{emis}≈470 nm could also be encountered. On the other hand, contrary to minor presence of $FI_{sync470}$ expressing very low intensities as 0.0857-0.695, predominant $FI_{sync280}$ displayed changes in the range of 21.8-48.5 (Figure 4.28).

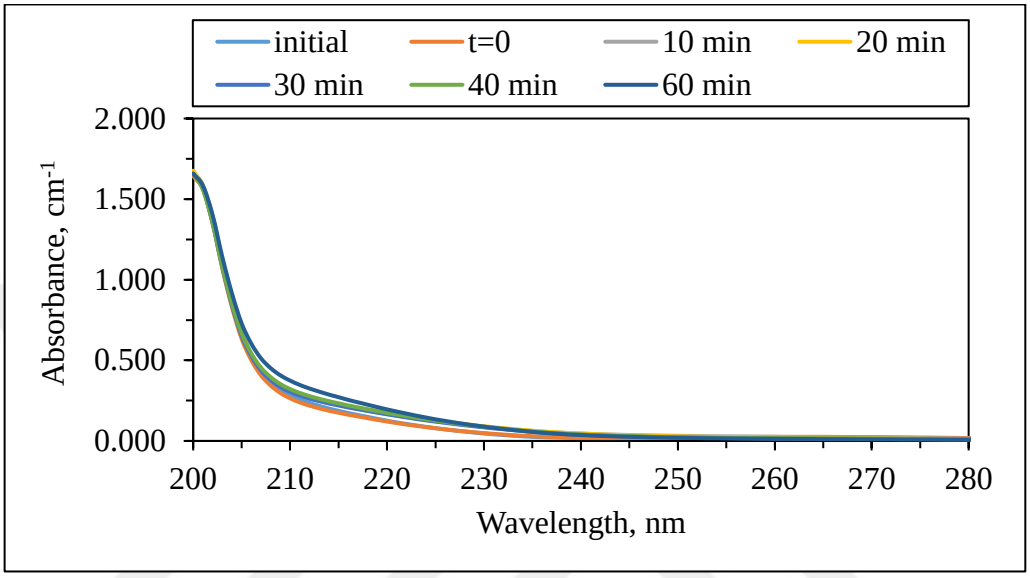

Figure 4.26. UV-vis absorption spectra of organic matter: Irradiation time dependent *E. coli* inactivation in IsoT solution upon TiO_2 solar photocatalytic treatment.

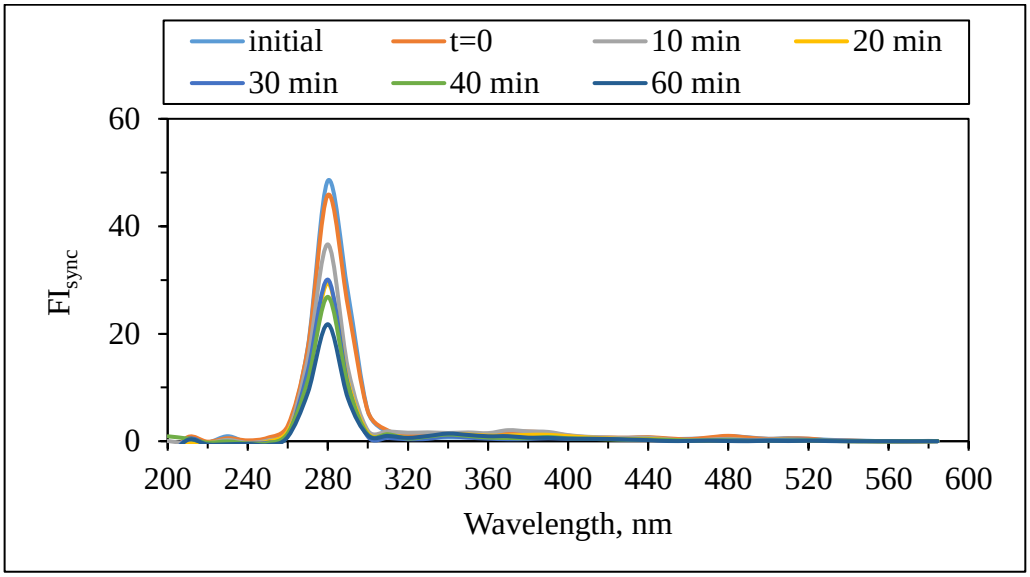

Figure 4.27. Synchronous scan fluorescence spectra of organic matter: Irradiation time dependent *E. coli* inactivation in IsoT solution upon TiO_2 solar photocatalytic treatment.

NPOC expressed variations in the range of 2.17-8.69 mg/L (Figure 4.28). NPOC content increased up to t_{irr}=20 min (2.17-8.08 mg/L) due to the release of organics from damaged and/or

destructed *E. coli* cells, followed by a sharp decrease at t_{irr}=30 min (3.35 mg/L) and again followed by an increasing trend during solar photocatalytic treatment. All UV-vis parameters displayed quite low values. The highest UV_{254} displayed variations in the range of 0.0162-0.0287 the highest for t_{irr}=10 min (0.0287) and the lowest for t_{irr}=60 min. $Color_{436}$ excluding t=0 and t_{irr}=10 min, and UV_{365} of t_{irr}=20 min and 60 min conditions were detected quite low as ≤ 0.0003 due to the non-existence and subsequent degradation of color forming moieties of the released organic matrix upon irradiation and the usage of IsoT solution as an aqueous matrix. Accordingly, $SCoA_{436}$, $SUVA_{365}$, $SUVA_{280}$, $SUVA_{254}$, $SFI_{sync470}$, and $SFI_{sync280}$ parameters were calculated and presented in Figure 4.29.

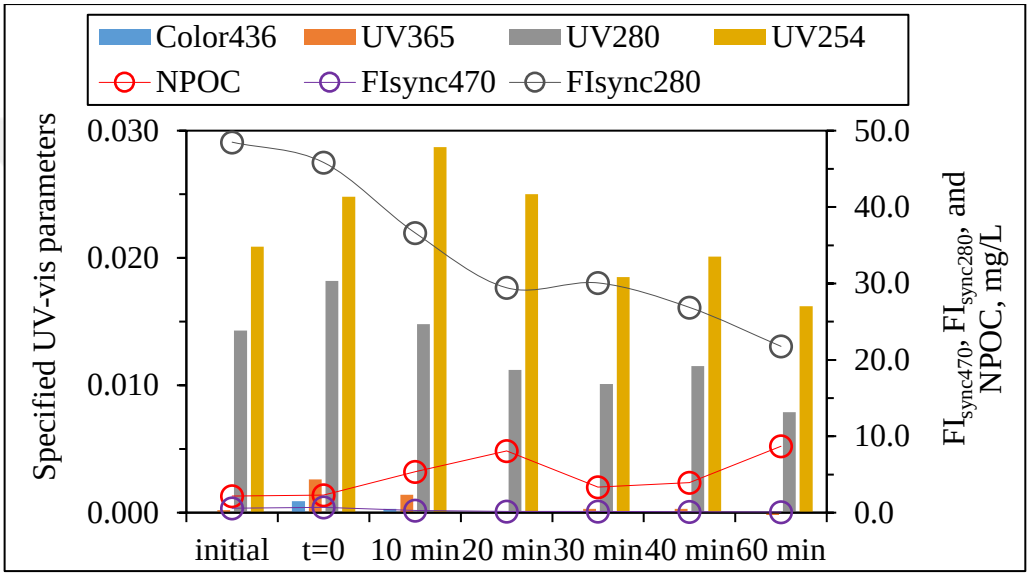

Figure 4.28. Specified UV-vis and fluroscence parameters of organic matter: Irradiation time dependent *E. coli* inactivation in IsoT solution upon TiO_2 solar photocatalytic treatment.

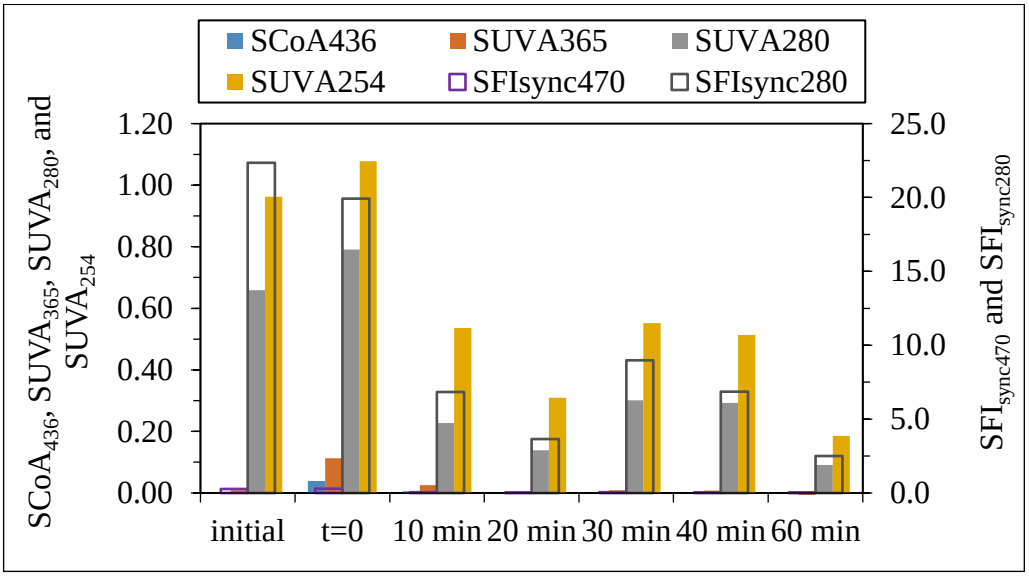

Figure 4.29. Specific UV-vis and fluroscence parameters of organic matter: Irradiation time dependent *E. coli* inactivation in IsoT solution upon TiO_2 solar photocatalytic treatment.

$SUVA_{254}$ displayed variations during TiO_2 photocatalysis in between 0.186-1.08 L/m mg, expressing differences in both UV_{254} and NPOC removals. $SUVA_{280}$ expressed noticeable presence in the range of 0.091-0.791 L/m mg being the highest for t=0 and the lowest for t_{irr}=60 min. However, due to almost insignificant presence of $Color_{436}$ and UV_{365}, calculated $SCoA_{436}$ and $SUVA_{365}$ of initial, t_{irr}=20 min, 30 min, 40 min and 60 min conditions displayed quite low presence as ≤ 0.009. Furthermore, $SFI_{sync470}$ displayed quite insignificant presence in the range of 0.010-0.302 however $SFI_{sync280}$ varied in the range of 2.51-22.3. The key fluorophoric group was accepted as $SFI_{sync280}$.

For simplicity purposes, based on the irradiation time dependent variations in UV-vis and fluorescence spectroscopic properties along with NPOC data, characteristic properties of organic matter under initial condition, upon introduction of TiO_2 (t=0) and TiO_2 solar photocatalytic treatment for irradiation period of 60 min were presented in Table 4.12.

Table 4.12. Characteristic properties of organic matter present in TiO_2 solar photocatalytic treatment of *E. coli* in IsoT solution.

Irradiation time, min	UV-vis Spectroscopic Parameters, cm^{-1}				NPOC, mg/L	$SUVA_{254}$, L/m mg	$FI_{sync280}$	$SFI_{sync280}$	FI
	$Color_{436}$	UV_{365}	UV_{280}	UV_{254}					
Initial	0.0000	0.0002	0.0143	0.0209	2.17	0.963	48.5	22.3	1.64
t=0	0.0009	0.0026	0.0182	0.0248	2.30	1.08	45.8	19.9	1.64
60 min	0.0000	0.0000	0.0079	0.0162	8.69	0.186	21.8	2.51	1.06

No remarkable difference was detected between the initial and t=0 conditions of TiO_2 solar photocatalytic treatment of *E. coli* in IsoT solution revealing insignificant surface interactions. Upon t_{irr}=60 min at which 5.90 log reduction of *E. coli* in IsoT was attained (Table 4.11), released organic matter expressed the following UV-vis parameters (cm^{-1}); UV_{280}: 0.0079, UV_{254}: 0.0162, and NPOC as 8.69 mg/L. $Color_{436}$ and UV_{365} of samples upon t_{irr}=60 min could not be noticed due to absence of color forming moieties in the structure of the organic matrix released to the aqueous medium. Quite high NPOC content at t_{irr}=60 min expressed very low $SUVA_{254}$ as 0.186 L/m mg representing that the remaining organic matter could still be expressing hydrophilic and aliphatic character (Edzwald et al., 1985). A decrease in $FI_{sync280}$ was attained due to degraded protein content of *E. coli* debris. $SFI_{sync280}$ displayed a decrease at t_{irr}=60 min in accordance with the increased NPOC content due to the released organic material from bacteria. On the other hand, under initial, t=0, and t_{irr}=60 min conditions, minor $FI_{sync470}$ were recorded as 0.593, 0.695, and 0.0857, respectively. Degraded organic content released from damaged *E. coli* caused a decrease in $FI_{sync470}$ at t_{irr}=60 min also be encountered as negligible. $SFI_{sync470}$ of initial, t=0, and t_{irr}=60 min conditions were calculated as 0.273, 0.302, and 0.010, respectively. In the absence of HA, $FI_{sync470}$ and $SFI_{sync470}$ were detected as considerably lower

than λ_{emis}=280 nm of the same parameters as expected. Insignificant presence of fluorophoric regions at λ_{emis}=470 nm indicated that the organic matrix was mainly composed of aromatic moieties that were attributed to the presence of aromatic amino acids as further evidenced by EEM fluorescence contour plots (Figure 4.30). Although reaction matrix did not contain any humic matter, FI of t_{irr}=60 min was calculated as 1.06. This very low FI might specify the fluorophores present in the remaining organic matter due to complete reduction of bacteria under the specified conditions.

Irradiation time dependent EEM fluorescence contour plots of organic matter emerged and removed during *E. coli* inactivation in IsoT solution by TiO_2 solar photocatalytic treatment were displayed in Figure 4.30.

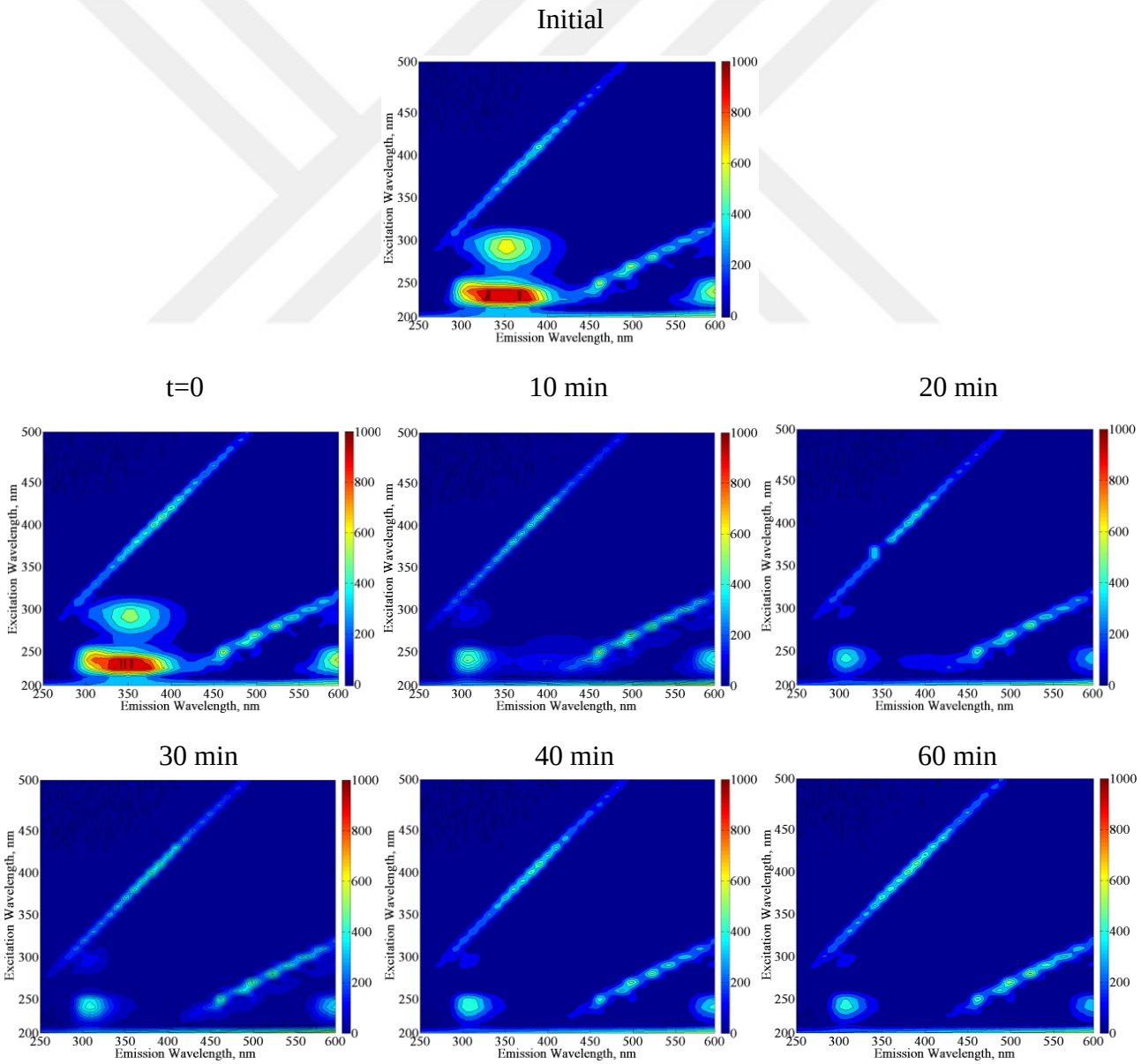

Figure 4.30. EEM fluorescence contour plots of organic matter: Irradiation time dependent *E. coli* inactivation in IsoT solution upon TiO_2 solar photocatalytic treatment.

EEM fluorescence contour plots displayed the presence of Regions I, II and IV indicating that the fluorophores were mainly originated from microbial by-products and proteins under all irradiation conditions. Throughout the irradiation periods, released microbial by-products and proteins from *E. coli* cells showed a decreasing trend in accordance with the solar photocatalytic degradation of released organic matter and reduction of *E. coli*. Moreover, different from the solar photolytic treatment of *E. coli* in IsoT solution (Figure 4.6), fluorescence intensities were detected as lower than photolytic process.

4.2.1.3. Mechanistic evaluation of *E. coli* inactivation upon TiO_2 solar photocatalytic treatment in IsoT solution. Upon irradiation, as inactivation products of TiO_2 solar photocatalytic treatment of *E. coli* in IsoT solution, total K, protein, and carbohydrate contents present in initial, t=0, and t_{irr}=60 min samples were presented in Table 4.13.

Table 4.13. Total K, protein, and carbohydrate contents of time dependent *E. coli* inactivation in IsoT solution upon TiO_2 solar photocatalytic treatment.

TiO_2 solar photocatalytic treatment	*E. coli* in IsoT solution		
	Initial	t=0	60 min
Total K, mg/L	1.76	0.91	0.96
Protein, mg/L	3.06	2.83	4.20
Carbohydrate, mg/L	0.891	1.19	1.61

Total K content showed an immediate adsorptive removal at t=0, as 48 %; and displayed almost no difference till the end of 60 min irradiation period. Stable total K content between t=0 and t_{irr}=60 min conditions could be due to both by adsorption of released K^+ ions onto oppositely charged ruptured *E. coli* cell wall particles and/or onto the negatively charged sites of TiO_2 particles.

Initial protein content of *E. coli* in IsoT solution was determined as 3.06 mg/L. Zhang and colleagues reported that flagellar assembly of *E. coli* did not detach during photocatalytic process (Zhang et al., 2019). Even if it was not possible to fully detach flagellar assembly with solar photocatalytic treatment, adsorbed TiO_2 particles onto flagella, fimbriae or pili could cause splitting of these structures, which could be the cause of high initial protein concentrations. At the end of t_{irr}=60 min treatment period, both protein and carbohydrate contents displayed increasing trends. Protein contents were plotted against $FI_{sync280}$ and NPOC data in order to detect if there could be any relationship between these parameters, and strong correlations were detected as R^2=0.94 and R^2=0.97,

respectively. Furthermore, a strong correlation was detected as R^2=0.84 when carbohydrate contents plotted against NPOC data.

4.2.1.4. Organic matter formation and removal upon TiO_2 solar photocatalytic treatment of *E. coli* in WM solution. UV-vis absorption and synchronous scan fluorescence spectra of organic matter in WM solution were illustrated in Figures 4.31 and 4.32. Although humic-like trend was observed under all irradiation periods, UV absorption was completely diminished at λ > 250 nm. Irradiation time dependent absorbance changes were significantly similar to each other in UV wavelength range of λ=205-260 nm lacking the dominant presence of aromatic domains and color forming moieties ($Color_{436}$, UV_{365} and UV_{280}) that should be evident at longer wavelengths. On the other hand, absorbances detected at λ < 210 nm were characteristic to NO_3^- which was a component of WM solution (Krishnan and Guha, 1934; Edwards at el., 2001).

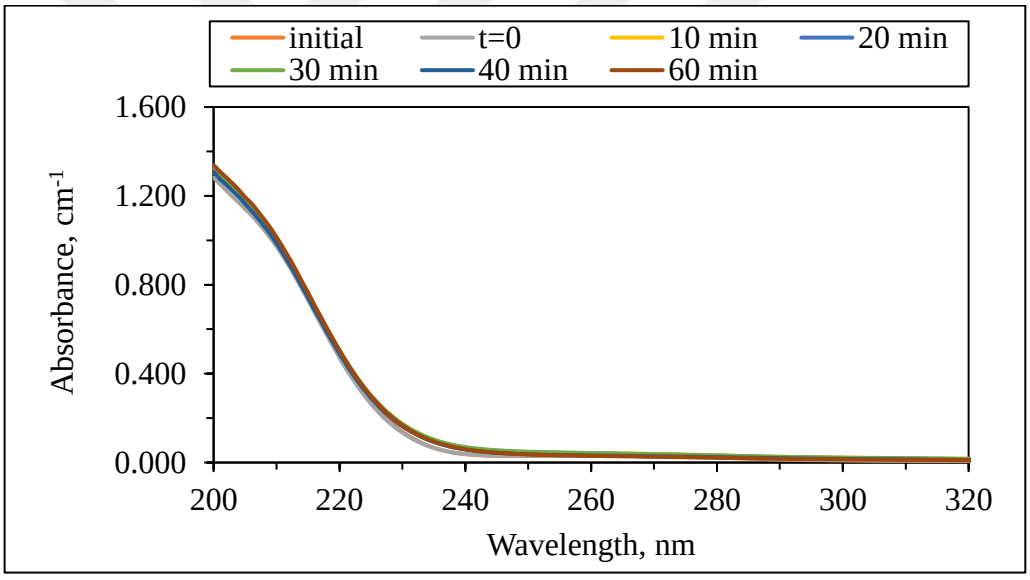

Figure 4.31. UV-vis absorption spectra of organic matter: Irradiation time dependent *E. coli* inactivation in WM solution upon TiO_2 solar photocatalytic treatment.

Synchronous scan fluorescence spectra of emerged organic matter displayed an intense peak at λ_{emis}=280 nm (Figure 4.32). An irradiation time dependent decreasing order in $FI_{sync280}$ data was observed up to t_{irr}=40 min (40.8-15.9) and intensity showed a slight increase at t_{irr}=60 min (19.1) of solar photocatalytic treatment indicating that degraded fluorophores could be reemerged during specified irradiation period. Contrary to the synchronous scan fluorescence spectra attained in IsoT solution (Figure 4.27), the presence of fluorophores was evident at λ_{emis} > 320 nm displaying a tailing effect rather than a well-defined peak. In the absence of humic matter in the solution matrix, insignificant $FI_{sync470}$ varying in between 0.206-2.98 were detected originating from released organics

from damaged *E. coli* cells. However, predominant $FI_{sync280}$ expressed changes in the range of 19.1-52.2 due to released aromatic protein content from bacteria (Figure 4.33). The main fluorophoric group was accepted as $FI_{sync280}$.

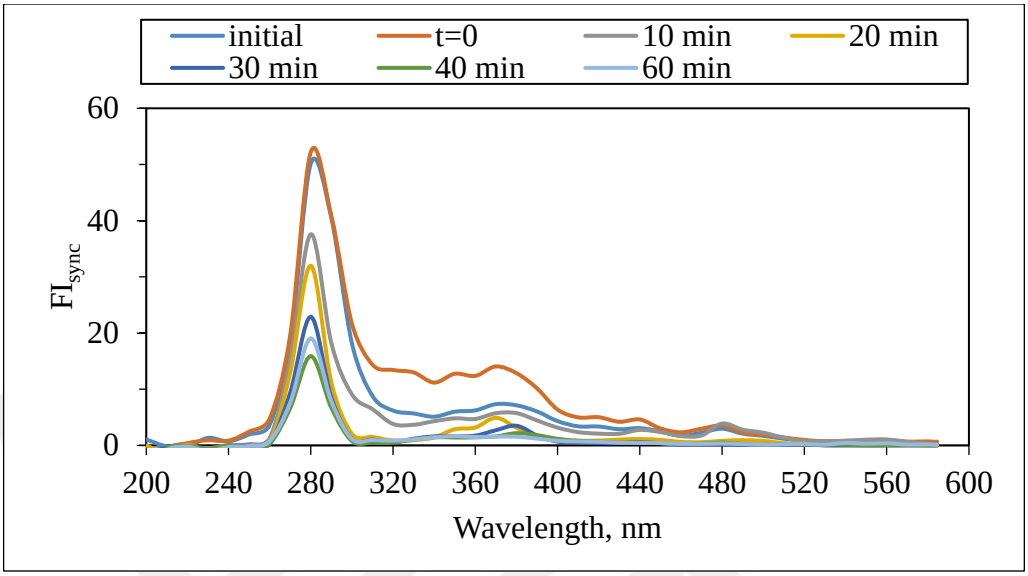

Figure 4.32. Synchronous scan fluorescence spectra of organic matter: Irradiation time dependent *E. coli* inactivation in WM solution upon TiO_2 solar photocatalytic treatment.

NPOC content increased up to t_{irr}=30 min (1.51-11.2 mg/L) with respect to *E. coli* inactivation (6.41E+05 CFU/mL for t=0; 2.50E+03 CFU/mL for t_{irr}=30 min) resulting in release of organics from damaged and destructed *E. coli* cells, followed by a sharp decrease at t_{irr}=40 min (4.99 mg/L NPOC; 5.17E+02 CFU/mL *E. coli*) and slightly increased during solar photocatalytic treatment (Figure 4.33).

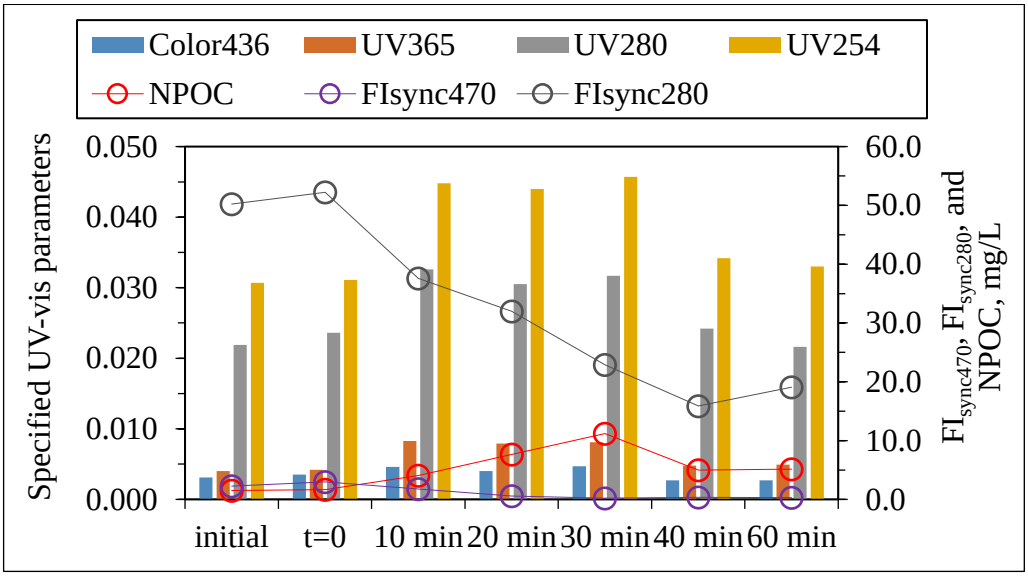

Figure 4.33. Specified UV-vis and fluroscence parameters of organic matter: Irradiation time dependent *E. coli* inactivation in WM solution upon TiO_2 solar photocatalytic treatment.

All UV-vis parameters displayed minor presence however, upon 30 min of irradiation period at which bacteria count decreased to 2.50E+03 CFU/mL (6.41E+05 CFU/mL *E. coli* for t=0) (Figure 4.25), the highest values were attained as $Color_{436}$: 0.0047, UV_{365}: 0.0081, UV_{280}: 0.0317, UV_{254}: 0.0457, and NPOC: 11.2 mg/L due to released organic matter from damaged bacteria cells. In the non-existence and subsequent degradation of color forming moieties of the released organic matter upon irradiation and the usage of WM solution, which was also a colorless solution, attained $Color_{436}$ and UV_{365} values were lower than UV_{280} and UV_{254}. Following prolonged irradiation periods, a decreasing trend could be visualized for both specified UV-vis parameters and NPOC contents.

Based on NPOC contents, $SCoA_{436}$, $SUVA_{365}$, $SUVA_{280}$, $SUVA_{254}$, $SFI_{sync470}$, and $SFI_{sync280}$ parameters were calculated and presented in Figure 4.34. As the most significant parameter, $SUVA_{254}$ displayed variations in the range of 0.408-2.03 L/m mg being the lowest for t_{irr}=30 min and the highest for initial conditions during TiO_2 solar photocatalytic treatment indicating differences in both UV_{254} and NPOC removals. Moreover, $SUVA_{280}$ was recognized as the second significant specific UV-vis parameter varied in the range of 0.283-1.45 L/m mg being the lowest for t_{irr}=30 min and the highest for initial conditions.

Furthermore, besides very low presence of $SFI_{sync470}$ changing in between 0.0184-1.78, $SFI_{sync280}$ showed significant existence varying in the range of 2.05-33.2. As expected quite low $SFI_{sync470}$ were calculated in accordance with almost insignificant $FI_{sync470}$ it could be most probably due to absence of humic matter as a solution matrix component.

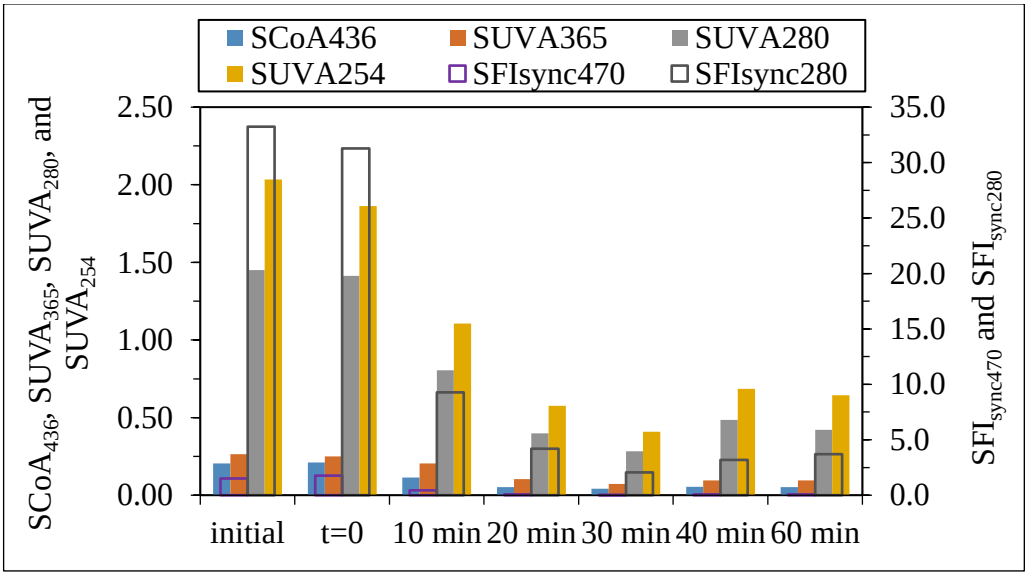

Figure 4.34. Specific UV-vis and fluroscence parameters of organic matter: Irradiation time dependent *E. coli* inactivation in WM solution upon TiO_2 solar photocatalytic treatment.

For comparison purposes, characteristic properties of organic matter under initial condition, upon introduction of TiO_2 (t=0) and at t_{irr}=60 min of TiO_2 solar photocatalytic inactivation of *E. coli* in WM solution medium were presented in Table 4.14.

Table 4.14. Characteristic properties of organic matter present in TiO_2 solar photocatalytic treatment of *E. coli* in WM solution.

Irradiation time, min	UV-vis Spectroscopic Parameters, cm^{-1}				NPOC, mg/L	$SUVA_{254}$, L/m mg	$FI_{sync280}$	$SFI_{sync280}$	FI
	$Color_{436}$	UV_{365}	UV_{280}	UV_{254}					
Initial	0.0031	0.0040	0.0219	0.0307	1.51	2.03	50.2	33.2	1.46
t=0	0.0035	0.0042	0.0236	0.0311	1.67	1.86	52.2	31.3	1.46
60 min	0.0027	0.0049	0.0216	0.0330	5.13	0.643	19.1	3.72	1.90

Upon irradiation period of 60 min TiO_2 solar photocatalytic treatment at which 3.73 log reduction of *E. coli* in WM was attained (Table 4.11), released organic matter expressed the following UV-vis parameters (cm^{-1}); $Color_{436}$: 0.0027, UV_{365}: 0.0049, UV_{280}: 0.0216, UV_{254}: 0.0330, and NPOC as 5.13 mg/L. As expressed previously, the negligible presence of both color forming moieties and UV_{365} were evidently noticed. Similar UV-vis spectroscopic parameters were recorded for initial, t=0 and t_{irr}=60 min irradiation periods revealing insignificant surface interactions.

As presented at Figure 4.34, all specific UV-vis parameters expressed quite low importance. But more importantly $SUVA_{254}$, which brings an insight to composition of the samples in terms of hydrophobicity and hydrophilicity, was calculated as 0.643 L/m mg at t_{irr}=60 min represented that the remaining organic matter could still be considered as having hydrophilic and aliphatic character (Edzwald et al., 1985).

$FI_{sync280}$ decreased to 19.1 after 60 min of irradiation period (50.2 for initial) as a result of degraded protein content. $SFI_{sync280}$ also displayed a decrease at t_{irr}=60 min in accordance with the increased NPOC due to the released organic material from decaying bacteria cells. Although an inconsistent trend was attained (Figure 4.33), $FI_{sync470}$ were quite insignificant as 2.27, 2.98, and 0.289 for initial, t=0, and t_{irr}=60 min conditions, respectively. Due to the degradation of released organic content from damaged *E. coli* cells, $FI_{sync470}$ decreased at t_{irr}=60 min as expected. $SFI_{sync470}$ values of initial, t=0, and t_{irr}=60 min conditions were calculated as 1.50, 1.78, and 0.0563, respectively.

On the other hand, FI value calculated under t_{irr}=60 min period was 1.90 most probably due to the presence of microbially derived organic material due to the prevailing destructive reaction conditions.

In a similar manner to the UV-vis absorbance and synchronous scan fluorescence analyses, EEM fluorescence contour plots of organic matter emerged and removed during irradiation time dependent *E. coli* inactivation in WM solution upon TiO_2 solar photocatalytic treatment were also followed and displayed in Figure 4.35.

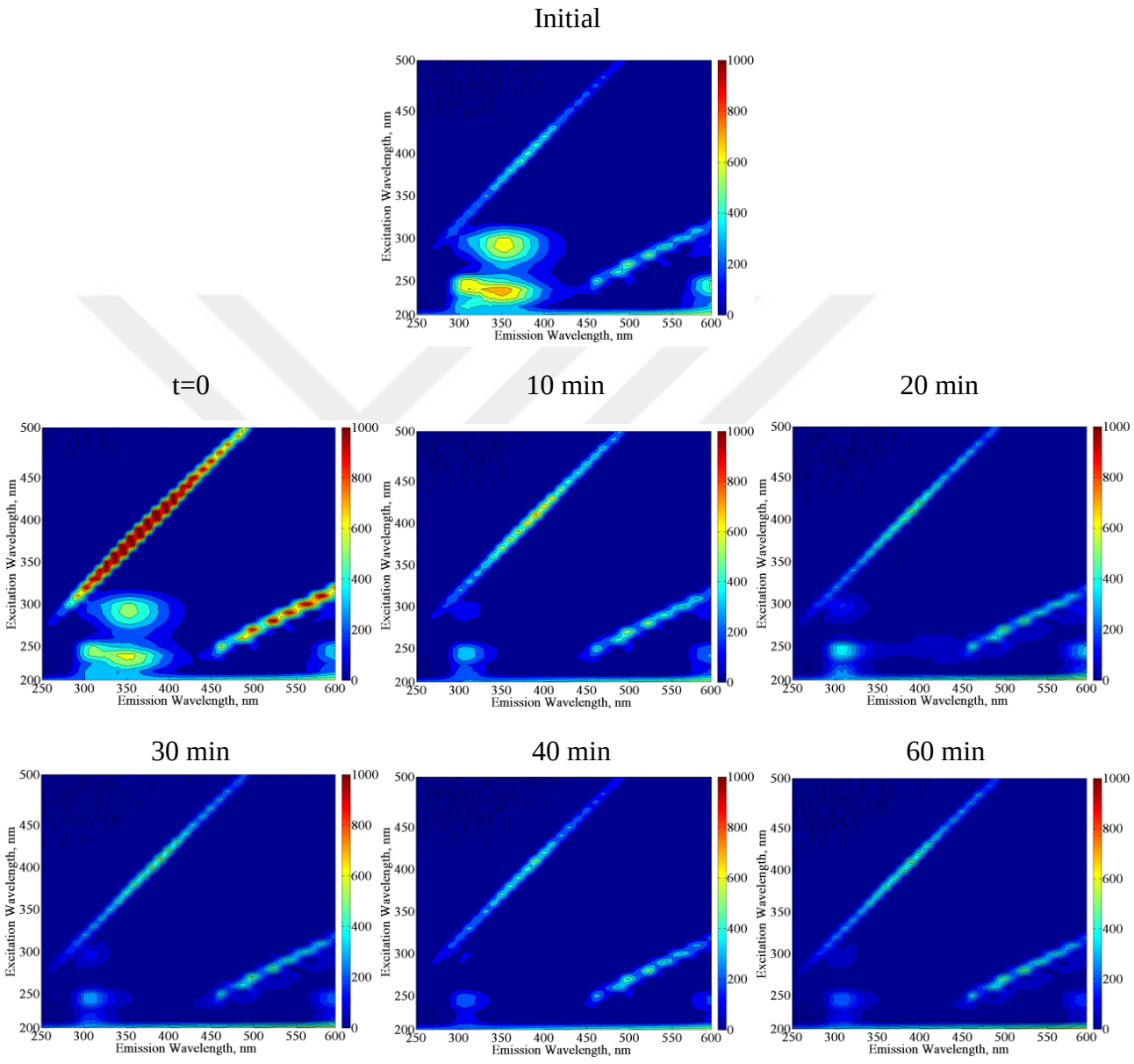

Figure 4.35. EEM fluorescence contour plots of organic matter: Irradiation time dependent *E. coli* inactivation in WM solution upon TiO_2 solar photocatalytic treatment.

EEM fluorescence counter plots displayed the presence of Regions I, II and IV expressing that the fluorophores were mainly originated from microbial by-products and proteins under all conditions in a decreasing manner with respect to increasing exposure to irradiation. Moreover, contrary to the solar photolytic (Figure 4.6) and TiO_2 solar photocatalytic treatment of *E. coli* in IsoT solution (Figure

4.30), regional fluorescence intensities were lower in the presence of aqueous medium composed of WM most probably due to lower UV_{254} and NPOC contents (Table 4.3, 4.12 and 4.14).

4.2.1.5. Mechanistic evaluation of *E. coli* inactivation upon TiO_2 solar photocatalytic treatment in WM solution. As inactivation products of TiO_2 solar photocatalytic treatment of *E. coli* in WM solution, total K, protein, and carbohydrate contents present in initial, t=0, and t_{irr}=60 min solutions were presented in Table 4.15.

Table 4.15. Total K, protein, and carbohydrate contents of time dependent *E. coli* inactivation in WM solution upon TiO_2 solar photocatalytic treatment.

TiO_2 solar photocatalytic treatment	*E. coli* in WM solution		
	Initial	t=0	60 min
Total K, mg/L	4.23	4.09	4.19
Protein, mg/L	0.961	0.710	8.15
Carbohydrate, mg/L	1.06	1.64	1.80

Total K content displayed a similar trend with the solar photocatalytic treatment inactivation kinetics of *E. coli* in IsoT solution (Table 4.13); at t=0, total K showed a slight adsorptive removal as 3.3 % and displayed almost no difference upon irradiation period of 60 min. Stable total K content between t=0 and t_{irr}=60 min of irradiation duration could be caused from the adsorption of released K^+ ions onto the ruptured *E. coli* cell wall particles having opposite surface charge and/or negatively charged sites of TiO_2 particles due to the preferential electrostatic interactions.

Upon TiO_2 solar photocatalytic treatment *E. coli* in WM solution, both protein and carbohydrate content expressed increased concentrations at the end of the 60 min treatment period. Dissimilar to the solar photolytic and photocatalytic treatment of *E. coli* in IsoT solution (Table 4.4 and 4.13), protein concentration showed a drastic increase after 60 min of irradiation (0.961 mg/L for initial; 8.15 mg/L for t_{irr}=60 min). Significantly increased protein content after 60 min of irradiation period was also detected in solar photolytic treatment of *E. coli* in WM solution (Table 4.6). Carbohydrate content did not display a significant increase at t_{irr}=60 min similar to IsoT solution condition (Table 4.13). However, it could be indicated that upon t_{irr}=60 min in IsoT and WM solutions, attained carbohydrate contents with the use of TiO_2 were higher than the ones obtained from solar photolytic treatment sets (Tables 4.4, 4.6 and 4.13). A strong correlation was detected as R^2=1.00 between protein and $FI_{sync280}$ as well as between protein and NPOC data. Carbohydrate contents were also plotted against NPOC and a moderate correlation was obtained as R^2=0.50.

4.2.1.6. Organic matter formation and removal upon TiO_2 solar photocatalytic treatment of *E. coli* in HA solution. UV-vis absorption (Figure 4.36) and synchronous scan fluorescence (Figure 4.37) spectral features of organic matter in reaction medium were presented. It should be noted that the absorbance of HA_i could be visualized as following a rather different trend in $\lambda < 235$ nm region as expected. Since sample designated as "initial" represented "HA and *E. coli*" solution followed by 0.45 μm filtration, organic matter exudates from *E. coli* would also be encountered in the UV-vis spectra. Upon introduction of TiO_2 (t=0) into the solution, absorbances displayed an increase especially between wavelength range of λ=215 nm and 385 nm. The reason could be attributed to mechanistic effect of TiO_2 on *E. coli* cell wall, TiO_2 particles adsorbed on bacteria cells could cause cell wall damage and consequently release of cytoplasmic organic content to the reaction medium that could be resulting in increased UV light absorption.

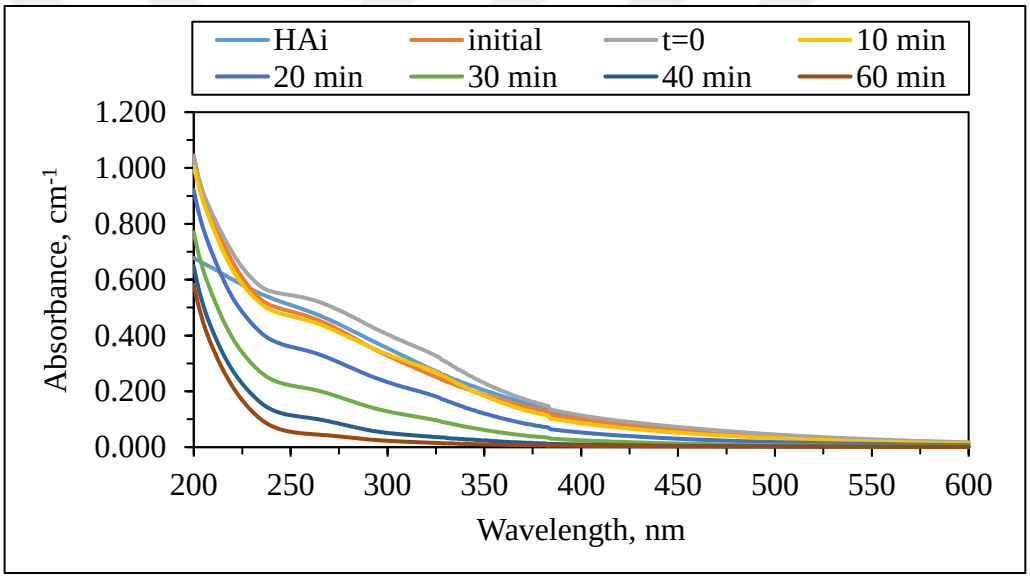

Figure 4.36. UV-vis absorption spectra of organic matter: Irradiation time dependent *E. coli* inactivation in HA solution upon TiO_2 solar photocatalytic treatment.

Irradiation time dependent absorbance changes were significantly different from each other in UV wavelength range of λ=200-500 nm due to the presence of aromatic domains and color forming moieties ($Color_{436}$, UV_{365} and UV_{280}) originating mainly from the structural properties of HA present either as remaining unreacted sub-fractions or degraded under irradiation via oxidation reactions, and also originating from the organic matter released by destructed *E. coli* cells via photocatalysis. Due to overlapping absorbance behavior, no discrimination would be assessed in between the compositional variations. On the other hand, as different from solar photolytic treatment of *E. coli* in HA solution (Figure 4.12), irradiation time dependent sequential degradation of organic matter was achieved with TiO_2 solar photocatalytic treatment.

Synchronous scan fluorescence spectra of emerged organic matter displayed a high intensity peak at λ_{emis}=370 nm and two minor peaks at λ_{emis}=440 nm and 480 nm indicating the presence of aromatic domains (Dujmov and Sučević, 1990) (Figure 4.37). However, HA_i and initial conditions displayed a rather different trend. After the introduction of TiO_2 into the solution (t=0), a drastic increase in fluorescence intensities was detected. The reason could be attributed to immediate interaction of photocatalyst with HA and *E. coli* cell surface, which could cause a mechanistic harm to bacteria via cell wall damage or degrade some EPS onto the cell wall. Moreover, released extracellular and/or intracellular organic matter from bacteria via mechanistic action of TiO_2 could behave like "in-situ generated humic-like matter" and contribute to enhanced intensity peaks of aromatic domains (Uyguner-Demirel et al., 2018).

On the other hand, due to masking effect of humic fluorophores on protein fluorophores, measured intensities at λ_{emis}=280 nm were quite low. After t_{irr}=10 min, an irradiation time dependent decreasing order in FI_{sync} data was observed with a significant decrease after irradiation period of 30 min. Furthermore, $FI_{sync470}$ and $FI_{sync280}$ displayed changes in the range of 1.24-99.9 and 7.81-91.5, respectively (Figure 4.38). $FI_{sync280}$ of HA_i could not be detected however after the addition of bacteria into HA solution i.e. the "initial" condition, $FI_{sync280}$ increased to 7.81 indicating the presence of proteinaceous components in solution.

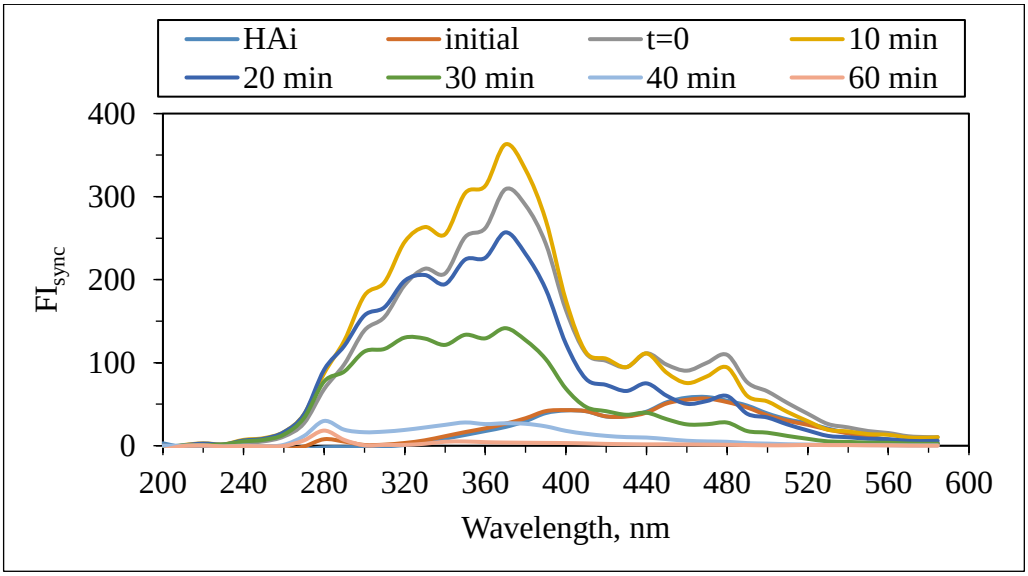

Figure 4.37. Synchronous scan fluorescence spectra of organic matter: Irradiation time dependent *E. coli* inactivation in HA solution upon TiO_2 solar photocatalytic treatment.

Along with the presence of HA solution, NPOC expressed considerable variations in the range of 4.78-20.9 mg/L (Figure 4.38). NPOC of sole HA solution (HA_i) and HA together with *E. coli*

(initial) was measured as 4.78 and 7.95 mg/L, respectively. After the introduction of bacteria, increased NPOC content was detected which could be due to mainly EPS of *E. coli*. At t=0 condition with the addition of TiO_2 into reaction medium, NPOC displayed a slight decrease as 6.59 mg/L. NPOC content increased from t_{irr}=10 min to 20 min (8.46-20.9 mg/L) due to the release of organics from damaged and/or destructed *E. coli* cells and along with the degradation of released cytoplasmic organic content from bacteria decreased at t_{irr}=30 min (13.2 mg/L), and showed another slight increase between t_{irr}=30 min and 40 min (15.2 mg/L), followed by a decreasing trend during solar photocatalytic treatment (5.68 mg/L).

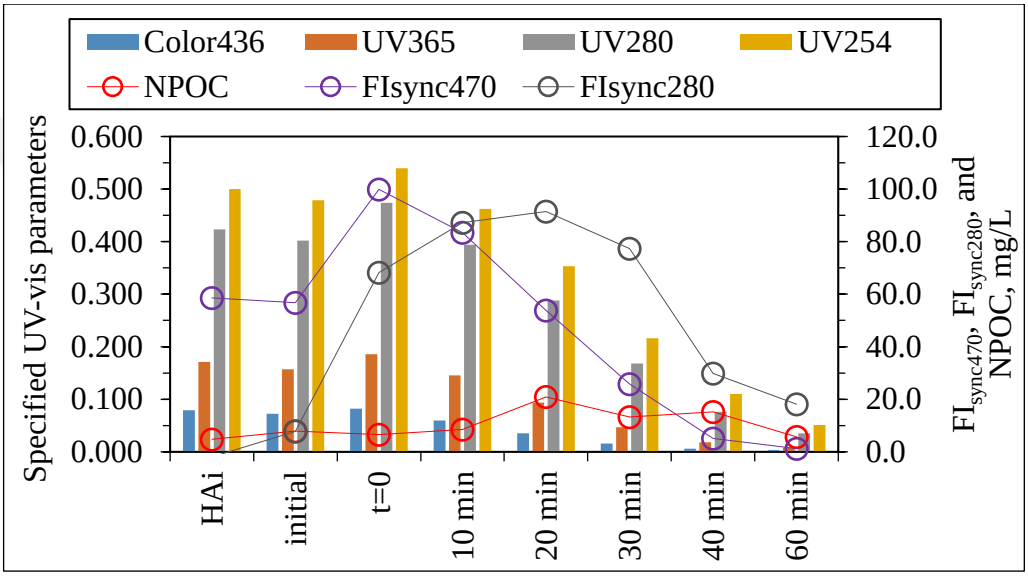

Figure 4.38. Specified UV-vis and fluroscence parameters of organic matter: Irradiation time dependent *E. coli* inactivation in HA solution upon TiO_2 solar photocatalytic treatment.

All UV-vis parameters expressed high presence due to the use of HA solution as a reaction medium (Figure 4.38). After t=0 condition, all specified UV-vis parameters followed a sequential decrease in comparison to solar photolytic treatment of *E. coli* in HA solution (Figure 4.14), which indicates the effectiveness of TiO_2 onto degradation of organic content in the solution. As the most significant parameter, UV_{254} showed changes in the range of 0.0509-0.5397, being the highest for t=0 condition and the lowest for t_{irr}=60 min condition. Moreover, at t_{irr}=60 min $Color_{436}$ was measured as 0.0033 due to subsequent degradation of color forming moieties originating from humic matter and released cytoplasmic organic content of bacteria.

Based on NPOC contents, $SCoA_{436}$, $SUVA_{365}$, $SUVA_{280}$, $SUVA_{254}$, $SFI_{sync470}$, and $SFI_{sync280}$ parameters were calculated and presented in Figure 4.39. $SUVA_{254}$ displayed variations in between 0.722-10.5 L/m mg during TiO_2 solar photocatalytic treatment showing differences in both UV_{254} and

NPOC removals. On the other hand, due to almost insignificant presence of $Color_{436}$ (0.0033) and UV_{365} (0.0081) at t_{irr}=60 min (Figure 4.38), calculated $SCoA_{436}$ and $SUVA_{365}$ displayed quite low presence as 0.039 and 0.118 L/m mg, respectively.

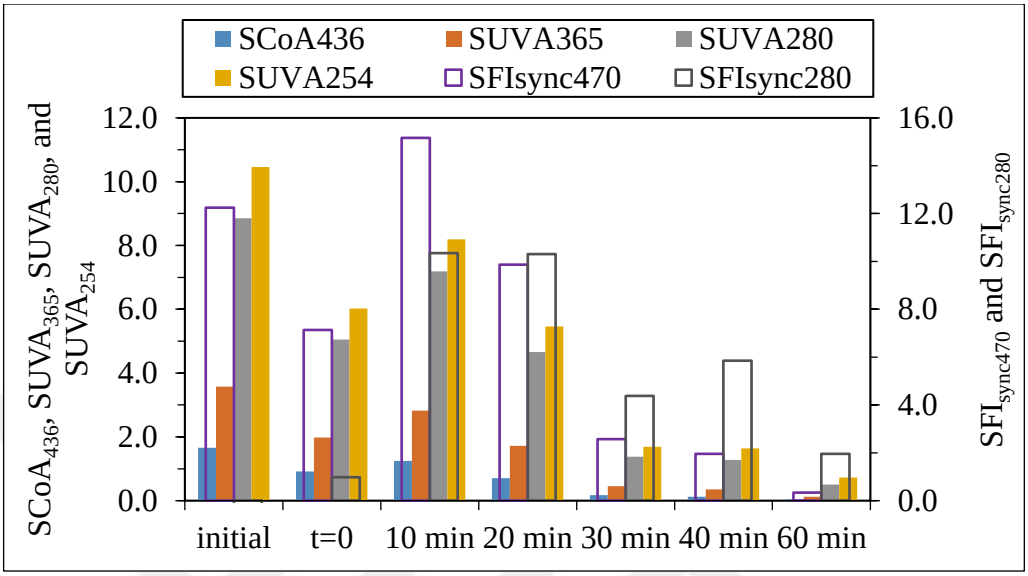

Figure 4.39. Specific UV-vis and fluroscence parameters of organic matter: Irradiation time dependent *E. coli* inactivation in HA solution upon TiO_2 solar photocatalytic treatment.

Furthermore, $SFI_{sync470}$ and $SFI_{sync280}$ expressed variations in the range of 0.337-15.2 and 0.982-10.3, respectively. In comparison to solar photolytic inactivation of *E. coli* in HA solution (Figure 4.15) relatively high $SFI_{sync280}$ values were calculated in the presence of TiO_2 as a bare photocatalyst specimen. According to undetected $FI_{sync280}$ of HA_i, $SFI_{sync280}$ could not be calculated either. Although $SFI_{sync280}$ of initial sample (0.982) and $SFI_{sync470}$ of irradiation period of 60 min condition (0.337) could be regarded as insignificant.

For comparative evaluation purposes, characteristic properties of organic matter under initial condition, upon introduction of TiO_2 (t=0) and at the end of TiO_2 solar photocatalytic inactivation of *E. coli* in HA solution for 60 min of solar light exposure were presented in Table 4.16.

Table 4.16. Characteristic properties of organic matter present in TiO_2 solar photocatalytic treatment of *E. coli* in HA solution.

Irradiation time, min	UV-vis Spectroscopic Parameters, cm^{-1}				NPOC, mg/L	$SUVA_{254}$, L/m mg	$FI_{sync470}$	$SFI_{sync470}$	FI
	$Color_{436}$	UV_{365}	UV_{280}	UV_{254}					
Initial	0.0724	0.1571	0.4017	0.4787	7.95	6.02	56.8	7.14	1.17
t=0	0.0819	0.1857	0.4738	0.5397	6.59	8.19	99.9	15.2	1.12
60 min	0.0033	0.0081	0.0351	0.0509	5.68	0.896	1.24	0.218	1.29

Upon 60 min of TiO_2 solar photocatalytic treatment of *E coli* in the presence of HA solution at which 1.45 log *E. coli* reduction was achieved (Table 4.11), released organic matter expressed the following UV-vis parameters (cm^{-1}); $Color_{436}$: 0.0033, UV_{365}: 0.0081, UV_{280}: 0.0351, UV_{254}: 0.0509, and NPOC as 5.68 mg/L. Due to degradation of both already present organic content originating from used HA solution and emerged organic matter from damaged bacteria, all specified UV-vis parameters and NPOC displayed a decrease after 60 min of irradiation period.

$SUVA_{254}$ of initial, t=0, and t_{irr}=60 min conditions were calculated as 6.02, 8.19, and 0.896 L/m mg, respectively. Edzwald and colleagues reported that $SUVA_{254} < 3$ indicates the presence of hydrophilic and aliphatic content however $SUVA_{254} > 4$ reveals the existence of hydrophobic and aromatic substances in solution (Edzwald et al., 1985). Therefore, it could be indicated that initial and t=0 solutions displayed hydrophobic and aromatic features while t_{irr}=60 min condition expressed hydrophilic and aliphatic characteristics due to degradation of aromatic organics throughout 60 min of solar photocatalytic treatment process. The use of HA solution as reaction medium caused relatively high NPOC and $SUVA_{254}$ at the beginning of the solar photocatalytic treatment (for initial and t=0 conditions) as expected.

$FI_{sync470}$ displayed a significant increase between the initial (56.8) and t=0 (99.9) conditions and decreased at t_{irr}=60 min (1.24) owing to degradation of organic content. According to recorded $FI_{sync470}$ and NPOC data, $SFI_{sync470}$ was calculated as 7.14, 15.2, and 0.218 for initial, t=0 and t_{irr}=60 min solutions, respectively. Moreover, $FI_{sync280}$ of initial, t=0 and t_{irr}=60 min conditions were recorded as 7.81, 68.2, and 18.2, respectively. Similar with $FI_{sync470,}$ $FI_{sync280}$ demonstrated a drastic increase between initial and t=0 samples, and due to degradation of released protein content resulted in a significant decrease in $FI_{sync280}$ at t_{irr}=60 min. $SFI_{sync280}$ of initial, t=0, and t_{irr}=60 min runs were calculated as 0.982, 10.3, and 1.96, respectively.

In the presence of HA, quite low $FI_{sync280}$ and $SFI_{sync280}$ values were detected in comparison with solar photolytic and photocatalytic treatment of *E. coli* in IsoT solution and WM conditions (Tables 4.3, 4.5, 4.12 and 4.14). It could be indicated that masking effect of HA on protein content could be the main cause of detected low $FI_{sync280}$ and $SFI_{sync280}$ values.

Furthermore, FI of initial, t=0, and t_{irr}=60 min conditions were calculated as 1.17, 1.12, and 1.29, respectively. According to literature, $FI \leq 1.4$ is attributed to presence of humic fluorophores (Sen-Kavurmaci and Bekbolet, 2014). All calculated FI values indicated the presence of fluorophores originating from present HA solution matrix as expected.

EEM fluorescence contour plots of organic matter emerged and removed during irradiation time dependent *E. coli* inactivation in HA solution by TiO_2 solar photocatalytic treatment were displayed in Figure 4.40.

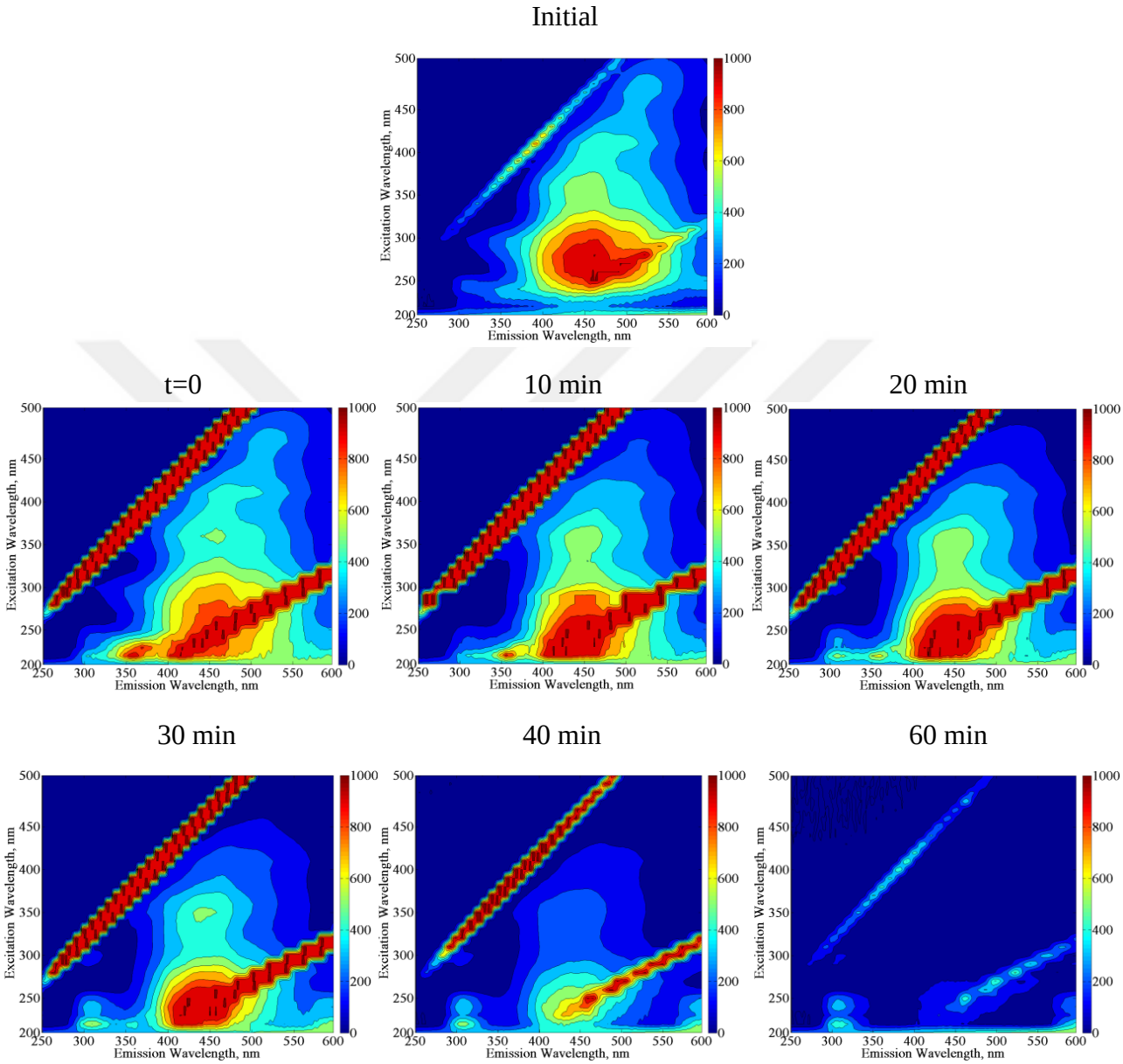

Figure 4.40. EEM fluorescence contour plots of organic matter. Irradiation time dependent *E. coli* inactivation in HA solution upon TiO_2 solar photocatalytic treatment.

EEM fluorescence contour plots displayed the presence of Regions III, and V indicating that the fluorophores were mainly originated from fulvic-like and humic-like organic fractions. Although microbial by-products and protein-like fluorophores were also still evident in solution, the presence of humic-like components might largely quenched protein-like ones (Wang et al., 2015). Following further irradiation periods, fulvic-like and humic-like fluorophores showed a decreasing trend in accordance with the solar photocatalytic degradation of HA, and reduction of *E. coli* counts.

However, alongside almost removed fluorescence intensities of Regions III, and V; Region I, which represents the presence of aromatic protein content, expressed remaining fluorescence intensities after 60 min of irradiation period. The reason could be attributed to remained high amount of *E. coli* (3.85E+04 CFU/mL) (Figure 4.25) in the solution after selected irradiation period. On the other hand, beside reduced intensities of EEM fluorescence contour plots at Regions III, and V, degradation of HA content could also be followed via UV-vis absorbance spectra (Figure 4.36), synchronous scan fluorescence spectra (Figure 4.37), NPOC contents (Figure 4.38).

4.2.1.7. Mechanistic evaluation of *E. coli* inactivation upon TiO_2 solar photocatalytic treatment in HA solution. As a result of bacteria inactivation upon TiO_2 solar photocatalytic treatment of *E. coli* in HA solution, total K, protein, and carbohydrate contents present in initial, t=0, and t_{irr}=60 min samples were presented in Table 4.17.

Table 4.17. Total K, protein, and carbohydrate contents of time dependent *E. coli* inactivation in HA solution upon TiO_2 solar photocatalytic treatment.

TiO_2 solar photocatalytic treatment	*E. coli* and HA		
	Initial	t=0	60 min
Total K, mg/L	0.53	0.49	0.66
Protein, mg/L	13.4	11.0	3.75
Carbohydrate, mg/L	2.77	2.92	2.24

Total K content showed an immediate adsorptive removal as 7.5 % along with the addition of photocatalyst into the solution (t=0) and slightly increased at t_{irr}=60 min condition expressing K^+ ion release from damaged bacteria cells. Detected low total K contents displayed similarity with solar photolytic treatment of *E. coli* in HA solution (Table 4.8), therefore it could be concluded that the presence of HA solution caused a significant inhibition of total K content detection.

Previous solar photolytic and photocatalytic treatments carried out with different solution matrixes (Tables 4.4, 4.6, 4.8, 4.10, 4.13, and 4.15) showed increased protein and carbohydrate concentrations after t_{irr}=60 min however TiO_2 solar photocatalytic treatment of *E. coli* in the presence of HA solution displayed decreasing trends for both protein (13.4-3.75 mg/L) and carbohydrate (2.77-2.24 mg/L) contents. Protein content showed a significant decrease (72 %) while carbohydrate concentration displayed almost no change (< 1 %). Both protein concentrations and $FI_{sync280}$ (Figure 4.38), and carbohydrate and NPOC contents (Table 4.16) showed no correlation with each other. On the other hand, when protein concentrations plotted against NPOC a strong correlation was obtained

as R^2=0.85. It could be indicated that decreasing trend of NPOC were related to the preferential decrease of protein content in comparison to carbohydrate content.

4.2.1.8. Organic matter formation and removal upon TiO_2 solar photocatalytic treatment of *E. coli* in "HA and WM" solution. UV-vis absorption and synchronous scan fluorescence spectra of organic matter in solution were presented in Figures 4.41 and 4.42. Irradiation time dependent absorbance changes were significantly different from each other in UV wavelength range of λ=200-400 nm due to the presence of aromatic domains and color forming moieties ($Color_{436}$, UV_{365} and UV_{280}) mainly originating from humic sub-fractions. UV-vis absorption spectra showed a drastic decrease after the introduction of photocatalyst into the reaction medium (t=0), which could be due to immediate adsorptive removal of present aromatic domains and color forming moieties via membrane filtration prior to UV-vis spectroscopic measurements. Similar to TiO_2 solar photocatalytic inactivation of *E. coli* in HA solution, irradiation time dependent sequential degradation of organic matter was achieved starting from t_{irr}=10 min (Figure 4.36). On the other hand, due to the use of NO_3^- containing WM solution as a component of aqueous reaction medium, different absorbance characteristics were observed at λ < 240 nm as expected.

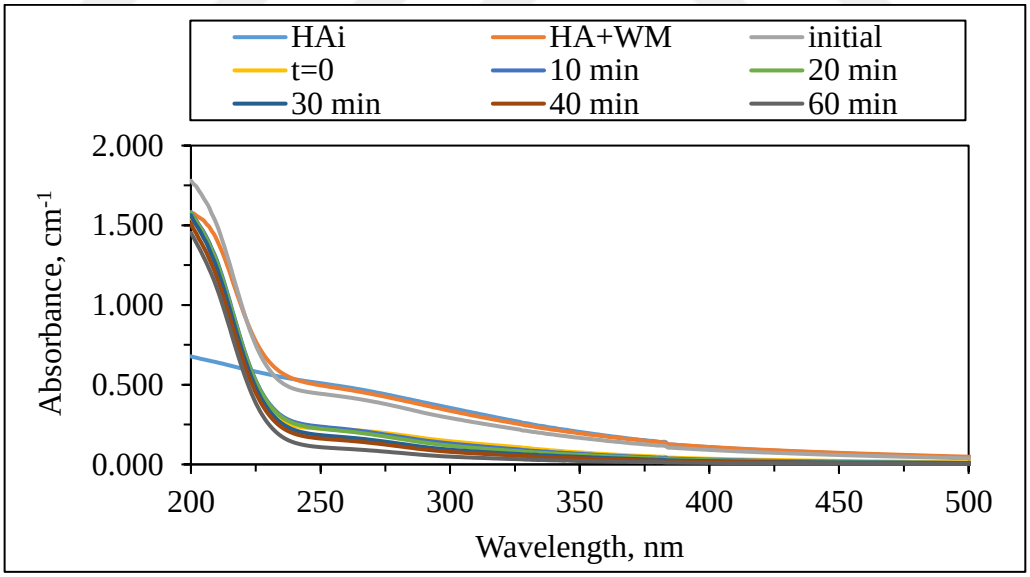

Figure 4.41. UV-vis absorption spectra of organic matter: Irradiation time dependent *E. coli* inactivation in "HA and WM" solution upon TiO_2 solar photocatalytic treatment.

Synchronous scan fluorescence spectra of emerged organic matter displayed an intensity peak at λ_{emis}=370 nm for t=0 and λ_{emis}=470 nm for HA_i, "HA and WM", initial and t_{irr}=10 min conditions (Figure 4.42). All irradiation period scans demonstrated minor peaks at λ_{emis}=280 nm, except HA_i and "HA and WM" solution. Obtained synchronous scan fluorescence spectra of HA_i was characteristic

to HA solution and in resemblance with the findings of Uyguner and Bekbolet (Uyguner and Bekbolet, 2005). Moreover, between wavelength range λ_{emis}=300-480 nm, various peaks could be visualized indicating the presence of aromatic domains in solutions (Dujmov and Sučević, 1990). The peaks obtained were in accordance with the presence and absence of the bacteria in the reaction medium. After introduction of TiO_2 into reaction solution, a significant increase in FI_{sync} data was observed, which could be originating from released cytoplasmic organic content of bacteria due to the mechanistic effect of TiO_2 on cell wall structure. From a general perspective, an irradiation time dependent decreasing order in $FI_{sync470}$ data was observed.

On the other hand, dominant $FI_{sync470}$ and comparatively low $FI_{sync280}$ displayed changes in the range of 2.78-186.3 and 4.20-63.6, respectively (Figure 4.43). $FI_{sync280}$ of HA_i could not be detected however $FI_{sync280}$ obtained in "HA and WM" solution was detected as 4.20. Along with the presence of HA solution as an aqueous matrix component, the main fluorophoric group was recognized as $FI_{sync470}$.

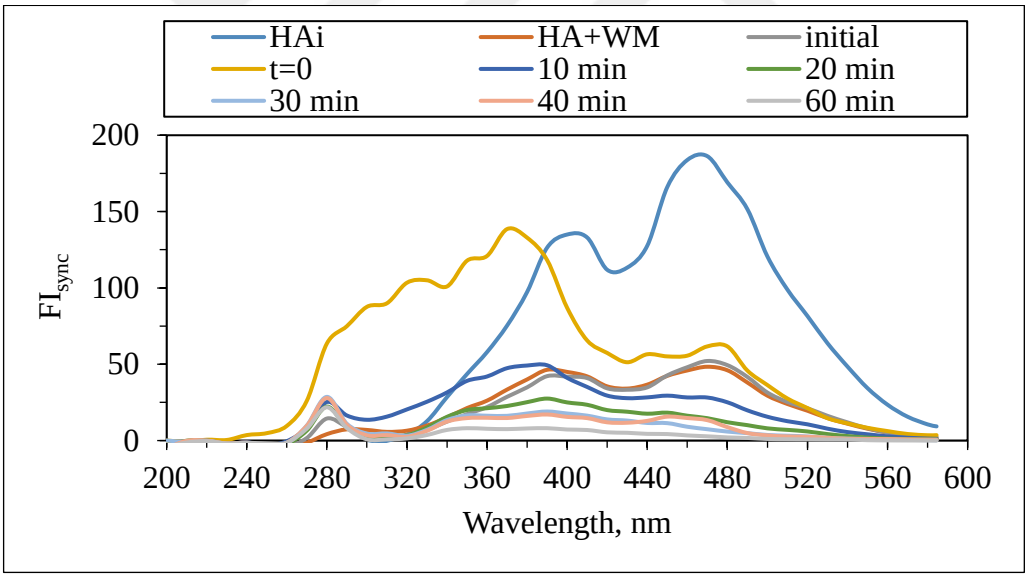

Figure 4.42. Synchronous scan fluorescence spectra of organic matter: Irradiation time dependent *E. coli* inactivation in "HA and WM" solution upon TiO_2 solar photocatalytic treatment.

NPOC expressed variations in the range of 4.78-21.5 mg/L (Figure 4.43). NPOC content slightly decreased between HA_i (4.78 mg/L) and "HA and WM" (4.38 mg/L) solution, after the addition of bacteria into the solution (initial) slightly increased (7.88 mg/L) and displayed 26.5 % immediate adsorptive removal after the addition of photocatalyst into the reaction matrix (t=0) (5.79 mg/L). At t_{irr}=10 min, NPOC showed a significant increase (16.5 mg/L) and followed by a decreasing trend up

to t_{irr}=30 min (12.3 mg/L), afterwards showed a sharp increase at t_{irr}=40 min (21.5 mg/L) and decreased until the end of solar photocatalytic treatment of 60 min (10.5 mg/L).

All UV-vis parameters expressed high presence due to the use of HA solution as a reaction medium component (Figure 4.43). Except t=0 condition, all specified UV-vis parameters followed a sequential decrease in comparison to solar photolytic treatment of *E. coli* in "HA and WM" solution (Figure 4.19). Similar to solar photocatalytic inactivation of *E. coli* in sole HA solution in the presence of TiO_2 (Figure 4.38), the use of TiO_2 expressed quite effective organic matter removal in comparison to solar photolytic treatment (Figure 4.19). As the most significant parameter, UV_{254} showed changes in the range of 0.1035-0.5000, being the highest for HA_i solution and the lowest for t_{irr}=60 min condition. According to undetected $FI_{sync280}$ of HA_i solution, its $SFI_{sync280}$ could not be calculated either.

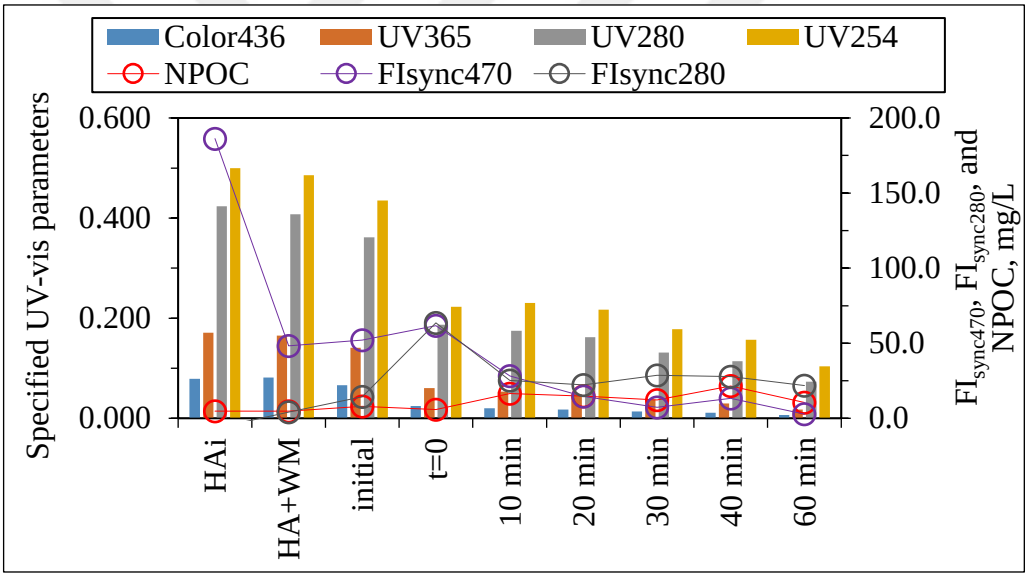

Figure 4.43. Specified UV-vis and fluroscence parameters of organic matter: Irradiation time dependent *E. coli* inactivation in "HA and WM" solution upon TiO_2 solar photocatalytic treatment.

Based on NPOC contents, all specific parameters as $SCoA_{436}$, $SUVA_{365}$, $SUVA_{280}$, $SUVA_{254}$, $SFI_{sync470}$, and $SFI_{sync280}$ were calculated and presented in Figure 4.44. As the most apparent parameter, $SUVA_{254}$ displayed variations in between 0.730-10.5 L/m mg during TiO_2 solar photocatalytic treatment expressing differences in both UV_{254} and NPOC removals. Furthermore, due to quite low presence of $Color_{436}$ (0.0069) and UV_{365} (0.0175) at t_{irr}=60 min condition (Figure 4.43), calculated $SCoA_{436}$ and $SUVA_{365}$ displayed quite low presence as 0.066 and 0.167, respectively. On the other hand, $SFI_{sync470}$ and $SFI_{sync280}$ expressed changes in the range of 0.265-39.0 and 0.871-11.0, respectively. The key fluorophoric group was recognized as $SFI_{sync470}$ in the presence of HA solution.

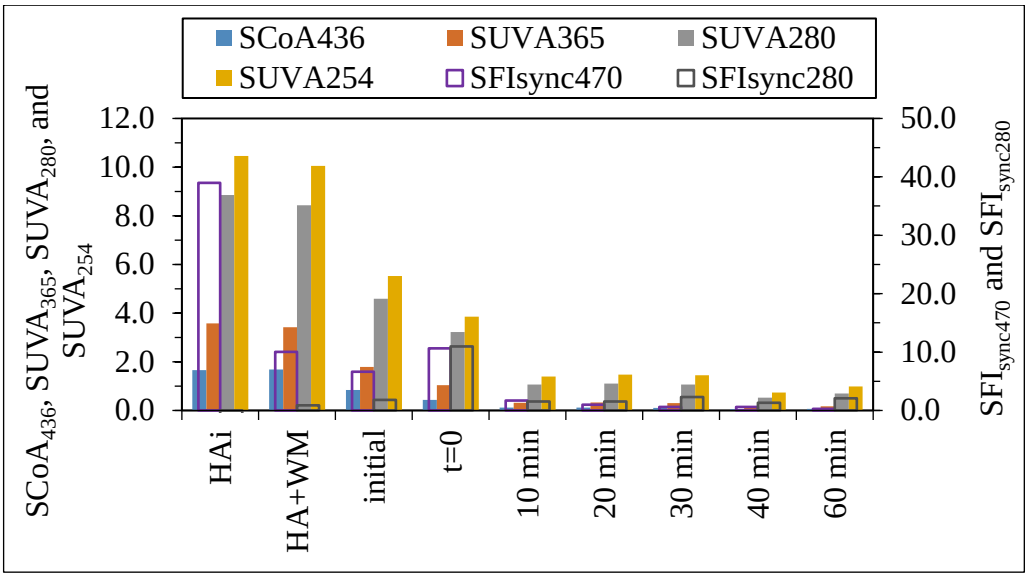

Figure 4.44. Specific UV-vis and fluroscence parameters of organic matter: Irradiation time dependent *E. coli* inactivation in "HA and WM" solution upon TiO_2 solar photocatalytic treatment.

For comparative evaluation purposes, characteristic properties of organic matter present under initial condition, upon introduction of TiO_2 (t=0) and at the end of TiO_2 solar photocatalytic inactivation of *E. coli* in "HA and WM" solution for 60 min of solar light exposure were presented in Table 4.18.

Table 4.18. Characteristic properties of organic matter present in TiO_2 solar photocatalytic treatment of *E. coli* in "HA and WM" solution.

Irradiation time, min	UV-vis Spectroscopic Parameters, cm^{-1}				NPOC, mg/L	$SUVA_{254}$, L/m mg	$FI_{sync470}$	$SFI_{sync470}$	FI
	$Color_{436}$	UV_{365}	UV_{280}	UV_{254}					
Initial	0.0664	0.1409	0.3614	0.4351	7.88	5.52	52.1	6.61	1.23
t=0	0.0248	0.0601	0.1867	0.2229	5.79	3.85	61.7	11.0	1.28
60 min	0.0069	0.0175	0.0734	0.1035	10.5	0.986	2.78	0.265	1.31

Upon irradiation period of 60 min TiO_2 solar photocatalytic treatment of *E coli* in "HA and WM" solution, 1.08 log *E. coli* reduction was achieved (Table 4.11), released organic matter expressed the following UV-vis parameters (cm^{-1}); $Color_{436}$: 0.0069, UV_{365}: 0.0175, UV_{280}: 0.0734, UV_{254}: 0.1035, and NPOC as 10.5 mg/L. $SUVA_{254}$ value at initial and t_{irr}=60 min conditions were detected as 5.52 and 0.986 L/m mg, respectively. Obtained $SUVA_{254}$ complied with the content of the solution matrix and indicate the degradation of organics at the end of 60 min irradiation period. The use of HA as solution matrix caused relatively high initial NPOC and $SUVA_{254}$ as expected. NPOC content of t_{irr}=60 min showed an increase due to HA content and released organic material from bacteria. Obtained $FI_{sync280}$ of initial, t=0 and t_{irr}=60 min solutions were detected as 14.4, 63.6, and 21.8,

respectively. $FI_{sync470}$ and $FI_{sync280}$ displayed similar patterns with treatment conducted in sole HA solution (Figure 4.38 and Table 4.16), with an increase at t=0 and a significant decreased at t_{irr}=60 min conditions. Furthermore, $SFI_{sync280}$ of initial, t=0, and t_{irr}=60 min runs were calculated as 1.83, 11.0, and 2.08, respectively. FI at t_{irr}=60 min was calculated as 1.31 indicating the presence of fluorophores originating from HA containing solution matrix as expected.

EEM fluorescence counter plots of organic matter emerged and removed during irradiation time dependent *E. coli* inactivation in "HA and WM" solution upon TiO_2 solar photocatalytic treatment were displayed in Figure 4.45.

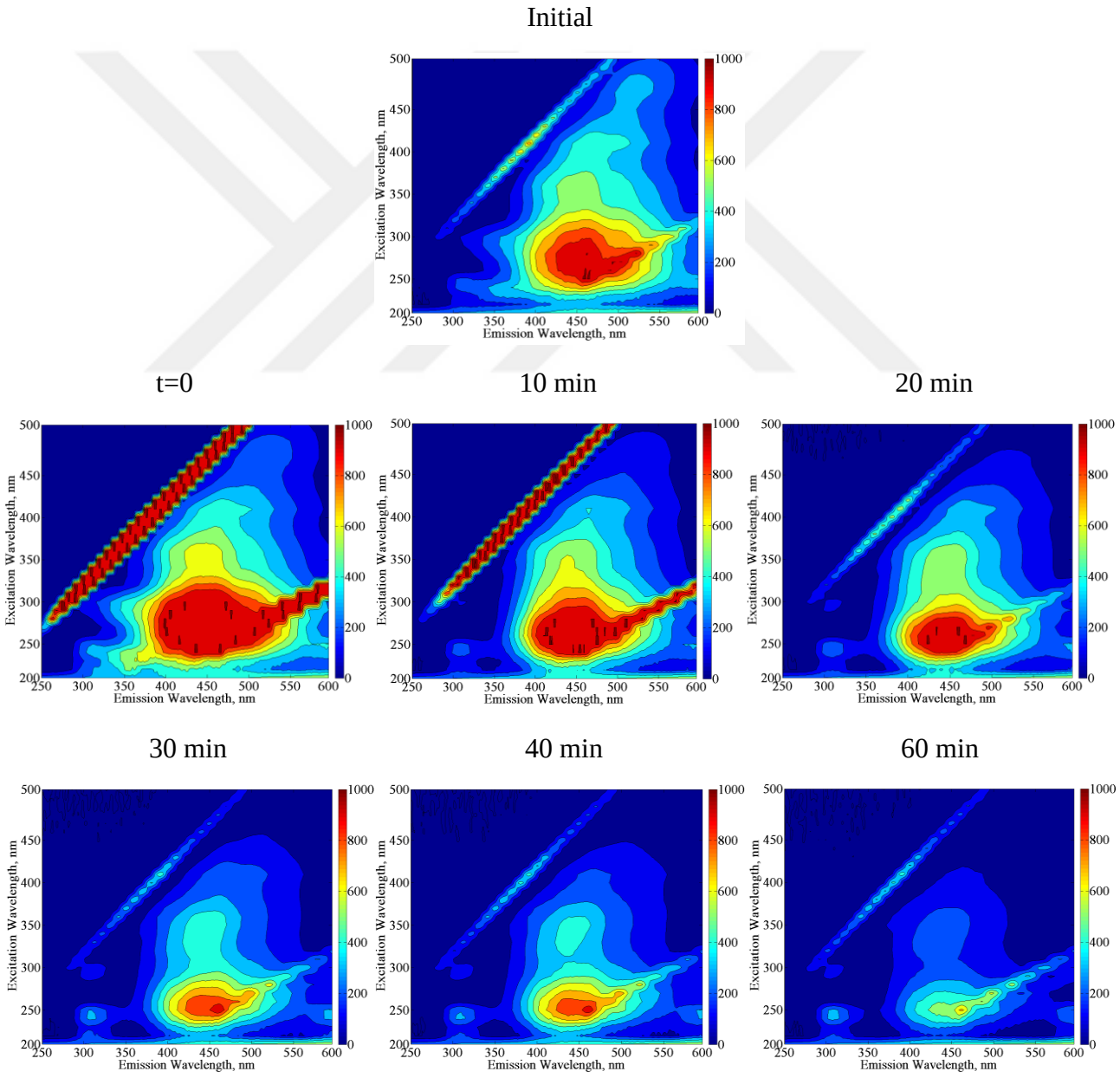

Figure 4.45. EEM fluorescence contour plots of organic matter: Irradiation time dependent *E. coli* inactivation in "HA and WM" solution upon TiO_2 solar photocatalytic treatment.

EEM fluorescence counter plots displayed the presence of Regions III, and V like solar photolytic *E. coli* inactivation in "HA and WM" solution (Figure 4.21). Presence of HA solution caused a masking effect over the Region I, II and IV owing to the quenching of the fluorophores of protein like materials by humic-like materials (Wang et al., 2015). Following further irradiation periods, fulvic-like and humic-like components of the sample showed a decreasing trend in accordance with the solar photocatalytic degradation of HA and reduction of *E. coli* (Figures 4.25 and 4.43). EEM fluorescence contour plots of *E. coli* in the presence of both HA and WM components showed similarities with solar photocatalytic *E. coli* inactivation in sole HA solution (Figure 4.40). Cell enumerations of *E. coli* in HA solution (3.85E+04 CFU/mL), and *E. coli* in "HA and WM" solution (5.55E+04 CFU/mL) after 60 min of irradiation were detected as relatively close to each other although HA contents showed differences (Table 4.16 and 4.18). Following treatment of *E. coli* in "HA and WM" solution, less HA degradation was observed than sole HA conditions which could also be followed via reduced intensities at Region III and V of EEM contour plots, UV-vis absorption spectra, and synchronous scan fluorescence spectra (Figures 4.36, 4.37 and 4.40). It could be attributed that the presence of WM solution as an experimental media content could cause the formation of WM solution dependent regional profiles in EEM fluorescence contour plots. Recorded data showed that retardation effect exerted by WM components was only perceived by HA rather than directly on *E. coli* most probably due to repulsive electrostatic forces.

4.2.1.9. Mechanistic evaluation of *E. coli* inactivation upon TiO_2 solar photocatalytic treatment in "HA and WM" solution. As inactivation products of TiO_2 solar photocatalytic treatment of *E. coli* in "HA and WM" solution, total K, protein, and carbohydrate contents present in initial, t=0, and t_{irr}=60 min samples were presented in Table 4.19.

Table 4.19. Total K, protein, and carbohydrate contents of time dependent *E. coli* inactivation in "HA and WM" solution upon TiO_2 solar photocatalytic treatment.

TiO_2 solar photocatalytic treatment	*E. coli* in "HA and WM"		
	Initial	t=0	60 min
Total K, mg/L	4.51	4.49	4.07
Protein, mg/L	13.9	7.83	5.72
Carbohydrate, mg/L	3.93	2.24	1.48

Total K content showed a slight decrease between initial and t_{irr}=60 min conditions. An insignificant adsorptive removal of total K (< 0.5 %) was attained at t=0 condition. Total K decrease at the end of 60 min irradiation period could be related to the low bacteria LRV as 1.08 (Table 4.11).

It could be indicated that, *E. coli* cells remaining intact and/or having undamaged cell walls after 60 min treatment period could not display K^+ ion release. Moreover, additional K^+ ion contents originating from WM solution, could compensate released K^+ ion content via leakage from the cells, and thereby protect bacteria from destruction via the retardation of cell wall damage.

Upon TiO_2 solar photocatalytic treatment, *E. coli* in "HA and WM" solution displayed a decrease in both protein (13.9-5.72 mg/L) and carbohydrate (3.93-1.48 mg/L) contents at the end of t_{irr}=60 min period. Similar findings were also detected from TiO_2 solar photocatalytic treatment of *E. coli* in sole HA solution (Table 4.17). Contrary to the data of *E. coli* in HA solution, NPOC increased after t_{irr}=60 min for *E. coli* in "HA and WM" solution (Tables 4.16 and 4.18). Moreover, EEM counter plots attained at t_{irr}=60 min displayed the presence of humic-like and fulvic-like fluorophores (Figure 4.45), therefore; it could be concluded that EEM counter plots and NPOC data correlated well with each other instead of protein/carbohydrate contents and NPOC. No correlation was detected either between $FI_{sync280}$ and protein contents or between NPOC and protein/carbohydrate concentrations.

4.2.1.10. Comparative evaluation of different experimental matrixes on TiO_2 solar photocatalytic inactivation mechanism of *E. coli.* As TiO_2 solar photocatalytic inactivation products, total K, protein, and carbohydrate concentrations along with bacteria enumerations in different solution matrixes were compiled from Figure 4.25, Tables 4.13, 4.15, 4.17, 4.19 and presented in Figure 4.46. Total K contents varied in between 0.49-4.51 mg/L being the lowest for t=0 sample of *E. coli* in HA solution and the highest for initial sample of *E. coli* in "HA and WM" solution. Total K content in WM solution displayed higher presence as expected due to the existence of medium constituents. No significant difference of total K contents was determined in between initial, t=0, and t_{irr}=60 min conditions upon solar photocatalysis of *E. coli* in WM, HA and "HA and WM" matrixes. Protein and carbohydrate contents of *E. coli* in IsoT solution indicated increased values at t_{irr}=60 min (4.20 mg/L protein; 1.61 mg/L carbohydrate) contrary to the decrease attained in total K content (0.96 mg/L). Furthermore, total K contents were plotted against *E. coli* cell counts in order to detect if there could be any correlation between these parameters, initial and t=0 conditions showed a strong correlation, as $R^2 > 0.83$, except the presence of IsoT solution, however t_{irr}=60 min runs displayed no correlation between these two parameters. Covering all conditions protein contents varied in between 0.710-13.9 mg/L being the lowest for t=0 sample of *E. coli* in WM solution and the highest for initial sample of *E. coli* in "HA and WM" condition. Similarly, carbohydrate contents varied in between 0.89-3.93 mg/L being the lowest for initial condition of *E. coli* in IsoT solution and the highest for initial sample of *E. coli* in "HA and WM" solution.

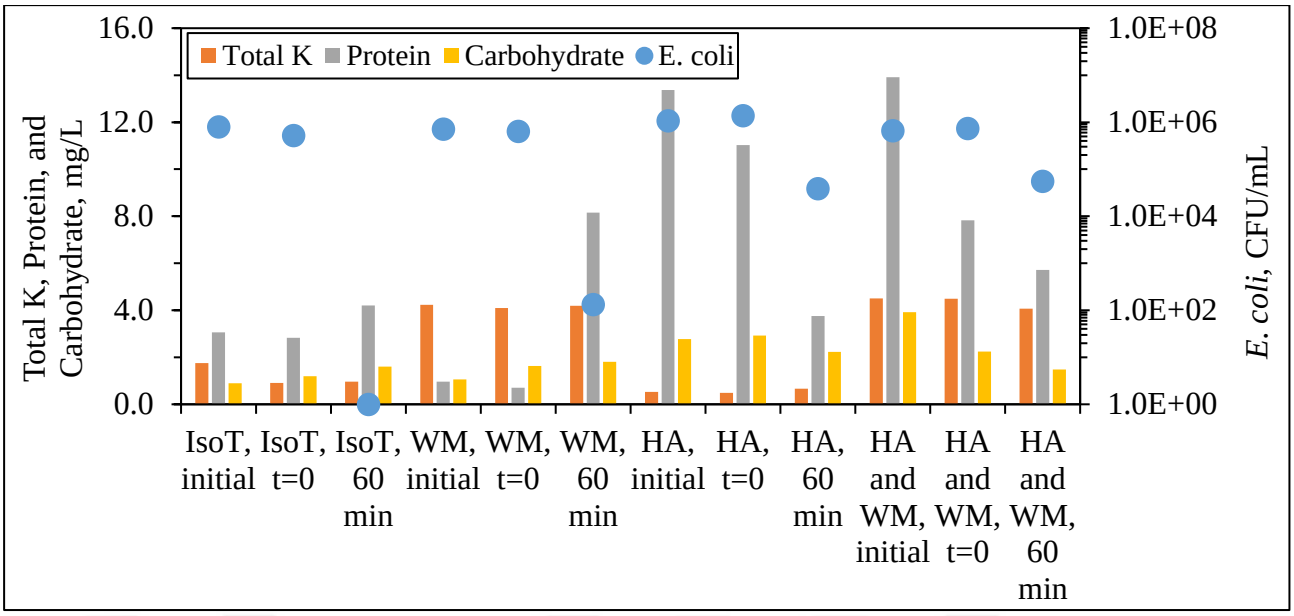

Figure 4.46. Initial, t=0, and t_{irr}=60 min total K, protein, carbohydrate contents, and bacteria enumeration results of *E. coli* inactivation upon TiO_2 solar photocatalytic treatment in various aqueous matrixes.

The highest protein concentration at t_{irr}=60 min was determined in the presence of WM components (8.15 mg/L). While protein contents of *E. coli* in WM solution initial (0.96 mg/L) and t=0 min (0.71 mg/L) conditions revealed lowest ones, at t_{irr}=60 min the highest protein release was detected. In sole IsoT solution, initial (0.89 mg/L) and t=0 (1.19 mg/L) conditions displayed lower carbohydrate contents than other experimental conditions. Contrary to the inactivation profiles in IsoT and WM solutions expressing increasing trend in both protein and carbohydrate contents after 60 min irradiation, samples containing sole HA solution displayed decreased organic matter content. It could be indicated that, the presence of HA solution caused an enhancement for both protein and carbohydrate contents of initial and t=0 conditions. *E. coli* inactivation at the end of 60 min irradiation time decreased in the presence of HA solution, and the use of sole HA solution as reaction matrix affected *E. coli* inactivation more negatively than the presence of "HA and WM" solution.

Released and degraded protein and carbohydrate contents and bacteria LRV of TiO_2 solar photocatalytic treatment of *E. coli* in different solution matrixes were given in Figure 4.47. Released protein and carbohydrate concentrations of *E. coli* in IsoT and WM conditions were calculated by subtracting initial data from the concentrations obtained at t_{irr}=60 min condition (Figure 4.47 Left). While released protein and carbohydrate concentrations of IsoT and WM matrixes could be calculated, in HA and "HA and WM" solutions, degradation of protein and carbohydrate contents should also be encountered. Released protein content was lower for *E. coli* in IsoT solution (1.14 mg/L). However, almost no difference was detected between released carbohydrate contents for both

IsoT (0.72 mg/L) and WM (0.74 mg/L) solutions. LRV of *E. coli* was inversely proportional to protein release for IsoT (5.9) and WM (3.7) matrixes. No direct correlation was detected between bacteria LRV and released protein and carbohydrate contents for *E. coli* in IsoT and WM solution conditions.

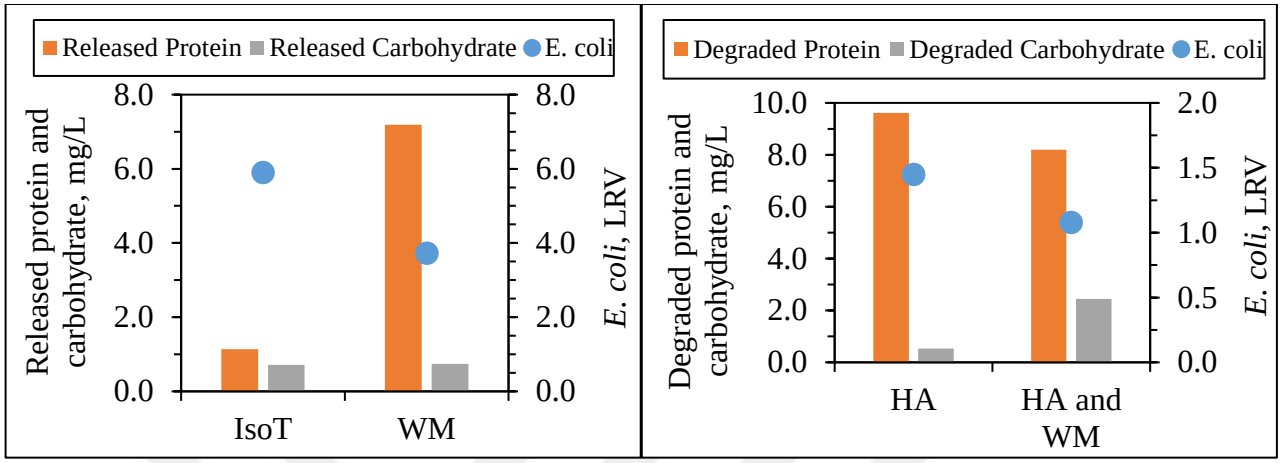

Figure 4.47. Released (Left) and degraded (Right) protein and carbohydrate contents, and bacteria LRV of *E. coli* inactivation upon TiO_2 solar photocatalytic treatment in various aqueous matrixes.

Degraded protein and degraded carbohydrate concentrations of *E. coli* in HA and "HA and WM" conditions were calculated by subtracting detected concentrations of t_{irr}=60 min conditions from initial condition data (Figure 4.47 Right). Solar photocatalytic treatments containing HA solution showed a decrease of protein and carbohydrate contents. It could be due to extra organic matter coming from HA and high bacteria survival. Due to low *E. coli* inactivation, protein and carbohydrate content arising from bacteria were inhibited, therefore it could be indicated that the protein and carbohydrate concentrations determined were mostly originating from HA content of the samples. Under photolytic conditions, there were no degradation detected for protein and carbohydrate contents (Figure 4.23), it could be attributed to the use of TiO_2 showing selectivity towards organic matrix rather than bacteria. It could be concluded that LRV of *E. coli* is directly proportional to protein degradation but inversely proportional to carbohydrate degradation.

Upon solar photocatalytic treatment of *E. coli* in different solution matrixes, the attained protein and carbohydrate contents, $FI_{sync280}$, UV_{280}, and NPOC under initial, t=0, and t_{irr}=60 min conditions were given in Figure 4.48. Protein concentrations and UV_{280} displayed an increase in the presence of HA solution, like solar photolytic treatment (Figure 4.24). Similar data were obtained for $FI_{sync280}$ of initial and t=0 conditions in IsoT and WM matrixes. The highest $FI_{sync280}$ (68.2) and UV_{280} (0.4738) were measured in HA solution upon introduction of TiO_2 (t=0) into the solution matrix. A strong correlation was detected between protein and $FI_{sync280}$ data as $R^2 > 0.81$ except for sole HA solution.

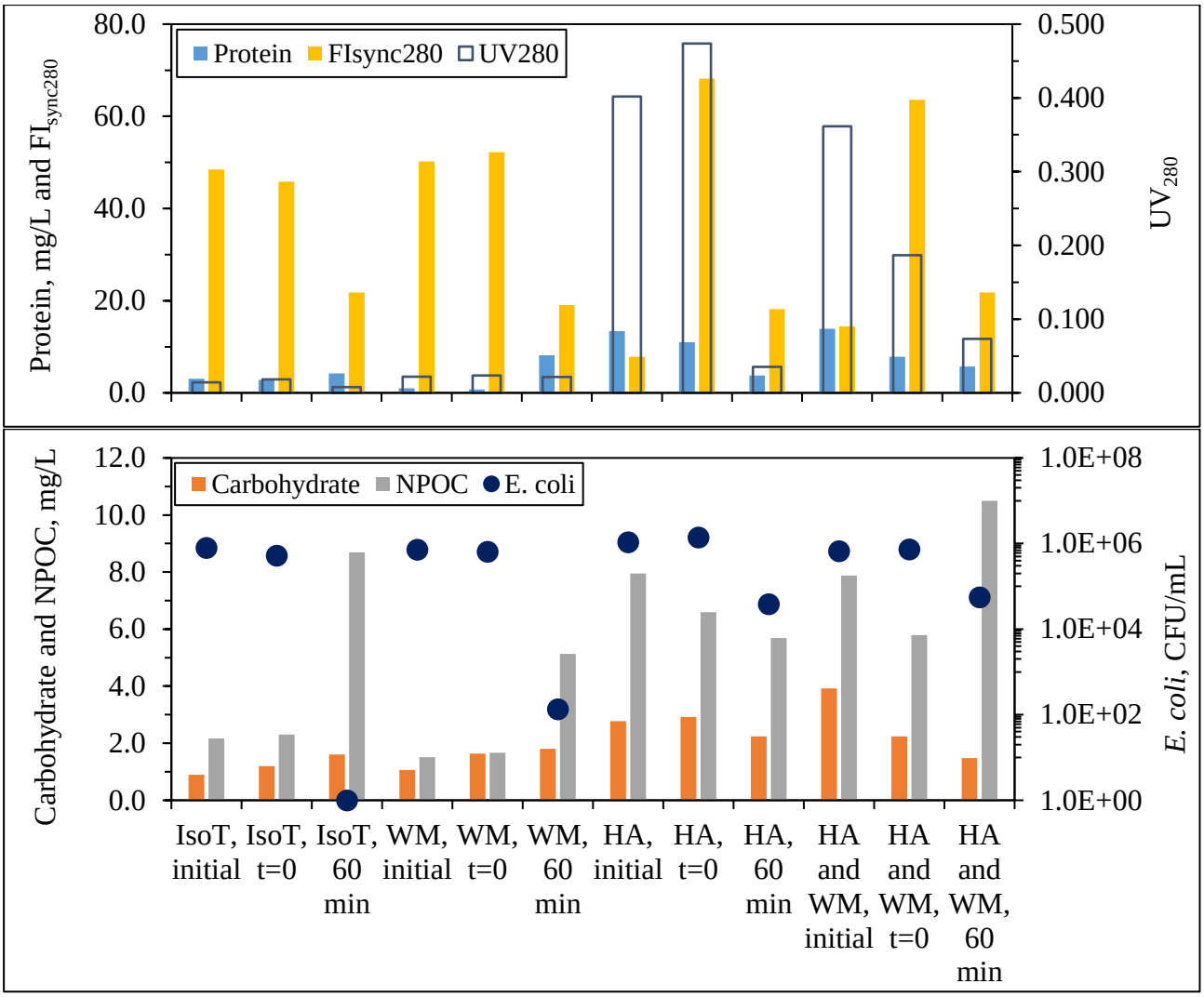

Figure 4.48. Initial, t=0, and t_{irr}=60 min protein and carbohydrate contents, $FI_{sync280}$, UV_{280}, NPOC, and bacteria enumeration results of TiO_2 solar photocatalytic treatment of *E. coli* in various aqueous matrixes.

NPOC contents were detected as higher than carbohydrate concentrations for all conditions. The highest NPOC content (10.5 mg/L) and the lowest *E. coli* inactivation efficiency (5.55E+04 CFU/mL) was obtained in case that "HA and WM" solution was used upon t_{irr}=60 min exposure. The second high NPOC was detected in IsoT solution at t_{irr}=60 min (8.69 mg/L) with complete bacteria inactivation signified by LRV as 5.90 (Table 4.11).

It could be concluded that final (t_{irr}=60 min) NPOC content of "HA and WM" solution mostly originated from HA present either as remaining unreacted and/or degraded sub-fractions under irradiation via oxidation reactions rather than *E. coli* inactivation. Moreover, a strong correlation between carbohydrate and NPOC contents as $R^2 > 0.82$ were detected, excluding the presence of sole WM solution.

4.2.2. SynTiO$_2$ Solar Photocatalytic Inactivation of *E. coli*

4.2.2.1. SynTiO$_2$ solar photocatalytic *E. coli* inactivation under specified reaction conditions, reductions, and kinetics. *E. coli* suspension (N_o=4.37E+05 CFU/mL) was prepared in IsoT solution and was subjected to solar photocatalytic treatment using SynTiO$_2$. Upon irradiation period of 30 min, *E. coli* count decreased to 1.90E+02 CFU/mL. Following light exposure of t_{irr}=60 min, complete *E. coli* inactivation was detected. Under these conditions LRV was 5.64 and reduction was 99.999 %. Upon preparation of *E. coli* suspension in WM solution expressing an initial count as N_o=6.33E+05 CFU/mL, for an irradiation period of 30 min, *E. coli* count decreased to 6.00E+02 CFU/mL. Upon light exposure of t_{irr}=60 min, *E. coli* count decreased to 2.85E+01 CFU/mL revealing LRV as 4.35 and reduction as 99.99 %. *E. coli* (N_o=1.69E+05 CFU/mL) suspension was prepared in HA solution for an irradiation period of 30 min, *E. coli* count decreased to 1.67E+02 CFU/mL. Following light exposure of t_{irr}=60 min, *E. coli* count reached to 3.35E+01 CFU/mL revealing LRV as 3.70 and reduction as 99.9 %. *E. coli* (N_o=5.31E+05 CFU/mL) suspension was prepared in a solution of "HA and WM" components and was subjected to an irradiation period of 30 min in which *E. coli* count decreased to 2.21E+03 CFU/mL. Upon light exposure of t_{irr}=60 min, *E. coli* count decreased to 4.67E+02 CFU/mL revealing LRV as 3.06 and reduction as 99.9 %.

Based on these results, the effect of solution matrix could be displayed in terms of LRV of *E. coli* in an increasing order as: "HA and WM" < HA < WM < IsoT. *E. coli* inactivation profiles and first order kinetic parameters were presented in Figure 4.49 and Table 4.20.

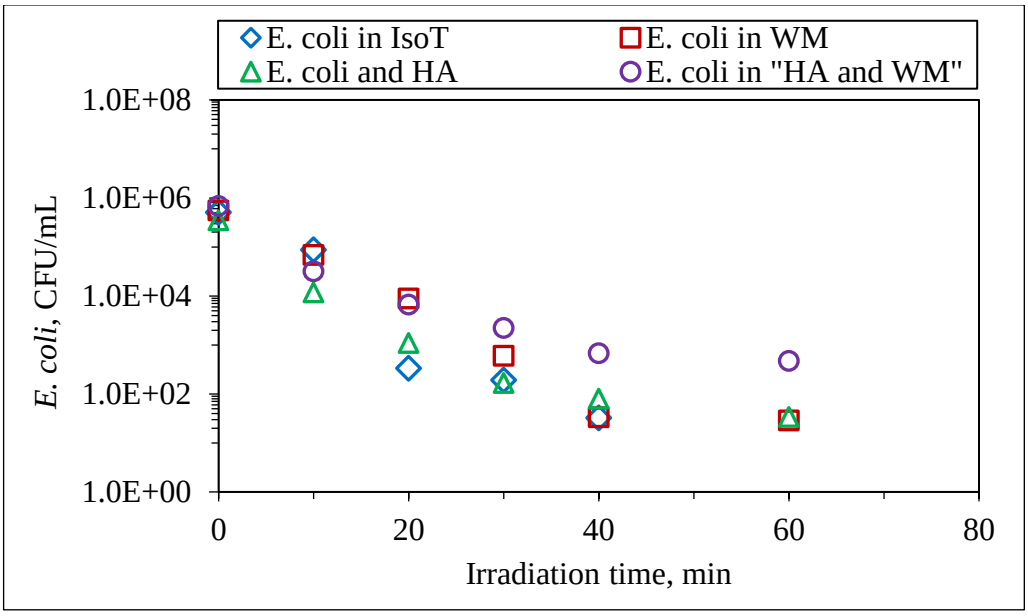

Figure 4.49. Irradiation time dependent *E. coli* inactivation upon SynTiO$_2$ solar photocatalytic treatment in various solution matrixes.

$SynTiO_2$ solar photocatalytic treatment of *E. coli* in IsoT solution resulted in a rather fast reduction with k=0.254 min^{-1} and half-life as 2.73 min. In the presence of "HA and WM", a reaction rate constant of k=0.117 min^{-1} and half-life as 5.92 min were attained. The effect of reaction medium could also be expressed in terms of inactivation reaction rate constant (k, min^{-1}) in a decreasing order as; IsoT > WM > HA > "HA and WM". Irrespective of the minor differences in initial bacteria counts, inactivation rates (CFU/mL min) were calculated as follows; 1.14E+05 > 1.11E+05 > 6.21E+04 > 2.54E+04 for WM, IsoT, "HA and WM", and HA, respectively.

Table 4.20. $SynTiO_2$ solar photocatalytic treatment of *E. coli*: Inactivation parameters.

Matrix	First order kinetic model			LRV	Reduction, %
	k, min^{-1}	$t_{1/2}$, min	R, CFU/mL min		
E. coli in IsoT	0.254	2.73	1.11E+05	5.64	99.999
E. coli in WM	0.180	3.85	1.14E+05	4.35	99.99
E. coli and HA	0.150	4.62	2.54E+04	3.70	99.9
E. coli in HA and WM	0.117	5.92	6.21E+04	3.06	99.9

$SynTiO_2$ solar photocatalytic treatment of *E. coli* in IsoT solution showed the highest bacteria reduction percentage among other media, as 99.999 %. Similar *E. coli* LRV was achieved with TiO_2 solar photocatalytic treatment (Table 4.11).

Due to constituents present in WM solution used in $SynTiO_2$ solar photocatalytic treatment, *E. coli* displayed lower % reduction than *E. coli* in IsoT solution in correlation with the findings attained upon use of TiO_2 in IsoT and WM solutions (Table 4.11).

In the presence of HA, decreased *E. coli* cell counts resulted in reduction as 99.9 % upon use of $SynTiO_2$ photocatalyst specimen as being 2.5 times higher than LRV upon use of TiO_2 (Table 4.11). It could be indicated that while TiO_2 displayed selectivity for HA, $SynTiO_2$ was more selective towards *E. coli*.

Upon $SynTiO_2$ solar photocatalytic inactivation of *E. coli* in "HA and WM" solution, showed the same bacteria reduction percentage with HA, as 99.9 % however slightly lower LRV was attained in "HA and WM" solution. Although similar data were obtained with use of sole HA solution, these bacteria inactivation values were detected way higher than those with TiO_2 (Table 4.11). The diverse efficiencies of these TiO_2 specimens could confirm that $SynTiO_2$ had higher selectivity to *E. coli* rather than organic matrix. Moreover, Turkten and Cinar, having worked with the same $SynTiO_2$, achieved lower organic matter removals than TiO_2, in accordance with the assumption of $SynTiO_2$ selectivity against bacteria (Turkten and Cinar, 2017).

4.2.2.2. Organic matter formation and removal upon SynTiO$_2$ solar photocatalytic treatment of *E. coli* in IsoT solution. UV-vis absorption and synchronous scan fluorescence spectra of organic matter remaining in solution were presented in Figures 4.50 and 4.51. Irradiation time dependent absorbance changes at $\lambda < 280$ nm were significantly similar to each other in the absence of aromatic domains and color forming moieties. Similar UV spectral features were also attained from solar photolytic (Figure 4.2) and TiO$_2$ solar photocatalytic treatments of *E. coli* in IsoT solution (Figure 4.26).

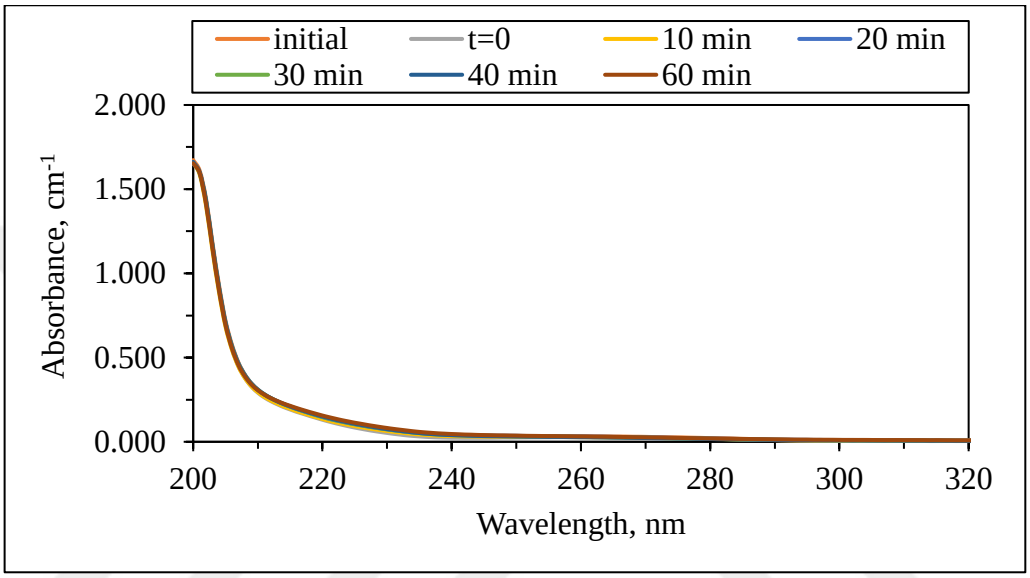

Figure 4.50. UV-vis absorption spectra of organic matter: Irradiation time dependent *E. coli* inactivation in IsoT solution upon SynTiO$_2$ solar photocatalytic treatment.

Synchronous scan fluorescence spectra of emerged organic matter displayed an intense peak at λ_{emis}=280 nm. (Figure 4.51). The major peak was accompanied with a tailing effect in lower intensities in longer emission wavelengths as compared to the main peak intensity at λ_{emis}=280 nm as $FI_{sync}\approx$50. Further evaluation would also consider minor peak intensity at λ_{emis}=470 nm to maintain a basis for comparison upon use of HA. From a general perspective, an irradiation time dependent decreasing order in $FI_{sync280}$ data was observed. On the other hand, contrary to minor presence of $FI_{sync470}$ expressing almost insignificant intensities in the range of 0.0216-0.532, predominant $FI_{sync280}$ displayed changes in between 31.5-53.1 (Figure 4.52).

All UV-vis parameters displayed very low values (Figure 4.52). The highest UV_{254} was attained upon t_{irr}=60 min (0.0341) as could also be considered as similar to t_{irr}=20 min (0.0332) although variations were insignificant. UV_{280} varied in between 0.0164-0.0218 being the lowest for t_{irr}=40 min and the highest for initial samples. Due to non-existence and subsequent degradation of color forming moieties of the released organic matrix upon irradiation and the usage of IsoT solution, quite low

$Color_{436}$ and UV_{365} values were attained. NPOC content showed a slight decrease between t=0 and t_{irr}=10 min (4.16-4.09 mg/L) and increased up to t_{irr}=40 min (5.65 mg/L) due to the release of organics from damaged and destructed *E. coli* cells, followed by a sharp decrease at t_{irr}=60 min (4.25 mg/L).

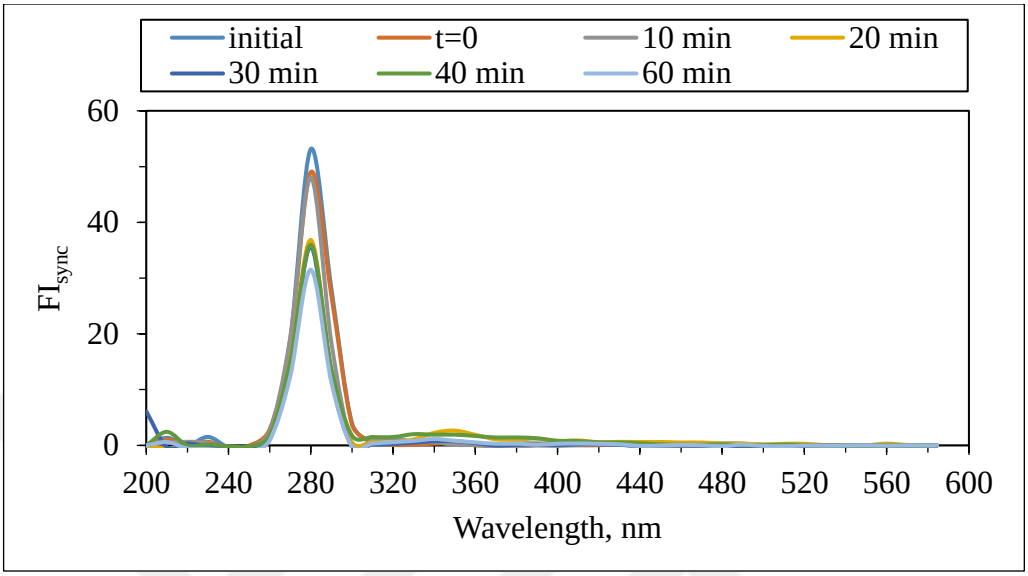

Figure 4.51. Synchronous scan fluorescence spectra of organic matter: Irradiation time dependent *E. coli* inactivation in IsoT solution upon $SynTiO_2$ solar photocatalytic treatment.

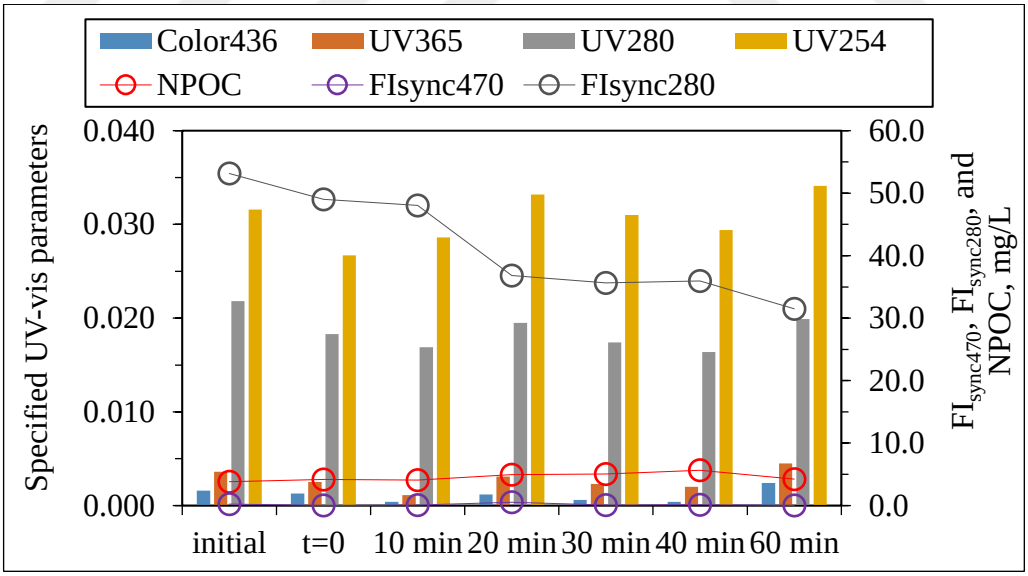

Figure 4.52. Specified UV-vis and fluroscence parameters of organic matter: Irradiation time dependent *E. coli* inactivation in IsoT solution upon $SynTiO_2$ solar photocatalytic treatment.

Based on NPOC contents, $SCoA_{436}$, $SUVA_{365}$, $SUVA_{280}$, $SUVA_{254}$, $SFI_{sync470}$, and $SFI_{sync280}$ were calculated (Figure 4.53). $SUVA_{254}$ displayed variations (0.520-0.827 L/m mg) during $SynTiO_2$ solar photocatalytic treatment with respect to varying trends in both UV_{254} and NPOC removals. Almost insignificant presence of color forming moieties also reflected in insignificant $SCoA_{436}$

profiles in accordance with slight variations in NPOC data determined under all conditions as 3.82-5.26 mg/L. Most important difference could be related to SFI_{syn280} as almost decreasing by half ratio. Besides $SFI_{sync470}$ displayed quite insignificant presence in the range of 0.00519-0.0621, $SFI_{sync280}$ as the main flurophoric group in the absence of HA, expressed variations in between 6.37-13.9.

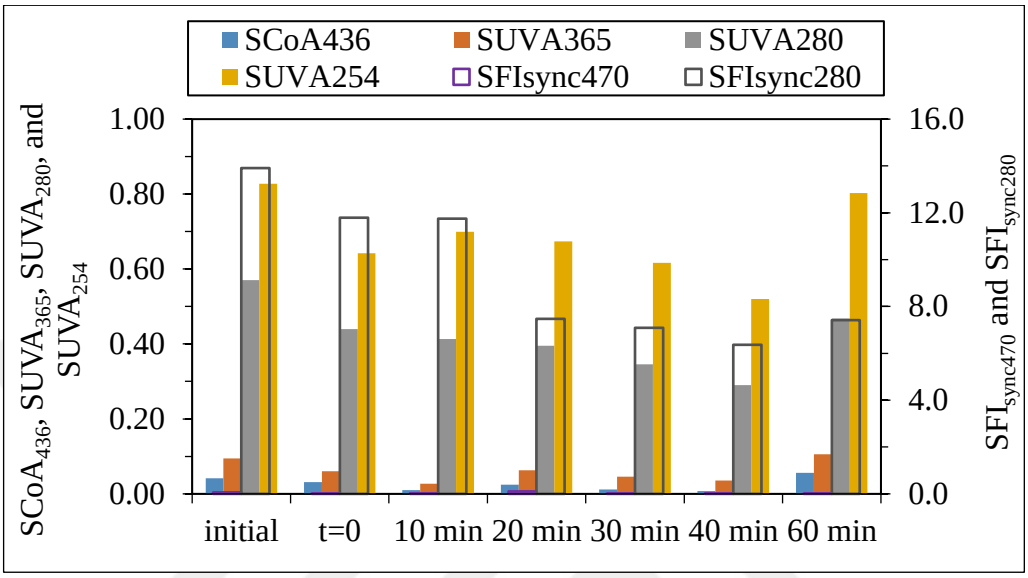

Figure 4.53. Specific UV-vis and fluroscence parameters of organic matter: Irradiation time dependent *E. coli* inactivation in IsoT solution upon $SynTiO_2$ solar photocatalytic treatment.

Characteristic properties of organic matter under initial conditions, upon introduction of $SynTiO_2$ (t=0) and upon $SynTiO_2$ solar photocatalytic inactivation of *E. coli* in IsoT solution exposed to irradiation for 60 min were presented in Table 4.21.

Table 4.21. Characteristic properties of organic matter present in $SynTiO_2$ solar photolytic treatment of *E. coli* in IsoT solution.

Irradiation time, min	UV-vis Spectroscopic Parameters, cm^{-1}				NPOC, mg/L	$SUVA_{254}$, L/m mg	$FI_{sync280}$	$SFI_{sync280}$	FI
	$Color_{436}$	UV_{365}	UV_{280}	UV_{254}					
Initial	0.0016	0.0036	0.0218	0.0316	3.82	0.827	53.1	13.9	1.39
t=0	0.0013	0.0025	0.0183	00267	4.16	0.642	49.0	11.8	1.63
60 min	0.0024	0.0045	0.0199	0.0341	4.25	0.802	31.5	7.41	1.90

There was no significant difference between the slightly increasing order of UV-vis spectroscopic parameters recorded under all conditions. Upon irradiation period of 60 min at which 5.64 log reduction of *E. coli* in IsoT solution (Table 4.20) was attained, released organic matter expressed the very low UV-vis parameters, along with organic contents NPOC as 4.25 mg/L. $SUVA_{254}$ value at t_{irr}=60 min as 0.802 L/m mg represents that the remaining organic matter could be

considered having hydrophilic and aliphatic character (Edzwald et al., 1985). Owing to the degradation of protein content, $FI_{sync280}$ displayed a decreasing trend at the end of 60 min irradiation period. $SFI_{sync280}$ value showed slight decrease at t_{irr}=60 min in accordance with the increased NPOC due to the released organic material from bacteria. According to very low $FI_{sync470}$ and NPOC data, calculated $SFI_{sync470}$ were insignificant under all conditions. At t_{irr}=60 min, FI was calculated as 1.90, in accordance with the microbially derived organic content of the experiment solution.

EEM fluorescence contour plots of organic matter emerged and removed during irradiation time dependent *E. coli* inactivation in IsoT solution during $SynTiO_2$ solar photocatalytic treatment were displayed in Figure 4.54.

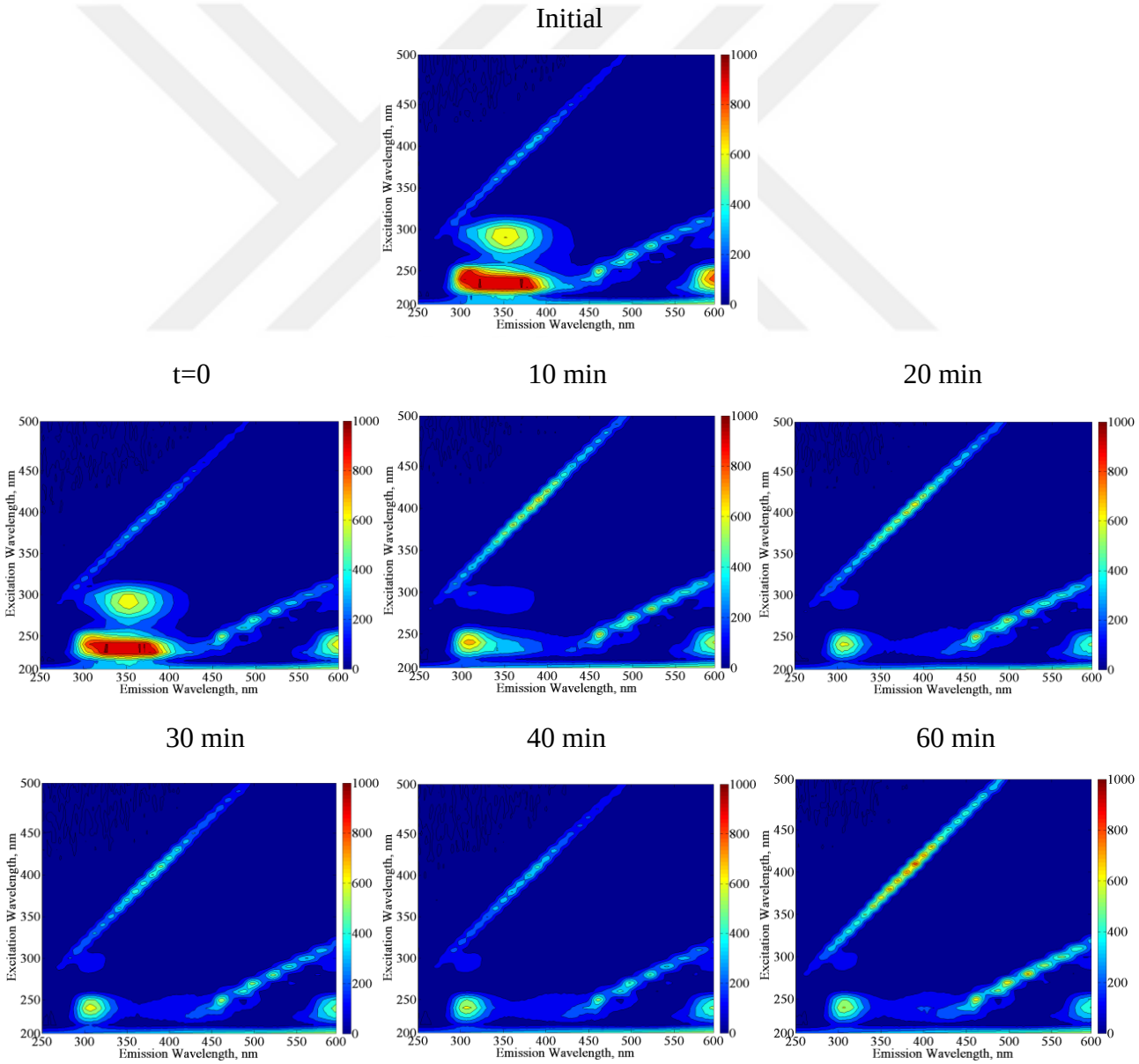

Figure 4.54. EEM fluorescence contour plots of organic matter: Irradiation time dependent *E. coli* inactivation in IsoT solution upon $SynTiO_2$ solar photocatalytic treatment.

EEM fluorescence contour plots displayed the presence of Regions I, II and IV expressing that the fluorophores were mainly originated from microbial by-products and proteins under all irradiation conditions. Throughout 60 min irradiation period, released microbial by-products and proteins from *E. coli* cells showed a decreasing trend in accordance with the solar photocatalytic degradation of released organic matter and reduction of *E. coli*. However, at t_{irr}=60 min fluorescence intensities were detected as higher than the ones of TiO_2 solar photocatalytic treatment of *E. coli* in IsoT solution (Figure 4.30). Furthermore, decreasing intensities at Region I and II representing the presence of aromatic proteins could also be correlated with the irradiation time dependent decreasing order of $FI_{sync280}$ data (Figures 4.51 and 4.52).

4.2.2.3. Mechanistic evaluation of *E. coli* inactivation upon SynTiO_2 solar photocatalytic treatment in IsoT solution. As bacteria inactivation products total K, protein, and carbohydrate contents present in initial, t=0, and t_{irr}=60 min samples of SynTiO_2 solar photocatalytic treatment of *E. coli* in IsoT solution were presented in Table 4.22.

Table 4.22. Total K, protein, and carbohydrate contents of time dependent *E. coli* inactivation in IsoT solution upon SynTiO_2 solar photocatalytic treatment.

SynTiO_2 solar photocatalytic treatment	*E. coli* in IsoT solution		
	Initial	t=0	60 min
Total K, mg/L	1.18	0.97	1.07
Protein, mg/L	3.54	3.95	5.86
Carbohydrate, mg/L	2.34	3.15	45.0

Total K content displayed immediate adsorptive removal as 17.8 % at t=0, which could be resulting from K^+ ion adsorption onto negatively charged *E. coli* and/or TiO_2 surfaces. At the end of 60 min irradiation period, total K content slightly increased due to released K^+ ions from damaged bacteria cells.

E. coli in IsoT solution upon SynTiO_2 solar photocatalytic treatment displayed increasing trend in both protein and carbohydrate contents. Protein contents were plotted against $FI_{sync280}$ and NPOC in order to detect if there is any correlation between these parameters; while protein contents and $FI_{sync280}$ displayed a strong correlation as R^2=1.00, protein concentrations and NPOC showed a moderate correlation as R^2=0.60. Carbohydrate concentration showed a drastic increase after 60 min of irradiation period (45.0 mg/L) that could be due to an unexpected condition. Various researchers reported that the use of strong acid may cause production of some degradation products which can

absorb light in the same spectral band with carbohydrates, resulting in overestimation of carbohydrate concentration (Josefsson et al. 1972; Dawson and Liebezeit, 1981). Moreover, Rao and Pattabiraman indicate that the presence of glycoproteins could be troublesome for detection of carbohydrate content (Rao and Pattabiraman, 1989). No significant correlation was detected between carbohydrate concentrations and NPOC data.

4.2.2.4. Organic matter formation and removal upon SynTiO$_2$ solar photocatalytic treatment of *E. coli* in WM solution. UV-vis absorption spectra of organic matter in reaction medium were presented in Figure 4.55. Irradiation time dependent absorbance changes displayed minor differences from each other in UV wavelength range of λ=200-280 nm in the absence of aromatic domains and color forming moieties (Color$_{436}$, UV$_{365}$ and UV$_{280}$) that should be measured in longer wavelengths. Initial solution expressed higher absorption at λ > 210 nm however t_{irr}=60 min condition displayed lower absorption at λ < 240 nm indicating that light absorbing moieties could be emerged and removed throughout the irradiation period.

Different from *E. coli* in IsoT solution conditions, the use of WM solution resulted in the detection of different absorbance characteristics at λ < 250 nm. Especially between λ=200-210 nm a shoulder effect was detected for all samples originating from the strong absorption spectrum of NO_3^- having its λ_{max} at approximately 200 nm (Krishnan and Guha, 1934; Edwards at el., 2001). Similar absorption behaviors could also be visualized with previous solar photolytic (Figure 4.7) and TiO$_2$ photocatalytic treatments carried out with WM solution (Figure 4.31).

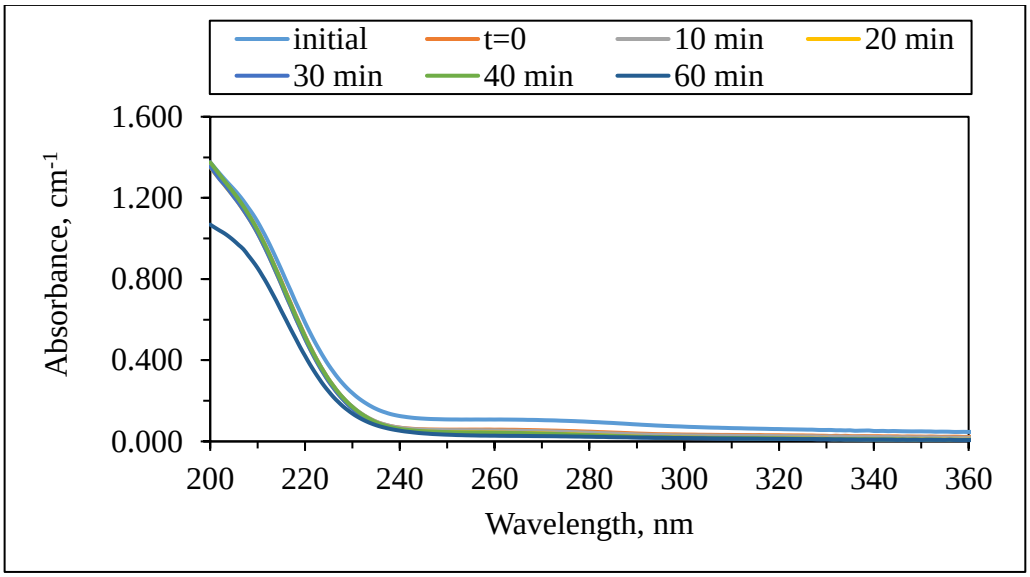

Figure 4.55. UV-vis absorption spectra of organic matter: Irradiation time dependent *E. coli* inactivation in WM solution upon SynTiO$_2$ solar photocatalytic treatment.

Synchronous scan fluorescence spectra of emerged organic matter displayed an intense peak at λ_{emis}=280 nm, although, a second peak at λ_{emis}=420 nm was observed for t=0 min condition (Figure 4.55). The emergence of the fluorophores at emission wavelength of 420 nm could be related to the conformational changes in the released organic matter upon use of SynTiO$_2$ expressing different surface properties in comparison to bare TiO$_2$ (Figure 4.32 and Appendix C). Furthermore, FI_{sync} data displayed a dramatic increase at t_{irr}=10 min displaying a broad spectrum followed which a reducing trend was attained during solar photocatalytic treatment. Fluorescence spectral shape resembled a mono peak at λ_{emis}=280 nm style as depicted previously in case of IsoT solution (Figure 4.51). Furthermore, very low $FI_{sync470}$ showed changes in between 0.220-4.32 however dominant $FI_{sync280}$ displayed variations in the range of 15.8-76.0. The key fluorophoric group was accepted as $FI_{sync280}$, in the absence of HA solution as an aqueous matrix component (Figure 4.57).

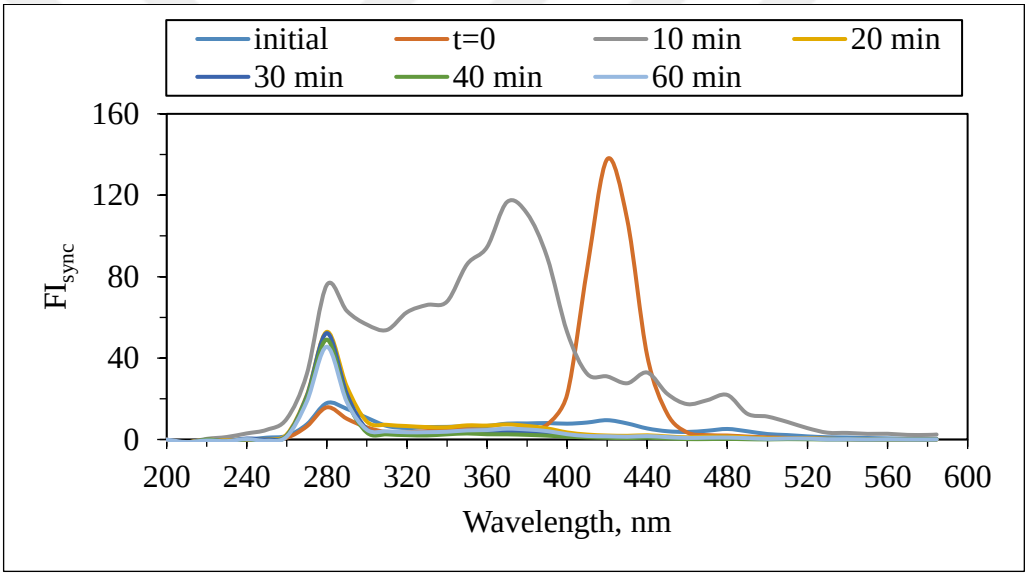

Figure 4.56. Synchronous scan fluorescence spectra of organic matter: Irradiation time dependent *E. coli* inactivation in WM solution upon SynTiO$_2$ solar photocatalytic treatment.

From a general perspective, NPOC expressed variations in the range of 1.81-11.7 mg/L (Figure 4.57). NPOC content significantly increased between initial (1.81 mg/L) and t=0 (7.17 mg/L) conditions which could be most probably due to mechanistic adverse effect of SynTiO$_2$ on *E. coli* cells, at t_{irr}=20 min (4.44 mg/L) NPOC declined and again increased until t_{irr}=30 min (11.7 mg/L) due to release of organics from damaged and destructed *E. coli* cells, and followed by a declining trend until t_{irr}=40 min (9.93 mg/L), further prolonged irradiation duration showed a slight increase up to 10.8 mg/L. The lowest NPOC content was determined under initial condition (1.81mg/L) representing the amount of organic matter present in WM solution following immediate filtration through 0.45 μm membrane filter. Therefore, approximately 10 mg/L NPOC was present in reaction

medium upon solar photocatalysis using SynTiO$_2$. On the other hand, UV$_{254}$ varied in between 0.0302-0.1080 was detected as the most significant UV-vis parameter.

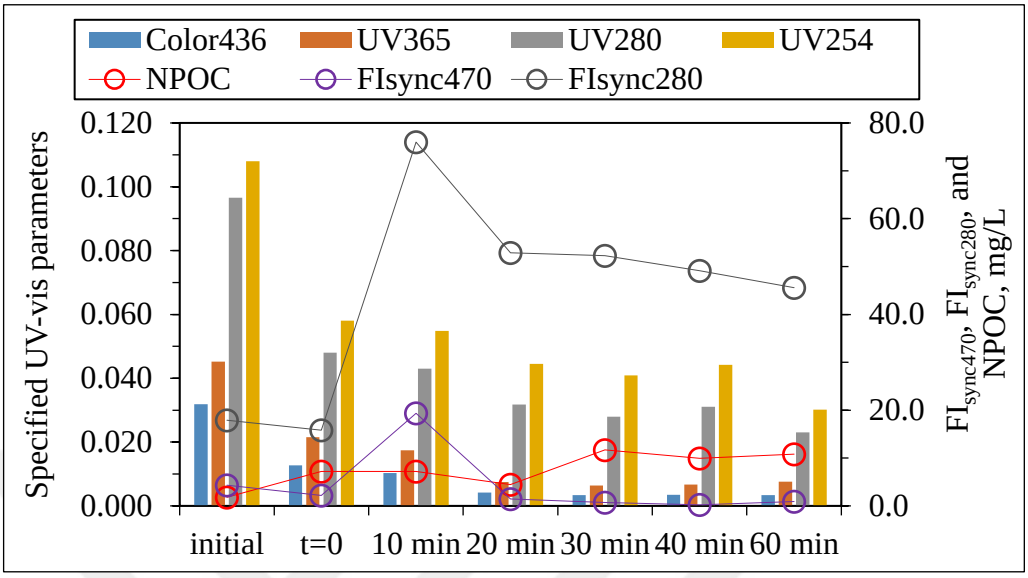

Figure 4.57. Specified UV-vis and fluroscence parameters of organic matter: Irradiation time dependent *E. coli* inactivation in WM solution upon SynTiO$_2$ solar photocatalytic treatment.

SCoA$_{436}$, SUVA$_{365}$, SUVA$_{280}$, SUVA$_{254}$, SFI$_{sync470}$, and SFI$_{sync280}$ were calculated and presented in Figure 4.58. After the introduction of SynTiO$_2$ into the system, all specific UV-vis parameters expressed a drastic decrease. As the most significant parameter, SUVA$_{254}$ displayed changes (0.280-5.97 L/m mg) during solar photocatalytic treatment in relation to concurrent differences in both UV$_{254}$ and NPOC removals. At t_{irr}=60 min, SUVA$_{254}$ displayed a significant decrease as 95.3 %.

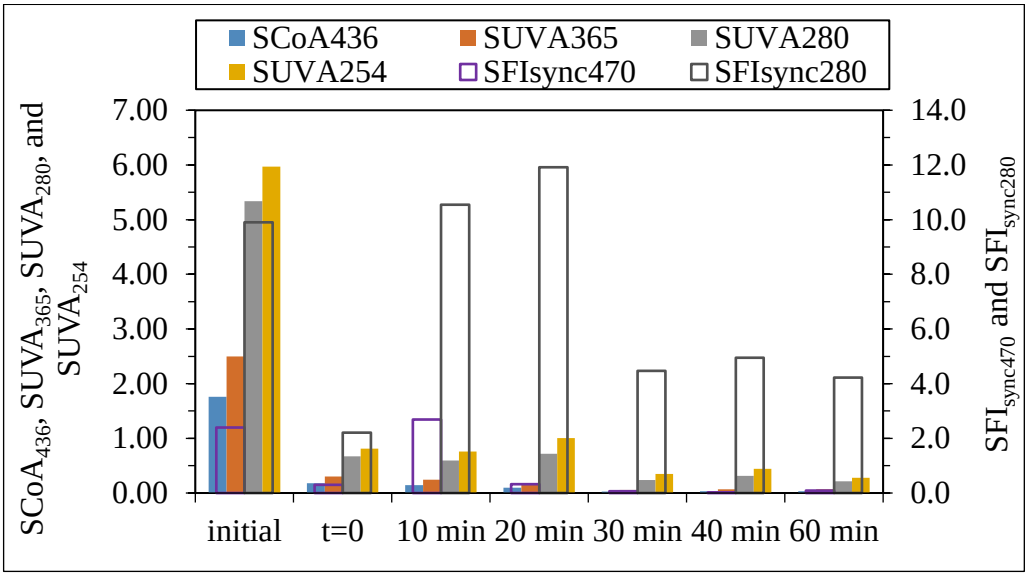

Figure 4.58. Specific UV-vis and fluroscence parameters of organic matter: Irradiation time dependent *E. coli* inactivation in WM solution upon SynTiO$_2$ solar photocatalytic treatment.

Due to non-existence and subsequent degradation of color forming moieties of the released organic matter upon irradiation, calculated $SCoA_{436}$ and $SUVA_{365}$ were quite low. However, $SUVA_{280}$ as the secondly significant parameter, expressed variations in between 0.213-5.34 L/m mg being the lowest for t_{irr}=60 min and the highest for initial conditions. Furthermore, specific fluorescence parameter as $SFI_{sync470}$ and $SFI_{sync280}$ expressed variations in the range of 0.0221-2.68 and 2.21-11.9, respectively. The main fluorophoric group was accepted as $SFI_{sync280}$ and the most remarkable variation was noticed for $SFI_{sync280}$ being highest under 20 min of irradiation (11.9).

Characteristic properties of organic matter present under initial and t=0 conditions and following irradiation for 60 min $SynTiO_2$ solar photocatalytic inactivation of *E. coli* in WM solution were presented in Table 4.23.

Table 4.23. Characteristic properties of organic matter present in $SynTiO_2$ solar photolytic treatment of *E. coli* in WM solution.

Irradiation time, min	UV-vis Spectroscopic Parameters, cm^{-1}				NPOC, mg/L	$SUVA_{254}$, L/m mg	$FI_{sync280}$	$SFI_{sync280}$	FI
	$Color_{436}$	UV_{365}	UV_{280}	UV_{254}					
Initial	0.0319	0.0452	0.0966	0.108	1.81	5.97	17.9	9.90	1.48
t=0	0.0127	0.0215	0.0480	0.0580	7.17	0.809	15.8	2.21	1.33
60 min	0.0034	0.0076	0.0230	0.0302	10.8	0.280	45.6	4.22	1.74

Upon irradiation period of 60 min $SynTiO_2$ solar photocatalytic treatment at which 4.35 log reduction of *E. coli* in WM was attained (Table 4.20), released organic matter expressed the following UV-vis parameters (cm^{-1}); $Color_{436}$: 0.0034, UV_{365}: 0.0076, UV_{280}: 0.0230, UV_{254}: 0.0302, and NPOC as 10.8 mg/L. $SUVA_{254}$ value was calculated as 0.280 L/m mg upon t_{irr}=60 min represents that the remaining organic matter could be considered having hydrophilic and aliphatic character (Edzwald et al., 1985).

$FI_{sync280}$ increased at the end of t_{irr}=60 min, which could be related to the release of *E. coli* protein content. $SFI_{sync280}$ value displayed a decrease at t_{irr}=60 min in accordance with increased NPOC due to released organic material from bacteria. On the other hand, $FI_{sync470}$ displayed almost insignificant presence as 4.33, 2.16, and 0.908 for initial, t=0, and t_{irr}=60 min conditions, respectively. Owing to the degradation of released organic content from damaged *E. coli* cells, $FI_{sync470}$ expressed a decrease at t_{irr}=60 min. $SFI_{sync470}$ values of initial, t=0, and t_{irr}=60 min samples were calculated as 2.39, 0.301, and 0.0841, respectively. Furthermore, FI at t_{irr}=60 min was calculated as 1.74 which could mostly be related to the presence of microbially derived organic matter in solution (Sen-Kavurmaci and Bekbolet, 2014). Despite calculated FI was between the indication values of humic and microbially

derived organics, it could most probably stemming from microbial origin. Moreover, the presence of microbially derived organic content in t_{irr}=60 min solution could also be supported with EEM contour plots represented in following Figure 4.59.

EEM fluorescence contour plots of organic matter emerged and removed during irradiation time dependent *E. coli* inactivation in WM during SynTiO$_2$ solar photocatalytic treatment were displayed in Figure 4.59. EEM fluorescence contour plots displayed the presence of Regions I, II and IV expressing that the fluorophores were mainly originated from microbial by-products and proteins under all irradiation conditions.

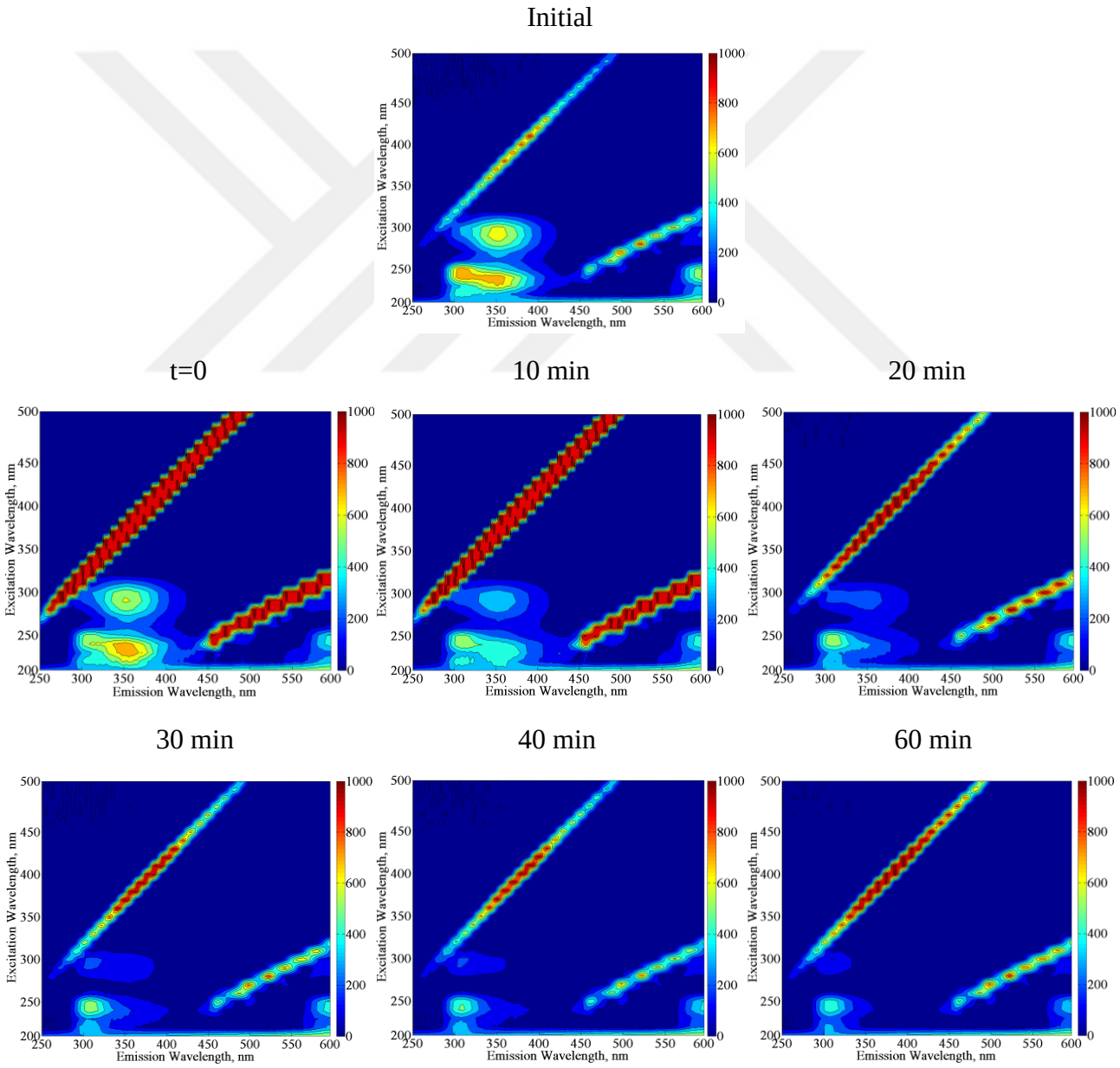

Figure 4.59. EEM fluorescence contour plots of organic matter: Irradiation time dependent *E. coli* inactivation in WM solution upon SynTiO$_2$ solar photocatalytic treatment.

Following further irradiation periods, released microbial by-products and protein content from *E. coli* cells showed a decreasing trend in accordance with the solar photocatalytic degradation of organic matter and reduction of *E. coli* which could be visualized by reduced fluorescence intensities of related regions. Furthermore, similar to previous solar photolytic (Figure 4.11) and TiO_2 solar photocatalytic treatment carried out in WM solution (Figure 4.35) lower regional fluorescence intensities were detected than IsoT solution conditions (Figures 4.6, 4.30, and 4.54). On the other hand, fluorescence intensities were detected as higher than TiO_2 solar photocatalytic treatment of *E. coli* in WM solution conditions (Figure 4.35).

4.2.2.5. Mechanistic evaluation of *E. coli* inactivation upon $SynTiO_2$ solar photocatalytic treatment in WM solution. Upon bacteria reduction, total K, protein, and carbohydrate contents present in initial, t=0, and t_{irr}=60 min samples of $SynTiO_2$ solar photocatalytic treatment of *E. coli* in WM solution were presented in Table 4.24.

Table 4.24. Total K, protein, and carbohydrate contents of time dependent *E. coli* inactivation in WM solution upon $SynTiO_2$ solar photocatalytic treatment.

$SynTiO_2$ solar photocatalytic treatment	*E. coli* in WM		
	Initial	t=0	60 min
Total K, mg/L	4.38	4.26	4.12
Protein, mg/L	2.35	2.85	14.8
Carbohydrate, mg/L	2.28	1.89	1.83

Total K content displayed a decreasing trend differing from *E. coli* behavior in WM solution under solar photolytic (Table 4.6) and photocatalytic conditions (Table 4.15). Immediate adsorptive removal of total K as 2.7 % was calculated at t=0 condition. Furthermore, decreased total K content after 60 min of irradiation period could be related to adsorption of released and/or present K^+ ions in WM solution onto both negatively charged *E. coli* and $SynTiO_2$ surface sites.

Upon $SynTiO_2$ solar photocatalysis, *E. coli* in WM solution displayed different trends for protein and carbohydrate evolution upon cell destruction. While protein content showed a significant increase (2.35-14.8 mg/L), carbohydrate content slightly decreased at the end of 60 min irradiation duration (2.28-1.83 mg/L). A similar inverse relation was also detected by fluorescence intensities as expressed by $FI_{sync280}$ and $FI_{sync470}$ (Figure 4.57). Both $FI_{sync280}$ and protein contents increased with a strong correlation as R^2=0.99. Protein contents and NPOC displayed a moderate correlation expressed as R^2=0.68 however carbohydrate and NPOC contents showed a strong correlation as R^2=0.91.

4.2.2.6. Organic matter formation and removal upon SynTiO$_2$ solar photocatalytic treatment of *E. coli* in HA solution. UV-vis absorption and synchronous scan fluorescence spectra of organic matter in HA solution were presented in Figures 4.60 and 4.61. Irradiation time dependent absorbance changes were significantly different from each other in UV wavelength range of λ=200-400 nm due to the presence of dense aromatic domains as well as color forming moieties (Color$_{436}$, UV$_{365}$ and UV$_{280}$). Despite the visualization of irradiation time dependent sequential degradation of organic matter, differences were more pronounced in the previous set of TiO$_2$ solar photocatalytic treatment (Figure 4.36).

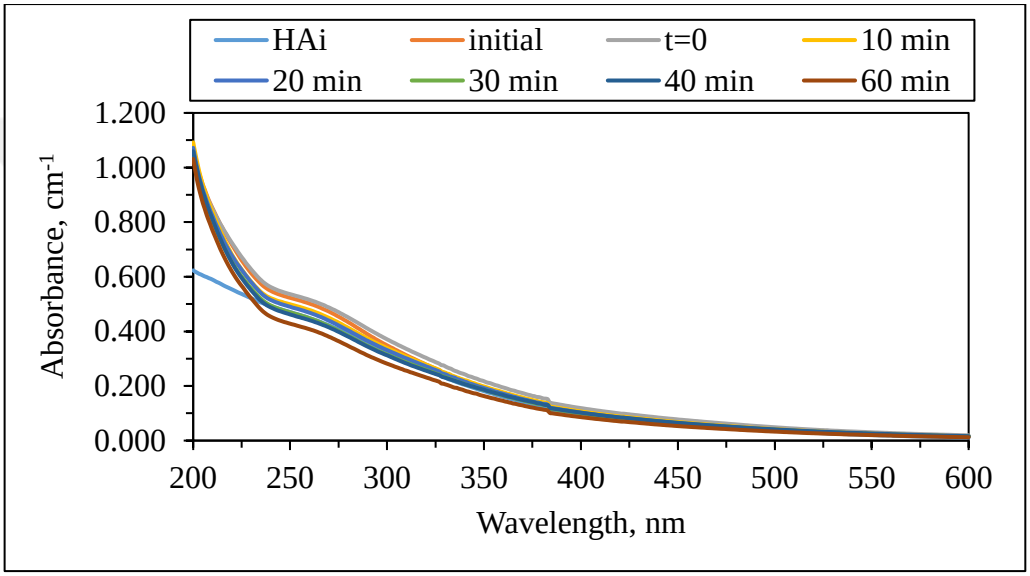

Figure 4.60. UV-vis absorption spectra of organic matter: Irradiation time dependent *E. coli* inactivation in HA solution upon SynTiO$_2$ solar photocatalytic treatment.

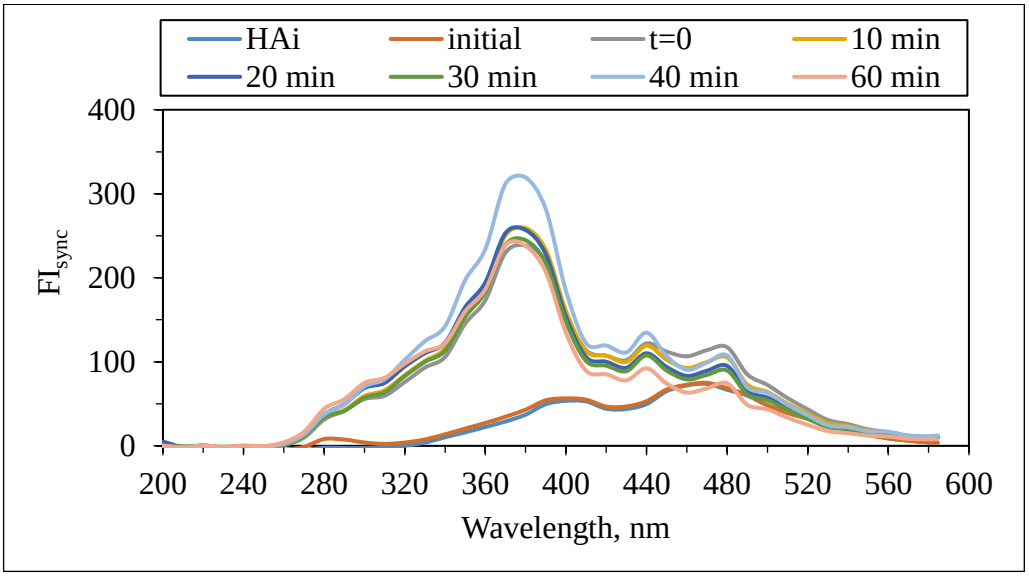

Figure 4.61. Synchronous scan fluorescence spectra of organic matter: Irradiation time dependent *E. coli* inactivation in HA solution upon SynTiO$_2$ solar photocatalytic treatment.

Synchronous scan fluorescence spectra of emerged organic matter displayed an intense peak at λ_{emis}=370 nm and two minor peaks at λ_{emis}=440 nm and 480 nm representing the presence of aromatic constituents in solution matrix (Dujmov and Sučević, 1990) (Figure 4.61). A relevant decrease in synchronous fluorescence intensities were observed following 40 min of irradiation. On the other hand, $FI_{sync470}$ and $FI_{sync280}$ displayed changes in the range of 68.4-99.7 and 8.03-44.0, respectively irrespective of the exposure periods. The predominant fluorophoric group referred to $FI_{sync470}$ in the presence of HA as the solution matrix was evident under all conditions along with $FI_{sync370}$. $FI_{sync280}$ of sole HA_i would not be expected, however $FI_{sync280}$ of the initial solution increased to 8.03 indicating the presence of protein content in the *E. coli* cell suspension (Figure 4.62).

From a general view, NPOC content expressed variations in the range of 4.74-23.1 mg/L. A drastic increase in NPOC content was attained upon t_{irr}=10 min (4.74-23.1 mg/L) due to the release of organics from damaged and/or destructed *E. coli* cells followed by a sharp decrease at t_{irr}=20 min (15.1 mg/L) and again displayed an increasing trend as observed during SynTiO$_2$ solar photocatalytic treatment (19.9 mg/L) (Figure 4.62).

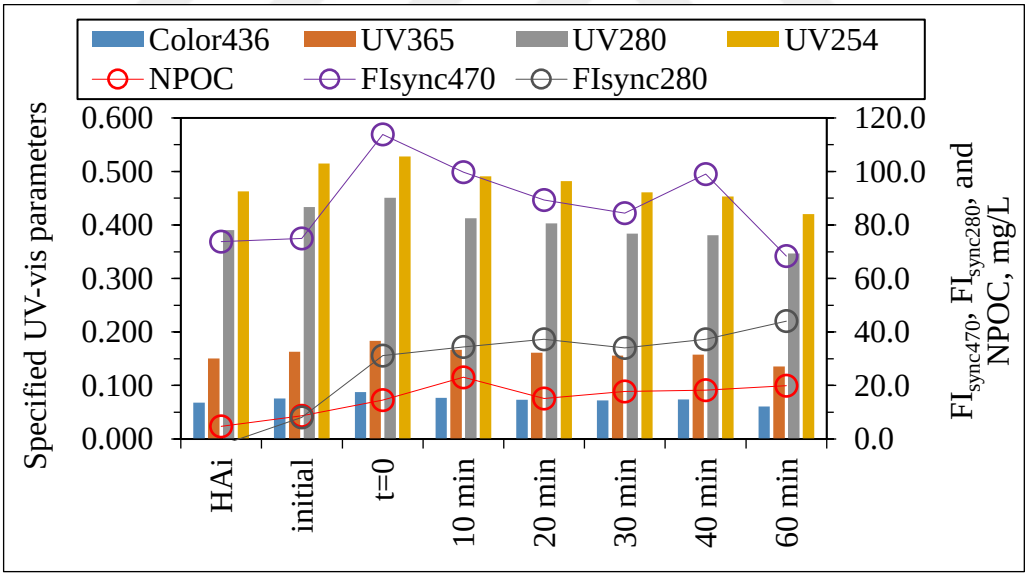

Figure 4.62. Specified UV-vis and fluroscence parameters of organic matter: Irradiation time dependent *E. coli* inactivation in HA solution upon SynTiO$_2$ solar photocatalytic treatment.

Along with the use of HA solution, all UV-vis parameters expressed high presence. After t=0 condition, all specified UV-vis parameters followed a decreasing trend however obtained decrease was rather low in comparison to TiO$_2$ solar photocatalytic treatment of *E. coli* in HA solution (Figure 4.38). UV_{254}, which was the most significant parameter displayed variations in the range of 0.4201-0.5283, being the highest for t=0 condition and the lowest for t_{irr}=60 min condition. Moreover,

especially $Color_{436}$ expressed very minor decrease at the end of 60 min light exposure in comparison to almost total removal obtained with the use of TiO_2 as a bare photocatalyst specimen. According to minor removal of NPOC and UV-vis parameters, it could be concluded that low organic content degradation was attained throughout 60 min of irradiation duration. Obtained data could support the interpretation was made about $SynTiO_2$ having higher selectivity against *E. coli* rather than HA in Section 4.2.2.1.

Based on NPOC data attained under all conditions, specific UV-vis parameters as $SCoA_{436}$, $SUVA_{365}$, $SUVA_{280}$, $SUVA_{254}$, $SFI_{sync470}$, and $SFI_{sync280}$ were calculated and presented in Figure 4.63. Most importantly, $SUVA_{254}$ displayed variations in between 2.11-9.76 L/m mg during $SynTiO_2$ solar photocatalytic treatment indicating concomitant differences in both UV_{254} and NPOC removals. The highest $SUVA_{254}$ was attained for sole HA solution.

Furthermore, specific fluorescence parameters as predominant $SFI_{sync470}$ and quite low $SFI_{sync280}$ expressed variations in the range of 3.44-15.6 and 0.929-2.47, respectively. Obtained $SFI_{sync280}$ values were almost insignificant. According to insignificant presence of $FI_{sync280}$ related to HA_i, $SFI_{sync280}$ would be irrelevant in comparison to $SFI_{sync470}$.

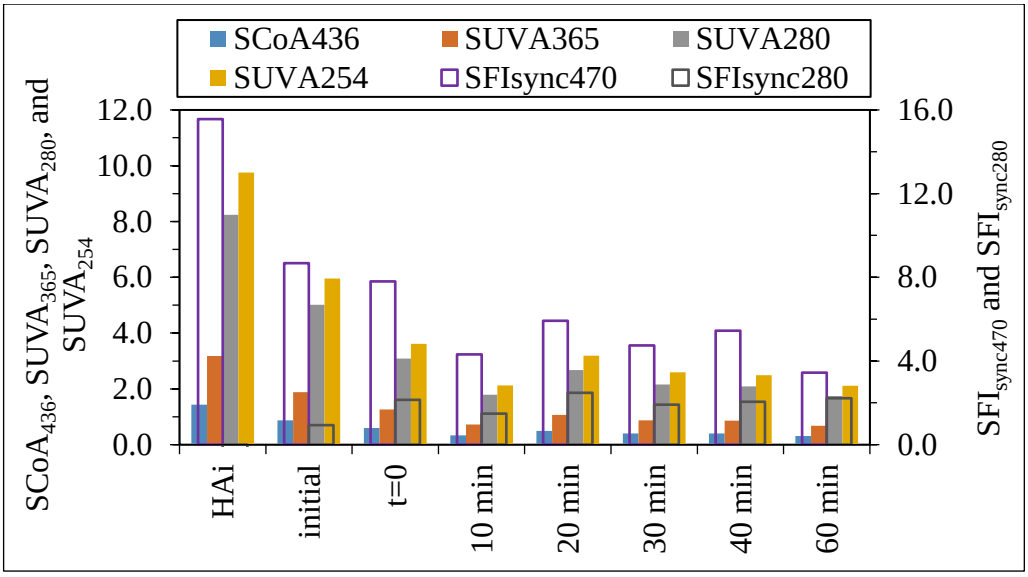

Figure 4.63. Specific UV-vis and fluroscence parameters of organic matter: Irradiation time dependent *E. coli* inactivation in HA solution upon $SynTiO_2$ solar photocatalytic treatment.

For comparative evaluation purposes, characteristic properties of organic matter present in solutions under initial condition, upon introduction of $SynTiO_2$ (t=0) and $SynTiO_2$ solar

photocatalytic inactivation of *E. coli* in HA solution exposed to irradiation for 60 min were presented in Table 4.25.

Table 4.25. Characteristic properties of organic matter present in $SynTiO_2$ solar photolytic treatment of *E. coli* in HA solution.

Irradiation time, min	UV-vis Spectroscopic Parameters, cm^{-1}				NPOC, mg/L	$SUVA_{254}$, L/m mg	$FI_{sync470}$	$SFI_{sync470}$	FI
	$Color_{436}$	UV_{365}	UV_{280}	UV_{254}					
Initial	0.0756	0.1629	0.4334	0.5150	8.65	5.95	75.0	8.67	1.08
t=0	0.0875	0.1836	0.4511	0.5283	14.6	3.62	114	7.80	1.10
60 min	0.0608	0.1358	0.3466	0.4201	19.9	2.11	68.4	3.44	1.16

Upon t_{irr}=60 min of $SynTiO_2$ solar photocatalytic treatment of *E coli* in HA solution, at which 3.70 log *E. coli* reduction (Table 4.20) was achieved, released organic matter expressed the following UV-vis parameters; $Color_{436}$: 0.0608, UV_{365}: 0.1358, UV_{280}: 0.3466, UV_{254}: 0.4201, and NPOC as 19.9 mg/L.

$SUVA_{254}$ of initial and following t_{irr}=60 min conditions of irradiation were calculated as 5.95 and 2.11 L/m mg, respectively. Detected decrease in $SUVA_{254}$ indicated the degradation of aromatic organics during 60 min of solar photocatalysis. The use of HA solution as reaction matrix caused relatively high initial NPOC and $SUVA_{254}$ as expected.

$FI_{sync470}$ displayed a significant increase at t=0 condition (75.0-114) and after 60 min of irradiation decreased below initial value (68.4) emphasizing degradation of released cytoplasmic organic matter from *E. coli*. According to changes in $FI_{sync470}$ and NPOC content, calculated $SFI_{sync470}$ displayed a decrease after t_{irr}=60 min. On the other hand, $FI_{sync280}$ measurements of initial, t=0 and t_{irr}=60 min conditions were detected as 8.03, 14.6 and 44.1, respectively. $FI_{sync280}$ demonstrated a significant increase at the end of 60 min solar light exposure due to the released protein content from *E. coli* cells. $SFI_{sync280}$ attained under initial, t=0, and t_{irr}=60 min conditions were calculated as 0.929, 2.13, and 2.21, respectively. After irradiation period of 60 min, FI was calculated as 1.16 indicating the presence of fluorophores emerging from humic matter present in experimental solution matrix as expected.

In a similar manner to the UV-vis absorbance and synchronous scan fluorescence analyses, EEM fluorescence contour plots of organic matter emerged and removed during irradiation time dependent *E. coli* inactivation in HA solution during $SynTiO_2$ solar photocatalytic treatment were also followed and displayed in Figure 4.64.

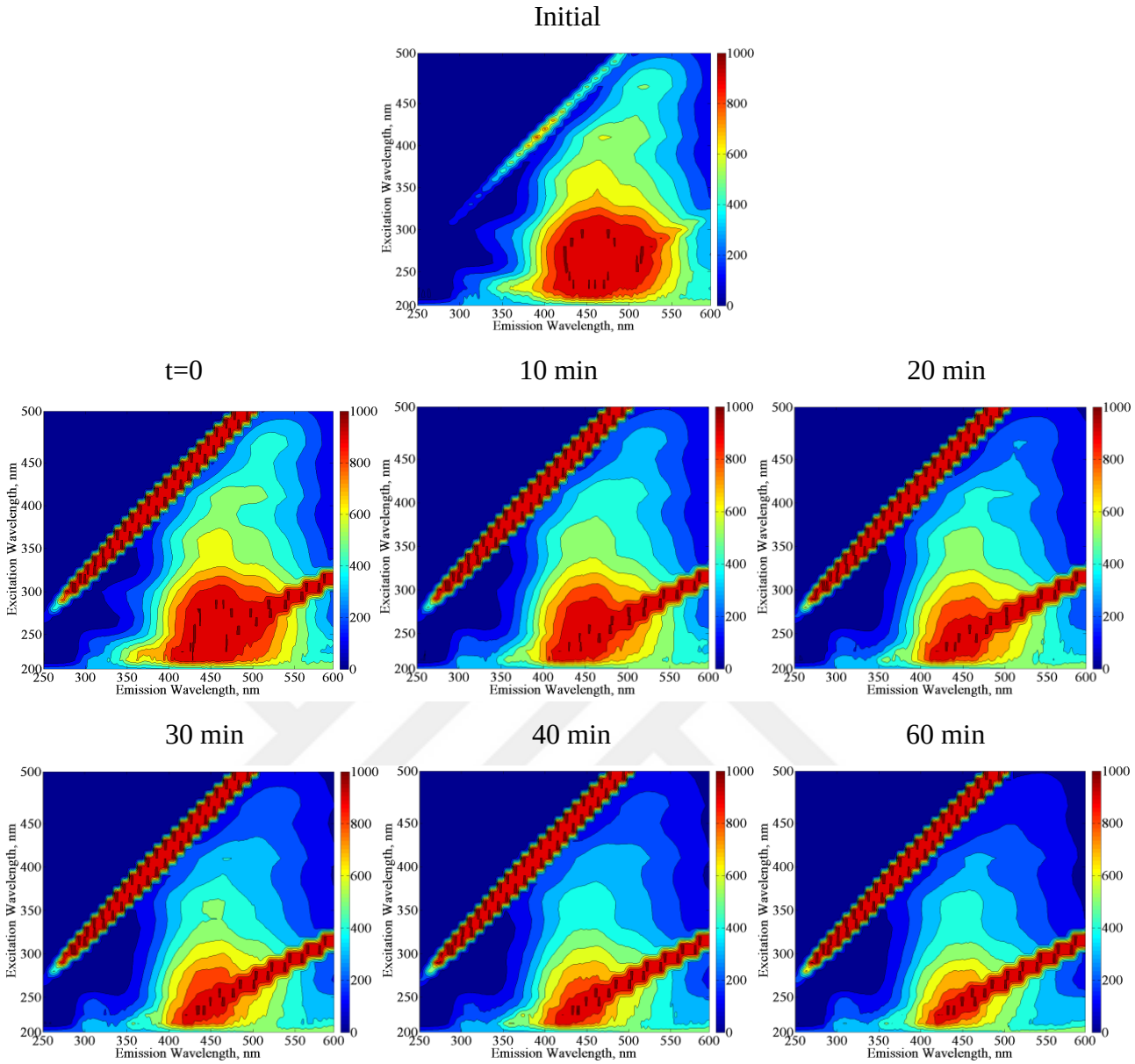

Figure 4.64. EEM fluorescence contour plots of organic matter: Irradiation time dependent *E. coli* inactivation in HA solution upon SynTiO$_2$ solar photocatalytic treatment.

EEM fluorescence contour plots of *E. coli* in HA solution upon SynTiO$_2$ solar photocatalytic treatment displayed the presence of Regions III, and V indicating that the fluorophores were mainly originated from fulvic-like and humic-like substances. Both humic-like and fulvic-like fluorophore intensities expressed a slight decrease throughout the irradiation periods revealing that organic matter having HA origin showed only minor degradation during t_{irr}=60 min. Besides EEM fluorescence contour plots showing almost no change of humic-like and fulvic-like fluorophores, high *E. coli* LRV as 3.70 was attained upon 60 min of irradiation period which also supported the selectivity of SynTiO$_2$ towards *E. coli*. It could be concluded that specified UV-vis parameters, NPOC data, and EEM fluorescence contour plots were complied with each other about degradation of organic content in solution. Moreover, EEM fluorescence contour plots displaying low organic matrix removal were

similar to the findings of Turkten and Cınar (Turkten and Cinar, 2017). Although released and degraded microbial by-products and protein-like fluorophores were present in solution, they could not exactly be identified due to possible masking effect of humic-like components (Wang et al., 2015).

4.2.2.7. Mechanistic evaluation of *E. coli* inactivation upon SynTiO$_2$ solar photocatalytic treatment in HA solution. Upon cell destruction of *E. coli* in HA solution via SynTiO$_2$ solar photocatalysis, released total K, protein, and carbohydrate contents under initial, t=0, and t_{irr}=60 min conditions were presented in Table 4.26.

Table 4.26. Total K, protein, and carbohydrate contents of time dependent *E. coli* inactivation in HA solution upon SynTiO$_2$ solar photocatalytic treatment.

SynTiO$_2$ solar photocatalytic treatment	*E. coli* and HA		
	Initial	t=0	60 min
Total K, mg/L	0.61	0.64	0.73
Protein, mg/L	8.82	7.93	11.1
Carbohydrate, mg/L	2.51	2.61	25.3

Total K content of *E. coli* in HA solution by solar photocatalytic treatment with SynTiO$_2$ displayed a slight increase between initial and t_{irr}=60 min conditions expressing K^+ ion release from damaged bacteria cells. Measured low total K concentrations showed similarity with both solar photolytic (Table 4.8) and TiO$_2$ solar photocatalytic treatment sets of *E. coli* in the presence of HA solution (Table 4.17).

Upon SynTiO$_2$ solar photocatalytic treatment of *E. coli* in HA solution, increase in both protein and carbohydrate contents were observed at the end of 60 min solar light exposure. Carbohydrate concentration showed significant increase (2.51-25.3 mg/L) while protein concentration displayed a slight increase (8.82-11.1 mg/L). A plausible explanation of this remarkable increase of carbohydrate concentration could be emerging from nondegraded humic sub-fractions along with released carbohydrate from *E. coli* cells upon solar photocatalysis. Moreover, high carbohydrate concentrations could be related with EEM counter plots having high intensities for fulvic-like and humic-like regions as Region III and V (Figure 4.64). $FI_{sync280}$ and NPOC data were plotted against protein concentrations to detect if there was any correlation, and neither $FI_{sync280}$ nor NPOC showed any correlation with protein contents. On the other hand, NPOC and carbohydrate concentrations displayed a moderate correlation with each other as R^2=0.72.

4.2.2.8. Organic matter formation and removal upon SynTiO$_2$ solar photocatalytic treatment of *E. coli* in "HA and WM" solution. UV-vis absorption and synchronous scan fluorescence spectra of organic matter remaining in "HA and WM" solution including *E. coli* cell inactivation products were presented in Figures 4.65 and 4.66, respectively. Irradiation time dependent absorbance changes were different from each other in UV wavelength range of λ=200-400 nm due to the presence of aromatic domains and color forming moieties (Color$_{436}$, UV$_{365}$ and UV$_{280}$) mainly originating from humic sub-fractions as also recorded sole HA spectral features. Irradiation time dependent sequential degradation of organic matter could be visualized throughout 60 min of irradiation period. In contradiction to previous set of TiO$_2$ solar photocatalytic treatment (Figure 4.36), no evident difference was observed between initial and t=0 conditions revealing insignificant surface interactions. On the other hand, absorbances detected at λ < 240 nm were characteristic to NO_3^- containing "HA and WM" solution.

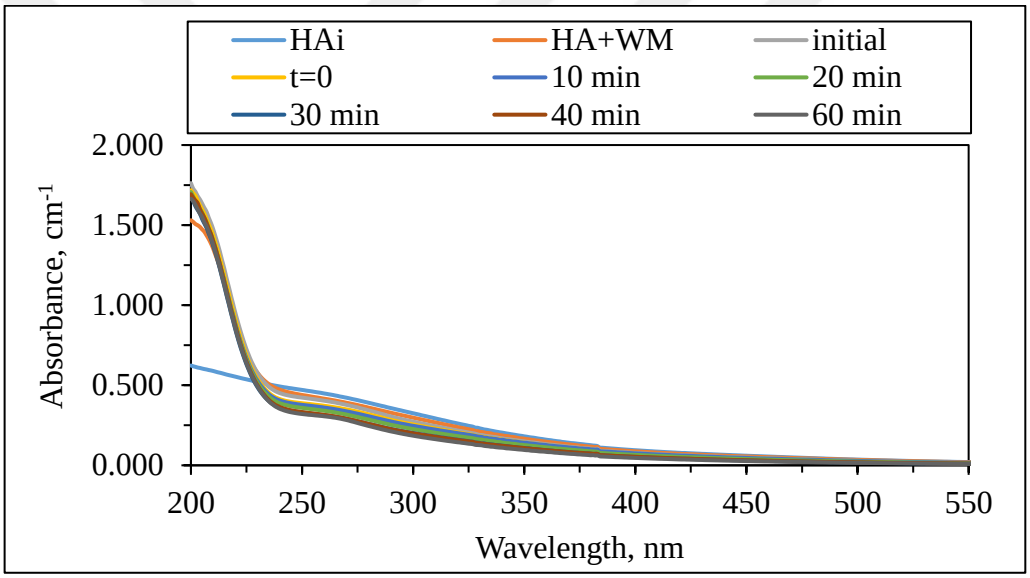

Figure 4.65. UV-vis absorption spectra of organic matter: Irradiation time dependent *E. coli* inactivation in "HA and WM" solution upon SynTiO$_2$ solar photocatalytic treatment.

Synchronous scan fluorescence spectra of the emerged organic matter displayed an intense peak at λ_{emis}=380 nm as was also observed in sole HA$_i$ solution (Figures 4.61 and 4.66). Besides the intense peaks at λ_{emis}=380 nm, two minor peaks at λ_{emis}=440 nm and 480 nm were detected as well. Similar peak wavelengths presenting the presence of aromatic hydrocarbons were also detected for *E. coli* in HA solution upon SynTiO$_2$ solar photocatalytic treatment (Figure 4.61). Similar to solar photolytic treatment of *E. coli* in "HA and WM" solution (Figure 4.18), "HA and WM" solution and initial condition, showed increased fluorescence intensities relative to sole HA$_i$ solution at λ_{emis} < 450 nm. After the addition of photocatalyst into solution matrix, a significant increase in FI$_{sync}$ data was observed relative to sole HA$_i$, "HA and WM", and initial conditions. It could be indicated that the

mechanistic effect of $SynTiO_2$ on bacteria cell wall could cause damaged cell wall structure and release of cytoplasmic organics resulting in increased FI_{sync} data. Similar findings could also be visualized with the use of TiO_2 (Figure 4.42). From a general perspective, FI_{sync} data did not follow an irradiation time dependent decreasing order. $FI_{sync380}$ data showed a decreasing trend between t_{irr}=10 min and 30 min conditions and followed by an increasing trend at 60 min of solar light exposure revealing that the re-emergence of removed fluorophoric groups following further irradiation periods.

Furthermore, $FI_{sync470}$ and $FI_{sync280}$ displayed changes in the range of 44.2-94.9 and 6.73-48.0, respectively (Figure 4.67). $FI_{sync280}$ of HA_i could not be detected however $FI_{sync280}$ in "HA and WM" solution was detected as 6.73. Due to the use of HA solution, the dominant fluorophoric group was accepted as $FI_{sync470}$.

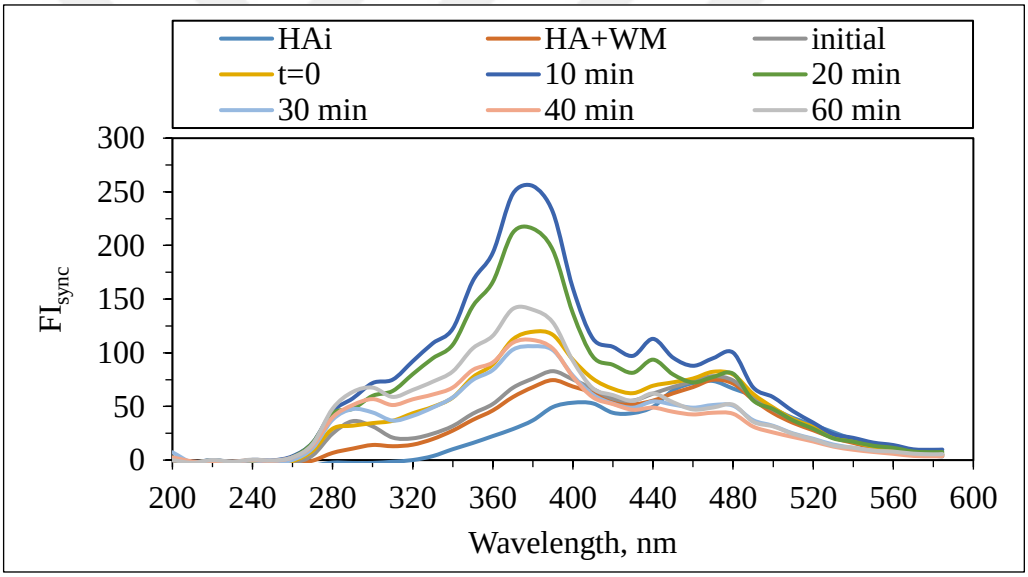

Figure 4.66. Synchronous scan fluorescence spectra of organic matter: Irradiation time dependent *E. coli* inactivation in "HA and WM" solution upon $SynTiO_2$ solar photocatalytic treatment.

Along with the presence of "HA and WM" solution as reaction matrix, NPOC expressed variations in the range of 4.87-18.3 mg/L (Figure 4.67). NPOC content showed an insignificant decrease between HA_i (4.87 mg/L) and "HA and WM" solution (4.77 mg/L) and increased up to t_{irr}=20 min (18.3 mg/L) due to release of organics from damaged and destructed *E. coli* cells, afterwards remained stable up to t_{irr}=30 min and followed by a decreasing trend until the end of 60 min solar light exposure duration (10.1 mg/L). According to almost remained stable *E. coli* enumerations at t_{irr}=40 min (6.75E+02 CFU/mL) and 60 min (4.67E+02 CFU/mL) (Figure 4.49), it

could be indicated that decreased NPOC content after t_{irr}=30 min could be related with degradation of both HA content and released cytoplasmic organic content from destructed *E. coli* cells.

Specified UV-vis parameters expressed a high presence due to the use of HA solution as a reaction matrix component. UV_{254}, as the most evident parameter, displayed changes in between 0.4626-0.3149. Excluding slightly increased UV_{254} at irradiation period of 40 min, UV_{254} showed a decreasing trend throughout the treatment, however obtained decrease could be considered as insignificant in comparison with TiO_2 solar photocatalytic treatment of *E. coli* in "HA and WM" solution (Figure 4.43). Similar lessened decrease in specified UV-vis parameters was also recorded upon solar photocatalytic *E. coli* inactivation in sole HA solution the presence of $SynTiO_2$ in comparison to use of TiO_2 as a bare photocatalyst specimen (Figures 4.38 and 4.62).

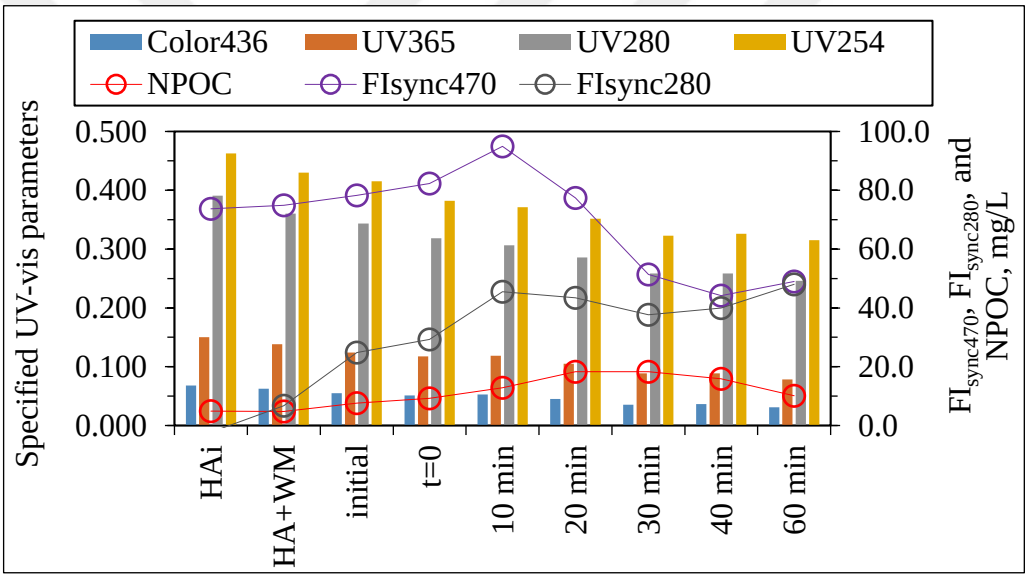

Figure 4.67. Specified UV-vis and fluroscence parameters of organic matter: Irradiation time dependent *E. coli* inactivation in "HA and WM" solution upon $SynTiO_2$ solar photocatalytic treatment.

Based on NPOC contents attained under all solar irradiation periods, specific UV-vis parameters as $SCoA_{436}$, $SUVA_{365}$, $SUVA_{280}$, $SUVA_{254}$, $SFI_{sync470}$, and $SFI_{sync280}$ were calculated and presented in Figure 4.68. as the most significant specific UV-vis parameter, $SUVA_{254}$ expressed changes in the range of 1.76-9.50 L/m mg during $SynTiO_2$ solar photocatalytic treatment indicating concomitant differences in both UV_{254} and NPOC removals. $SUVA_{254}$ showed a decreasing trend up to t_{irr}=30 min and increased at the end of t_{irr}=60 min. On the other hand, calculated $SFI_{sync470}$ and $SFI_{sync280}$ expressed variations in the range of 2.78-15.7 and 1.41-4.75, respectively. Due to the presence of HA

solution, $SFI_{sync470}$ displayed evident presence and accepted as the predominant fluorophoric group in compared to $SFI_{sync280}$.

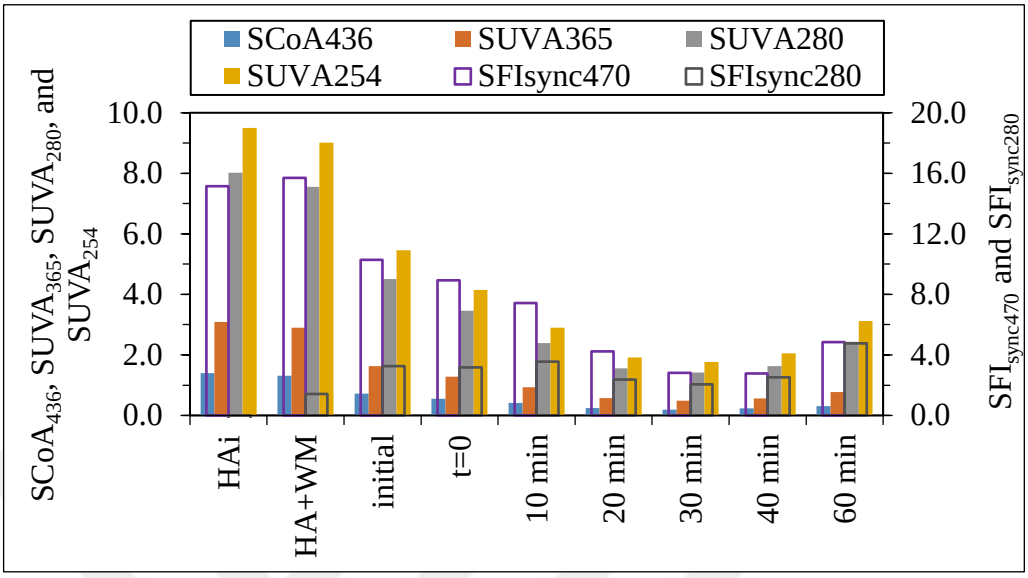

Figure 4.68. Specific UV-vis and fluroscence parameters of organic matter: Irradiation time dependent *E. coli* inactivation in "HA and WM" solution upon $SynTiO_2$ solar photocatalytic treatment.

Characteristic properties of organic matter present under initial and t=0 conditions, and t_{irr}=60 min of solar light exposure attained upon $SynTiO_2$ solar photocatalytic inactivation of *E. coli* in "HA and WM" solution were presented in Table 4.27.

Table 4.27. Characteristic properties of organic matter present in $SynTiO_2$ solar photolytic treatment of *E. coli* in "HA and WM" solution.

Irradiation time, min	UV-vis Spectroscopic Parameters, cm^{-1}				NPOC, mg/L	$SUVA_{254}$, L/m mg	$FI_{sync470}$	$SFI_{sync470}$	FI
	$Color_{436}$	UV_{365}	UV_{280}	UV_{254}					
Initial	0.0548	0.1242	0.3433	0.4155	7.61	5.46	78.3	10.3	1.17
t=0	0.0511	0.1176	0.3185	0.3821	9.21	4.15	82.3	8.94	1.19
60 min	0.0312	0.0784	0.2458	0.3149	10.1	3.12	49.0	4.85	1.26

Upon t_{irr}=60 min of $SynTiO_2$ solar photocatalytic treatment of *E coli* in " HA and WM" solution, 3.06 log *E. coli* reduction was achieved (Table 4.20), and released organic matter expressed the following UV-vis parameters; $Color_{436}$: 0.0312, UV_{365}: 0.0784, UV_{280}: 0.2458, UV_{254}: 0.3149, and NPOC as 10.1 mg/L. According to calculated $SUVA_{254}$, it could be indicated that initial and t=0 solutions displaying aromatic and hydrophobic features however after t_{irr}=60 min, organic content degraded and expressed mostly aliphatic and hydrophilic characteristics (Edzwald et al., 1985).

$FI_{sync470}$ and $SFI_{sync470}$ displayed a decrease at t_{irr}=60 min. However, $FI_{sync280}$ of initial, t=0, and t_{irr}=60 min conditions were detected as 24.8, 29.3, and 48.0, respectively and $SFI_{sync280}$ were calculated as 3.26, 3.18, and 4.75, respectively, showing an increased trend. FI of t_{irr}=60 min condition was calculated as 1.26 indicating the presence of fluorophores originating from HA content as expected.

EEM fluorescence contour plots of organic matter emerged and removed during irradiation time dependent *E. coli* inactivation in "HA and WM" solution during $SynTiO_2$ solar photocatalytic treatment were displayed in Figure 4.69.

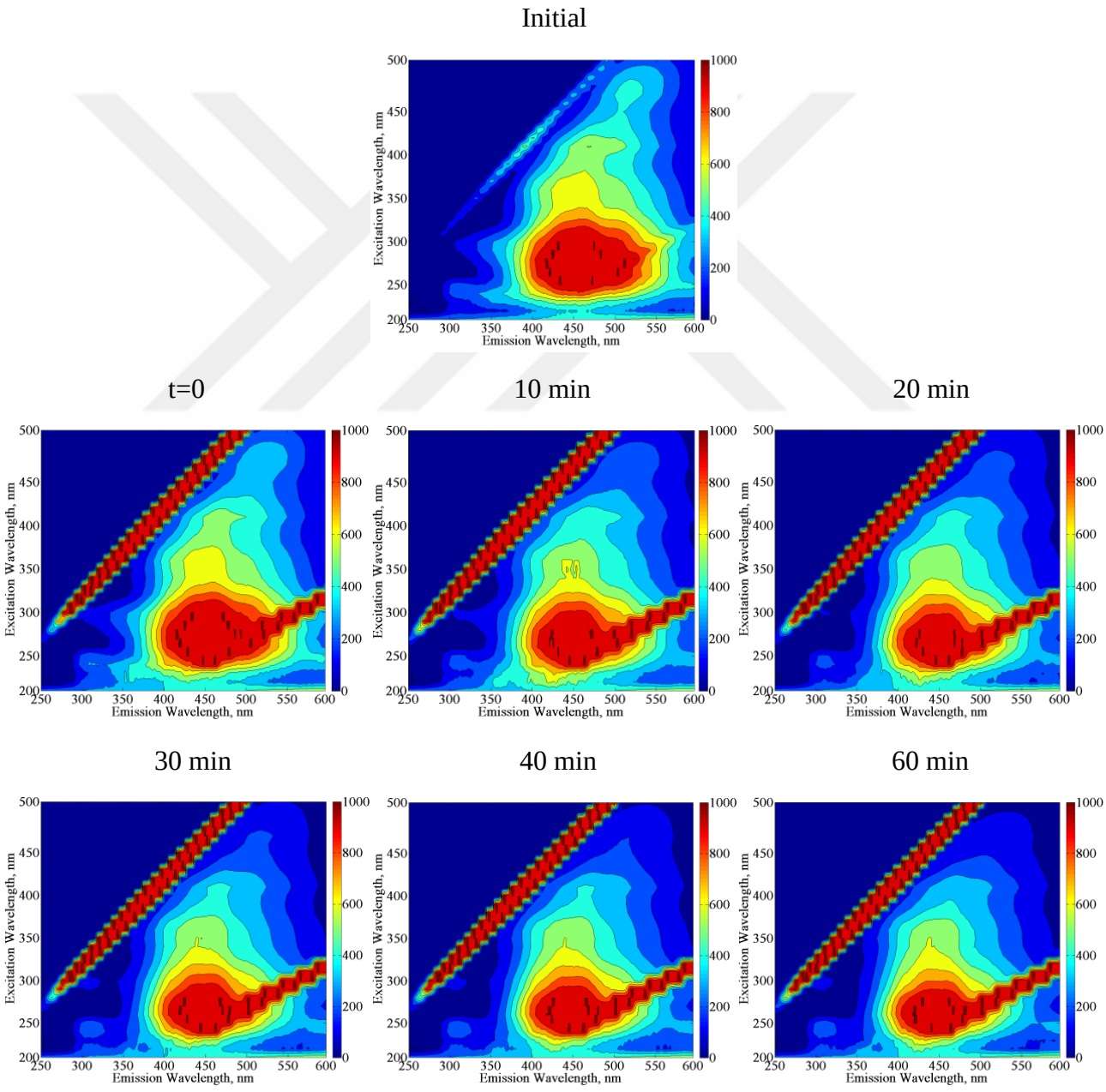

Figure 4.69. EEM fluorescence contour plots of organic matter: Irradiation time dependent *E. coli* inactivation in "HA and WM" solution upon $SynTiO_2$ solar photocatalytic treatment.

EEM fluorescence contour plots of *E. coli* in "HA and WM" solution upon $SynTiO_2$ solar photocatalytic treatment displayed the presence of Regions III, and V indicating that the fluorophores were mainly originated from fulvic-like and humic-like substances. Both humic-like and fulvic-like fluorophore intensities displayed a slight decrease throughout irradiation period of 60 min however they displayed more intense fluorescence in comparison to *E. coli* inactivation in HA solution (Figure 4.64). Similar finfings were also obtained from solar photolytic treatment of *E. coli* both in sole HA solution (Figure 4.16) and "HA and WM" solution (Figure 4.21). It could be indicated that the presence of WM in the solution matrix caused inhibition of HA degradation. Different from the TiO_2 solar photocatalytic treatment (Figure 4.45), $SynTiO_2$ expressed lower degradation of fulvic-like and humic-like substances. Moreover, Regions I, II and IV were quenched by fulvic-like and humic-like substances originating from HA as expected.

4.2.2.9. Mechanistic evaluation of *E. coli* inactivation upon $SynTiO_2$ solar photocatalytic treatment in "HA and WM" solution. Upon irradiation, as bacteria inactivation products of $SynTiO_2$ solar photocatalytic treatment of *E. coli* in "HA and WM" solution, total K, protein, and carbohydrate contents present in initial, t=0, and t_{irr}=60 min samples were presented in Table 4.28.

Table 4.28. Total K, protein, and carbohydrate content of time dependent *E. coli* inactivation in "HA and WM" solution upon $SynTiO_2$ solar photocatalytic treatment.

$SynTiO_2$ solar photocatalytic treatment	*E. coli* in "HA and WM"		
	Initial	t=0	60 min
Total K, mg/L	4.48	4.38	4.47
Protein, mg/L	6.65	5.95	13.3
Carbohydrate, mg/L	2.02	2.05	28.4

Total K content remained nearly constant under all conditions. The reason could be attributed to various attractive and repulsive electrostatic interactions as well as passive transport mechanism of *E. coli* cells regulating K^+ ion uptake from and/or release to reaction medium containing WM solution.

Upon solar photocatalytic treatment, substantial increase in both protein (6.65-13.3 mg/L) and carbohydrate (2.02-28.4 mg/L) concentrations were detected. Carbohydrate concentration showed higher increase than protein concentration similar to *E. coli* inactivation conducted in sole HA solution (Table 4.26). Protein contents and $FI_{sync280}$ displayed a strong correlation as R^2=0.93. Both protein and carbohydrate contents were plotted against NPOC separately and showed moderate correlations with each other as R^2=0.51 and R^2=0.60. Moreover, it could be concluded that increased

NPOC (Table 4.27) and intense EEM contour plots (Figure 4.69) were roughly correlated with detected high carbohydrate content.

4.2.2.10. Comparative evaluation of different experimental matrixes on $SynTiO_2$ solar photocatalytic inactivation mechanism of *E. coli.* Upon solar inactivation process via $SynTiO_2$ photocatalysis, total K, protein, and carbohydrate contents and bacteria enumerations attained in comparison to various conditions were given in Figure 4.70. Total K contents varied in between 0.61-4.48 mg/L being the lowest for the initial condition of *E. coli* in sole HA solution and the highest for the initial sample of *E. coli* in "HA and WM" solution. Total K content attained in WM containing treatments showed increased presence due to high total K concentration of sole WM solution (3.84 mg/L, Section 4.1.5). Considering total K concentrations of different matrix conditions individually, no significant difference was detected between initial, t=0 and t_{irr}=60 min conditions. Similar to previous treatments carried out in HA solution (Table 4.8 and 4.17), lower total K contents were obtained among other solution matrixes upon use of $SynTiO_2$ specimen. Except the presence of sole WM solution, total K and *E. coli* counts displayed a rough correlation as $R^2 > 0.71$.

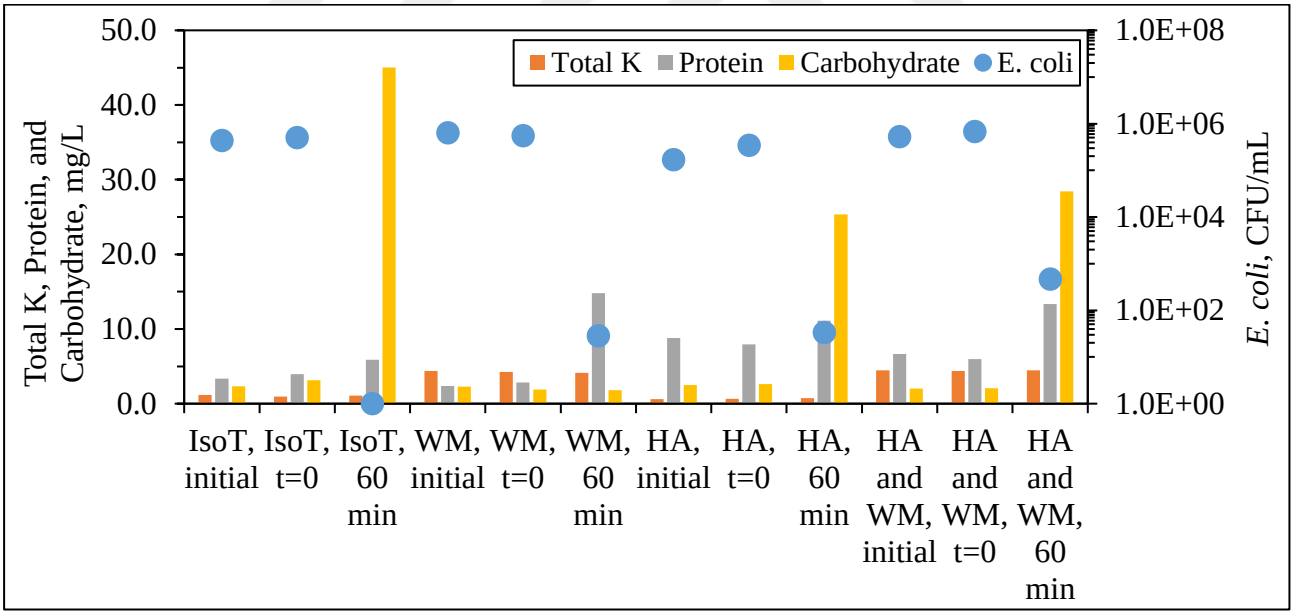

Figure 4.70. Initial, t=0, and t_{irr}=60 min total K, protein, and carbohydrate contents and bacteria enumeration results of *E. coli* inactivation upon $SynTiO_2$ solar photocatalytic treatment in various aqueous matrixes.

Covering all conditions, protein contents varied in between 2.35-14.8 mg/L being the lowest for initial and the highest for t_{irr}=60 min conditions of *E. coli* in WM solution. Similarly, carbohydrate contents varied in between 1.83-45.0 mg/L being the lowest upon treatment for t_{irr}=60 min of *E. coli* in WM solution whereas the highest for t_{irr}=60 min sample of *E. coli* in IsoT solution. Protein contents

under initial and t=0 conditions in HA solution containing reaction matrixes were higher than the case attained in IsoT and WM solutions. *E. coli* in IsoT solution for t_{irr}=60 min displayed a significant increase in carbohydrate content which could be resulting from an experimental error as explained in Section 4.2.2.3. Except inactivation profiles attained in WM solution, under all conditions an increasing trend for protein and carbohydrate contents were observed. *E. coli* inactivation upon t_{irr}=60 min showed a decrease in "HA and WM" solution (4.67E+02 CFU/mL) however the presence of sole HA did not cause a significant retardation effect on *E. coli* inactivation (3.35E+01 CFU/mL).

Released protein and carbohydrate contents, calculating by subtracting initial contents from the final contents attained upon t_{irr}=60 min, and bacteria LRV of SynTiO$_2$ solar photocatalytic treatment of *E. coli* in various solution matrixes were given in Figure 4.71. Calculation for WM solution revealed negative values indicating degradation of carbohydrate content. Released protein content was higher for WM solution (12.5 mg/L). It could be concluded that the presence of WM solution displayed selectivity towards degradation of carbohydrates rather than protein. Released carbohydrate content (42.7 mg/L) and LRV of *E. coli* (5.64) in IsoT solution were detected as the highest ones. *E. coli* LRV was inversely proportional to protein release for IsoT and WM solutions. Moreover, in the presence of HA and "HA and WM" solutions, *E. coli* LRV expressed inverse relation with released protein and carbohydrate concentrations. *E. coli* LRV were plotted against released protein concentration and no correlation was detected, whereas *E. coli* LRV and released carbohydrate contents displayed a strong correlation as R^2=0.84 excluding the presence of sole WM solution.

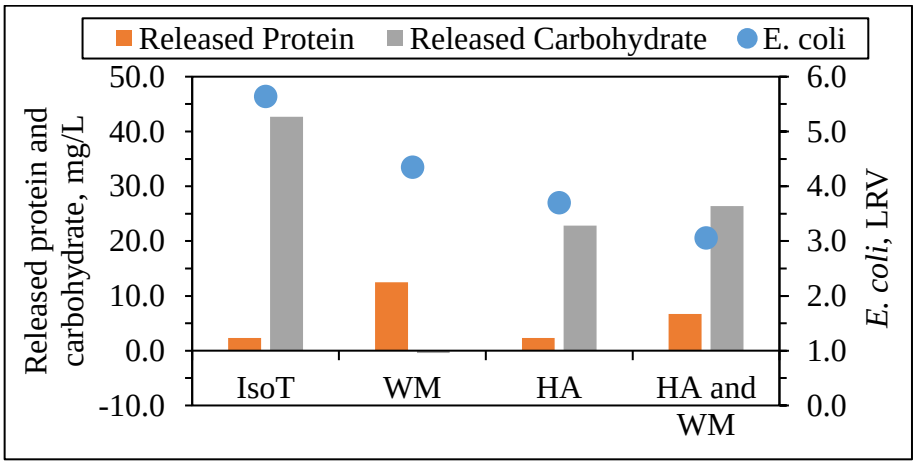

Figure 4.71. Released protein and carbohydrate content, and bacteria LRV of *E. coli* inactivation upon SynTiO$_2$ solar photocatalytic treatment in various aqueous matrixes.

Upon SynTiO$_2$ solar photocatalytic treatment of *E. coli* in various matrixes, the attained protein and carbohydrate contents, $FI_{sync280}$, UV_{280}, and NPOC data under initial, t=0, and t_{irr}=60 min

conditions were given in Figure 4.72. Similar UV_{280} values were obtained for initial, t=0, and t_{irr}=60 min samples of *E. coli* in IsoT solution. Both protein concentrations and UV_{280} showed an increasing trend for HA solution containing experimental conditions. All conditions, except HA initial solution, expressed higher $FI_{sync280}$ than protein contents. Moreover, a rough correlation as $R^2 > 0.67$ was detected between protein contents and $FI_{sync280}$ in the absence of WM solution.

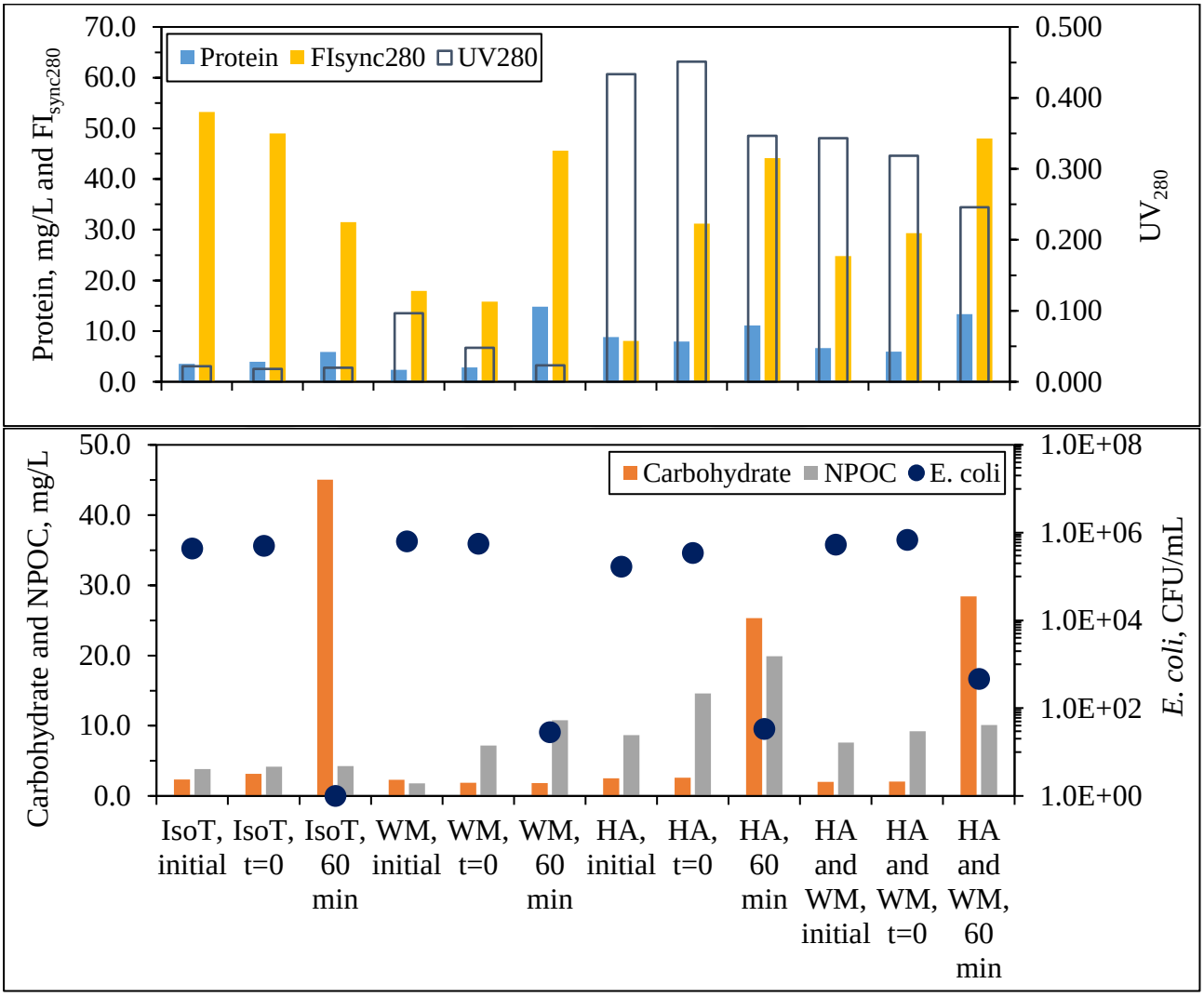

Figure 4.72. Initial, t=0, and t_{irr}=60 min protein and carbohydrate contents, $FI_{sync280}$, UV_{280}, NPOC, and bacteria enumeration results of $SynTiO_2$ solar photocatalytic treatment of *E. coli* in various aqueous matrixes.

Carbohydrate concentrations were higher than NPOC contents in t_{irr}=60 min samples of IsoT, HA and "HA and WM" solutions. NPOC measurements displayed an increasing trend under all experimental conditions. No correlation was detected between carbohydrate concentrations and NPOC in initial samples; however, t=0 and t_{irr}=60 min data displayed a rough correlation as $R^2 > 0.72$ except the presence of sole HA solution.

4.2.3. 0.25% Fe-TiO_2 Solar Photocatalytic Inactivation of *E. coli*

4.2.3.1. 0.25% Fe-TiO_2 solar photocatalytic *E. coli* inactivation under specified reaction conditions, reductions, and kinetics. *E. coli* suspension (N_o=1.18E+06 CFU/mL) was prepared in IsoT solution and subjected to solar photocatalytic treatment using 0.25% Fe-TiO_2 specimen. Upon irradiation for 30 min, *E. coli* cell count decreased to 3.45E+02 CFU/mL. Following prolonged light exposure of t_{irr}=60 min, *E. coli* cell count further decreased to 6.13E+01 CFU/mL. Under these conditions LRV was 4.28 and reduction was 99.99 %. Upon preparation of *E. coli* (N_o=9.17E+05 CFU/mL) suspension in WM solution, for an irradiation period of 30 min, *E. coli* count decreased to 2.16E+04 CFU/mL. Following light exposure of t_{irr}=60 min, *E. coli* count reached to 2.95E+03 CFU/mL revealing LRV as 2.49 and reduction as 99 %. In case that *E. coli* (N_o=6.13E+05 CFU/mL) suspension was prepared in HA solution, for an irradiation period of 30 min, *E. coli* count decreased to 9.79E+03 CFU/mL. Upon light exposure of t_{irr}=60 min, *E. coli* count diminished to 5.00E+03 CFU/mL expressing LRV as 2.09 and reduction as 99 %. *E. coli* (N_o=9.26E+05 CFU/mL) suspension was also prepared in a solution of "HA and WM" components and was subjected to an irradiation period of 30 min in which *E. coli* count decreased to 1.17E+05 CFU/mL. Following light exposure of t_{irr}=60 min, *E. coli* count declined to 6.73E+03 CFU/mL revealing LRV as 2.14 and reduction as 99 %. Based on these results, the effect of solution matrix could be displayed in terms of LRV of *E. coli* in an increasing order as: HA < "HA and WM" < WM < IsoT. *E. coli* inactivation profiles and first order kinetic parameters were presented in Figure 4.73 and Table 4.29.

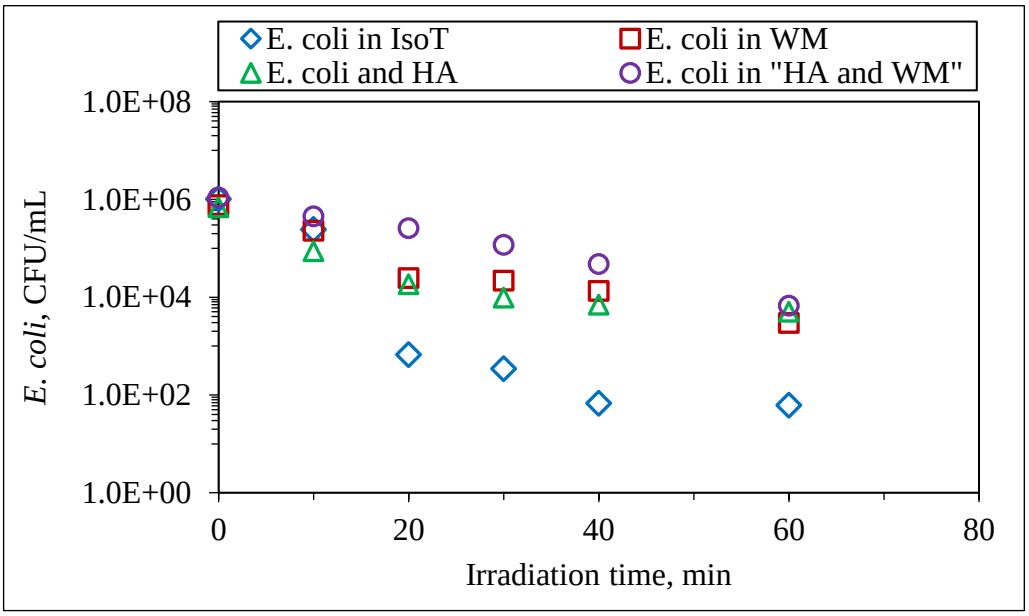

Figure 4.73. Irradiation time dependent *E. coli* inactivation upon 0.25% Fe-TiO_2 solar photocatalytic treatment in various solution matrixes.

0.25% Fe-TiO_2 solar photocatalytic treatment of *E. coli* in IsoT solution resulted in a rather fast reduction with k=0.174 min^{-1} and half-life as 3.98 min. In the presence of HA, a reaction rate constant of k=0.0774 min^{-1} and half-life as 8.95 min were attained. The effect of reaction medium could also be expressed in terms of inactivation reaction rate constant (k, min^{-1}) in a decreasing order as; IsoT > WM > "HA and WM" > HA. Irrespective of the minor differences in initial bacteria counts, inactivation rates (CFU/mL min) also followed the same trend as; 2.05E+05 > 8.16E+04 > 7.71E+04 > 4.74E+04 for IsoT, WM, "HA and WM", and HA, respectively.

Table 4.29. 0.25% Fe-TiO_2 solar photocatalytic treatment of *E. coli*: Inactivation parameters.

Matrix	First order kinetic model			LRV	Reduction, %
	k, min^{-1}	$t_{1/2}$, min	R, CFU/mL min		
E. coli in IsoT	0.174	3.98	2.05E+05	4.28	99.99
E. coli in WM	0.0890	7.79	8.16E+04	2.49	99
E. coli and HA	0.0774	8.95	4.74E+04	2.09	99
E. coli in "HA and WM"	0.0833	8.32	7.71E+04	2.14	99

Solar photocatalytic treatment of *E. coli* in IsoT solution with 0.25% Fe-TiO_2 showed the highest bacteria reduction percentage among other experiment media, as 99.99 %. However, its LRV, which was detected as 4.28, was lower than the results of TiO_2 (Table 4.11) and SynTiO_2 (Table 4.20). Birben and colleagues studied with several doped TiO_2 types as; N-doped, Se-doped and Se-N co-doped under similar experimental conditions, except the use of deionized water as working solution, and they achieved rate constants (k, min^{-1}) as 0.153, 0.155 and 0.317 for N-doped, Se-N co-doped and Se-doped, respectively (Birben et al., 2017a). It could be indicated that 0.25% Fe-TiO_2 expressed a slightly higher reduction rate constant than N-doped and Se-N co-doped TiO_2 species. On the other hand, rate constant of Se-doped TiO_2 was higher than 0.25% Fe-TiO_2.

0.25% Fe-TiO_2 solar photocatalytic treatment of *E. coli* in WM solution showed lower % reduction (99 %) than *E. coli* in IsoT solution (99.99 %) due to the inhibition effect of WM components (Section 2.5). LRV for *E. coli* inactivation in WM solution was the lowest in comparison to either solar photolytic (Table 4.2) or TiO_2/SynTiO_2 photocatalytic treatments carried out so far (Tables 4.11 and 4.20).

The role of HA presence in *E. coli* inactivation using 0.25% Fe-TiO_2 solar photocatalysis could be explained as resulting in the lowest *E. coli* LRV as 2.09. It could be indicated that 0.25% Fe-TiO_2 had selectivity towards *E. coli* rather than organic matter like SynTiO_2 due to detected higher *E. coli* reduction than sole TiO_2. Birben and colleagues, having worked with the same 0.25% Fe-TiO_2, indicated that doped TiO_2 showed a retardation effect on HA removal rates compared to undoped

TiO_2 (Birben et al., 2017b). This information could support *E. coli* selectivity suggestion about 0.25% Fe-TiO_2. Moreover, in another study of Birben and colleagues, in which under similar experimental conditions other doped TiO_2 species were employed, reaction rate constants were 0.163, 0.110 and 0.096 min^{-1} for N-doped, Se-doped and Se-N co-doped, respectively (Birben et al., 2017a). Bacteria reduction rate constant of 0.25% Fe-TiO_2 as 0.0774 min^{-1} was considerably lower in comparison to other doped TiO_2 species. It could be concluded that in the presence of HA, N-doped TiO_2 has the fastest bacteria reduction among other doped TiO_2 species.

E. coli in "HA and WM" solution solar photocatalytic treatment with 0.25% Fe-TiO_2 showed higher bacteria LRV than HA, as 2.14. It could be indicated that, the addition WM solution displayed no significant retardation effect as different than the presence of only HA solution. In the view of these very close *E. coli* LRV of WM, HA and "HA and WM" solutions, it could be concluded that the presence of HA more negatively affects *E. coli* inactivation than WM solution. Irrespective of the minor differences in LRV of these three solution matrixes, similar bacteria reduction percentages were detected as 99 %.

4.2.3.2. Organic matter formation and removal upon 0.25% Fe-TiO_2 solar photocatalytic treatment of *E. coli* in IsoT solution. UV-vis absorption and synchronous scan fluorescence spectra of organic matter in solution were presented in Figures 4.74 and 4.75, respectively. Irradiation time dependent absorbance changes were significantly similar to each other in UV wavelength range of λ=200-250 nm displaying the absence of aromatic domains and color forming moieties ($Color_{436}$, UV_{365} and UV_{280}) that should be recorded in longer wavelengths as $\lambda \geq 280$ nm and extending to visible region. Detected absorbances at $\lambda < 210$ nm were characteristic to present IsoT solution (Tong et al., 2020). UV spectral features displayed similarities to the ones attained upon solar photolytic (Figure 4.2) and photocatalytic treatments with the use of bare TiO_2 specimens as TiO_2 (Figure 4.26) and SynTiO_2 (Figure 4.50).

Synchronous scan fluorescence spectra of the emerged organic matter displayed an intense peak at λ_{emis}=280 nm (Figure 4.75). Moreover, the presence of fluorophoric groups expressing very minor intensities at $\lambda_{emis}\approx$470 nm could also be encountered similar to findings attained with the solar photolytic treatment (Figure 4.3) and use of TiO_2 (Figure 4.27) and SynTiO_2 (Figure 4.51) specimens in solar photocatalytic treatments. An irradiation time dependent decreasing order in $FI_{sync280}$ was observed throughout the experiment. On the other hand, contrary to very low intensities of $FI_{sync470}$ in the range of 0.0948-0.752, dominant $FI_{sync280}$ displayed changes in between 24.1-51.0. In the absence of HA as solution matrix, the key fluorophoric group was recognized as $FI_{sync280}$.

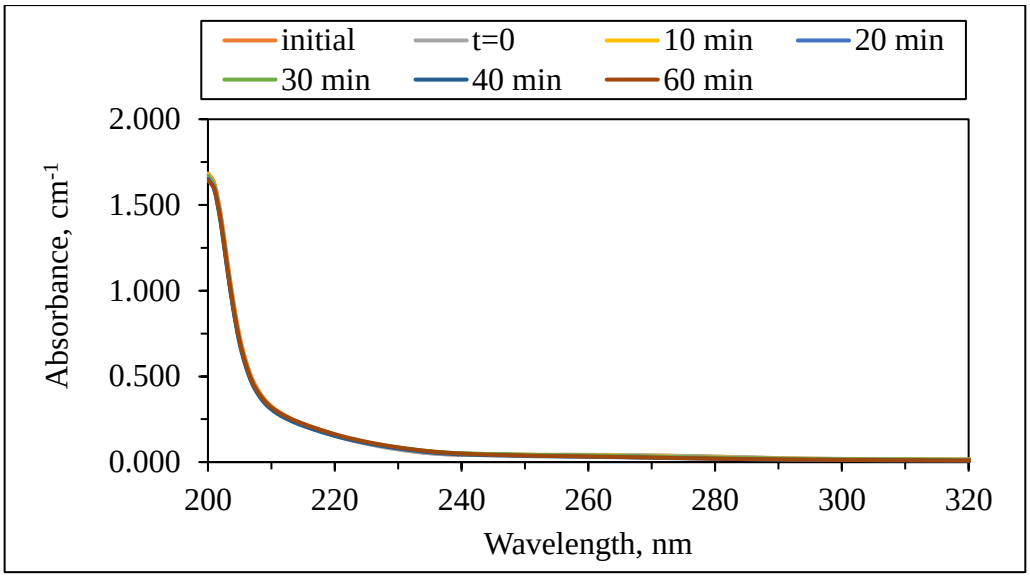

Figure 4.74. UV-vis absorption spectra of organic matter: Irradiation time dependent *E. coli* inactivation in IsoT solution upon 0.25% Fe-TiO_2 solar photocatalytic treatment.

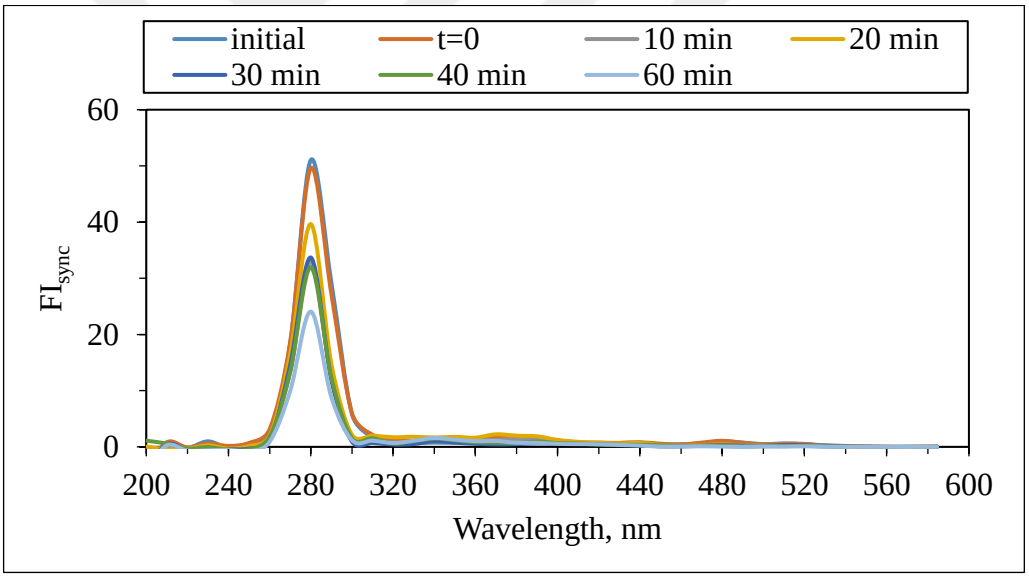

Figure 4.75. Synchronous scan fluorescence spectra of organic matter: Irradiation time dependent *E. coli* inactivation in IsoT solution upon 0.25% Fe-TiO_2 solar photocatalytic treatment.

From a general perspective, NPOC data expressed variations in the range of 0.847-4.07 mg/L (Figure 4.76). NPOC content increased up to t_{irr}=20 min (0.847-4.01 mg/L) due to the release of organics from the damaged and destructed *E. coli* cells, followed by a minor fluctuation trend up to t_{irr}=40 min (3.69-4.07 mg/L) and then decreased to 2.91 mg/L during solar photocatalytic treatment. As the most significant specified UV-vis parameter, UV_{254} displayed variations in the range of 0.0337-0.0422. The highest UV_{254} was attained for initial condition (0.0422) as could also be considered as similar to t=0 (0.0418) and t_{irr}=10 min (0.0417) conditions although variations were insignificant.

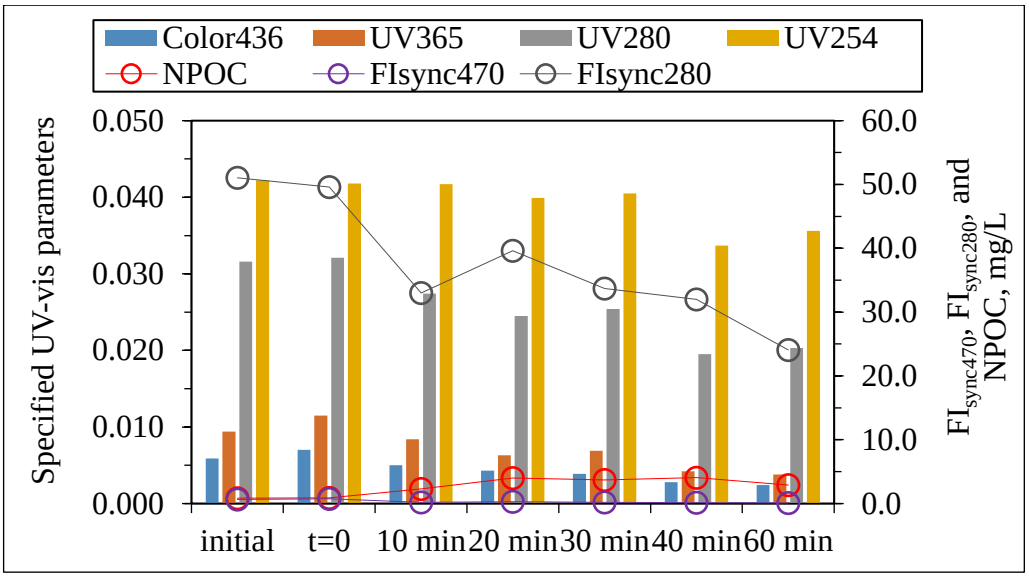

Figure 4.76. Specified UV-vis and fluroscence parameters of organic matter: Irradiation time dependent *E. coli* inactivation in IsoT solution upon 0.25% Fe-TiO_2 solar photocatalytic treatment.

Based on NPOC contents, all UV-vis and fluorescence specific parameters as $SCoA_{436}$, $SUVA_{365}$, $SUVA_{280}$, $SUVA_{254}$, $SFI_{sync470}$, and $SFI_{sync280}$ parameters were calculated (Figure 4.77). Most importantly, $SUVA_{254}$ displayed variations (0.828-4.982 L/m mg) during 0.25% Fe-TiO_2 solar photocatalytic treatment indicating concomitant differences in both UV_{254} and NPOC removals.

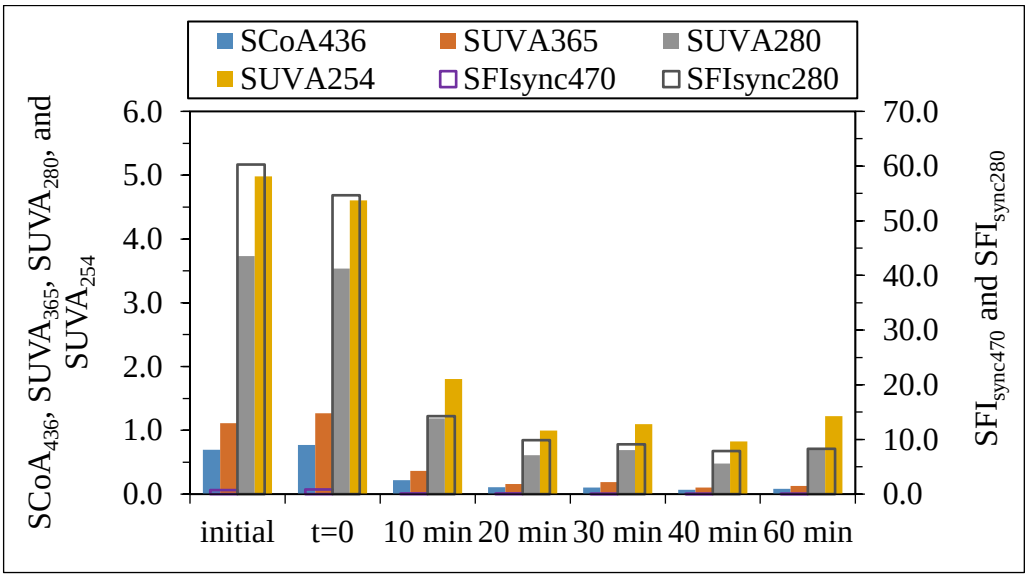

Figure 4.77. Specific UV-vis and fluroscence parameters of organic matter: Irradiation time dependent *E. coli* inactivation in IsoT solution upon 0.25% Fe-TiO_2 solar photocatalytic treatment.

Although $SCoA_{436}$, $SUVA_{365}$, $SUVA_{280}$ were also presented, respective specified parameters were very low in comparison to total NPOC contents of the organic matter. Similar findings were

reported upon use of bare TiO_2 specimens as TiO_2 (Figure 4.28) and $SynTiO_2$ (Figure 4.52). The role of Fe doping of TiO_2 could not be visualized under the specified experimental conditions.

In a similar manner, $SFI_{sync470}$ expressed variations in the range of 0.0326-0.829 expressing insignificant contribution of fluorophores detected at λ_{emis}=470 nm. As indicated above, $SFI_{sync280}$ expressed considerable variations in the range of 7.86-60.3. The main fluorophoric group was accepted as $SFI_{sync280}$ similar to previous solar photocatalytic treatments conducted with the use of TiO_2 (Figure 4.29) and $SynTiO_2$ (Figure 4.53) in IsoT solution.

For simplicity purposes, based on the irradiation time dependent variations in UV-vis and fluorescence spectroscopic properties along with NPOC data, characteristic properties of organic matter under initial condition, upon introduction of 0.25% Fe-TiO_2 (t=0) and at the end of 0.25% Fe-TiO_2 solar photocatalytic treatment for irradiation period of 60 min were presented in Table 4.30.

Table 4.30. Characteristic properties of organic matter present in 0.25% Fe-TiO_2 solar photocatalytic treatment of *E. coli* in IsoT solution.

Irradiation time, min	UV-vis Spectroscopic Parameters, cm^{-1}				NPOC, mg/L	$SUVA_{254}$, L/m mg	$FI_{sync280}$	$SFI_{sync280}$	FI
	$Color_{436}$	UV_{365}	UV_{280}	UV_{254}					
Initial	0.0059	0.0094	0.0316	0.0422	0.847	4.98	51.1	60.3	1.33
t=0	0.0070	0.0115	0.0321	0.0418	0.908	4.60	49.6	54.6	1.68
60 min	0.0024	0.0038	0.0203	0.0356	2.91	1.22	24.1	8.27	1.84

Upon irradiation for 60 min in 0.25% Fe-TiO_2 solar photocatalytic treatment at which 4.28 log reduction of *E. coli* in IsoT was attained (Table 4.29), released organic matter expressed the following UV-vis parameters (cm^{-1}); $Color_{436}$: 0.0024, UV_{365}: 0.0038, UV_{280}: 0.0203, UV_{254}: 0.0356, and NPOC as 2.91 mg/L. After t_{irr}=60 min, calculated $SUVA_{254}$ as 1.22 L/m mg represents that the remaining organic matter could be considered having hydrophilic and aliphatic character (Edzwald et al., 1985).

Due to the degradation of protein content, $FI_{sync280}$ displayed a decrease at the end of 60 irradiation period. $SFI_{sync280}$ expressed a decrease after t_{irr}=60 min in accordance with the increased NPOC content due to released organic material from bacteria. Moreover, $FI_{sync470}$ of initial, t=0, and t_{irr}=60 min conditions were detected as 0.624, 0.753, and 0.0948, respectively. Almost insignificant $SFI_{sync470}$ of initial, t=0, and t_{irr}=60 min conditions were calculated as 0.737, 0.829, and 0.0326, respectively. At t_{irr}=60 min, FI was calculated as 1.84 that could mostly be related to microbially derived organic matter. Similar finding was also reported by Birben and colleagues for N-doped TiO_2 (Birben et al., 2017a).

EEM fluorescence contour plots of organic matter emerged and removed during irradiation time dependent *E. coli* inactivation in IsoT solution during 0.25% Fe-TiO_2 solar photocatalytic treatment were displayed in Figure 4.78.

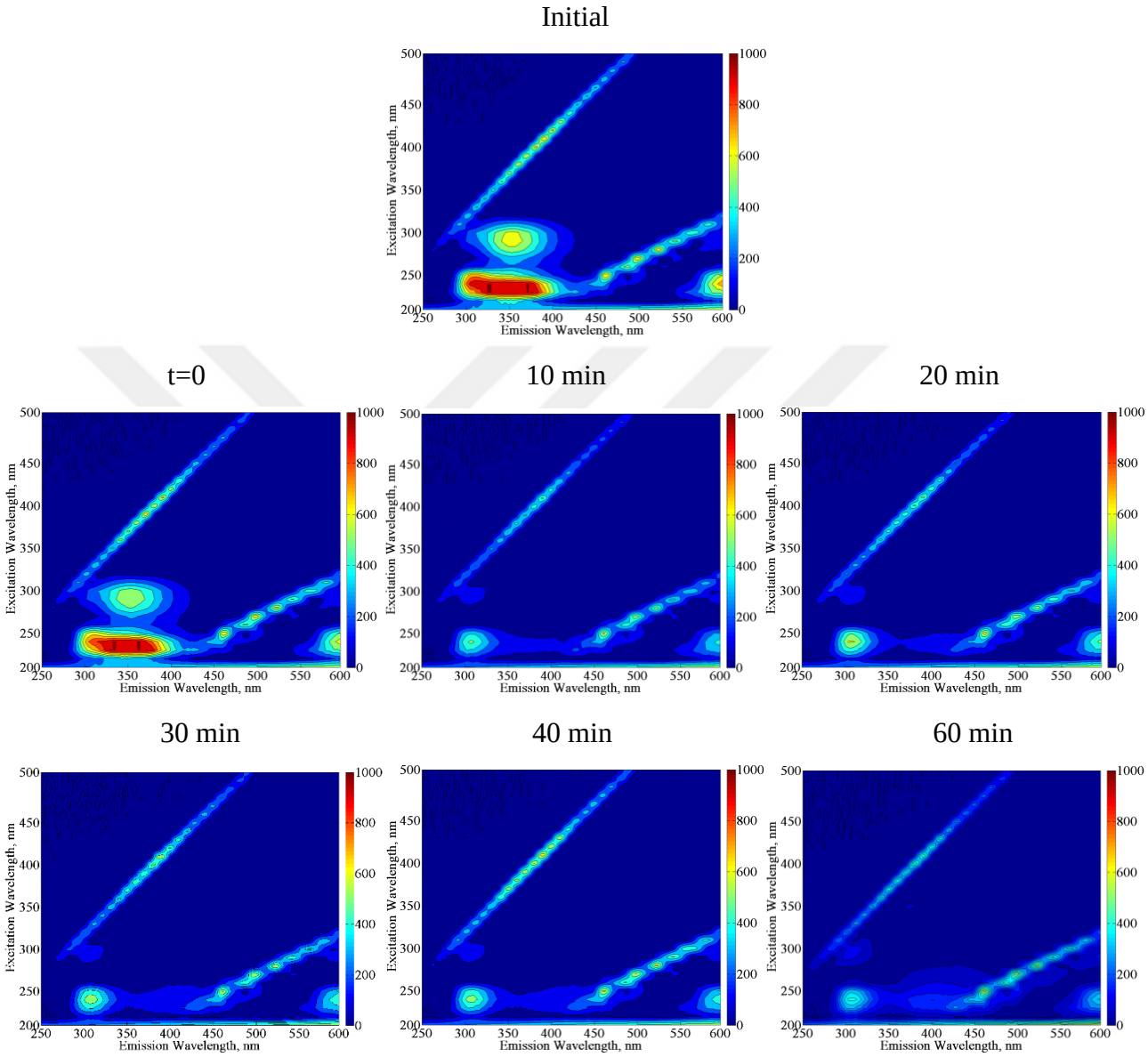

Figure 4.78. EEM fluorescence contour plots of organic matter: Irradiation time dependent *E. coli* inactivation in IsoT solution upon 0.25% Fe-TiO_2 solar photocatalytic treatment.

EEM fluorescence contour plots displayed the presence of Regions I, II and IV expressing that the fluorophores were mainly originated from microbial by-products and proteins under all irradiation conditions. Following further irradiation periods, released microbial by-products and proteins from *E. coli* cells showed a decreasing trend in accordance with the solar photocatalytic degradation of organic matter and reduction of *E. coli*. However, fluorescence intensities displayed quite low changes after 30 min of irradiation period in accordance with relatively close *E. coli* enumeration

results obtained between t_{irr}=30 min (3.45E+02 CFU/mL) and 60 min (6.13E+01 CFU/mL) (Figure 4.73). Moreover, EEM contour plots of 0.25% Fe-TiO_2 solar photocatalytic treatment of *E. coli* in IsoT solution have more intense results than TiO_2 solar photocatalytic treatment in IsoT solution (Figure 4.30) which could be resulting from the lower bacteria reduction percentage of 0.25% Fe-TiO_2 (LRV as 5.90 for TiO_2; LRV as 4.28 for 0.25% Fe-TiO_2 solar photocatalytic inactivation of *E. coli* in IsoT solution) (Tables 4.11 and 4.29).

4.2.3.3. Mechanistic evaluation of *E. coli* inactivation upon 0.25% Fe-TiO_2 solar photocatalytic treatment in IsoT solution. Upon irradiation, as bacteria inactivation products of 0.25% Fe-TiO_2 solar photocatalytic treatment of *E. coli* in IsoT solution, total K, protein, and carbohydrate contents present in initial, t=0, and t_{irr}=60 min samples were presented in Table 4.31.

Table 4.31. Total K, protein, and carbohydrate contents of time dependent *E. coli* inactivation in IsoT solution upon 0.25% Fe-TiO_2 solar photocatalytic treatment.

0.25% Fe-TiO_2 solar photocatalytic treatment	*E. coli* in IsoT solution		
	Initial	t=0	60 min
Total K, mg/L	1.35	1.12	1.15
Protein, mg/L	1.20	1.07	6.44
Carbohydrate, mg/L	1.58	2.18	6.00

Total K content displayed a slight fluctuation as 0.23 mg/L similar to SynTiO_2 (Table 4.22). At t=0, total K showed an immediate adsorption removal as 17.0 % and decreased from 1.35 mg/L (initial) to 1.12 mg/L. After irradiation period of 60 min, almost the same total K concentration was detected with t=0 condition. The reason could be attributed to adsorption of released K^+ ions from damaged bacteria onto negatively charged *E. coli* cell wall particles and/or 0.25% Fe-TiO_2 particles having dominantly negatively charges sites at experimental pH (≈7) due to its pH_{zpc} as 4.80 (Birben et al., 2017).

E. coli in IsoT solution upon 0.25% Fe-TiO_2 solar photocatalytic treatment showed increase in both protein and carbohydrate content at the end of 60 min treatment period. Similar increase was detected for protein and carbohydrate contents after 60 min of irradiation period. Protein concentrations were plotted against $FI_{sync280}$ in order to detect if there is any correlation between these parameters; and a strong correlation as R^2=1.00 was detected. Furthermore, NPOC data were plotted against protein and carbohydrate concentrations separately, both parameters displayed strong correlations with NPOC as R^2=1.00 and R^2=0.99, respectively.

4.2.3.4. Organic matter formation and removal upon 0.25% Fe-TiO_2 solar photocatalytic treatment of *E. coli* in WM solution. UV-vis absorption spectra of organic matter in solution were presented in Figure 4.79. Irradiation time dependent absorbance changes were significantly similar to each other in UV wavelength range of λ=200-320 nm in the slight presence of aromatic domains and color forming moieties ($Color_{436}$, UV_{365} and UV_{280}) originating from the components of WM solution. UV-vis absorption spectra obtained from organic matter in WM solution displayed a declining trend without any absorption peaks complying UV-vis absorption spectra of humic substance which was represented in Section 2.4. (Figure 2.16a). However, the use of NO_3^- containing WM solution resulted in high light absorption at λ < 210 nm originating from the presence of NO_3^- having its λ_{max} at approximately 200 nm (Krishnan and Guha, 1934; Edwards at el., 2001).

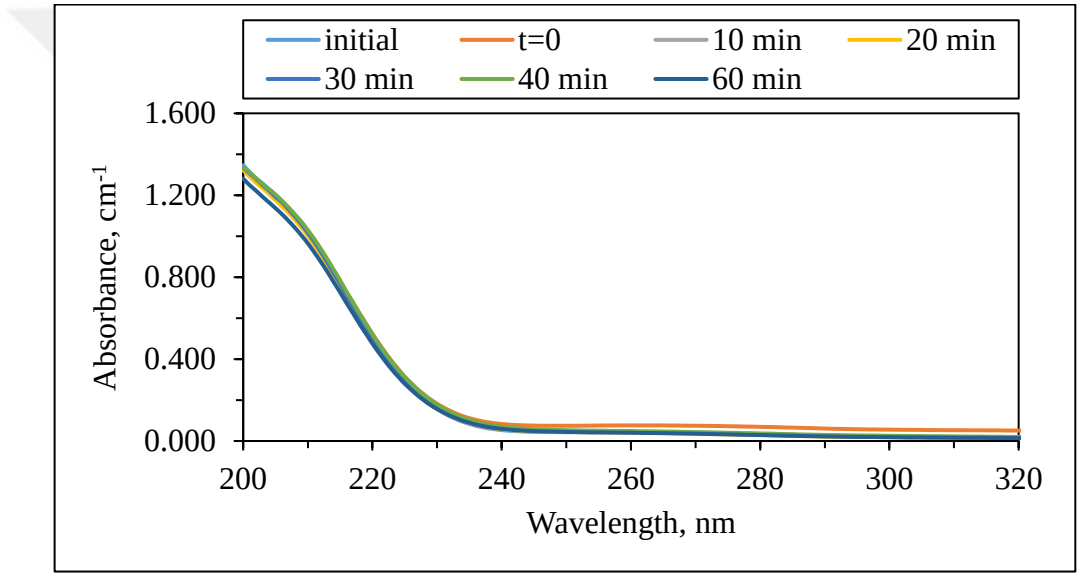

Figure 4.79. UV-vis absorption spectra of organic matter: Irradiation time dependent *E. coli* inactivation in WM solution upon 0.25% Fe-TiO_2 solar photocatalytic treatment.

Synchronous scan fluorescence spectra of emerged organic matter displayed an intense peak at λ_{emis}=280 nm (Figure 4.80). FI_{sync} data displayed a significant increase at t_{irr}=40 min followed by a declining trend during solar photocatalytic treatment. It could be indicated that fluorophoric groups could be reemerged and degraded again throughout specified irradiation period. The presence of fluorophores was evident at λ_{emis} > 300 nm displaying a tailing effect rather than a well-defined peak. Moreover, the presence of fluorophoric groups expressing very minor intensities at λ_{emis}≈470 nm could also be encountered similar to findings attained in IsoT solution (Figure 4.75). Furthermore, in the absence of humic content, $FI_{sync470}$ displayed almost featureless intensities in the range of 0.293-1.47 however dominant $FI_{sync280}$ expressed variations in between 34.6-52.6. The main fluorophoric groups were accepted as $FI_{sync280}$.

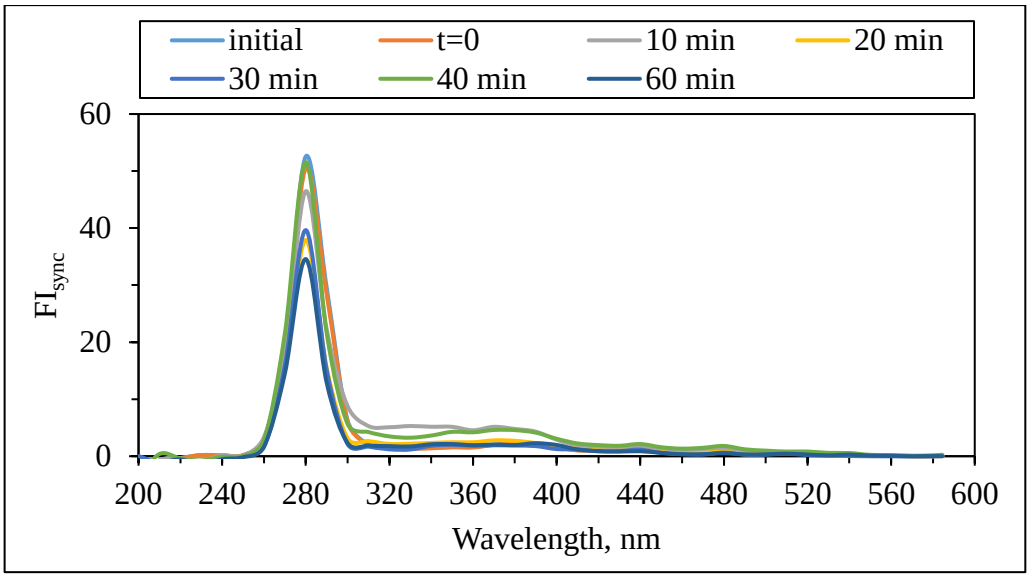

Figure 4.80. Synchronous scan fluorescence spectra of organic matter: Irradiation time dependent *E. coli* inactivation in WM solution upon 0.25% Fe-TiO_2 solar photocatalytic treatment.

NPOC expressed variations in the range of 0.755-2.46 mg/L (Figure 4.81). NPOC content displayed a minor decrease between initial (0.957 mg/L) and t=0 (0.755 mg/L) due to adsorptive removal of organic content after introduction of photocatalyst into the system, and then followed by an increasing trend up to t_{irr}=30 min (2.46 mg/L) originating from released organics from the damaged and destructed *E. coli* cells and decreased during solar photocatalytic treatment (1.88 mg/L).

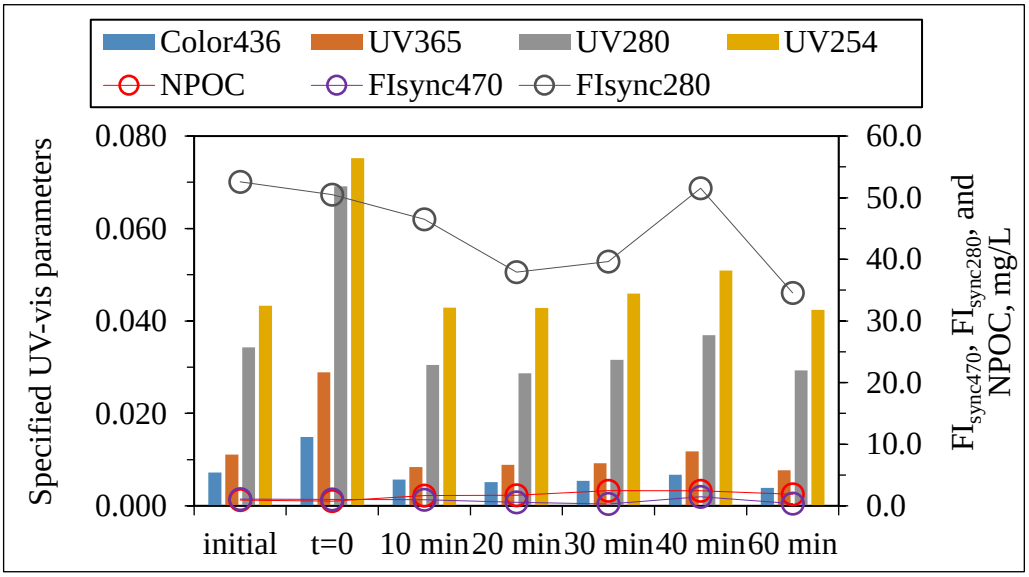

Figure 4.81. Specified UV-vis and fluroscence parameters of organic matter: Irradiation time dependent *E. coli* inactivation in WM solution upon 0.25% Fe-TiO_2 solar photocatalytic treatment.

Similar to previous solar photolytic (Figure 4.9) and photocatalytic treatments of *E. coli* in WM solution (Figures 4.33 and 4.57), all UV-vis displayed quite low presence. On the other hand, $Color_{436}$

and UV_{365} expressed lower presence than UV_{280} and UV_{254} due to non-existence and subsequent degradation of color forming moieties of the released organic matrix upon irradiation, and the use of WM solution, which was a colorless solution as well. As the most significant UV-vis parameter, UV_{254} displayed variations in between 0.0424 and 0.0752 being the lowest for t_{irr}=60 min and the highest for t=0 conditions. The role of Fe doping of TiO_2 could not be visualized under the specified experimental conditions.

Based on NPOC contents, $SCoA_{436}$, $SUVA_{365}$, $SUVA_{280}$, $SUVA_{254}$, $SFI_{sync470}$, and $SFI_{sync280}$ parameters were calculated and presented in Figure 4.82. $SUVA_{254}$ displayed variations in the range of 1.87-9.96 L/m mg during 0.25% Fe-TiO_2 solar photocatalytic treatment expressing differences in both UV_{254} and NPOC removals. Due to minor presence of $Color_{436}$ and UV_{365}, calculated $SCoA_{436}$ and $SUVA_{365}$ was almost insignificant. On the other hand, calculated specific UV-vis and fluroscence parameters presented higher presence from prior solar photolytic (Figure 4.10) and photocatalytic treatments conducted in WM solution (Figures 4.34 and 4.58).

Moreover, due to the absence of humic matter in the solution matrix, $SFI_{sync470}$ displayed almost insignificant presence in between 0.119-1.38 however owing to released protein content from damaged bacteria cells, $SFI_{sync280}$ expressed variations in the range of and 18.4-66.8. The highest $SFI_{sync470}$ and $SFI_{sync280}$ was calculated for t=0 condition in accordance with the lowest NPOC content of the sample. The predominant fluorophoric group was recognized as $SFI_{sync280}$ in the absence of HA solution as solution media.

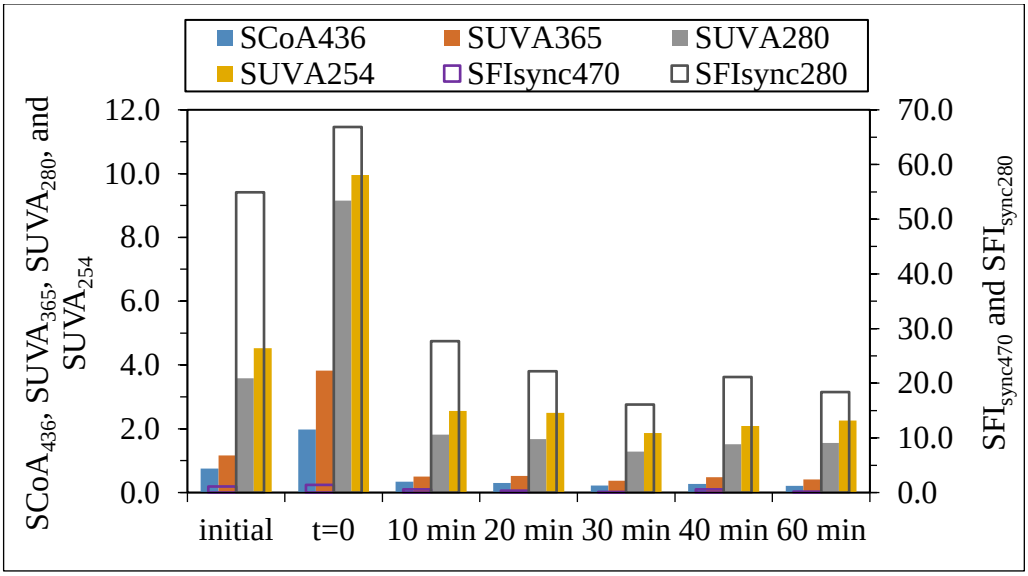

Figure 4.82. Specific UV-vis and fluroscence parameters of organic matter: Irradiation time dependent *E. coli* inactivation in WM solution upon 0.25% Fe-TiO_2 solar photocatalytic treatment.

Characteristic properties of organic matter present under initial condition, upon introduction of 0.25% Fe-TiO_2 (t=0) and at the end of 0.25% Fe-TiO_2 solar photocatalytic treatment for irradiation period of 60 min were presented in Table 4.32.

Table 4.32. Characteristic properties of organic matter present in 0.25% Fe-TiO_2 solar photolytic treatment of *E. coli* in WM solution.

Irradiation time, min	UV-vis Spectroscopic Parameters, cm^{-1}				NPOC, mg/L	$SUVA_{254}$, L/m mg	$FI_{sync280}$	$SFI_{sync280}$	FI
	$Color_{436}$	UV_{365}	UV_{280}	UV_{254}					
Initial	0.0072	0.0111	0.0343	0.0433	0.957	4.53	52.6	54.9	1.32
t=0	0.0149	0.0289	0.0691	0.0752	0.755	9.96	50.5	66.8	1.23
60 min	0.0039	0.0077	0.0293	0.0424	1.88	2.26	34.6	18.4	1.74

Upon solar photocatalytic treatment using 0.25% Fe-TiO_2 specimen for irradiation period of 60 min, where 2.49 log reduction of *E. coli* in WM was attained (Table 4.29), released organic matter expressed the following UV-vis parameters (cm^{-1}); $Color_{436}$: 0.0039, UV_{365}: 0.0077, UV_{280}: 0.0293, UV_{254}: 0.0424, and NPOC as 1.88 mg/L.

$SUVA_{254}$ was calculated as 4.53, 9.95, and 2.26 L/m mg at for initial, t=0, and t_{irr}=60 min conditions, respectively. According to findings of Edzwald and colleagues, $SUVA_{254} < 3$ indicates the presence of hydrophilic and aliphatic content and $SUVA_{254} > 4$ reveals hydrophobic and aromatic substances (Edzwald et al., 1985). It could be indicated that initial and t=0 solutions had hydrophobic and aromatic characteristics however t_{irr}=60 min showed hydrophilic and aliphatic features. Decreased $SUVA_{254}$ could be due to degradation of aromatic organics after 60 min of irradiation period.

$FI_{sync280}$ decreased at t_{irr}=60 min due to degradation of protein content released from damaged *E. coli* cells. At the same time, calculated $SFI_{sync280}$ displayed a decrease at t_{irr}=60 min in accordance with the increased NPOC due to released proteins from bacteria. On the other hand, $FI_{sync470}$ were detected as 1.08, 1.04, and 0.352 for initial, t=0, and t_{irr}=60 min conditions, respectively. Owing to the degradation of released organic content from damaged *E. coli* cells, $FI_{sync470}$ at t_{irr}=60 min expressed a decline. $SFI_{sync470}$ of initial, t=0, and t_{irr}=60 min conditions were calculated as 1.13, 1.38, and 0.187, respectively.

FI of initial, t=0, and t_{irr}=60 min conditions were calculated as 1.32, 1.23, and 1.74, respectively. $FI \leq 1.4$ represents the presence of humic fluorophores originating from the presence of humic matter and $FI \geq 1.9$ indicates the existence of microbially derived organic material (Sen-Kavurmaci and

Bekbolet, 2014). Besides the absence of HA as a solution matrix, calculated FI values of initial and t=0 samples was as less than 1.4, the reason could be attributed to the formation of "in-situ generated humic-like matter" originating from extracellular and/or intracellular organic matter founding in the structure of *E. coli* (Uyguner-Demirel et al., 2018). After 60 min of irradiation period, calculated FI was 1.74 which could mostly be related to microbially derived organic content, was the same with Se-N co-doped TiO_2 presented by Birben and colleagues (Birben et al., 2017a).

EEM fluorescence contour plots of organic matter emerged and removed during irradiation time dependent *E. coli* inactivation in WM solution during 0.25% Fe-TiO_2 solar photocatalytic treatment were displayed in Figure 4.83.

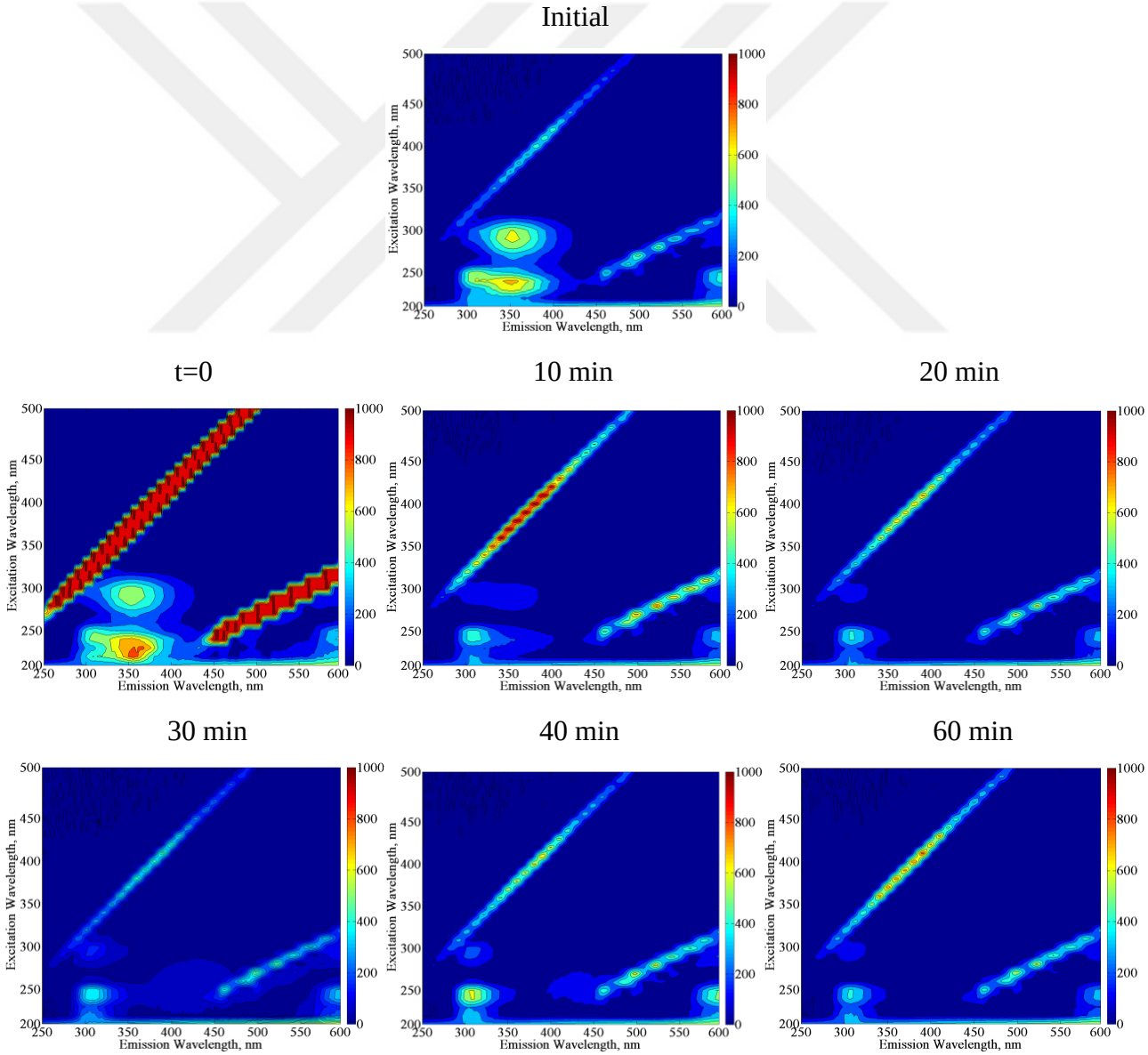

Figure 4.83. EEM fluorescence contour plots of organic matter: Irradiation time dependent *E. coli* inactivation in WM solution upon 0.25% Fe-TiO_2 solar photocatalytic treatment.

EEM fluorescence contour plots displayed the presence of Regions I, II and IV expressing that the fluorophores were mainly originated from microbial by-products and proteins under all irradiation conditions. Following further irradiation times released microbial by-products and proteins from *E. coli* cells showed a decreasing trend in accordance with the solar photocatalytic degradation of organic matter and reduction of *E. coli*. However, at 40 min of irradiation period, increased intensities could be visualized at Region I. It could be indicated that, enhanced protein release from bacteria occurred at t_{irr}=40 min, increased protein content could also be followed via $FI_{sync280}$ data at t_{irr}=40 min (Figure 4.81). Moreover, different from TiO_2 solar photocatalytic treatment of *E. coli* in WM solution (Figure 4.35), higher fluorescence intensities were detected from EEM fluorescence contour plots with the use of 0.25% Fe-TiO_2.

4.2.3.5. Mechanistic evaluation of *E. coli* inactivation upon 0.25% Fe-TiO_2 solar photocatalytic treatment in WM solution. Upon irradiation, as bacteria inactivation products of 0.25% Fe-TiO_2 solar photocatalytic treatment of *E. coli* in WM, total K, protein, and carbohydrate contents present in initial, t=0, and t_{irr}=60 min samples were presented in Table 4.33.

Table 4.33. Total K, protein, and carbohydrate contents of time dependent *E. coli* inactivation in WM solution upon 0.25% Fe-TiO_2 solar photocatalytic treatment.

0.25% Fe-TiO_2 solar photocatalytic treatment	*E. coli* in WM solution		
	Initial	t=0	60 min
Total K, mg/L	4.11	4.16	3.98
Protein, mg/L	1.79	1.29	9.15
Carbohydrate, mg/L	2.81	0.911	4.44

Total K content displayed a slight increase at t=0 which could be resulting from K^+ ion release from *E. coli* cells after adsorption of photocatalyst particles onto the cell surface. After an irradiation period of 60 min, total K content showed a decrease (3.98 mg/L), that could be due to K^+ ion intake via passive transport by bacteria. Moreover, the reason of high bacteria count result at t_{irr}=60 min as 2.95E+03 CFU/mL (Figure 4.73) could be attributed to the use of excessive K^+ ions in solution by bacteria to maintain inner osmatic pressure of cells and increase the possibility of survival.

After solar photocatalytic treatment of *E. coli* in WM solution in the presence of 0.25% Fe-TiO_2, increased protein and carbohydrate concentrations were detected. However, increase in protein concentration (1.29 mg/L for t=0; 9.15 mg/L for t_{irr}=60 min) was more evident that than the increase in carbohydrate content (0.911 mg/L for t=0; 4.44 mg/L) after 60 min of solar irradiation period.

Protein contents were plotted against $FI_{sync280}$ and NPOC separately in order to detect if there is any correlation between these parameters; and protein concentrations displayed a strong correlation with both $FI_{sync280}$ and NPOC parameters as R^2=1.00 and R^2=0.99, respectively. Furthermore, carbohydrate and NPOC contents showed a strong correlation with each other as R^2=0.85, as well.

4.2.3.6. Organic matter formation and removal upon 0.25% Fe-TiO_2 solar photocatalytic treatment of *E. coli* in HA solution. UV-vis absorption and synchronous scan fluorescence spectra of organic matter in solution were presented in Figures 4.84 and 4.85. Irradiation time dependent absorbance changes were significantly different from each other in UV wavelength range of λ=200-400 nm due to the presence of aromatic domains, UV absorbing centers as well as color forming moieties ($Color_{436}$, UV_{365} and UV_{280}). On the other hand, HA_i displayed distinctly different trend in wavelength region below λ=230 as expected. Upon introduction of 0.25% Fe-TiO_2 (t=0) into the reaction medium, increased absorbances were recorded similar to TiO_2 solar photocatalytic treatment of *E. coli* in HA solution (Figure 4.36). It could be attributed to mechanistic effect of photocatalyst on *E. coli* cell wall, which could cause cell wall damage and release of organic matter into the solution. UV-vis absorption spectra did not follow an irradiation time dependent decreasing order in contradistinction to previous solar photocatalytic treatments carried out with undoped TiO_2 specimens (Figures 4.36 and 4.60). It could be indicating that emergence and removal of light absorbing centers could be pronounced throughout 60 min of irradiation duration. Moreover, higher absorbances were detected in accordance with bare TiO_2 specimens as TiO_2 (Figure 4.36) and $SynTiO_2$ (Figure 4.60).

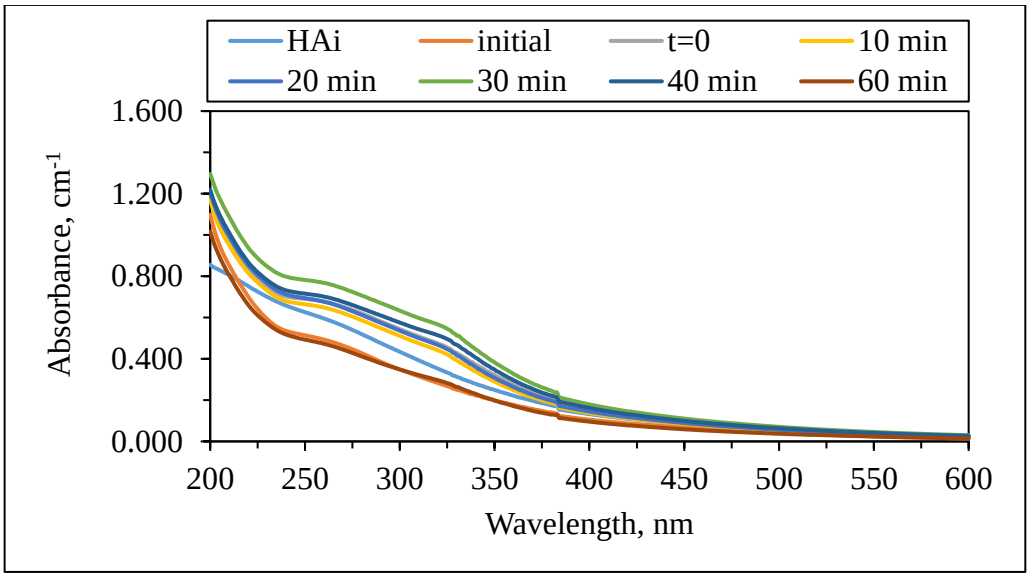

Figure 4.84. UV-vis absorption spectra of organic matter: Irradiation time dependent *E. coli* inactivation in HA solution upon 0.25% Fe-TiO_2 solar photocatalytic treatment.

Synchronous scan fluorescence spectra of emerged organic matter displayed an intense peak at λ_{emis}=370 nm and two minor peaks at λ_{emis}=440 nm and 480 nm representing the presence of aromatic hydrocarbons in the solution (Dujmov and Sučević, 1990) (Figure 4.85). After 30 min of irradiation period, FI_{sync} data displayed a declining trend. Moreover, in comparison to previous solar photolytic and photocatalytic treatments of *E. coli* in HA solution (Figures 4.13, 4.37, and 4.61), the highest synchronous scan fluorescence intensities were measured in the use of 0.25% Fe-TiO_2.

On the other hand, $FI_{sync470}$ and $FI_{sync280}$ displayed changes in the range of 60.7-198 and 9.96-114, respectively (Figure 4.86). $FI_{sync280}$ of sole HA_i could not be detected however $FI_{sync280}$ of initial solution increased to 9.96 indicating the presence of protein content in the solution. The main increase in $FI_{sync280}$ was detected between initial and t=0 conditions, therefore; it could be indicated that, detach of protein containing structures from cell wall and increased protein release due to cell wall damage could be occurred right after the photocatalyst and *E. coli* contact.

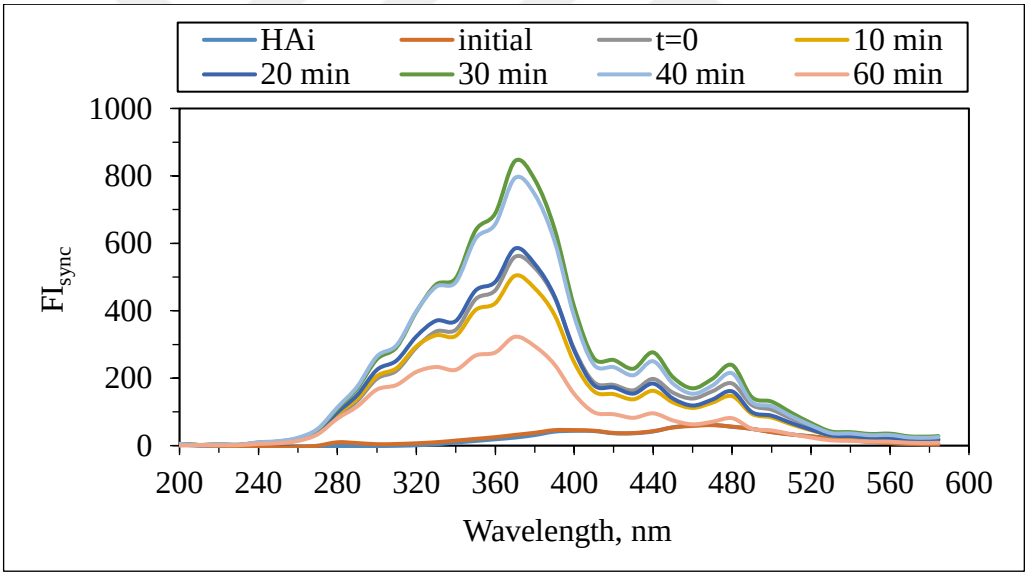

Figure 4.85. Synchronous scan fluorescence spectra of organic matter: Irradiation time dependent *E. coli* inactivation in HA solution upon 0.25% Fe-TiO_2 solar photocatalytic treatment.

Along with the presence of HA solution, NPOC expressed variations in the range of 4.21-6.67 mg/L (Figure 4.86). NPOC content increased up to t=0 condition (4.42-6.22 mg/L) and followed by a decreased trend in t_{irr}=10 min (4.21 mg/L) and again followed by fluctuations in a range of 4.21-6.67 mg/L during solar photocatalytic treatment. The highest NPOC was detected at t_{irr}=60 min due to released organic content from bacteria. Specified UV-vis parameters expressed higher presence relative to previous solar photolytic (Figure 4.14) and photocatalytic treatment sets of *E. coli* in HA solution (Figures 4.38 and 4.62). However, variations in UV-vis parameters did not followed an

irradiation time dependent order. As the most significant parameter, UV_{254} showed changes in the range of 0.4851-0.7778, being the highest for t_{irr}=30 min and the lowest for irradiation period of 60 min conditions.

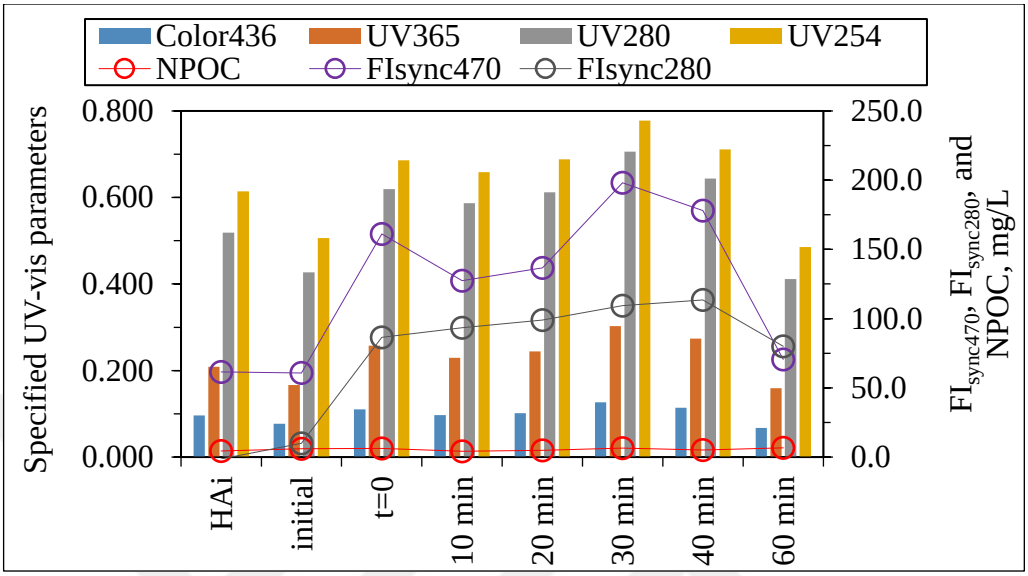

Figure 4.86. Specified UV-vis and fluroscence parameters of organic matter: Irradiation time dependent *E. coli* inactivation in HA solution upon 0.25% Fe-TiO_2 solar photocatalytic treatment.

Based on NPOC contents, $SCoA_{436}$, $SUVA_{365}$, $SUVA_{280}$, $SUVA_{254}$, $SFI_{sync470}$, and $SFI_{sync280}$ parameters were calculated and presented in Figure 4.87. $SUVA_{254}$ displayed variations in between 7.27-14.3 L/m mg during 0.25% Fe-TiO_2 solar photocatalytic treatment expressing differences in both UV_{254} and NPOC removals.

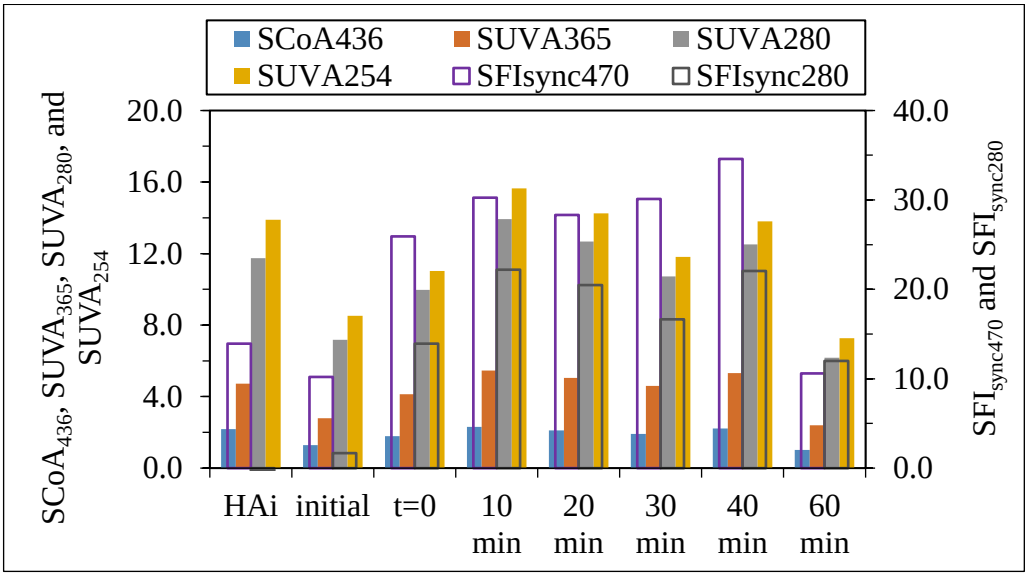

Figure 4.87. Specific UV-vis and fluroscence parameters of organic matter: Irradiation time dependent *E. coli* inactivation in HA solution upon 0.25% Fe-TiO_2 solar photocatalytic treatment.

Furthermore, $SFI_{sync470}$ and $SFI_{sync280}$ expressed variations in the range of 10.2-34.6 and 1.67-22.2, respectively. In the presence of HA solution as a reaction matrix, the key fluorophoric group was recognized as $FI_{sync470}$. According to undetected $FI_{sync280}$ of HA_i, $SFI_{sync280}$ could not be calculated as well.

Characteristic properties of organic matter present under initial and t=0 conditions, and at the end of solar photocatalytic inactivation of *E. coli* in HA solution for 60 min of irradiation period using 0.25% Fe-TiO_2 were presented in Table 4.34.

Table 4.34. Characteristic properties of organic matter present in 0.25% Fe-TiO_2 solar photolytic treatment of *E. coli* in HA solution.

Irradiation time, min	UV-vis Spectroscopic Parameters, cm^{-1}				NPOC, mg/L	$SUVA_{254}$, L/m mg	$FI_{sync470}$	$SFI_{sync470}$	FI
	$Color_{436}$	UV_{365}	UV_{280}	UV_{254}					
Initial	0.0767	0.1663	0.4270	0.5064	5.95	8.51	60.7	10.2	1.05
t=0	0.1106	0.2573	0.6197	0.6858	6.22	11.0	161	25.9	1.08
60 min	0.0674	0.1595	0.4114	0.4851	6.67	7.27	70.6	10.6	1.16

Upon 60 min solar photocatalytic treatment of *E coli* in the presence of HA solution at which 2.09 log *E. coli* reduction was achieved (Table 4.29), released organic matter expressed the following UV-vis parameters (cm^{-1}); $Color_{436}$: 0.0674, UV_{365}: 0.1595, UV_{280}: 0.4114, UV_{254}: 0.4851, and NPOC as 6.67 mg/L. $SUVA_{254}$ of initial, t=0, and t_{irr}=60 min solutions were calculated as 8.51, 11.0, and 7.27 L/m mg, respectively. The use of HA solution as reaction medium caused relatively high initial NPOC and $SUVA_{254}$ as expected. All calculated $SUVA_{254}$ values were higher than 4 (Figure 4.86), indicating that throughout the 60 min light exposure, samples solutions displayed hydrophobic and aromatic characteristics (Edzwald et al., 1985). Moreover, synchronous scan fluorescence spectra revealing the presence of aromatic hydrocarbons in the solutions (Figure 4.85) could be correlated with high $SUVA_{254}$ data.

$FI_{sync470}$ increased at t_{irr}=60 min due to both released organic content from damaged *E. coli* cells and present HA solution. At the end of the irradiation period of 60 min $SFI_{sync470}$ almost remained the same as the initial in accordance with slightly increased NPOC. On the other hand, $FI_{sync280}$ measurements of initial, t=0 and t_{irr}=60 min conditions were detected as 9.96, 86.5, and 80.0, respectively. According to NPOC and $FI_{sync280}$, $SFI_{sync280}$ of initial, t=0, and t_{irr}=60 min conditions were calculated as 1.67, 13.9, and 12.0, respectively. FI at t_{irr}=60 min was calculated as 1.16 indicating the presence of fluorophores coming from humic matter containing solution matrix as expected. Similar FI values were also presented by Birben and colleagues (Birben et al., 2017a).

EEM fluorescence contour plots of organic matter emerged and removed during irradiation time dependent *E. coli* inactivation in HA solution during 0.25% Fe-TiO_2 solar photocatalytic treatment were displayed in Figure 4.88.

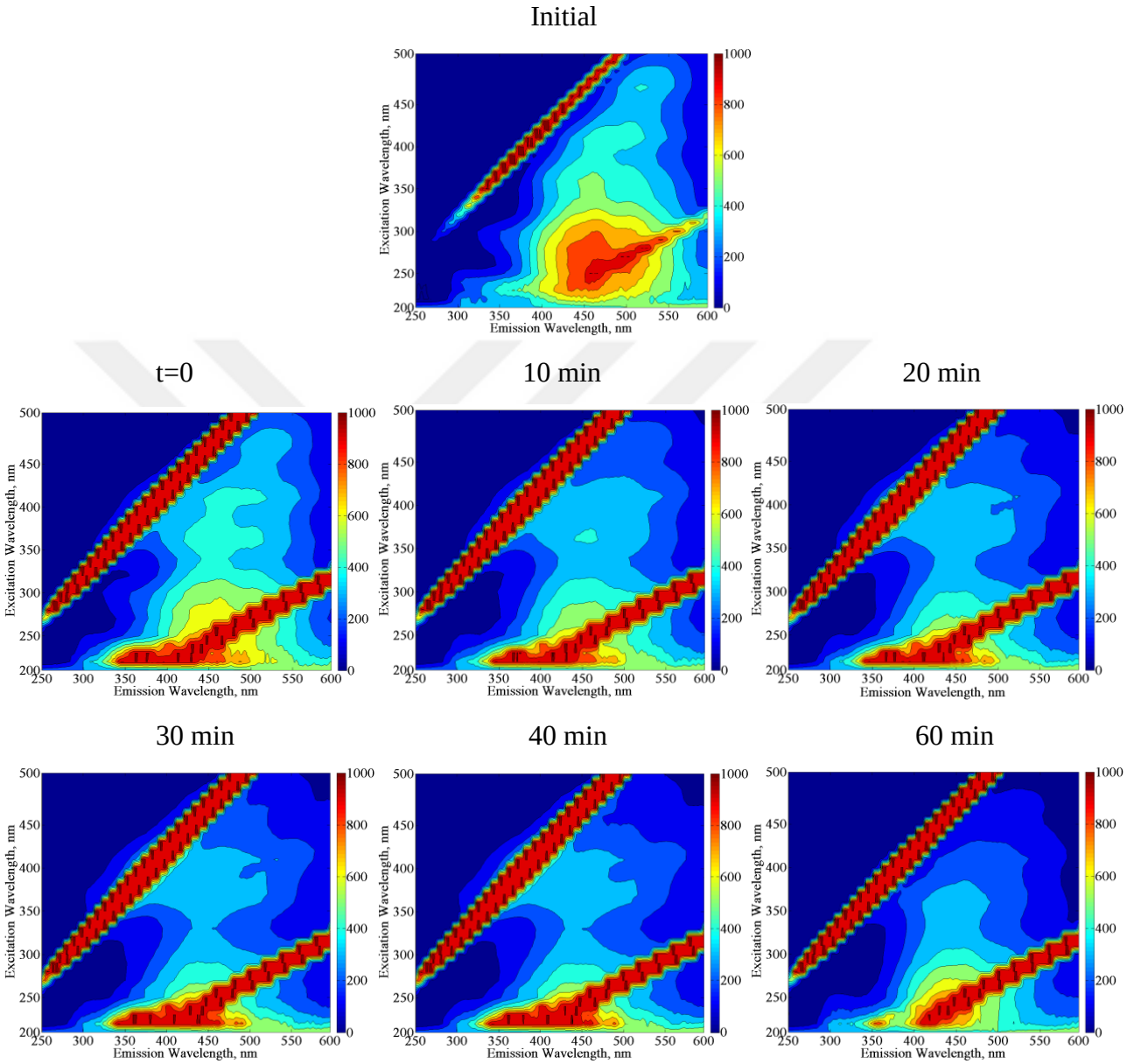

Figure 4.88. EEM fluorescence contour plots of organic matter: Irradiation time dependent *E. coli* inactivation in HA solution upon 0.25% Fe-TiO_2 solar photocatalytic treatment.

EEM fluorescence contour plots of *E. coli* inactivation in HA solution upon 0.25% Fe-TiO_2 solar photocatalytic treatment displayed the presence of Regions III, and V indicating that the fluorophores were mainly originated from fulvic-like and humic-like substances. Humic-like fluorophore intensities displayed a decreasing trend throughout the treatment period however at t_{irr}=60 min fulvic-like fluorescence intensities expressed an increase, which could be attributed to transformation from humic-like region to fulvic-like with increased humic matter degradation. Moreover, visualized

decreased fluorescence intensities were very low with respect to TiO_2 solar photocatalytic treatment (Figure 4.40). It could be indicated that 0.25% Fe-TiO_2 had a selectivity towards bacteria on contrary to TiO_2 displaying lower *E. coli* reduction (*E. coli* LRV as 2.09 for 0.25% Fe-TiO_2; *E. coli* LRV as 1.45 for TiO_2) (Figures 4.11 and 4.29) and higher organic content degradation (Figures 4.38 and 4.86). Moreover, besides EEM contour plot at t_{irr}=60 min showing similarities with SynTiO_2 (Figure 4.64), with the use of 0.25% Fe-TiO_2 lower intensities were attained, therefore; it could be concluded that 0.25% Fe-TiO_2 had lower bacteria selectivity than SynTiO_2.

4.2.3.7. Mechanistic evaluation of *E. coli* inactivation upon 0.25% Fe-TiO_2 solar photocatalytic treatment in HA solution. Upon destruction of bacteria cells in HA solution via 0.25% Fe-TiO_2 solar photocatalytic treatment, released total K, protein, and carbohydrate contents of in initial, t=0, and t_{irr}=60 min solutions were presented in Table 4.35.

Table 4.35. Total K, protein, and carbohydrate contents of time dependent *E. coli* inactivation in HA solution upon 0.25% Fe-TiO_2 solar photocatalytic treatment.

0.25% Fe-TiO_2 solar photocatalytic treatment	*E. coli* and HA		
	Initial	t=0	60 min
Total K, mg/L	0.59	0.44	0.45
Protein, mg/L	10.4	9.52	14.3
Carbohydrate, mg/L	2.50	3.09	3.61

Total K content showed an immediate adsorptive removal as 25.0 % at t=0 and remained stable at t_{irr}=60 min. Low total K content detected at t_{irr}=60 min could be resulting from the adsorption of K^+ ions onto oppositely charged *E. coli*, photocatalyst, and/or HA surfaces and removal via membrane filtration applied prior to total K analysis. Similar low total K contents were also obtained from previous solar photolytic and photocatalytic experiment sets carried out in HA solution (Tables 4.8, 4.17, and 4.26) complying with the suggestion that HA has an inhibitory effect on the detection of total K concentration.

E. coli in HA solution upon 0.25% Fe-TiO_2 solar photocatalytic treatment displayed increase in both protein and carbohydrate contents at the end of 60 min irradiation period. Protein concentration showed a higher increase (10.4-14.3 mg/L) than carbohydrate concentration (2.50-3.61 mg/L). In comparison with treatments conducted in the presence of IsoT and WM solutions, higher initial protein (10.4 mg/L) and carbohydrate (2.50 mg/L) contents were detected due to the presence of HA solution. No correlation was detected between $FI_{sync280}$ and protein content however NPOC

measurements displayed strong correlations with both protein and carbohydrate concentrations as R^2=0.72 and R^2=0.97, respectively.

4.2.3.8. Organic matter formation and removal upon 0.25% Fe-TiO_2 solar photocatalytic treatment of *E. coli* in "HA and WM" solution. UV-vis absorption and synchronous scan fluorescence spectra of organic matter in solution were presented in Figures 4.89 and 4.90. Irradiation time dependent absorbance changes were different from each other in UV wavelength range of λ=200-400 nm due to the presence of aromatic domains and color forming moieties ($Color_{436}$, UV_{365} and UV_{280}). UV-vis absorption spectra did not follow an irradiation time dependent decreasing order similar to previous SynTiO_2 solar photocatalytic treatment of *E. coli* in sole HA solution (Figures 4.84). On the other hand, the use of "HA and WM" solution as a reaction medium, caused distinctly different trend in UV absorption at λ < 240 nm as expected.

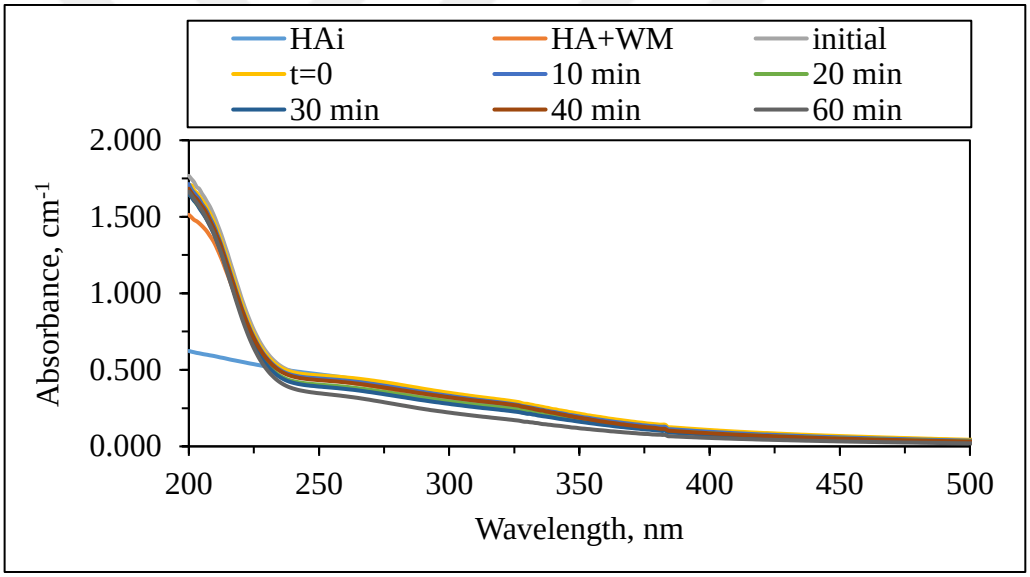

Figure 4.89. UV-vis absorption spectra of organic matter: Irradiation time dependent *E. coli* inactivation in "HA and WM" solution upon 0.25% Fe-TiO_2 solar photocatalytic treatment.

Synchronous scan fluorescence spectra of emerged organic matter displayed an intense peak at λ_{emis}=370 nm and two minor peaks at λ_{emis}=440 nm and 470 nm (Figure 4.90). On the other hand, data at λ_{emis}=370 nm displayed the highest presence in comparison with previous treatment sets conducted in the presence of "HA and WM" solution (Figures 4.18, 4.42, and 4.66) and expressed variations in the range of 13.0-593. From a general perspective, FI_{sync} data displayed an increase between t_{irr}=30 min and 40 min and followed by a drastic decrease at t_{irr}=60 min. Furthermore, similar to TiO_2 and SynTiO_2 solar photocatalytic inactivation of *E. coli* in "HA and WM" solution (Figures 4.42 and 4.66), t=0 condition expressed a significant increase in FI_{sync} data. The reason could be

attributed to the possible mechanistic effect of photocatalyst on cell wall structure, causing release of cytoplasmic organic content from *E. coli* cells.

Moreover, $FI_{sync470}$ and $FI_{sync280}$ displayed changes in the range of 52.1-130 and 43.1-103, respectively (Figure 4.91). In the presence of HA solution as a constituent of aqueous reaction matrix, $FI_{sync470}$ expressed higher intensities than $FI_{sync280}$ as expected and recognized as the main fluorophoric group. On the other hand, $FI_{sync280}$ "HA and WM" solution and initial condition could not be detected however t=0 displayed an $FI_{sync280}$ as 63.5.

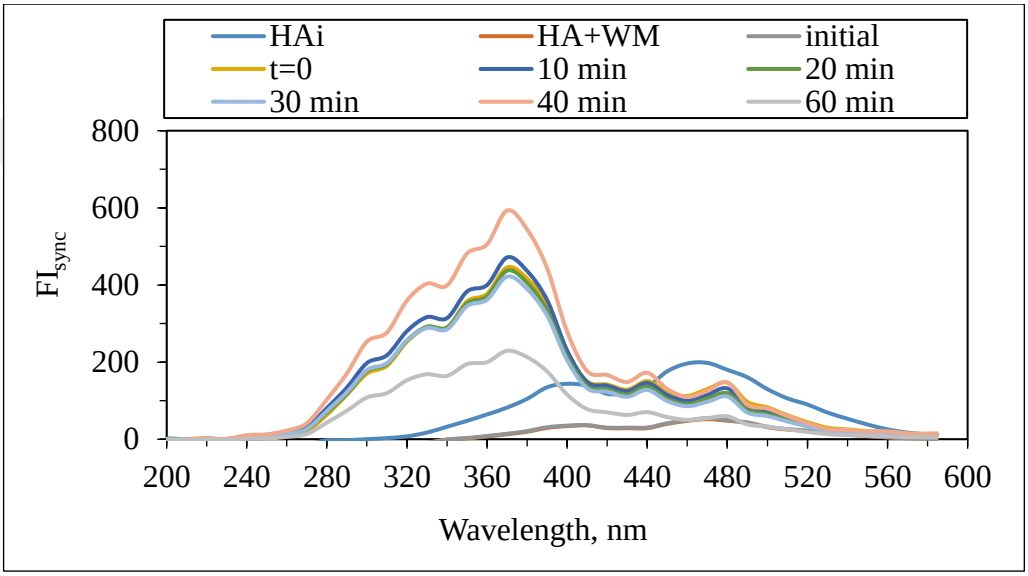

Figure 4.90. Synchronous scan fluorescence spectra of organic matter: Irradiation time dependent *E. coli* inactivation in "HA and WM" solution upon 0.25% Fe-TiO_2 solar photocatalytic treatment.

From a general perspective, NPOC expressed variations in the range of 4.24-5.97 mg/L (Figure 4.91). NPOC content increased after the introduction of bacteria into "HA and WM" solution (4.24-5.97 mg/L) and slightly decreased after the addition of 0.25% Fe-TiO_2 (4.54 mg/L) due to immediate adsorptive removal or organic content as 24.0 %. An increasing trend in NPOC content was recorded up to t_{irr}=20 min (5.46 mg/L) due to the release of organics from damaged and destructed *E. coli* cells and followed by a decrease until t_{irr}=40 min (4.74 mg/L) then again expressed a slight increase during solar photocatalytic treatment (4.88 mg/L).

Specified UV-vis parameters did not follow a continuous irradiation time dependent order similar to SynTiO_2 solar photocatalytic *E. coli* inactivation conducted in the presence of sole HA solution (Figure 4.86). As the most significant parameter, UV_{254} expressed variations in between 0.3395-0.4589, being the highest for t=0 and the lowest for t_{irr}=60 min conditions. A decreasing trend

was observed in all specified UV-vis parameters between t=0 and t_{irr}=30 min conditions, however a significant increase and a drastic decrease followed each other at t_{irr}=40 min and 60 min conditions, respectively.

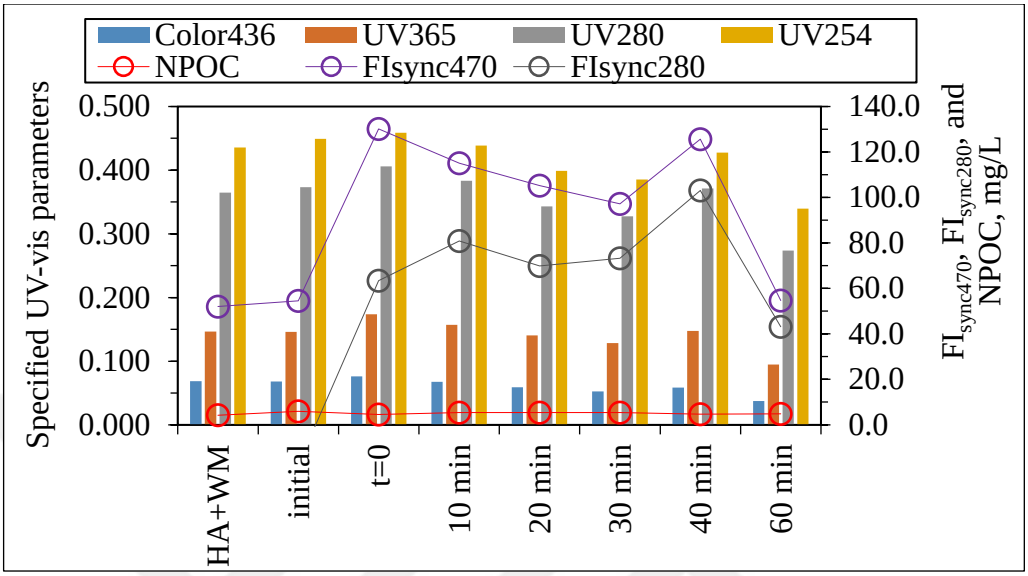

Figure 4.91. Specified UV-vis and fluroscence parameters of organic matter: Irradiation time dependent *E. coli* inactivation in "HA and WM" solution upon 0.25% Fe-TiO_2 solar photocatalytic treatment.

Based on NPOC contents, $SCoA_{436}$, $SUVA_{365}$, $SUVA_{280}$, $SUVA_{254}$, $SFI_{sync470}$, and $SFI_{sync280}$ parameters were calculated and presented in Figure 4.92.

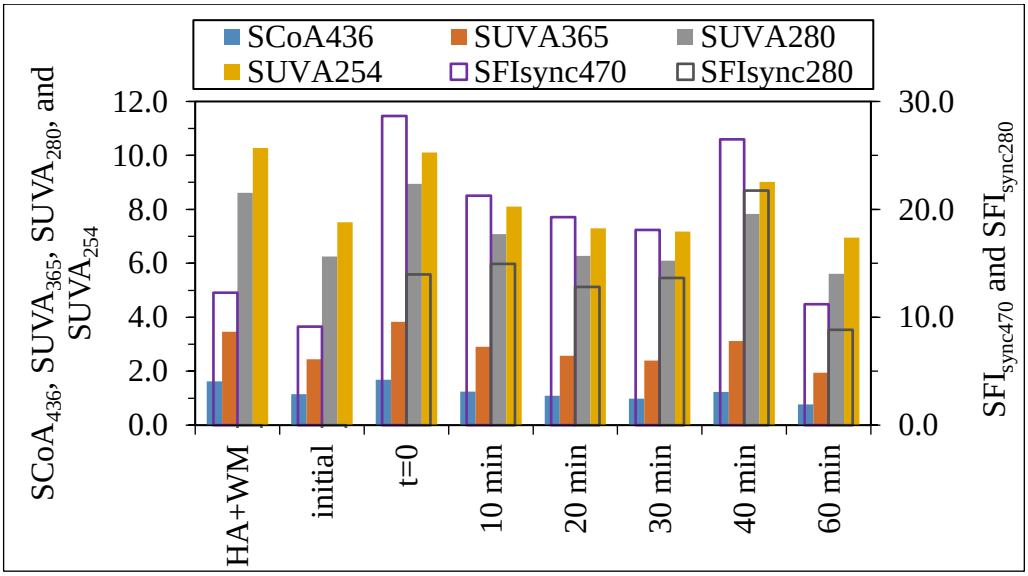

Figure 4.92. Specific UV-vis and fluroscence parameters of organic matter: Irradiation time dependent *E. coli* inactivation in "HA and WM" solution upon 0.25% Fe-TiO_2 solar photocatalytic treatment.

As the most evident specific UV-vis parameter, $SUVA_{254}$ displayed variations in the range of 6.96-100 L/m mg during 0.25% Fe-TiO_2 solar photocatalytic treatment indicating differences in both UV_{254} and NPOC removals. In accordance with obtained specified UV-vis parameters and NPOC contents (4.24-5.97 mg/L), calculated specific UV-vis parameter displayed similar emergence and removal pattern with specified UV-vis parameters (Figure 4.91).

On the other hand, $SFI_{sync470}$ and $SFI_{sync280}$ expressed variations in the range of 9.13-28.7 and 8.84-21.7, respectively. The dominant fluorophoric group was accepted as $SFI_{sync470}$ due to its remarkable presence in comparison to $SFI_{sync280}$. According to undetected $FI_{sync280}$ of "HA and WM" solution and initial condition, their $SFI_{sync280}$ could not be calculated either.

Characteristic properties of organic matter upon initial and t=0 conditions, and at the end of 0.25% Fe-TiO_2 solar photocatalytic inactivation of *E. coli* in "HA and WM" solution for 60 min were presented in Table 4.36.

Table 4.36. Characteristic properties of organic matter present in 0.25% Fe-TiO_2 solar photolytic treatment of *E. coli* in "HA and WM" solution.

Irradiation time, min	UV-vis Spectroscopic Parameters, cm^{-1}				NPOC, mg/L	$SUVA_{254}$, L/m mg	$FI_{sync470}$	$SFI_{sync470}$	FI
	$Color_{436}$	UV_{365}	UV_{280}	UV_{254}					
Initial	0.0683	0.1461	0.3732	0.4494	5.97	7.53	54.5	9.13	1.16
t=0	0.0763	0.1737	0.4060	0.4589	4.54	10.1	130	28.7	1.21
60 min	0.0377	0.0948	0.2736	0.3395	4.88	6.96	54.8	11.2	1.27

Upon t_{irr}=60 min 0.25% Fe-TiO_2 solar photocatalytic treatment of *E coli* in the presence of "HA and WM" at which 2.14 log *E. coli* reduction was achieved (Table 4.29), released organic matter expressed the following UV-vis parameters (cm^{-1}); $Color_{436}$: 0.0377, UV_{365}: 0.0948, UV_{280}: 0.2736, UV_{254}: 0.3395, and NPOC as 4.88 mg/L. The use of HA solution as a matrix component caused relatively high initial NPOC and $SUVA_{254}$ as expected. NPOC expressed a decrease after 60 min of irradiation time indicating degradation of organics. $SUVA_{254}$ at t_{irr}=60 min was calculated as 6.96 L/m mg indicating the remaining organic content in solution displayed aromatic and hydrophobic characteristics (Edzwald et al., 1985).

$FI_{sync470}$ decreased at t_{irr}=60 min due to degradation of organic content released from damaged *E. coli* cells and organic matrix content. At the end of 60 min treatment period $SFI_{sync470}$ increased in accordance with decreased NPOC. Moreover, $FI_{sync280}$ of initial, t=0 and t_{irr}=60 min conditions were determined as ≤0.01, 63.5, and 43.1 respectively. According to NPOC and $FI_{sync280}$ measurements,

$SFI_{sync280}$ values of initial, t=0, and t_{irr}=60 min conditions were calculated as ≤0.01, 14.0, and 8.84 respectively. FI of t_{irr}=60 min was calculated as 1.27 indicating the presence of fluorophores originating from humic content as expected.

EEM fluorescence contour plots of organic matter emerged and removed during irradiation time dependent *E. coli* inactivation in "HA and WM" solution by 0.25% Fe-TiO_2 solar photocatalytic treatment were displayed in Figure 4.93.

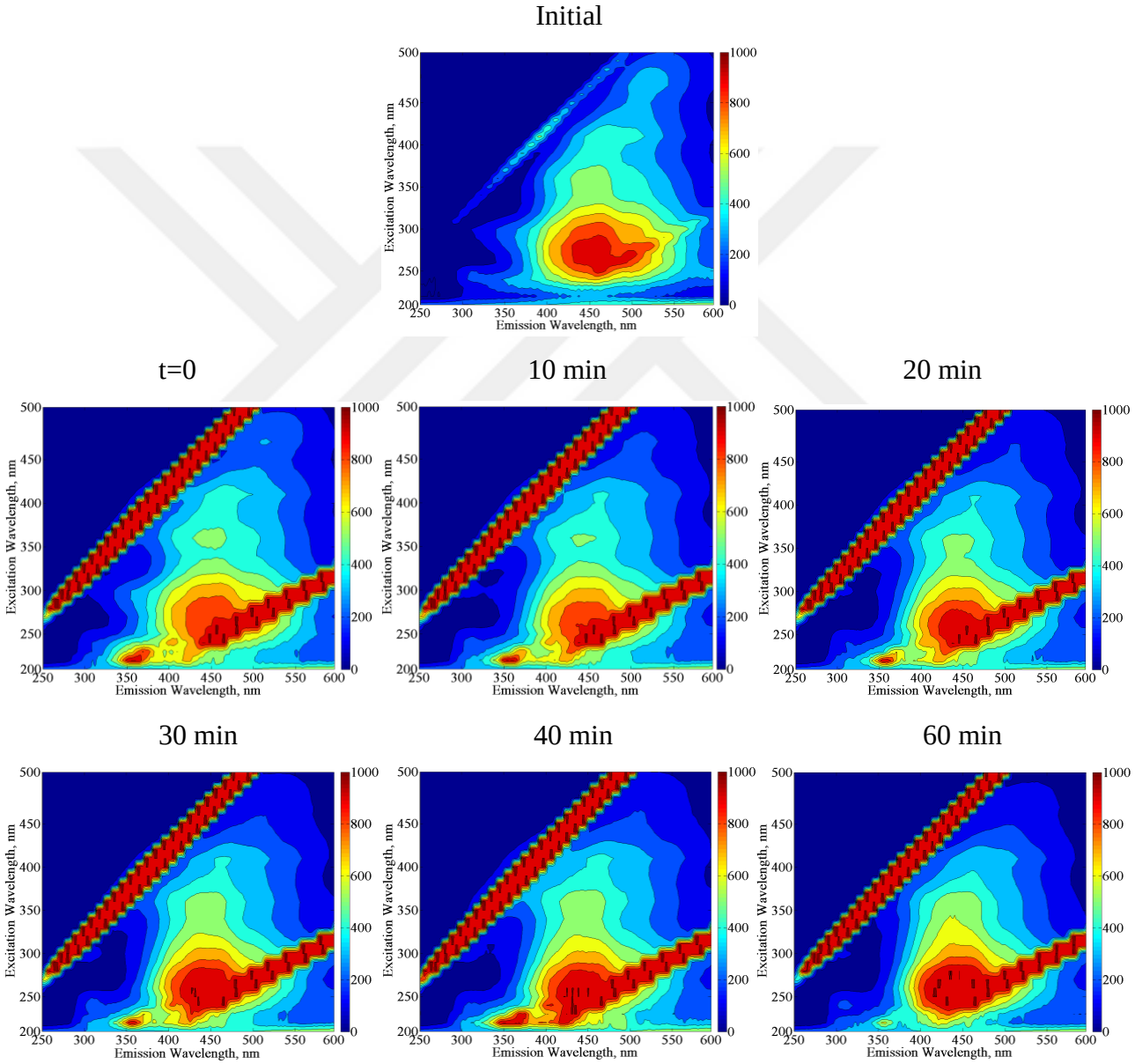

Figure 4.93. EEM fluorescence contour plots of organic matter: Irradiation time dependent *E. coli* inactivation in "HA and WM" solution upon 0.25% Fe-TiO_2 solar photocatalytic treatment.

EEM fluorescence contour plots of *E. coli* in "HA and WM" solution upon 0.25% Fe-TiO_2 solar photocatalytic treatment displayed the presence of Regions III, and V indicating that the fluorophores

were mainly originated from fulvic-like and humic-like substances. Humic-like fluorophore intensities displayed a slight decrease throughout the treatment however they had more intense fluorescence than *E. coli* in HA solution set (Figure 4.88) which is a similar pattern that was detected from previous "HA and WM" solar photolytic and photocatalytic treatments (Figures 4.21, 4.45, and 4.69). After t_{irr}=30 min, intensity of fulvic-like fluorophore displayed an increase while humic-like fluorophore intensities decreased slightly, which could be attributed to a shift of treated high molecular size HA towards lower molecular size fractions (Birben et al., 2017b).

4.2.3.9. Mechanistic evaluation of *E. coli* inactivation upon 0.25% Fe-TiO_2 solar photocatalytic treatment in "HA and WM" solution. As inactivation products of 0.25% Fe-TiO_2 solar photocatalytic treatment of *E. coli* in "HA and WM" solution, total K, protein, and carbohydrate contents present in initial, t=0, and t_{irr}=60 min solutions were presented in Table 4.37.

Table 4.37. Total K, protein, and carbohydrate contents of time dependent *E. coli* inactivation in "HA and WM" solution upon 0.25% Fe-TiO_2 solar photocatalytic treatment.

0.25% Fe-TiO_2 solar photocatalytic treatment	*E. coli* in "HA and WM"		
	Initial	t=0	60 min
Total K, mg/L	4.36	4.29	4.23
Protein, mg/L	12.6	4.35	16.6
Carbohydrate, mg/L	4.66	2.65	5.49

Total K content showed a decrease at t_{irr}=60 min which could be resulting from the adsorption of K^+ ions onto oppositely charged *E. coli*, photocatalyst, and HA surfaces. Moreover, at t=0 condition total K displayed 1.61 % of immediate adsorptive removal however it was lower than calculated adsorptive total K content removals of IsoT and HA solutions (17.0 % for *E. coli* in IsoT and 25.0 % for *E. coli* and HA). Due to the use of WM solution as an aqueous matrix component, higher total K concentrations were obtained in comparison with IsoT (Table 4.31) and sole HA solutions (Table 4.35).

0.25% Fe-TiO_2 solar photocatalytic treatment of *E. coli* in "HA and WM" solution expressed an increase in both protein and carbohydrate concentration after t_{irr}=60 min owing to release of cell components from *E. coli*. While protein concentration showed a significant increase (12.6-16.6 mg/L), carbohydrate concentration increased slightly (4.66-5.49 mg/L). Protein concentrations displayed no correlation with either $FI_{sync280}$ or NPOC data. Furthermore, no correlation was detected between NPOC and carbohydrate contents.

4.2.3.10. Comparative evaluation of different experimental matrixes on 0.25% Fe-TiO_2 solar photocatalytic inactivation mechanism of *E. coli.* Total K, protein, and carbohydrate concentrations and bacteria enumerations attained upon 0.25% Fe-TiO_2 solar photocatalytic treatment of *E. coli* in different solution matrixes in comparison with initial, t=0 and t_{irr}=60 min samples were given in Figure 4.94. Total K contents varied in between 0.44-4.36 mg/L being the lowest for t=0 condition of *E. coli* in HA solution and the highest for initial sample of *E. coli* in "HA and WM" solution. Total K content of WM solution containing conditions displayed higher concentrations as expected. Except the presence of sole HA solution, a rough correlation as $R^2 > 0.75$, was detected between total K contents and bacteria counts of initial and t_{irr}=60 solutions, however t=0 data displayed no correlation.

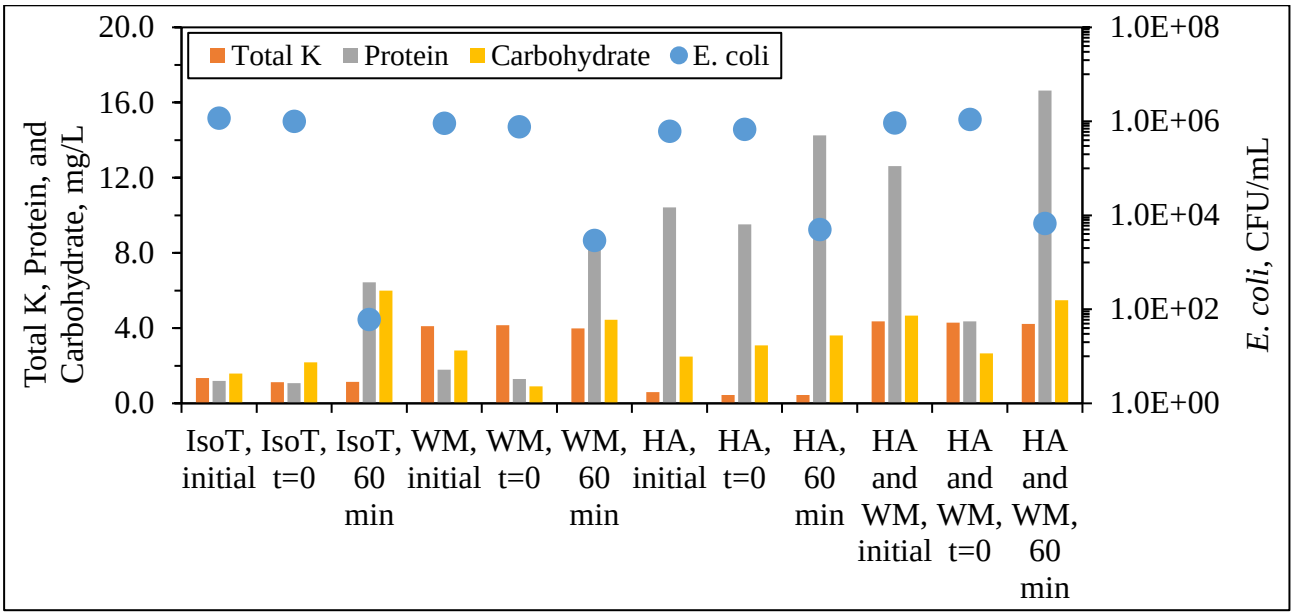

Figure 4.94. Initial, t=0, and t_{irr}=60 min total K, protein, and carbohydrate contents and bacteria enumeration results of *E. coli* inactivation upon 0.25% Fe-TiO_2 solar photocatalytic treatment in various aqueous matrixes.

Covering all conditions protein contents varied in between 1.07-16.6 mg/L being the lowest for t=0 sample of *E. coli* in IsoT solution and the highest for t_{irr}=60 min sample of *E. coli* in "HA and WM" solution. Similarly, carbohydrate contents varied in between 0.91-6.00 mg/L being the lowest for t=0 condition of *E. coli* in WM solution and the highest for t_{irr}=60 min sample of *E. coli* in IsoT solution. At t_{irr}=60 min, all solar photocatalytic treatment conditions displayed increased protein contents, with the highest being detected from "HA and WM" solution (16.6 mg/L). All carbohydrate contents at t_{irr}=60 min displayed increasing trends with respect to their initial conditions. Although similar bacteria counts were obtained from WM, HA and "HA and WM" solutions, there were no resemblance detected between protein and carbohydrate contents. Only total K content of WM and "HA and WM" solutions showed similarities due to the presence of WM solution as reaction medium.

Released protein and carbohydrate contents were calculated by subtracting initial data from the final contents attained upon irradiation period of 60 min and represented with *E. coli* LRV in Figure 4.95. Despite the higher LRV of IsoT solution as 4.28, released protein content was detected as the highest in *E. coli* in WM solution (7.36 mg/L) which could be attributed to the degradation of released proteins in IsoT solution. In the presence of HA and "HA and WM" solutions, *E. coli* showed similar LRV (2.09 for *E. coli* in HA solution; 2.14 for *E. coli* in "HA and WM" solution) and in accordance with that, their released protein and carbohydrate concentrations were also detected as close to each other. It could be indicated that released carbohydrate contents of WM, HA and "HA and WM" solutions were directly proportional to decreased LRV of bacteria. Furthermore, both released protein and carbohydrate concentrations were plotted against LRV of *E. coli* individually to detect if there was any correlation between these parameters. In the absence of IsoT solution, released protein concentrations and bacteria LRV showed a strong correlation as R^2=1.0. Moreover, released carbohydrate concentrations and LRV of *E. coli* displayed a strong correlation for all solutions as R^2=0.99.

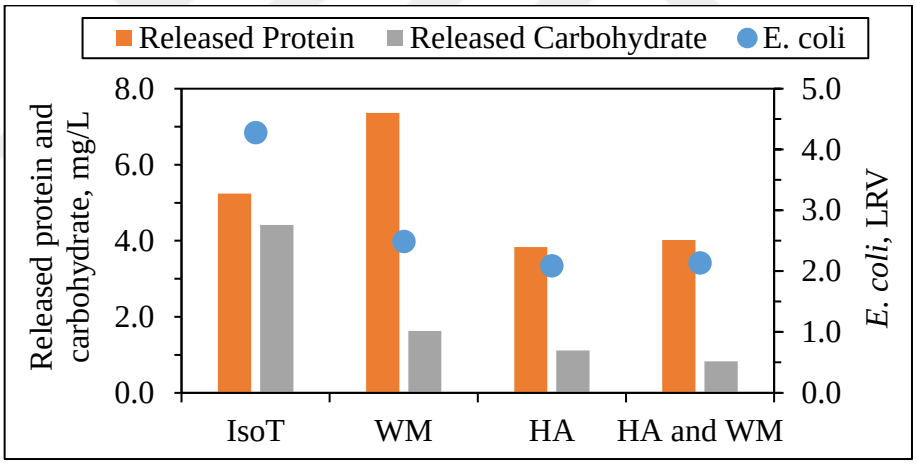

Figure 4.95. Released protein and carbohydrate contents, and bacteria LRV of *E. coli* inactivation upon 0.25% Fe-TiO_2 solar photocatalytic treatment in various aqueous matrixes.

Upon 0.25% Fe-TiO_2 solar photocatalytic treatment of *E. coli* in different solution matrixes, the attained protein and carbohydrate contents, $FI_{sync280}$, UV_{280} and NPOC data under initial, t=0, and t_{irr}=60 min conditions were given in Figure 4.96. In the presence of HA solution, protein contents and UV_{280} showed increased presence similar to the finding obtained from solar photolytic (Figure 2.24) and SynTiO_2 photocatalytic treatments (Figure 4.72). Similar protein concentrations and $FI_{sync280}$ were detected between initial and t=0 conditions in both IsoT and WM solutions. $FI_{sync280}$ data showed a significant increase after addition of photocatalyst to the solution matrix in only sole HA solution.

$FI_{sync280}$ of "HA and WM" initial sample was detected as ≤ 0.01. Excluding the presence of sole HA matrix, $FI_{sync280}$ and protein data expressed a strong correlation as $R^2 > 0.90$.

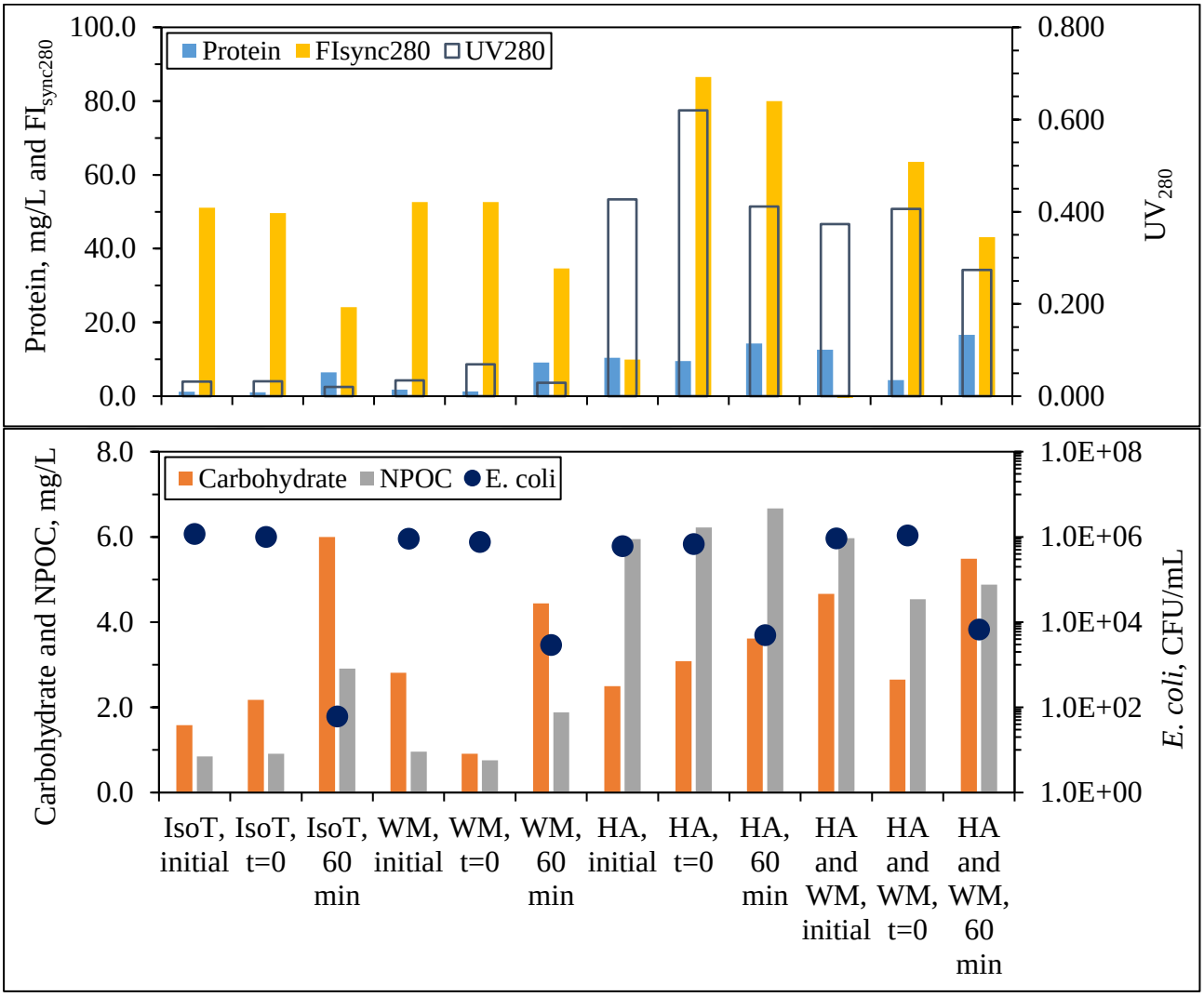

Figure 4.96. Initial, t=0, and t_{irr}=60 min protein and carbohydrate contents, $FI_{sync280}$, UV_{280}, NPOC, and bacteria enumeration results of 0.25% Fe-TiO_2 solar photocatalytic treatment of *E. coli* in various aqueous matrixes.

HA containing conditions displayed higher NPOC than carbohydrate contents, except t_{irr}=60 min condition of "HA and WM" solution. *E. coli* in IsoT and WM solutions showed significant increase in carbohydrate content at t_{irr}=60 min, due to released organics from damaged cells. It could be indicated that the presence of HA solution was directly proportional to NPOC content which also complied with the data of previous solar photolytic (Figure 4.24) and photocatalytic treatments (Figures 4.48 and 4.72). In the absence of sole HA solution, NPOC and carbohydrate contents displayed a strong correlation as R^2=0.86 for initial conditions. However, t=0 and t_{irr}=60 min samples showed a strong correlation as $R^2 > 0.88$ except in the use of sole WM solution.

4.2.4. 0.50% Fe-TiO_2 Solar Photocatalytic Inactivation of *E. coli*

4.2.4.1. 0.50% Fe-TiO_2 solar photocatalytic *E. coli* inactivation under specified reaction conditions, reductions, and kinetics. *E. coli* suspension (N_o=6.18E+05 CFU/mL) was prepared in IsoT solution and subjected to solar photocatalytic treatment using 0.50% Fe-TiO_2 specimen. Upon an irradiation period of 40 min, *E. coli* count decreased to 3.34E+03 CFU/mL. Following further light exposure of t_{irr}=60 min, *E. coli* count decreased to 2.23E+03 CFU/mL. Under these conditions LRV was 2.44 and reduction was 99 %. Upon preparation of *E. coli* (N_o=6.71E+05 CFU/mL) suspension in WM solution, for an irradiation period of 40 min, *E. coli* count decreased to 2.04E+03 CFU/mL. Following prolonged light exposure of t_{irr}=60 min, *E. coli* count reached to 2.18E+02 CFU/mL revealing LRV as 3.49 and reduction as 99.9 %. *E. coli* (N_o=6.25E+05 CFU/mL) suspension was prepared in HA solution and for an irradiation period of 40 min, *E. coli* count decreased to 1.29E+03 CFU/mL. Following further light exposure of t_{irr}=60 min, *E. coli* count declined to 2.71E+02 CFU/mL expressing LRV as 3.36 and reduction as 99.9 %. *E. coli* (N_o=5.34E+05 CFU/mL) suspension was prepared in a solution comprising of "HA and WM" components and was subjected to an irradiation period of 40 min in which *E. coli* count decreased to 3.54E+04 CFU/mL. Upon light exposure of t_{irr}=60 min, *E. coli* count further diminished to 7.74E+03 CFU/mL revealing LRV as 1.84 and reduction as 96.8 %. Based on these results, the effect of solution matrix could be displayed in terms of LRV of *E. coli* in an increasing order as: "HA and WM" < IsoT < HA < WM. Irradiation time dependent *E. coli* inactivation profiles and first order kinetic parameters were presented in Figure 4.97 and Table 4.38.

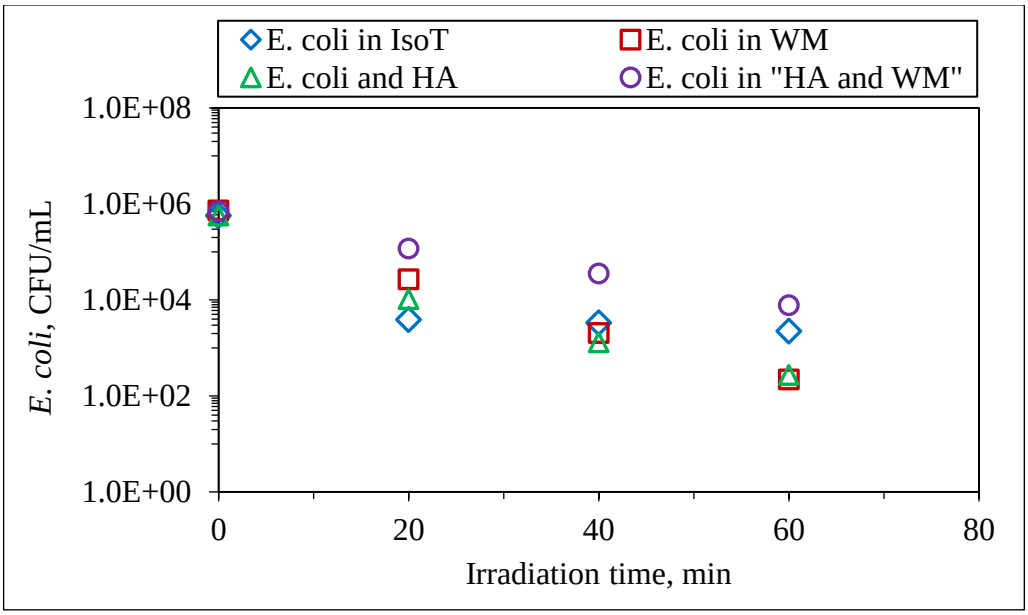

Figure 4.97. Irradiation time dependent *E. coli* inactivation upon 0.50% Fe-TiO_2 solar photocatalytic treatment in various solution matrixes.

0.50% Fe-TiO_2 solar photocatalytic treatment of *E. coli* in WM solution resulted in a rather fast reduction with k=0.135 min^{-1} and half-life as 5.13 min. In the presence of "HA and WM" solution, a reaction rate constant of k=0.0734 min^{-1} and half-life as 9.44 min was attained. The effect of reaction medium could also be expressed in terms of inactivation reaction rate constant (k, min^{-1}) in a decreasing order as; WM > HA > IsoT > "HA and WM". Irrespective of the minor differences in initial bacteria counts, inactivation rates (CFU/mL min) also followed the same trend as; 9.06E+04 > 7.81E+04 > 5.19E+04 > 3.92E+04 for WM, HA, IsoT, "HA and WM", respectively.

Table 4.38. 0.50% Fe-TiO_2 solar photocatalytic treatment of *E. coli*: Inactivation parameters.

Matrix	First order kinetic model			LRV	Reduction, %
	k, min^{-1}	$t_{1/2}$, min	R, CFU/mL min		
E. coli in IsoT	0.0839	8.26	5.19E+04	2.44	99
E. coli in WM	0.135	5.13	9.06E+04	3.49	99.9
E. coli and HA	0.125	5.54	7.81E+04	3.36	99.9
E. coli in "HA and WM"	0.0734	9.44	3.92E+04	1.84	96.8

E. coli in IsoT solution solar photocatalytic treatment with 0.50% Fe-TiO_2 experiment showed lower bacteria reduction than WM and HA aqueous media, as 99 %. *E. coli* LRV was obtained as 2.44. Different from the previous sets of solar photolytic (Table 4.2) and photocatalytic experiments (Tables 4.11, 4.20, and 4.29) *E. coli* in IsoT solution displayed lower LRV from WM and HA solutions. It could be resulting from the presence of optimal osmotic conditions provided by 0.85 % IsoT solution. Moreover, detected reaction rate constant as 0.0839 was lower than N-doped, Se-doped, and Se-N co-doped TiO_2 results presented by Birben and colleagues (Birben et al., 2017a).

0.50% Fe-TiO_2 solar photocatalytic treatment of *E. coli* in WM solution displayed the highest *E. coli* LRV among other experiment media, as 3.49. Higher bacteria reduction results could be explained with the presence of common anions and cations in the WM solution. The presence of anions and cations could cause production of increased amount of ROS thus enhance the inactivation rate of bacteria.

In the presence of HA solution, similar reduction of bacteria was detected with *E. coli* in WM condition, as 99.9 % however LRV showed a slight decrease as 0.13. According to the study of Birben and colleagues, it could be concluded that 0.50% Fe-TiO_2 showed a faster reduction rate than Se-doped and Se-N co-doped but slower than N-doped TiO_2 (Birben et al., 2017a). Also, LRV of *E. coli* in the presence of 0.50% Fe-TiO_2 was detected as higher than that in the presence of 0.25% Fe-TiO_2 (Table 4.29) therefore it could be concluded that 0.50% Fe-TiO_2 displayed higher selectivity against *E. coli*, rather than HA.

E. coli in "HA and WM" solution upon solar photocatalytic treatment with 0.50% Fe-TiO_2 showed the lowest bacteria reduction, as 96.8 % which could be due to retardation effect of the presence of both WM and HA solutions. It could be resulting from the beneficial role of "HA and WM" solution on *E. coli* survival by acting as a nutrient source and giving resistance to bacteria.

4.2.4.2. Organic matter formation and removal upon 0.50% Fe-TiO_2 solar photocatalytic treatment of *E. coli* in IsoT solution. UV-vis absorption and synchronous scan fluorescence spectra of organic matter in solution were presented in Figures 4.98 and 4.99. Irradiation time dependent absorbance changes were significantly similar to each other in UV wavelength range of λ=200-280 nm in the absence of aromatic domains and color forming moieties ($Color_{436}$, UV_{365}, and UV_{280}) that should be measured in longer wavelengths. The highest absorption was detected at t_{irr}=60 min between λ=205 nm and 320 nm resembling with the UV-vis absorption spectra feature of t_{irr}=60 min sample of TiO_2 solar photocatalytic treatment (Figure 4.26).

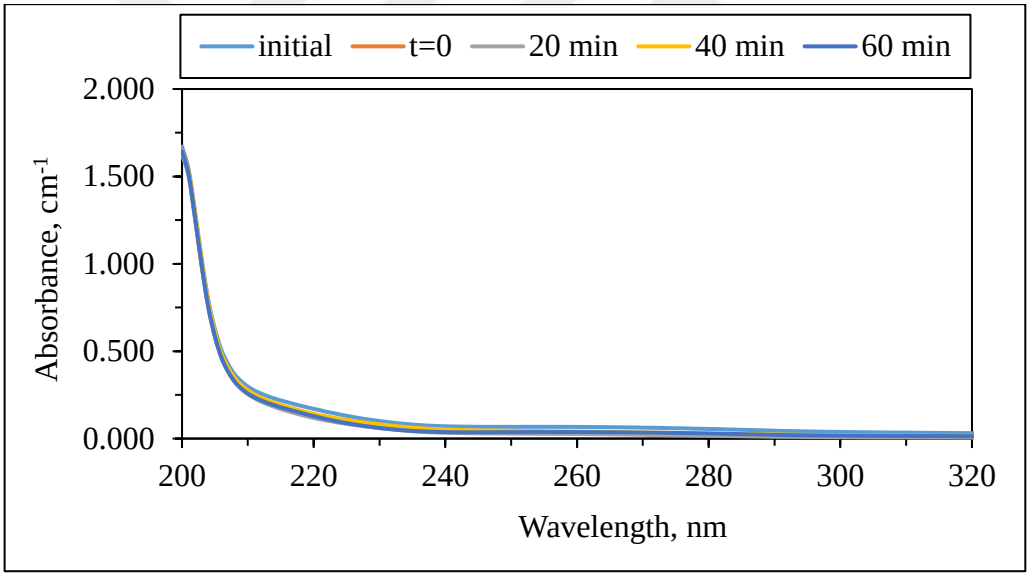

Figure 4.98. UV-vis absorption spectra of organic matter: Irradiation time dependent *E. coli* inactivation in IsoT solution upon 0.50% Fe-TiO_2 solar photocatalytic treatment.

Synchronous scan fluorescence spectra of emerged organic matter displayed an intense peak at λ_{emis}=280 nm, especially at t_{irr}=20 and 40 min (Figure 4.99). The highest intensity at λ_{emis}=280 nm was detected at t_{irr}=20 min (32.8) due to released protein content from damaged bacteria and following t_{irr}=40 min, intensity at λ_{emis}=280 nm displayed a slight decrease (27.4) however it also expressed a minor peak at λ_{emis}=320 nm representing the presence of aromatic hydrocarbons originating from released organic content from bacteria (Dujmov and Sučević, 1990). Moreover, the presence of fluorophoric groups expressing very minor intensities as FI_{sync}≈6.5 could also be

encountered at λ_{emis} > 320 nm. From a general perspective, after t_{irr}=20 min, an irradiation time dependent decreasing order in $FI_{sync280}$ was observed. On the other hand, in the absence of humic matter $FI_{sync470}$ expressed very low intensities as in between 0.486-2.54 however dominant $FI_{sync280}$ displayed changes in the range of and 8.97-32.8.

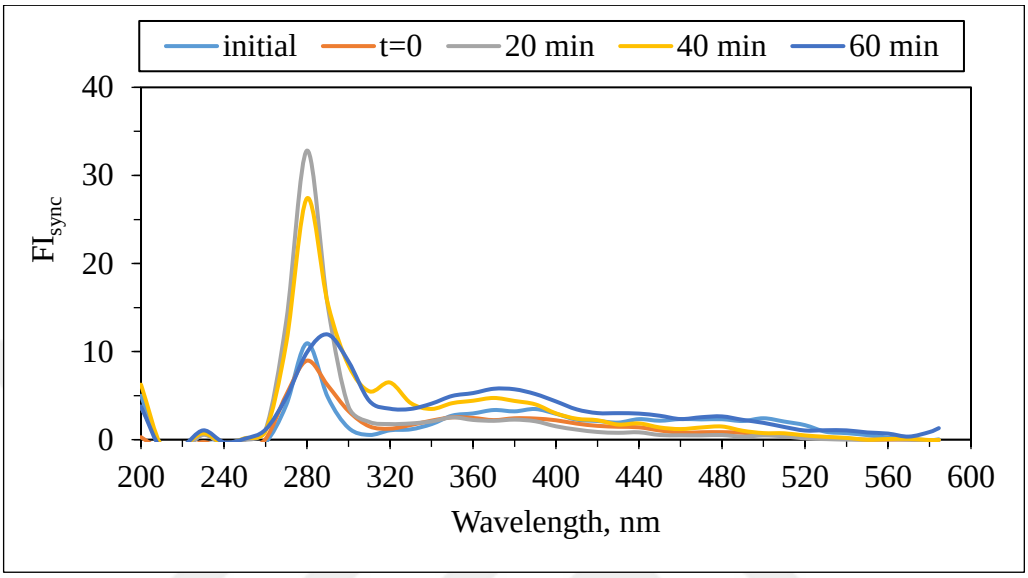

Figure 4.99. Synchronous scan fluorescence spectra of organic matter: Irradiation time dependent *E. coli* inactivation in IsoT solution upon 0.50% Fe-TiO_2 solar photocatalytic treatment.

NPOC expressed variations in the range of 3.47-6.09 mg/L (Figure 4.100). NPOC content increased between initial (3.85 mg/L) and t=0 (6.09 mg/L) and decreased up to t_{irr}=20 min (3.47 mg/L) and again increased to t_{irr}=40 min (5.35 mg/L) due to the release of organics from damaged and destructed *E. coli* cells and followed by a decreasing trend during solar photocatalytic treatment. Specified UV-vis parameters displayed higher values from previous solar photolytic (Figure 4.4) and photocatalytic treatment sets (Figures 4.28, 4.52, and 4.76) carried out in the presence of IsoT solution. The highest data was detected at initial condition as 0.0131 for $Color_{436}$, 0.0213 for UV_{365}, 0.0551 for UV_{280}, and 0.0670 for UV_{254}. All specified UV-vis parameters expressed variations throughout the irradiation duration however a decrease was detected after 60 min of irradiation period.

Based on NPOC contents, $SCoA_{436}$, $SUVA_{365}$, $SUVA_{280}$, $SUVA_{254}$, $SFI_{sync470}$, and $SFI_{sync280}$ parameters were calculated and presented in Figure 4.101. $SUVA_{254}$ displayed variations in the range of 0.626-1.74 L/m mg during solar photocatalytic treatment in the presence of 0.50% Fe-TiO_2 expressing differences in both UV_{254} and NPOC removals. Despite quite low presence of specific UV-vis parameters, they expressed a significant decrease at t=0 condition and followed by an increasing trend until the end of 60 min irradiation period. Furthermore, besides almost insignificant

$SFI_{sync470}$ varied in between 0.137-0.597, $SFI_{sync280}$ expressed changes in the range of and 1.47-9.45. In accordance with the highest $FI_{sync280}$ of irradiation period of 20 min as 32.8 (Figures 4.99 and 4.100), $SFI_{sync280}$ of the same condition (9.45) was calculated as the highest among initial and other irradiation period conditions. In the absence of HA as a solution matrix component, the main fluorophoric group was accepted as $SFI_{sync280}$ similar to previous solar photolytic (Figure 4.5) and photocatalytic *E. coli* inactivation treatments carried out in the presence of IsoT solution (Figures 4.29, 4.53, and 4.77). The role of Fe doping dose of TiO_2 could not be visualized under the specified experimental conditions.

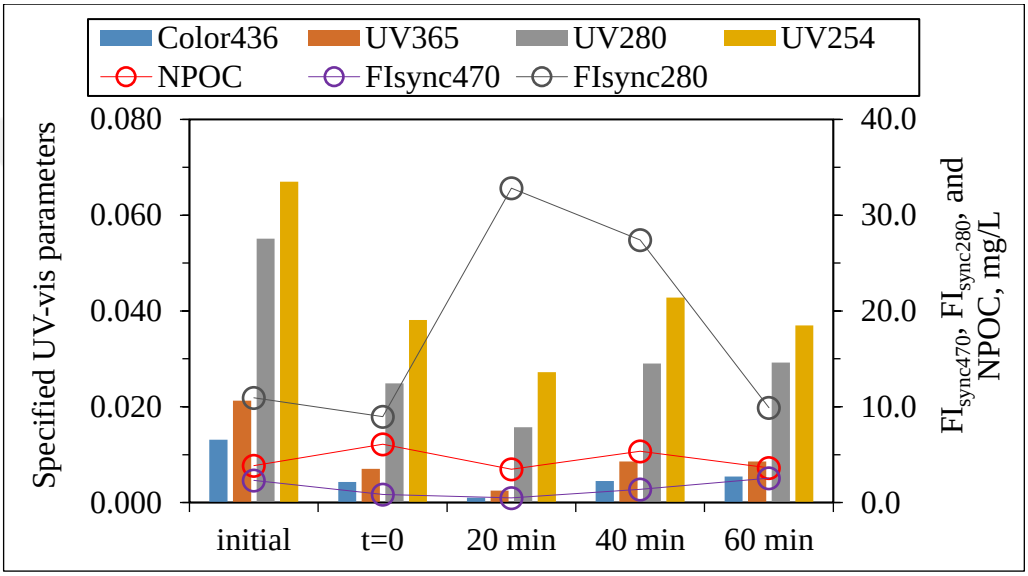

Figure 4.100. Specified UV-vis and fluroscence parameters of organic matter: Irradiation time dependent *E. coli* inactivation in IsoT solution upon 0.50% Fe-TiO_2 solar photocatalytic treatment.

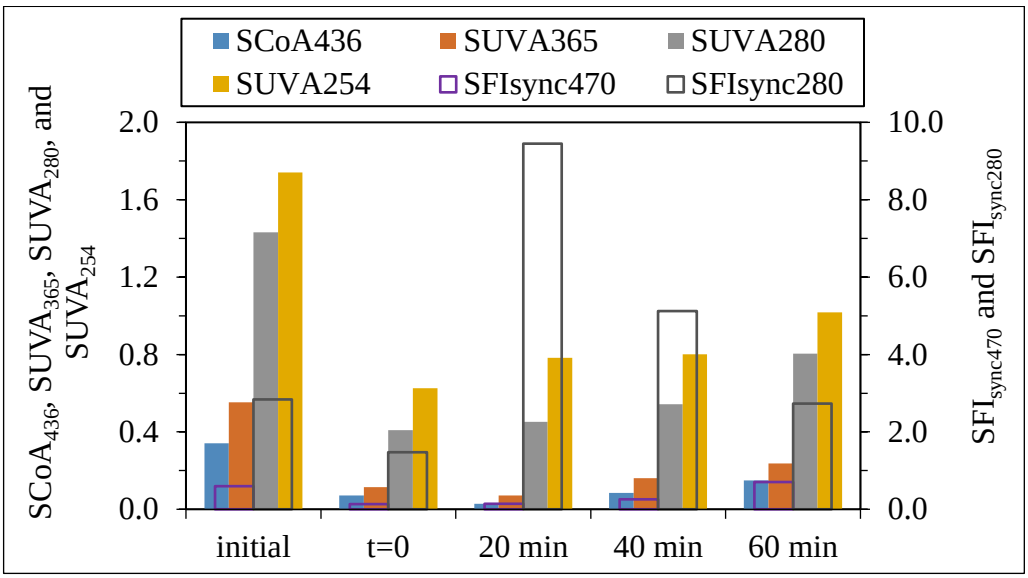

Figure 4.101. Specific UV-vis and fluroscence parameters of organic matter: Irradiation time dependent *E. coli* inactivation in IsoT solution upon 0.50% Fe-TiO_2 solar photocatalytic treatment.

For simplicity purposes, based on the irradiation time dependent variations in UV-vis and fluorescence spectroscopic properties along with NPOC data, characteristic properties of organic matter under initial condition, upon introduction of 0.50% Fe-TiO_2 (t=0) and at the end of 0.50% Fe-TiO_2 solar photocatalytic for irradiation period of 60 min were presented in Table 4.39.

Table 4.39. Characteristic properties of organic matter present in 0.50% Fe-TiO_2 solar photolytic treatment of *E. coli* in IsoT solution.

Irradiation time, min	UV-vis Spectroscopic Parameters, cm^{-1}				NPOC, mg/L	$SUVA_{254}$, L/m mg	$FI_{sync280}$	$SFI_{sync280}$	FI
	$Color_{436}$	UV_{365}	UV_{280}	UV_{254}					
Initial	0.0131	0.0213	0.0551	0.0670	3.85	1.74	10.9	2.84	1.48
t=0	0.0043	0.0070	0.0249	0.0381	6.09	0.626	8.97	1.47	2.05
60 min	0.0054	0.0086	0.0292	0.0370	3.63	1.02	9.92	2.73	1.49

Upon irradiation of 60 min at which 2.44 log reduction of *E. coli* in IsoT solution was attained (Table 4.38), released organic matter expressed the following UV-vis parameters (cm^{-1}); $Color_{436}$: 0.0054, UV_{365}: 0.0086, UV_{280}: 0.0292, UV_{254}: 0.0370, and NPOC as 3.63 mg/L. At the end of irradiation period of 60 min, $SUVA_{254}$ was calculated as 1.02 L/m mg represents that the remaining organic matter could be considered as having hydrophilic and aliphatic character (Edzwald et al., 1985).

Due to release and degradation of proteins, $FI_{sync280}$ showed some fluctuation throughout the irradiation period. According to $FI_{sync280}$ and NPOC contents, calculated $SFI_{sync280}$ also exhibited similar variations. On the other hand, initial, t=0, and t_{irr}=60 min $FI_{sync470}$ data were detected as 2.30, 0.837, and 2.54, respectively. Owing to the release of organics, $FI_{sync470}$ increased at the end of 60 min of irradiation period. $SFI_{sync470}$ values of initial, t=0, and t_{irr}=60 min conditions were calculated as 0.597, 0.137, and 0.701, respectively. FI was calculated as 1.49, which was in between the region of humic fluorophores and microbially derived fluorophores, after irradiation period of 60 min (Sen-Kavurmaci and Bekbolet, 2014). The reason could be attributed to degradation of released organic content from damaged and/or destructed bacteria cells.

In accordance with the UV-vis absorbance and synchronous scan fluorescence analyses, EEM fluorescence contour plots of organic matter emerged and removed during irradiation time dependent *E. coli* inactivation in IsoT solution during solar photocatalytic treatment in the presence of 0.50% Fe-TiO_2 were also followed and illustrated in Figure 4.102. EEM fluorescence contour plots displayed the presence of Regions I, II and IV expressing that the fluorophores were mainly originated from microbial by-products and proteins under all irradiation conditions.

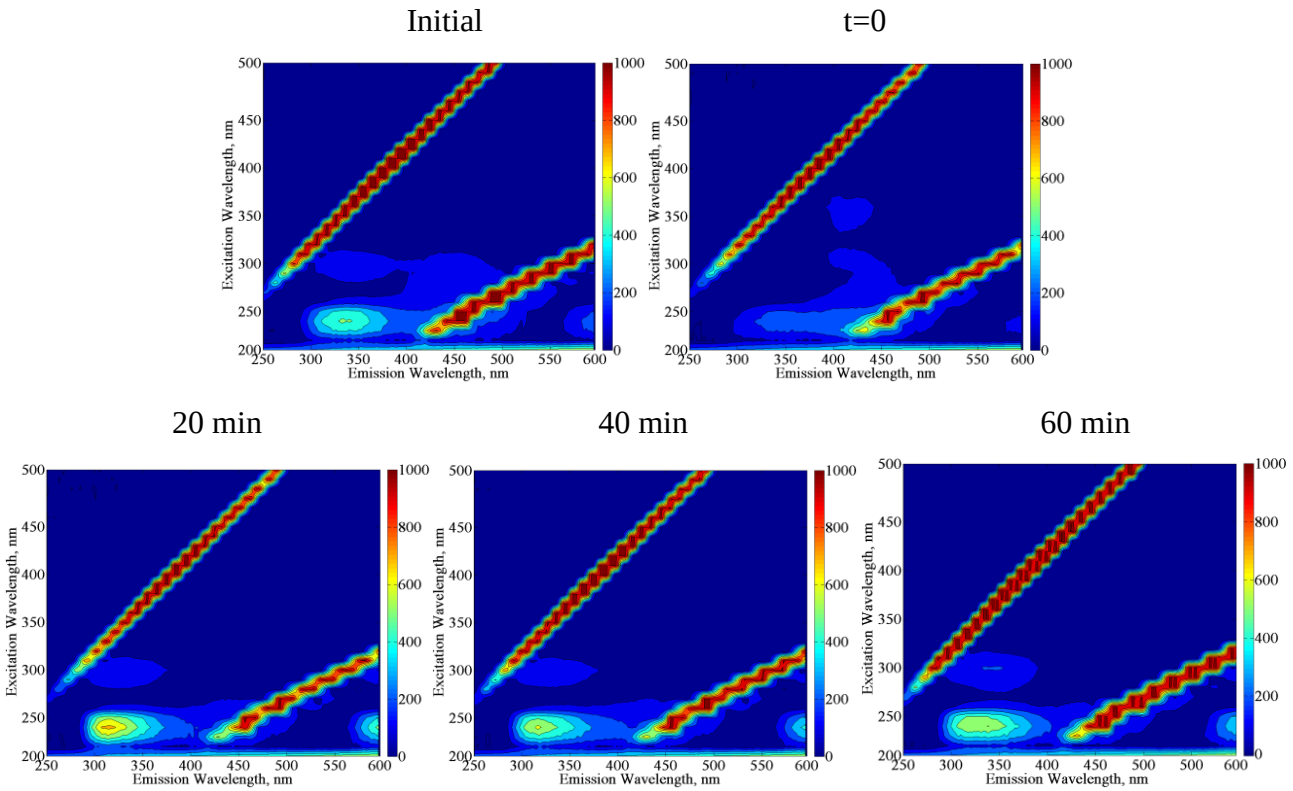

Figure 4.102. EEM fluorescence contour plots of organic matter: Irradiation time dependent *E. coli* inactivation in IsoT solution upon 0.50% Fe-TiO_2 solar photocatalytic treatment.

Decreased fluorescence intensities were detected at t=0 which could be attributed to the immediate adsorptive removal of organics in the presence of photocatalyst. At t_{irr}=20 min, increased intensities were detected at Region I due to the increased protein release from bacteria. The presence of improved protein release could also be followed by increase in $FI_{sync280}$ (Figures 4.99 and 4.100) and $SFI_{sync280}$ (Figure 4.101). After 20 min of irradiation, released microbial by-products and proteins from *E. coli* cells showed a decreasing trend in accordance with the solar photocatalytic degradation of released organic matter and reduction of *E. coli*. Fluorescence intensities were displayed quite low decrease after 20 min of irradiation period in accordance with relatively close *E. coli* enumeration results obtained from t_{irr}=20 min (3.87E+03 CFU/mL), 40 min (3.34E+03 CFU/mL), and 60 min (2.23E+03 CFU/mL) (Figure 4.97). EEM contour plots of 0.50% Fe-TiO_2 solar photocatalytic treatment of *E. coli* in IsoT solution displayed more intense fluorescence after t_{irr}=20 min than 0.25% Fe-TiO_2 solar photocatalytic treatment in IsoT solution (Figure 4.78). However, both solar photocatalytic treatment sets expressed quite low changes in fluorescence intensities and bacteria counts (Figures 4.73 and 4.97) after t_{irr}=20 min.

Besides increased NPOC contents of t=0 and t_{irr}=40 min (Figure 4.100), there was no increased fluorescence could be visualized by EEM contour plot of these conditions. The reason could be

attributed to either the masking effect of released polysaccharides on protein contents of the samples or the presence of organic content other than proteins which could contribute the enhanced NPOC detection.

4.2.4.3. Mechanistic evaluation of *E. coli* inactivation upon 0.50% Fe-TiO_2 solar photocatalytic treatment in IsoT solution. During irradiation, as bacteria inactivation products of 0.50% Fe-TiO_2 solar photocatalytic treatment of *E. coli* in IsoT solution, total K, protein, and carbohydrate contents present in initial, t=0, and t_{irr}=60 min samples were presented in Table 4.40.

Table 4.40. Total K, protein, and carbohydrate contents of time dependent *E. coli* inactivation in IsoT solution upon 0.50% Fe-TiO_2 solar photocatalytic treatment.

0.50% Fe-TiO_2 solar photocatalytic treatment	*E. coli* in IsoT solution		
	Initial	t=0	60 min
Total K, mg/L	1.08	1.00	0.83
Protein, mg/L	1.28	3.64	5.52
Carbohydrate, mg/L	2.12	2.20	25.9

Total K content displayed a decrease in both t=0 and irradiation period of 60 min conditions. 7.4 % of total K showed an immediate adsorptive removal at t=0. Moreover, further decrease of total K content at t_{irr}=60 min could be due to adsorption of released K^+ ions onto oppositely charged *E. coli* cell wall and/or surface of photocatalyst particles and removal by membrane filtration prior total K analysis.

E. coli in IsoT solution upon solar photocatalytic treatment in the presence of 0.50% Fe-TiO_2 displayed increase in both protein and carbohydrate contents at the end of 60 min treatment period. Carbohydrate concentration showed a significant increase (25.9 mg/L) while protein concentration displayed a slight increase (5.52 mg/L). Glycoproteins that are present in the structure of *E. coli*, and Fe^{3+} released from doped-TiO_2 could interfere with the carbohydrate determination process and result in high carbohydrate concentration at the end of irradiation period of 60 min (Martens and Frankenburger, 1990, Rao and Pattabiraman, 1989). Birben and colleagues reported that when sole 0.25% Fe-TiO_2 was irradiated for 60 min in deionized water, 0.013 mg/L iron release was detected (Birben et al., 2017b). However, released Fe^{3+} analysis of both t=0 and t_{irr}=60 min solutions of *E. coli* in IsoT solution upon solar photocatalytic treatment in the presence of 0.50% Fe-TiO_2 were detected as below detection limit (BDL). No correlations were detected neither between NPOC and protein or carbohydrate concentrations, nor between $FI_{sync280}$ and protein contents.

4.2.4.4. Organic matter formation and removal upon 0.50% Fe-TiO_2 solar photocatalytic treatment of *E. coli* in WM solution. UV-vis absorption and synchronous scan fluorescence spectra of organic matter in solution were presented in Figures 4.103 and 4.104. Irradiation time dependent absorbance changes were significantly similar to each other in UV wavelength range of λ=200-280 nm in the absence of aromatic domains and color forming moieties ($Color_{436}$, UV_{365}, and UV_{280}) that should be measured in longer wavelengths. Only t=0 condition displayed higher absorption than following irradiation period conditions at λ > 220 nm. Similar absorption feature of t=0 was also detected with the use of 0.25% Fe-TiO_2 upon solar photocatalytic treatment of *E. coli* in WM solution (Figure 4.79). On the other hand, absorbance detected at λ < 210 nm were characteristic to NO_3^- which was a component of WM solution (Krishnan and Guha, 1934; Edwards at el., 2001).

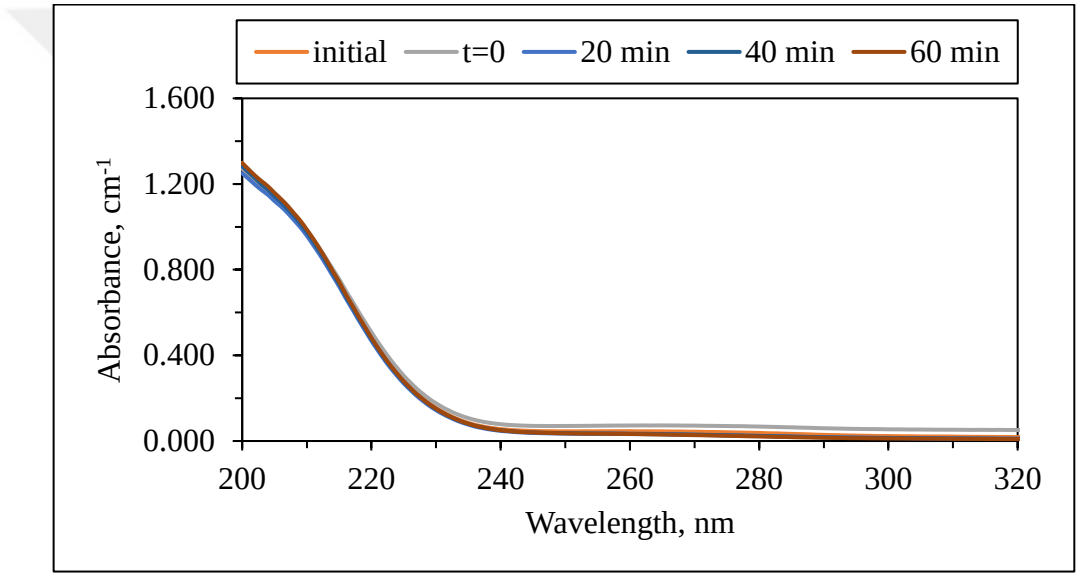

Figure 4.103. UV-vis absorption spectra of organic matter: Irradiation time dependent *E. coli* inactivation in WM solution upon 0.50% Fe-TiO_2 solar photocatalytic treatment.

Synchronous scan fluorescence spectra of the emerged organic matter displayed an intense peak at λ_{emis}=280 and a minor peak at λ_{emis}=420 nm revealing the presence of protein and aromatic hydrocarbon content, respectively (Figure 4.104). At λ_{emis}=280 nm, FI_{sync} data showed a significant increase at t_{irr}=20 min and followed by a decreasing trend. However, decreased fluorescence intensities at λ_{emis}=420 nm until 40 min of irradiation time, displayed a drastic increase at t_{irr}=60 min that could be originating from released aromatic organic content from damaged and destructed *E. coli* cells. Obtained changes in FI_{sync} data was not follow an irradiation time dependent decreasing or increasing order which could be indicating that the presence of both degradation and reemergence of fluorophoric groups could be visualized during specified irradiation period. Furthermore, contrary to minor presence of $FI_{sync470}$ in the range of 0.570-2.74, $FI_{sync280}$ displayed variations significant

presence in between 8.71-30.7. The key fluorophoric groups were accepted as $FI_{sync280}$, in the absence of humic matter in solution.

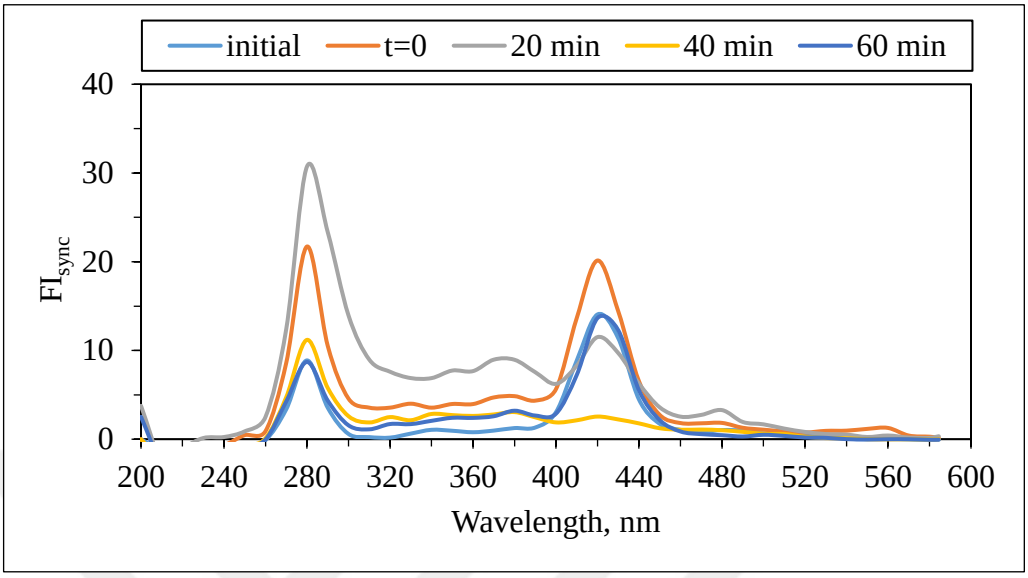

Figure 4.104. Synchronous scan fluorescence spectra of organic matter: Irradiation time dependent *E. coli* inactivation in WM solution upon 0.50% Fe-TiO_2 solar photocatalytic treatment.

From a general perspective, NPOC expressed variations in the range of 1.40-6.12 mg/L (Figure 4.105). NPOC content displayed an insignificant decrease between initial (1.49 mg/L) and t=0 (1.40 mg/L) and increased up to t_{irr}=20 min (3.33 mg/L) due to release of organics from damaged and destructed *E. coli* cells, then decreased up to t_{irr}=40 min (3.08 mg/L) and followed by a sharp increase during solar photocatalytic treatment (6.12 mg/L).

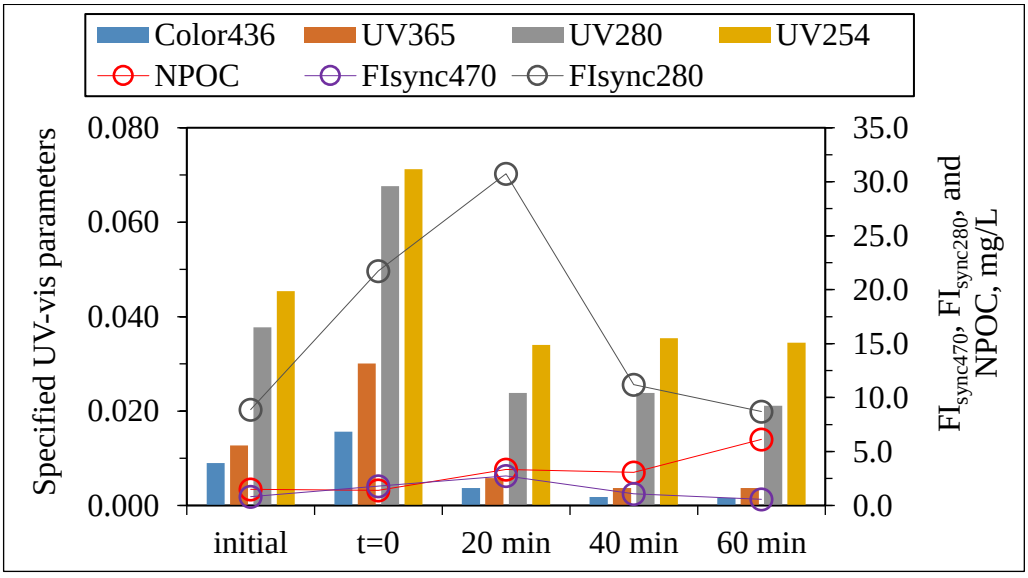

Figure 4.105. Specified UV-vis and fluroscence parameters of organic matter: Irradiation time dependent *E. coli* inactivation in WM solution upon 0.50% Fe-TiO_2 solar photocatalytic treatment.

All UV-vis parameters displayed quite low presence however as the most significant parameter, UV_{254} expressed changes in between 0.0340-0.0712 being the lowest for t_{irr}=20 min which could also be considered as similar to t_{irr}= 40 min (0.0354) and 60 min (0.0345), and the highest for t=0 condition.

Based on NPOC contents, $SCoA_{436}$, $SUVA_{365}$, $SUVA_{280}$, $SUVA_{254}$, $SFI_{sync470}$, and $SFI_{sync280}$ parameters were calculated and presented in Figure 4.106. $SUVA_{254}$ displayed variations in between 0.563-5.09 L/m mg during 0.50% Fe-TiO_2 solar photocatalytic treatment indicating the differences in both UV_{254} and NPOC removals. Furthermore, $SFI_{sync470}$ displayed almost featureless presence in the range of 0.0931-1.28 however dominant $SFI_{sync280}$ expressed variations in between 1.42-15.4.

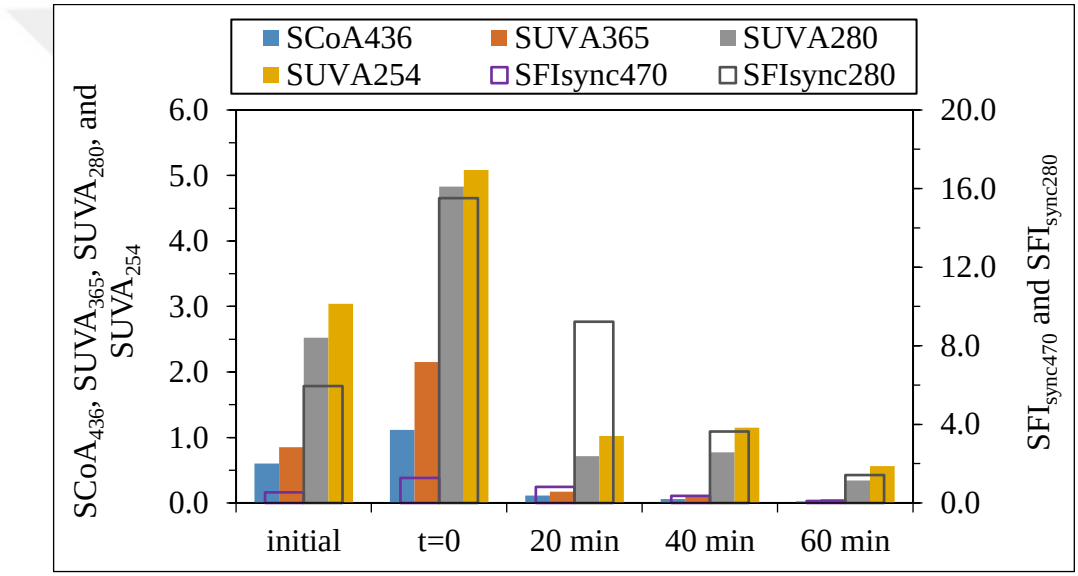

Figure 4.106. Specific UV-vis and fluroscence parameters of organic matter: Irradiation time dependent *E. coli* inactivation in WM solution upon 0.50% Fe-TiO_2 solar photocatalytic treatment.

Characteristic properties of organic matter present under initial condition, upon introduction of 0.25% Fe-TiO_2 (t=0) and at the end of 0.50% Fe-TiO_2 solar photocatalytic treatment for irradiation period of 60 min were presented in Table 4.41.

Table 4.41. Characteristic properties of organic matter present in 0.50% Fe-TiO_2 solar photolytic treatment of *E. coli* in WM solution.

Irradiation time, min	UV-vis Spectroscopic Parameters, cm^{-1}				NPOC, mg/L	$SUVA_{254}$, L/m mg	$FI_{sync280}$	$SFI_{sync280}$	FI
	$Color_{436}$	UV_{365}	UV_{280}	UV_{254}					
Initial	0.0090	0.0127	0.0377	0.0454	1.49	3.04	8.88	5.95	1.35
t=0	0.0156	0.0301	0.0676	0.0712	1.40	5.09	21.7	15.5	1.21
60 min	0.0016	0.0037	0.0211	0.0345	6.12	0.563	8.71	1.42	1.92

Upon an irradiation period of 60 min, 3.49 log reduction of *E. coli* in WM solution was attained in the presence of 0.50% Fe-TiO_2 specimen (Table 3.38). Released organic matter expressed the following UV-vis parameters (cm^{-1}); $Color_{436}$: 0.0016, UV_{365}: 0.0037, UV_{280}: 0.0211, UV_{254}: 0.0345, and NPOC as 6.12 mg/L. $SUVA_{254}$ was calculated as 0.563 L/m mg at t_{irr}=60 min representing that the remaining organic matter could still be considered as having hydrophilic and aliphatic character (Edzwald et al., 1985). The decrease of $SUVA_{254}$ between t=0 (5.09 L/m mg) and t_{irr}=60 min conditions could be attributed to the degradation of present organic content in the solution during irradiation period. Owing to the degradation of released protein content from damaged *E. coli* cells, $FI_{sync280}$ showed a decrease at t_{irr}=60 min. $SFI_{sync280}$ decreased at t_{irr}=60 min in accordance with the increased NPOC due to released organic material from bacteria. Furthermore, $FI_{sync470}$ of initial, t=0, and t_{irr}=60 min runs were detected as 0.803, 1.79, and 0.570, respectively. $SFI_{sync470}$ values of initial, t=0, and t_{irr}=60 min conditions were calculated as 0.538, 1.28, and 0.0931, respectively. Due to the presence of microbially derived organic material, FI at t_{irr}=60 min was calculated as 1.92, as expected.

EEM fluorescence contour plots of organic matter emerged and removed during irradiation time dependent *E. coli* inactivation in WM solution during solar photocatalytic treatment in the presence of 0.50% Fe-TiO_2 were displayed in Figure 4.107.

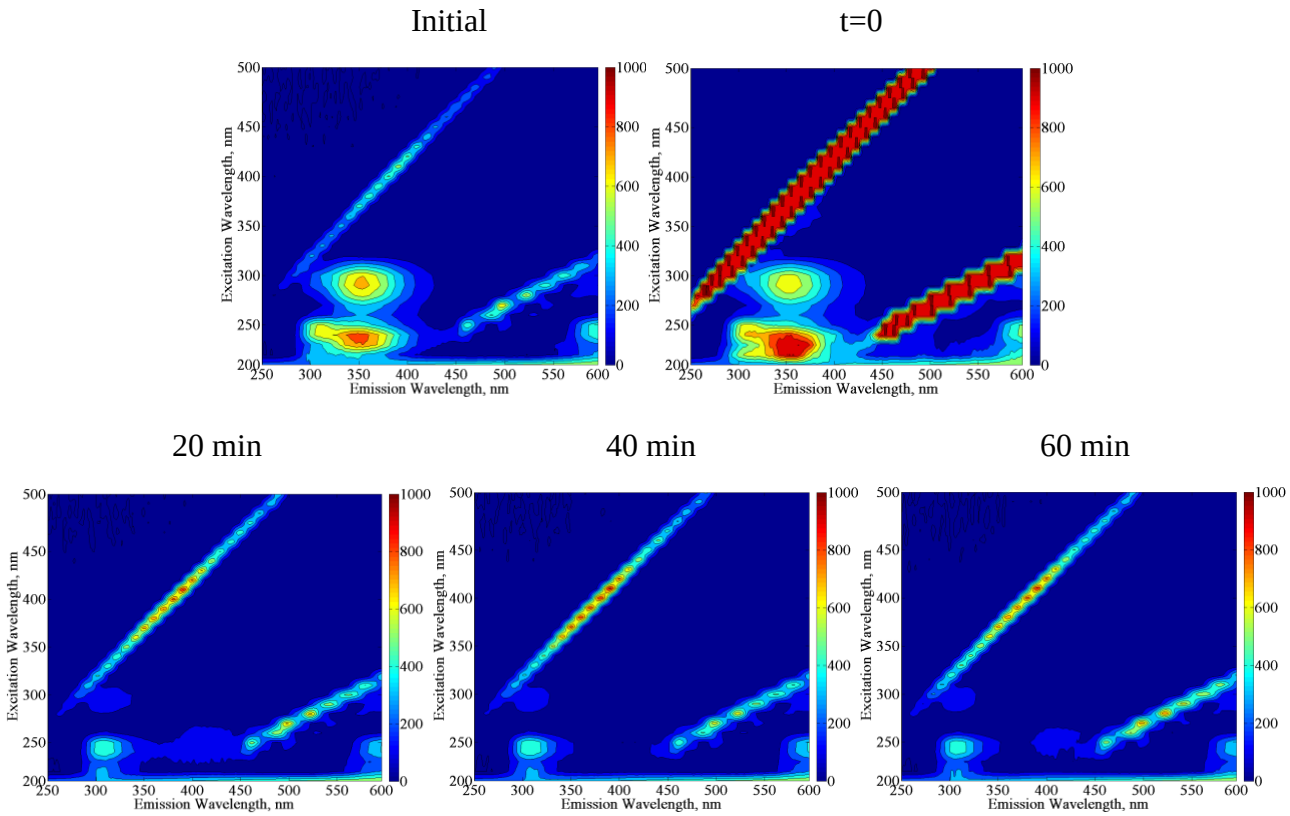

Figure 4.107. EEM fluorescence contour plots of organic matter: Irradiation time dependent *E. coli* inactivation in WM solution upon 0.50% Fe-TiO_2 solar photocatalytic treatment.

EEM fluorescence contour plots displayed the presence of Regions I, II, and IV expressing that the fluorophores were mainly originated from microbial by-products and proteins under all irradiation conditions. Obtained increased intensities of Regions I, II, and IV at t=0 condition could be attributed to cell wall damage occurred right after the introduction of photocatalyst into the solution, similar increases could also be followed by synchronous scan fluorescence spectra (Figure 4.104), specified UV-vis parameters (Figure 4.105), and specific UV-vis and fluroscence parameters (Figure 4.106). Following further irradiation period released microbial by-products and proteins from *E. coli* cells showed a decreasing trend in accordance with the solar photocatalytic degradation of organic matter and reduction of *E. coli*. Moreover, EEM contour plots of *E. coli* in IsoT solution (Figure 4.102) have higher intensities than *E. coli* in WM solution which could be resulting from the lower bacteria LRV of *E. coli* in IsoT solution condition (LRV as 2.44 for *E. coli* in IsoT solution; LRV as 3.49 for *E. coli* in WM solution) (Figure 4.38), also released protein content of *E. coli* in WM solution could possibly be removed throughout the irradiation and result in lower intensities as well.

4.2.4.5. Mechanistic evaluation of *E. coli* inactivation upon 0.50% Fe-TiO_2 solar photocatalytic treatment in WM solution. As *E. coli* inactivation products of solar photocatalytic treatment of *E. coli* in WM solution in the presence of 0.50% Fe-TiO_2, total K, protein, and carbohydrate contents present in initial, t=0, and t_{irr}=60 min samples were presented in Table 4.42.

Table 4.42. Total K, protein, and carbohydrate contents of time dependent *E. coli* inactivation in WM solution upon 0.50% Fe-TiO_2 solar photocatalytic treatment.

0.50% Fe-TiO_2 solar photocatalytic treatment	*E. coli* in WM solution		
	Initial	t=0	60 min
Total K, mg/L	4.12	3.86	3.91
Protein, mg/L	1.08	1.10	14.7
Carbohydrate, mg/L	0.618	1.25	3.21

Total K content showed a slight fluctuation like TiO_2 solar photocatalytic treatment (Table 4.15). At t=0, total K content displayed an immediate adsorptive removal as 6.3 % and after irradiation period of 60 min, a slight increase in total K was obtained owing to release of K^+ ions from damaged bacteria cells.

Upon introduction of 0.25% Fe-TiO_2 into the solution (t=0), protein content expressed almost insignificant increase at t=0 however carbohydrate content increased higher than the half of initial condition. Increased carbohydrate content at t=0 could be correlated with increased data obtained

from synchronous scan fluorescence spectra (Figure 4.104), specified UV-vis parameters (Figure 4.105), specific UV-vis and fluroscence parameters (Figure 4.106), and increased EEM intensities at Region IV representing microbial by-products (Figure 4.107). Both protein and carbohydrate contents increased at t_{irr}=60 min. Besides minor increase in carbohydrate content at t_{irr}=60 min (0.618-3.21 mg/L), protein concentration displayed a significant increase (1.08-14.7 mg/L), similar increase in protein content was also detected from SynTiO_2 solar photocatalytic treatment in WM solution (Table 4.24). Protein and $FI_{sync280}$ showed no correlation with each other however NPOC displayed strong correlations with both protein and carbohydrate contents as R^2=1.00 and R^2=0.94, respectively.

4.2.4.6. Organic matter formation and removal upon 0.50% Fe-TiO_2 solar photocatalytic treatment of *E. coli* in HA solution. UV-vis absorption and synchronous scan fluorescence spectra of organic matter in solution were presented in Figures 4.108 and 4.109. Irradiation time dependent absorbance changes were significantly different from each other in UV wavelength range of λ=200-400 nm due to the presence of aromatic domains and color forming moieties ($Color_{436}$, UV_{365}, and UV_{280}). The absorbance of HA_i expressed a rather different trend in λ < 235 nm region as expected. Upon addition of bacteria into the solution (initial), due to organic matter exudates from *E. coli* following 0.45 μm filtration increased absorbances were detected. Moreover, further increase of absorbances at UV region were recorded after the introduction of 0.50% Fe-TiO2 into the reaction medium due to released cytoplasmic organic content from bacteria via mechanistic effect of photocatalyst adsorbed onto the cell wall. On the other hand, after t=0 condition, UV-vis absorption spectra followed an irradiation time dependent decreasing order during 60 min of irradiation period.

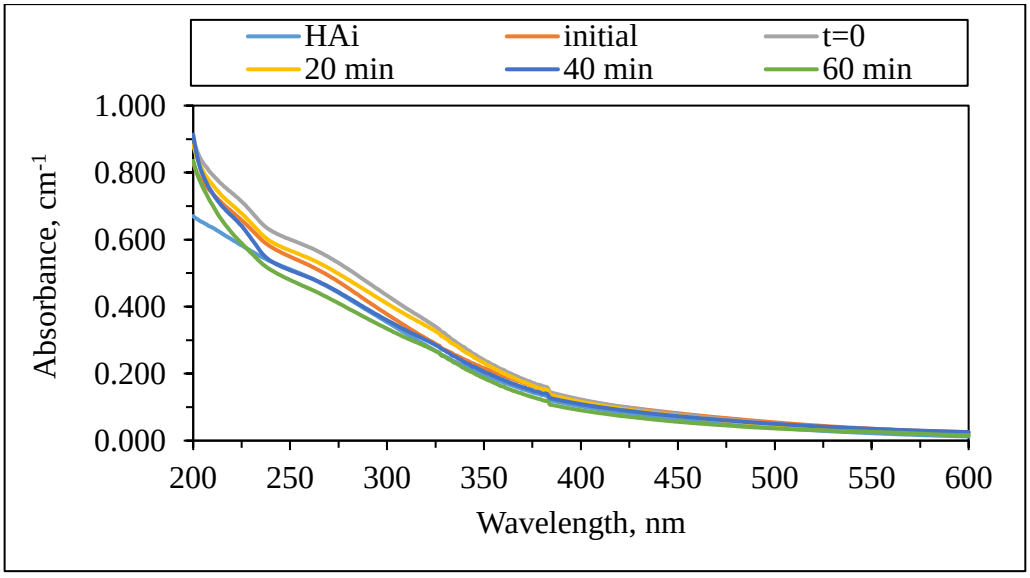

Figure 4.108. UV-vis absorption spectra of organic matter: Irradiation time dependent *E. coli* inactivation in HA solution upon 0.50% Fe-TiO_2 solar photocatalytic treatment.

Synchronous scan fluorescence spectra of emerged organic matter displayed intense peaks at λ_{emis}=370 nm and two minor peaks at λ_{emis}=440 nm and 480 nm that represent the presence of aromatic hydrocarbons in the solution as expected (Dujmov and Sučević, 1990) (Figure 4.109). Significant increase in FI_{sync} data, especially for $FI_{sync370}$, were observed at t_{irr}= 20 min and 40 min conditions, which could be indicating that the increased released of organic content from damaged bacteria cells. Furthermore, in the presence of HA solution, evidently present $FI_{sync470}$ expressed changes in the range of 67.8-106 however $FI_{sync280}$ displayed lower presence varied in between 4.76-83.7 as expected (Figure 4.110). The main fluorophoric group referred to $FI_{sync470}$ in the presence of HA as the solution matrix was evident under all conditions along with $FI_{sync370}$.

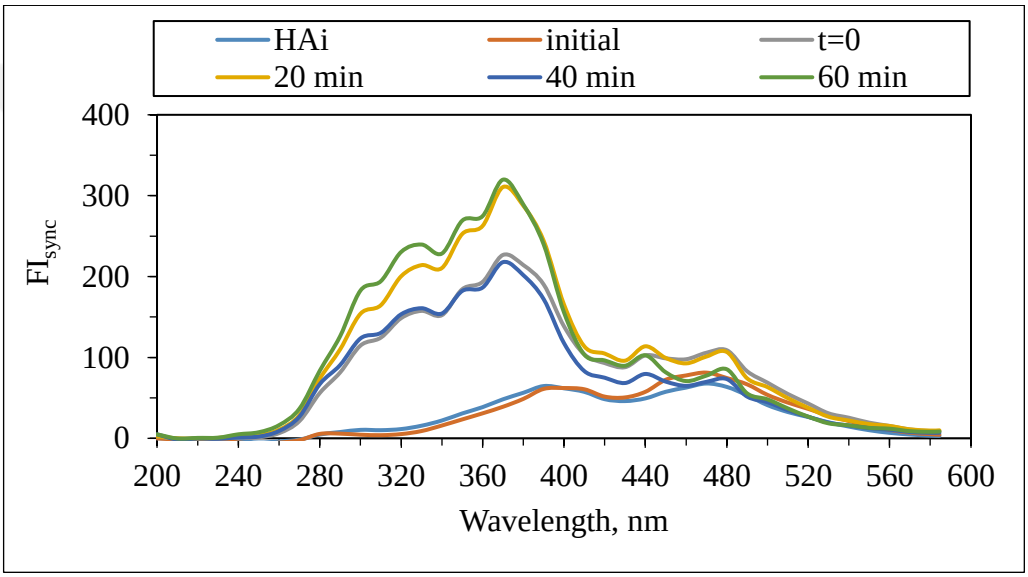

Figure 4.109. Synchronous scan fluorescence spectra of organic matter: Irradiation time dependent *E. coli* inactivation in HA solution upon 0.50% Fe-TiO_2 solar photocatalytic treatment.

In the presence of HA solution, NPOC contents expressed variations in the range of 5.27-13.7 mg/L (Figure 4.110). NPOC content increased between HA_i (5.52 mg/L) and initial (7.57 mg/L) due to introduction of bacteria into the solution but decreased up to t=0 (5.27 mg/L) owing to immediate adsorptive removal of organic content as 30.4 %. Afterwards, NPOC displayed fluctuations up to 0.44 mg/L until t_{irr}=40 min (5.31 mg/L) and a sharp increase was observed as 13.7 mg/L due to release of organics from damaged and destructed *E. coli* cells during solar photocatalytic treatment. The highest NPOC release was attained upon irradiation of 60 min. All UV-vis parameters expressed high presence due to the use of HA solution. After t=0 condition, all specified UV-vis parameters followed a sequential decreasing trend similar to TiO_2 and SynTiO_2 solar photocatalytic treatment sets (Figures 4.38 and 4.62). However, demonstrated decreasing trend was not evident as in TiO_2 solar

photocatalytic treatment. As the most significant parameter UV_{254} expressed variations in the range of 0.4688-0.5911.

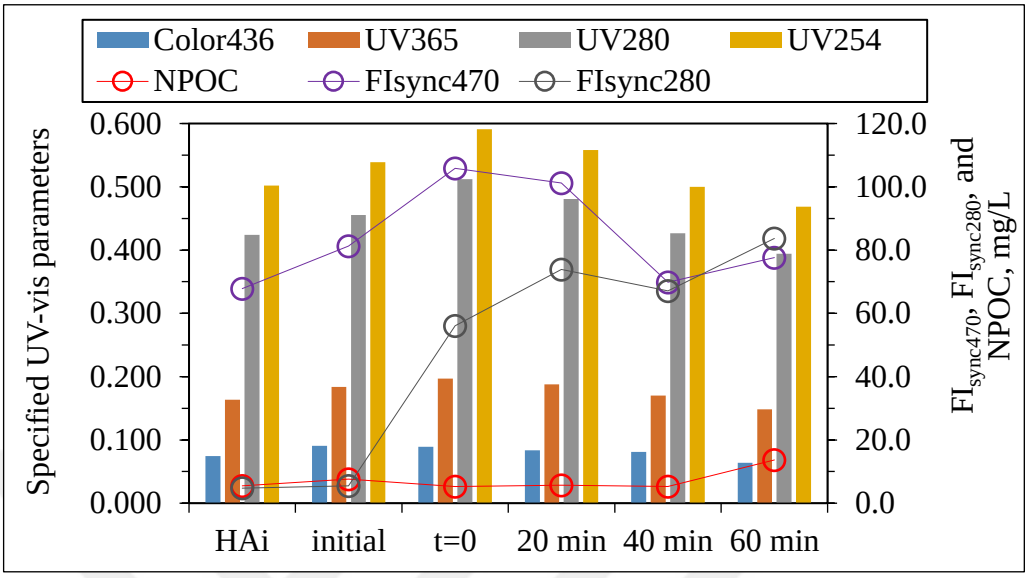

Figure 4.110. Specified UV-vis and fluroscence parameters of organic matter: Irradiation time dependent *E. coli* inactivation in HA solution upon 0.50% Fe-TiO_2 solar photocatalytic treatment.

Based on NPOC contents attained under all conditions, $SCoA_{436}$, $SUVA_{365}$, $SUVA_{280}$, $SUVA_{254}$, $SFI_{sync470}$, and $SFI_{sync280}$ parameters were calculated and presented in Figure 4.111.

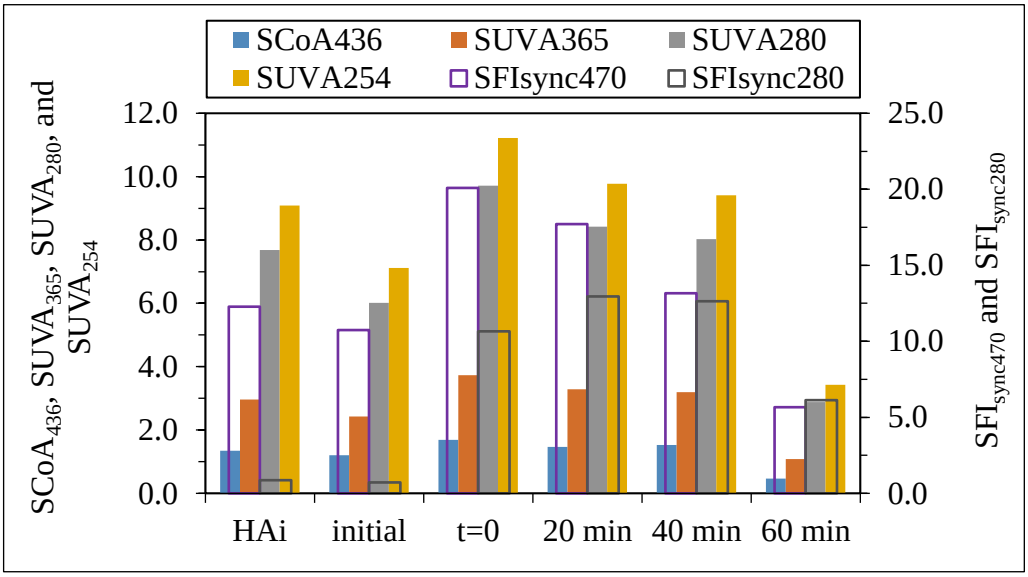

Figure 4.111. Specific UV-vis and fluroscence parameters of organic matter: Irradiation time dependent *E. coli* inactivation in HA solution upon 0.50% Fe-TiO_2 solar photocatalytic treatment.

Most importantly, $SUVA_{254}$ displayed variations in the range of 3.43-11.2 L/m mg during solar photocatalytic treatment in the presence of 0.50% Fe-TiO_2 expressing differences in both UV_{254} and

NPOC removals. Furthermore, $SFI_{sync470}$ and $SFI_{sync280}$ expressed variations in the range of 5.68-20.1 and 0.728-12.9, respectively. In presence of HA solution as a reaction medium, the predominant fluorophoric group was accepted as $SFI_{sync470}$.

For comparative evaluation purposes, characteristic properties of organic matter under initial condition, upon introduction of 0.50% Fe-TiO_2 (t=0) and at the end of 0.50% Fe-TiO_2 solar photocatalytic inactivation of *E. coli* in HA solution for 60 min of irradiation period were presented in Table 4.43.

Table 4.43. Characteristic properties of organic matter present in 0.50% Fe-TiO_2 solar photolytic treatment of *E. coli* in HA solution.

Irradiation time, min	UV-vis Spectroscopic Parameters, cm^{-1}				NPOC, mg/L	$SUVA_{254}$, L/m mg	$FI_{sync470}$	$SFI_{sync470}$	FI
	$Color_{436}$	UV_{365}	UV_{280}	UV_{254}					
Initial	0.0909	0.1837	0.4552	0.5390	7.57	7.12	81.3	10.7	1.04
t=0	0.0891	0.1967	0.5119	0.5911	5.27	11.2	106	20.1	1.05
60 min	0.0641	0.1486	0.3942	0.4688	13.7	3.43	77.6	5.68	1.17

Upon 60 min of irradition period, upon solar photocatalytic treatment in the presence of 0.50% Fe-TiO_2, 3.36 log *E. coli* reduction was achieved in HA solution (Table 4.38). Released organic matter expressed the following UV-vis parameters (cm^{-1}); $Color_{436}$: 0.0641, UV_{365}: 0.1486, UV_{280}: 0.3942, UV_{254}: 0.4688, and NPOC as 13.7 mg/L.

$SUVA_{254}$ of initial, t=0, and following irradiation period of 60 min condition were calculated as 7.12, 11.2, and 3.43 L/m mg, respectively. At the beginning of the treatment, sample solutions (initial and t=0) displayed hydrophobic and aromatic features however after t_{irr}=60 min aromaticity of the organic content showed a significant decrease and expressed almost completely aliphatic characteristics (Edzwald et al., 1985). The presence of HA as solution matrix caused relatively high initial NPOC and $SUVA_{254}$ as expected.

$FI_{sync470}$ displayed a decrease at t_{irr}=60 min due to degradation of organic matter in solution however detected $FI_{sync280}$ followed a different pattern. $FI_{sync280}$ measurements of initial, t=0 and t_{irr}=60 min conditions were detected as 5.51, 56.1, and 83.7, respectively. Released proteins from damaged bacteria caused an increase in $FI_{sync280}$ data at the end of 60 min of irradiation time. In accordance with increased NPOC at t_{irr}=60 min, $SFI_{sync470}$ decreased by almost half with respect to initial condition. On the other hand, $SFI_{sync280}$ values of initial, t=0, and t_{irr}=60 min samples were calculated as 0.728, 10.6, and 6.12, respectively. After solar light exposure of 60 min, FI was

calculated as 1.17 indicating the presence of fluorophores emerging from present humic matter in the solution as expected.

EEM fluorescence contour plots of organic matter emerged and removed during irradiation time dependent *E. coli* inactivation in HA solution during 0.50% Fe-TiO_2 solar photocatalytic treatment were displayed in Figure 4.112.

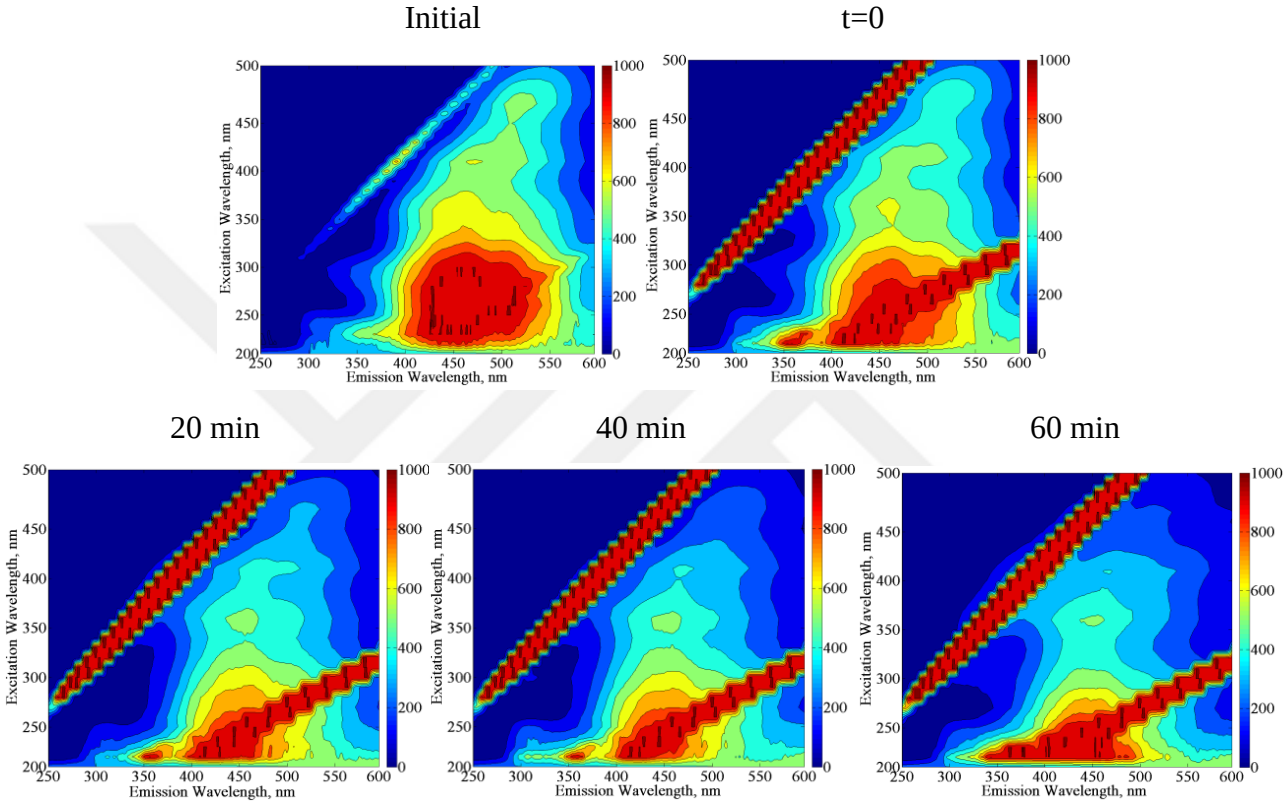

Figure 4.112. EEM fluorescence contour plots of organic matter: Irradiation time dependent *E. coli* inactivation in HA solution upon 0.50% Fe-TiO_2 solar photocatalytic treatment.

EEM fluorescence contour plots of *E. coli* in HA solution upon solar photocatalytic treatment in the presence of 0.50% Fe-TiO_2 displayed the presence of Regions III, and V indicating that the fluorophores were mainly originated from fulvic-like and humic-like substances. Due to the quenching effect of humic-like components on microbial by-products and protein-like fluorophores, and encapsulation of proteins by humic substances, the presence of Region I, II and IV could not significantly be identified as expected (Tomaszewski et al., 2011; Wang et al., 2015). Both humic-like and fulvic-like fluorophore intensities displayed a decreasing trend throughout the 60 min irradiation period however the decrease was very low with respect to TiO_2 solar photocatalytic treatment (Figure 4.40). It could be attributed that 0.50% Fe-TiO_2 has a selectivity towards bacteria rather than organic matrix similar to the behavior of SynTiO_2 and 0.25% Fe-TiO_2 specimens.

Moreover, EEM contour plots of 0.50% Fe-TiO_2 have similarities with 0.25% Fe-TiO_2 (Figure 4.88) but displayed higher intensities than 0.25% Fe-TiO_2; therefore, it could be concluded that 0.50% Fe-TiO_2 has higher affinity for bacteria than 0.25% Fe-TiO_2.

4.2.4.7. Mechanistic evaluation of *E. coli* inactivation upon 0.50% Fe-TiO_2 solar photocatalytic treatment in HA solution. As *E. coli* inactivation products of 0.50% Fe-TiO_2 solar photocatalytic treatment in HA solution, total K, protein, and carbohydrate contents present in initial, t=0, and t_{irr}=60 min samples were presented in Table 4.44.

Table 4.44. Total K, protein, and carbohydrate contents of time dependent *E. coli* inactivation in HA solution upon 0.50% Fe-TiO_2 solar photocatalytic treatment.

0.50% Fe-TiO_2 solar photocatalytic treatment	*E. coli* and HA		
	Initial	t=0	60 min
Total K, mg/L	0.54	0.57	0.57
Protein, mg/L	8.55	8.75	11.3
Carbohydrate, mg/L	3.02	3.99	77.9

Low total K concentrations were obtained from *E. coli* in the presence of HA solution as expected. Total K content showed a slight increase after initial condition and remained stable between t=0 and t_{irr}=60 min conditions. Same total K content of t=0 and t_{irr}=60 min solutions could be due to the elimination of released K^+ ions, which adsorbed onto bacteria, HA and photocatalyst surfaces, by membrane filtration taking place prior to total K analysis.

E. coli in HA solution upon solar photocatalytic treatment in the presence of 0.50% Fe-TiO_2 displayed increase in both protein (8.55-11.3 mg/L) and carbohydrate (3.02-77.9 mg/L) content at t_{irr}=60 min. Protein concentrations were plotted against $FI_{sync280}$ and a moderate correlation was detected as R^2=0.66. Carbohydrate concentration showed an unexpected significant increase after 60 min of irradiation period (77.9 mg/L) which could be due to an experimental error or by reason of the presence of some interfering compounds like cellulosic fibers and other insoluble carbohydrates, or NO_3^- and Fe^{3+} (Martens and Frankenberger, 1990). Moreover, investigators reported that when humic material is treated with H_2SO_4, which was used in phenol-sulfuric acid method, it could give absorbance in the range of λ=350-500 nm and may interfere with the total carbohydrate determination (Sieburth and Jensen, 1969; Meadows and Campbell, 1978). Leached Fe^{3+} content was measured in both t=0 and t_{irr}=60 min samples as 0.032 mg/L and 0.051 mg/L, respectively. Therefore, the reason of high carbohydrate content of t_{irr}=60 min could be attributed to presence of HA, Fe^{3+}, and

glycoproteins originating from bacteria. On the other hand, NPOC displayed strong correlations with either protein and carbohydrate contents as R^2=0.89 and R^2=0.92, respectively.

4.2.4.8. Organic matter formation and removal upon 0.50% Fe-TiO_2 solar photocatalytic treatment of *E. coli* in "HA and WM" solution. UV-vis absorption spectra of organic matter in solution were recorded and presented in Figure 4.113. Irradiation time dependent absorbance changes were significantly different from each other in UV wavelength range of λ=200-400 nm due to the presence of aromatic domains and color forming moieties ($Color_{436}$, UV_{365}, and UV_{280}).

Different from HA_i, the use of "HA and WM" solution matrix, absorbance characteristics displayed a different trend at λ < 260 nm. Especially between λ=200-210 nm a shoulder was detected due to the strong absorption spectrum of NO_3^- having its λ_{max} at approximately 200 nm (Krishnan and Guha, 1934; Edwards at el., 2001). Similar absorption behaviors could also be visualized with previous solar photolytic (Figure 4.17) and photocatalytic treatment sets carried out in the presence of "HA and WM" solution (Figures 4.41, 4.65, and 4.89). On the other hand, UV-vis absorption spectra displayed an irradiation time dependent decreasing order during 60 min solar light exposure duration.

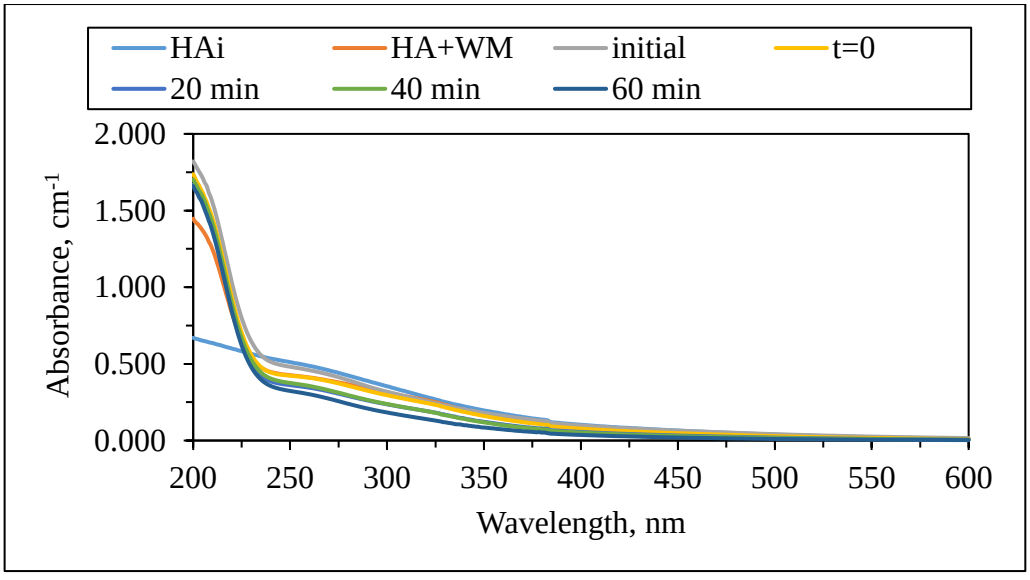

Figure 4.113. UV-vis absorption spectra of organic matter: Irradiation time dependent *E. coli* inactivation in "HA and WM" solution upon 0.50% Fe-TiO_2 solar photocatalytic treatment.

Synchronous scan fluorescence spectra of the emerged organic matter displayed an intense peak at λ_{emis}=370 nm and a minor peak at λ_{emis}=480 nm (Figure 4.114). Similar to TiO_2 solar photocatalytic treatment of *E. coli* conducted in "HA and WM" solution, with the addition of 0.50% Fe-TiO_2 into

the reaction matrix (t=0), a drastic increase in FI_{sync} data was recorded. It could be indicated that, due to the mechanistic effect of photocatalyst on the cell wall causing release of cytoplasmic material of bacteria, FI_{sync} could be increase with increased organic matter content in solution. From a general view, FI_{sync} data displayed an increase between t_{irr}=20 min and 40 min and followed by a significant decrease at t_{irr}=60 min.

Furthermore, despite predominant $FI_{sync470}$ expressing variations in between 28.1-95.0, quite low $FI_{sync280}$ displayed changes in the range of 4.07-70.8 (Figure 4.115). The key fluorophoric group was recognized as $FI_{sync470}$ due to the presence of HA in the solution matrix.

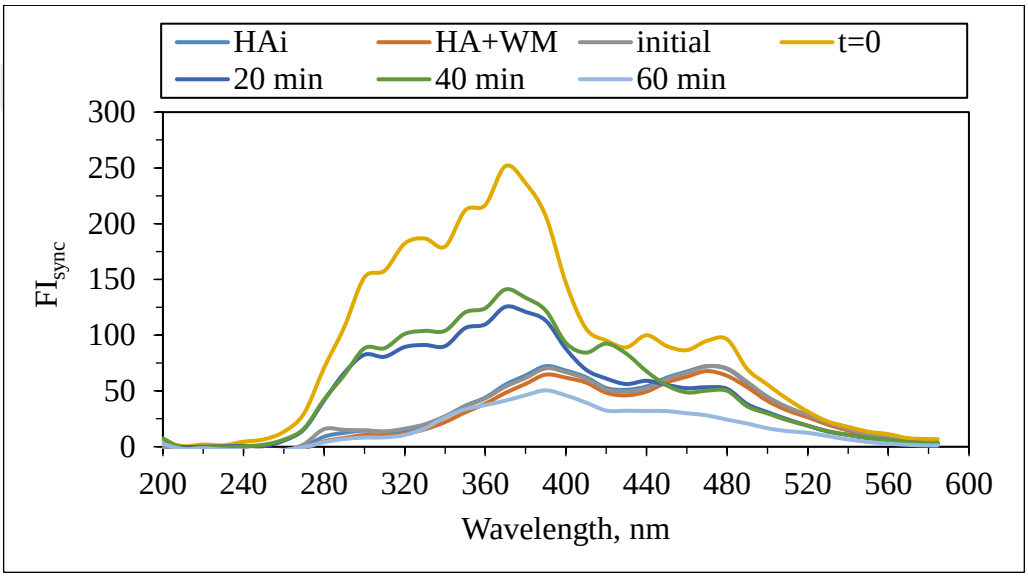

Figure 4.114. Synchronous scan fluorescence spectra of organic matter: Irradiation time dependent *E. coli* inactivation in "HA and WM" solution upon 0.50% Fe-TiO_2 solar photocatalytic treatment.

Along with the presence of "HA and WM" solution, NPOC expressed variations in the range of 4.76-12.9 mg/L (Figure 4.115). NPOC content slightly decrease between HA_i (4.83 mg/L) and "HA and WM" solutions (4.76 mg/L). After the addition of *E. coli* into the reaction solution (initial condition), a significant increase was recorded in NPOC content (7.07 mg/L). However, at t=0 condition due to an immediate adsorptive removal of organics as 25.9 %, NPOC content displayed a drastic decrease (5.24 mg/L). Afterwards, NPOC expressed fluctuations in a range of 0.38 mg/L up to t_{irr}=40 min (5.62 mg/L) and followed by a sharp increase (12.9 mg/L) due to the release of organics from damaged and destructed bacterial cells during solar photocatalytic treatment. Detected NPOC increase in between t_{irr}=40 min and 60 min could also be well correlated with increased bacteria inactivation at t_{irr}= 60 min (3.54E+04 CFU/mL for t_{irr}= 40 min; 7.74E+03 CFU/mL for t_{irr}= 60 min) (Figure 4.97). On the other hand, all specified UV-vis parameters displayed an irradiation time

dependent decreasing order, except slightly increased UV_{280} and UV_{254} at t_{irr}=40 min condition. As the most evident parameter, UV_{254} expressed changes in the range of 0.3151-0.5020, being the highest for HA_i solution and the lowest for t_{irr}=60 min condition.

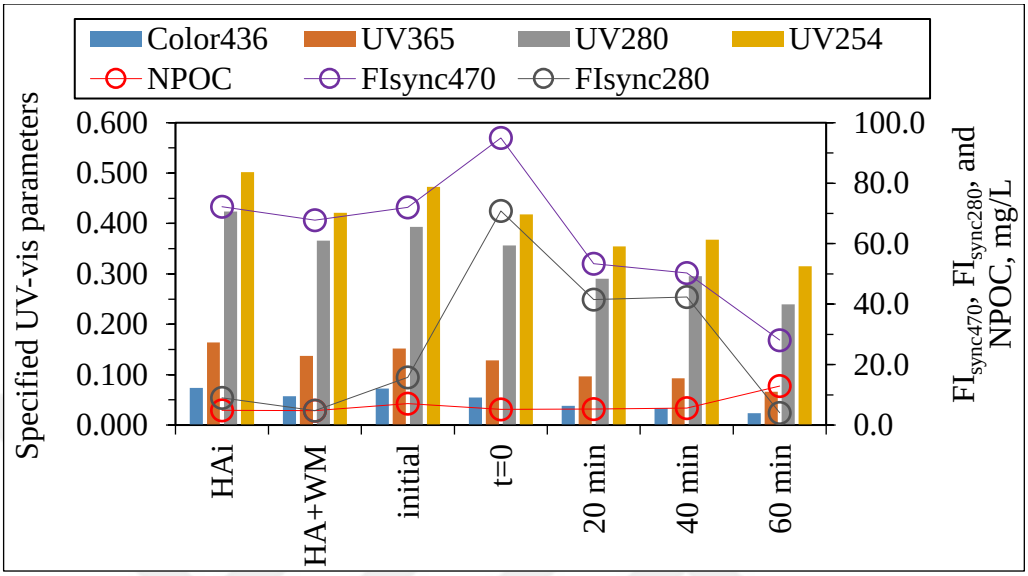

Figure 4.115. Specified UV-vis and fluroscence parameters of organic matter: Irradiation time dependent *E. coli* inactivation in "HA and WM" solution upon 0.50% Fe-TiO_2 solar photocatalytic treatment.

Based on NPOC contents, $SUVA_{365}$, $SUVA_{280}$, $SUVA_{254}$, $SFI_{sync470}$, and $SFI_{sync280}$ parameters were calculated and presented in Figure 4.116.

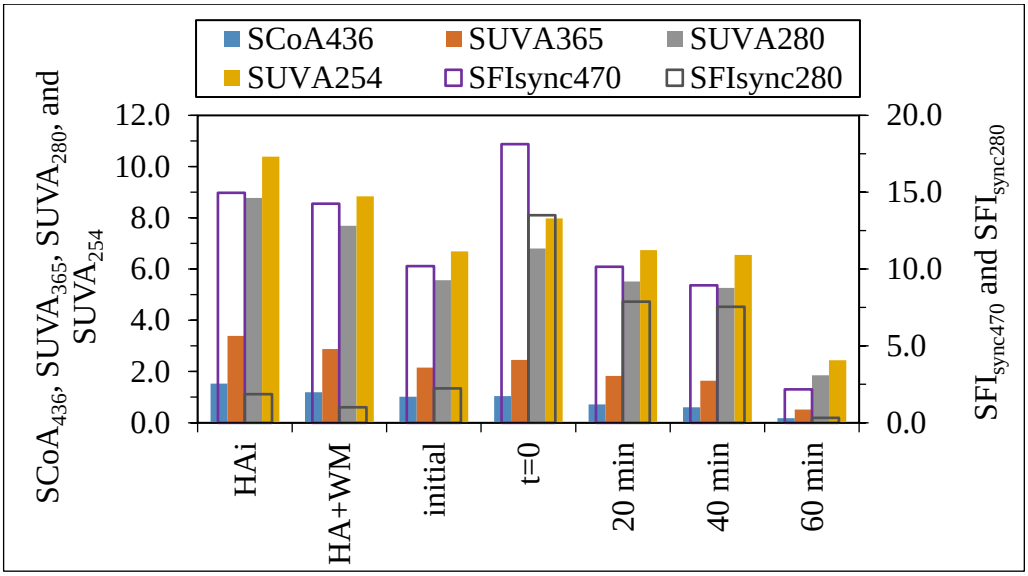

Figure 4.116. Specific UV-vis and fluroscence parameters of organic matter: Irradiation time dependent *E. coli* inactivation in "HA and WM" solution upon 0.50% Fe-TiO_2 solar photocatalytic treatment.

$SUVA_{254}$, as the most significant specific UV-vis parameter, displayed changes in between 2.45-10.4 L/m mg during 0.50% Fe-TiO_2 solar photocatalytic treatment expressing the differences in both UV_{254} and NPOC removals. On the other hand, $SFI_{sync470}$ and $SFI_{sync280}$ expressed variations in the range of 2.18-18.1 and 0.316-7.89, respectively. Due to remarkable presence of $SFI_{sync470}$ in comparison to $SFI_{sync280}$, it was accepted as the dominant fluorophoric group.

For comparative evaluation purposes, characteristic properties of organic matter under initial condition, upon introduction of 0.50% Fe-TiO_2 (t=0) and at the end of 0.50% Fe-TiO_2 solar photocatalytic inactivation of *E. coli* in "HA and WM" solution for 60 min of solar light exposure were presented in Table 4.45.

Table 4.45. Characteristic properties of organic matter present in 0.50% Fe-TiO_2 solar photolytic treatment of *E. coli* in "HA and WM" solution.

Irradiation time, min	UV-vis Spectroscopic Parameters, cm^{-1}				NPOC, mg/L	$SUVA_{254}$, L/m mg	$FI_{sync470}$	$SFI_{sync470}$	FI
	$Color_{436}$	UV_{365}	UV_{280}	UV_{254}					
Initial	0.0724	0.1520	0.3935	0.4727	7.07	6.69	72.0	10.2	1.14
t=0	0.0544	0.1286	0.3567	0.4182	5.24	7.98	95.0	18.1	1.19
60 min	0.0234	0.0661	0.2395	0.3151	12.9	2.45	28.1	2.18	1.27

Upon solar photocatalytic treatment in the presence of 0.50% Fe-TiO_2 for t_{irr}=60 min, at which 1.84 log *E. coli* reduction was achieved in "HA and WM" solution (Table 4.38), released organic matter expressed the following UV-vis parameters (cm^{-1}); $Color_{436}$: 0.0234, UV_{365}: 0.0661, UV_{280}: 0.2395, UV_{254}: 0.3151, and NPOC as 12.9 mg/L.

$SUVA_{254}$ of initial, t=0, and t_{irr}=60 min conditions were calculated as 6.69, 7.98, and 2.45 L/m mg, respectively. According to findings of Edzwald and colleagues, $SUVA_{254} < 3$ indicates that sample display hydrophilic and aliphatic features however $SUVA_{254} > 4$ reveals hydrophobic and aromatic characteristics of solution (Edzwald et al., 1985). Therefore, it could be indicated that whereas initial and t=0 conditions showed hydrophobic and aromatic features, t_{irr}=60 min condition expressed hydrophilic and aliphatic characteristics due to degradation of aromatic organics throughout 60 min of solar light exposure duration. On the other hand, the presence of HA solution as a rection matrix constituent caused relatively high initial NPOC and $SUVA_{254}$ as expected.

$FI_{sync470}$ decreased at t_{irr}=60 min due to degradation of organic content arising from damaged *E. coli* cells and organic matrix. At the end of 60 min irradiation period, calculated $SFI_{sync470}$ decreased in accordance with increased NPOC content. On the other hand, $FI_{sync280}$ measurements of initial, t=0

and t_{irr}=60 min conditions were detected as 15.8, 70.8, and 4.07, respectively. Furthermore, $SFI_{sync280}$ values of initial, t=0, and t_{irr}=60 min conditions were calculated as 2.23, 13.5, and 0.316, respectively. Due to degradation of both humic content and released cytoplasmic organics containing proteins, $FI_{sync280}$ and consequently $FI_{sync280}$ showed a decrease after 60 min of solar irradiation period. FI was calculated as 1.27 for t_{irr}=60 min conditions indicating the presence of fluorophores emerging from present humic matter in experimental solution matrix as expected (Sen-Kavurmaci and Bekbolet, 2014).

In accordance with the UV-vis absorbance and synchronous scan fluorescence spectroscopic analyses, EEM fluorescence contour plots of organic matter during irradiation time dependent *E. coli* inactivation in "HA and WM" solution under 0.50% Fe-TiO_2 solar photocatalytic treatment conditions were also followed and illustrated in Figure 4.117. It should be indicated that both emergence and removal mechanisms were prevailing under the specified conditions.

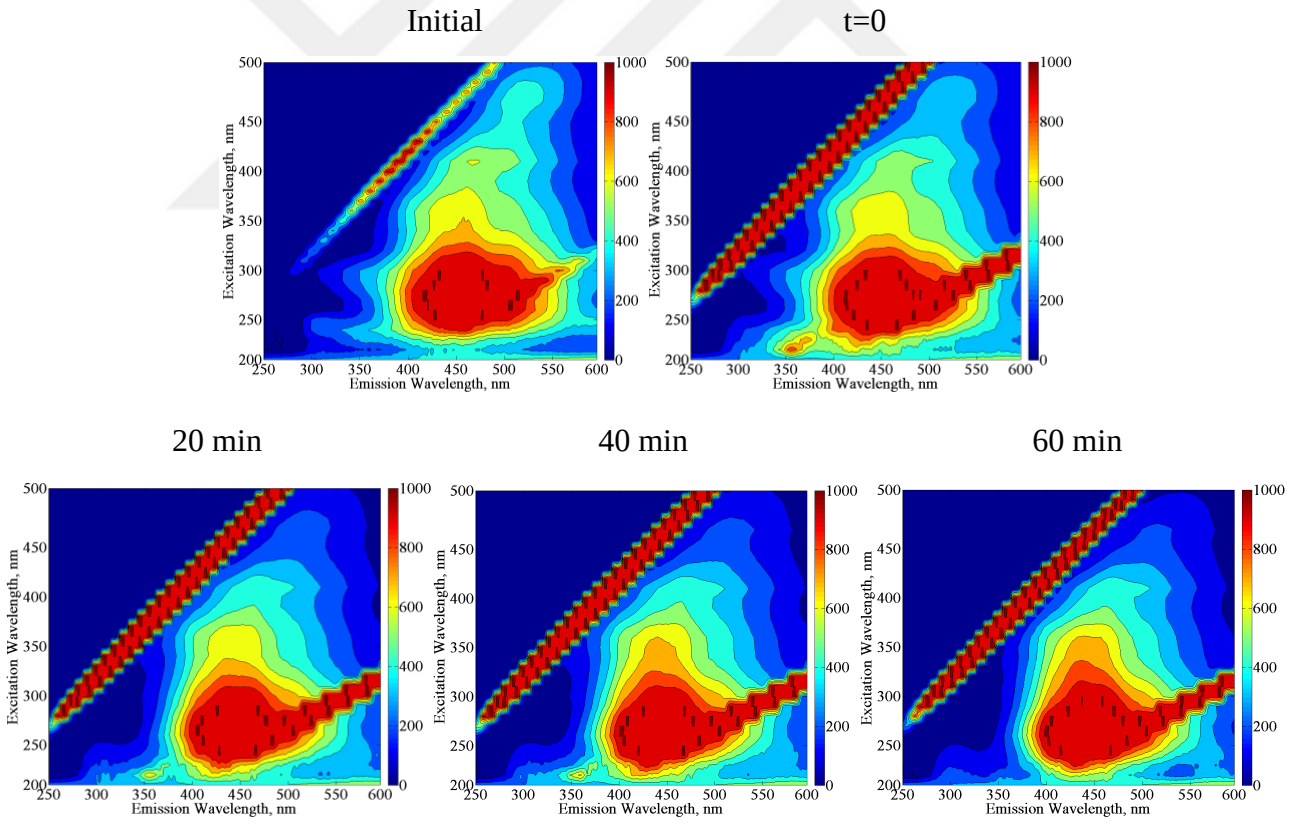

Figure 4.117. EEM fluorescence contour plots of organic matter: Irradiation time dependent *E. coli* inactivation in "HA and WM" solution upon 0.50% Fe-TiO_2 solar photocatalytic treatment.

EEM fluorescence contour plots of *E. coli* in the presence of "HA and WM" solution upon 0.50% Fe-TiO_2 solar photocatalytic treatment displayed the presence of Regions III, and V indicating that the fluorophores were mainly originated from fulvic-like and humic-like substances. Both humic-like

and fulvic-like fluorophore intensities displayed a decreasing trend throughout 60 min solar light exposure period. However, solar photocatalytic treatment conducted in "HA and WM" solution expressed more intense fluorescence than the ones attained for *E. coli* in HA solution (Figure 4.112) most probably due to retardation effect of WM components on organic matter degradation and bacteria cell destruction. Intensity differences between EEM contour plots of treatments carried out with sole HA and "HA and WM" solution could also be correlated with *E. coli* count obtained at t_{irr}=60 min (2.71E+02 CFU/mL for *E. coli* in sole HA solution and 7.74E+03 CFU/mL for *E. coli* in "HA and WM" solution) (Figure 4.97).

4.2.4.9. Mechanistic evaluation of *E. coli* inactivation upon 0.50% Fe-TiO_2 solar photocatalytic treatment in "HA and WM" solution. Upon solar irradiation, as inactivation products of 0.50% Fe-TiO_2 solar photocatalytic treatment of *E. coli* in "HA and WM" solution total K, protein, and carbohydrate contents present in initial, t=0, and t_{irr}=60 min solutions were presented in Table 4.46.

Table 4.46. Total K, protein, and carbohydrate contents of time dependent *E. coli* inactivation in "HA and WM" solution upon 0.50% Fe-TiO_2 solar photocatalytic treatment.

0.50% Fe-TiO_2 solar photocatalytic treatment	*E. coli* in "HA and WM"		
	Initial	t=0	60 min
Total K, mg/L	4.61	4.42	4.35
Protein, mg/L	6.47	4.66	10.0
Carbohydrate, mg/L	2.73	1.95	4.25

Total K content showed a decreasing trend, which could be resulting from the adsorption of released K^+ ions onto negatively charged *E. coli*, photocatalyst and/or HA surfaces. On the other hand, 4.1 % of immediate adsorptive total K removal was calculated for t=0 condition. A similar pattern was also observed upon solar photocatalytic treatment of *E. coli* in "HA and WM" solution in the presence of 0.25% Fe-TiO_2 (Table 4.37).

E. coli in the presence of "HA and WM" solution upon solar photocatalytic treatment using 0.50% Fe-TiO_2 displayed increase in both protein (6.47-10.0 mg/L) and carbohydrate content (2.37-4.25 mg/L) at the end of 60 min irradiation period due to release of cell components from damaged *E. coli* and the presence of humic matter in solution matrix. Increase in both protein and carbohydrate concentrations could be expressed with strong correlations with increased NPOC content, where R^2 values were calculated as 0.99 for both relations. On the other hand, protein contents were plotted against $FI_{sync280}$ data and a strong correlation was obtained between these parameters as R^2=0.73.

4.2.4.10. Comparative evaluation of different experimental matrixes on 0.50% Fe-TiO_2 solar photocatalytic inactivation mechanism of *E. coli.* Total K, protein, and carbohydrate concentrations and bacteria enumerations of 0.50% Fe-TiO_2 solar photocatalytic treatment of *E. coli* in different solution matrixes in comparison with initial, t=0, and t_{irr}=60 min conditions were given in Figure 4.118. Total K contents varied in between 0.54-4.61 mg/L being the lowest for initial sample of *E. coli* in HA solution and the highest for initial condition of *E. coli* in "HA and WM" solution. Total K content of WM containing reaction media displayed higher presence than IsoT and HA solutions as expected. Except *E. coli* in HA solution, other matrixes showed a decreasing trend in total K concentrations during t_{irr}=60 min. The lowest total K contents were obtained from *E. coli* in HA solution, also previous solar photolytic (Figure 4.22) and photocatalytic treatment runs (Figures 4.46, 4.70, and 4.94) displayed similar patterns. Total K contents were plotted against *E. coli* counts and except the presence of sole WM solution a strong correlation was detected as $R^2 > 0.92$.

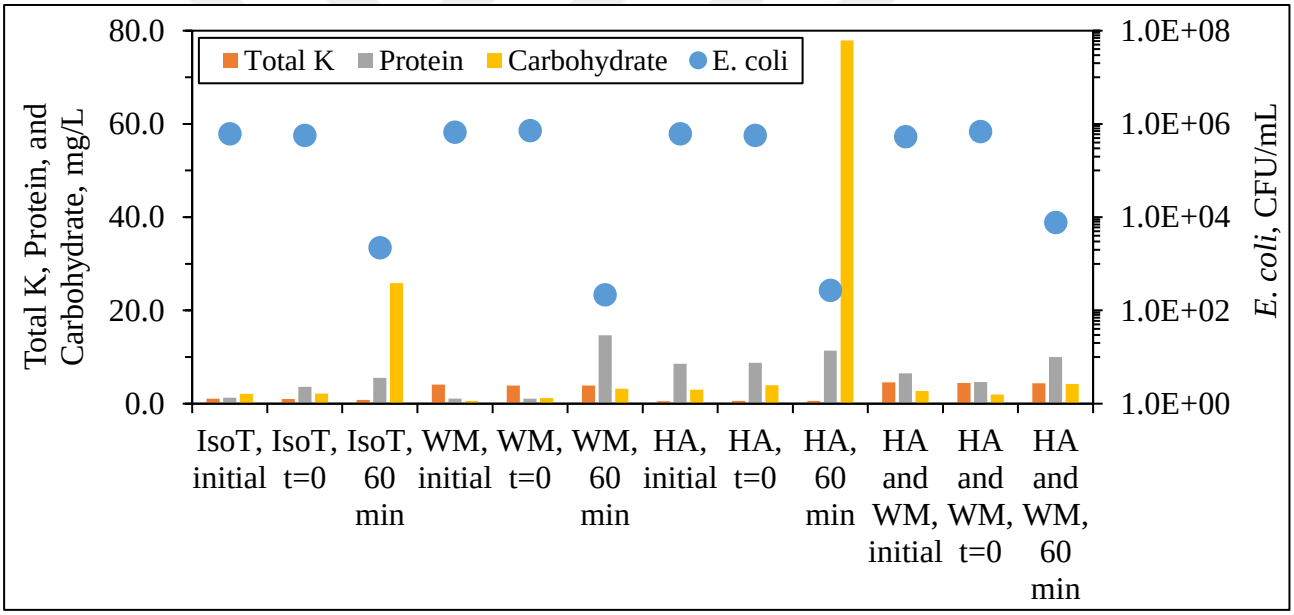

Figure 4.118. Initial, t=0, and t_{irr}=60 min total K, protein, and carbohydrate contents and bacteria enumeration results of *E. coli* inactivation upon 0.50% Fe-TiO_2 solar photocatalytic treatment in various aqueous matrixes.

Covering all conditions protein contents varied in between 1.08-14.7 mg/L being the lowest for initial sample of *E. coli* in WM solution and the highest for t_{irr}=60 min sample of the same reaction matrix. Similarly, carbohydrate concentrations varied in between 0.62-77.9 mg/L being the lowest for initial sample of *E. coli* in WM solution and the highest for t_{irr}=60 min sample of *E. coli* in HA solution. At the end of t_{irr}=60 min, all treatment sets displayed increased protein contents. In the presence of sole HA solution, initial (8.55 mg/L) and t=0 (8.75 mg/L) samples showed higher protein

concentrations than other initial and t=0 condition. Moreover, all carbohydrate concentrations at t_{irr}=60 min displayed an increasing trend with respect to their initial contents.

Released protein and carbohydrate concentrations and bacteria LRV of 0.50% Fe-TiO_2 solar photocatalytic treatment of *E. coli* in different solution matrixes were given in Figure 4.119. Released protein and carbohydrate concentrations were calculated by subtracting initial data from final contents attained upon t_{irr}=60 min. In the presence of sole WM and HA solutions, *E. coli* showed similar LRV however their released protein and carbohydrate contents were detected as significantly different from each other. The highest released protein content was obtained from WM solution (13.6 mg/L) which complied with the findings of previous solar photocatalytic treatment sets (Figures 4.47, 4.71, and 4.95). In the presence of sole HA solution, the highest carbohydrate release (74.9 mg/L) was detected which could be due to the released carbohydrate content from bacteria and present organic matrix, and also possible experimental error and/or interferences which were indicated at Section 4.2.4.7. Between *E. coli* LRV and released protein contents a strong correlation was detected as R^2=0.91 except the presence of sole HA solution matrix. Furthermore, released carbohydrate content and LRV of *E. coli* showed a strong correlation in the absence of sole WM solution as R^2=0.99.

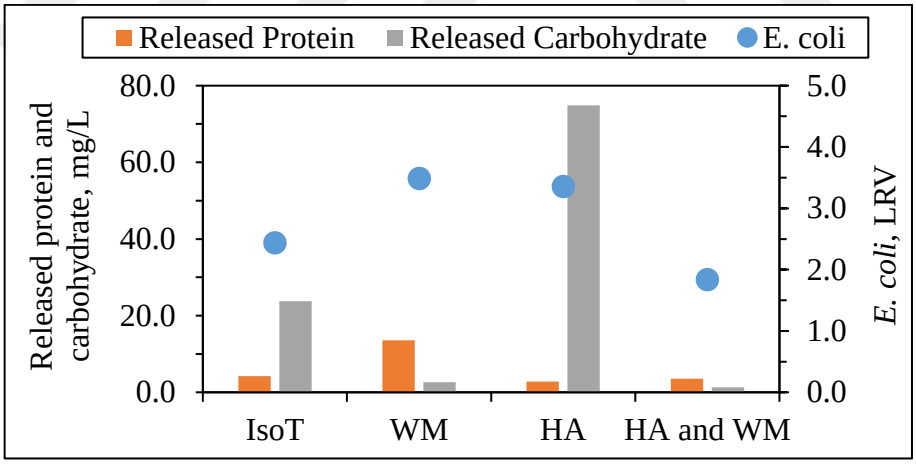

Figure 4.119. Released protein and carbohydrate contents, and bacteria LRV of *E. coli* inactivation upon 0.50% Fe-TiO_2 solar photocatalytic treatment in various aqueous matrixes.

Upon 0.50% Fe-TiO_2 solar photocatalytic treatment of *E. coli* in different solution matrixes, the attained protein and carbohydrate contents, $FI_{sync280}$, UV_{280} and NPOC data under initial, t=0, and t_{irr}=60 min conditions were given in Figure 4.120. UV_{280} values increased in HA solution containing reaction matrixes, like previous solar photolytic (Figure 4.24) and photocatalytic treatment sets (Figures 4.48, 4.72, and 4.96). The presence of HA solution caused the detection of higher protein concentrations for initial and t=0 conditions. In the presence of "HA and WM" solution, $FI_{sync280}$ data

showed a significant increase after addition of photocatalyst into the solution. Except the presence of sole HA solution, initial protein concentration and $FI_{sync280}$ displayed a strong correlation as R^2=0.94, however no correlation was detected for t=0 and t_{irr}=60 min conditions.

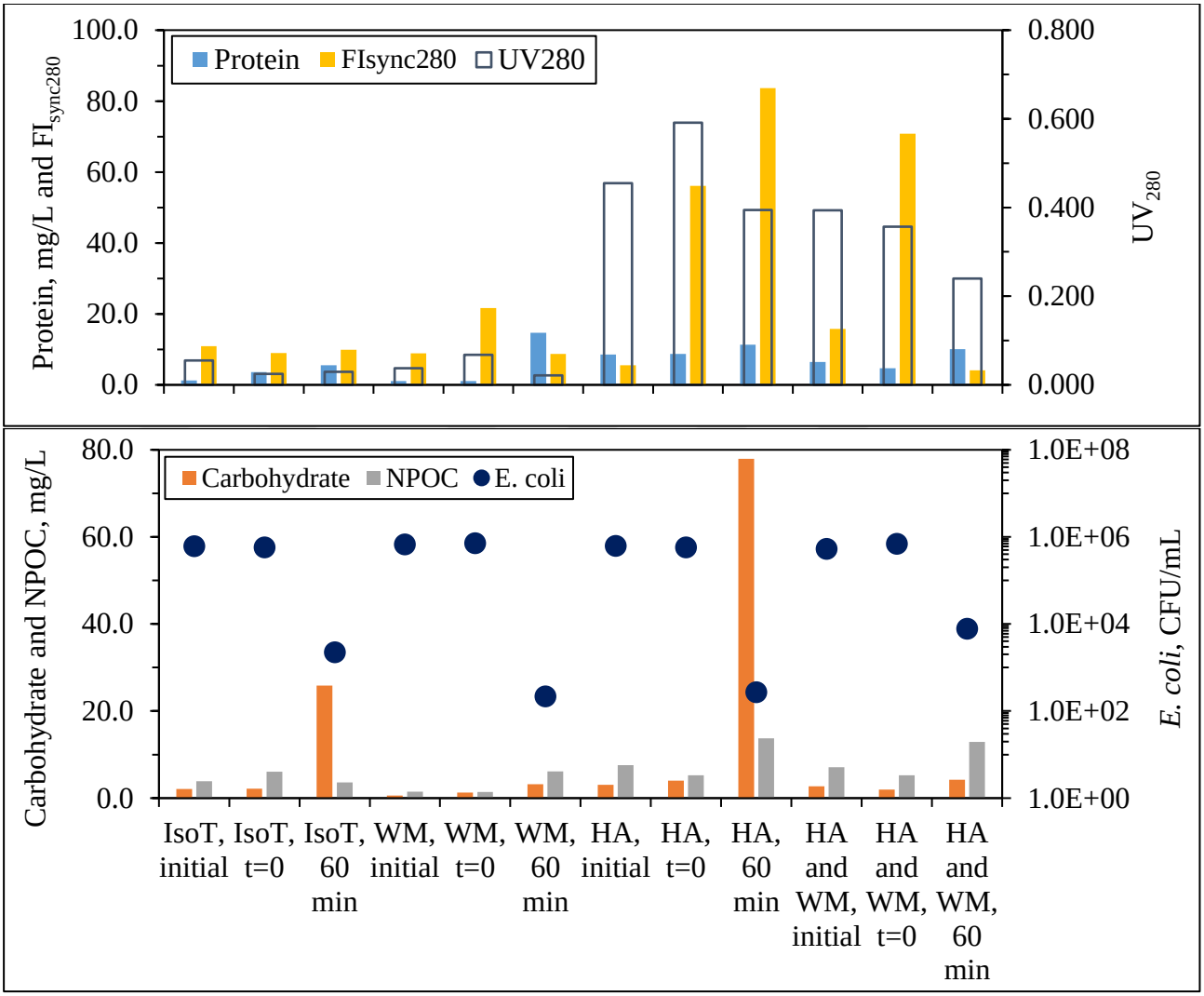

Figure 4.120. Initial, t=0, and t_{irr}=60 min protein and carbohydrate contents, $FI_{sync280}$, UV_{280}, NPOC, and bacteria enumeration results of 0.50% Fe-TiO_2 solar photocatalytic treatment of *E. coli* in various aqueous matrixes.

E. coli in IsoT solution showed a significant increase in carbohydrate content at t_{irr}=60 min due to organics released from damaged bacteria. In the presence of sole HA solution, higher NPOC contents were obtained for initial and t_{irr}=60 min samples. A strong correlation as R^2 = 0.93 was detected for initial carbohydrate and NPOC concentrations. Moreover, for t=0 condition a strong correlation was detected as R^2=0.99 in the absence of sole HA solution. Different from initial and t=0 conditions, carbohydrate and NPOC contents of t_{irr}=60 min displayed a rough correlation as R^2=0.74 in the absence of "HA and WM" solution.

4.2.5. 0.25% Fe-SynTiO$_2$ Solar Photocatalytic Inactivation of *E. coli*

4.2.5.1. 0.25% Fe-SynTiO$_2$ solar photocatalytic *E. coli* inactivation under specified reaction conditions, reductions, and kinetics. *E. coli* suspension (N_o=4.03E+05 CFU/mL) was prepared in IsoT solution and subjected to solar photocatalytic treatment using 0.25% Fe-SynTiO$_2$ as a Fe-doped photocatalyst specimen. Upon irradiation period of 30 min, *E. coli* count decreased to 2.20E+03 CFU/mL. Following further light exposure of t_{irr}=60 min, *E. coli* count decreased to 5.60E+02 CFU/mL. Under these conditions LRV was 2.86 and reduction was 99 %. Upon preparation of *E. coli* suspension (N_o=2.23E+05 CFU/mL) in WM solution, for an irradiation period of 30 min, *E. coli* count decreased to 1.18E+02 CFU/mL. Upon prolonged light exposure of t_{irr}=60 min, *E. coli* count decreased to 4.00E+01 CFU/mL revealing LRV as 3.75 and reduction as 99.9 %. *E. coli* (N_o=2.62E+05 CFU/mL) suspension was prepared in HA solution and exposed to an irradiation period of 30 min, *E. coli* count decreased to 6.71E+02 CFU/mL. Following further light exposure of t_{irr}=60 min, *E. coli* count decreased to 4.00E+01 CFU/mL revealing LRV as 3.82 and reduction as 99.9 %. *E. coli* (N_o=7.83E+05 CFU/mL) suspension was prepared in a solution composed of "HA and WM" components and was subjected to an irradiation period of 30 min in which *E. coli* count decreased to 8.51E+03 CFU/mL. Following light exposure of t_{irr}=60 min, *E. coli* count decreased to 2.49E+03 CFU/mL revealing LRV as 2.50 and reduction as 99 %. Based on these results, the effect of solution matrix could be displayed in terms of LRV of *E. coli* in an increasing order as: "HA and WM" < IsoT < WM < HA. *E. coli* inactivation profiles and first order kinetic parameters were presented in Figure 4.121 and Table 4.47.

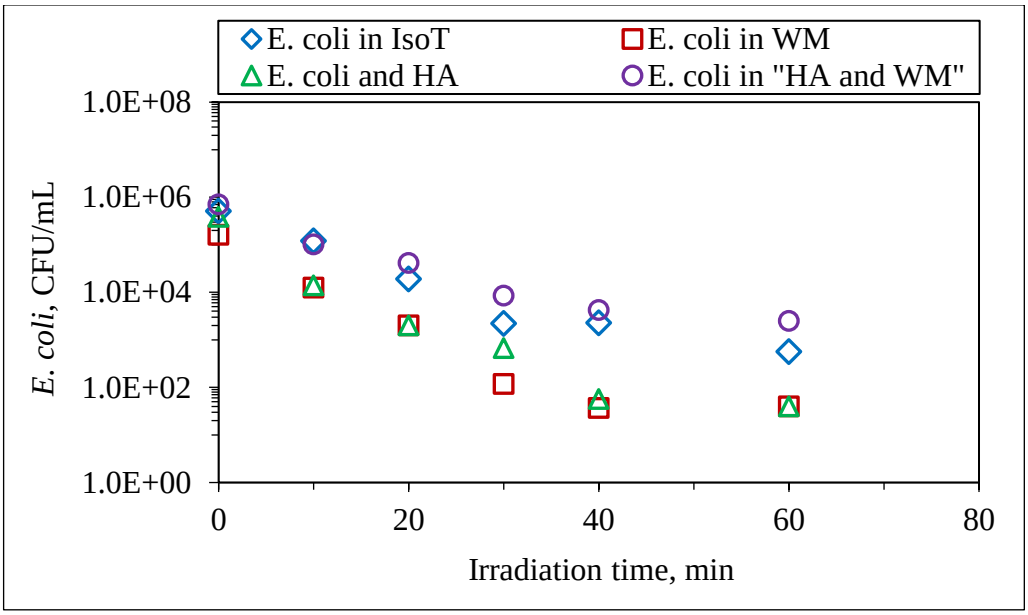

Figure 4.121. Irradiation time dependent *E. coli* inactivation upon 0.25% Fe-SynTiO$_2$ solar photocatalytic treatment in various solution matrixes.

0.25% Fe-SynTiO$_2$ solar photocatalytic treatment of *E. coli* in the presence of HA solution resulted in a rather fast removal with k=0.152 min^{-1} and half-life as 4.56 min. In the presence of "HA and WM" solution, a reaction rate constant of k=0.0943 min^{-1} and half-life as 7.35 min were attained. The effect of reaction media on bacteria inactivation could also be expressed in terms of inactivation reaction rate constant (k, min^{-1}) in a decreasing order as; HA > WM > IsoT > "HA and WM". Irrespective of the minor differences in initial bacteria counts, inactivation rates (CFU/mL min) followed as; 7.38E+04 > 4.67E+04 > 3.98E+04 > 3.26E+04 for "HA and WM", IsoT, HA and WM solutions, respectively.

Table 4.47. 0.25% Fe-SynTiO$_2$ solar photocatalytic treatment of *E. coli*: Inactivation parameters.

Matrix	First order kinetic model			LRV	Removal, %
	k, min^{-1}	$t_{1/2}$, min	R, CFU/mL min		
E. coli in IsoT	0.116	5.97	4.67E+04	2.86	99.7
E. coli in WM	0.146	4.75	3.26E+04	3.75	99.9
E. coli and HA	0.152	4.56	3.98E+04	3.82	99.9
E. coli in "HA and WM"	0.0943	7.35	7.38E+04	2.50	99.7

E. coli in IsoT solution upon solar photocatalytic treatment with 0.25% Fe-SynTiO$_2$ experiment showed lower bacteria reduction than WM and HA media, as 99.7 %. The reason could be attributed the use of IsoT solution providing higher resistance to bacteria against solar photocatalytic process due to optimal osmotic pressure. However, obtained *E. coli* LRV as 2.86 was lower than LRV of 0.25% Fe-TiO$_2$ (4.28) (Table 4.29) could be indicating no relevance between same doping concentration among bare TiO$_2$ species as TiO$_2$ and SynTiO$_2$. Moreover, detected reaction rate constant as 0.116 was lower than N-doped, Se-doped, and Se-N co-doped TiO$_2$ results presented by Birben and colleagues (Birben et al., 2017a).

0.25% Fe-SynTiO$_2$ solar photocatalytic treatment of *E. coli* in WM solution showed higher bacteria reduction than IsoT, as 99.9 %. Common anions and cations present in the solution could cause production of extra ROSs and enhanced bacteria inactivation rate.

In the presence of HA solution, 0.25% Fe-SynTiO$_2$ solar photocatalytic treatment of *E. coli* displayed the highest *E. coli* LRV among other experiment media, as 3.82. Due to this high LRV it could be suggested that 0.25% Fe-SynTiO$_2$ has selectivity against bacteria rather than organic matrix. Moreover, Birben and colleagues, which they work with other doped TiO$_2$ species on the degradation of HA and reduction of *E. coli*, achieved higher reaction rate with N-doped and lower reaction rates with Se-doped and Se-N co-doped TiO$_2$ photocatalyst specimens than 0.25% Fe-SynTiO$_2$ (Birben et al., 2017a).

0.25% Fe-SynTiO$_2$ solar photocatalytic treatment of *E. coli* in "HA and WM" solution displayed the lowest bacteria LRV, as 2.50. It could be owing to two different effects of solution matrix as inhibition on the photocatalytic removal process of bacteria and providing resistance to bacteria by playing a role as a nutrient source.

4.2.5.2. Organic matter formation and removal upon 0.25% Fe-SynTiO$_2$ solar photocatalytic treatment of *E. coli* in IsoT solution. UV-vis absorption and synchronous scan fluorescence spectra of organic matter in solution were presented in Figures 4.122 and 4.123. Irradiation time dependent absorbance changes were significantly similar to each other in UV wavelength range of λ=200-290 nm excluding the presence of aromatic domains and color forming moieties that should be measured in longer wavelengths. UV spectral features expressed similarities to the ones attained upon solar photolytic (Figure 4.2) and photocatalytic treatments (Figures 4.26, 4.50, 4.74 and 4.98).

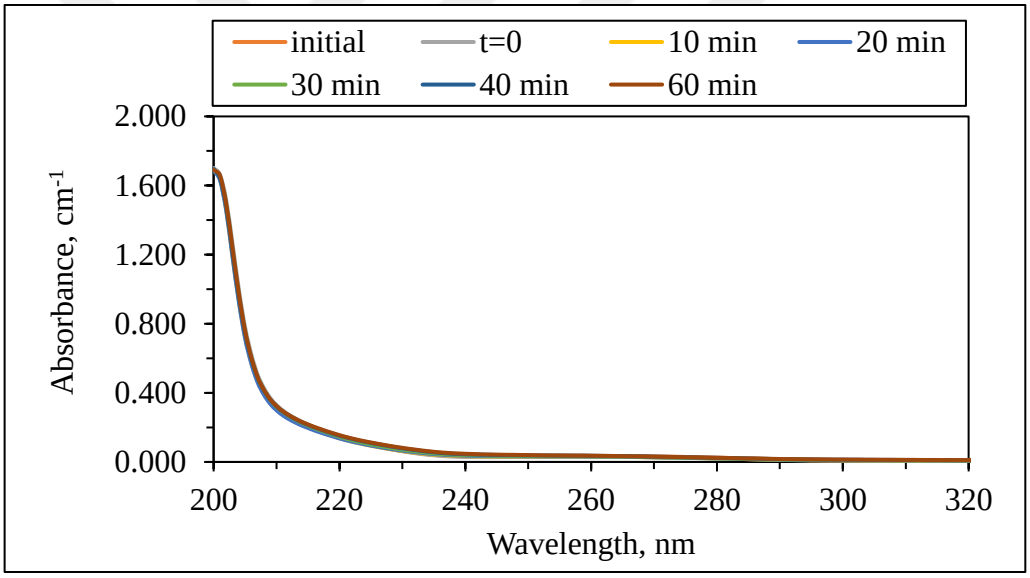

Figure 4.122. UV-vis absorption spectra of organic matter: Irradiation time dependent *E. coli* inactivation in IsoT solution upon 0.25% Fe-SynTiO$_2$ solar photocatalytic treatment.

Synchronous scan fluorescence spectra of the emerged organic matter displayed an intense peak at λ_{emis}=280 nm for all irradiation periods and also a minor peak was detected at λ_{emis}=440 nm of t_{irr}=10 min datum representing the presence of aromatic hydrocarbons originating from released organic content from bacteria (Dujmov and Sučević, 1990) (Figure 4.123). Furthermore, the presence of fluorophoric groups expressing very minor intensities as FI_{sync} < 5.5 could also be encountered at λ_{emis} > 300 nm. Similar low peaks around FI_{sync}=2-10 were also detected from solar photolytic (Figure 4.3) and 0.50% Fe-TiO$_2$ solar photocatalytic treatment (Figure 4.99) of *E. coli* in IsoT solution conditions. An irradiation time dependent decreasing order in $FI_{sync280}$ data was observed. On the

other hand, despite quite low presence of $FI_{sync470}$ varied between 0.499-2.72, in the presence of bacteria dominant $FI_{sync280}$ displayed changes in the range of 12.9-25.8.

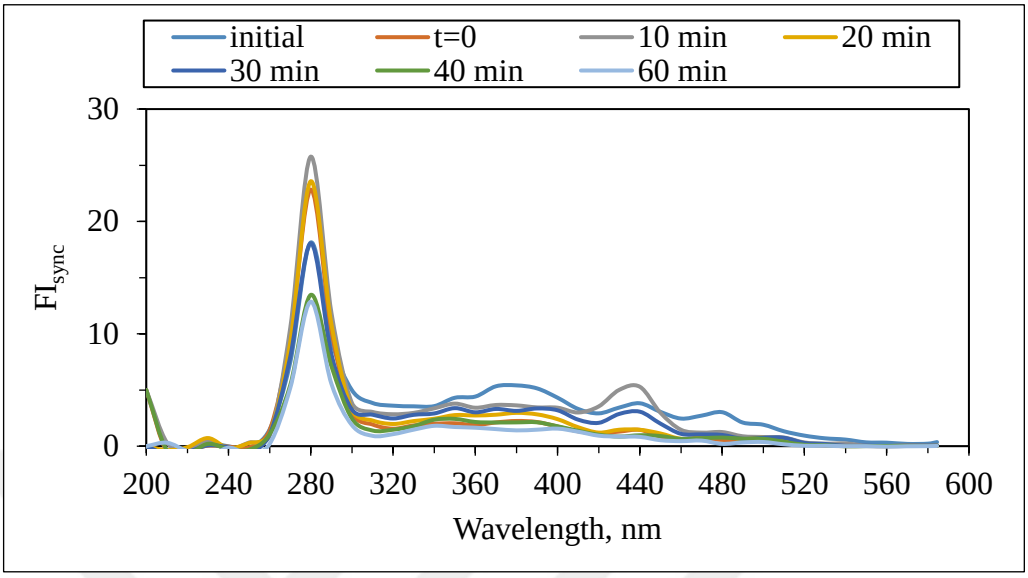

Figure 4.123. Synchronous scan fluorescence spectra of organic matter: Irradiation time dependent *E. coli* inactivation in IsoT solution upon 0.25% Fe-SynTiO$_2$ solar photocatalytic treatment.

NPOC contents slightly increased between initial (3.82 mg/L) and t=0 min (4.16 mg/L) and besides slight decrease at t_{irr}=10 min (4.09 mg/L), followed by an increasing trend until t_{irr}=40 min (5.65 mg/L) due to the release of organics from damaged and destructed *E. coli* cells, then displayed a sharp decrease at t_{irr}=60 min (4.25 mg/L) (Figure 4.124).

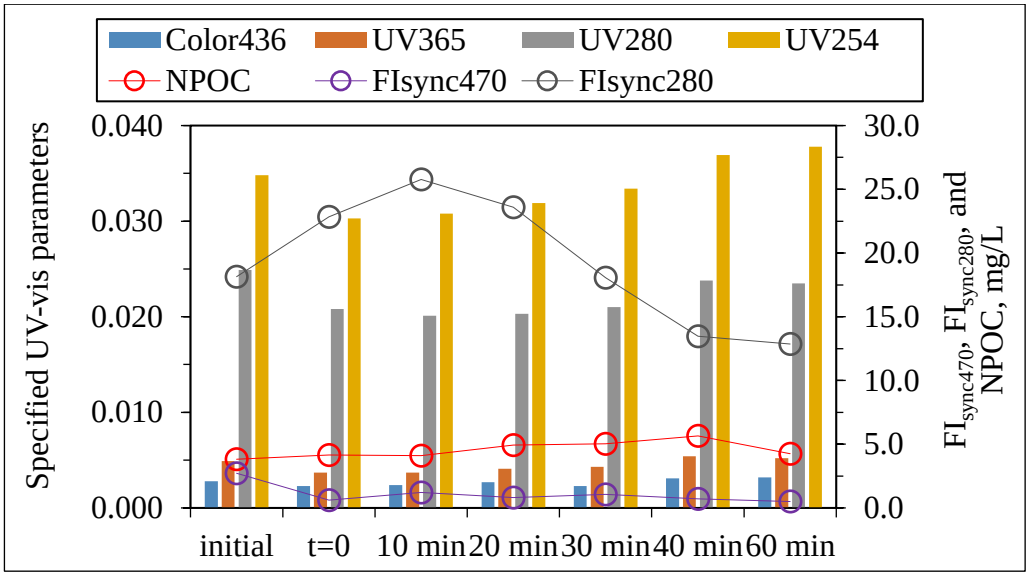

Figure 4.124. Specified UV-vis and fluroscence parameters of organic matter: Irradiation time dependent *E. coli* inactivation in IsoT solution upon 0.25% Fe-SynTiO$_2$ solar photocatalytic treatment.

All UV-vis parameters displayed quite low presence (Figure 4.124). The highest UV_{254} was attained upon t_{irr}=60 min (0.0378) as could also be considered as similar to t_{irr}=40 min (0.0369) although variations were insignificant. UV_{280} displayed almost insignificant changes varied in between 0.0201-0.0249. Due to non-existence and subsequent degradation of color forming moieties of the released organic matrix upon irradiation and the usage of IsoT solution, $Color_{436}$ and UV_{365} expressed minor presence similar to previous solar photolytic (Figure 4.4) and photocatalytic treatment sets (Figures 4.28, 4.52, 4.76, and 4.100). The role of both Fe doping of TiO_2 and 0.25% Fe doping on different TiO_2 specimens as TiO_2 and $SynTiO_2$ could not be visualized under the specified experimental conditions.

Based on NPOC contents expressing variations in the range of 3.82-5.65 mg/L, $SCoA_{436}$, $SUVA_{365}$, $SUVA_{280}$, $SUVA_{254}$, $SFI_{sync470}$, and $SFI_{sync280}$ parameters were calculated and presented in Figure 4.125. As the most significant parameter, $SUVA_{254}$ displayed changes in the range of 0.653-0.911 L/m mg during 0.25% Fe-$SynTiO_2$ solar photocatalytic treatment expressing differences in both UV_{254} and NPOC removals. The highest $SUVA_{254}$ was calculated for initial (0.911 L/m mg) condition as could also be considered as similar to t_{irr}=60 min (0.889 L/m mg). Moreover, $SUVA_{280}$ displayed noticeable presence varied in between 0.412-0.652 L/m mg being the highest for initial and the lowest for irradiation period of 20 min conditions. Although $SCoA_{436}$ and $SUVA_{365}$ were also presented, respective specified parameters were very low in comparison to total NPOC contents of the organic matter present in solution.

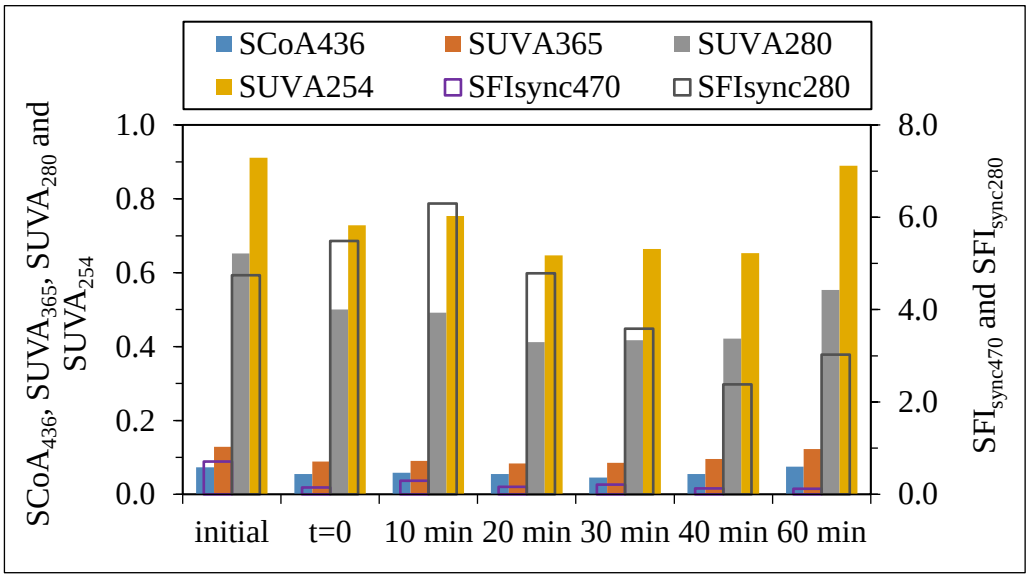

Figure 4.125. Specific UV-vis and fluroscence parameters of organic matter: Irradiation time dependent *E. coli* inactivation in IsoT solution upon 0.25% Fe-$SynTiO_2$ solar photocatalytic treatment.

Furthermore, $SFI_{sync470}$ displayed very low chances in between 0.117-0.712 expressing insignificant contribution of fluorophores detected at λ_{emis}=470 nm. However, $SFI_{sync280}$ expressed considerable variations in the range of 2.38-6.30. In the absence of HA as a solution matrix component, the predominant fluorophoric group was accepted as $SFI_{sync280}$.

For simplicity purposes, based on the irradiation time dependent variations in UV-vis and fluorescence spectroscopic properties along with NPOC data, characteristic properties of organic matter under initial condition, upon introduction of 0.25% Fe-SynTiO_2 (t=0) and at the end of solar photocatalytic for irradiation period of 60 min were presented in Table 4.48.

Table 4.48. Characteristic properties of organic matter present in 0.25% Fe-SynTiO_2 solar photolytic treatment of *E. coli* in IsoT solution.

Irradiation time, min	UV-vis Spectroscopic Parameters, cm^{-1}				NPOC, mg/L	$SUVA_{254}$, L/m mg	$FI_{sync280}$	$SFI_{sync280}$	FI
	$Color_{436}$	UV_{365}	UV_{280}	UV_{254}					
Initial	0.0028	0.0049	0.0249	0.0348	3.82	0.911	18.1	4.75	1.33
t=0	0.0023	0.0037	0.0208	0.0303	4.16	0.728	22.8	5.49	1.65
60 min	0.0032	0.0052	0.0235	0.0378	4.25	0.117	12.9	3.03	1.77

There was no significant difference detected between the initial, t=0 and t_{irr}=60 min UV-vis spectroscopic parameter results of 0.25% Fe-SynTiO_2 solar photocatalytic treatment of *E. coli* in IsoT solution. Upon irradiation period of 60 min at which 2.86 log reduction of *E. coli* in IsoT solution was attained (Table 4.47), released organic matter expressed the following specified UV-vis parameters (cm^{-1}); $Color_{436}$: 0.0032, UV_{365}: 0.0052, UV_{280}: 0.0235, UV_{254}: 0.0378, and NPOC as 4.25 mg/L. $SUVA_{254}$ value at t_{irr}=60 min was calculated as 0.117 L/m mg, which could be considered as insignificant, represents that the remaining organic matter could be having hydrophilic and aliphatic character (Edzwald et al., 1985).

Due to degradation of protein content, $FI_{sync280}$ displayed a decrease at the end of t_{irr}=60 min. Moreover, $SFI_{sync280}$ expressed a decrease at t_{irr}=60 min (4.75 for initial; 3.03 for t_{irr}=60 min) in accordance with the increased NPOC. Furthermore, $FI_{sync470}$ of initial, t=0, and t_{irr}=60 min conditions were detected as 2.72, 0.623, and 0.499, respectively. According to $FI_{sync470}$ and NPOC, calculated $SFI_{sync470}$ of initial, t=0, and t_{irr}=60 min samples, as 0.712, 0.150, and 0.117, respectively, were almost insignificant. FI at t_{irr}=60 min was calculated as 1.77 which was between indication value of organic matter, originating from humic matter or microbial content (Sen-Kavurmaci and Bekbolet, 2014). Calculated FI could mostly be related to microbially derived organic matter. Similar finding was also reported by Birben and colleagues for N-doped TiO_2 (Birben et al., 2017a).

EEM fluorescence contour plots of organic matter emerged and removed during irradiation time dependent *E. coli* inactivation in IsoT solution during 0.25% Fe-SynTiO$_2$ solar photocatalytic treatment were displayed in Figure 4.126.

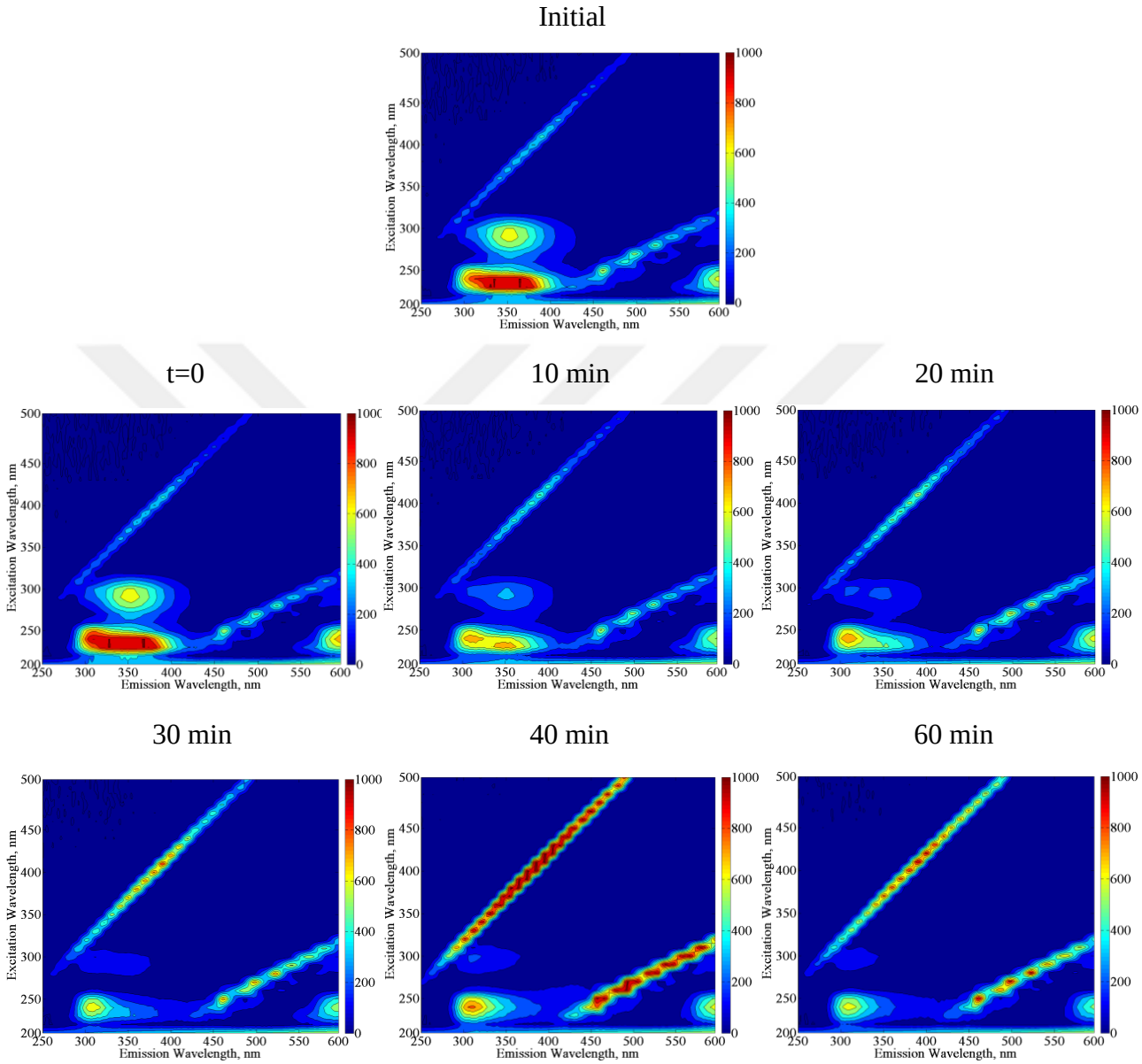

Figure 4.126. EEM fluorescence contour plots of organic matter: Irradiation time dependent *E. coli* inactivation in IsoT solution upon 0.25% Fe-SynTiO$_2$ solar photocatalytic treatment.

EEM fluorescence contour plots displayed the presence of Regions I, II and IV expressing that the fluorophores were mainly originated from microbial by-products and proteins under all irradiation conditions. Following further irradiation periods released microbial by-products and proteins from *E. coli* cells showed a decreasing trend in accordance with the solar photocatalytic degradation of organic matter and reduction of *E. coli*. Moreover, it could be indicated that due to lower bacteria reduction of 0.25% Fe-SynTiO$_2$ than SynTiO$_2$ (*E. coli* LRV as 2.86 for 0.25% Fe-SynTiO$_2$; *E. coli*

LRV as 5.64 for $SynTiO_2$) (Tables 4.20 and 4.47), EEM contour plots of 0.25% Fe-$SynTiO_2$ have more intense results than $SynTiO_2$ solar photocatalytic treatment (Figure 4.54).

4.2.5.3. Mechanistic evaluation of *E. coli* inactivation upon 0.25% Fe-$SynTiO_2$ solar photocatalytic treatment in IsoT solution. As bacteria inactivation products of 0.25% Fe-$SynTiO_2$ solar photocatalytic treatment of *E. coli* in IsoT solution, total K, protein, and carbohydrate contents present in initial, t=0, and t_{irr}=60 min solutions were presented in Table 4.49.

Table 4.49. Total K, protein, and carbohydrate contents of time dependent *E. coli* inactivation in IsoT solution upon 0.25% Fe-$SynTiO_2$ solar photocatalytic treatment.

0.25% Fe-$SynTiO_2$ solar photocatalytic treatment	*E. coli* in IsoT solution		
	Initial	t=0	60 min
Total K, mg/L	1.94	0.85	1.05
Protein, mg/L	3.83	4.33	4.94
Carbohydrate, mg/L	1.52	1.27	78.0

Total K content showed an immediate adsorptive removal as 56.2 % at t=0, and slightly increased at t_{irr}=60 min due to K^+ ion release from *E. coli* cells having damaged cell walls. Similar high immediate adsorptive removal of total K was also detected from TiO_2 solar photocatalytic treatment carried out with IsoT solution (48.0 %) (Section 4.2.1.3).

E. coli in IsoT solution upon 0.25% Fe-$SynTiO_2$ solar photocatalytic treatment displayed increase in both protein and carbohydrate content at the end of 60 min treatment period. No correlation was detected between protein concentrations and $FI_{sync280}$ results however a strong correlation was obtained from protein and NPOC contents as R^2=0.82. Carbohydrate content significantly increased at t_{irr}=60 min (78.0 mg/L) and similar finding was also detected from $SynTiO_2$ solar photocatalytic treatment of *E. coli* in IsoT solution (45.0 mg/L) (Table 4.22). The usage of H_2SO_4 at the carbohydrate concentration determination process, which could cause the formation of degradation products absorbing light in the same spectral band with carbohydrates, and the presence of glycoproteins and Fe^{3+} could be the cause of unexpected high carbohydrate results (Dawson and Liebezeit, 1981; Martens and Frankenburger, 1990; Josefsson et al. 1972; Rao and Pattabiraman, 1989). However, for both t=0 and irradiation period of 60 min conditions of *E. coli* in IsoT solution upon solar photocatalytic treatment in the presence of 0.25% Fe-$SynTiO_2$ Fe^{3+} release was detected as BDL. On the other hand, carbohydrate and NPOC concentrations displayed a strong correlation as R^2=1.00.

4.2.5.4. Organic matter formation and removal upon 0.25% Fe-SynTiO$_2$ solar photocatalytic treatment of *E. coli* in WM solution. UV-vis absorption and synchronous scan fluorescence spectra of organic matter in WM solution were presented in Figures 4.127 and 4.128. Irradiation time dependent absorbance changes were significantly similar to each other in UV wavelength range of λ=200-280 nm in the absence of aromatic domains and color forming moieties (Color$_{436}$, UV$_{365}$, and UV$_{280}$) that should be measured in longer wavelengths. A slightly increasing trend in between λ=240 nm and 280 nm could be visualized under all irradiation period conditions, which could be due to released organic aromatic content from lysed *E. coli* cells and EPS surrounding cell wall (Birben et al., 2021a). Similar absorption pattern was also detected from previous solar photolytic (Figure 4.7) and photocatalytic treatments carried out in the presence of WM solution (Figures 4.31, 4.55, 4.79, and 4.103).

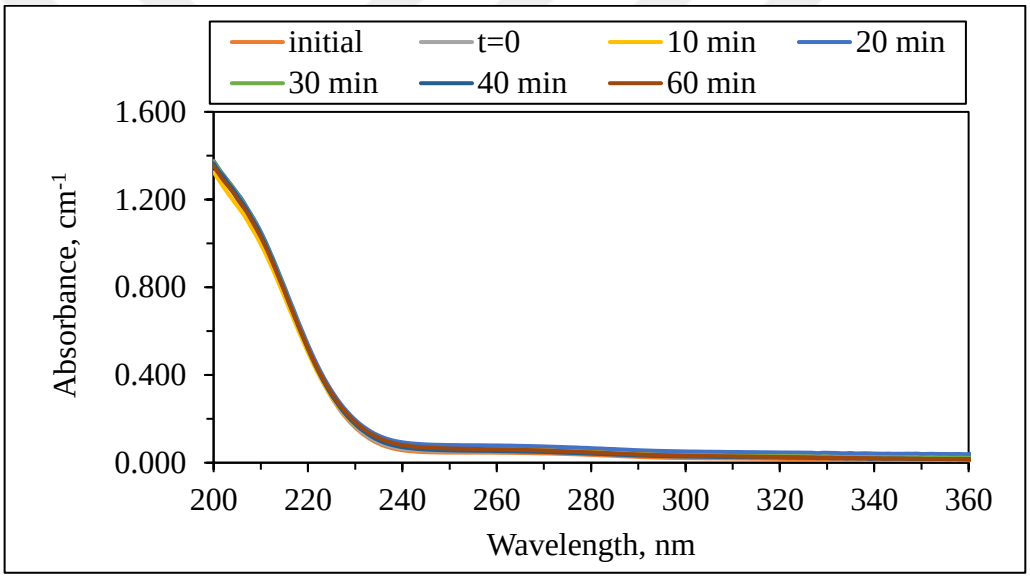

Figure 4.127. UV-vis absorption spectra of organic matter: Irradiation time dependent *E. coli* inactivation in WM solution upon 0.25% Fe-SynTiO$_2$ solar photocatalytic treatment.

Synchronous scan fluorescence spectra of the emerged organic matter displayed minor peaks at λ_{emis}=280 nm as FI$_{sync}$ in the range of 14.6-23.5. However, initial, t=0, t_{irr}=10 min and 30 min samples displayed intense peaks at λ_{emis}=420 nm. The highest FI$_{sync}$ as 213 was detected from t_{irr}=10 min at λ_{emis}=420 nm, representing the presence of aromatic hydrocarbons (Dujmov and Sučević, 1990), could be attributed to carbohydrate release from bacteria. Intense peaks at λ_{emis}=420 nm were also attained in previous solar photolytic (Figure 4.8), SynTiO$_2$ (Figure 4.56) and 0.50% Fe-TiO$_2$ (Figure 4.104) photocatalytic treatment sets carried out in WM solution however the highest FI$_{sync}$ (213) was detected upon 0.25% Fe-SynTiO$_2$ solar photocatalytic treatment of *E. coli* in WM solution. On the

other hand, $FI_{sync470}$ displayed minor presence in the range of 1.19-4.56 however predominant $FI_{sync280}$ expressed changes in between 14.6-23.5.

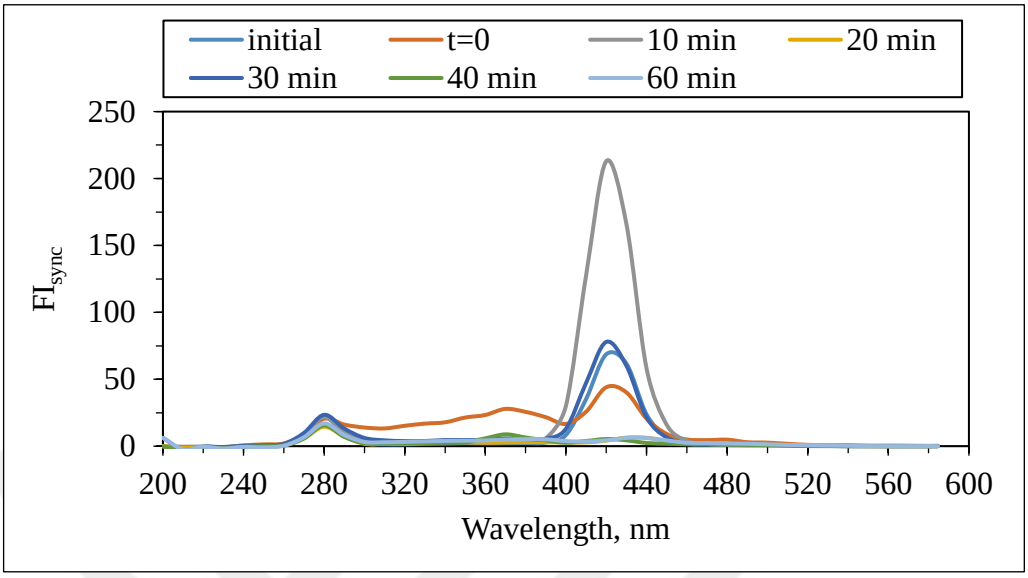

Figure 4.128. Synchronous scan fluorescence spectra of organic matter: Irradiation time dependent *E. coli* inactivation in WM solution upon 0.25% Fe-SynTiO$_2$ solar photocatalytic treatment.

All UV-vis parameters displayed very low presence however as the most significant parameter, UV_{254} expressed variations in between 0.0459-0.0798 (Figure 4.129). UV_{280}, as the second evident UV-vis parameter, displayed changed in the range of 0.0357-0.0665. The highest UV_{254} and UV_{280} values were recorded upon t_{irr}=20 min condition.

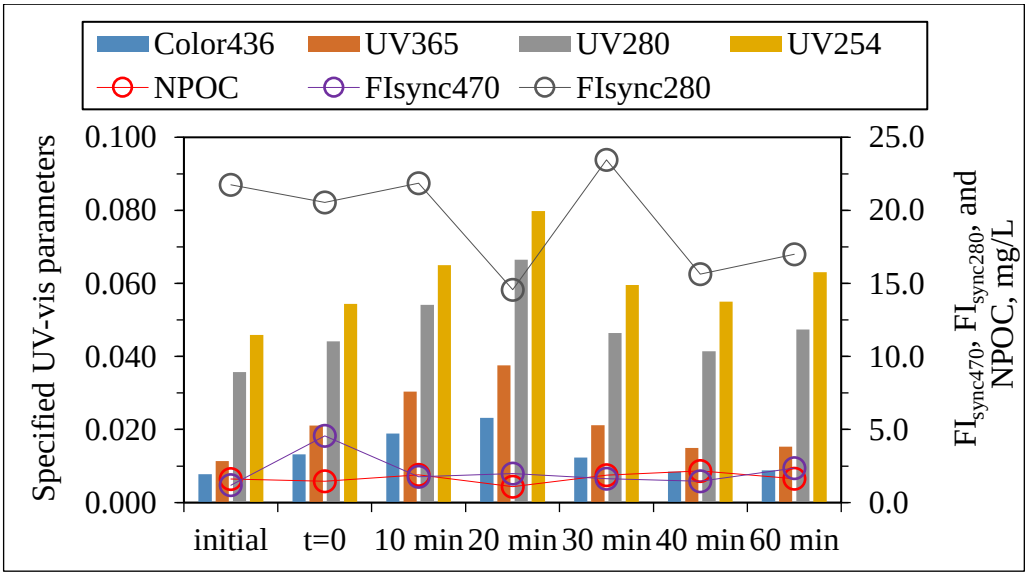

Figure 4.129. Specified UV-vis and fluroscence parameters of organic matter: Irradiation time dependent *E. coli* inactivation in WM solution upon 0.25% Fe-SynTiO$_2$ solar photocatalytic treatment.

Furthermore, due to absence and subsequent degradation of color forming moieties of the released extracellular/intracellular organic matrix upon irradiation and the usage of WM solution, $Color_{436}$ and UV_{365} expressed quite low presence similar to previous sets of *E. coli* inactivation in WM solution upon solar photolytic (Figure 4.9) and photocatalytic treatments (Figures 4.33, 4.57, 4.81, and 4.105).

From a general perspective, NPOC expressed changes in the range of 1.09-2.17 mg/L (Figure 4.129). NPOC content displayed a minor decrease between initial (1.62 mg/L) and t=0 (1.47 mg/L) conditions, followed by an increase at t_{irr}=10 min (1.89 mg/L) and decreased at t_{irr}=20 min (1.09 mg/L). an increasing trend was visualized up to following further irradiation period of 40 min (2.17 mg/L) and NPOC displayed a decrease at t_{irr}=60 min (1.64 mg/L). The role of 0.25% Fe doping on different TiO_2 specimens as TiO_2 and $SynTiO_2$ could not be visualized under the specified experimental conditions.

Based on NPOC contents, $SCoA_{436}$, $SUVA_{365}$, $SUVA_{280}$, $SUVA_{254}$, $SFI_{sync470}$, and $SFI_{sync280}$ were calculated and presented in Figure 4.130. $SUVA_{254}$ displayed variations in the range of 2.54-7.32 L/m mg during 0.25% Fe-$SynTiO_2$ solar photocatalytic treatment indicating differences in both UV_{254} and NPOC removals. On the other hand, besides quite low $SFI_{sync470}$ displaying changes in between 0.601-6.05, $SFI_{sync280}$ expressed variations in the range of 6.41-27.2. The main fluorophoric group was recognized as $SFI_{sync280}$ in the absence of HA solution as reaction medium.

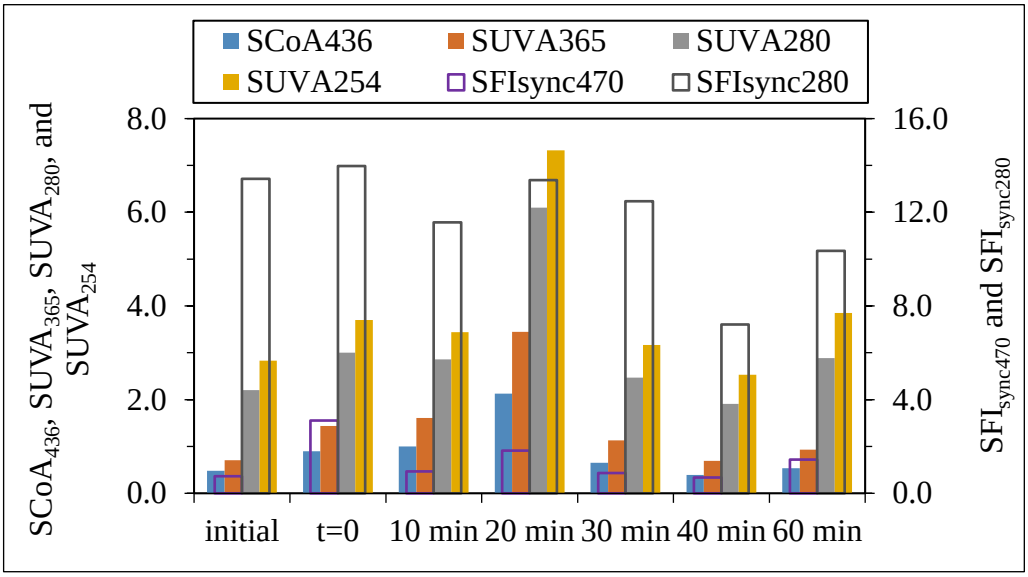

Figure 4.130. Specific UV-vis and fluroscence parameters of organic matter: Irradiation time dependent *E. coli* inactivation in WM solution upon 0.25% Fe-$SynTiO_2$ solar photocatalytic treatment.

Characteristic properties of organic matter under initial condition, upon introduction of 0.25% Fe-SynTiO$_2$ as photocatalyst specimen (t=0), and at the end of the 0.25% Fe-SynTiO$_2$ solar photocatalytic inactivation of *E. coli* in WM solution for irradiation period of 60 min were presented in Table 4.50.

Table 4.50. Characteristic properties of organic matter present in 0.25% Fe-SynTiO$_2$ solar photolytic treatment of *E. coli* in WM solution.

Irradiation time, min	UV-vis Spectroscopic Parameters, cm^{-1}				NPOC, mg/L	SUVA$_{254}$, L/m mg	FI$_{sync280}$	SFI$_{sync280}$	FI
	Color$_{436}$	UV$_{365}$	UV$_{280}$	UV$_{254}$					
Initial	0.0078	0.0114	0.0357	0.0459	1.62	2.83	21.8	13.4	1.39
t=0	0.0132	0.0211	0.0441	0.0544	1.47	3.70	20.5	14.0	1.30
60 min	0.0088	0.0153	0.0474	0.0631	1.64	3.85	17.0	10.4	1.49

Upon irradiation period of 60 min 0.25% Fe-SynTiO$_2$ solar photocatalytic treatment at which 3.75 log reduction of *E. coli* in WM solution was attained (Table 4.47), released organic matter expressed the following UV-vis parameters (cm^{-1}); Color$_{436}$: 0.0088, UV$_{365}$: 0.0153, UV$_{280}$: 0.0474, UV$_{254}$: 0.0631, and NPOC as 1.64 mg/L.

After irradiation period of 60 min, SUVA$_{254}$ was calculated as 3.85 L/m mg. Edzwald and colleagues reported that, SUVA$_{254}$ < 3 indicates the presence of hydrophilic and aliphatic content and SUVA$_{254}$ > 4 reveals hydrophobic and aromatic substances (Edzwald et al., 1985). It could be indicated that calculated SUVA$_{254}$ as 3.85 L/m mg would be denoted the higher presence of hydrophobic and aromatic groups in the solution.

FI$_{sync280}$ showed a decrease at t_{irr}=60 min due to degradation of released protein content from damaged bacteria. SFI$_{sync280}$ displayed a decrease at t_{irr}=60 min according to increased NPOC. On the other hand, in the absence of humic matter as a component of reaction solution quite low FI$_{sync470}$ were detected as 1.19, 4.56, and 2.37 for initial, t=0, and t_{irr}=60 min conditions, respectively. Based on FI$_{sync470}$ and NPOC data, SFI$_{sync470}$ of initial, t=0, and t_{irr}=60 min samples were calculated as 0.733, 3.12, and 1.44, respectively.

After irradiation period of 60 min, FI was calculated as 1.49, which was in between the region indicating the presence of humic fluorophores and microbially derived fluorophores (Sen-Kavurmaci and Bekbolet, 2014). The reason of closeness the FI value to the fluorophores originating humic matter could be attributed to degradation of released organic content from damaged *E. coli* cells.

EEM fluorescence contour plots of organic matter emerged and removed during irradiation time dependent *E. coli* inactivation in WM solution during 0.25% Fe-SynTiO$_2$ solar photocatalytic treatment were displayed in Figure 4.131.

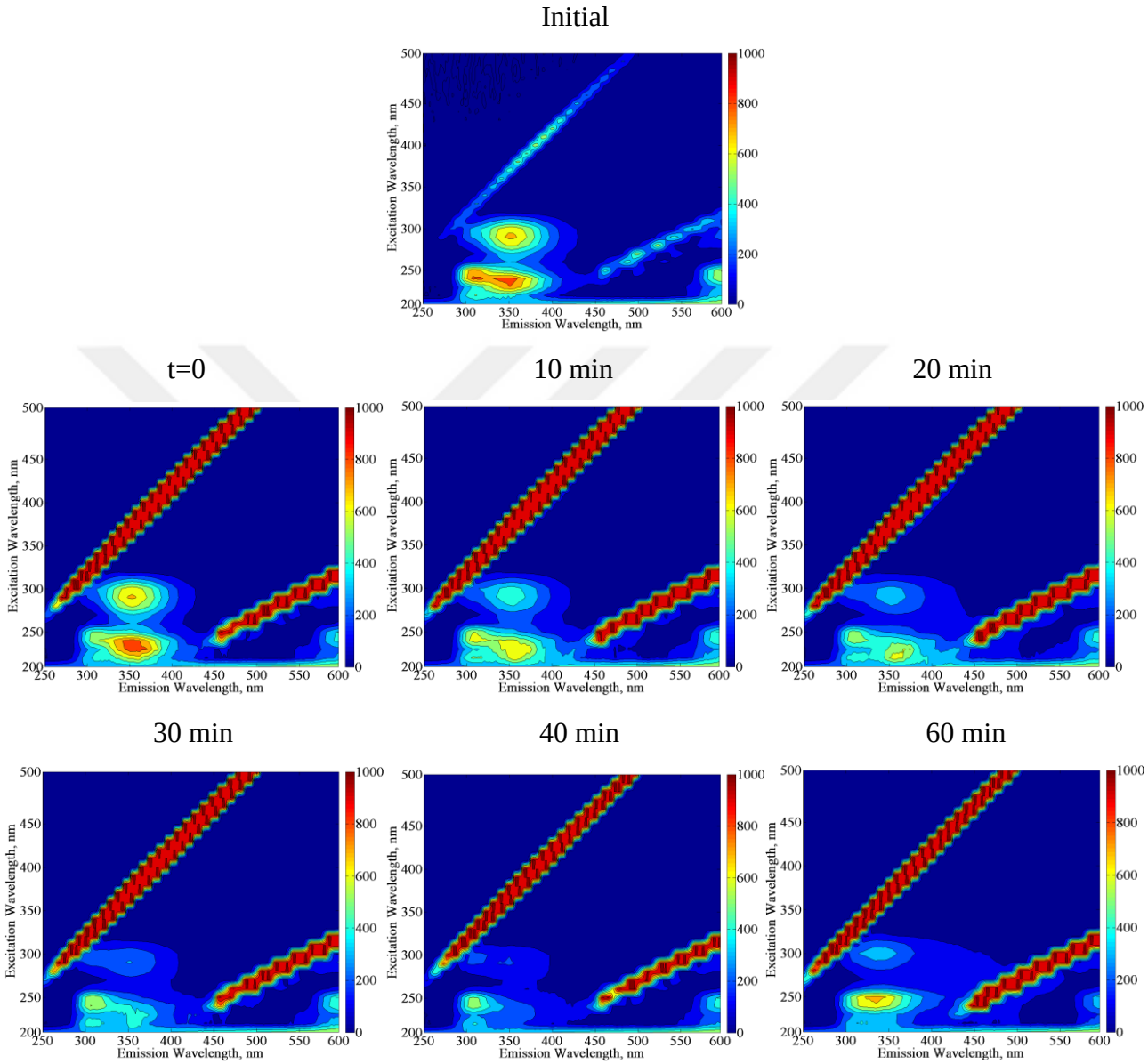

Figure 4.131. EEM fluorescence contour plots of organic matter: Irradiation time dependent *E. coli* inactivation in WM solution upon 0.25% Fe-SynTiO$_2$ solar photocatalytic treatment.

EEM fluorescence contour plots displayed the presence of Regions I, II and IV expressing that the fluorophores were mainly originated from microbial by-products and proteins under all irradiation conditions. Following further irradiation times released microbial by-products and proteins from *E. coli* cells showed a decreasing trend however at t_{irr}=60 min intensities of Region I, II and IV showed an increase. Moreover, at the end of 60 min of irradiation period, Region III representing the presence of fulvic-like fluorophores displayed increased intensities. Also, bacteria count showed a slight

increase between t_{irr}=40 min (3.70E+01 CFU/mL) and 60 min (4.00E+01 CFU/mL) indicating that the presence of bacteria propagation. It could be attributed that bacteria used anions and cations not only to resist the solar photocatalytic process but to reproduce and this propagation caused an increase in the intensities of EEM fluorescence contour plots.

4.2.5.5. Mechanistic evaluation of *E. coli* inactivation upon 0.25% Fe-SynTiO$_2$ solar photocatalytic treatment in WM solution. Upon irradiation total K, protein, and carbohydrate contents present in initial, t=0, and t_{irr}=60 min samples of 0.25% Fe-SynTiO$_2$ solar photocatalytic treatment of *E. coli* in WM solution were presented in Table 4.51.

Table 4.51. Total K, protein, and carbohydrate contents of time dependent *E. coli* inactivation in WM solution upon 0.25% Fe-SynTiO$_2$ solar photocatalytic treatment.

0.25% Fe-SynTiO$_2$ solar photocatalytic treatment	*E. coli* in WM solution		
	Initial	t=0	60 min
Total K, mg/L	4.11	4.04	3.97
Protein, mg/L	1.80	2.18	6.95
Carbohydrate, mg/L	1.95	3.16	74.7

Immediate adsorptive removal of total K content at t=0 was calculated as 1.7 %. Total K content showed a decreasing trend which could be due to released K^+ ion adsorption onto negatively charged ruptured *E. coli* cell wall and photocatalyst surfaces. Similar decreasing pattern was also obtained from SynTiO$_2$ solar photocatalytic treatment of *E. coli* in WM solution (Table 4.24).

E. coli in WM solution upon solar photocatalytic treatment in the presence of 0.25% Fe-SynTiO$_2$ specimen displayed increase in both protein and carbohydrate content at the end of 60 min treatment period however carbohydrate concentration showed a significant increase (1.95-74.7 mg/L) like *E. coli* in IsoT solution condition (Table 4.49). Although detection of slight increase in bacteria count, measured carbohydrate concentration was fairly high than expected, therefore; it could be mentioned that the presence of some experimental errors or interferences. The presence of glycoproteins, Fe^{3+}, and NO_3^- which was a component of WM solution, could be the cause of interferences affecting carbohydrate determination process (Martens and Frankenberger, 1990; Rao and Pattabiraman, 1989). However, Fe^{3+} release was detected as BDL for both t=0 and t_{irr}=60 min conditions. On the other hand, protein concentrations were plotted against $FI_{sync280}$ and a strong correlation was obtained as R^2=0.96. Moreover, NPOC content displayed a strong correlation with both protein and carbohydrate contents as R^2=0.95 and R^2=0.97, respectively.

4.2.5.6. Organic matter formation and removal upon 0.25% Fe-SynTiO$_2$ solar photocatalytic treatment of *E. coli* in HA solution. UV-vis absorption and synchronous scan fluorescence spectra of organic matter in solution were presented in Figures 4.132 and 4.133. Irradiation time dependent absorbance changes were significantly similar to each other in UV wavelength range of λ=200-400 nm due to the presence of aromatic domains and color forming moieties (Color$_{436}$, UV$_{365}$, and UV$_{280}$). Irradiation time dependent sequential degradation of organic matter was not detected in contradiction to previous sets of solar photocatalytic treatment of *E. coli* in HA solution carried out with TiO$_2$, SynTiO$_2$, and 0.50% Fe-TiO$_2$ (Figures 4.36, 4.60, and 4.108). It should be indicated that, the absorbance of HA$_i$ could be visualized a rather different trend at λ < 235 nm, as expected.

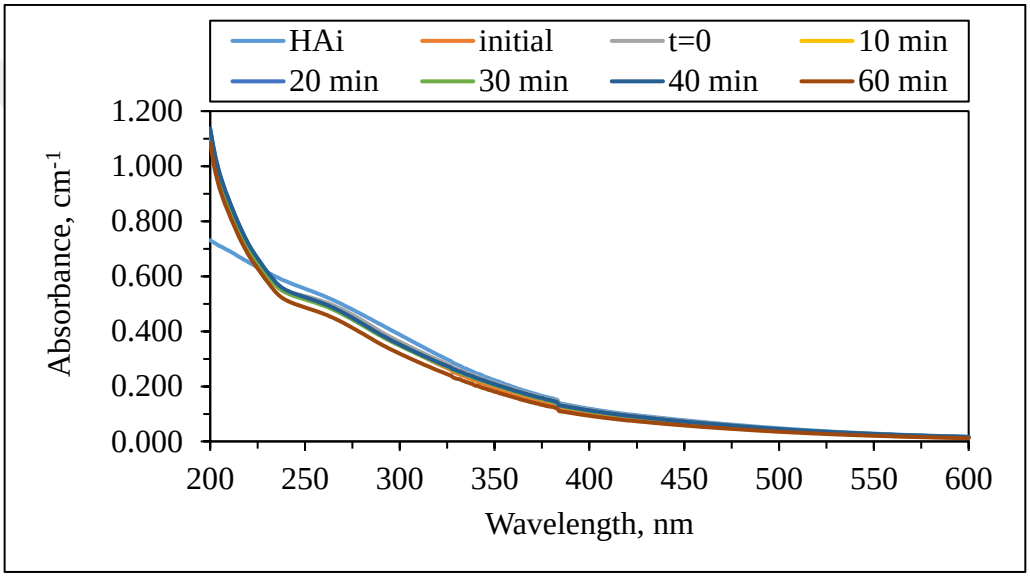

Figure 4.132. UV-vis absorption spectra of organic matter: Irradiation time dependent *E. coli* inactivation in HA solution upon 0.25% Fe-SynTiO$_2$ solar photocatalytic treatment.

Synchronous scan fluorescence spectra of the emerged organic matter displayed an intense peak at λ$_{emis}$=380 nm and two minor peaks at λ$_{emis}$=440 and 480 nm representing the presence of aromatic hydrocarbons (Dujmov and Sučević, 1990) (Figure 4.133). Due to masking effect of humic fluorophores on protein fluorophores, measured intensities at λ$_{emis}$=280 nm was quite low as expected. After t$_{irr}$=30 min, an irradiation time dependent decreasing order in FI$_{sync}$ data was observed with a significant decrease after irradiation period of 40 min.

On the other hand, FI$_{sync470}$ and FI$_{sync280}$ displayed changes in the range of 55.3-119 and 8.71-27.4, respectively (Figure 4.134). In the presence of HA as solution matrix, the predominant fluorophoric groups were recognized as FI$_{sync470}$. FI$_{sync280}$ of HA$_i$ could not be detected however after

the introduction of bacteria into HA solution i.e. the "initial" condition, $FI_{sync280}$ increased to 8.71 indicating the presence of of proteinaceous components in solution.

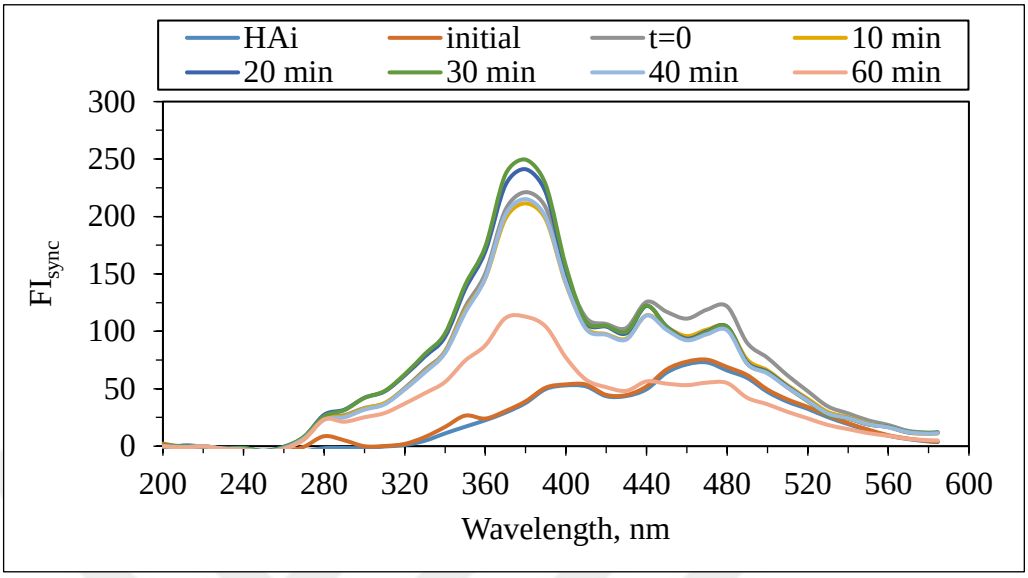

Figure 4.133. Synchronous scan fluorescence spectra of organic matter: Irradiation time dependent *E. coli* inactivation in HA solution upon 0.25% Fe-SynTiO$_2$ solar photocatalytic treatment.

All UV-vis parameters expressed high presence due to the use of HA solution as expected (Figure 4.134). Specified UV-vis parameters displayed a decrease at t_{irr}=60 min. Most importantly, UV_{254} expressed variations in the range of 0.4777-0.5446 being the highest for HA_i solution and the lowest for t_{irr}=60 min condition.

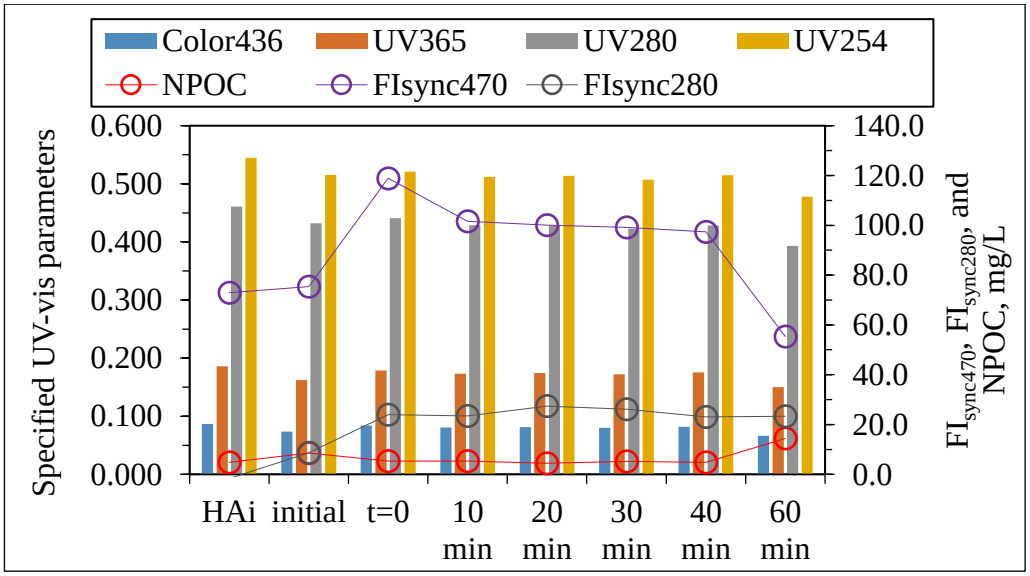

Figure 4.134. Specified UV-vis and fluroscence parameters of organic matter: Irradiation time dependent *E. coli* inactivation in HA solution upon 0.25% Fe-SynTiO$_2$ solar photocatalytic treatment.

However, obtained differences in specified UV-vis parameters were quite low and similar to $SynTiO_2$ solar photocatalytic treatment of *E. coli* in HA solution (Figure 4.62). Moreover, obtained data could be supported that the interpretation which was made about 0.25% Fe-$SynTiO_2$ having higher selectivity against *E. coli* rather than HA in Section 4.2.5.1.

Along with the presence of HA solution, NPOC expressed considerable variations in the range of 4.46-14.4 mg/L (Figure 4.134). NPOC content increased between HA_i (4.76 mg/L) and initial (8.48 mg/L) due to possibly EPS content of introduced bacteria, then followed a decreasing trend up to t_{irr}=20 min (4.46 mg/L) due to degradation of organics both originating from HA and *E. coli* content. Afterward, followed by an increase to t_{irr}=30 min (5.17 mg/L) and again followed by a decrease to t_{irr}=40 min (4.75 mg/L) and displayed a sharp increase at t_{irr}=60 min (14.4 mg/L) due to further release of organics from damaged and destructed *E. coli* cells.

Based on NPOC contents, $SCoA_{436}$, $SUVA_{365}$, $SUVA_{280}$, $SUVA_{254}$, $SFI_{sync470}$, and $SFI_{sync280}$ parameters were calculated and presented in Figure 4.135. $SUVA_{254}$ displayed variations in between 3.32-11.5 L/m mg during 0.25% Fe-$SynTiO_2$ solar photocatalytic treatment expressing differences in both UV_{254} and NPOC removals.

Furthermore, $SFI_{sync470}$ and $SFI_{sync280}$ expressed variations in the range of 3.84-22.4 and 1.03-6.14, respectively. The key fluorophoric group was accepted as $SFI_{sync470}$ in the presence of HA solution. According to undetected $FI_{sync280}$ of HA_i solution, $SFI_{sync280}$ could not be calculated as well.

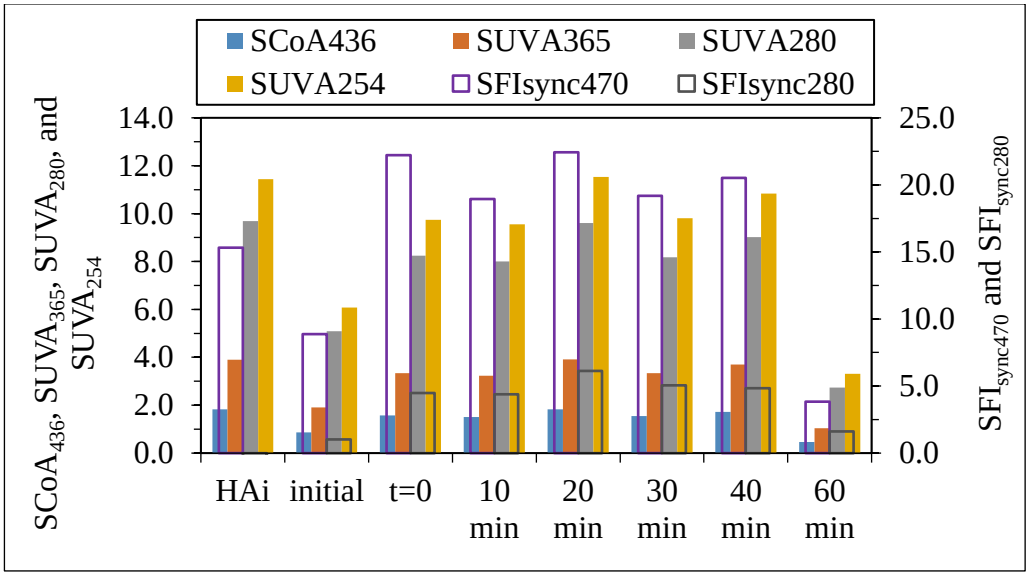

Figure 4.135. Specific UV-vis and fluroscence parameters of organic matter: Irradiation time dependent *E. coli* inactivation in HA solution upon 0.25% Fe-$SynTiO_2$ solar photocatalytic treatment.

Characteristic properties of organic matter under initial condition, upon introduction of 0.25% Fe-SynTiO$_2$ (t=0) and at the end of 0.50% Fe-TiO$_2$ solar photocatalytic inactivation of *E. coli* in HA solution for 60 min of irradiation period were presented in Table 4.52.

Table 4.52. Characteristic properties of organic matter present in 0.25% Fe-SynTiO$_2$ solar photolytic treatment of *E. coli* in HA solution.

Irradiation time, min	UV-vis Spectroscopic Parameters, cm^{-1}				NPOC, mg/L	SUVA$_{254}$, L/m mg	FI$_{sync470}$	SFI$_{sync470}$	FI
	Color$_{436}$	UV$_{365}$	UV$_{280}$	UV$_{254}$					
Initial	0.0736	0.1622	0.4320	0.5154	8.48	6.08	75.3	8.88	1.05
t=0	0.0840	0.1789	0.4408	0.5208	5.35	9.73	119	22.2	1.06
60 min	0.0661	0.1501	0.3931	0.4777	14.4	3.32	55.3	3.84	1.10

Upon t_{irr}=60 min of 0.25% Fe-SynTiO$_2$ solar photocatalytic treatment of *E coli* in HA solution, at which 3.82 log *E. coli* reduction was achieved (Table 4.47), released organic matter expressed the following UV-vis parameters (cm^{-1}); Color$_{436}$: 0.0661, UV$_{365}$: 0.1501, UV$_{280}$: 0.3931, UV$_{254}$: 0.4777, and NPOC as 14.4 mg/L.

SUVA$_{254}$ of initial, t=0, and t_{irr}=60 min conditions were calculated as 6.08, 9.73, and 3.32 L/m mg, respectively. Differences in SUVA$_{254}$ could be indicate that initial and t=0 solutions expressed hydrophobic and aromatic features however after t_{irr}=60 min with the degradation of organic matter, aromaticity of the organic content displayed a significant decrease and expressed almost completely aliphatic characteristics (Edzwald et al., 1985). On the other hand, the use of HA solution as aqueous medium caused relatively high initial NPOC and SUVA$_{254}$ as expected.

FI$_{sync470}$ expressed a decrease at t_{irr}=60 min due to degradation of organic content. Calculated SFI$_{sync470}$ displayed a decrease at t_{irr}=60 min in accordance with the increased NPOC. On the other hand, FI$_{sync280}$ measurements of initial, t=0 and t_{irr}=60 min conditions were detected as 8.71, 23.9, and 23.4, respectively. FI$_{sync280}$ demonstrated an increase at t_{irr}=60 min due to released protein content from bacteria. SFI$_{sync280}$ of initial, t=0, and t_{irr}=60 min runs were calculated based on NPOC and FI$_{sync280}$ data, as 1.03, 4.47, and 1.62, respectively. Moreover, FI at t_{irr}=60 min was calculated as 1.10 representing the presence of fluorophores originating from humic content present in reaction solution as expected.

In a similar manner to the UV-vis absorbance and synchronous scan fluorescence analyses, EEM fluorescence contour plots of organic matter emerged and removed during irradiation time dependent

E. coli inactivation in HA solution upon 0.25% Fe-SynTiO$_2$ solar photocatalytic treatment were displayed in Figure 4.136.

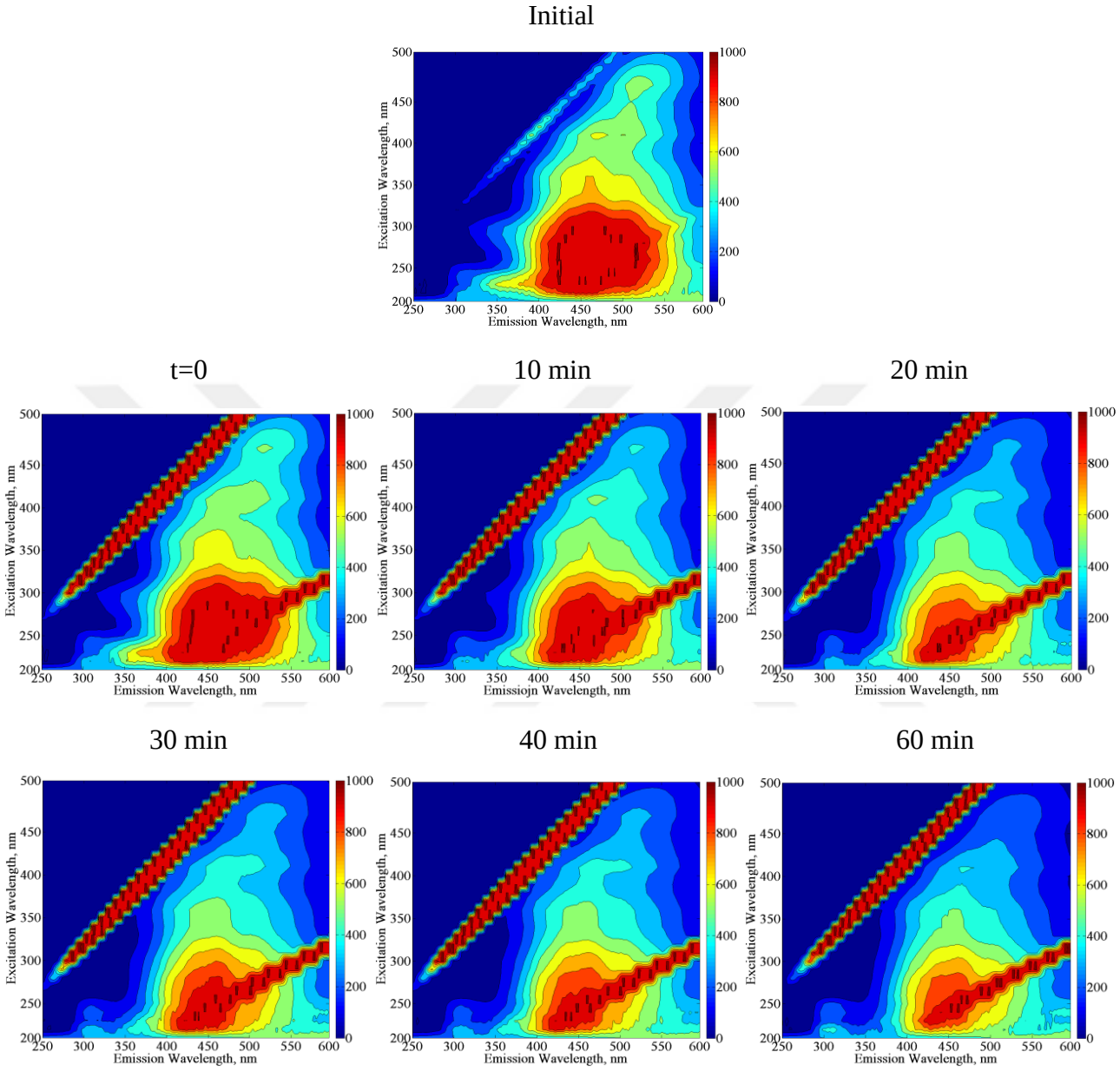

Figure 4.136. EEM fluorescence contour plots of organic matter: Irradiation time dependent *E. coli* inactivation in HA solution upon 0.25% Fe-SynTiO$_2$ solar photocatalytic treatment.

EEM fluorescence contour plots of 0.25% Fe-SynTiO$_2$ solar photocatalytic treatment of *E. coli* in HA solution displayed the presence of Regions III, and V indicating that the fluorophores were mainly originated from fulvic-like and humic-like substances. Both humic-like and fulvic-like fluorophore intensities displayed a decreasing trend throughout solar irradiation duration however obtained intensities at t_{irr}=60 min were quite high with respect to TiO$_2$ solar photocatalytic treatment (Figure 4.40). It could be concluded that 0.25% Fe-SynTiO$_2$ has a selectivity towards bacteria

irrespective to TiO_2 due to higher bacteria LRV of 0.25% Fe-SynTiO_2 (*E. coli* LRV as 1.45 for TiO_2; *E. coli* LRV as 3.82 for 0.25% Fe-SynTiO_2) (Tables 4.11 and 4.47).

4.2.5.7. Mechanistic evaluation of *E. coli* inactivation upon 0.25% Fe-SynTiO_2 solar photocatalytic treatment in HA solution. As bacteria inactivation products of 0.25% Fe-SynTiO_2 solar photocatalytic treatment of *E. coli* in HA solution, total K, protein, and carbohydrate contents present in initial, t=0, and t_{irr}=60 min solutions were presented in Table 4.53.

Table 4.53. Total K, protein, and carbohydrate contents of time dependent *E. coli* inactivation in HA solution upon 0.25% Fe-SynTiO_2 solar photocatalytic treatment.

0.25% Fe-SynTiO_2 solar photocatalytic treatment	*E. coli* and HA		
	Initial	t=0	60 min
Total K, mg/L	0.55	0.55	0.63
Protein, mg/L	7.05	8.78	13.5
Carbohydrate, mg/L	2.80	3.12	25.7

Total K content displayed no immediate adsorptive removal at t=0, following t_{irr}=60 min showed a slight increase expressing the presence of K^+ ion release from *E. coli* cells after 60 min of irradiation. Similar inhibited total K contents were also obtained from previous solar photolytic (Table 4.8) and photocatalytic treatment sets (Tables 4.17, 4.26, 4.35, and 4.44) carried out in the presence of HA solution.

Upon 0.25% Fe-SynTiO_2 solar photocatalytic treatment of *E. coli* in HA solution, both protein and carbohydrate contents displayed increase in at the end of t_{irr}=60 min. No correlation was detected when protein concentrations were plotted against $FI_{sync280}$ data. Carbohydrate concentration showed higher increase (2.80-25.7 mg/L) than protein concentration (7.05-13.5 mg/L) after 60 min of solar irradiation period. Detected significantly increased carbohydrate concentration as 25.7 mg/L could be due to remaining humic content and released carbohydrate content from bacteria. Increased NPOC content (Figure 4.134) and the presence of relatively intense EEM contour plots at t_{irr}=60 min (Figure 4.136) could support increased protein and carbohydrate contents at t_{irr}=60 min. Protein concentrations and NPOC displayed a moderate correlation with each other as R^2=0.67 however carbohydrate and NPOC contents showed a strong correlation as R^2=0.88. Moreover, 0.029 mg/L of Fe^{3+} release was detected at t_{irr}=60 min, which could be result in increased carbohydrate concentration due to the interfering presence of Fe^{3+} to total carbohydrate determination process (Martens and Frankenberger, 1990).

4.2.5.8. Organic matter formation and removal upon 0.25% Fe-SynTiO$_2$ solar photocatalytic treatment of *E. coli* in "HA and WM" solution. UV-vis absorption and synchronous scan fluorescence spectra of organic matter in solution were presented in Figures 4.137 and 4.138. Irradiation time dependent absorbance changes were significantly different from each other in UV wavelength range of λ=200-400 nm due to the presence of aromatic domains and color forming moieties (Color$_{436}$, UV$_{365}$, and UV$_{280}$).

Different from previous sets of solar photolytic (Figure 4.17) and photocatalytic treatments conducted in "HA and WM" solution (Figures 4.41, 4.65, 4.89 and 4.113), except "HA and WM" solution and initial condition, quite low absorbances were detected at λ < 250 nm. On the other hand, similar to TiO$_2$ solar photocatalytic treatment (Figure 4.41), after the introduction of photocatalyst into the solution (t=0), a drastic decrease was attained at λ < 230 nm, which revealing significant surface interactions.

Moreover, UV-vis absorption spectra did not follow an irradiation time dependent decreasing order similar to 0.25% Fe-TiO$_2$ solar photocatalytic treatment of *E. coli* in "HA and WM" solution (Figures 4.89). The reason could be attributed that the re-emergence of removed light absorbing centers following further irradiation periods.

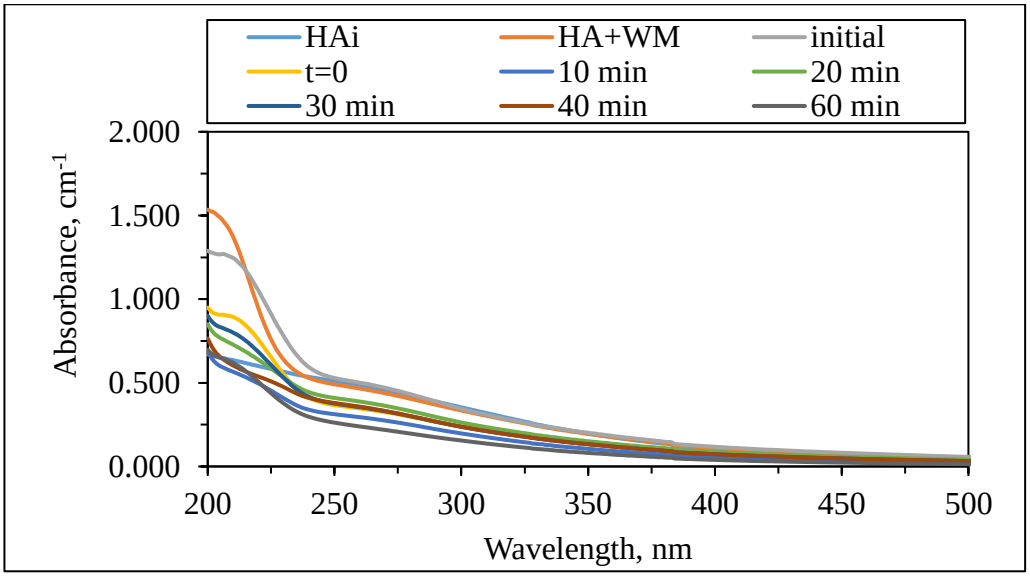

Figure 4.137. UV-vis absorption spectra of organic matter: Irradiation time dependent *E. coli* inactivation in "HA and WM" solution upon 0.25% Fe-SynTiO$_2$ solar photocatalytic treatment.

Synchronous scan fluorescence spectra of emerged organic matter displayed two intense peaks at λ$_{emis}$=390 nm and 470 nm, and a minor peak at λ$_{emis}$=280 nm, due to presence of HA solution as a

matrix component, as expected (Figure 4.138). After the introduction of photocatalyst into the aqueous reaction solution (t=0) an increase in FI_{sync} at λ_{emis} < 410 nm, especially at λ_{emis} < 300 nm was detected. It could be indicated that released cytoplasmic content from *E. coli* with the mechanistic effect of present photocatalyst contained higher proteinaceous content than aromatic hydrocarbons. The most significant decrease in FI_{sync} data was observed after t_{irr}=40 min.

Furthermore, $FI_{sync470}$ and $FI_{sync280}$ displayed changes in the range of 29.3-68.7 and 1.14-31.9, respectively (Figure 4.139). The predominant fluorophoric group was determined as $FI_{sync470}$ due to the use of HA solution as a reaction medium constituent.

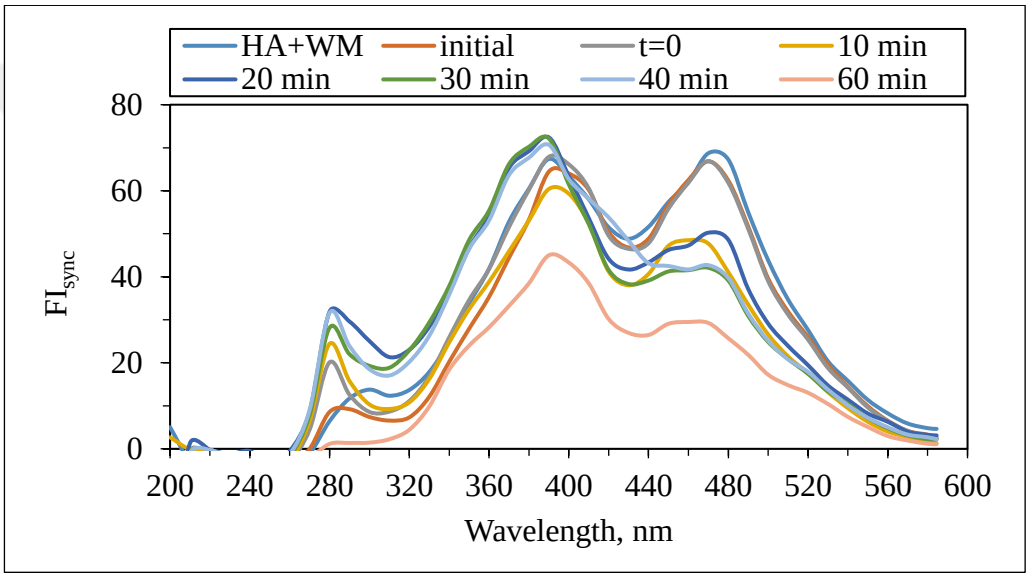

Figure 4.138. Synchronous scan fluorescence spectra of organic matter: Irradiation time dependent *E. coli* inactivation in "HA and WM" solution upon 0.25% Fe-SynTiO$_2$ solar photocatalytic treatment.

NPOC contents expressed variations in the range of 4.56-5.52 mg/L (Figure 4.139). NPOC content displayed a decreasing trend up to t=0 condition (5.52-4.63 mg/L), revealing an immediate adsorptive removal as 16.1 %, and slightly increased up to t_{irr}=10 min (5.02 mg/L) due to release of cytoplasmic organic content from damaged bacteria, and followed by a decreasing trend until t_{irr}=30 min (4.56 mg/L). Afterwards NPOC showed an increasing trend during prolonged solar light irradiation period of 60 min (5.37 mg/L) due to release of organics from damaged and destructed *E. coli* cells. Moreover, obtained increase in NPOC content could also be roughly correlated with continuous but slowed down bacteria decrease between irradiation period of 30 min and 60 min conditions (8.51E+03 CFU/mL for t_{irr}=30 min; 4.24E+03 CFU/mL for t_{irr}=40 min; 2.49E+03 CFU/mL for t_{irr}=60 min) (Figure 4.121).

All specified UV-vis parameters displayed a significant decrease at t=0 condition due to adsorptive removal or organic content via membrane filtration prosess applied prior to spectroscopic analysis (Figure 4.139). Besides an increase recorded at t_{irr}=20 min, specified UV-vis parameters expressed a decrease at t_{irr}=60 min. On the other hand, between t_{irr}=20 min and 40 min quite low differences were measured in specified UV-vis and NPOC parameters however, almost 1 log bacteria reduction was achieved among indicated irradiation periods (4.15E+04 CFU/mL for t_{irr}=20 min; 4.24E+03 CFU/mL for t_{irr}=40 min) (Figure 4.121). Therefore, it could be indicated that between these irradiation periods solar photocatalytic system worked against the destruction of *E. coli* rather than the degradation of already present and released organic content in the solutions. On the other hand, as the most significant parameter, UV_{254} displayed variations in the range of 0.2521-0.5166, being the highest for initial solution and the lowest for t_{irr}=60 min condition.

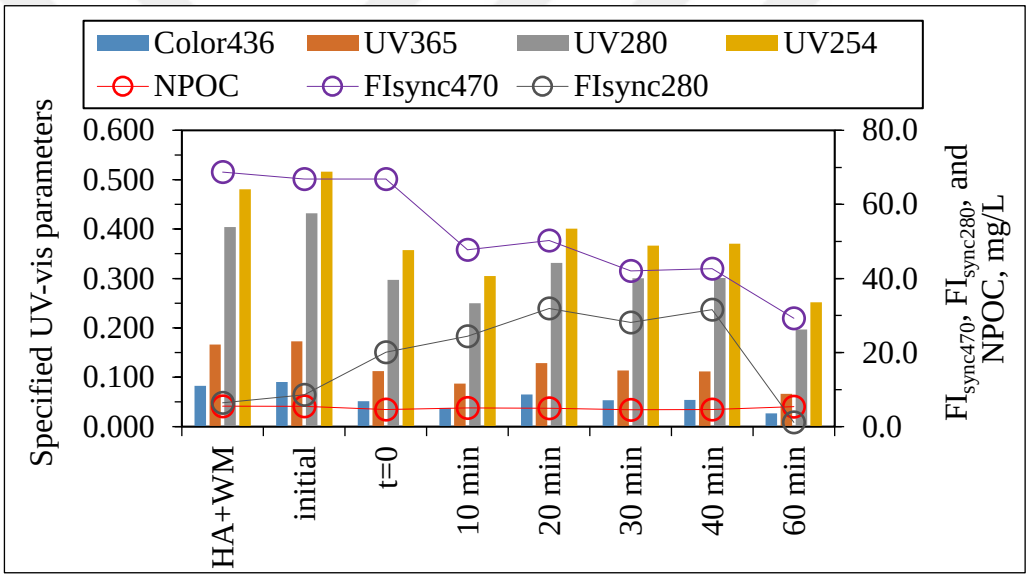

Figure 4.139. Specified UV-vis and fluroscence parameters of organic matter: Irradiation time dependent *E. coli* inactivation in "HA and WM" solution upon 0.25% Fe-SynTiO$_2$ solar photocatalytic treatment.

Based on NPOC contents of the samples, all specific parameters as $SCoA_{436}$, $SUVA_{365}$, $SUVA_{280}$, $SUVA_{254}$, $SFI_{sync470}$, and $SFI_{sync280}$ were calculated and presented in Figure 4.140. $SUVA_{254}$ displayed variations in between 4.70-9.46 L/m mg during 0.25% Fe-SynTiO$_2$ solar photocatalytic treatment indicating the differences in both UV_{254} and NPOC removals. Similar to behavior of specified UV-vis parameters (Figure 4.139), all calculated specific UV-vis and fluorescence parameters expressed insignificant changes between t_{irr}=20 min and 40 min conditions. On the other hand, beside predominant $SFI_{sync470}$ displaying variations in the range of 5.45-14.4, quite low $SFI_{sync280}$ expressed changes in between 0.213-6.83.

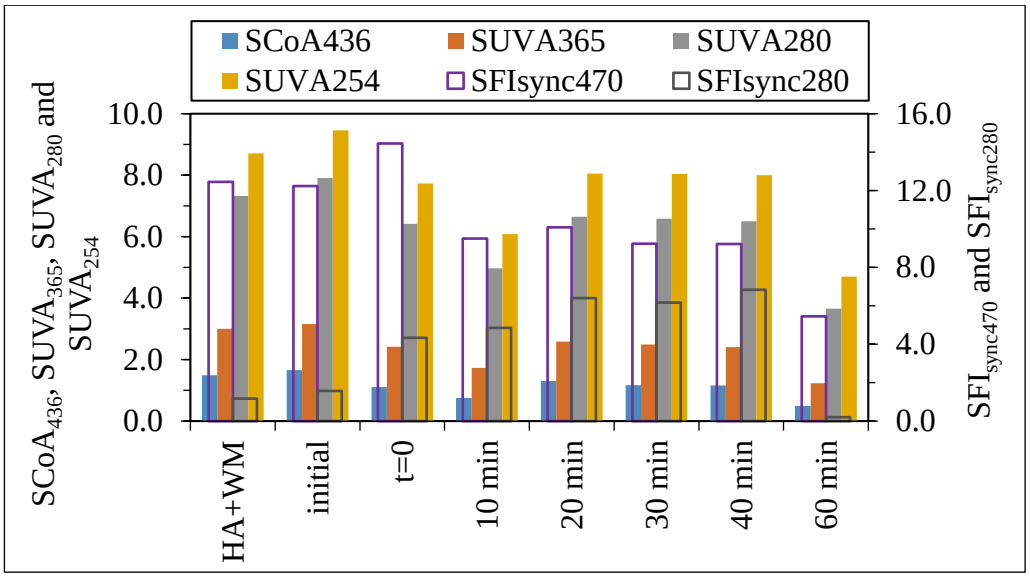

Figure 4.140. Specific UV-vis and fluroscence parameters of organic matter: Irradiation time dependent *E. coli* inactivation in "HA and WM" solution upon 0.25% Fe-SynTiO$_2$ solar photocatalytic treatment.

Characteristic properties of organic matter under initial condition, at t=0 condition, and at the end of the 0.25% Fe-SynTiO$_2$ solar photocatalytic inactivation of *E. coli* in "HA and WM" solution for 60 min were presented in Table 4.54.

Table 4.54. Characteristic properties of organic matter present in 0.25% Fe-SynTiO$_2$ solar photolytic treatment of *E. coli* in "HA and WM" solution.

Irradiation time, min	UV-vis Spectroscopic Parameters, cm^{-1}				NPOC, mg/L	SUVA$_{254}$, L/m mg	FI$_{sync470}$	SFI$_{sync470}$	FI
	Color$_{436}$	UV$_{365}$	UV$_{280}$	UV$_{254}$					
Initial	0.0904	0.1726	0.4317	0.5166	5.46	9.46	66.8	12.2	1.18
t=0	0.0512	0.1122	0.2970	0.3577	4.63	7.73	66.9	14.4	1.19
60 min	0.0267	0.0663	0.1965	0.2521	5.37	4.70	29.3	5.45	1.26

Upon t$_{irr}$=60 min solar photocatalytic treatment of *E coli* in "HA and WM" solution in the presence of 0.25% Fe-SynTiO$_2$, at which 2.50 log *E. coli* reduction was achieved (Table 4.47), released organic matter expressed the following UV-vis parameters (cm^{-1}); Color$_{436}$: 0.0267, UV$_{365}$: 0.0663, UV$_{280}$: 0.1965, UV$_{254}$: 0.2521, and NPOC as 5.37 mg/L. After irradiation period of 60 min, SUVA$_{254}$ was calculated as 4.69, indicating that the presence of hydrophobic and aromatic substances in solution (Edzwald et al., 1985). The use of HA solution caused relatively high initial NPOC and SUVA$_{254}$ values as expected. FI$_{sync470}$ showed a decrease at t$_{irr}$=60 min due to degradation of organic content released from damaged *E. coli* cells and already present organic matrix content. After solar light exposure period of 60 min SFI$_{sync470}$ decreased while NPOC result displayed a slight decrease

based on initial content. Moreover, $FI_{sync280}$ of initial, t=0 and irradiation period of 60 min conditions were recorded as 8.57, 20.1, and 1.14, respectively. $SFI_{sync280}$ of initial, t=0, and t_{irr}=60 min samples were calculated as 1.57, 4.34, and 0.213, respectively. Due to degradation of released cytoplasmic protein content, both $FI_{sync280}$ and $SFI_{sync280}$ displayed a decrease at t_{irr}=60 min condition. FI at t_{irr}=60 min was calculated as 1.26 expressing the presence of fluorophores coming from present HA solution as expected.

EEM fluorescence contour plots of organic matter emerged and removed during irradiation time dependent *E. coli* inactivation in "HA and WM" solution during 0.25% Fe-SynTiO$_2$ solar photocatalytic treatment were displayed in Figure 4.141.

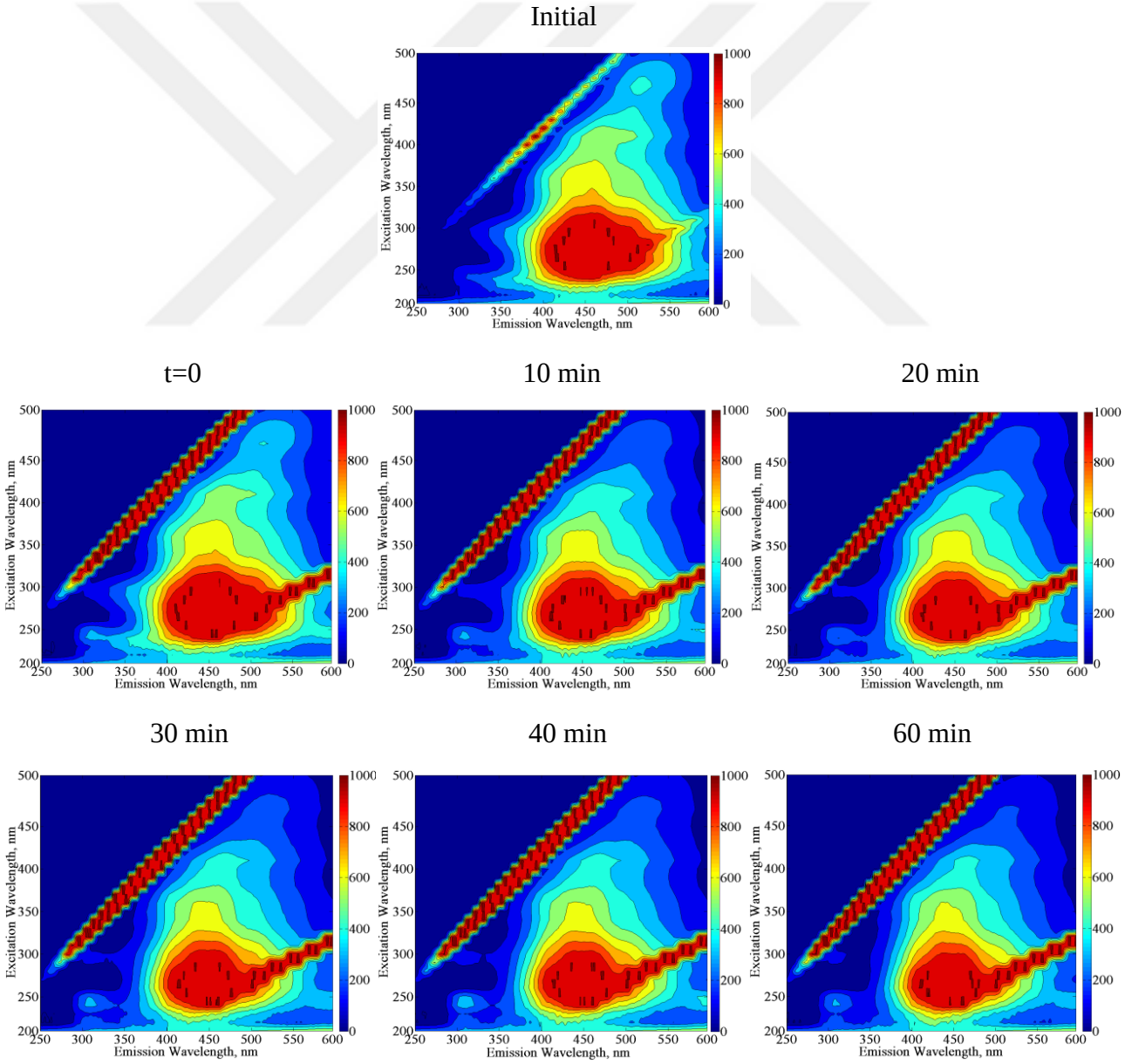

Figure 4.141. EEM fluorescence contour plots of organic matter: Irradiation time dependent *E. coli* inactivation in "HA and WM" solution upon 0.25% Fe-SynTiO$_2$ solar photocatalytic treatment.

EEM fluorescence contour plots of *E. coli* in "HA and WM" solution upon 0.25% Fe-SynTiO$_2$ solar photocatalytic treatment displayed the presence of Regions III, and V indicating that the fluorophores were mainly originated from fulvic-like and humic-like substances. Both humic-like and fulvic-like fluorophore intensities displayed a decrease throughout irradiation period of 60 min however, more intense fluorescence could be visualized relative to *E. coli* in HA solution (Figure 4.136). The reason could be attributed to the presence of WM solution which acting a retardation effect on both reduction of *E. coli* and degradation of humic content.

4.2.5.9. Mechanistic evaluation of *E. coli* inactivation upon 0.25% Fe-SynTiO$_2$ solar photocatalytic treatment in "HA and WM" solution. Total K, protein, and carbohydrate contents present in initial, t=0, and t_{irr}=60 min samples, as bacteria inactivation products of 0.25% Fe-SynTiO$_2$ solar photocatalytic treatment of *E. coli* in "HA and WM" solution were presented in Table 4.55.

Table 4.55. Total K, protein, and carbohydrate contents of time dependent *E. coli* inactivation in "HA and WM" solution upon 0.25% Fe-SynTiO$_2$ solar photocatalytic treatment.

0.25% Fe-SynTiO$_2$ solar photocatalytic treatment	*E. coli* in "HA and WM"		
	Initial	t=0	60 min
Total K, mg/L	4.59	4.47	4.41
Protein, mg/L	5.10	4.79	10.2
Carbohydrate, mg/L	5.01	4.52	36.2

Total K content displayed an immediate adsorptive removal at t=0 as 2.61 % and followed by a further decrease at t_{irr}=60 min condition. Decreased total K content at 60 min of irradiation period could be due to the adsorption of K^+ ions onto negatively charged *E. coli*, photocatalyst and HA surfaces, and elimination with membrane filtration prior to total K analysis. Similar trends were also obtained from previous Fe-doped solar photocatalytic treatment sets carried out in the presence of "HA and WM" solution (Tables 4.37 and 4.46).

E. coli in "HA and WM" solution upon 0.25% Fe-SynTiO$_2$ solar photocatalytic treatment displayed increased protein (5.10-10.2 mg/L) and carbohydrate concentration (5.01-36.2 mg/L) results at the end of t_{irr}=60 min treatment period. A moderate correlation was obtained between protein and $FI_{sync280}$ data as R^2=0.68. Carbohydrate content showed higher increase than protein. This significantly increased carbohydrate concentration could be due to possible extra absorbance at λ=350-500 nm, which includes the measured absorbance value of carbohydrate determination as λ=490 nm, originating from H_2SO_4 treated remaining humic content (Sieburth and Jensen, 1969;

Meadows and Campbell, 1978). Furthermore, released Fe^{3+} concentration at t_{irr}=60 min was detected as 0.008 mg/L, which could also cause an interference in carbohydrate determination process (Martens and Frankenberger, 1990). There were no correlations detected between NPOC contents and neither protein nor carbohydrate concentrations.

4.2.5.10. Comparative evaluation of different experimental matrixes on 0.25% Fe-SynTiO$_2$ solar photocatalytic inactivation mechanism of *E. coli*. Total K, protein, and carbohydrate concentrations and bacteria count results of 0.25% Fe-SynTiO$_2$ solar photocatalytic treatment of *E. coli* in different solution matrixes in comparison with initial, t=0, and t_{irr}=60 min conditions were given in Figure 4.142. Total K contents varied in between 0.55-4.59 mg/L being the lowest for initial and t=0 samples of *E. coli* in HA solution and the highest for initial sample of *E. coli* in "HA and WM" solution. WM solution containing samples displayed higher total K contents than IsoT and HA solutions. Except *E. coli* in HA solution solar photocatalytic treatment set, total K concentrations expressed a decreasing trend. In the absence of sole WM solution, total K contents and *E. coli* counts displayed a strong correlation as $R^2 > 0.89$.

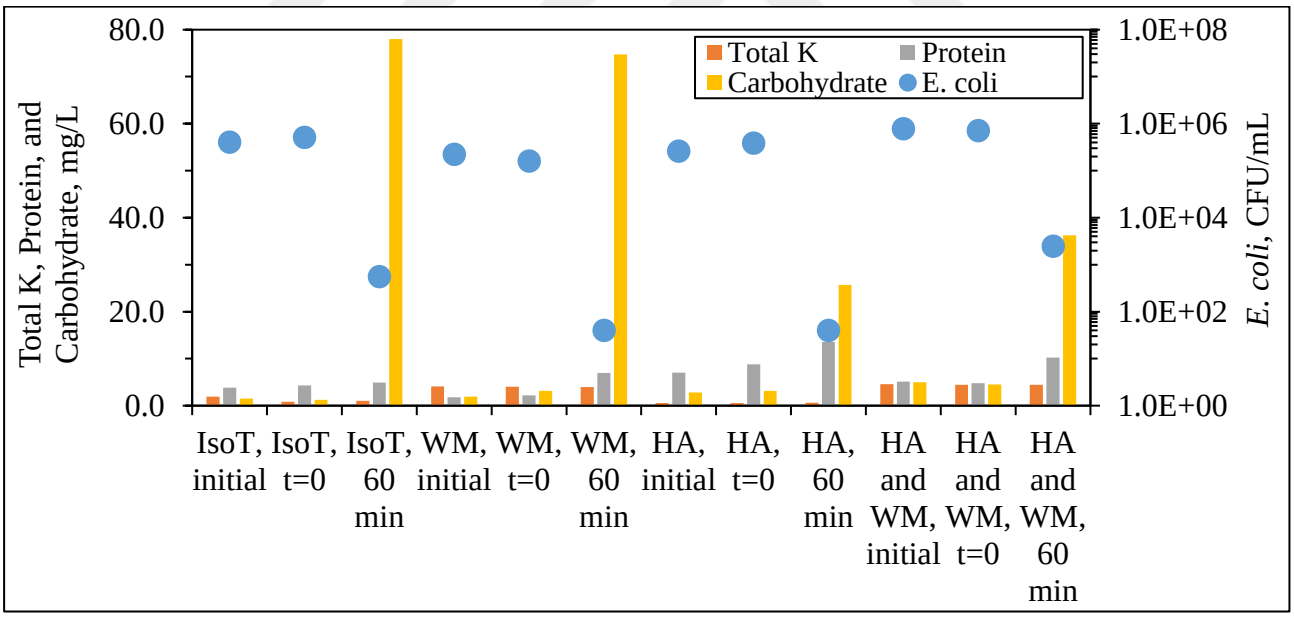

Figure 4.142. Initial, t=0, and t_{irr}=60 min total K, protein, and carbohydrate contents and bacteria enumeration results of *E. coli* inactivation upon 0.25% Fe-SynTiO$_2$ solar photocatalytic treatment in various aqueous matrixes.

Covering all conditions protein contents varied in between 1.80-13.5 mg/L being the lowest for initial sample of *E. coli* in WM solution and the highest for t_{irr}=60 min sample of *E. coli* in HA solution. Similarly, carbohydrate contents varied in between 1.27-78.0 mg/L being the lowest for t=0 condition and the highest for t_{irr}=60 min sample of *E. coli* in IsoT solution. At t_{irr}=60 min, all matrix

conditions displayed increased protein and carbohydrate concentrations. The highest protein concentrations for initial (7.05 mg/L), t=0 (8.78 mg/L), and t_{irr}=60 min (13.5 mg/L) samples were detected in only HA solution matrix. On the other hand, *E. coli* in IsoT, WM and "HA and WM" solution conditions showed significantly increased t_{irr}=60 min carbohydrate concentrations, which could be resulting from an experimental error as explained in Sections 4.2.5.3, 4.2.5.5, and 4.2.5.9.

Released protein and carbohydrate concentrations and bacteria LRV of 0.25% Fe-SynTiO$_2$ solar photocatalytic treatment of *E. coli* in various solution matrixes were given in Figure 4.143. Released protein and carbohydrate concentrations were calculated by subtracting initial from t_{irr}=60 min contents. While WM solution displayed the highest released protein in previous solar photocatalytic treatment sets (Figures 4.47, 4.71, 4.95, and 4.119), upon 0.25% Fe-SynTiO$_2$ solar photocatalytic treatment the highest released protein was obtained from HA solution as 6.49 mg/L. Moreover, LRV of *E. coli* in HA solution was detected as the highest as 3.82. It could be concluded that high bacteria LRV caused the highest released protein concentration. The highest released carbohydrate content was calculated for IsoT solution as 76.5 mg/L complying with its highest t_{irr}=60 min carbohydrate content. A strong correlation was detected between released protein contents and *E. coli* LRV as R^2 = 0.97 except the presence of "HA and WM" solution; however, there was no correlation detected between released carbohydrate concentrations and bacteria LRV.

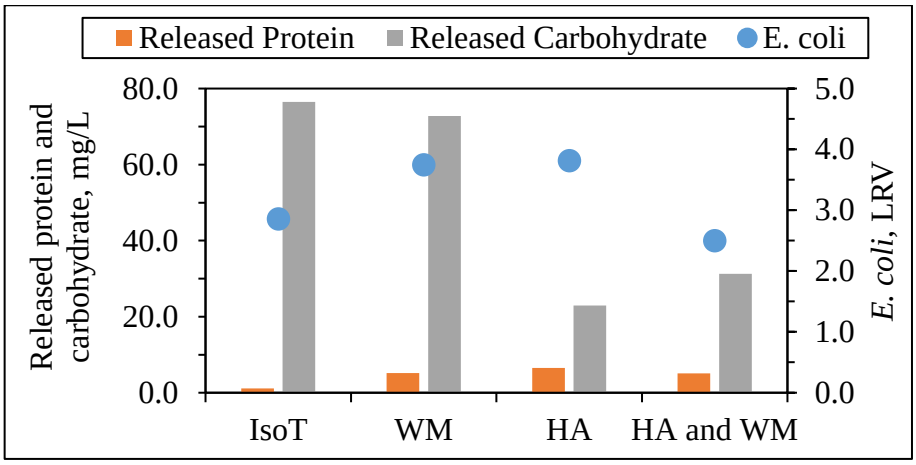

Figure 4.143. Released protein and carbohydrate contents, and bacteria LRV of *E. coli* inactivation upon 0.25% Fe-SynTiO$_2$ solar photocatalytic treatment in various aqueous matrixes.

Upon 0.25% Fe-SynTiO$_2$ solar photocatalytic treatment of *E. coli* in different solution matrixes, the attained protein and carbohydrate contents, $FI_{sync280}$, UV_{280} and NPOC data under initial, t=0, and irradiation period of 60 min conditions were given in Figure 4.144. In the presence of HA solution, higher UV_{280} values were recorded similar to previous solar photolytic (Figure 4.24) and

photocatalytic treatment sets (Figures 4.48, 4.72, 4.96, and 4.120). The use of HA solution as a matrix component resulted in the detection of higher protein contents for initial and t=0 conditions. In the presence of sole HA solution, $FI_{sync280}$ data showed a significant increase at t=0 condition as 23.9. Excluding the presence of "HA and WM" solution, protein concentrations and $FI_{sync280}$ showed a strong correlation as $R^2 > 0.83$.

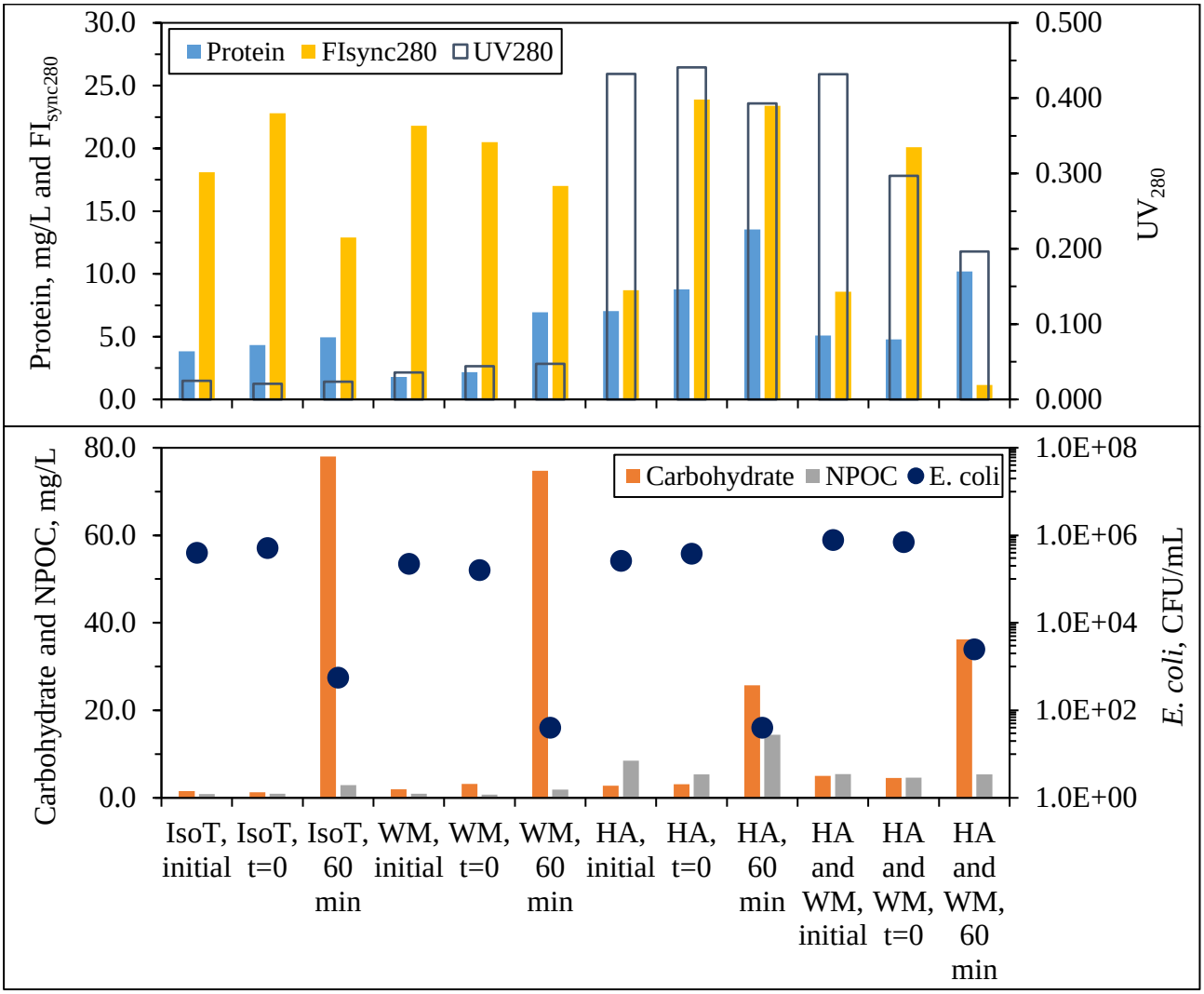

Figure 4.144. Initial, t=0, and t_{irr}=60 min protein and carbohydrate contents, $FI_{sync280}$, UV_{280}, NPOC, and *E. coli* enumeration results of 0.25% Fe-SynTiO_2 solar photocatalytic treatment of *E. coli* in various solution matrixes.

Higher NPOC contents were obtained in conditions containing HA solution, besides increased NPOC of initial and t=0 samples, increased carbohydrate concentrations were detected as well. IsoT and WM solutions expressed significantly high carbohydrate concentrations at t_{irr}=60 min, however NPOC content did not show any substantial increase, which supporting the assumption of the presence of an experimental error in carbohydrate determination process. Carbohydrate and NPOC contents displayed a rough correlation as $R^2 > 0.63$, except the presence of sole HA solution.

4.2.6. 0.50% Fe-SynTiO$_2$ Solar Photocatalytic Inactivation of *E. coli*

4.2.6.1. 0.50% Fe-SynTiO$_2$ solar photocatalytic *E. coli* inactivation under specified reaction conditions, reductions, and kinetics. *E. coli* suspension (N_o=5.42E+05 CFU/mL) was prepared in IsoT solution and subjected to solar photocatalytic treatment using 0.50% Fe-SynTiO$_2$. Upon irradiation period of 40 min, *E. coli* count decreased to 1.81E+03 CFU/mL. Following prolonged light exposure of t_{irr}=60 min, *E. coli* count declined to 3.80E+01 CFU/mL. Under these conditions LRV was 4.15 and reduction was 99.99 %. Upon preparation of *E. coli* (N_o=5.95E+05 CFU/mL) suspension in WM solution, for an irradiation period of 40 min, *E. coli* count decreased to 2.79E+02 CFU/mL. Following further light exposure of t_{irr}=60 min, *E. coli* count reached to 1.33E+02 CFU/mL revealing LRV as 3.65 and reduction as 99.9 %. *E. coli* (N_o=6.44E+05 CFU/mL) suspension was prepared in HA solution and for an irradiation period of 40 min, *E. coli* count decreased to 7.21E+02 CFU/mL. Upon light exposure of t_{irr}=60 min, *E. coli* count diminished to 1.27E+02 CFU/mL revealing LRV as 3.71 and reduction as 99.9 %. *E. coli* (N_o=5.74E+05CFU/mL) suspension was prepared in "HA and WM" components and was subjected to an irradiation period of 40 min in which *E. coli* count decreased to 1.01E+04 CFU/mL. Following prolonged light exposure of t_{irr}=60 min, *E. coli* count decreased to 3.38E+03 CFU/mL revealing LRV as 2.23 and reduction as 99 %.

Based on these results, the effect of solution matrix could be displayed in terms of LRV of *E. coli* in an increasing order as: "HA and WM" < WM < HA < IsoT. *E. coli* inactivation profiles and first order kinetic parameters were presented in Figure 4.145 and Table 4.65.

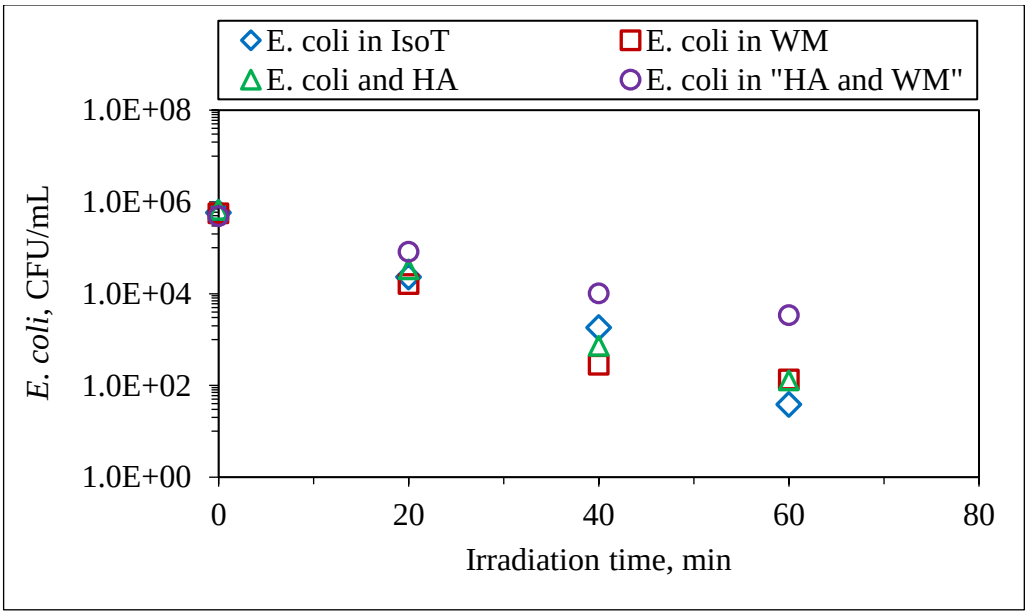

Figure 4.145. Irradiation time dependent *E. coli* inactivation upon 0.50% Fe-SynTiO$_2$ solar photocatalytic treatment in various solution matrixes.

Solar photocatalytic treatment of *E. coli* in the presence of 0.50% Fe-SynTiO$_2$ in IsoT solution resulted in a rather fast removal with k=0.158 min^{-1} and half-life as 4.39 min. In the presence of "HA and WM" solution, a reaction rate constant of k=0.0850 min^{-1} and half-life as 8.15 min were attained. The effect of reaction medium could also be expressed in terms of inactivation reaction rate constant (k, min^{-1}) in a decreasing order as; IsoT > HA > WM > "HA and WM". Irrespective of the minor differences in initial bacteria counts, inactivation rates (CFU/mL min) were ordered as; 9.53E+04 > 8.69E+04 > 8.56E+04 > 4.88E+04 for HA, WM, IsoT, and "HA and WM", respectively.

Table 4.56. 0.50% Fe-SynTiO$_2$ solar photocatalytic treatment of *E. coli*: Inactivation parameters.

Matrix	First order kinetic model			LRV	Reduction, %
	k, min^{-1}	$t_{1/2}$, min	R, CFU/mL min		
E. coli in IsoT	0.158	4.39	8.56E+04	4.15	99.99
E. coli in WM	0.146	4.75	8.69E+04	3.65	99.9
E. coli in HA	0.148	4.68	9.53E+04	3.71	99.9
E. coli in "HA and WM"	0.0850	8.15	4.88E+04	2.23	99

Solar photocatalytic treatment of *E. coli* in IsoT solution in the presence of 0.50% Fe-SynTiO$_2$ displayed the highest bacteria reduction among other experimental media, as 99.99 %. According to a recent study of Birben and colleagues, reaction rate constant of 0.50% Fe-SynTiO$_2$, which was detected as 0.158 min^{-1}, was higher than the rate constants of N-doped and Se-N co-doped TiO$_2$ and lower than Se-doped TiO$_2$ (Birben et al., 2017a).

E. coli in WM solution upon solar photocatalytic treatment with 0.50% Fe-SynTiO$_2$ displayed lower reduction than *E. coli* in IsoT solution, as 99.9 %. The presence of WM solution produced an inhibitory effect on the inactivation of bacteria.

E. coli inactivation in the presence of HA solution upon 0.50% Fe-SynTiO$_2$ solar photocatalytic treatment displayed the same *E. coli* reduction with WM solution as, 99.9 %. However, LRV of *E. coli* was slightly higher than that in WM solution, as 3.71. Considering high *E. coli* LRV, it could be suggested that 0.50% Fe-SynTiO$_2$ has selectivity towards bacteria rather than organic matrix. A reaction rate constant of 0.148 min^{-1} was obtained for HA solution condition. Birben and colleagues achieved a higher reaction rate constant with N-doped TiO$_2$ and lower reaction rate constants with Se-doped and Se-N co-doped TiO$_2$ species on the degradation of HA and *E. coli* (Birben et al., 2017a).

Solar photocatalytic treatment of *E. coli* in "HA and WM" solution showed the lowest bacteria reduction as 99 %. The presence of both HA and WM could retard the bacteria inactivation by inhibiting the process or giving resistance to bacteria.

4.2.6.2. Organic matter formation and removal upon 0.50% Fe-SynTiO$_2$ solar photocatalytic treatment of *E. coli* in IsoT solution. UV-vis absorption and synchronous scan fluorescence spectra of organic matter in solution were presented in Figures 4.146 and 4.147. Irradiation time dependent absorbance changes were significantly similar to each other in UV wavelength range of λ=200-240 nm in the absence of aromatic domains and color forming moieties (Color$_{436}$, UV$_{365}$, and UV$_{280}$) that should be measured in longer wavelengths. Moreover, resembling with TiO$_2$ (Figure 4.26) and 0.50% Fe-TiO$_2$ (Figure 4.98) solar photocatalytic treatments, the highest absorption was detected at t_{irr}=60 min in the wavelength range of λ=205-320 nm.

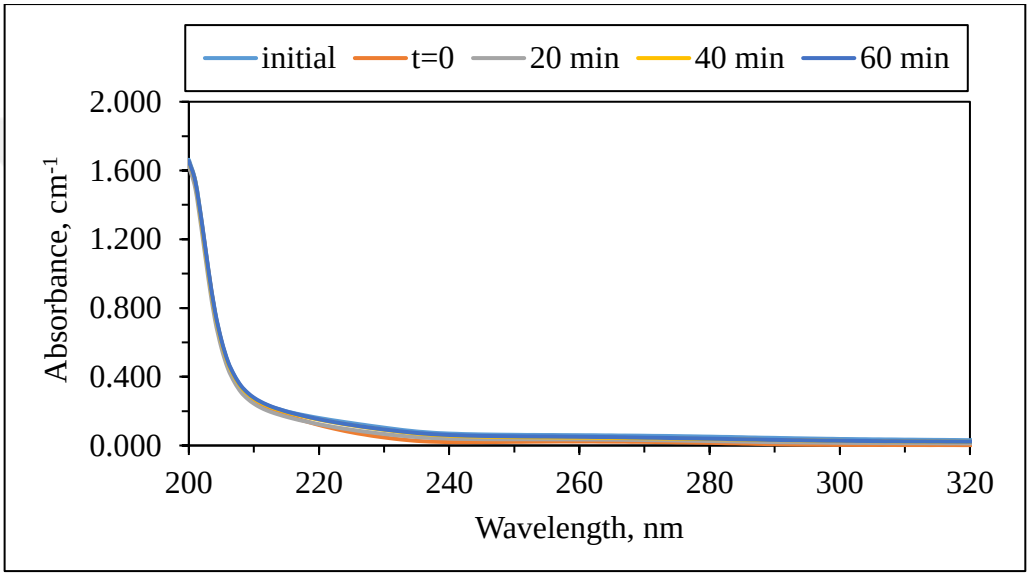

Figure 4.146. UV-vis absorption spectra of organic matter: Irradiation time dependent *E. coli* inactivation in IsoT solution upon 0.50% Fe-SynTiO$_2$ solar photocatalytic treatment.

Synchronous scan fluorescence spectra of emerged organic matter displayed an intense peak at λ_{emis}=280 nm (Figure 4.147). An irradiation time dependent decreasing order in $FI_{sync280}$ data was observed up to t_{irr}=40 min and no significant difference was detected between t_{irr}=40 min and 60 min. On the other hand, the presence of fluorophoric groups expressing very minor intensities as FI_{sync} < 5.5 could also be encountered at λ_{emis} > 300 nm. Similar minor peaks around FI_{sync}=2-10 were also detected from solar photolytic (Figure 4.3), 0.50% Fe-TiO$_2$ (Figure 4.99), and 0.25% Fe-SynTiO$_2$ (Figure 4.123) solar photocatalytic treatment of *E. coli* in IsoT solution conditions. Moreover, beside very low $FI_{sync470}$ displaying changes in between 0.587-2.27, predominant $FI_{sync280}$ expressed variations in the range of 7.12-29.0 in the absence of humic matter in solution matrix.

NPOC expressed variations in the range of 2.38-6.76 mg/L during 60 min of irradiation period (Figure 4.148). NPOC content increased between initial (2.38 mg/L) and t=0 (3.00 mg/L), remained

nearly stable up to t_{irr}=20 min (2.95 mg/L) and followed by a sharp increase at t_{irr}=40 min (6.76 mg/L) due to release of organics from damaged and destructed *E. coli* cells. Subsequently, a decreasing trend was observed at 60 min of solar photocatalytic treatment period (5.23 mg/L). Despite, all UV-vis parameters displayed quite low values, due to absence and adsorptive removal of color forming structures of released organic matter in the solution, $Color_{436}$ and UV_{365} values of t=0 condition could be considered as negligible (<0.0005). On the other hand, as the most significant parameter, UV_{254} displayed variations in the range of 0.0228-0.0612 being the highest for initial condition.

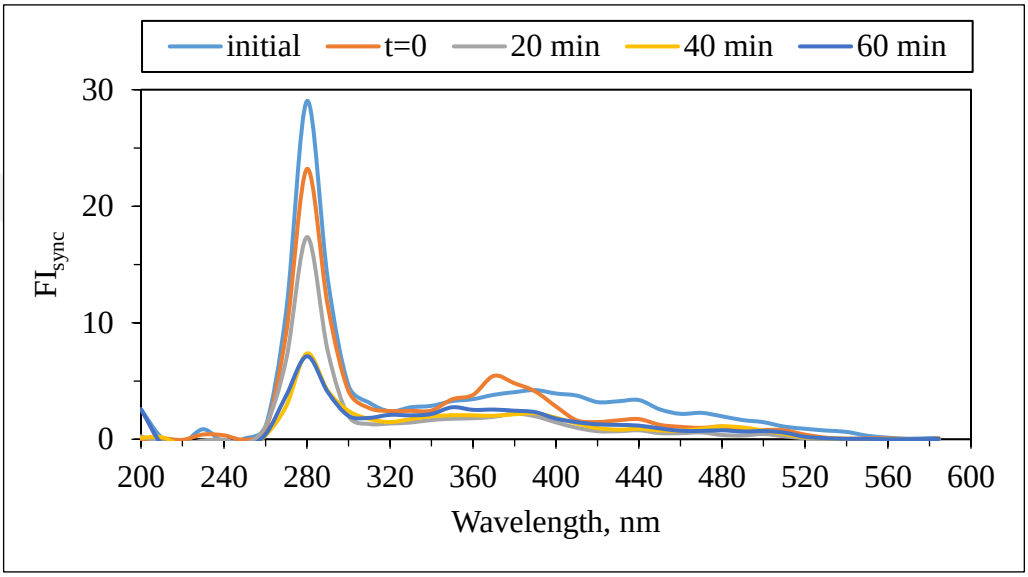

Figure 4.147. Synchronous scan fluorescence spectra of organic matter: Irradiation time dependent *E. coli* inactivation in IsoT solution upon 0.50% Fe-SynTiO$_2$ solar photocatalytic treatment.

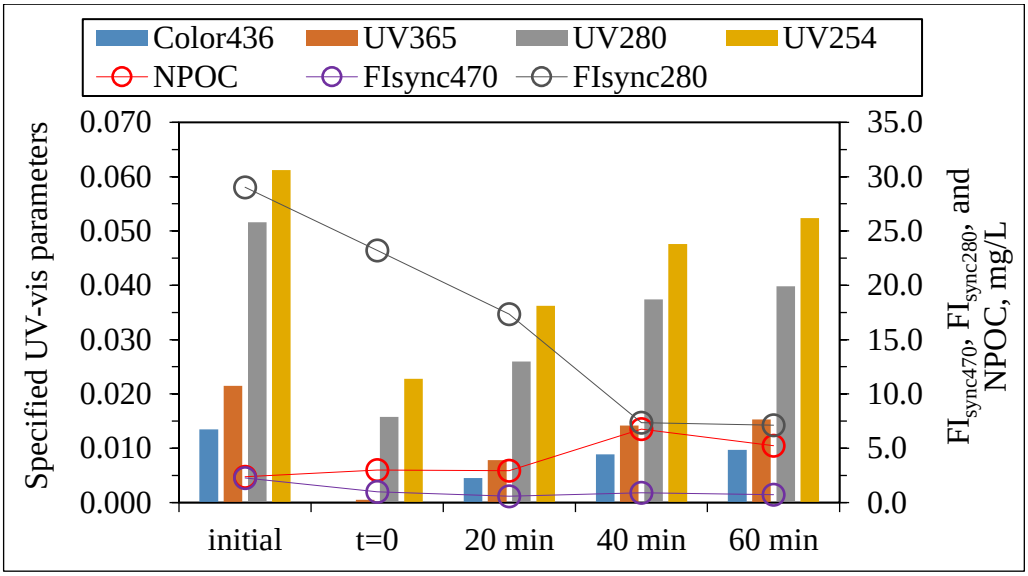

Figure 4.148. Specified UV-vis and fluroscence parameters of organic matter: Irradiation time dependent *E. coli* inactivation in IsoT solution upon 0.50% Fe-SynTiO$_2$ solar photocatalytic treatment.

Based on NPOC contents, $SCoA_{436}$, $SUVA_{365}$, $SUVA_{280}$, $SUVA_{254}$, $SFI_{sync470}$, and $SFI_{sync280}$ parameters were calculated and presented in Figure 4.149. $SUVA_{254}$ displayed variations in the range of 0.704-2.57 L/m mg during 0.50% Fe-SynTiO_2 solar photocatalytic treatment showing differences in both UV_{254} and NPOC removals. In accordance with negligible $Color_{436}$ and UV_{365} values of t=0 condition (Figure 4.148), $SCoA_{436}$ and $SUVA_{365}$ of t=0 solution were calculated as 0.000 and 0.017 L/m mg, respectively. Furthermore, $SFI_{sync470}$ displayed almost insignificant presence in the range of 0.132-0.954 however dominant $SFI_{sync280}$ expressed changes in between 1.09-12.2. The role of both Fe doping of TiO_2 and 0.50% Fe doping on different TiO_2 specimens as TiO_2 and SynTiO_2 could not be visualized under the specified experimental conditions.

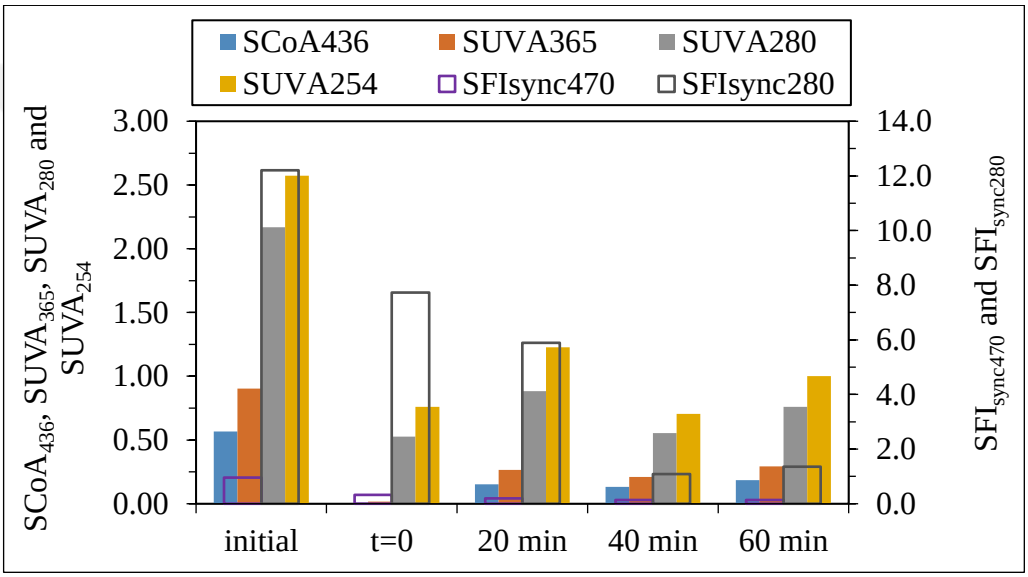

Figure 4.149. Specific UV-vis and fluroscence parameters of organic matter: Irradiation time dependent *E. coli* inactivation in IsoT solution upon 0.50% Fe-SynTiO_2 solar photocatalytic treatment.

Characteristic properties of organic matter under initial condition, upon t=0 condition, and at the end of 0.50% Fe-SynTiO_2 solar photocatalytic treatment of *E. coli* in IsoT solution for irradiation period of 60 min were presented in Table 4.57.

Table 4.57. Characteristic properties of organic matter present in 0.50% Fe-SynTiO_2 solar photocatalytic treatment of *E. coli* in IsoT solution.

Irradiation time, min	UV-vis Spectroscopic Parameters, cm^{-1}				NPOC, mg/L	$SUVA_{254}$, L/m mg	$FI_{sync280}$	$SFI_{sync280}$	FI
	$Color_{436}$	UV_{365}	UV_{280}	UV_{254}					
Initial	0.0135	0.0215	0.0516	0.0612	2.38	2.57	29.0	12.2	1.18
t=0	0.0000	0.0005	0.0158	0.0228	3.00	0.760	23.2	7.73	1.53
60 min	0.0097	0.0153	0.0398	0.0524	5.23	1.00	7.12	1.36	1.72

Upon irradiation period of 60 min of 0.50% Fe-SynTiO$_2$ solar photolytic treatment at which 4.15 log reduction of *E. coli* in IsoT solution was attained (Table 4.56), released organic matter expressed following UV-vis parameters (cm^{-1}); Color$_{436}$: 0.0097, UV$_{365}$: 0.0153, UV$_{280}$: 0.0398, UV$_{254}$: 0.0524, and NPOC as 5.23 mg/L. SUVA$_{254}$ at t_{irr}=60 min was calculated as 1.00 L/m mg represents that remaining organic matter could be considered having hydrophilic and aliphatic character (Edzwald et al., 1985). Due to degradation of released protein content, FI$_{sync280}$ displayed a decrease at the end of 60 min of irradiation period. SFI$_{sync280}$ also expressed a decrease at t_{irr}=60 min, in accordance with the increased NPOC result. On the other hand, FI$_{sync470}$ of initial, t=0, and t_{irr}=60 min conditions were detected as 2.27, 0.978, and 0.721, respectively. Based on FI$_{sync470}$ and NPOC data, SFI$_{sync470}$ values of initial, t=0, and t_{irr}=60 min samples were calculated as 0.954, 0.326, and 0.138, respectively. After 60 min of irradiation period, FI was calculated as 1.72 which could mostly be associated with the presence of microbially derived organic matter. Similar finding was also reported by Birben and colleagues for N-doped TiO$_2$ (Birben et al., 2017a).

EEM fluorescence contour plots of organic matter emerged and removed during irradiation time dependent *E. coli* inactivation in IsoT solution during 0.50% Fe-SynTiO$_2$ solar photocatalytic treatment were displayed in Figure 4.150.

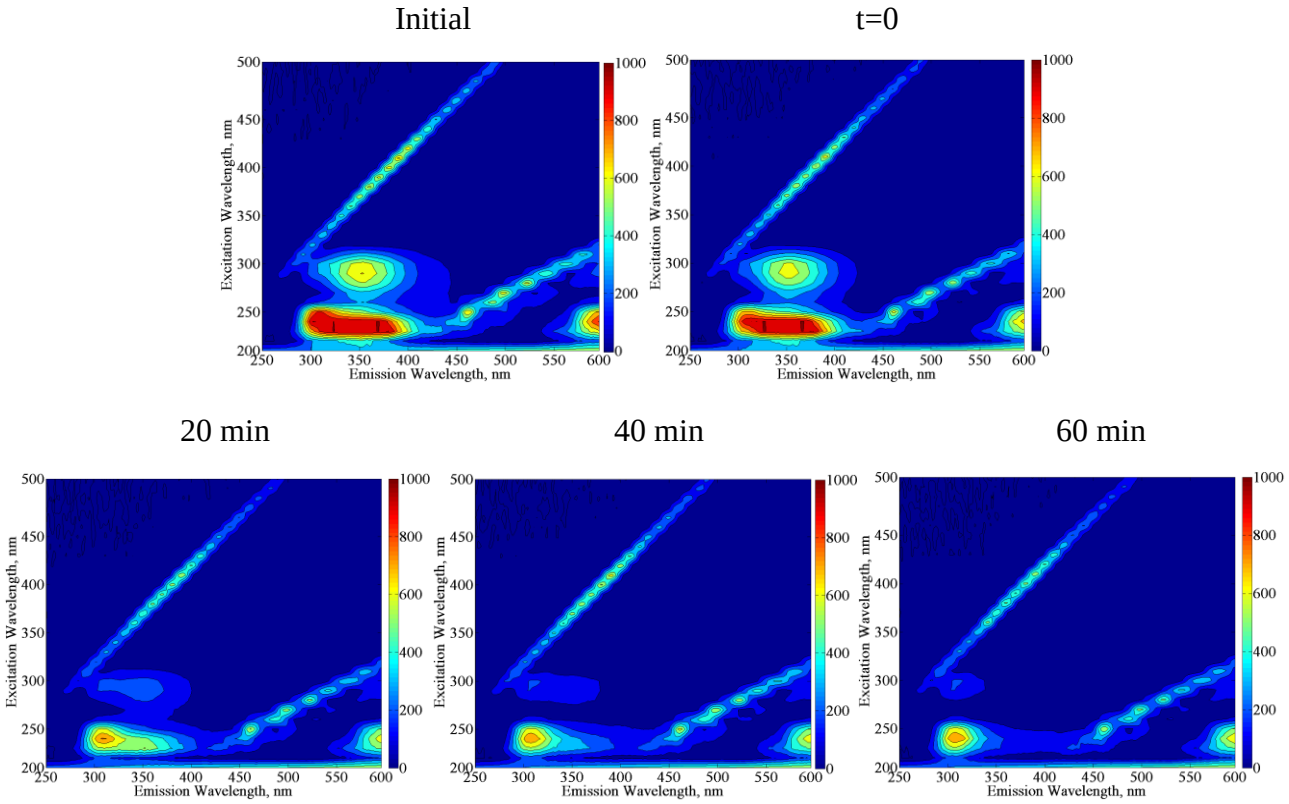

Figure 4.150. EEM fluorescence contour plots of organic matter: Irradiation time dependent *E. coli* inactivation in IsoT solution upon 0.50% Fe-SynTiO$_2$ solar photocatalytic treatment.

EEM fluorescence contour plots displayed the presence of Regions I, II and IV expressing that the fluorophores were mainly originated from microbial by-products and proteins under all irradiation conditions. Following further irradiation periods, released microbial by-products and proteins from *E. coli* cells showed a decreasing trend in accordance with the solar photocatalytic degradation of organic matter and reduction of *E. coli*. EEM contour plots displayed similarities with 0.25% Fe-SynTiO$_2$ (Figure 4.126) but displayed more intense results at 60 min of irradiation period. Significant irradiation time dependent decreasing trend of fluorescence intensities until t_{irr}=40 min especially at Region I and II could be roughly correlated with decreasing $FI_{sync280}$ data (Figures 4.147 and 4.148). Similar to minor decrease of $FI_{sync280}$ between t_{irr}=40 min and 60 min, EEM fluorescence contour plots displayed quite low decrease in intensities as well.

4.2.6.3. Mechanistic evaluation of *E. coli* inactivation upon 0.50% Fe-SynTiO$_2$ solar photocatalytic treatment in IsoT solution. From a general perspective, as inactivation products of 0.50% Fe-SynTiO$_2$ solar photocatalytic treatment of *E. coli* in IsoT solution total K, protein, and carbohydrate contents present in initial, t=0, and t_{irr}=60 min samples were presented in Table 4.58.

Table 4.58. Total K, protein, and carbohydrate contents of time dependent *E. coli* inactivation in IsoT solution upon 0.50% Fe-SynTiO$_2$ solar photocatalytic treatment.

0.50% Fe-SynTiO$_2$ solar photocatalytic treatment	*E. coli* in IsoT solution		
	Initial	t=0	60 min
Total K, mg/L	0.96	0.79	0.81
Protein, mg/L	0.683	1.95	5.85
Carbohydrate, mg/L	2.43	2.24	23.9

Total K content showed a similar trend with SynTiO$_2$ (Table 4.22) and 0.25% Fe-TiO$_2$ (Table 4.49) solar photocatalytic treatments. At t=0, total K expressed an immediate adsorptive removal as 17.7 %, and slightly increased at t_{irr}=60 min due to K^+ ion release from damaged bacteria cells.

E. coli in IsoT solution upon 0.50% Fe-TiO$_2$ solar photocatalytic treatment displayed increased protein and carbohydrate concentrations at the end of t_{irr}=60 min due to the release of organics from damaged bacteria cells. Carbohydrate content showed significant increase (23.9 mg/L) while protein concentration displayed a slight increase (5.85 mg/L). Protein concentrations were plotted against $FI_{sync280}$ and NPOC data separately and displayed strong correlations as R^2=1.00 with both parameters. Moreover, carbohydrate and NPOC concentrations displayed a strong correlation as R^2=0.95.

4.2.6.4. Organic matter formation and removal upon 0.50% Fe-SynTiO$_2$ solar photocatalytic treatment of *E. coli* in WM solution. UV-vis absorption and synchronous scan fluorescence spectra of organic matter in solution were presented in Figures 4.151 and 4.152. Irradiation time dependent absorbance changes displayed minor differences from each other in UV wavelength range of λ=200-500 nm in the slight presence of aromatic domains and color forming moieties (Color$_{436}$, UV$_{365}$, and UV$_{280}$) that should be measured in longer wavelengths. Irradiation period of 60 min condition expressed higher absorption at λ > 210 nm which could be due to released organic content from lysed *E. coli* cells and EPS surrounding cell wall (Birben et al., 2021a). However, all irradiation period conditions expressed higher absorption than previous solar photolytic and photocatalytic treatments carried out in the presence of WM solution (Figures 4.7, 4.31, 4.55, 4.79, 4.103, and 4.127).

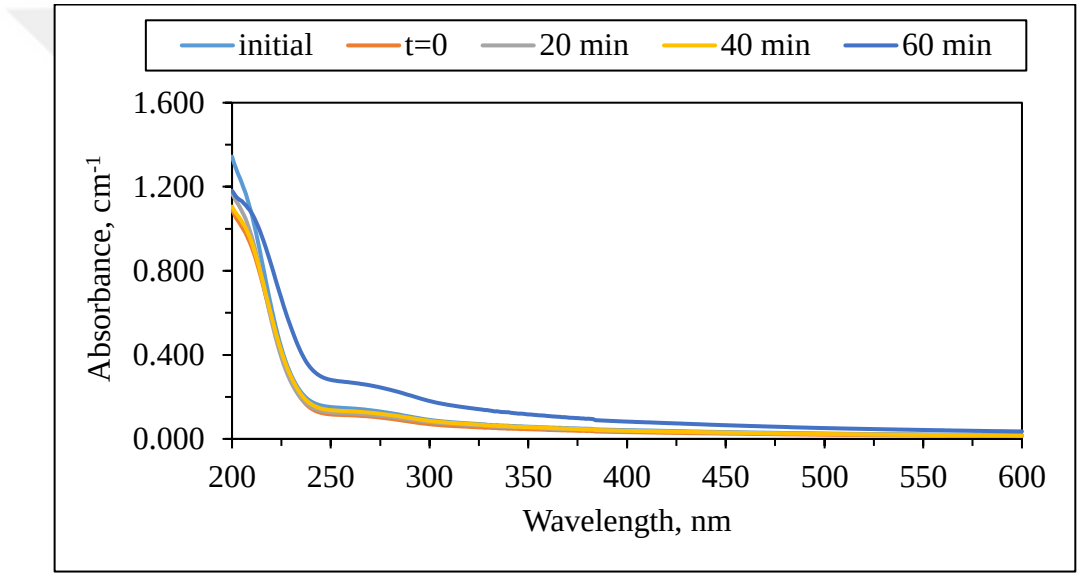

Figure 4.151. UV-vis absorption spectra of organic matter: Irradiation time dependent *E. coli* inactivation in WM solution upon 0.50% Fe-SynTiO$_2$ solar photocatalytic treatment.

Synchronous scan fluorescence spectra of all irradiation periods displayed a minor peak at λ_{emis}=280 nm however initial and t_{irr}=20 min samples expressed intense peaks at λ_{emis}=420 nm which could represent the release of organics from damaged bacteria (Figure 4.152). Despite lower intensities attained in 0.50% Fe-SynTiO$_2$ solar photocatalytic treatment of *E. coli* in WM solution, similar intense peaks at λ_{emis}=420 nm were also detected upon 0.25% Fe-SynTiO$_2$ solar photocatalytic treatment of *E. coli* in WM solution (Figure 4.128). An irradiation time dependent decreasing order in FI$_{sync}$ data at λ_{emis}=280 nm was noticeable. On the other hand, FI$_{sync470}$ expressed almost featureless presence in the range of 0.943-1.85 however due to existence of proteinaceous content originating from bacteria FI$_{sync280}$ expressed variations in between 14.6-22.1. In the absence of HA as a solution matrix component, predominant fluorophoric group was recognized as FI$_{sync280}$.

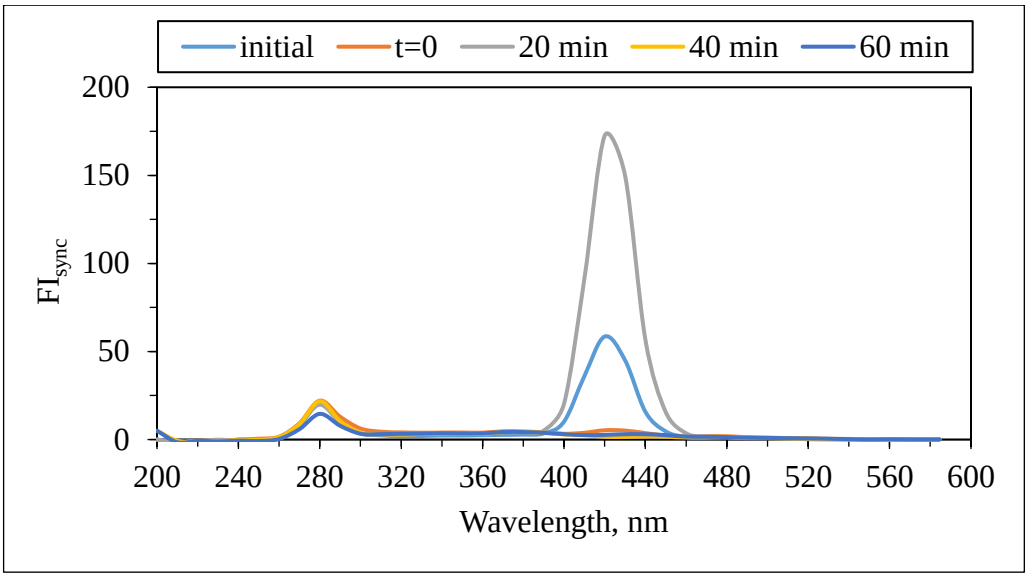

Figure 4.152. Synchronous scan fluorescence spectra of organic matter: Irradiation time dependent *E. coli* inactivation in WM solution upon 0.50% Fe-SynTiO$_2$ solar photocatalytic treatment.

All UV-vis parameters expressed low presence however obtained values were higher than prior solar photolytic (Figure 4.9) and photocatalytic treatments of *E. coli* in WM solution (Figures 4.33, 4.57, 4.81, 4.105 and 4.129). UV$_{254}$ which was the most significant parameter, displayed changes in the range of 0.1146-0.2748 being the highest for t_{irr}=60 min condition.

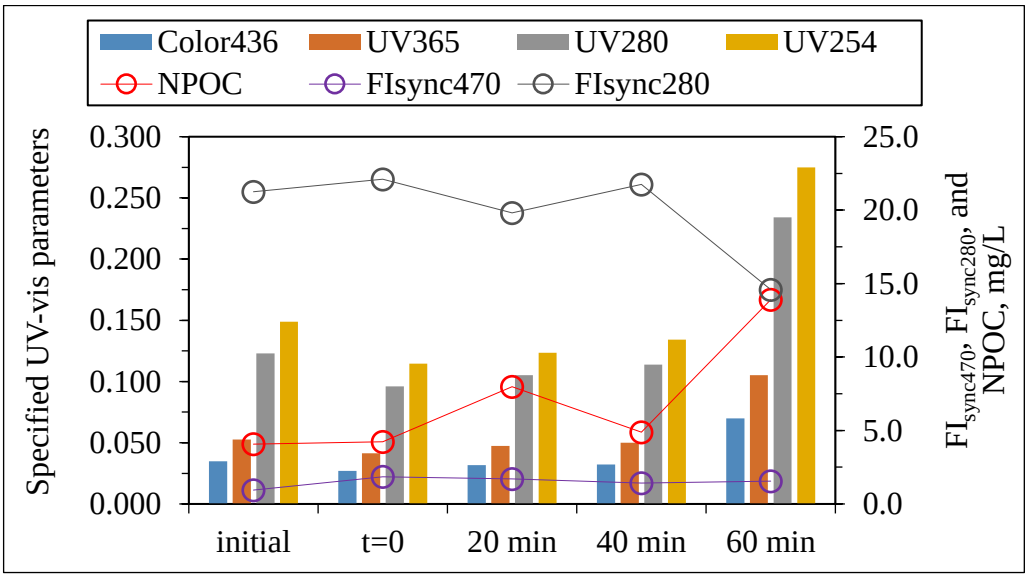

Figure 4.153. Specified UV-vis and fluroscence parameters of organic matter: Irradiation time dependent *E. coli* inactivation in WM solution upon 0.50% Fe-SynTiO$_2$ solar photocatalytic treatment.

NPOC content increased up to t_{irr}=20 min (4.07-7.97 mg/L) due to release of organics from damaged and destructed *E. coli* cells, then decreased up to t_{irr}=40 min (4.89 mg/L) and followed by a

sharp increase (13.9 mg/L) during the solar photocatalytic treatment. Significantly increased NPOC at t_{irr}=60 min could also be correlated with high UV_{254}, which is also a surrogate parameter of DOC.

Based on NPOC contents, $SCoA_{436}$, $SUVA_{365}$, $SUVA_{280}$, $SUVA_{254}$, $SFI_{sync470}$, and $SFI_{sync280}$ parameters were calculated and presented in Figure 4.154. $SUVA_{254}$ displayed changes in between 1.55-3.66 L/m mg during 0.50% Fe-SynTiO$_2$ solar photocatalytic treatment indicating differences in both UV_{254} and NPOC removals. Furthermore, $SFI_{sync470}$ displayed almost insignificant presence varied in between 0.112-0.436 however $SFI_{sync280}$ expressed variations in the range of 1.05-5.22. The key fluorophoric group was accepted as $SFI_{sync280}$.

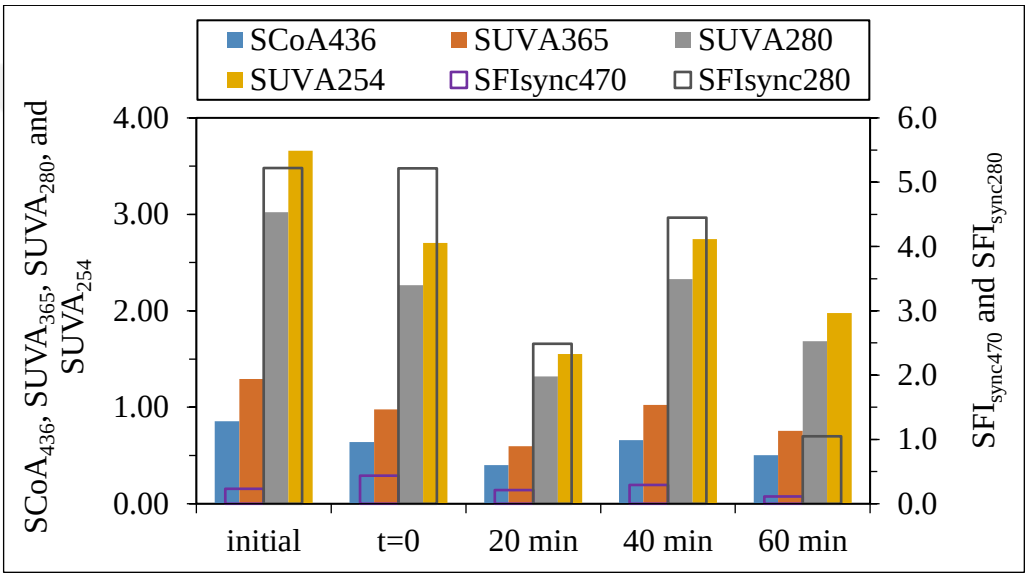

Figure 4.154. Specific UV-vis and fluroscence parameters of organic matter: Irradiation time dependent *E. coli* inactivation in WM solution upon 0.50% Fe-SynTiO$_2$ solar photocatalytic treatment.

Characteristic properties of organic matter under initial condition, upon introduction of 0.50% Fe-SynTiO$_2$ (t=0) and at the end of 0.50% Fe-SynTiO$_2$ solar photocatalytic treatment for irradiation period of 60 min were presented in Table 4.59.

Table 4.59. Characteristic properties of organic matter present in 0.50% Fe-SynTiO$_2$ solar photocatalytic treatment of *E. coli* in WM solution.

Irradiation time, min	UV-vis Spectroscopic Parameters, cm^{-1}				NPOC, mg/L	$SUVA_{254}$, L/m mg	$FI_{sync280}$	$SFI_{sync280}$	FI
	$Color_{436}$	UV_{365}	UV_{280}	UV_{254}					
Initial	0.0348	0.0526	0.1230	0.1489	4.07	3.66	21.3	5.22	1.60
t=0	0.0271	0.0415	0.0960	0.1146	4.24	2.70	22.1	5.21	1.49
60 min	0.0699	0.1052	0.2341	0.2748	13.9	1.98	14.6	1.05	1.45

Upon 60 min of solar photocatalytic treatment in the presence of 0.50% Fe-SynTiO$_2$ at which 3.65 log reduction of *E. coli* in WM solution was attained (Table 4.56), released organic matter expressed the following UV-vis parameters (cm^{-1}); Color$_{436}$: 0.0699, UV$_{365}$: 0.1052, UV$_{280}$: 0.2341, UV$_{254}$: 0.2748, and NPOC as 13.9 mg/L. SUVA$_{254}$ was calculated as 1.98 L/m mg at t_{irr}=60 min, indicating that samples solution displayed the presence of hydrophilic and aliphatic content (Edzwald et al., 1985). Owing to the degradation of released protein content from *E. coli* cells, FI$_{sync280}$ decreased at t_{irr}=60 min. SFI$_{sync280}$ displayed a decrease at t_{irr}=60 min in accordance with the increased NPOC result. On the other hand, FI$_{sync470}$ were detected as 0.943, 1.85, and 1.56 for initial, t=0, and t_{irr}=60 min conditions, respectively. According to FI$_{sync470}$ and NPOC results, SFI$_{sync470}$ of initial, t=0, and t_{irr}=60 min samples were calculated as 0.232, 0.436, and 0.112, respectively. After irradiation period of 60 min, FI was calculated as 1.45, which was in between the region of humic fluorophores and microbially derived fluorophores (Sen-Kavurmaci and Bekbolet, 2014). The reason could be attributed to degradation of released organic content from damaged bacteria.

EEM fluorescence contour plots of organic matter emerged and removed during irradiation time dependent *E. coli* inactivation in WM solution during 0.50% Fe-SynTiO$_2$ solar photocatalytic treatment were displayed in Figure 4.155.

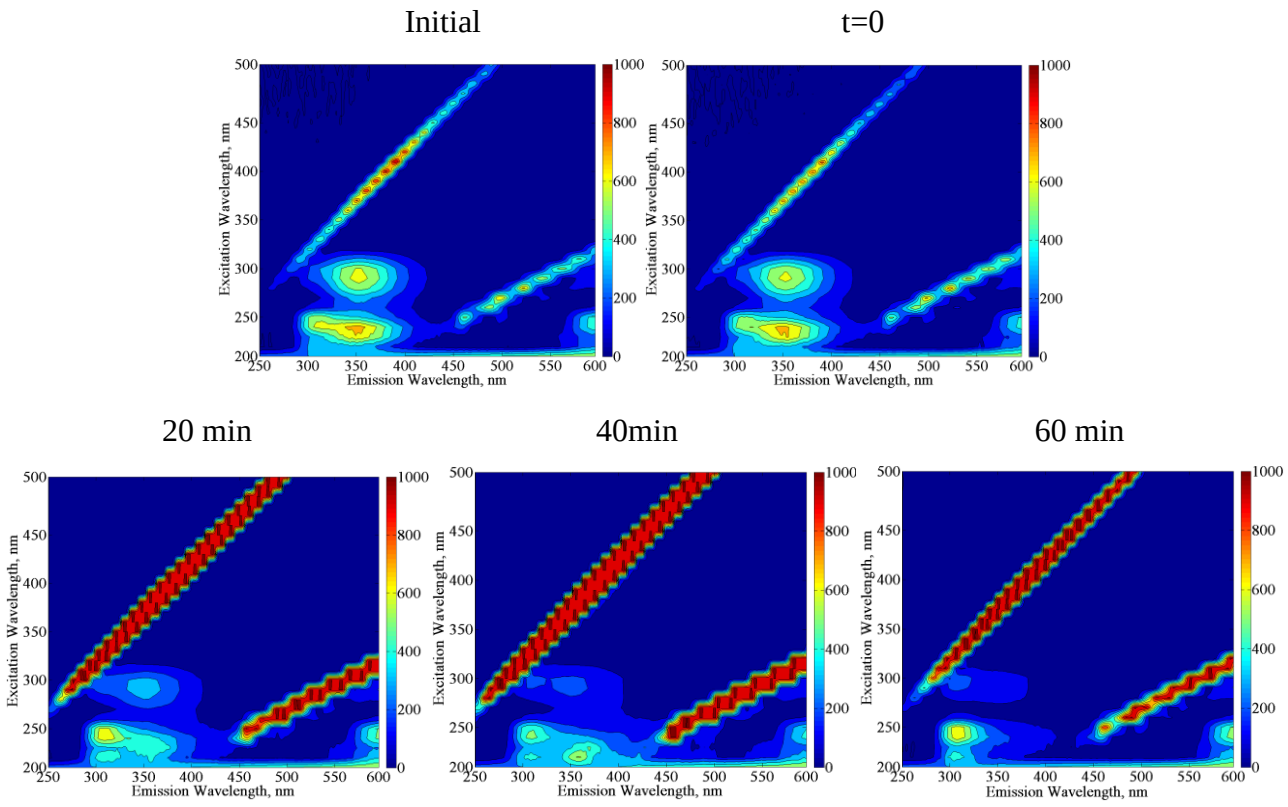

Figure 4.155. EEM fluorescence contour plots of organic matter: Irradiation time dependent *E. coli* inactivation in WM solution upon 0.50% Fe-SynTiO$_2$ solar photocatalytic treatment.

EEM fluorescence contour plots displayed the presence of Regions I, II and IV expressing that the fluorophores were mainly originated from microbial by-products and proteins under all irradiation conditions. Following further irradiation times released microbial by-products and proteins from *E. coli* cells showed a decreasing trend in accordance with the solar photocatalytic degradation of released organic matter and reduction of *E. coli*. However, fluorescence intensities of Region I which indicating the existence of aromatic proteins showed an increase at t_{irr}=60 min, similar to increase in UV_{280} which also represent the presence of aromatic proteins especially tyrosine and tryptophane containing ones (Edelhoch, 1948). The reason could be attributed to the release of proteins from damaged *E. coli* cells after 60 min of irradiation period. Moreover, EEM contour plots of 0.50% Fe-SynTiO_2 have lower intensities than 0.25% Fe-SynTiO_2 solar photocatalytic treatment of *E. coli* in WM solution (Figure 4.131).

4.2.6.5. Mechanistic evaluation of *E. coli* inactivation upon 0.50% Fe-SynTiO_2 solar photocatalytic treatment in WM solution. As *E. coli* inactivation products of 0.50% Fe-SynTiO_2 solar photocatalytic treatment of *E. coli* in WM solution, total K, protein, and carbohydrate contents present in initial, t=0, and t_{irr}=60 min samples were presented in Table 4.60.

Table 4.60. Total K, protein, and carbohydrate contents of time dependent *E. coli* inactivation in WM solution upon 0.50% Fe-SynTiO_2 solar photocatalytic treatment.

0.50% Fe-SynTiO_2 solar photocatalytic treatment	*E. coli* in WM solution		
	Initial	t=0	60 min
Total K, mg/L	4.32	3.91	3.89
Protein, mg/L	1.03	1.15	10.7
Carbohydrate, mg/L	1.80	2.06	47.0

Total K content showed a declining trend that is similar to measurements detected from SynTiO_2 (Table 4.24) and 0.25% Fe-SynTiO_2 (Table 4.51) solar photocatalytic treatment of *E. coli* in WM solution. An immediate adsorptive removal of total K as 9.5 % was calculated at t=0. Further decrease of total K concentration could be resulting from adsorption of released K^+ ions onto oppositely charged *E. coli* cell wall particles and photocatalyst surfaces.

E. coli in WM solution upon 0.50% Fe-SynTiO_2 solar photocatalytic treatment displayed increase in both protein and carbohydrate content at t_{irr}=60 min. Carbohydrate concentration showed a significant increase (1.08-47.0 mg/L) after 60 min of irradiation period, like *E. coli* in IsoT solution upon SynTiO_2 solar photocatalytic treatment (Table 4.22). Released Fe^{3+} concentration was detected

as 0.006 mg/L after an irradiation time of 60 min. The presence of NO_3^- in WM solution, use of Fe^{3+} doped photocatalyst, and the presence of glycoproteins founding in *E. coli* structure could be interference factors for carbohydrate determination process and the cause of detected high carbohydrate content (Martens and Frankenberger, 1990; Rao and Pattabiraman, 1989). $FI_{sync280}$ and protein contents displayed a strong correlation with each other as R^2=0.99. Moreover, both protein and carbohydrate concentrations showed a strong correlation with NPOC data as R^2=1.00.

4.2.6.6. Organic matter formation and removal upon 0.50% Fe-SynTiO$_2$ solar photocatalytic treatment of *E. coli* in HA solution. UV-vis absorption and synchronous scan fluorescence spectra of organic matter in solution were presented in Figures 4.156 and 4.157. Irradiation time dependent absorbance changes were similar to each other in UV wavelength range of λ=200-400 nm due to the presence of aromatic domains and color forming moieties ($Color_{436}$, UV_{365}, and UV_{280}). Upon introduction of bacteria into the solution (initial), due to exudating organic matter from *E. coli* following 0.45 μm filtration process increased absorbances were detected. UV-vis absorption spectra did not follow an irradiation time dependent decreasing order similar to previous sets of solar photocatalytic treatment of *E. coli* in HA solution in the presence of 0.25% Fe-TiO$_2$ (Figure 4.84) and 0.25% Fe-SynTiO$_2$ (Figure 4.132). It could be indicated that emergence and removal of light absorbing centers could be pronounced throughout 60 min of irradiation duration.

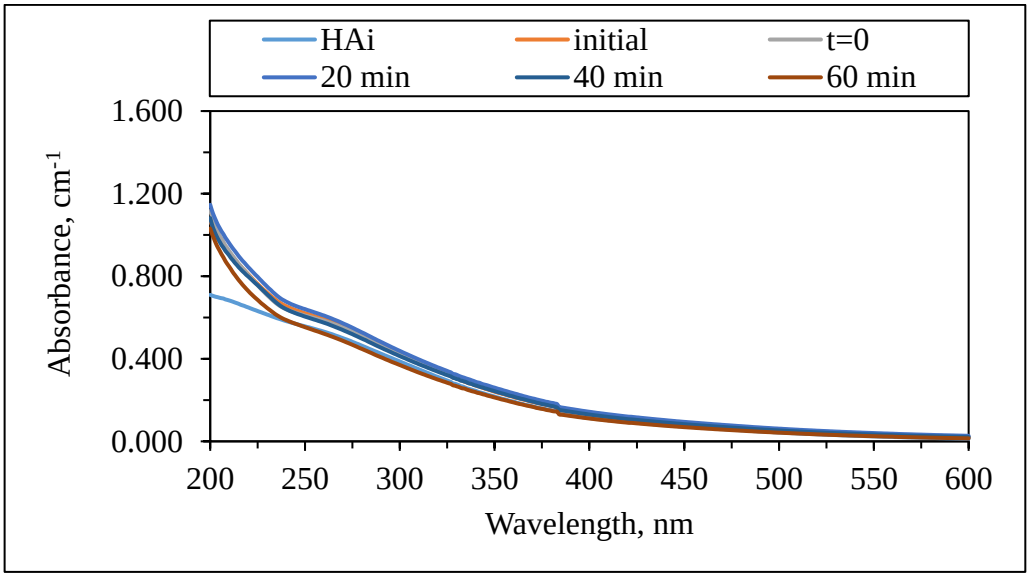

Figure 4.156. UV-vis absorption spectra of organic matter: Irradiation time dependent *E. coli* inactivation in HA solution upon 0.50% Fe-SynTiO$_2$ solar photocatalytic treatment.

Synchronous scan fluorescence spectra of emerged organic matter displayed intense peaks at λ_{emis}=390 nm and 470 nm indicating the presence of aromatic hydrocarbons in the solution as

expected (Dujmov and Sučević, 1990) (Figure 4.157). From a general perspective, after the fluorescence intensity increase at t=0 condition, an irradiation time dependent sequential decreasing order in FI_{sync} data was observed. The reason of increased FI_{sync} at t=0 could be attributed to immediate interaction of 0.50% Fe-SynTiO$_2$ with HA and *E. coli* cell surface causing mechanistic damage to bacteria cell wall and cytoplasmic organic matter release.

On the other hand, $FI_{sync470}$ and $FI_{sync280}$ displayed changes in the range of 41.8-81.9 and 1.02-13.5, respectively (Figure 4.158). Due to the presence of HA solution as reaction medium, $FI_{sync470}$ were recognized as the predominant fluorophoric group, as expected. $FI_{sync280}$ of HA_i and initial conditions could not be detected however at t=0 condition, $FI_{sync280}$ increased to 11.8 representing the presence of proteinaceous content in the sample, which also support the occurrence of mechanistic bacteria cell wall damage of in the presence of photocatalyst specimen.

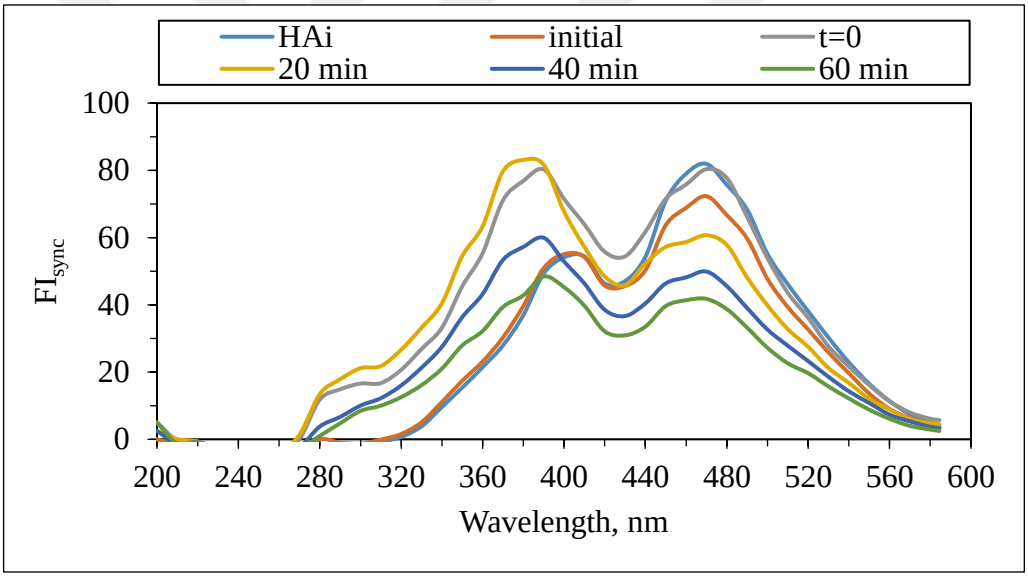

Figure 4.157. Synchronous scan fluorescence spectra of organic matter: Irradiation time dependent *E. coli* inactivation in HA solution upon 0.50% Fe-SynTiO$_2$ solar photocatalytic treatment.

Along with the presence of HA solution, NPOC expressed variations in the range of 5.76-14.9 mg/L (Figure 4.158). NPOC content showed an increasing trend (5.76-14.9) throughout the solar photocatalytic treatment due to release of organics from damaged and destructed *E. coli* cells, that consistent with gradually decreased *E. coli* counts (Figure 4.145).

Specified UV-vis parameters expressed high presence due to use of HA solution (Figure 4.158). As the most significant parameter, UV_{254} showed changes in between 0.5406-0.6281, being the highest for irradiation period of 20 min and the lowest for 60 min irradiation period conditions. All

other specified UV-vis parameters followed a similar trend with UV_{254} which could be due to release of cytoplasmic organic content at t_{irr}=20 min and its degradation occurred during further irradiation periods.

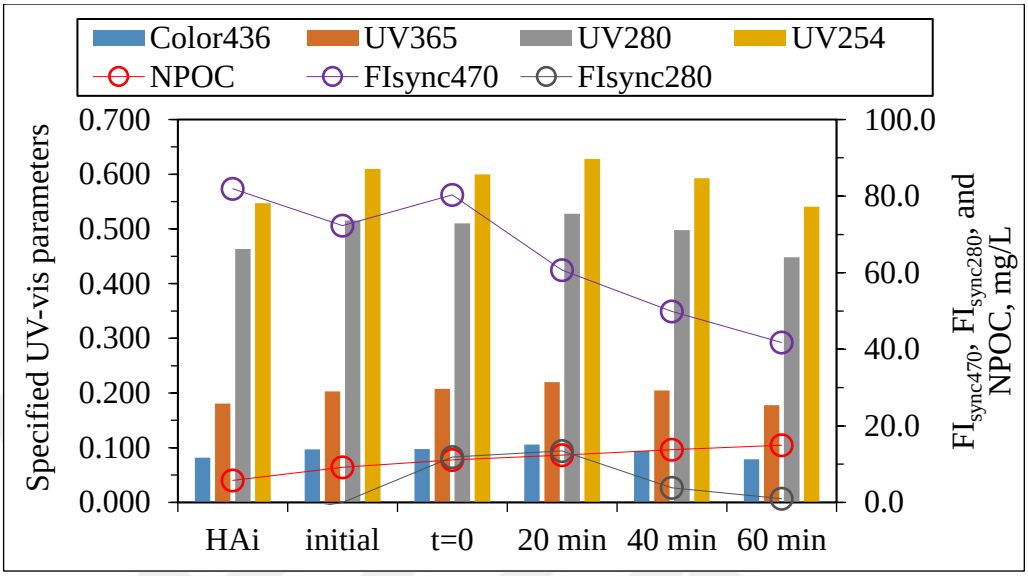

Figure 4.158. Specified UV-vis and fluroscence parameters of organic matter: Irradiation time dependent *E. coli* inactivation in HA solution upon 0.50% Fe-SynTiO$_2$ solar photocatalytic treatment.

Based on NPOC contents, $SCoA_{436}$, $SUVA_{365}$, $SUVA_{280}$, $SUVA_{254}$, $SFI_{sync470}$, and $SFI_{sync280}$ parameters were calculated and presented in Figure 4.159. $SUVA_{254}$ displayed a decreasing trend (9.50-3.62 L/m mg) during solar photocatalytic treatment indicating differences in both UV_{254} and NPOC removals.

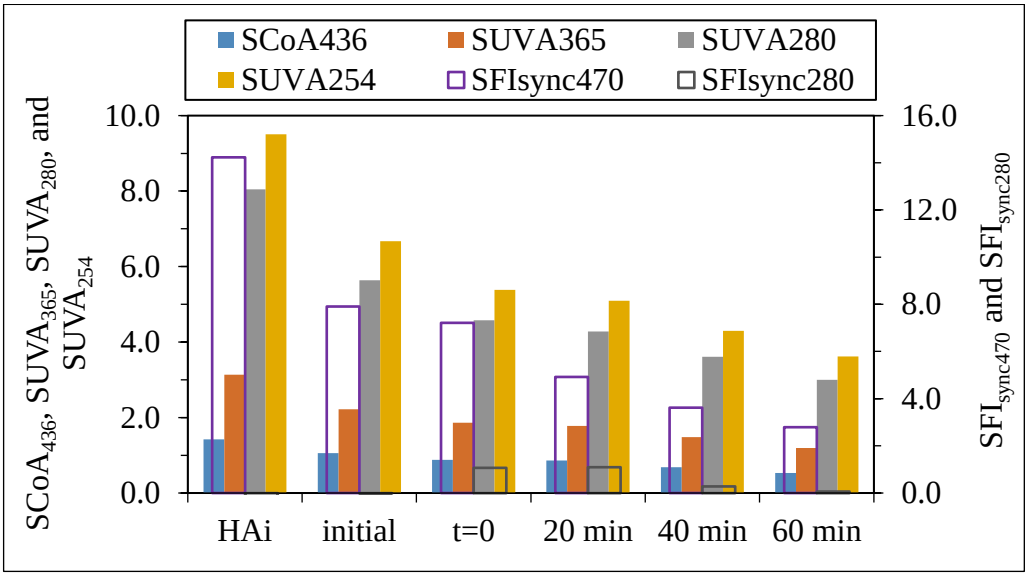

Figure 4.159. Specific UV-vis and fluroscence parameters of organic matter: Irradiation time dependent *E. coli* inactivation in HA solution upon 0.50% Fe-SynTiO$_2$ solar photocatalytic treatment.

Furthermore, despite dominant $SFI_{sync470}$ displaying changes in between 2.80-14.2, almost insignificant $SFI_{sync280}$ expressed variations in the range of 0.0684-1.09. $SFI_{sync470}$ was accepted as the main fluorophoric group due to its remarkable presence in comparison to $SFI_{sync280}$. Moreover, according to undetected $FI_{sync280}$ of HA_i and initial conditions, $SFI_{sync280}$ could not be detected either.

For simplicity purposes, based on the irradiation time dependent variations in UV-vis and fluorescence spectroscopic properties along with NPOC data, characteristic properties of organic matter under initial condition, upon introduction of 0.50% Fe-SynTiO$_2$ (t=0) and at the end of 0.50% Fe-SynTiO$_2$ solar photocatalytic for irradiation period of 60 min were presented in Table 4.61.

Table 4.61. Characteristic properties of organic matter present in 0.50% Fe-SynTiO$_2$ solar photocatalytic treatment of *E. coli* in HA solution.

Irradiation time, min	UV-vis Spectroscopic Parameters, cm^{-1}				NPOC, mg/L	$SUVA_{254}$, L/m mg	$FI_{sync470}$	$SFI_{sync470}$	FI
	$Color_{436}$	UV_{365}	UV_{280}	UV_{254}					
Initial	0.0970	0.2027	0.5154	0.6099	9.15	6.67	72.3	7.91	1.03
t=0	0.0974	0.2074	0.5102	0.5998	11.1	5.38	80.4	7.21	1.04
60 min	0.0787	0.1777	0.4479	0.5406	14.9	3.62	41.8	2.80	1.08

Upon t_{irr}=60 min of solar photocatalytic treatment of *E coli* in HA solution at which 3.71 log *E. coli* reduction was achieved (Table 4.56), released organic matter expressed the following UV-vis parameters (cm^{-1}); $Color_{436}$: 0.0787, UV_{365}: 0.1777, UV_{280}: 0.4479, UV_{254}: 0.5406, and NPOC as 14.9 mg/L. Similar UV-vis spectroscopic parameter results were detected from initial and t=0 conditions revealing insignificant surface interactions. After irradiation period of 60 min, $SUVA_{254}$ was calculated as 3.62 L/m mg representing that the remaining organic matter could be considered having hydrophilic and aliphatic character, indicating the occurrence of humic content degradation (Edzwald et al., 1985).

$FI_{sync470}$ displayed a decrease at the end of t_{irr}=60 min due to degradation of organic matter content. In accordance with the increased NPOC, $SFI_{sync470}$ displayed a decrease at t_{irr}=60 min, as well. Moreover, $FI_{sync280}$ measurements of initial, t=0 and t_{irr}=60 min samples were detected as 0.00, 11.8, and 1.02, respectively. Similar to data of $FI_{sync470,}$ $FI_{sync280}$ demonstrated a decreasing trend between t=0 and t_{irr}=60 min conditions owing to degradation of released protein content. $SFI_{sync280}$ of initial, t=0, and t_{irr}=60 min conditions were calculated as $\leq$ 0.001, 1.06, and 0.0684, respectively. Moreover, FI was calculated as 1.08 at 60 min of irradiation period, representing the presence of fluorophores originating from used HA solution as an aqueous medium in the solar photocatalytic treatment, as expected.

In a similar manner to the UV-vis absorbance and synchronous scan fluorescence analyses, irradiation time dependent EEM fluorescence contour plots of organic matter emerged and removed during *E. coli* inactivation in HA solution upon 0.50% Fe-SynTiO$_2$ solar photocatalytic treatment were also followed and displayed in Figure 4.160.

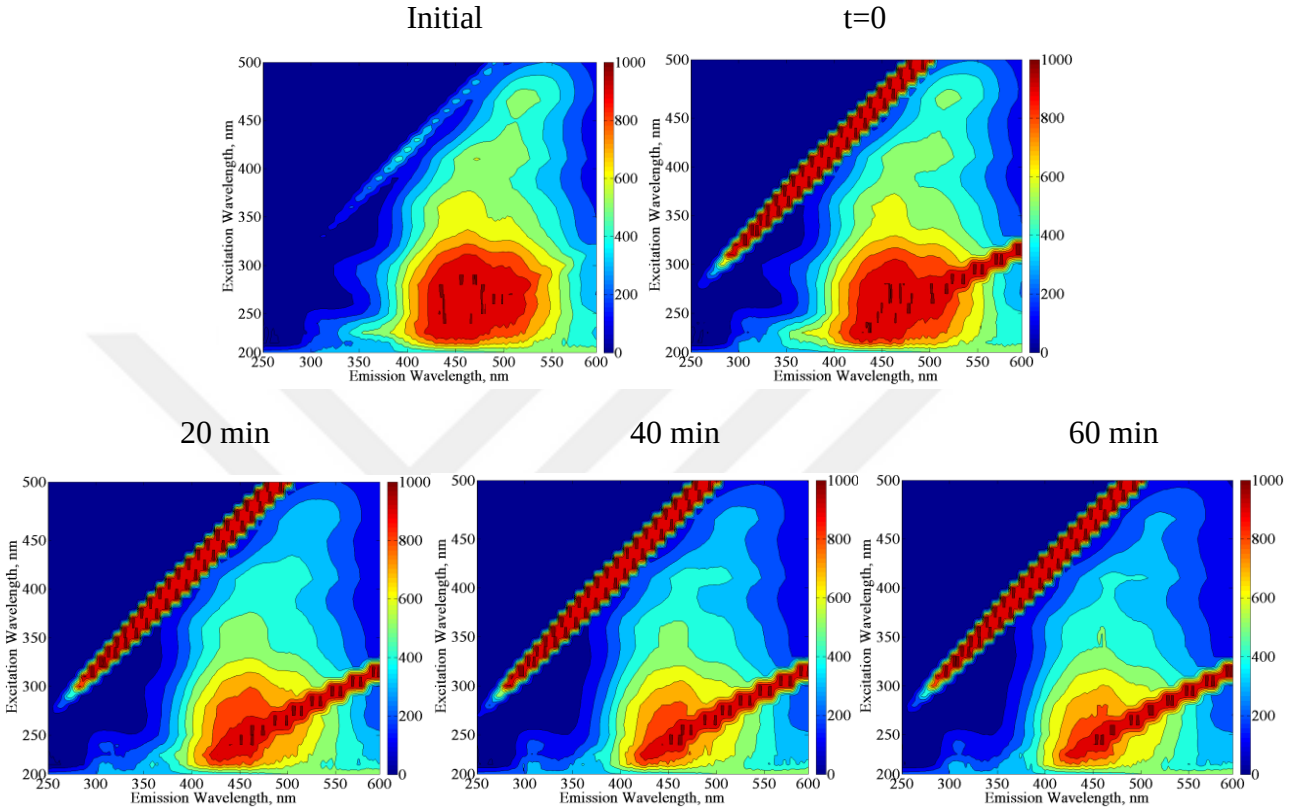

Figure 4.160. EEM fluorescence contour plots of organic matter: Irradiation time dependent *E. coli* inactivation in HA solution upon 0.50% Fe-SynTiO$_2$ solar photocatalytic treatment.

EEM fluorescence contour plots of 0.50% Fe-SynTiO$_2$ solar photocatalytic treatment of *E. coli* in the presence of HA solution displayed the presence of Regions III, and V indicating that the fluorophores were mainly originated from fulvic-like and humic-like substances. Both humic-like and fulvic-like fluorophore intensities slightly decreased throughout the 60 min of treatment period. It could be concluded that 0.50% Fe-SynTiO$_2$ has a selectivity towards bacteria in contradiction to TiO$_2$ having lower bacteria LRV (LRV as 1.08 for TiO$_2$; LRV as 3.71 for 0.50% Fe-SynTiO$_2$) (Tables 4.11 and 4.56) and less intense EEM contour plots (Figure 4.40).

4.2.6.7. Mechanistic evaluation of *E. coli* inactivation upon 0.50% Fe-SynTiO$_2$ solar photocatalytic treatment in HA solution. As bacteria inactivation products of 0.50% Fe-SynTiO$_2$ solar photocatalytic treatment of *E. coli* in HA solution, total K, protein, and carbohydrate contents present in initial, t=0, and t_{irr}=60 min solutions, were presented in Table 4.62.

Table 4.62. Total K, protein, and carbohydrate contents of time dependent *E. coli* inactivation in HA solution upon 0.50% Fe-SynTiO$_2$ solar photocatalytic treatment.

0.50% Fe-SynTiO$_2$ solar photocatalytic treatment	*E. coli* and HA		
	Initial	t=0	60 min
Total K, mg/L	0.51	0.55	0.61
Protein, mg/L	10.8	9.67	16.2
Carbohydrate, mg/L	3.49	3.16	4.14

Total K content showed an increasing trend during 60 min of solar light exposure which was also detected from SynTiO$_2$ solar photocatalytic treatment of *E. coli* in HA solution (Table 4.26). Release of K^+ ions from damaged bacteria cells caused increased total K concentration at the end of 60 min irradiation period.

E. coli in HA solution upon solar photocatalytic treatment displayed an increase in both protein and carbohydrate content at t_{irr}=60 min. Protein concentration (10.8-16.2 mg/L) showed a higher increase than carbohydrate content (3.49-4.14 mg/L). Similar pattern was also detected from solar photocatalytic treatment with 0.25% Fe-TiO$_2$ in the presence of HA solution (Table 4.35). Increase in protein concentrations displayed a strong correlation with NPOC data as R^2=0.77 however, increased carbohydrate and NPOC contents showed a moderate correlation with each other as R^2=0.61. On the other hand, no correlation was detected between protein concentrations and $FI_{sync280}$.

4.2.6.8. Organic matter formation and removal upon 0.50% Fe-SynTiO$_2$ solar photocatalytic treatment of *E. coli* in "HA and WM" solution. UV-vis absorption and synchronous scan fluorescence spectra of organic matter in solution were presented in Figures 4.161 and 4.162, respectively. Irradiation time dependent absorbance changes were different from each other in UV wavelength range of λ=200-350 nm, except HA_i solution, due to the presence of aromatic domains and color forming moieties ($Color_{436}$, UV_{365}, and UV_{280}). The reason of different absorbance characteristics of HA_i solution at λ < 240 nm could be attributed to the absence of NO_3^- containing WM solution in the aqueous medium.

Contrary to previous *E. coli* inactivation sets of solar photolytic (Figure 4.17) and photocatalytic treatments in the presence of "HA and WM" solution (Figures 4.41, 4.65, 4.89, 4.113, and 4.137), with the use of 0.50% Fe-SynTiO$_2$ a sequential irradiation time dependent increasing trend was observed in UV-vis absorption spectra. The reason could be attributed to continuing cytoplasmic

organic content release from damaged *E. coli* cells, also in accordance with low bacteria LRV as 2.23 (Table 4.26).

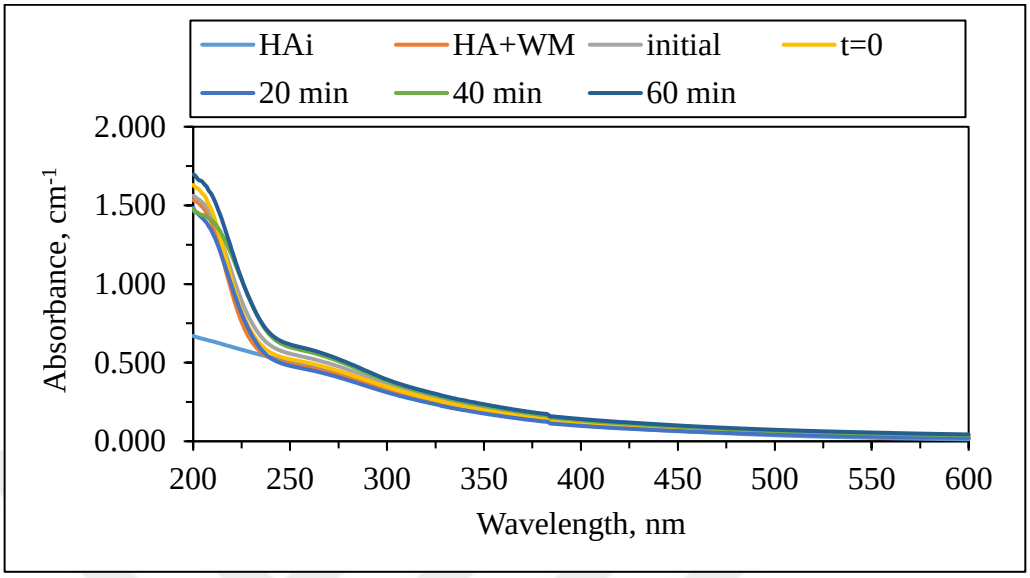

Figure 4.161. UV-vis absorption spectra of organic matter: Irradiation time dependent *E. coli* inactivation in "HA and WM" solution upon 0.50% Fe-SynTiO$_2$ solar photocatalytic treatment.

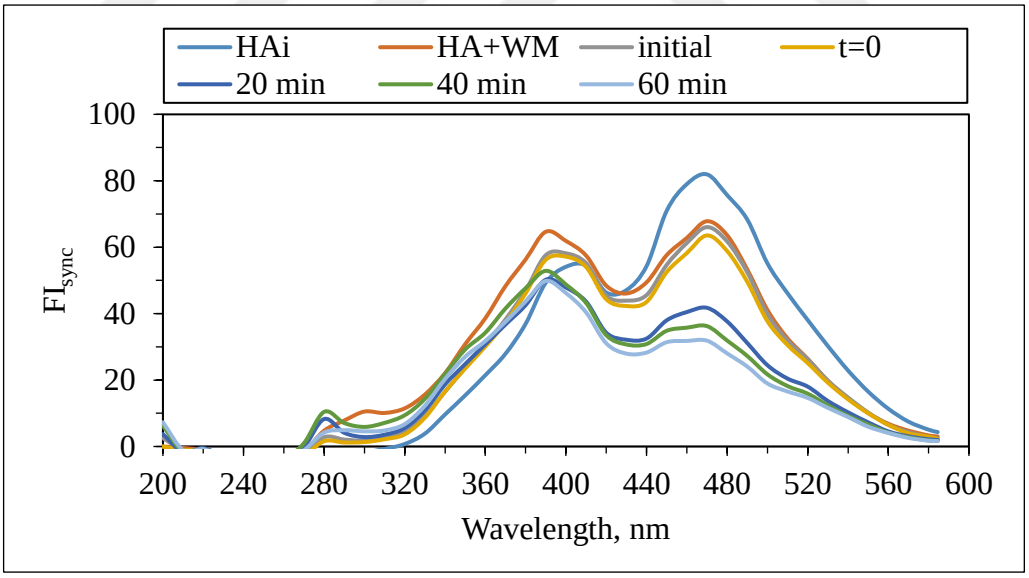

Figure 4.162. Synchronous scan fluorescence spectra of organic matter: Irradiation time dependent *E. coli* inactivation in "HA and WM" solution upon 0.50% Fe-SynTiO$_2$ solar photocatalytic treatment.

Synchronous scan fluorescence spectra of emerged organic matter displayed intense peaks at λ_{emis}=390 nm and 470 nm (Figure 4.162) in the presence of humic content, as excepted. A drastic decrease at λ_{emis}=390 nm was detected between t=0 and t_{irr}=20 min conditions representing that the degradation of humic content in the solution. At t_{irr}=20 min and 40 min conditions, minor peaks at

λ_{emis}=280 nm were detected expressing release of protein content from bacteria. Moreover, similar to solar photolytic (Figure 4.18) and SynTiO$_2$ solar photocatalytic inactivation of *E. coli* in "HA and WM" solution (Figure 4.66), both in "HA and WM" solution and after addition of bacteria into the reaction solution (initial and t=0 conditions), increased fluorescence intensities were observed relative to sole HA$_i$ condition at λ_{emis} < 410 nm. From a general perspective, an irradiation time dependent decreasing order in FI$_{sync}$ data was observed.

On the other hand, FI$_{sync470}$ and FI$_{sync280}$ displayed changes in the range of 31.9-81.9 and 1.60-10.4, respectively (Figure 4.163). Due to the use of HA solution as an aqueous matrix component FI$_{sync470}$ displayed dominant presence and accepted as the key fluorophoric group. FI$_{sync280}$ of HA$_i$ could not be detected however FI$_{sync280}$ of "HA and WM" solution was detected as 4.76.

From a general perspective, NPOC contents expressed variations in the range of 5.76-13.4 mg/L (Figure 4.163). NPOC content increased between HA$_i$ solution (5.76 mg/L) and t=0 condition (7.10 mg/L) and decreased up to t_{irr}=20 min (6.33 mg/L) followed by a sharp increase until t_{irr}=40 min (13.4 mg/L) due to the release of organics from damaged and destructed *E. coli* cells. Subsequently a decreasing trend (11.5 mg/L) was observed during solar photocatalytic treatment.

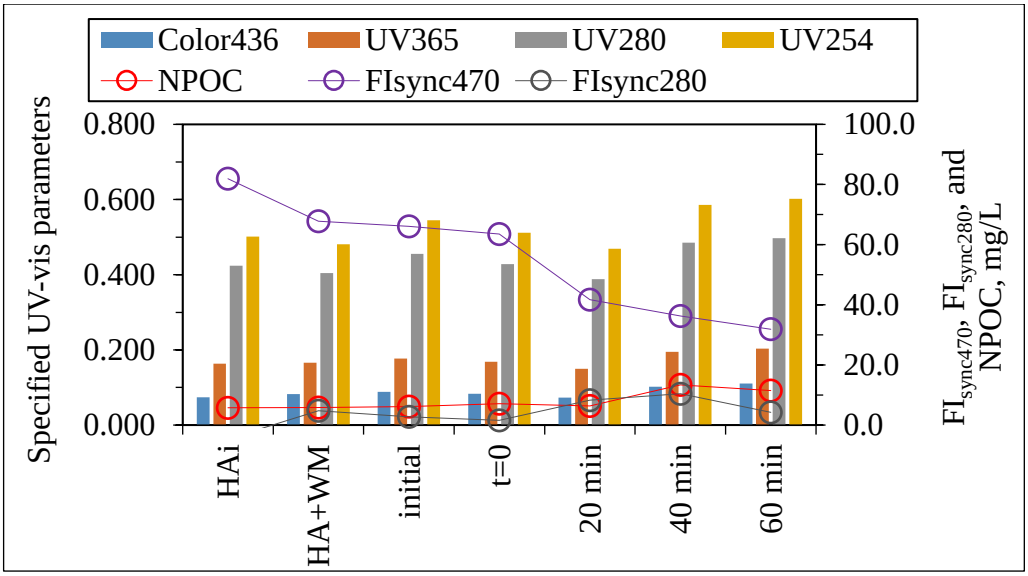

Figure 4.163. Specified UV-vis and fluroscence parameters of organic matter: Irradiation time dependent *E. coli* inactivation in "HA and WM" solution upon 0.50% Fe-SynTiO$_2$ solar photocatalytic treatment.

In the presence of HA solution as a reaction matrix component, all specified UV-vis parameters and FI$_{sync470}$ displayed significant presence. As the most evident parameter UV$_{254}$ expressed

variations in between 0.4690-0.6023, being the lowest for t_{irr}=20 min and the highest for t_{irr}=60 min conditions with a remarkable increase at t_{irr}=40 min (0.5855). Moreover, detected increase in all specified UV-vis parameters could be roughly correlated with decreased bacteria counts between irradiation period of 20 min and 40 min (8.17E+04 CFU/mL for t_{irr}=20 min; 1.01E+04 CFU/mL for t_{irr}=40 min) (Figure 4.145). It could be indicated that with the destruction of bacteria, release of cytoplasmic organic content could be enhanced and caused an increase in specified UV-vis parameters and also $FI_{sync280}$. Moreover, according to inverse relation between $FI_{sync280}$ and $FI_{sync470}$ at t_{irr}=40 min, it could be indicated that the released organic content from bacteria could probably had proteinaceous characteristics.

Based on NPOC contents, all specific UV-vis and fluorescence parameters as, $SCoA_{436}$, $SUVA_{365}$, $SUVA_{280}$, $SUVA_{254}$, $SFI_{sync470}$, and $SFI_{sync280}$ parameters were calculated and presented in Figure 4.164. As the most significant parameter, $SUVA_{254}$ displayed variations in between 4.38-8.87 L/m mg during 0.50% Fe-SynTiO$_2$ solar photocatalytic treatment expressing differences in both UV_{254} and NPOC removals.

Furthermore, despite dominant $SFI_{sync470}$ displaying changes in between 2.71-14.2, quite low $SFI_{sync280}$ expressed variations in the range of 0.225-1.31. Along with the use of HA solution as an aqueous medium component, $SFI_{sync470}$ was accepted as the main fluorophoric group. According to undetected $FI_{sync280}$ of HA_i solution, its $SFI_{sync280}$ could not be calculated either.

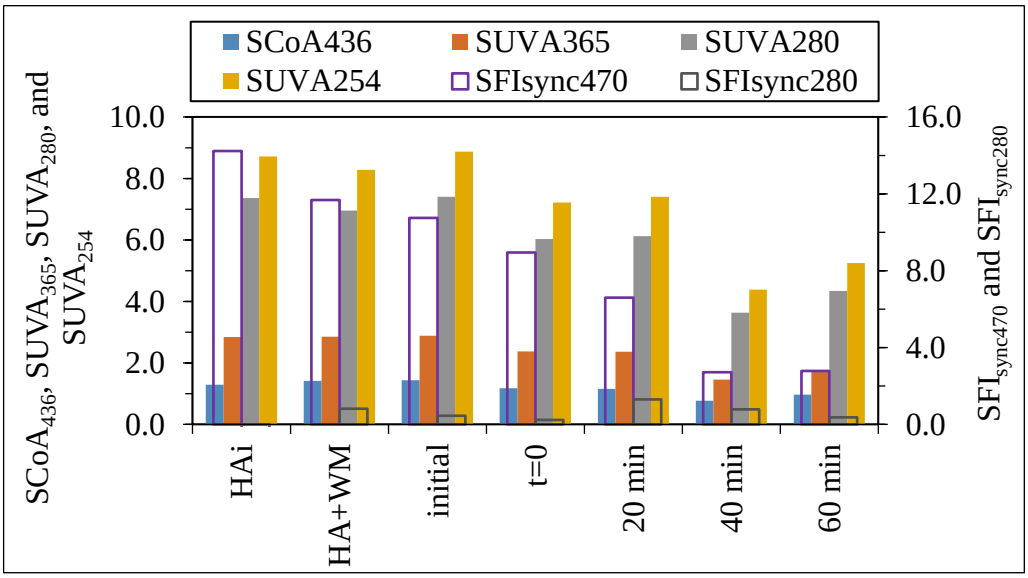

Figure 4.164. Specific UV-vis and fluroscence parameters of organic matter: Irradiation time dependent *E. coli* inactivation in "HA and WM" solution upon 0.50% Fe-SynTiO$_2$ solar photocatalytic treatment.

For comparative evaluation purposes, characteristic properties of organic matter under initial condition, upon introduction of 0.50% Fe-SynTiO$_2$ (t=0), and at the end of 0.50% Fe-SynTiO$_2$ solar photocatalytic inactivation of *E. coli* in "HA and WM" solution for 60 min of solar light exposure were presented in Table 4.63.

Table 4.63. Characteristic properties of organic matter present in 0.50% Fe-SynTiO$_2$ solar photocatalytic treatment of *E. coli* in "HA and WM" solution.

Irradiation time, min	UV-vis Spectroscopic Parameters, cm^{-1}				NPOC, mg/L	SUVA$_{254}$, L/m mg	FI$_{sync470}$	SFI$_{sync470}$	FI
	Color$_{436}$	UV$_{365}$	UV$_{280}$	UV$_{254}$					
Initial	0.0881	0.1772	0.4551	0.5451	6.15	8.87	66.1	10.7	1.15
t=0	0.0835	0.1682	0.4280	0.5119	7.10	7.21	63.6	8.95	1.16
60 min	0.1108	0.2030	0.4973	0.6023	11.5	5.25	31.9	2.78	1.25

Upon t_{irr}=60 min of solar photocatalytic treatment of *E coli* in "HA and WM" solution, at which 2.23 log *E. coli* reduction was achieved (Table 4.56), released organic matter expressed the following UV-vis parameters (cm^{-1}); Color$_{436}$: 0.1108, UV$_{365}$: 0.2030, UV$_{280}$: 0.4973, UV$_{254}$: 0.6023, and NPOC as 11.5 mg/L. With respect to increased UV-vis parameters and NPOC content at t_{irr}=60 min, it could be indicated that cytoplasmic organic content release generated throughout the irradiation period and its complete removal could not be achieved in determined irradiation period.

SUVA$_{254}$ of initial, t=0, and t_{irr}=60 min conditions were calculated as 8.87, 7.21, and 5.25 L/m mg, respectively. Calculated SUVA$_{254}$ values were > 4, therefore; it could be indicated that besides a decrease of SUVA$_{254}$ at t_{irr}=60 min, which revealing the degradation of aromatic organic matter in solution, all samples expressed hydrophobic and aromatic characteristics (Edzwald et al., 1985).

FI$_{sync470}$ decreased at t_{irr}=60 min due to degradation of organic content originating from damaged *E. coli* cells and HA containing organic matrix. At the end of t_{irr}=60 min, calculated SFI$_{sync470}$ showed a decrease in accordance with increased NPOC. On the other hand, FI$_{sync280}$ of initial, t=0 and t_{irr}=60 min samples were detected as 2.79, 1.60, and 4.20, respectively. Different from FI$_{sync470}$, FI$_{sync280}$ demonstrated an increase at the end of 60 min irradiation period due to released protein content from bacteria. Furthermore, SFI$_{sync280}$ values of initial, t=0, and t_{irr}=60 min conditions were calculated as 0.454, 0.225, and 0.366, respectively. FI at 60 min irradiation period was calculated as 1.25 indicating the presence of fluorophores coming from present humic matter in solution, as expected.

In accordance with the UV-vis absorbance and synchronous scan fluorescence spectroscopic analyses, EEM fluorescence contour plots of organic matter during irradiation time dependent *E. coli*

inactivation in “HA and WM” solution under 0.50% Fe-SynTiO$_2$ solar photocatalytic treatment conditions were also followed and illustrated in Figure 4.165. It should be noted that both emergence and removal mechanisms were prevailing under the specified conditions.

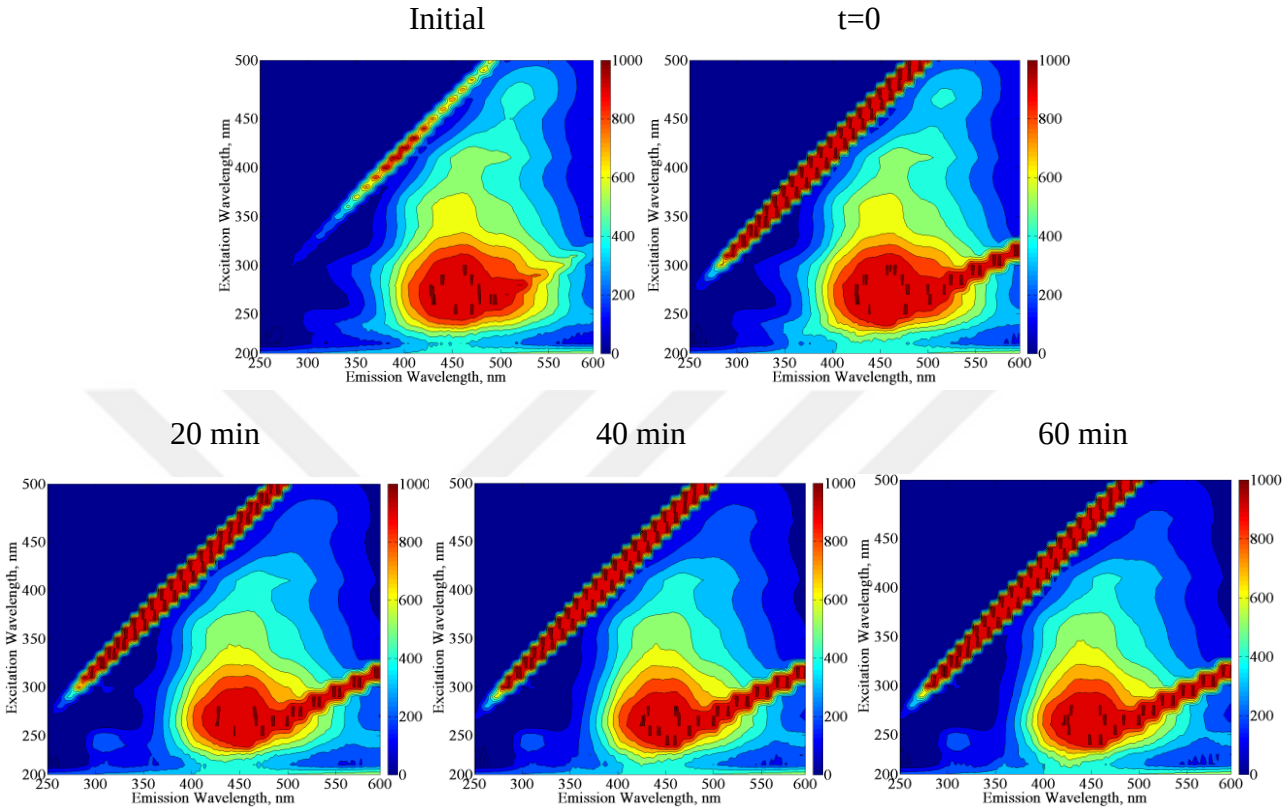

Figure 4.165. EEM fluorescence contour plots of organic matter: Irradiation time dependent *E. coli* inactivation in “HA and WM” solution upon 0.50% Fe-SynTiO$_2$ solar photocatalytic treatment.

EEM fluorescence contour plots of *E. coli* in “HA and WM” solution upon 0.50% Fe-SynTiO$_2$ solar photocatalytic treatment displayed the presence of Regions III, and V indicating that the fluorophores were mainly originated from fulvic-like and humic-like substances. Both humic-like and fulvic-like fluorophore intensities displayed a slight decrease throughout the treatment period of 60 min however detection of relatively high intensities at irradiation period of 60 min could be indicated that, due to the presence of WM solution as a reaction matrix constituent, a retardation effect could be observed on both degradation of organic matter content and inactivation rate of bacteria.

4.2.6.9. Mechanistic evaluation of *E. coli* inactivation upon 0.50% Fe-SynTiO$_2$ solar photocatalytic treatment in “HA and WM” solution. As bacteria inactivation products of 0.50% Fe-SynTiO$_2$ solar photocatalytic treatment of *E. coli* in “HA and WM” solution, total K, protein, and carbohydrate contents present in initial, t=0, and t_{irr}=60 min samples, were presented in Table 4.64.

Table 4.64. Total K, protein, and carbohydrate contents of time dependent *E. coli* inactivation in "HA and WM" solution upon 0.50% Fe-SynTiO$_2$ solar photocatalytic treatment.

0.50% Fe-SynTiO$_2$ solar photocatalytic treatment	*E. coli* in "HA and WM"		
	Initial	t=0	60 min
Total K, mg/L	4.56	4.43	4.36
Protein, mg/L	7.45	16.3	22.8
Carbohydrate, mg/L	3.01	6.41	84.2

Total K content displayed an immediate adsorptive removal at t=0 condition, as 2.85 %. A slight total K content decrease was detected throughout t_{irr}=60 min. Similar pattern was also detected from previous Fe-doped TiO$_2$ sets carried out in "HA and WM" solution (Tables 4.37, 4.46, and 4.55).

E. coli in "HA and WM" solution upon 0.50% Fe-SynTiO$_2$ solar photocatalytic treatment displayed increase in both protein (7.45-22.8 mg/L) and carbohydrate (3.01-84.2 mg/L) content at t_{irr}=60 min. No correlation detected between protein and $FI_{sync280}$ data. Carbohydrate concentration at t_{irr}=60 min displayed the highest concentration detected (84.2 mg/L), which could be due to some experimental errors and/or interferences. Moreover, released Fe^{3+} concentration at the end of 60 min irradiation period was detected as 0.009 mg/L. On the other hand, there could be some interfering factors resulting in the detection of high carbohydrate concentration such as; *i*) the use of H_2SO_4 as a strong acid in phenol sulfuric acid method could cause some degradation products which could absorb light in the same band with carbohydrates, *ii*) H_2SO_4 treated humic matter could give extra absorbance in the same spectral band used in the method, *iii*) NO_3^- coming from WM solution, *iv*) the use of Fe^{3+} doped photocatalyst, and *v*) glycoprotein content founding in bacteria (Dawson and Liebezeit, 1981; Josefsson et al. 1972; Martens and Frankenberger, 1990; Meadows and Campbell, 1978; Rao and Pattabiraman, 1989; Sieburth and Jensen, 1969). Despite a number of possible interferences, NPOC content displayed strong correlations with both protein and carbohydrate concentrations as R^2=0.82 and R^2=0.98, respectively.

4.2.6.10. Comparative evaluation of different experimental matrixes on 0.50% Fe-SynTiO$_2$ solar photocatalytic inactivation mechanism of *E. coli.* Total K, protein, and carbohydrate concentrations and bacteria enumeration results of 0.50% Fe-SynTiO$_2$ solar photocatalytic treatment of *E. coli* in different solution matrixes in comparison with initial, t=0, and t_{irr}=60 min samples were given in Figure 4.166. Total K contents varied in between 0.51-4.56 mg/L being the lowest for initial sample of *E. coli* in HA solution and the highest for initial solution of *E. coli* in "HA and WM" solution. WM solution containing conditions showed higher total K contents as expected. Total K and *E. coli* counts

of initial and t=0 conditions displayed a strong correlation as $R^2 > 0.91$ except the presence of IsoT solution. Moreover, a strong correlation was detected between t_{irr}=60 min conditions as R^2=1.00, in the absence of sole WM solution.

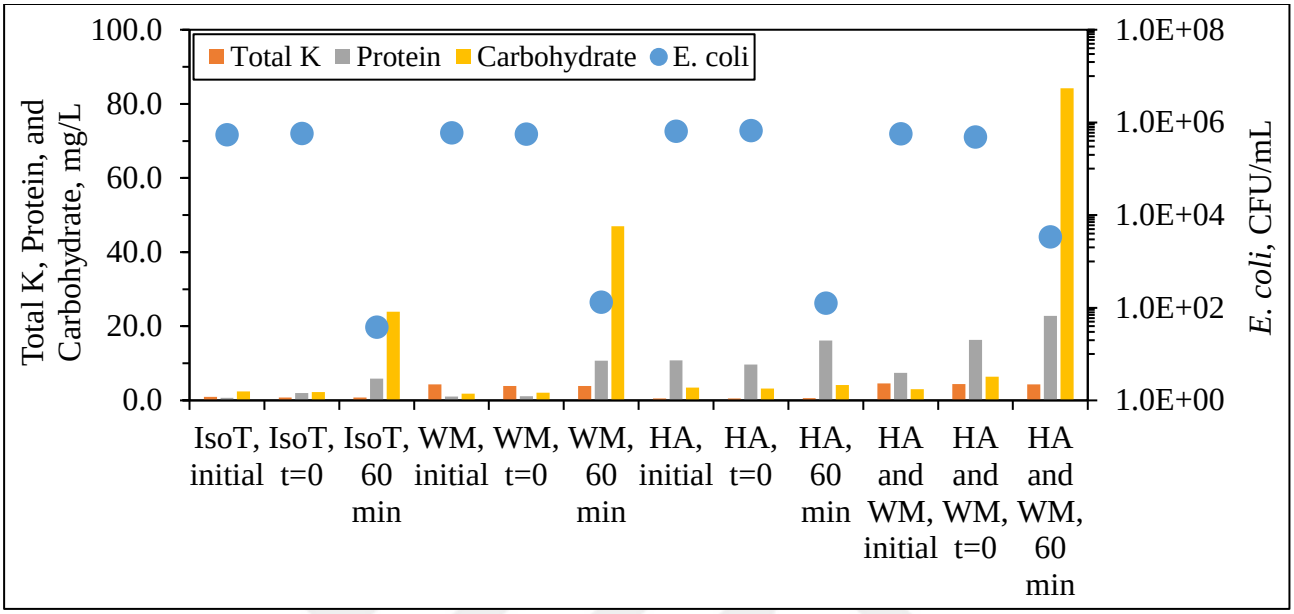

Figure 4.166. Initial, t=0, and t_{irr}=60 min total K, protein, and carbohydrate contents and bacteria enumeration results of *E. coli* inactivation upon 0.50% Fe-SynTiO$_2$ solar photocatalytic treatment in various aqueous matrixes.

Covering all conditions protein contents varied in between 0.68-22.8 mg/L being the lowest for initial sample of *E. coli* in IsoT solution and the highest for t_{irr}=60 min sample of *E. coli* in "HA and WM" solution. Similarly, carbohydrate contents varied in between 1.80-84.2 mg/L being the lowest for initial sample of *E. coli* in WM solution and the highest for t_{irr}=60 min condition of *E. coli* in "HA and WM" solution. Protein concentration of all treatment sets displayed an increasing order except sole HA solution which displayed a slight decrease between initial (3.49 mg/L) and t=0 (3.16 mg/L) conditions. Except t_{irr}=60 min condition of *E. coli* in sole HA solution, all carbohydrate concentrations expressed a significant increase at the end of 60 min irradiation period being the highest for "HA and WM" solution (84.2 mg/L). The possible experimental errors could be the reason of detected extremely high carbohydrate content were given in Section 4.2.6.9.

Released protein and carbohydrate contents and bacteria LRV of 0.50% Fe-SynTiO$_2$ solar photocatalytic treatment of *E. coli* in various solution matrixes were given in Figure 4.167. Released protein and carbohydrate contents were calculated by subtracting initial concentrations from t_{irr}=60 min ones. The highest released protein (15.4 mg/L) and carbohydrate contents (81.2 mg/L), and the lowest bacteria LRV (2.23) were obtained in the presence of "HA and WM" solution. While both

WM and HA solutions had similar *E. coli* LRV (3.65 for *E. coli* in WM solution; 3.71 for *E. coli* in HA solution), released carbohydrate content of *E. coli* in HA solution (0.653 mg/L) was detected as significantly lower than WM solution (45.2 mg/L); therefore, it could be mentioned that degradation of released carbohydrate content occurred in the presence of HA solution. Beside high *E. coli* LRV detected from HA solution as 3.71, degradation of released carbohydrate content could be indicated that 0.50% Fe-SynTiO$_2$ displayed both high bacteria inactivation efficiency and organic matter degradation at the same time. *E. coli* LRV were plotted against released protein content and a strong correlation as R^2=0.89 was obtained, however released carbohydrate contents and *E. coli* LRV showed a moderate correlation as R^2=0.70.

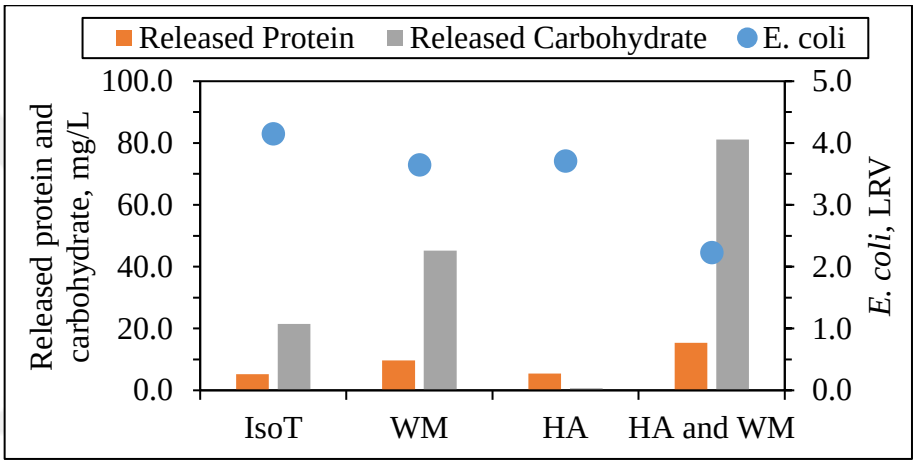

Figure 4.167. Released protein and carbohydrate contents, and bacteria LRV of *E. coli* inactivation upon 0.50% Fe-SynTiO$_2$ solar photocatalytic treatment in various solution matrixes.

Upon 0.50% Fe-SynTiO$_2$ solar photocatalytic treatment of *E. coli* in different solution matrixes, the attained protein and carbohydrate contents, $FI_{sync280}$, UV_{280} and NPOC data under initial, t=0, and t_{irr}=60 min conditions were given in Figure 4.168. In the presence of HA solution, high UV_{280} values were obtained similar to previous solar photolytic (Figure 4.24) and photocatalytic treatments (Figures 4.48, 4.72, 4.96, 4.120, and 4.143). Moreover, the presence of HA solution caused higher protein contents for all samples. $FI_{sync280}$ data showed a significant increase in both IsoT and WM solution for initial, t=0, and t_{irr}=60 conditions. On the other hand, initial $FI_{sync280}$ data of HA solution was detected as $\leq$ 0.001. A strong correlation as $R^2 > 0.93$ was detected between protein concentrations and $FI_{sync280}$ of initial and t=0 samples, whereas t_{irr}=60 min showed no correlation between these two parameters. The highest NPOC contents were detected from *E. coli* in HA solution (9.15 mg/L for initial; 11.1 mg/L for t=0; 14.9 mg/L for t_{irr}=60 min). Treatments conducted in IsoT and WM solutions displayed similar patterns for carbohydrate and NPOC contents, however higher concentration were detected for WM solution.

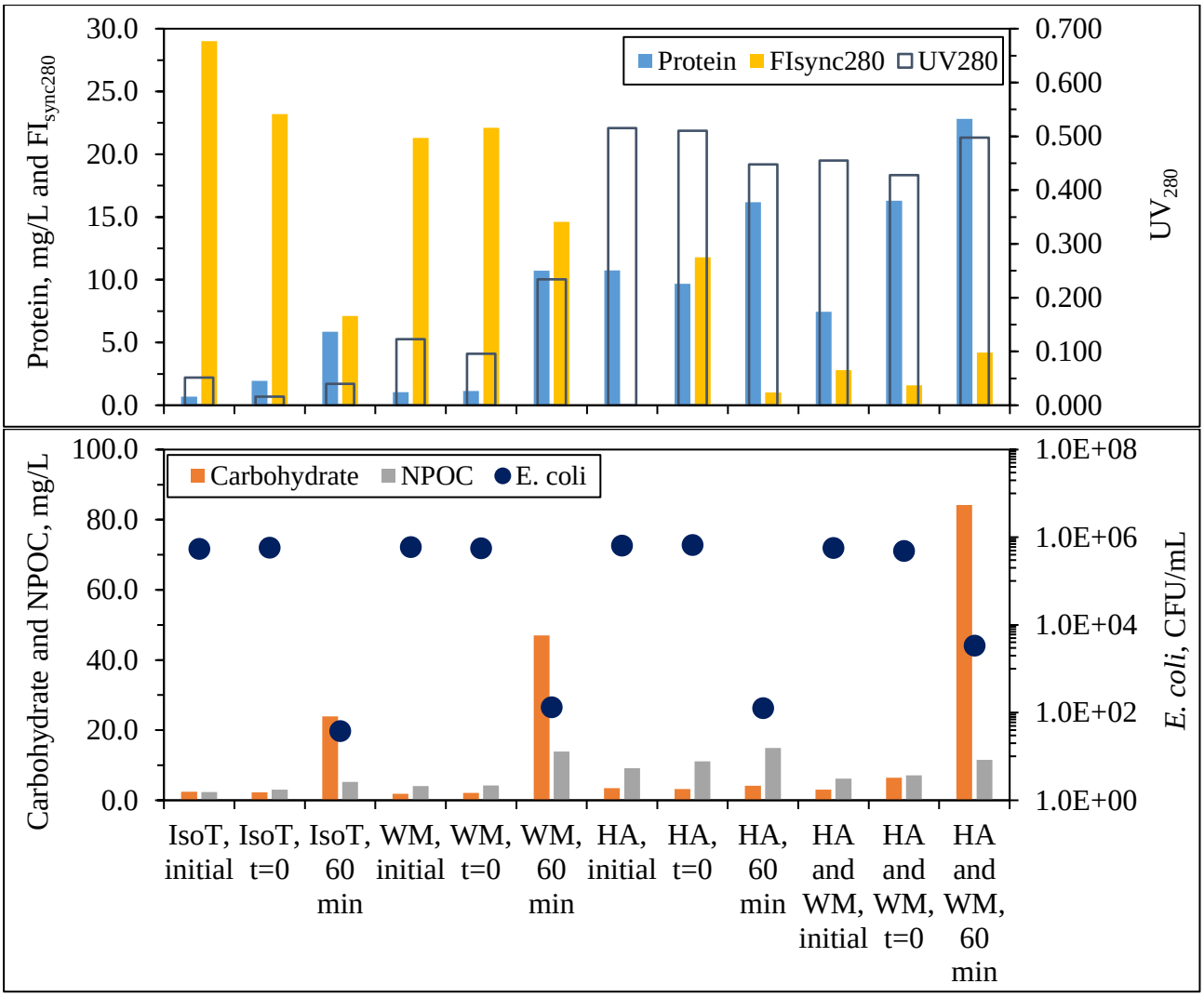

Figure 4.168. Initial, t=0, and t_{irr}=60 min protein and carbohydrate contents, $FI_{sync280}$, UV_{280}, NPOC, and bacteria enumeration results of 0.50% Fe-SynTiO$_2$ solar photocatalytic treatment of *E. coli* in various aqueous matrixes.

Except significantly different carbohydrate content of WM (47.0 mg/L) and sole HA (4.14 mg/L) solutions at irradiation period of 60 min condition, they displayed resembling NPOC contents (13.9 mg/L for *E. coli* in WM solution; 14.9 mg/L for *E. coli* in HA solution) and bacteria counts (1.33E+02 CFU/mL for *E. coli* in WM solution; 1.27E+02 CFU/mL for *E. coli* in HA solution). It could be concluded that in WM solution, only released organic content from bacteria was the source of NPOC, whereas both released organic material from bacteria and present HA content contributed to measured NPOC for sole HA solution condition. Initial carbohydrate and NPOC contents showed a rough correlation for all reaction matrixes as R^2=0.66; however, t=0 conditions showed a strong correlation except the presence of sole HA solution as R^2=0.89. Different from these irradiation time correlations, t_{irr}=60 min conditions displayed a strong correlation as R^2=0.93, excluding the presence of IsoT solution.

4.3. Comparative Evaluation of *E. coli* Inactivation Upon Use of Photocatalyst Specimens

4.3.1. Comparative Efficiency Evaluation of Different Photocatalyst Specimens on *E. coli* Inactivation in IsoT Solution

In the presence of sole IsoT solution, irradiation time dependent solar photocatalytic *E. coli* inactivation profiles and first order kinetic parameters upon use of undoped and Fe-doped photocatalyst specimens were compiled from respective figures and tables and presented in Figure 4.169 and Table 4.65 in a comparative manner.

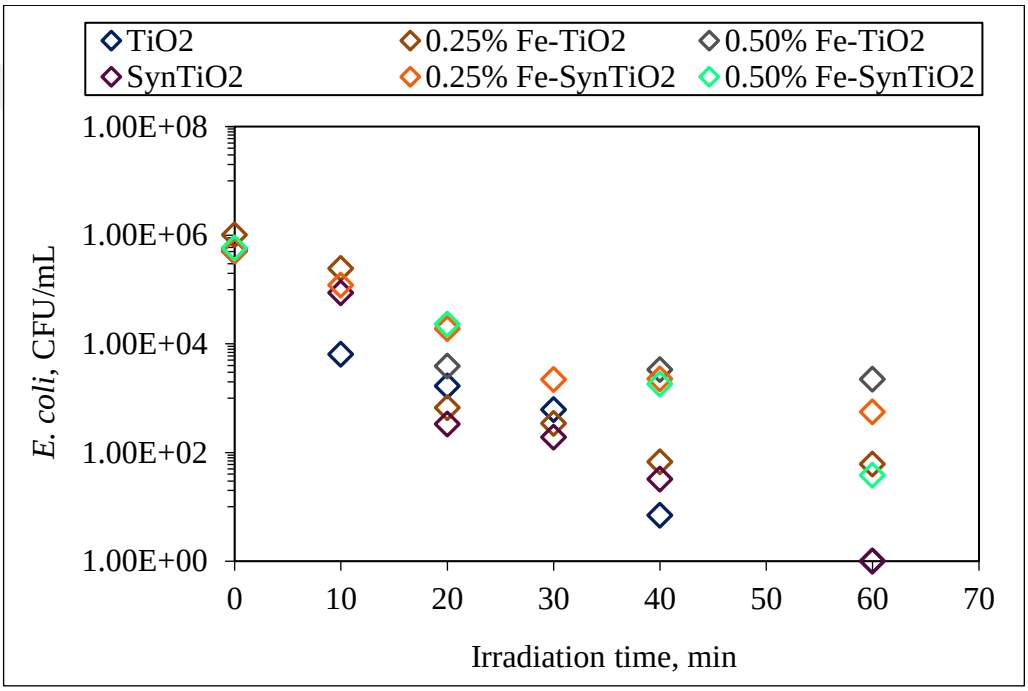

Figure 4.169. Irradiation time dependent *E. coli* inactivation in IsoT solution upon solar photocatalytic treatments performed in the presence of undoped and Fe-doped TiO_2 specimens.

Table 4.65. Solar photocatalytic treatment of *E. coli* in IsoT solution performed in the presence of undoped and Fe-doped TiO_2 specimens: Inactivation parameters.

E. coli in IsoT solution solar photocatalytic treatment	First order kinetic model			LRV	Reduction, %
	k, min^{-1}	$t_{1/2}$, min	R, CFU/mL min		
TiO_2	0.248	2.79	1.97E+05	5.90	99.999
$SynTiO_2$	0.254	2.73	1.11E+05	5.64	99.999
0.25% Fe-TiO_2	0.174	3.98	2.05E+05	4.28	99.99
0.50% Fe-TiO_2	0.0839	8.26	5.19E+04	2.44	99
0.25% Fe-$SynTiO_2$	0.116	5.97	4.67E+04	2.86	99.7
0.50% Fe-$SynTiO_2$	0.158	4.39	8.56E+04	4.15	99.99

Irradiation time dependent continuous reduction of *E. coli* in IsoT solution was achieved under all solar photocatalytic treatment conditions using all TiO_2 specimens. The effect of each photocatalyst could be expressed in terms of inactivation reaction rate constant (k, min^{-1}) in an increasing order as; 0.50% Fe-TiO_2 < 0.25% Fe-SynTiO_2 < 0.50% Fe-SynTiO_2 < 0.25% Fe-TiO_2 < TiO_2 < SynTiO_2. In general, bacteria reduction percentages obtained from some photocatalysts showed the same efficiencies in a decreasing order as; TiO_2 = SynTiO_2 > 0.25% Fe-TiO_2 = 0.50% Fe-SynTiO_2 > 0.25% Fe-SynTiO_2 > 0.50% Fe-TiO_2. Besides the similar bacteria reductions of some photocatalysts, LRV of *E. coli* displayed differences and could be expressed in an increasing order as; 0.50% Fe-TiO_2 < 0.25% Fe-SynTiO_2 < 0.50% Fe-SynTiO_2 < 0.25% Fe-TiO_2 < SynTiO_2 < TiO_2. Except the change observed for bare TiO_2 and SynTiO_2 specimens, Fe-doped photocatalyst specimens displayed the same order for both bacteria LRV and inactivation reaction rate constants. The most effective photocatalyst was detected as TiO_2 while the least effective one 0.50% Fe-TiO_2. The highest bacteria LRV of bare TiO_2 could be due to its high BET surface area as 57.6 m^2/g (Table C.2) (Birben et al., 2015).

It could be indicated that Fe-doping in differing concentrations showed no significant difference on the efficiency of bacteria inactivation, whereas the most effective Fe-doped TiO_2 specimen was 0.25% Fe-TiO_2 in IsoT solution. Yalcin and colleagues reported that 0.25% Fe-TiO_2 displayed the highest degradation rate among the other dopant concentrations upon use of 4-nitrophenol as a model organic compound (Yalcin et al., 2010). The reason for higher inactivation rate of 0.25% Fe-TiO_2 could be related to the increased amount of $HO^{\bullet}$ formation due to generated vacancies on TiO_2 surface by Fe^{3+} doping process. Formed oxygen vacancies on the photocatalyst surface could adsorb more water molecules and during irradiation, high amount of $HO^{\bullet}$ radicals as the main ROS could from via radical reactions as explained by basic photocatalysis mechanism in Section 2.3.1 (Equations 2.1-2.8).

On the other hand, 0.25% Fe-TiO_2 exhibited the lowest crystallite particle size among other Fe-doped photocatalysts as 16.4 nm which could generate various agglomerate sizes resulted in higher photocatalytic activity (Table C.1.) (Yalcin et al., 2010). Moreover, 0.25% Fe-doped TiO_2 specimen displayed heterogenous aggregate formations, smaller crystallite particles containing straight edges and sharp corners, which indicates the presence of large variety of shape and distribution causing high grade of porosity, therefore; it could be indicated that previously reported crystallite particle size properties of 0.25% Fe-doped TiO_2 could cause mechanic inactivation effect on *E. coli* (Yalcin et al., 2010). The second effective Fe-doped photocatalyst was detected as 0.50% Fe-SynTiO_2, exhibiting comparatively less agglomeration behavior (Turkten and Cinar, 2019). Agglomeration could lead to

altered surface attractions prevailing in between *E. coli* and photocatalyst specimen resulting in attachment of particles onto comparatively higher cell surface area (6.0 μm^2) to be exposed to irradiation. Under these conditions, light harvesting capacity of the 0.50% Fe-SynTiO_2 could be affected leading to lower efficiency on the ROS formation.

4.3.1.1. Comparative mechanistic evaluation of *E. coli* inactivation in IsoT solution upon solar photocatalytic treatments performed in the presence of undoped and Fe-doped TiO_2 specimens. As inactivation products of bare and Fe-doped TiO_2 solar photocatalytic treatments of *E. coli* in the presence of IsoT solution, total K, protein, and carbohydrate concentrations of initial, t=0, and t_{irr}=60 min conditions were given in Figure 4.170.

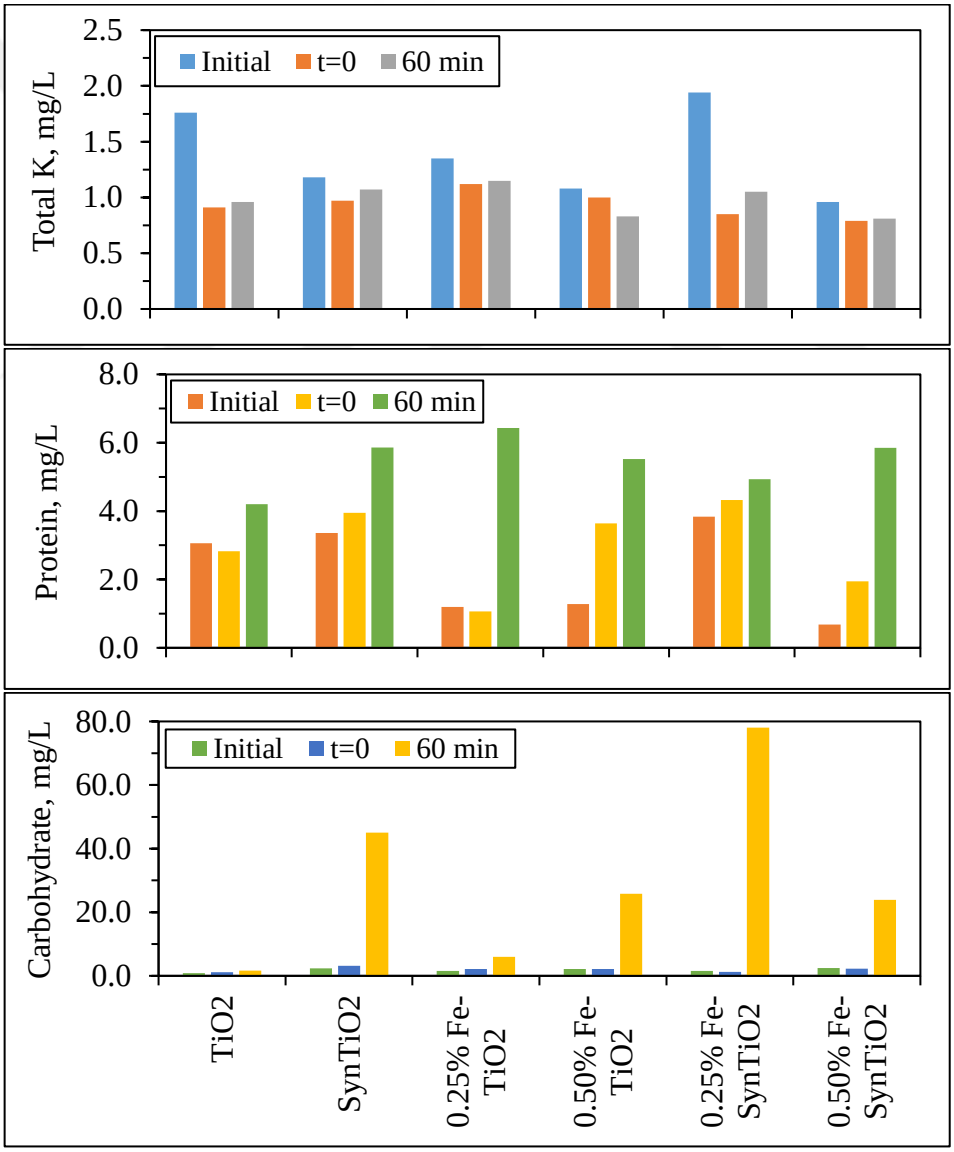

Figure 4.170. Initial, t=0, and t_{irr}=60 min total K, protein, and carbohydrate contents of *E. coli* inactivation in IsoT solution upon solar photocatalytic treatments performed in the presence of bare and Fe-doped TiO_2 specimens.

From a general perspective, all total K contents displayed variations in the range of 0.79-1.94 mg/L. Instantaneous adsorptive removal of total K at t=0 condition expressed changes in between 7.4-56 %. Maximum adsorptive removal of total K was detected upon use of 0.25% Fe-TiO_2 however, 0.50% Fe-TiO_2 displayed the lowest initial adsorptive removal at t=0 condition. Moreover, varying trend of total K contents could be related most probably to the passive and active transport mechanisms of *E. coli* as well as by attractive surface interactions of the charged sites.

Protein contents displayed variations in the range of 0.683-6.44 mg/L. Under all experimental conditions, protein concentrations increased at the end of t_{irr}=60 min irradiation, however maximum protein release was detected upon use of 0.25% Fe-TiO_2 as 6.44 mg/L. The presence of proteinaceous organic compounds was very clearly presented by respective UV-vis absorbance (Figures 4.74 and 4.76) synchronous scan fluorescence spectral features (Figure 4.75) as well as EEM fluorescence contour plots (Figures 4.78).

Under all conditions, carbohydrate contents displayed variations in the range of 0.891-78.0 mg/L. All concentrations showed an increase in carbohydrate contents at irradiation period of 60 min however maximum carbohydrate release was detected as 78.0 mg/L in case that 0.25% Fe-SynTiO_2 was utilized as the photocatalyst specimen.

As presented, the most efficient photocatalyst specimen in IsoT solution could be visualized as undoped TiO_2 specimen expressing the effective degradation mechanism upon solar photocatalysis as was also represented by NPOC contents (Figure 4.28, Table 4.12). On the other hand, it should be noted that, related to measured high carbohydrate contents at t_{irr}=60 with the use of SynTiO_2 (45.0 mg/L) and 0.25% Fe-SynTiO_2 (78.0 mg/L), and possible experimental errors due to the present interfering factors which widely explained in Section 3.2.3.3, comparative evaluation of photocatalyst specimens according to carbohydrate contents could cause erroneous conclusions.

4.3.2. Comparative Efficiency Evaluation of Different Photocatalyst Specimens on *E. coli* Inactivation in WM Solution

In the presence of sole WM solution, irradiation time dependent solar photocatalytic *E. coli* inactivation profiles and first order kinetic parameters upon use of undoped and Fe-doped photocatalyst specimens were compiled from respective figures and tables and presented in Figure 4.171 and Table 4.66 in a comparative manner. Solar irradiation time dependent continuous reduction of *E. coli* in WM solution was displayed upon solar photocatalysis using both undoped and Fe-doped

TiO_2 specimens. As could be visualized from logarithmic decay profiles, *E. coli* cells were effectively inactivated upon solar photocatalytic treatment processes using the specified specimens either as undoped or Fe doped forms in WM solution. Although variations were considerably evident in between the efficiencies of the employed photocatalyst specimens, upon irradiation period of 60 min, 2.95E+03 CFU/mL *E. coli* cells were still present upon use of 0.25% Fe-TiO_2 whereas only 2.85E+01 CFU/mL *E. coli* cells were present upon use of SynTiO_2. Therefore, the effect of reaction medium could be successfully expressed in terms of inactivation reaction rate constant (k, min^{-1}) in an increasing order as; 0.25% Fe-TiO_2 < TiO_2 < 0.50% Fe-TiO_2 < 0.25% Fe-SynTiO_2 ≤ 0.50% Fe-SynTiO_2 < SynTiO_2 (Table 4.66).

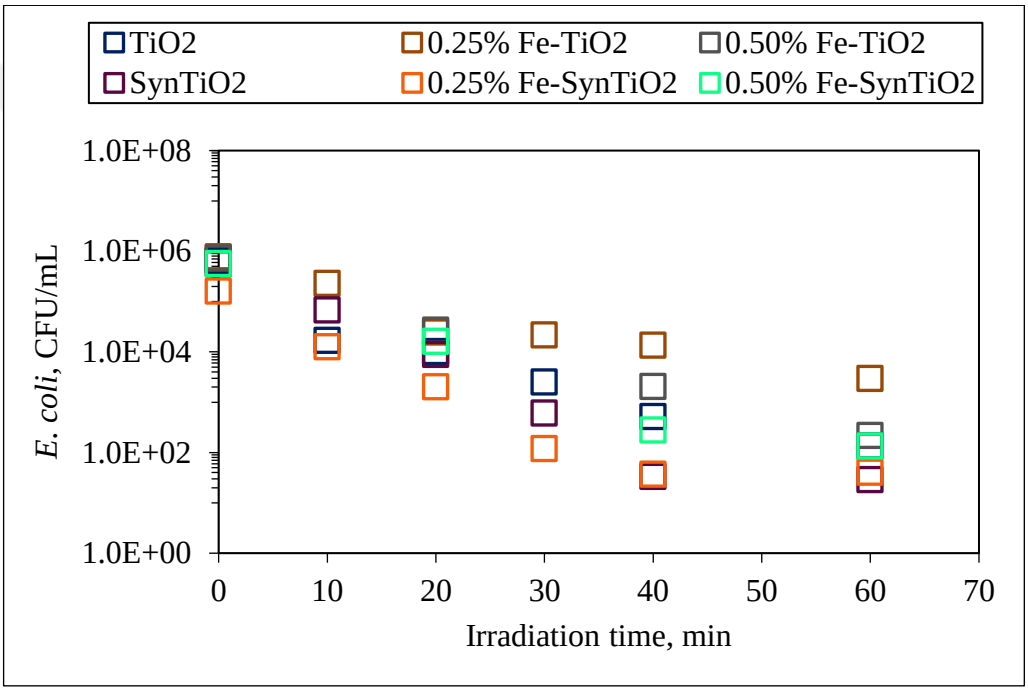

Figure 4.171. Irradiation time dependent *E. coli* inactivation in WM solution upon solar photocatalytic treatments performed in the presence of undoped and Fe-doped TiO_2 specimens.

Table 4.66. Solar photocatalytic treatment of *E. coli* in WM solution performed in the presence of undoped and Fe-doped TiO_2 specimens: Inactivation parameters.

E. coli in WM solution solar photocatalytic treatment	First order kinetic model			LRV	Reduction, %
	k, min^{-1}	$t_{1/2}$, min	R, CFU/mL min		
TiO_2	0.132	5.25	9.44E+04	3.73	99.9
SynTiO_2	0.180	3.85	1.14E+05	4.35	99.99
0.25% Fe-TiO_2	0.0891	7.78	8.17E+04	2.49	99
0.50% Fe-TiO_2	0.135	5.13	9.06E+04	3.49	99.9
0.25% Fe-SynTiO_2	0.146	4.75	3.26E+04	3.75	99.9
0.50% Fe-SynTiO_2	0.146	4.75	8.69E+04	3.65	99.9

The effect of photocatalyst specimens on *E. coli* inactivation in WM solution could also be displayed in terms of reduction percentage of *E. coli* in an increasing order as; 0.25% Fe-TiO_2 < 0.50% Fe-TiO_2 = 0.50% Fe-$SynTiO_2$ = TiO_2 = 0.25% Fe-$SynTiO_2$ < $SynTiO_2$. However, although *E coli* reduction percentages (e.g., 99.9 %) were the same, respective bacteria LRV displayed differences in the range of 3.49-3.75. LRV of *E. coli* inactivation followed an increasing order as; 0.25% Fe-TiO_2 < 0.50% Fe-TiO_2 < 0.50% Fe-$SynTiO_2$ < TiO_2 < 0.25% Fe-$SynTiO_2$ < $SynTiO_2$. It could be indicated that, except 0.25% Fe-TiO_2 specimen, other Fe-doped photocatalysts showed no significant efficiency difference. The most effective photocatalyst upon *E. coli* inactivation in WM solution was observed as $SynTiO_2$ while the least effective one 0.25% Fe-TiO_2 specimen.

4.3.2.1. Comparative mechanistic evaluation of *E. coli* inactivation in WM upon solar photocatalytic treatment with undoped and Fe-doped TiO_2 specimens. As solar photocatalytic inactivation products of bare and Fe-doped TiO_2 solar photocatalytic treatments of *E. coli* in the presence of WM components, total K, protein, and carbohydrate contents under initial, t=0, and t_{irr}=60 min conditions were given in Figure 4.172.

Total K contents displayed variations in the range of 3.86-4.38 mg/L. Except 0.25% Fe-TiO2, all photocatalyst specimens displayed an immediate adsorptive removal of total K content at t=0 condition in the range of 1.7-9.5 %. Maximum adsorptive removal % of total K content was attained in the case of 0.50% Fe-$SynTiO_2$. Moreover, all experiment conditions showed decreased total K concentrations at the end of 60 min irradiation period. Depending on the resultant cell counts depicted in respective Figure 4.171, the role of K^+ ion transportation mechanisms in and out of the cell wall via passive and active transport should also be considered under all conditions. It should be noted that excessive amount of K ions present in WM solution could be used by bacteria to compensate released K^+ ion content and protect bacteria from destruction by retarding of cell wall damage.

Furthermore, due to the presence of common anions and cations in WM solution, various electrostatic attractive and repulsive forces between charged species should take place resulting in varying surface interactions both onto photocatalyst specimens and bacteria surface. The effect of pH_{zpc} of photocatalyst specimens (TiO_2: 6.25; $SynTiO_2$: 6.40; 0.25% Fe-TiO_2: 4.80) played the dominant role specifically on t=0 conditions and during solar photocatalytic treatment under irradiation conditions covering the formation of charged cell fractions (Birben et al., 2015, 2017b).

From a general perspective, protein contents displayed variations in the range of 0.710-14.8 mg/L. All protein concentrations showed an increase following t_{irr}=60 min however the highest

protein content was detected as 14.8 mg/L upon use of SynTiO$_2$ specimen. Under these conditions, both UV-vis absorbance (Figures 4.55 and 4.57) and synchronous scan fluorescence spectral features (Figure 4.56) as well as EEM fluorescence contour plots (Figure 4.59) proved the existence of protein like components in reaction medium.

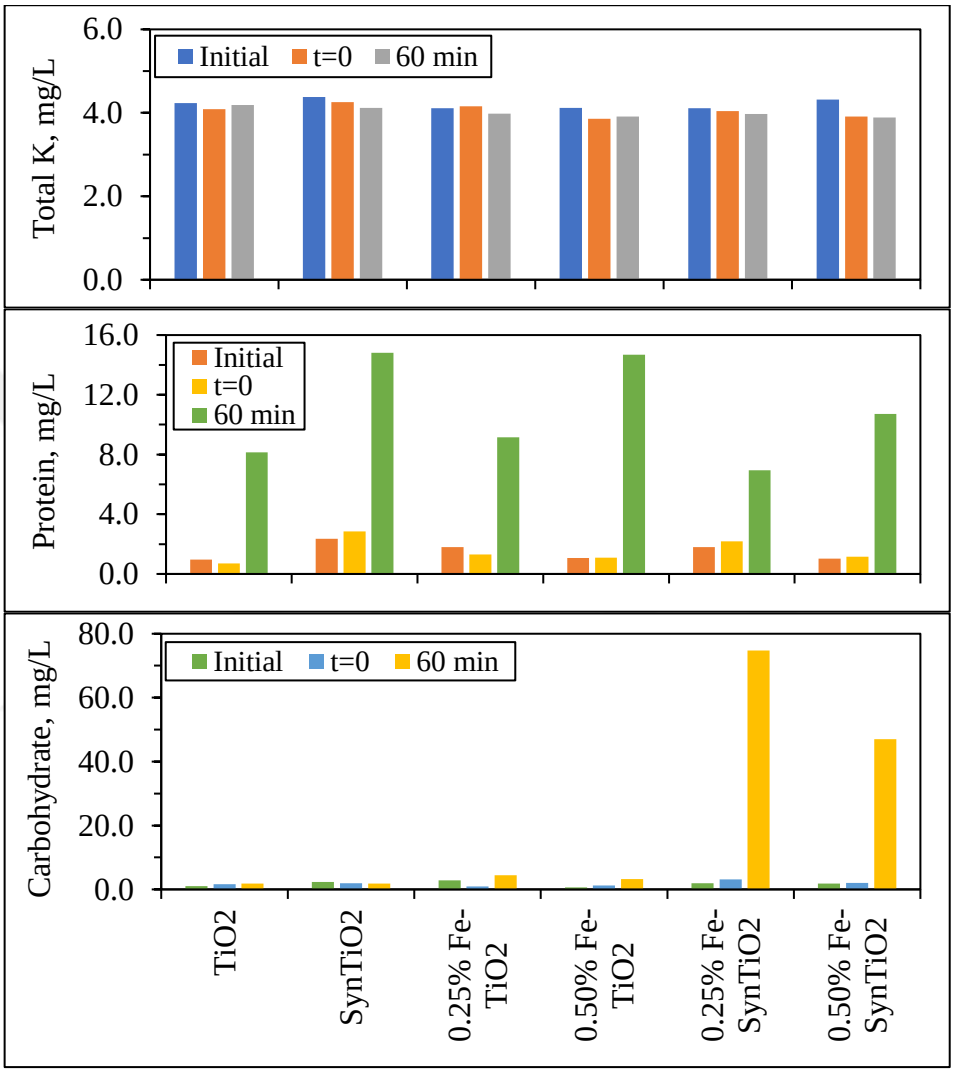

Figure 4.172. Initial, t=0, and t_{irr}=60 min total K, protein, and carbohydrate contents of *E. coli* inactivation in WM solution upon solar photocatalytic treatments performed in the presence of bare and Fe-doped TiO$_2$ specimens.

From a general perspective, carbohydrate contents displayed variations in the range of 0.618-74.7 mg/L. However, upon use of undoped and Fe-doped TiO$_2$ specimens almost all carbohydrate contents were quite low as < 4 mg/L for initial and t=0 conditions, expressing insignificant role of Fe doping on TiO$_2$. Since carbohydrate contents could not be followed by spectroscopic techniques, it could only be related to the selectivity of photocatalysis towards the organic fractions exhibiting carbohydrate structures mainly composed of hydrophilic groups. Deprotonation of these groups could

be neutralized by counter ions e.g., K^+ ions formed through cell lysis or by cations present as WM constituent (Bythell et al., 2018). Although an analogous approach could also be related to the behavior of $SynTiO_2$ (< 2 mg/L at t_{irr}=60 min), Fe-doping significantly affected the reaction mechanism excluding the degradation of carbohydrate components. Increasing Fe dopant concentration of $SynTiO_2$ from 0.25% to 0.50% did not reflect as a dopant concentration role, therefore lower carbohydrate content was found as 47 mg/L. The reason could be attributed to the surface morphological properties of Fe-doped Syn TiO_2 specimens rather than the selectivity or efficiency of photocatalysis. Similar trend was also observed upon use undoped and 0.25% Fe-doped TiO_2 specimens during solar photocatalytic inactivation of *E. coli* in IsoT solution revealing carbohydrate contents as ~ < 5 mg/L (Figure 4.170). Further increase in Fe doping of TiO_2 resulted in substantial increase in carbohydrate content as 25 mg/L. The reason could only be related to the sole presence of Cl^- anion in solution exerting considerably less ion effect. Contrary to these findings, $SynTiO_2$ either as undoped or doped forms expressed varying carbohydrate contents under all conditions proceeding through different reaction mechanism. Interestingly, upon use of 0.25% Fe-$SynTiO_2$ in the presence of either IsoT solution (78.0 mg/L) or WM solution (74.7 mg/L) almost similar carbohydrate contents were still present in reaction medium (Figures 4.170 and 4.172).

4.3.3. Comparative Efficiency Evaluation of Different Photocatalyst Specimens on *E. coli* Inactivation in HA Solution

In the presence of sole HA solution, irradiation time dependent solar photocatalytic *E. coli* inactivation profiles and first order kinetic parameters upon use of undoped and Fe-doped photocatalys specimens were compiled from respective figures and tables and presented in Figure 4.173 and Table 4.67 in a comparative manner.

Irradiation time dependent continuous reduction of *E. coli* in HA solution was achieved under all solar photocatalytic treatment conditions using undoped and Fe-doped TiO_2 specimens. Although differences were considerably evident in between the efficiencies of the employed photocatalyst specimens, upon t_{irr}=60 min, 3.85E+04 CFU/mL *E. coli* cells were still present upon use of bare TiO_2 whereas only 3.35E+01 CFU/mL *E. coli* cells were present upon use of undoped $SynTiO_2$. Therefore, the effect of photocatalyst specimens could be expressed in terms of inactivation reaction rate constant (k, min^{-1}) in an increasing order as; TiO_2 < 0.25% Fe-TiO_2 < 0.50% Fe-TiO_2 < 0.50% Fe-$SynTiO_2$ < $SynTiO_2$ < 0.25% $SynTiO_2$. The effect of different photocatalysts on *E. coli* inactivation in the presence of sole HA solution could also be displayed in terms of *E. coli* reduction percentage in a decreasing order as; $SynTiO_2$ = 0.50% Fe-TiO_2 = 0.25% Fe-$SynTiO_2$ = 0.50% Fe-$SynTiO_2$ >

0.25% Fe-TiO_2 > TiO_2. Besides the same bacteria reduction percentage of some photocatalysts (e.g., 99.9 %), LRV of *E. coli* displayed changes in between 3.36-3.82. *E. coli* LRV of all conditions could be displayed in an increasing order as; TiO_2 < 0.25% Fe-TiO_2 < 0.50% Fe-TiO_2 < SynTiO_2 < 0.50% Fe-SynTiO_2 < 0.25% Fe-SynTiO_2.

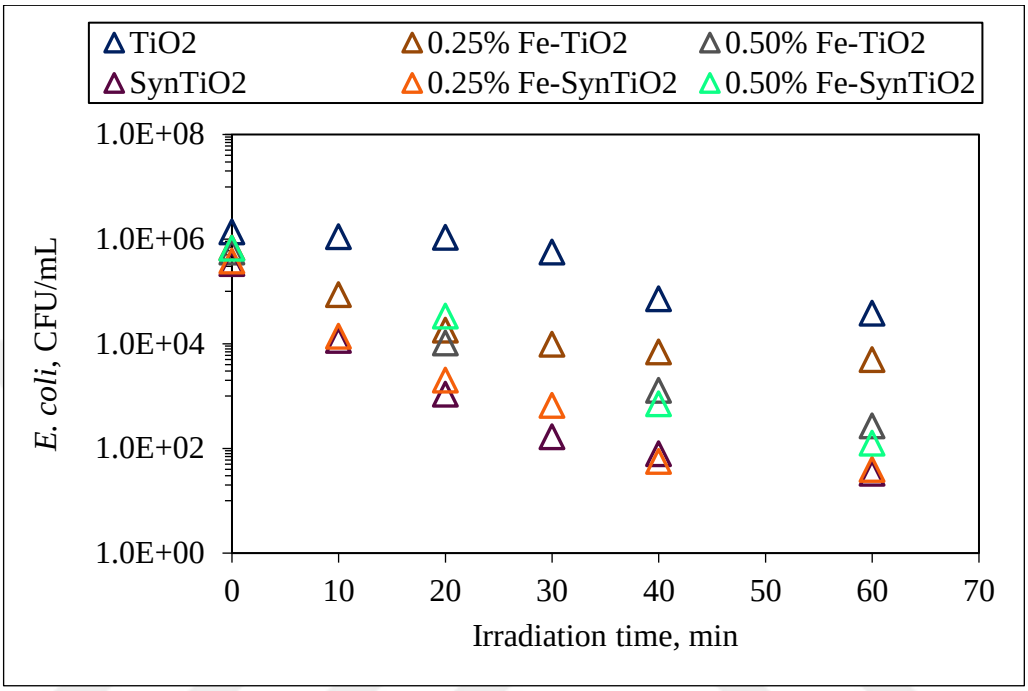

Figure 4.173. Irradiation time dependent *E. coli* inactivation in HA solution upon solar photocatalytic treatments performed in the presence of undoped and Fe-doped TiO_2 specimens.

Table 4.67. Solar photocatalytic treatment of *E. coli* in HA solution performed in the presence of undoped and Fe-doped TiO_2 specimens: Inactivation parameters.

E. coli in HA solution solar photocatalytic treatment	First order kinetic model			LRV	Reduction, %
	k, min^{-1}	$t_{1/2}$, min	R, CFU/mL min		
TiO_2	0.0672	10.3	7.26E+04	1.45	90
SynTiO_2	0.150	4.62	2.54E+04	3.70	99.9
0.25% Fe-TiO_2	0.0774	8.95	4.74E+04	2.09	99
0.50% Fe-TiO_2	0.125	5.54	7.81E+04	3.36	99.9
0.25% Fe-SynTiO_2	0.152	4.56	3.98E+04	3.82	99.9
0.50% Fe-SynTiO_2	0.148	4.68	9.53E+04	3.71	99.9

The most effective photocatalyst in the presence of HA solution was detected as 0.25% Fe-SynTiO_2 and the least effective one as bare TiO_2 specimen. Related to detected inactivation rate constants and LRV upon use of various photocatalyst specimens, it could be concluded that SynTiO_2 and its Fe-doped species displayed selectivity towards *E. coli* however TiO_2 and its Fe-doped species

expressed selectivity against humic matter in solution. The reason could be attributed that the different crystallite particle sizes of photocatalyst specimens (Table C.1). Besides lower crystallite particle sizes of bare TiO_2 (22.3 nm) and Fe-doped TiO_2 specimens (16.4 nm for 0.25% Fe-TiO_2; 19.9 nm for 0.50% Fe-TiO_2), bare SynTiO_2 (33.1 nm) and Fe-doped SynTiO_2 specimens (20.7 nm for 0.25% Fe-SynTiO_2; 23.7 nm for 0.50% Fe-SynTiO_2) displayed higher crystallite particle sizes (Turkten and Cinar, 2019; Turkten, 2016; Turkten et al., 2019; Yalcin et al., 2010). It could be indicated that photocatalyst specimens having lower crystallite particle sizes, namely TiO_2 species, display selectivity toward the removal of organic matter however higher crystallite particle sized SynTiO_2 species showed selectivity against bacteria inactivation.

Furthermore, findings of Birben and colleagues indicating that 0.25% Fe-TiO_2 showed a retardation effect on HA removal rates compared to undoped TiO_2, supporting the order of 0.25% Fe-TiO_2 and bare TiO_2 in the aspect of inactivation rate constants and bacteria LRV. It could be indicated that 0.25% Fe-TiO_2 has slightly more selectivity towards bacteria than TiO_2. Researchers reported that the surface interactions between HA and surface of Fe-doped photocatalysts could be the cause of slower degradation rates of HA upon solar photocatalytic treatment (Birben et al., 2017b).

4.3.3.1. Comparative mechanistic evaluation of *E. coli* inactivation in HA solution upon solar photocatalytic treatments performed in the presence of undoped and Fe-doped TiO_2 specimens. As inactivation products of bare and Fe-doped TiO_2 solar photocatalytic treatments of *E. coli* in the presence of sole HA solution, total K, protein, and carbohydrate contents of initial, t=0, and t_{irr}=60 min conditions were given in Figure 4.170.

From a general view, total K contents expressed changes in the range of 0.44-0.73 mg/L. In the presence of HA solution, total K contents displayed lower presence from IsoT solution conditions (Figure 4.170). Different from IsoT and WM solution conditions, in the presence of HA solution, immediate adsorptive removal of total K content at t=0 condition was only calculated upon use of bare TiO_2 and 0.25% Fe-TiO_2 specimens as 7.5 and 25 %, respectively. Moreover, except 0.25% Fe-TiO_2, all other conditions, showed increased total K concentrations at the end of 60 min irradiation period, which was a pattern that did not detected in the presence of IsoT and WM solutions (Figures 4.170 and 4.172).

Under all conditions, protein contents expressed changes in the range of 3.75-16.2 mg/L. The use of bare TiO_2 as a photocatalyst resulted in a degradation in protein content at t_{irr}=60 min (13.4-3.75 mg/L). It could be indicated that, expressed protein degradation could be associated with

obtained lower bacteria inactivation rate of TiO_2 and could also support the suggestion about selectivity of TiO_2 against organic content rather than bacteria. On the other hand, solar photocatalytic treatments conducted in the presence of bare $SynTiO_2$ and all Fe-doped photocatalyst specimens displayed increased protein contents at the end of 60 min irradiation period, being the highest for 0.50% Fe-$SynTiO_2$ condition as 16.2 mg/L. Under these conditions, despite the masking effect of humic-like matter on protein-like ones, both UV-vis absorbance (Figures 4.156 and 4.158) and synchronous scan fluorescence spectral features (Figure 4.157) as well as EEM fluorescence contour plots (Figure 4.160) proved the existence of protein like components in reaction medium.

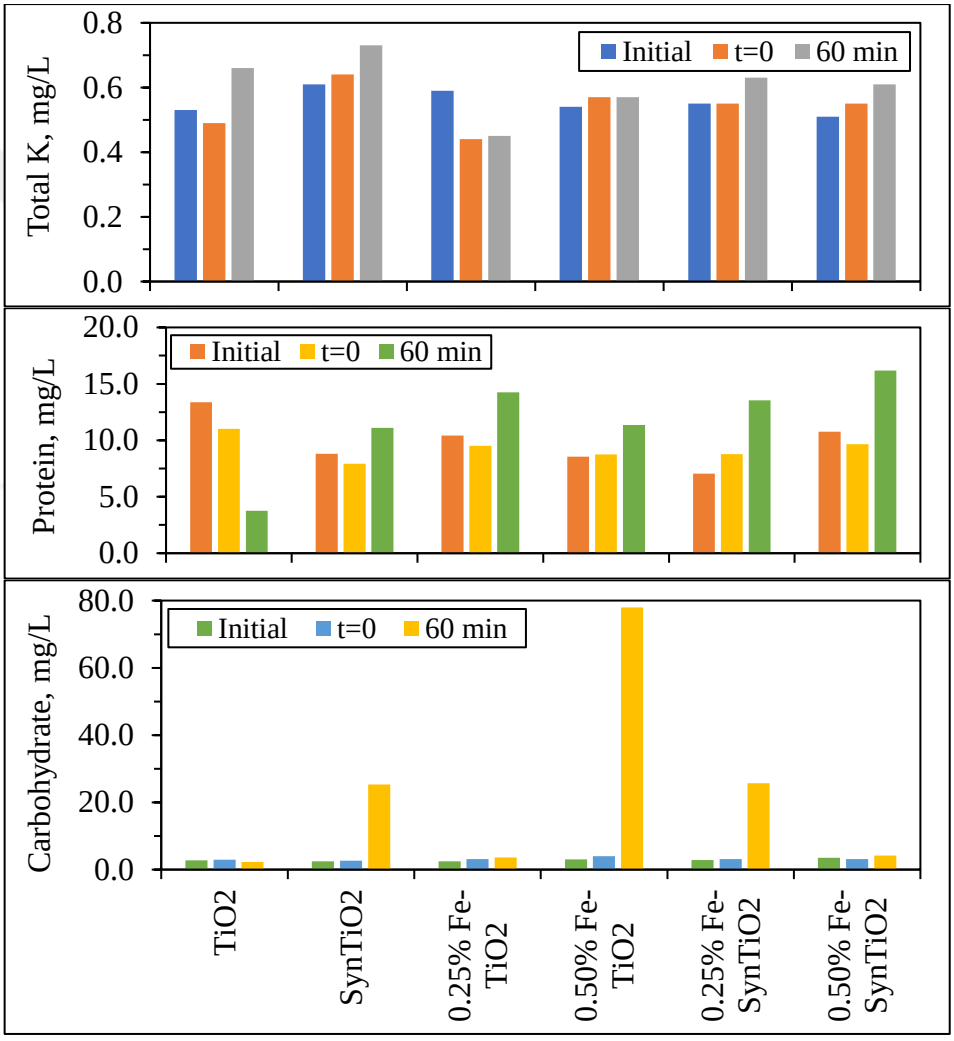

Figure 4.174. Initial, t=0, and t_{irr}=60 min total K, protein, and carbohydrate contents of *E. coli* inactivation in HA solution upon solar photocatalytic treatments performed in the presence of bare and Fe-doped TiO_2 specimens.

Carbohydrate contents displayed variations in the range of 2.24-77.9 mg/L. However, upon use of undoped and Fe-doped TiO_2 specimens almost all carbohydrate contents were quite low as < 5 mg/L for initial and t=0 conditions, expressing insignificant role of Fe doping on TiO_2. Similar trend

was also observed for initial and t=0 conditions upon use undoped and Fe-doped TiO_2 photocatalyst specimens during solar photocatalytic inactivation of *E. coli* in IsoT and WM solutions revealing carbohydrate contents as < 4 mg/L (Figure 4.170).

On the other hand, similar to degradation of protein content in the presence of undoped TiO_2 after irradiation period of 60 min, degraded carbohydrate content (2.77-2.24 mg/L) was detected upon use of TiO_2. All other conditions showed an increase in carbohydrate contents at the end of 60 min solar light exposure period however maximum carbohydrate content was detected as 77.9 mg/L in case that 0.50% Fe-TiO_2 was used as the photocatalyst specimen.

4.3.4. Comparative Efficiency Evaluation of Different Photocatalyst Specimens on *E. coli* Inactivation in "HA and WM" Solution

In the presence of "HA and WM" solution, irradiation time dependent solar photocatalytic *E. coli* inactivation profiles and first order kinetic parameters upon use of undoped and Fe-doped photocatalyst specimens were compiled from respective figures and tables and presented in Figure 4.175 and Table 4.68 in a comparative manner.

Irradiation time dependent continuous reduction of *E. coli* in "HA and WM" solution was achieved under all solar photocatalytic treatment conditions using undoped and Fe-doped TiO_2 specimens. However, after irradiation time of 40 min, TiO_2, SynTiO_2, and 0.25% Fe-SynTiO_2 displayed a retardation in *E. coli* reduction (Figure 4.175). Although variations were considerably evident in between the efficiencies of the employed photocatalyst specimens, upon irradiation period of 60 min, 5.50E+04 CFU/mL *E. coli* cells were still present upon use of bare TiO_2 whereas only 4.67E+02 CFU/mL *E. coli* cells were present upon use of SynTiO_2. Based on these results, the effect of photocatalysts could be expressed in terms of inactivation reaction rate constant (k, min^{-1}) in an increasing order as; TiO_2 < 0.50% Fe-TiO_2 < 0.25% Fe-TiO_2 < 0.50% Fe-SynTiO_2 < 0.25% SynTiO_2 < SynTiO_2.

The effects of photocatalyst specimens on bacteria inactivation in "HA and WM" solution could also be expressed in terms of reduction percentage of *E. coli* in a decreasing order as; SynTiO_2 > 0.25% Fe-SynTiO_2 > 0.50% Fe-SynTiO_2 = 0.25% Fe-TiO_2 > 0.50% Fe-TiO_2 > TiO_2. However, although bacteria reduction percentages (e.g., 99 %) were the same, respective bacteria LRV displayed variations in between 2.14-2.23. LRV of *E. coli* inactivation in "HA and WM" solution followed an increasing order as; TiO_2 < 0.50% Fe-TiO_2 < 0.25% Fe-TiO_2 < 0.50% Fe-SynTiO_2 <

0.25% Fe-SynTiO$_2$ < SynTiO$_2$. It could be indicated that, 0.25% Fe-SynTiO$_2$ expressed higher bacteria inactivation efficiency among other Fe-doped photocatalyst specimens. On the other hand, the most effective photocatalyst upon *E. coli* inactivation in "HA and WM" solution was observed as SynTiO$_2$ while the least effective one bare TiO$_2$ specimen.

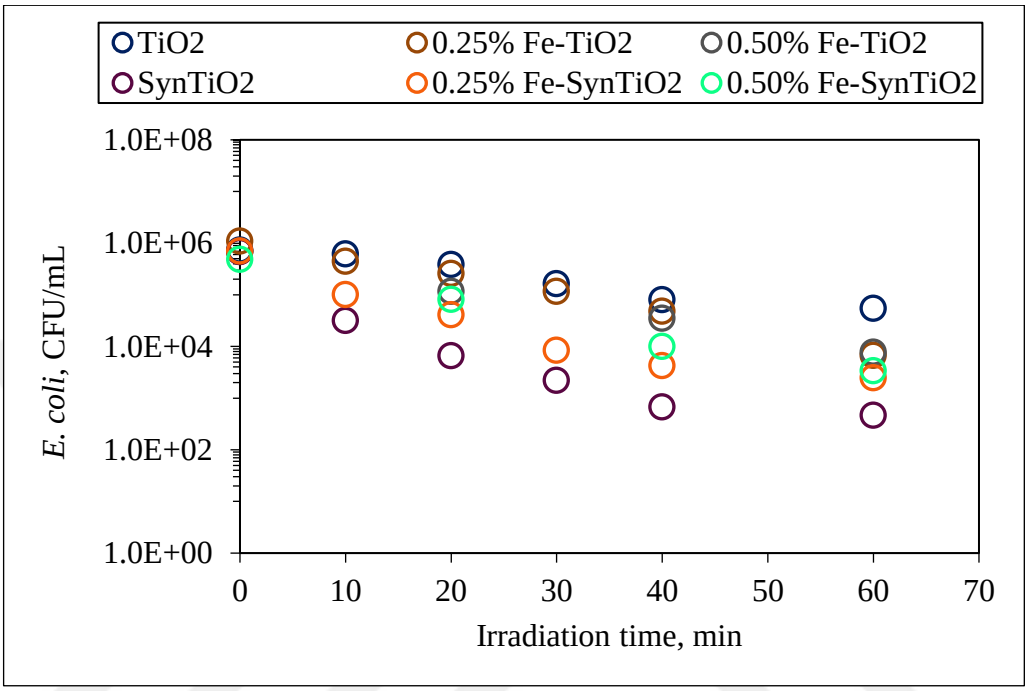

Figure 4.175. Irradiation time dependent *E. coli* inactivation in "HA and WM" solution upon solar photocatalytic treatments performed in the presence of undoped and Fe-doped TiO$_2$ specimens.

Table 4.68. Solar photocatalytic treatment of *E. coli* in "HA and WM" solution performed in the presence of undoped and Fe-doped TiO$_2$ specimens: Inactivation parameters.

E. coli in "HA and WM" solution solar photocatalytic treatment	First order kinetic model			LRV	Reduction, %
	k, min^{-1}	$t_{1/2}$, min	R, CFU/mL min		
TiO$_2$	0.0488	14.2	3.22E+04	1.08	90
SynTiO$_2$	0.117	5.92	6.21E+04	3.06	99.9
0.25% Fe-TiO$_2$	0.0834	8.31	7.72E+04	2.14	99
0.50% Fe-TiO$_2$	0.0734	9.44	3.92E+04	1.84	96.8
0.25% Fe-SynTiO$_2$	0.0943	7.35	7.38E+04	2.50	99.7
0.50% Fe-SynTiO$_2$	0.0850	8.15	4.88E+04	2.23	99

From a general perspective, related to inactivation rate constants and LRV of *E. coli* upon use of different photocatalyst specimens, it could be concluded that SynTiO$_2$ and Fe-doped SynTiO$_2$ specimens, having higher crystallite particle sizes, displayed selectivity towards *E. coli* however TiO$_2$ and Fe-doped TiO$_2$ specimens, having lower crystallite particle sizes, expressed selectivity against

humic matter present in reaction solution (Table C.1.). Similar trend was also observed from sole HA solution conditions.

Moreover, Birben and colleagues reported that 0.25% Fe-TiO_2 showed a retardation effect on HA removal rates compared to bare TiO_2, which complies with higher bacteria inactivation rate constant and LRV obtained in case that 0.25% Fe-TiO_2 was used as the photocatalyst specimen (Birben et al., 2017b). Therefore, it could be indicated that 0.25% Fe-TiO_2 has selectivity towards bacteria rather than HA content on contrary to bare TiO_2 specimen.

Based on inactivation rate constants and LRV of *E. coli* inactivation in "HA and WM" solution, undoped and Fe-doped SynTiO_2 specimens displayed quite close results with each other however bare SynTiO_2 expressed higher *E. coli* LRV and bacteria inactivation rate constant than 0.50% Fe-SynTiO_2 specimen. However, Turkten and Cinar reported that 0.50% Fe-SynTiO_2 displayed a slight agglomeration and higher degradation percentage of 4-nitrophenol as a model organic compound than SynTiO_2 and 0.50% Fe-SynTiO_2 (Turkten and Cinar, 2019). Therefore, it could be concluded that 0.50% Fe-SynTiO_2 most probably tend to display selectivity towards organic matter degradation rather than bacteria inactivation on contrary to bare SynTiO_2 specimen.

4.3.4.1. Comparative mechanistic evaluation of *E. coli* inactivation in "HA and WM" solution upon solar photocatalytic treatments performed in the presence of undoped and Fe-doped TiO_2 specimens.

As solar photocatalytic inactivation products of bare and Fe-doped TiO_2 solar photocatalytic treatments of *E. coli* in "HA and WM" solution components, total K, protein, and carbohydrate contents under initial, t=0, and t_{irr}=60 min conditions were given in Figure 4.176.

Under all conditions, total K contents displayed variations in the range of 4.07-4.61 mg/L. Due to the presence of WM solution as a reaction matrix constituent, total K contents expressed higher presence than IsoT (Figure 4.170) and sole HA solution (Figure 4.174) conditions as expected. All photocatalyst specimens displayed immediate adsorptive removal of total K the range of 0.44-4.1 % at t=0 condition. Moreover, all conditions showed decreased total K concentrations at the end of 60 min irradiation period.

Protein contents expressed changes in between 4.35-22.8 mg/L under all conditions. In the presence of bare TiO_2, protein content displayed a decreasing trend at t_{irr}=60 min (3.93-1.48 mg/L) on contradiction to the increasing trend obtained upon use of other photocatalyst specimens. Degradation of proteinaceous matter could be associated with obtained lower bacteria inactivation

rates in case that TiO_2 used as bare photocatalyst and could support the suggestion about selectivity of TiO_2 against organic content rather than bacteria. Similar protein degradation and release patterns were also detected solar photocatalytic treatments conducted in sole HA solution conditions (Figure 4.174).

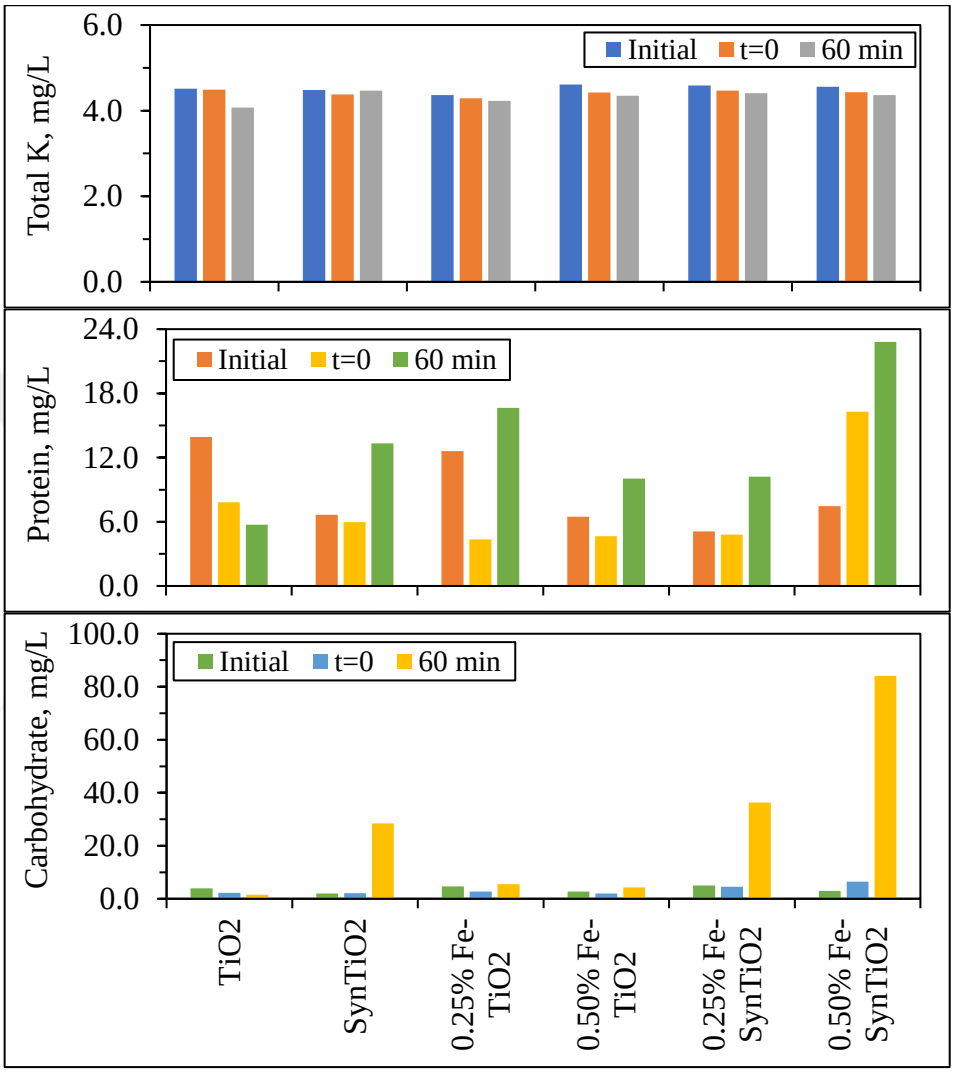

Figure 4.176. Initial, t=0, and t_{irr}=60 min total K, protein, and carbohydrate contents of *E. coli* inactivation in "HA and WM" solution upon solar photocatalytic treatments performed in the presence of bare and Fe-doped TiO_2 specimens.

Upon with the use of bare $SynTiO_2$ and all Fe-doped photocatalyst specimens, protein contents showed an increase at the end of 60 min irradiation period and maximum protein concentration was detected as 22.8 mg/L in the presence of 0.50% Fe-$SynTiO_2$. Under these conditions, despite the masking effect of humic-like fluorophores on protein-like ones, the presence of proteinaceous organic compounds was clearly presented by respective UV-vis absorbance (Figures 4.161 and 163), synchronous scan fluorescence spectral features (Figure 4.162) as well as EEM fluorescence contour

plots (Figures 4.165). Interestingly, solar photocatalytic treatments upon use of 0.50% Fe-SynTiO_2 in the presence of either sole HA solution (16.2 mg/L) or "HA and WM" solution (22.8 mg/L) high protein contents were still present in reaction medium (Figures 4.174 and 4.176).

From a general view, carbohydrate contents displayed variations in the range of 1.48-84.2 mg/L. Upon use of undoped and Fe-doped TiO_2 specimens all carbohydrate concentrations were quite low as < 6.5 mg/L for initial and t=0 conditions, expressing insignificant role of Fe doping on TiO_2. On the other hand, bare TiO_2 specimen displayed a degradation effect on carbohydrate content at t_{irr}=60 min (3.93-1.48 mg/L) similar to detected decrease in protein content. Similar trend was also detected upon use of undoped TiO_2 in sole HA solution condition (Figure 4.174). All other photocatalyst specimens showed increased carbohydrate concentrations at the end of 60 min solar light irradiation period and maximum carbohydrate content was detected as 84.2 mg/L in the case that 0.50% Fe-SynTiO_2.

4.4. Endotoxin Release Upon Solar Photolytic and Photocatalytic Inactivation of *E. coli* in Various Aqueous Solutions

Endotoxins are noxious substances present outside of the cell wall of Gram-negative bacteria. LPS which are a component of outer membrane of Gram-negative bacteria e.g., *E. coli*, consists of three parts as: O polysaccharide, core polysaccharide, and lipid A (Figure 4.177). The lipid A portion of LPS is the endotoxin of *E. coli*, therefore; it should be noted that endotoxins are not metabolic products, they are a natural part of the cell wall. Endotoxin release could occur when bacteria die, cell wall undergo to lysis and during the bacterial multiplication (Prescott et al., 1993; Tortora et al., 2018). Moreover, it should be indicated that endotoxins are not necessarily specific to infectious *E. coli* serotype O157:H7 due to presence of endotoxins in the outer membrane structure of all Gram-negative bacteria.

Major health related impacts could be expressed as that endotoxins have a great spectrum of biological activities on mammals and some of the main ones are pyrogenicity, leukopenia and septic shock. Basically, pyrogens are fever inducing agents of Gram-negative bacteria represented by endotoxins and pyrogenicity is probably the first recognized activity of endotoxins (Galanos, 1998).

During solar photolytic and photocatalytic inactivation processed, endotoxins could be released as inactivation by-products of bacteria. In this study, potential release of *E. coli* endotoxins was followed under different irradiation period conditions as well as control conditions as sole HA

solution, IsoT solution, WM solution, and distilled-deionized water. Limiting value of LAL analysis kit was determined as 0.125 EU/mL according to pure dialysis water having pyrogen-free characteristics (Glorieux et al., 2012).

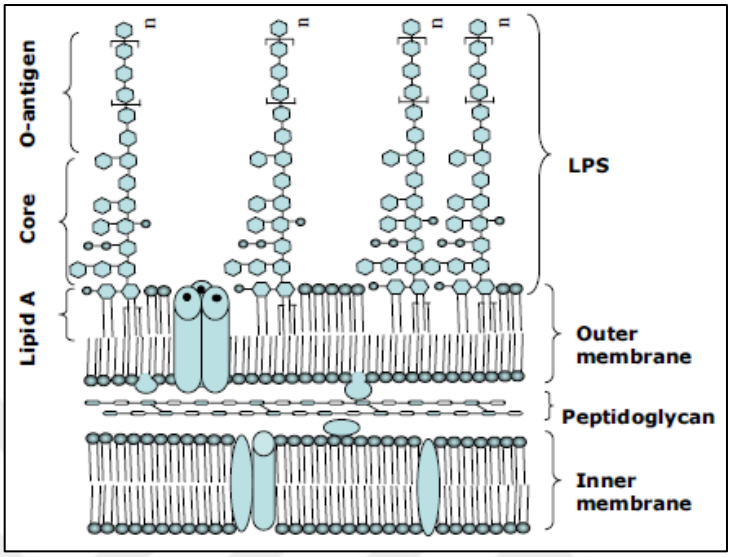

Figure 4.177. Schematic diagram of LPS structure and positioning on Gram-negative bacteria cell wall (Cardoso et al., 2006).

All selected solutions were subjected to LAL analysis and displayed endotoxin content as > 0.125 EU/mL including control conditions. Due to the detection of endotoxin content in sole HA, IsoT and WM solution conditions in the absence of *E. coli*, it could be considered that the probability of false positive determinations. Moreover, even distilled-deionized water expressed endotoxin content more than 0.125 EU/mL, therefore; positive endotoxin contents of sole reaction matrixes could be due to the lack of pyrogen-free water conditions rather than false positive endotoxin determinations. On the other hand, it should be noted that sterile and pyrogen-free indicates different conditions, sterile means absence of any viable microorganism while pyrogen-free means non-existence of fever causing substances. Consequently, it could be indicated that endotoxin analysis should be cautiously interpreted in the absence of pyrogen-free water conditions. However, degradation of endotoxin content originated from *E. coli* destruction under UV and solar irradiation conditions upon use of various photocatalyst specimens were reported in literature (Gadgil and Kodialbail, 2021; Sunada et al., 1998; Sreeja and Shetty, 2016, 2017). It should be emphasized that by-products released upon cell lysis e.g., carbohydrates were not considered in all of the aforementioned publications contrary to the findings reported in this study. Therefore, a comprehensive approach covering all aspects of cell destruction resulting in utmost removal of any live bacteria should be followed by characterization of complex organic matrix unless otherwise complete mineralization is achieved.

5. CONCLUSION

In this study, solar photolytic and photocatalytic inactivation of *E. coli* in various reaction matrixes was successfully achieved and characterized. Photocatalysis was performed under simulated solar irradiation conditions (wavelength range of λ=290 nm to 800 nm and light intensity, I_o=250 W/m^2) using different TiO_2 based photocatalyst specimens i.e., TiO_2 (P-25), SynTiO_2 (sol-gel synthesized) and Fe-doped counterparts as 0.25% and 0.50%. HA solution was used to represent NOM in aqueous medium. Saline solution (IsoT) was considered as baseline medium and aqueous solution containing common anions and cations defined water matrix (WM) was also employed.

Most significantly, simultaneous reduction of *E. coli* cell counts and degradation of organic matter could be attained under different experimental conditions upon solar irradiation. A retardation effect in the presence of "HA and WM" solution as mimicking natural surface water conditions was observed upon all solar photolytic and photocatalytic conditions regardless of changing photocatalyst specimens either bare or Fe-doped types. However, the significant role of "HA and WM" solution occurring via both photo initiated self-reactions and adsorptive interactions should be cautiously interpreted.

Photocatalyst specimens displayed different effectiveness upon use of IsoT, WM, sole HA, and "HA and WM" solutions. Solar photocatalytic inactivation of *E. coli* in IsoT solution under the presence of bare TiO_2 specimen was effectively achieved leading LRV as 5.90 excluding all possible adverse effects on inactivation process. However, in the presence of "HA and WM" solution, undoped TiO_2 was observed as the least effective photocatalyst specimen expressing *E. coli* LRV as 1.08. Attained enhanced retardation of *E. coli* inactivation in "HA and WM" solution should be evaluated considering present binary and ternary interactions between reaction medium components. In the presence of common anion and cation containing WM solution, solar photocatalytic *E. coli* inactivation was achieved successfully upon use of bare SynTiO_2 expressing LRV as 4.35. Moreover, upon use of sole HA solution as a reaction medium, the most effective *E. coli* reduction was attained in the presence of 0.25% Fe-SynTiO_2 specimen expressing LRV as 3.82. On the other hand, undoped SynTiO_2 was observed as the most effective photocatalyst specimen on *E. coli* inactivation in "HA and WM" solution revealing bacteria LRV as 3.06. As an overall evaluation expressed by first order kinetic rate constants, except upon use of 0.25% Fe-TiO_2, all solar photolytic and photocatalytic treatments displayed the least effectiveness on *E. coli* reduction in "HA and WM" solution conditions. Therefore, it should be noted that, bacteria inactivation efficiencies of different photocatalyst specimens were directly related to present aqueous medium conditions.

Organic matter released and removed upon solar photolytic and photocatalytic inactivation of *E. coli* could be effectively characterized by UV-vis and fluorescence spectroscopic techniques and quantified by NPOC contents. Based on applied EEM fluorescence contour plots relating to *E. coli* inactivation upon solar irradiation, properties of in-situ produced organic matter could be deeply investigated. Application of EEM fluorescence spectroscopy displayed detailed information about qualification of organic inactivation products by distinguishing them from humic features originating from background reaction matrixes. Moreover, emergence of microbial by-products and protein-like fluorophores were evidently identified by EEM fluorescence features.

Bacteria inactivation products as total K^+, protein and carbohydrate contents significantly revealed the destruction of *E. coli* cell wall. However, K^+ ion release from damaged cells should be carefully distinguished from already present K^+ ion content originating from WM condition especially while working with low initial bacteria counts. In the presence of high NOM contents, the accuracy of inactivation product concentrations (protein and carbohydrate) could considerably be affected via cage effect and/or encapsulation of lower molecular weight fractions by higher molecular weight fractions of humic substances due to re-conformational arrangements. On the other hand, it should be kept in mind that effect of filtration applied prior to analysis could cause elimination of some inactivation products due to prevailing electrostatic interactions between matrix constituents, therefore; remaining organic and inorganic substances in solution could not be regarded as representing exact content prior to filtration. It should be emphasized that membrane filtration did not exert any effect on *E. coli* cell counts thereby inactivation efficiencies due to the applied sampling procedure prior to filtration step.

Considering diverse physicochemical features of natural water systems containing NOM along with inorganic components, due to probable retardation effects on microorganism inactivation efficiencies of various photocatalyst specimens, direct solar light initiated reactions should be taken into consideration as well. Thus, simultaneously operating reactions ensued remarkable efficiencies on both *E. coli* cell count reduction as well as degradation of complex organic matter using bare TiO_2 and VLA TiO_2 specimens.

REFERENCES

Abdullah, M., Low, G.K.C., Matthews, R.W., 1990. Effects of common inorganic anions on rates of photocatalytic oxidation of organic carbon ove illuminated titanium dioxide. Journal of Physical Chemistry, 94, 6820-6825.

Acra, A., Karahagopian, Y., Raffoul, Z., Dajani, R., 1980. Disinfection of oral rehydration solutions by sunlight. The Lancet, 1257-1258.

Acra, A., Raffoul, Z., Karahagopian, Y., 1984. Solar disinfection of drinking water and oral rehydration solutions: Guidelines for household application in developing countries. UNICEF, Beirut, Lebanon.

Acra, A., Jurdi, M., Mu'allem, H., Karahagopian, Y., Raffoul, Z., 1989. Sunlight as disinfectant. The Lancet, 280.

Adachi, Y., Kobayashi, A., Kobayashi, M., 2012. Structure of colloidal flocs in relation to dynamic properties of unstable suspension. International Journal of Polymer Science, 2012, 574878, doi: 10.1155/2012/574878.

Adhikari, S., Banerjee, A., Eswar, N.K., Sarkar, D., Madras, G., 2015. Photocatalytic inactivation of *E. coli* by ZnO-Ag nanoparticles under solar radiation. Royal Society of Chemistry, 5, 51067-51077.

Aguer, J.P., Richard, C., 1993. Use of furoin as probe molecule for the involvement of singlet oxygen in aqueous phase photoinduced transformations. Toxicological and Environmental Chemistry, 39, 217-227.

Aguer, J.P., Richard, C., 1996. Reactive species produced on irradiation at 365 nm of aqueous solutions of humic acids. Journal of Photochemistry and Photobiology A: Chemistry, 93, 193-198.

Aguer, J.P., Richard, C., Andreux, F., 1999. Effect of light on humic substances: Production of reactive species. Analusis, 27, 5, 387-390.

Aiken, G.R., McKnight, D.M., Wershaw, R.L. (Eds.), 1985. Humic Substances in Soil, Sediment and Water, Wiley, New York, U.S.A.

Alberts, J.J., Takács, M., 2004. Total luminescence spectra of IHSS standard and reference fulvic acids, humic acids and natural organic matter: Comparison of aquatic and terrestrial source terms. Organic Geochemistry, 35, 243-256.

Aldsworth, T.G., Sharman, R.L., Dodd, C.E.R., 1999. Bacterial suicide through stress. Cellular and Molecular Life Sciences, 56, 378-383.

Alegre, M.L., Gerones, M., Rosso, J.A., Bertolotti, S.G., Braun, A.M., Martire, D.O., Gonzalez, M.C., 2000. Kinetic study of the reactions of chlorine atoms and $Cl_2^{\bullet-}$ radical anions in aqueous solutions. 1. Reaction with benzene. Journal of Physical Chemistry A, 104, 3117-3125.

An, H., Smith, D., 2005. Determination of Reducing and Nonreducing Sugars Using the Phenol-Sulfuric Acid Assay. In: Wrolstad, R.E., Acree, T.E., Decker, E.A., Penner, M.H., Reid, D.S., Schwartz, S.J., Shoemaker., C.F., Smith, D., Sporns, P. (Eds.), Handbook of Food Analytical Chemistry: Water, Proteins, Enzymes, Lipids, and Carbohydrates, 653-655, John Wiley & Sons., Inc., New Jersey, U.S.A.

An, T., Sun, H., Li, G., 2017. Photoelectrocatalytic Inactivation Mechanism of Bacteria. In: An, T., Zhao, H., Wong, P.K. (Eds.), Advances in Photocatalytic Disinfection, Green Chemistry and Sustainable Technology, Springer-Verlag GmbH, Berlin, Germany.

APHA, AWWA, WPCF, 2012. Standard Methods for the Examination of Water and Wastewater, 22nd Ed., American Public Health Association, American Water Works Association, Water Environment Federation Washington D.C., USA.

Artem'yev, V.Y., 1970. Carbohydrates in bottom sediments of the central Pacific. Oceanology, 10, 508-513.

Artifon, V., Zanardi-Lamardo, E., Fillmann, G., 2019. Aquatic organic matter: Classification and interaction with organic microcontaminants. Science of the Total Environmet, 649, 1620-1635.

Baker, A., Tipping, E., Thacker, S.A., Gondar, D., 2008. Relating dissolved organic matter fluorescence and functional properties. Chemosphere, 73, 1765-1772.

Beagle, S.D., Lockless, S.W., 2020. Unappreciated roles for K^+ channels in bacterial physiology. Trends in Microbiology, doi: 10.1016/j.tim.2020.11.005.

Bekbolet, M., 1997. Photocatalytic bactericidal activity of TiO_2 in aqueous suspensions of *E. coli*. Water Science and Technology, 35, 95-100.

Bekbolet, M., 2007. Photocatalytic Inactivation of Microorganisms in Drinking Water. In: Nikolau, A., Selcuk, H., Rizzo, L. (Eds.), Control of Disinfection By-Products in Drinking Water Systems, 97-117, NOVA Science Publishers Inc., New York, U.S.A.

Bekbolet, M., 2020. An Overview of Photocatalytic Drinking Water Treatment. In: Naddeo, V., Balakrishnan, M., Choo, K., (Eds.), Frontiers in Water-Energy-Nexus—Nature-Based Solutions, Advanced Technologies and Best Practices for Environmental Sustainability, 247-248, Springer Nature Switzerland AG, Switzerland.

Bekbolet, M., Araz, C.V., 1996. Inactivation of *Escherichia coli* by photocatalytic oxidation. Chemosphere, 32, 959-965.

Bekbolet, M., Balcioglu, I., 1996. Photocatalytic degradation kinetics of humic acids in aqueous TiO_2 disperisons: The influence of hydrogen peroxide and bicarbonate ion. Water Science and Technology, 34, 9, 73.

Bekbolet, M., Ozkosemen, G., 1996. A preliminary investigation on the photocatalytic degradation of a model humic acid. Water Science and Technology, 33, 6, 189-194.

Bekbolet, M., Boyacioglu, Z., Ozkaraova, B., 1998. The influence of solution matrix on the photocatalytic removal of color from natural waters. Water Science and Technology, 38,155-162.

Bekbolet, M., Tomruk, A., 1998. Photocatalytic Treatment of Drinking Water: Applications on Microorganisms and NOM. The 1998 European Workshop on Water and Air Treatment by Advanced Oxidation Technologies: Innovative and Commercial Applications. EPFL Lausanne, Oct 11-14, Switzerland.

Bekbolet, M., Sen-Kavurmaci, S., 2015. Effect of photocatalytic oxidation on molecular size distribution profiles of humic acid. Photochemical and Photobiological Sciences, 14, 576-582.

Bekbolet, M., Turkten, N., 2020. Solar Photocatalytic Degradation of Humic Acids Using Copper-Doped TiO_2. In: Naddeo, V., Balakrishnan, M., Choo, K., (Eds.), Frontiers in Water-Energy-Nexus—Nature-Based Solutions, Advanced Technologies and Best Practices for Environmental Sustainability, 257-260, Springer Nature Switzerland AG, Switzerland.

Beranek, R., 2011. (Photo)electrochemical methods for the determination of the band edge positions of TiO_2-based nanomaterials. Advances in Physical Chemistry, 2011, doi: 10.1155/2011/786759.

Bertani, G., 1951. Studies on lysogenesis. I. The mode of phage liberation by lysogenic *Escherichia coli.* Journal of Bacteriology, 62, 293-300.

Birben, N.C., Uyguner-Demirel, C.S., Sen-Kavurmacı, S., Gurkan, Y.Y., Turkten, N., Cinar, Z., Bekbolet, M., 2015. Comparative evaluation of anion doped photocatalysts on the mineralization and decolorization of natural organic matter. Catalysis Today, 240, 124-131.

Birben, N.C., Tomruk, A., Bekbolet, M., 2017a. The role of visible light active TiO_2 specimens on the solar photocatalytic disinfection of *E. coli*. Environmental Science and Pollution Research, 24, 12618-12627.

Birben N.C., Uyguner-Demirel C.S., Sen-Kavurmaci S., Gurkan Y.Y., Turkten N., Cinar Z., Bekbolet M., 2017b. Application of Fe-doped TiO_2 specimens for the solar photocatalytic degradation of humic acid. Catalysis Today, 281, 78-84.

Birben, N.C., Lale, E., Pelosato, R., Uyguner-Demirel, C.S., Sora, I.N., Bekbolet, M., 2021a. Photocatalytic bactericidal performance of $LaFeO_3$ under solar light: Kinetics, spectroscopic and mechanistic evaluation. Water, 13, 1135, doi: 10.3390/w13091135.

Birben, N.C., Lale, E., Uyguner-Demirel, C.S., Bekbolet, M., 2021b. Elucidation of in-situ produced oreganic matrix effect on the solar photo/photocatalytic inactivation of *E. coli*. Catalysis Today, doi: 10.1016/j.cattod.2021.04.025.

Blake, D.M., Maness, P.C., Huang, Z., Wolfrum, E.J., Huang, J., Jacoby, W.A., 1999. Application of the photocatalytic chemistry of titanium dioxide to disinfection and the killing of cancer cells. Separation and Purification Reviews, 28, 1-50.

Blough, N.V., Zepp, R.G., 1995. Reactive Oxygen Species in Natural Waters. In: Foote, C., Valentine, J., Greenberg, A., Liebman, J.F. (Eds.), Active Oxygen in Chemistry, 280-332, Chapman and Hill, New York, U.S.A.

Bose, B., Chatterjee, S.N., 1995. Correlation between UVA-induced changes in microviscosity, permeability, and malondialdehyde formation in liposomal membrane. Journal of Photochemistry and Photobiology, B, 28, 149-153.

Bosshard, F., Berney, M., Scheifele, M., Weilenmann, H.U., Egli, T., 2009. Solar disinfection (SODIS) and subsequent dark storage of *Salmonella typhimurium* and *Shigella flexneri* monitored by flow cytometry. Microbiology-Sgm, 155, 1310-1317.

Bosshard, F., Bucheli, M., Meur, Y., Egli, T., 2010a. The respiration chain is the cell's Achilles' heel during UVA inactivation in *Escherichia coli*. Microbiology, 156, 2006-2015.

Bosshard, F., Riedel, K., Schneider, T., Geiser, C., Bucheli, M., Egli, T., 2010b. Protein oxidation and aggregation in UVA-irradiated *Escherichia coli* cells as signs of accelerated cellular senescence. Environmental Microbiology, 12, 2931-2945.

Brock, T.D., Madigan, M.T., Martinko, J.M., Parker, J., 2000. Brock Biology of Microorganisms, 9th Edition, Prentice Hall International, New Jersey, U.S.A.

Brummer, Y., Cui, S.W., 2005. Phenol-sulfuric acid assay. In: Cui, S.W. (Eds.), Food Carbohydrates: Chemistry, Physical Properties, and Applications, 70-72, CRC Press, Taylor & Francis Group, Boca Raton, Florida, U.S.A.

Buffle, J., 1984. Natural Organic Matter and Metal-Organic Interactions in Aquatic Systems. In: Sigel, H. (Eds.), Metal Ions in Biological Systems, 18, 165-221, Marcel Dekker, Inc., New York, U.S.A.

Buffle, J., 1988. Complexation Reactions in Aquatic Systems: An Analytical Approach, Ellis Horwood, Chichester, West Sussex, U.K.

Busse, M.M., Becker, M., Applegate, B.M., Camp Jr., J.W., Blatchley III, E.R., 2019. Responses of *Salmonella typhimurium* LT2, *Vibrio harveyi*, and *Cryptosporidium parvum* to UVB and UVA radiation. Chemical Engineering Journal, 371, 647-656.

Buthiyappan, A., Aziz, A.R.A., Daud, W.M.A.W., 2016. Recent advances and prospects of catalytic advanced oxidation process in treating textile effluents. Reviews in Chemical Engineering, 32, 1-47.
Butler, S.M., Camilli, A., 2005. Going against the grain: Chemotaxis and infection in *Vibrio cholera*. Nature Reviews Microbiology, 3, 611-620.

Byrne, J.A., Dunlop, P.S.M., Hamilton, J.W.J., Fernández-Ibáñez, P., Polo-López, I., Sharma, P.K., Vennard, A.S.M., 2015. A review of heterogeneous photocatalysis for water and surface disinfection. Molecules, 20, 5574-5615.

Bythell, B.J., Rabus, J.M., Wagoner, A.R., Abutokaikah, M.T., Maître, P., 2018. Sequence ion structures and dissociation chemistry of deprotonated sucrose anions. Journal of The American Society for Mass Spectromety, 29, 2380-2393.

Cabiscol, E., Tamarit, J., Ros, J., 2000. Oxidative stress in bacteria and protein damage by reactive oxygen species. International Microbiology, 3, 3-8.

Cantwell, R.E., Hofmann, R., Templeton, M.R., 2008. Interactions between humic matter and bacteria when disinfecting water with UV light. Journal of Applied Microbiology, 105, 25-35.

Cardoso, P.G., Macedo, G.C., Azevedo, V., Oliveira, S.C., 2006. *Brucella spp* noncanonical LPS: structure, biosynthesis, and interaction with host immune system. Microbial Cell Factories, 5, 13, doi:10.1186/1475-2859-5-13.

Carey, J.H., Lawrence, J., Tosine, H.M., 1976. Photo-dechlorination of PCDBs in presence of titanium-dioxide in aqueous suspensions. Bulletin of Environmental Contamination and Toxicology, 16, 697-701.

Carratala, A., Calado, A.D., Mattle, M.J., Meierhofer, R., Luzi, S., Khon, T., 2016. Solar disinfection of viruses in polyethylene terephthalate bottles. Applied and Environmental Microbiology, 82, 1, 279-288.

Carré, G., Hamon, E., Ennahar, S., Estner, M., Lett, M-C., Horvatovich, P., Gies, J-P., Keller, V., Keller, N., Andre, P., 2014. TiO_2 photocatalysis damages lipids and proteins in *Escherichia coli*. Applied and Environmental Microbiology, 80, 2573-2581.

Castro-Alférez, M., Polo-López, M.I., Fernández-Ibáñez, P., 2016. Intracellular mechanisms of solar water disinfection. Scientific Reports, 6:38145, doi: 10.1038/srep38145.

Centi, G., Perathoner, S., 2005. Use of Solid Catalysts in Promoting Water Treatment and Remediation Technologies. In: Spivey, J.J. (Eds.), Catalysis: Volume 18, 46-71, The Royal Society of Chemistry, Cambridge, U.K.

Chen, H.Y., Zahraa, O., Bouchy, M., 1997. Inhibition of the adsorption and photocatalytic degradation of an organic contaminant in an aqueous suspension of TiO_2 by inorganic ions. Journal of Photochemistry and Photobiology A, Chemistry, 108, 37-44.

Chiang, S.M., Schellhorn, H.E., 2012. Regulators of oxidative stress response genes in *Escherichia coli* and their functional conservation in bacteria. Archives of Biochemistry and Biophysics, 525, 161-169.

Chick, H., 1908. An investigation of the laws of disinfection. The Journal of Hygiene, 8, 1, 92-158.

Cho, Y., Choi, W., Lee, C.-H., Hyeon, T., Lee, H.-I., 2001. Visible light-induced degradation of carbon tetrachloride on dye-sensitized TiO_2. Environmental Science and Technology, 35, 966-970.

Choppin, G.R., Allard, B., 1985. The complexes of actinides with naturally occurring organic compounds. In: Freeman, A.J., Keller, C. (Eds.), Handbook on the Physics and Chemistry of the Actinides, 407-429, Elsevier Science Publishers B.V., Amsterdam, The Netherlands.

CHROMagar ECC Product Leaflet. http://www.chromagar.com/fichiers/1559127431LF_EXT_003_EF_V8.0.pdf?PHPSESSID=6fe616535612c2fbb5966d02cb2804c4. Date accessed July 2019.

Clark, D.P., 1989. The fermentation pathways of *Escherichia coli*. FEMS Microbiology Reviews, 5, 223-234.

Coble, P.G., 1996. Characterization of marine and terrestrial DOM in seawater using excitation-emission matrix spectroscopy. Marine Chemistry, 51, 325-346.

Conroy, R.M., Elmore-Meegan, M., Joyce, T., McGuigan, K.G., Barnes, J., 1996. Solar disinfection of drinking water and diarrhoea in Maasai children: a controlled field trial. The Lancet, 348, 1695-1697.

Cooper, W.J., Zika, R.G., Petasne, R.G., Fischer, A.M., 1988a. Sunlight-induced photochemistry of humic substances in natural waters: major reactive species. Advances in Chemistry, 219, 333-362.

Cooper, W.J., Zika, R.G., Petasne, R.G., Plane, J.M.C., 1988b. Photochemical formation of H_2O_2 in natural waters exposed to sunlight. Environmental Science and Technology, 22, 1156-1160.

Corpe, W. A. 1970. Attachment of marine bacteria to solid surfaces. In: Manly, R. S. (Eds.), Adhesion in biological systems, 73-87, Academic Press, Inc., New York, U.S.A.

Curtis, T.P., Mara, D.D., Silva, S.A., 1992. Influence of pH, oxygen and humic substances on ability of sunlight to damage fecal coliforms in waste stabilization pond water. Applied and Environmental Microbiology, 58, 1335-1343.

Dalle-Donne, I., Rossi, R., Giustarini, D., Milzani, A., Colombo, R., 2003. Protein carbonyl groups as biomarkers of oxidative stress. Clinica Chimica Acta, 329, 23-38.

Dalrymple, O.K., Stefanakos, E., Trotz, M.A., Goswami, D.Y., 2010. A review of the mechanisms and modeling of photocatalytic disinfection. Applied Catalysis B: Environmental, 98, 27-38.

Dalrymple O., Isaac, W., Stefanakos, E., Trotz, M., Goswami, D., 2011. Lipid vesicles as model membranes in photocatalytic disinfection studies. Journal of Photochemistry and Photobiology A, 221, 64-70.

Dalrymple, O.K., Goswami, D.Y., 2017. Mechanistic Modeling of Photocatalytic Water Disinfection. In: An, T., Zhao, H., Wong, P.K. (Eds.), Advances in Photocatalytic Disinfection, Green Chemistry and Sustainable Technology, Springer Nature, Berlin, Germany.

Dawson, R., Liebezeit, G., 1981. The Analytical Methods for the Characterization of Organics in Seawater. In: Duursma, E.K., Dawson, R. (Eds.), Marine Organic Chemistry: Evolution, Composition Interactions and Chemistry of Organic Matter in Seawater, Oceanography Series, 31, 445-446, Amsterdam, The Netherlands.

de Melo, B.A.G., Motta, F.L., Santana, M.H.A., 2016. Humic acids: Structural properties and multiple functionalities for novel technological developments. Materials Science and Engineering: C, 62, 967-974.

Decho, A.W., 2011. Extracellular Polymeric Substances (EPS). In: Reitner, J., Thiel, V. (Eds.), Encyclopedia of Geobiology, Encyclopedia of Earth Sciences Series, 359-391, Springer, Dordrecht, Germany, doi: 10.1007/978-1-4020-9212-1_86.

Demchick, P., Koch., A.L., 2006. The permeability of the wall fabric of *Escherichia coli* and *Bacillus subtilis*. Journal of Bacteriology, 178, 768-773.

Dobosz, A., Sobczyński, A., 2003. The influence of silver additives on titania photoactivity in the photooxidation of phenol. Water Research, 37, 1489-1496.

Downes, A., Blunt, T.P., 1877a. The influence of light upon the development of bacteria. Nature, 218.

Downes, A., Blunt, T.P., 1877b. Researches on the effect of light upon *Bacteria* and other organisms. Proceedings of the Royal Society of London, 28, 488-501.

Downes, A., Blunt, T.P., 1878. On the influence of light upon protoplasm. Proceedings of the Royal Society of London, 28, 199-212.

Duboc, P., Marison, I., von Stockar, U., 1999. Quantitative calorimetry and biochemical engineering. In: Kemp, R.B. (Eds.), Handbook of Thermal Analysis and Calorimetry Vol. 4: from Molecules to Man, 267-365, Elsevier, Amsterdam, The Netherlands.

Dubois, M., Gilles, K.A., Hamilton, J.K., Rebers, P.A., Smith, F., 1956. Colorimetric method for determination of sugars and related substances. Analytical Chemistry, 28, 350-356.

Dujmov, J., Sučević, P., 1990. Application of synchronous fluorescence spectroscopy for characterization of the aromatic hydrocarbons in sediments of the middle Adriatic. Chemistry and Ecology, 4, 189-195.

Dworkin M., Falkow, S., Rosenberg, E., Schleifer, K.H., Stackebrandt, E. (Eds.), 2006. The Prokaryotes, A handbook on the Biology of Bacteria, Volume 1: Symbiotic Association, Biotechnology, Applied Microbiology, 3rd Edition, Springer Science + Bussiness Media, Inc., New York, U.S.A.

Eboigbodin, K.E., Biggs, C.A., 2008. Characterization of extracellular polymeric substances produced by *Escherichia coli* using infrared spectroscopic, proteomic, and aggregation studies. Biomacromolecules, 9, 686-695.

Edelhoch, H., 1967. Spectroscopic determination of tryptophan and tyrosine in proteins. Biochemistry, 6, 7, 1948-1954.

Edwards, A.C., Hooda, P.S., Cook, Y., 2001. Determination of nitrate in water containing dissolved organic carbon by ultraviolet spectroscopy. International Journal of Environmental Analytical Chemistry, 80, 1, 49-59.

Edzwald, J.K., Becker, W.C., Wattier, K.L, 1985. Surrogate parameters for monitoring organic matter and THM precursors. Research and Technology, Journal AWWA, 77, 4, 122-132.

Eisenstark, A., 1987. Mutagenic and lethal effects of near-ultraviolet radiation (290-400 nm) on bacteria and phage. Environmental and Molecular Mutagenesis, 10, 317-337.

Engebretson, R.R., von Wandruszka, R., 1994. Microorganization in dissolved humic acids. Environmental Science and Technology, 28, 11, 1934-1941.

EPA, 1991. Guidance Manual for Compliance with the Filtration and Disinfection Requirements for Public Water Systems Using Surface Water Sources. U.S. Environmental Protection Agency, Washington, D.C., U.S.A.

Espinoza, L.A.T., Frimmel, F.H., 2009. A simple simulation of the degradation of natural organic matter in homogeneous and heterogeneous advanced oxidation processes. Water Research, 43, 3902-3909.

Fetsch, D., Hradilova, E.M., Mendez, P., Havel, J., 1998. Capillary zone electrophoresis study of aggregation of humic substances. Journal of Chromatagraphy A, 817, 313-323.

Folin, O., Ciocalteu V., 1927. On tyrosine and tryptophane determinations in proteins. The Journal of Biological Chemistry, LXXIII, 2, 627-650.

Foyer, C.H., Lelandais, M., Kunert, K.J., 1994. Photooxidative stress in plants. Physiologia Plantarum, 92, 696-717.

Frank, S.N., Bard, A.J., 1977. Heterogeneous photocatalytic oxidation of cyanide ion in aqueous-solutions at TiO_2 powder. Journal of the American Chemical Society, 99, 303-304.

Fujishima, A., Honda, K., 1972. Electrochemical photolysis of water at a semiconductor electrode. Nature, 37, 238.

Fujishima, A., Rao, T.N., Tryk, D.A., 2000. Titanium dioxide photocatalysis. Journal of Photochemistry and Photobiology, C, 1, 1-21.

Fung, A.K.M., Chiu, B.K.W., Lam, M.H.W., 2003. Surface modification of TiO_2 by a ruthenium (II) polypyridly complex via silyl-linkage for the sensitized photocatalytic degradation of carbon tetrachloride by visible irradiation. Water Research, 37, 1939-1947.

Futsaether, C.M., Kjeldstad, B., Johnsson, A., 1995. Intracellular pH changes induced in *Propionibacterium acnes* by UVA radiation and blue light. Journal of Photochemistry and Photobiology, B, 31, 125-131.

Gadgil, D.J., Kodialbail, V.S., 2021. Suspended and polycaprolactone immobilized Ag @TiO_2/polyaniline nanocomposites for water disinfection and endotoxin degradation by visible and solar light-mediated photocatalysis. Environmental Science and Pollution Research, 28, 12780-12791.

Gaffney, J.S., Marley, N.A., Clark, S.B., 1996. Humic/Fulvic Acids and Organic Colloidal Materials in the Environment. In: Gaffney, J.S., Marley, N.A., Clark, S.B. (Eds.), Humic and Fulvic Acids, ACS Symposium Series, 651, 2-17, American Chemical Society, Washington, D.C., U.S.A.

Galanos, C., 1998. Endotoxin (Lipopolysaccharide (LPS)). Encyclopedia of Immunology, 806-807, ISBN: 0-12-226765-6.

Gerchakov, S. M., Hatcher, P.G., 1972. Improved technique for analysis of carbohydrates in sediments. Limnology and Oceanography, 17, 938-943.

Gjessing, E.T., 1976. Physical and Chemical Characteristics of Aquatic Humus, Ann Arbor Science Publishers Inc., Ann Arbor, Michigan, U.S.A.

Glaze, W.H., Kand, J.W., Chapin, D.H., 1987. The chemistry of water treatment processes involving ozone, hydrogen peroxide and UV-radiation. Ozone: Science and Engineering, 9, 335-352.

Glorieux, G., Neirynck, N., Veys, N., Vanholder, R., 2012. Dialysis water and fluid purity: more than endotoxin. Nephrology Dialysis Transplantation, 27, 4010-4021.

Gogniat, G., Thyssen, M., Denis, M., Pulgarin, C., Dukan, S., 2006. The bactericidal effect of TiO_2 photocatalysis involves adsorption onto catalyst and the loss of membrane integrity. FEMS Microbiology Letters, 258, 1, 18-24.

Gonenc, D., Bekbolet, M., 2001. Interactions of hypochlorite ion and humic acid: Photolytic and photocatalytic pathways. Water Science and Technology, 44, 5, 205.

Gourmelon, M., Cillard J., Pommepuy, M., 1994. Visible light damage to *Escherichia coli* in seawater: oxidative stress hypothesis. Journal of Applied Bacteriology, 77, 105-112.

Grigor'ev, A.E., Makarov, I.E., Pikaev, A.K., 1987. Formation of Cl_2^- in the bulk of solution during radiolysis of concentrated aqueous solutions of chlorides. Khimiya Vysokikh Energii, 21, 2, 123-126.

Gupta, R., Modak, J., 2020. Bacterial lysis via photocatalysis – A critical mechanistic review. ChemCatChem, 12, 2148-2170.

Haberhauer, G., Bednar, W., Gerzabek, M.H., Rosenberg, E., 2000. Application of MALDI-TOF-MS to the Characterization of Fulvic Acids. In: Gabbour, E.A., Davies, G., (Eds.), Humic Substances – Versatile Components of Plants, Soil and Water, 143-152, The Royal Society of Chemistry, Cambridge, U.K.

Halliwell, B., Gutteridge, J.M.C., 1989. Free Radicals in Biology and Medicine, 2nd Ed., Oxford University Press, New York, U.S.A.

Harper, J.C., Christensen, P.A., Egerton, T.A., Curtis, T.P., Gunlazuardi, J., 2001. Effect of catalyst type on the kinetics of the photoelectrochemical disinfection of water inoculated with *E. coli*. Journal of Applied Electrochemistry, 31, 623-628.

Helali, S., Polo-López, M.I., Fernández-Ibáñez, P., Ohtani, B., Amano, F., Malato, S., Guillard, C., 2014. Solar photocatalysis: A green technology for *E. coli* contaminated water disinfection. Effect of concentration and different types of suspended catalyst. Journal of Photochemistry and Photobiology, A, 276, 31-40.

Herbert, D., Phipps, P.J., Strange, R.E., 1971. Chapter III: Chemical Analysis of Microbial Cells. Methods in Microbiology, 5, Part B, 209-344.

Hessler, C.M., Wu, M.Y., Xue, Z., Choi, H., Seo, Y., 2012. The influence of capsular extracellular polymeric substances on the interaction between TiO_2 nanoparticles and planktonic bacteria. Water Research, 46, 4687-4696.

Hidaka, H., Horikoshi, S., Serpone, N., Knowland, J., 1997. In vitro photochemical damage to DNA, RNA and their bases by an inorganic sunscreen agent on exposure to UVA and UVB radiation. Journal of Photochemistry and Photobiology A, 111, 205-213.

Hirakawa, K., Mori, M., Yoshida, M., Oikawa, S., Kawanishi, S., 2004. Photo-irradiated titanium dioxide catalyzes site specific DNA damage via generation of hydrogen peroxide. Free Radical Research, 38, 439-447.

Hogg, S., 2005. Essential Microbiology. John Wiley and Sons Ltd., West Sussex, U.K.

Hoigné, J., 1990. Formulation and Calibration of Environmental Reaction Kinetics; Oxidations by Aqueous Photooxidants as an Example. In: Stumm, W., (Eds), Aquatic Chemical Kinetics, 43-70, Wiley, New York, U.S.A.

Huang, W-J., Fang, G-C., Wang, C-C., 2005. The determination and fate of disinfection by-products from ozonation of polluted raw water. Science of the Total Environment, 345, 261-272.

Huang, G.C., Xia, D.H., An, T.C., Ng, T.W., Yip, H.Y., Li, G.Y., Zhao, H.J., Wong, P.K., 2015. Dual roles of capsular extracellular polymeric substances in the photocatalytic inactivation of *Escherichia coli*: comparison of *E. coli* BW25113 with its isogenic mutants. Applied Environmental Microbiology, 81, 5174-5183.

IARC, 2012. A review of human carcinogens. Part D: Radiation / IARC Working Group on the Evaluation of Carcinogenic Risks to Humans, Lyon, France.

Ingraham, J., 1999. Effect of Temperature, pH, Water Acidity, and Pressure on Growth in *Escherichia coli* and *Salmonella typhimurium*. In: Neidhardt, C.F. (Eds.), Cellular and Molecular Biology, 1543, American Society for Microbiology, Washington, D.C., U.S.A.

IUPAC, 2004. International Union of Pure and Applied Chemistry, Compendium of Chemical Terminology, Gold Book, http://goldbook.iupac.org/pdf/goldbook.pdf. Date accessed June 2018.

Jagger, J., 1981. Near-UV radiation effects on microorganisms. Photochemistry and Photobiology, 34, 761-768.

Jayson, G.G., Parsons, B.J., Swallow, A.J., 1973. Some simple, high reactive, inorganic chloride derivatives in aqueous solution. Their formation using pulses of radiation and their role in the mechanism of the Fricke dosimeter. Journal of Chemical Society, Faraday Transactions 1: Physical Chemistry in Condensed Phases, 69, 1597-1607.

Jiang, X., Manawan, M., Feng, T., Qian, R., Zhao, T., Zhou G., Kong F., Wang, Q., Dai, S., Pan, J.H., 2017. Anatase and rutile in Evonik aeroxide P25: Heterojunctioned or individual nanoparticles? Catalysis Today, 300, 12-17.

Joost, U., Juganson, K., Visnapuu, M., Mortimer, M., Kahru, A., Nõmmiste, E., Joost, U., Kisand, V., Ivask, A., 2015. Photocatalytic antibacterial activity of nano-TiO_2 (anatase)-based thin films: Effects on *Escherichia coli* cells and fatty acids. Journal of Photochemistry and Photobiology, B, 142, 178-185.

Josefsson, B., Uppstrøm, L., Østling, G., 1972. Automatic spectrophotometric procedures for the determination of the total amount of dissolved carbohydrates in seawater. Deep-Sea Research, 19, 385-395.

Joyce, T., Kenny, V., McGuigan, K., Barnes, J., 1992. Disinfection of water by sunlight. The Lancet, 340, 921.

Joyce, T.M., McGuigan, K.G., Elmore-Meegan, M., Conroy, R.M., 1996. Inactivation of fecal bacteria in drinking water by solar heating. Applied and Environmental Microbiology, 62, 399-402.

Kehoe, S.C., Joyce, T.M., Ibrahim, P., Gillespie, J.B., Shahar, R.A., McGuigan, K.G., 2001. Effect of agitation, turbidity, aluminum foil reflectors and container volume on the inactivation efficiency of batch-process solar disinfectors. Water Research, 35, 1061-1065.

Kilic, M., Cinar, Z., 2009. A quantum mechanical approach to TiO_2 photocatalysis. Journal of Advanced Oxidation Technologies, 12, 1, 37-46.

Kiwi, J., Nadtochenko, V., 2005. Evidence for the mechanism of photocatalytic degradation of the bacterial wall membrane at the TiO_2 interface by ATR-FTIR and laser kinetic spectroscopy. Langmuir, 21, 4631-4641.

Koli, V.B., Delekar, S.D., Pawar, S.H., 2016. Photoinactivation of bacteria by using Fe-doped TiO_2-MWCNTs nanocomposites. Journal of Material Sciences: Materials in Medicine, 27, 177.

Kormann, C., Bahnemann, D.W., Hoffmann, M.R., 1991. Photolysis of chloroform and other organic molecules in aqueous TiO_2 suspensions. Environmental Science and Technology, 25, 494-500.

Kotzias, D., Parlar, H., Korte, F., 1982. Photoreaktivität organischer chemikalien in wäßrigen systemen in gegenwart von nitraten und nitriten. Naturwissenschaften, 69, 444-445.

Krishnan, K.S., Guha, A.C., 1934. The absorption spectra of nitrates and nitrites in relation to their photo-dissociation. Proceedings of the Indian Academy of Sciences – Section A, 1, 242-249.

Lawand, T.A., Alward, R., Odeyemi, O., Hahn, J., Kandpal, T.C., Ayoub, J., 1988. Solar Water Disinfection, Proceedings of a Workshop Held at the Brace Research Institute, Montreal, Quebec, 15-17 August 1988, Canada.

Leenheer, J.A., Croué, J.P., 2003. Characterizing aquatic dissolved organic matter. Environmental Science and Technology, 18A-26A.

Lettmann, C., Hinrichs, H., Maier, W.F., 2001. Combinatorial discovery of new photocatalysts for water purification with visible light. Angewandte Chemie International Edition, 40, 3160-3164.

Leung, T.Y., Chan, C.Y., Hu, C., Yu, J.C., Wong, P.K., 2008. Photocatalytic disinfection of marine bacteria using fluorescent light. Water Research, 42, 4827-4837.

Levin, J., Bang, F.B., 1968. Clottable protein in Limulus: Its localization and kinetics of its coagulation by endotoxin. Thrombosis et Diathesis Haemorrhagica, 19, 1, 186-197.

Levy, E.M., 1974. Flagellar elongation as a moving boundary problem. Bulletin of Mathematical Biology, 36, 265-273.

Li, X.Z., Li, F.B., Yang, C.L., Ge, W.K., 2001. Photocatalytic activity of WO_x-TiO_2 under visible light irradiation. Journal of Photochemistry and Photobiology, A, 141, 209-217.

Liu, Y., Li, J., Qui, X.F., Burda, C., 2007. Bactericidal activity of nitrogen-doped metal oxide nanocatalysts and the influence of bacterial extracellular polymeric substances (EPS). Journal of Photochemistry and Photobiology A, 190, 94-100.

Lobedank, J., Bellmann, E., Bendig, J., 1997. Sensitized photocatalytic oxidation of herbicides using natural sunlight. Journal of Photochemistry and Photobiology, A, 108, 89-93.

Long, M., Brame, J., Qin, F., Bao, J., Li, Q., Alvarez, P.J.J, 2017. Phosphate changes effect of humic acids on TiO_2 photocatalysis: From inhibition to mitigation of electron hole recombination. Environmental Science and Technology, 51, 514-521.

Lowry, O.H., Rosenbrough, N.J., Farr, A.L., Randall, R.J., 1951. Protein measurement with the Folin phenol reagent. Journal of Biological Chemistry, 193, 265-275.

Lu, Z.X., Zhou, Z.L., Zhang, Z.L., Shi, W.L., Xie, Z.X., Xie, H.Y., Pang, D.W., Shen, P., 2003. Cell damage induced by photocatalysis of TiO_2 thin films. Langmuir, 19, 8765-8768.

Lyon, D.Y., Fortner, J.D., Sayes, C.M., Colvin, V.L., Hughes, J.B., 2005. Bacterial cell association and antimicrobial activity of a C_{60} water suspension. Environmental Toxicology and Chemistry, 24, 11, 2757-2762.

MacCarthy, P., Malcolm, R.L., Clapp, C.E., Bloom, P.R., 1990. An Introduction to Soil Humic Substances. In: MacCarthy, P., Malcolm, R.L., Clapp, C.E., Bloom, P.R. (Eds.), Humic Substances in Soil and Crop Sciences: Selected Reading, 1-12, American Society of Agronomy and Soil Sciences Society of America, Madison, Wisconsin, U.S.A.

Macnab, R.M., 1979. Locomotion in microbial plants. In: Haupt, W. and Feinleib, M.E. (Eds.), Encyclopedia of plant physiology, 7, 207-223, Springer-Verlag, Berlin, Germany.

Macnab, R.M., Han, D.P., 1983. Asynchronous switching of flagellar motors on single bacterial cell. Cell, 32, 109-117.

Madigan, M.T., Martinko, J.M. (Eds.), 2006. Brock Biology of Microorganisms, 11th Edition, Pearson Education, Inc., Upper Saddle River, New Jersey, U.S.A.

Maji, D., Chatterjee, S., 2011. Importance of water quality in dialysis and need for endotoxin testing, https://www.qcin.org/nbqp/conclave2011/Presentation/Dr_Soma_Chatterjee.pdf. Date accessed May 2018.

Manahan, S.E., 1999. Environmental Chemistry, 7th Edition, Lewis Publishers, Florida, U.S.A.

Mansilla, H.D., Yeber, M.C., Freer, J., Rodríguez, J., Baeza, J., 1997. Homogeneous and heterogeneous advanced oxidation of a bleaching effluent from the pulp and paper industry. Water Science and Technology, 4, 273-278.

Mao, J., Hu, W., Schmidt-Rohr, K., Davies, G., Ghabbour, E.A., Xing, B., 1998. Structure and Elemental Composition of Humic Acids: Comparison of Solid-State ^{13}C NMR Calculations and Chemical Analysis. In: Davies, G., Ghabbour, E.A. (Eds.), Humic Substances – Structures, Properties and Uses, 79-90, The Royal Society of Chemistry, Cornwall, U.K.

Maraccini, P.A., Wenk, J., Boehm, A.B., 2016. Photoinactivation of eight health-relevant bacterial species: Determining the importance of the exogenous indirect mechanism. Environmental Science and Technology, 50, 5050-5059.

Martens, D.A., Frankenberger Jr., W.T., 1990. Quantification of soil saccharides by spectrophotometric methods. Soil Biology and Biochemistry, 22, 8, 1173–1175.

Marugán, J., van Grieken, R., Sordo, C., Cruz, C., 2008. Kinetics of the photocatalytic disinfection of *Escherichia coli* suspensions. Applied Catalysis B: Environmental, 82, 27-36.

Marugán, J., van Grieken, R., Pablos, C., Sordo, C., 2010. Analogies and differences between photocatalytic oxidation of chemicals and photocatalytic inactivation of microorganisms. Water Research, 44, 3, 789-796.

Matilainen, A., Sillanpää, M., 2010. Removal of natural organic matter from drinking water by advanced oxidation processes. Chemosphere, 80, 351-365.

Matsunaga, T., 1985. Sterilization with particulate photosemiconductor. Journal of Antibacterial and Antifungal Agents, 13, 211-220.

Matsunaga, T., Tomoda, R., Nakajima, T., Wake, H., 1985. Photoelectrochemical sterilization of microbial cells by semiconductor powders. FEMS Microbiology Letters, 29, 211-214.

Matthews, R.W., 1988. Kinetics of photocatalytic oxidation of organic solutes over titanium dioxide. Journal of Catalysis, 111, 264-272.

Matthews, R.W., Mahlman, H.A., Sworski, T.J., 1972. Elementary processes in the radiolysis of aqueous sulfuric acid solutions. Determinations of both G_{OH}, and $Gso_4^{-1,2}$. Journal of Physical Chemistry, 76, 9 ,1265-1272.

Mattle, M.J., Vione, D., Khon, T., 2015. Conceptual model and experimental framework to determine the contributions of direct and indirect photoreactions to the solar disinfection of MS2, phiX174, and adenovirus. Environmental Science and Technology, 49, 334-342.

McGuigan, K.G., Joyce, T.M., Conroy, R.M., Gillespie, J.B., Elmore-Meegan, M., 1998. Solar disinfection of drinking water contained in transparent plastic bottles: Characterizing the bacterial inactivation process. Journal of Applied Microbiology, 84, 1138-1148.

McGuigan, K.G., Joyce, T.M., Conroy, R.M., 1999. Solar disinfection: Use of sunlight to decontaminate drinking water in developing countries. Journal of Medical Microbiology, 48, 785-787.

McGuigan, K.G., Conroy, R.M., Mosler, H-J., Preez, M., Ubomba-Jaswa, E., Fernandez-Ibañez, P., 2012. Solar water disinfection (SODIS): A review from bench-top to roof-top. Journal of Hazardous Materials, 235-236, 29-46.

McKnight, D.M., Boyer, E.W., Westerhoff, P.K., Doran, P.T., Kulbe, T., Andersen D.T., 2001. Spectrofluorometric characterization of dissolved organic matter for indication of precursor organic material and aromaticity. Limnology and Oceanography, 46, 38-48.

Meadows, P. S., Campbell, J.I., 1978. An Introduction to Marine Science, 2nd Edition, John Wiley and Sons, New York, U.S.A.

Miles, A.A., Misra, S.S., 1938. The estimation of the bactericidal power of the blood. Epidemiology and Infection, 38, 6, 732-749.

Montgomery, M.A., Elimelech, M., 2007. Water and sanitation in developing countries: including health in the equation. Environmental Science and Technology, 41, 1, 17-24.

Nada, M., Jayalath, S., Gillan, E.G., Grassian, V.H., Larsen, S.C., 2019. Chapter 20 - Zeolites and Mesoporous Silica: From Greener Synthesis to Surface Chemistry of Environmental and Biological Interactions. In: Douhal, A., Anpo, M. (Eds.), Chemistry of Silica and Zeolite-Based Materials, Volume 2, 1st Edition, 375-397, Elsevier, Amsterdam, The Netherlands.

Neihof, R.A., Echols, W.H., 1973. Physicochemical studies of microbial cell walls. I. Comparative electrophoretic behavior of intact cells and isolated cell walls. Biocihimica et Biophysica Acta, 318, 23-32.

Ng, W., 2018. Zeta potential of *Escherichia coli* DH5α grown in different growth media. PeerJ Preprints, doi: 10.7287/peerj.preprints.26697v1.

Ng, W., Ting, Y.P., 2017. Zeta potential of bacteria cells: Effect of wash buffers. PeerJ Preprints, doi: 10.7287/peerj.preprints.110v7.

Nieuwenhuijsen, M.J., Toledano, M.B., Eaton, N.E., Fawell, J., Elliott, P., 2000. Chlorination disinfection byproducts in water and their association with adverse reproductive outcomes: A review. Occupational and Environmental Medicine, 57, 73-85.

Ollis, D.F., Pelizzetti, E., Serpone, N., 1991. Photocatalyzed destruction of water contaminants. Environmental Science and Technology, 25, 1523-1529.

Overmann, J., 2006. Principles of Enrichment, Isolation, Cultivation and Preservation of Prokaryotes. In: Dworkin M., Falkow, S., Rosenberg, E., Schleifer, K.H., Stackebrandt, E. (Eds.), The Prokaryotes, A Handbook on the Biology of Bacteria, Volume 1: Symbiotic Association, Biotechnology, Applied Microbiology, 3rd Edition, 80-136, Springer Science + Bussiness Media, Inc., New York, USA.

Pagano, T., Bida, M., Kenny, J.E., 2014. Trends in levels of allochthonous dissolved organic carbon in natural water: A review of potential mechanism under a changing climate. Water, 6, 2862-2897.

Panagiotopoulos, C., Sempere, R., 2005. Analytical methods for the determination of sugars in marine samples: A historical perspective and future directions. Limnology and Oceanography: Methods, 3, 419-454.

Park, S., Imlay, J.A., 2003. High levels of intracellular cysteine promote oxidative DNA damage by driving the Fenton reaction. Journal of Bacteriology, 185, 6, 1942-1950.

Parsons, S. (Eds.), 2004. Advanced Oxidation Processes for Water and Wastewater Treatment, IWA Publishing, London, U.K.

Phelps, E.B., 1909. Disinfection of sewage and sewage filter effluents with a chapter on the putrescibility and stability of sewage effluents. U.S. Geology Survey Water Supply Paper, 229.

Phillips, R., Kondev, J., Theriot, J., Garcia, H.J., 2013. Physical Biology of the Cell, 2nd Ed., Garland Science, Taylor & Francis Group, LLC, U.S.A.

Planchon, M., Ferrari, R., Guyot, F., Gélabert, A., Menguy, N., Chanéac, C., Thill, A., Benedetti, M.F., Spalla, O., 2013. Interaction between *Escherichia coli* and TiO_2 nanoparticles in natural and artificial waters. Colloids and Surfaces B: Biointerfaces, 102, 158-164.

Prescott, L.M., Harley, J.P., Klein, D.A., 1993. Microbiology, 2nd Edition, William C. Brown Publishers, Dubuque, Iowa, U.S.A.

Pulgarin, C., 2015. Fe vs. TiO_2 Photo-assisted processes for enhancing the solar inactivation of bacteria in water. Chimia, 69, 7-9.

Rao, P., Pattabiraman, T.N., 1989. Reevaluation of the phenol-sulfuric acid reactionfor the estimation of hexoses and pentoses. Analytic Biochemistry, 181, 18–22.

Reddy, P.V.L., Hernandez-Viezcas, J.A., Peralta-Videa, J.R., Gardea-Torresdey, J.L., 2016. Lessons learned: Are engineered nanomaterials toxic to terrestrial plants? Science of the Total Environment, 568, 470-479.

Reddy, P.V.L., Kavitha, B., Reddy, P.A.K., Kim, K-H., 2017. TiO_2-based photocatalytic disinfection of microbes in aqueous media: A review. Environmental Research, 154, 296-303.

Reed, R.H., 1997. Solar inactivation of faecal bacteria in water: The critical role of oxygen. Letters in Applied Microbiology, 24, 276-280.

Reed, R.H., Mani, S.K., Meyer, V., 2000. Solar photo-oxidative disinfection of drinking water: preliminary field observations. Letters in Applied Microbiology, 30, 432-436.

Reed, R.W., Reed, G.B., 1948. “Drop plate” method of counting viable bacteria. Canadian Journal of Research, 26, 317-326.

Reinhold, R.B., Fine, J., 1971. A technique for quantitative measurement of endotoxin in human plasma. Proceedings of the Society for Experimental Biology and Medicine, 137, 1, 334-340.

Ren, J., Wang, W., Zhang, L., Chang, J., Hu, S., 2009. Photocatalytic inactivation of bacteria by photocatalyst Bi_2WO_6 under visible light. Catalysis Communications, 10, 1940-1943.

Rengifo-Herrera, J.A., Rincón, A.G., Pulgarin, C., 2013. Waterborne *Escherichia coli* Inactivation by TiO_2 Photoassisted Processes: A Brief Overview. In: Pichat, P. (Eds.), Photocatalysis and Water Purification: From Fundamentals to Recent Applications, 295-309, WILEY-VCH Verlag GmbH & Co. KGaA, Weinheim, Germany.

Reuter, J.H., Perdue, E.M., 1977. Importance of heavy metal-organic matter interactions in natural waters. Geochimica et Cosmochimica Acta, 41, 325-334.

Reynolds, D.M., 2003. Rapid and direct determination of tryptophan in water using synchronous fluorescence spectroscopy. Water Research, 3055-3060.

Richardson, S.D., Simmons, J.E., Rice, G., 2002. Disinfection byproducts: The next generation, Environmental Science and Technology, 36, 198A-205A.

Richardson, S.D., Plewa, M.J., Wagner, E.D., Schoeny, R., DeMarini, D.M., 2007. Occurrence, genotoxicity, and carcinogenicity of regulated and emerging disinfection by-products in drinking water: A review and roadmap for research. Mutation Research, 636, 178-242.

Rincón, A.G., Pulgarin, C., 2004. Effect of pH, inorganic ions, organic matter and H_2O_2 on *E. coli* K12 photocatalytic inactivation by TiO_2 implications in solar water disinfection. Applied Catalysis B: Environmental, 51, 283-302.

Romazzoni, E., Giannakis, S., Giovannetti, R., Vione, D., Pulgarin, C., 2020. Detrimental vs. beneficial influence of ions during solar (SODIS) and photo-Fenton disinfection of *E. coli* in water: (Bi)carbonate, chloride, nitrate and nitrite effects. Applied Catalysis B: Environmental, 270, 118877.

Rosenbaum, J.L., Child, F.M., 1967. Flagellar regeneration in protozoan flagellates. The Journal of Cell Biology, 34, 345-364.

Saha, S.K., Brewer, C.F., 1994. Determination of the concentrations of oligosaccharides, complex type carbohydrates, and glycoproteins using the phenol-sulfuric acid method. Carbohydrate Research, 254, 157-167.

Saito, T., Iwase, T., Horie, J., Morioka, T., 1992. Mode of photocatalytic bactericidal action of powdered semiconductor TiO_2 on mutans streptococci. Journal of Photochemistry and Photobiology, B: Biology, 14, 369-379.

Sammartano, L.J., Tuveson, R.W., 1987. *Escherichia coli* strains carrying the cloned cytochrome *d* terminal oxidase complex are sensitive to near-UV inactivation. Journal of Bacteriology, 169, 5304-5307.

Sangchay, W., Ubonchonlakat, K., 2015. Photocatalytic disinfection of water containing *E. coli* using Fe^{3+} doped TiO_2 thin films coated on glass fibers. Digest Journal of Nanomaterials and Biostructures, 10, 1, 283-290.

Sapan, C.V., Lundblad, R.L., Price, N.C., 1999. Colorimetric protein assay techniques. Biotechnology and Applied Biochemistry, 29, 99-108.

Schenk, G.O., 1963. Photosensitization. Industrial and Engineering Chemistry, 55, 6, 40-43.

Scully, N.M., Cooper, W.J., Tranvik, L.J., 2003. Photochemical effects on microbial activity in natural waters: the interaction of reactive oxygen species and dissolved organic matter. FEMS Microbiology Ecology, 46, 353-357.

Senesi, N., 1990. Molecular and quantitative aspects of the chemistry of fulvic acid and its interactions with metal ions and organic chemicals: The fluorescence spectroscopy approach. Analytica Chimica Acta, 232, 77-106.

Sen-Kavurmaci, S., Bekbolet, M., 2014. Tracing TiO_2 photocatalytic degradation of humic acid in the presence of clay particles by excitation-emission matrix (EEM) fluorescence spectra. Journal of Photochemistry and Photobiology, A, 282, 0, 53-61.

Smith, E.J., Davison, W., Hamilton-Taylor, J., 2002. Methods for preparing synthetic freshwaters. Water Research, 36, 1286-1296.

Sichel, C., Blanco, J., Malato, S., Fernández-Ibáñez, P., 2007. Effects of experimental conditions on *E. coli* survival during solar photocatalytic water disinfection. Journal of Photochemistry and Photobiology, A, 189, 239-246.

Sieburth, J. McN., Jensen, A., 1969. Studies on algal substances in sea. II. The formation of gelbstoff (humic material) by exudates of Phaeophyta. Journal of Experimental Marine Biology and Ecology, 3, 275-289.

Simon-Deckers, A., Loo, S., Mayne-L'Hermite, M., Herlin-Boime, N., Menguy, N., Reynaud, C., Gouget, B., Carriere, M., 2009. Size-, composition- and shape-dependent toxicological impact of metal oxide nanoparticles and carbon nanotubes towards bacteria. Environmental Science and Technology, 43, 8423-8429.

Singh, S., Brocker, C., Koppaka, V., Chen, Y., Jackson, B.C., Matsumoto, A., Thompson, D.C., Vasiliou, V., 2013. Aldehyde dehydrogenases in cellular responses to oxidative/electrophilic stress. Free Radical Biology and Medicine, 56, 89-101.

Singleton, P., 1997. Bacteria in Biology, Biotechnology and Medicine 4th Edition. John Wiley and Sons, Inc., Ney Jersey, U.S.A.

Sommer, B., Marino, A., Solarte, Y., Salas, M.L., Dierolf, C., Valiente, C., Mora, D., Rechsteiner, R., Setter, P., Wirojanagud, W., Ajarmeh, H., Al-Hassan, A., Wegelin, M., 1997. SODIS-an emerging water treatment process. Journal of Water Supply: Research and Technology – AQUA, 46, 127-137.

Sreeja, S., Shetty, K.V., 2016. Microbial disinfection of water with endotoxin degradation by photocatalysis using Ag@TiO_2 core shell nanoparticles. Environmental Science and Pollution Research, 23, 18154-18764.

Sreeja, S., Shetty, K.V., 2017. Photocatalytic water disinfection under solar irradiation by Ag@TiO_2 core-shell structured nanoparticles. Solar Energy, 157, 236-243.

Stevenson, J., 1982. Humus Chemistry: Genesis, Composition, Reactions. John Wiley and Sons, New York, Inc., U.S.A.

Sucher, N.J., Carles, M.C., Nowortny, J., Bak, T., 2012. Photocatalytic water disinfection on oxide semiconductors: part 2-sytucture, functional properties and reactivity of microbial agents. Advances in Applies Ceramics, 111, 16-33.

Suffet, I.H., MacCarthy, P. (Eds.), 1989. Aquatic Humic Substances, Influence of Fate and Treatment of Pollutants, Advances in Chemistry Series, American Chemical Society, Washington D.C., U.S.A.

Sun, D.D., Tay, J.H., Tan, K.M., 2003. Photocatalytic degradation of *E. coliform* in water. Water Research, 37, 3452-3462.

Sun, H., Li, G., Nie, X., Shi, H., Wong, P.-K., Zhao, H., An, T., 2014. Systematic approach to in-depth understanding of photoelectrocatalytic bacterial inactivation mechanisms by tracking the decomposed building blocks. Environmental Science and Technology, 48, 9412-9419.

Sun, H., Li, G., An, T., 2017. Bacterial Oxidative Stress Responses and Cellular Damage Caused by Photocatalytic and Photoelectrocatalytic Inactivation. In: An, T., Zhao, H., Wong, P.K. (Eds.), Advances in Photocatalytic Disinfection, Green Chemistry and Sustainable Technology, 259-272, Springer-Verlag GmbH, Berlin, Germany.

Sunada, K., Kikuchi, Y., Hashimoto, K., Fujishima, A., 1998. Bactericidal and detoxification effects of TiO_2 thin film photocatalysts. Environmental Science and Technology, 32, 5, 726-728.

Sunada, K., Watanabe, T., Hashimoto, K., 2003. Studies on photokilling of bacteria on TiO_2 thin film. Journal of Photochemistry and Photobiology, A, 156, 227-233.

Suryo Rahmanto, A., Pattison, D.I., Davies, M.J., 2012. Photo-oxidation-induced inactivation of the selenium-containing protective enzymes thioredoxin reductase and glutathione peroxidase. Free Radical Biology and Medicine, 53, 1308-1316.

Thurman, E.M., 1985. Organic Geochemistry of Natural Waters, 1st Edition, Springer, Dordrecht, The Netherlands.

Thwaites, J.J., Mendelson, N.H., 1991. Mechanical Behavior of Bacterial Cell Walls. In: Luisa, B., Tempest, D. (Eds.), Advances in Microbial Physiology, 32, 173-222, Academic Press Limited, Massachusetts, U.S.A.

Tomaszewski, J.E., Schwarzenbach, R.P., Sander, M., 2011. Protein encapsulation by humic substances. Environmental Science and Technology, 45, 6003-6010.

Tong, A., Tang, X., Zhang, F., Wang, B., 2020. Study on the shift of ultraviolet spectra in aqueous solution with variations of the concentration. Spectrochimica Acta Part A: Molecular and Biomolecular Spectroscopy, 234, 118259, doi: 10.1016/j.saa.2020.118259.

Tortora, G.J., Funke, B.R., Case, C.L., 2018. Microbiology an Introduction, 13th Edition, Pearson Education, Inc., New York, U.S.A.

Turkten, N., 2016. Pirinç Kapçığı Şablonlu Yeni TiO_2 Mikroküreleri: Sentezi, Karakterizasyonu ve Fotokatalitik Aktivitesi, Ph.D. Thesis, Yıldız Technical University, Turkey.

Turkten, N., Cinar, Z., 2017. Photocatalytic decolorization of azo dyes on TiO_2: Prediction of mechanism via conceptual DFT. Catalysis Today, 287, 169-175.

Turkten, N., Cinar, Z., 2019. Preparation, Characterization and Photocatalytic Properties of Iron-doped TiO_2 Photocatalysts. 4th International Porous and Powder Materials Symposium and Exhibition Proceedings Book, 87-90.

Turkten, N., Cinar, Z., Tomruk, A., Bekbolet, M., 2019. Copper-doped TiO_2 photocatalysis: application to drinking water by humic matter degradation. Environmental Science and Pollution Research, 26, 36, 36096-36106.

Tuveson, R.W., Sammartano, L.J., 1986. Sensitivity of *HemA* mutant *Escherichia coli* cells to inactivation by near-UV light depends on the level of supplementation with delta-aminolevulinic acid. Photochemistry and Photobiology, 43, 621-626.

UNICEF, 2009. Soap, Toilets and Taps – A Foundation for Healthy Children. How UNICEF Supports Water, Sanitation and Hygiene, New York, U.S.A.

Uyguner, C.S., Bekbolet, M., 2005. A comparative study on the photocatalytic degradation of humic substances of various origins. Desalination, 176, 167-176.

Uyguner, C.S., Bekbolet, M., 2007. A Review on the Photocatalytic Degradation of Humic Substances. In: Nikolau, A., Selcuk, H., Rizzo L., (Eds), Advances in Control of Disinfection By-Products in Drinking Water Systems, 419-446, NOVA Science Publishers Inc., New York, USA.

Uyguner, C.S., Bekbolet, M., 2009. Application of photocatalysis for the removal of natural organic matter in simulated surface and ground waters. Journal of Advanced Oxidation Technologies, 12, 87-92.

Uyguner, C.S., Bekbolet, M., Swietlik, J., 2007. Natural Organic Matter: Definitions and Characterization. In: Nikolau, A., Selcuk, H., Rizzo L., (Eds), Advances in Control of Disinfection By-Products in Drinking Water Systems, 253-277, NOVA Science Publishers Inc., New York, USA.

Uyguner-Demirel, C.S., Bekbolet, M., 2011. Significance of analytical parameters for the understanding of natural organic matter in relation to photocatalytic oxidation. Chemosphere, 84, 1009-1031.

Uyguner-Demirel, C.S., Birben, N.C., Bekbolet, M., 2013. Key role of common anions on the photocatalytic degradation profiles of the molecular size fractions of humic acids. Catalysis Today, 209, 122-126.

Uyguner-Demirel, C.S., Birben, N.C., Bekbolet, M., 2017. Elucidation of background organic matter matrix effect on photocatalytic treatment of contaminants using TiO_2: A review, Catalysis Today, 284, 202-214.

Uyguner-Demirel, C.S., Birben, N.C., Bekbolet, M., 2018. A comprehensive review on the use of second generation TiO_2 photocatalysts: Microorganism inactivation. Chemosphere, 211, 420-448.

Uyguner-Demirel, C.S., Lale, E., Birben, N.C., Bekbolet, M., 2020. Solar Light-Initiated Photoinactivation of *E. coli*: Influence of Natural Organic Matter. In: Naddeo, V., Balakrishnan, M., Choo, K-H., (Eds.), Frontiers in Water-Energy-Nexus—Nature-Based Solutions, Advanced Technologies and Best Practices for Environmental Sustainability, 249-251, Springer Nature Switzerland AG, Switzerland.

Vale, G., Mehennaoui, K., Cambier, S., Libralato, G., Jomini, S., Domingos, R.F., 2016. Manufactured nanoparticles in the aquatic environment-biochemical responses on freshwater organisms: A critical overview. Aquatic Toxicology, 170, 162-174.

Valeur, B., 2002. Molecular Fluorescence, Principles and Applications, Wiley-VCH, Weinheim, Germany.

vanLoon, G.W., Duffy, S.J., 2000. Environmental Chemistry: A Global Perspective. Oxford University Press, Oxford, U.K.

Viel, M., Collet, F., Lanos, C., 2018. Chemical and multi-physical characterization of agro-resources' by-product as a possible raw building material. Industrial Crops and Products, 120, 214-237.

Vione, D., Minella, M., Maurino, V., Minero, C., 2014. Indirect photochemistry in sunlit surface waters: Photoinduced production of reactive transient species. Chemistry – A European Journal, 20, 10590-10606.

Vivar, M., Pichel, N., Fuentes, M., 2017. Solar disinfection of natural river water with low microbiological content (10-10^3 CFU/100 ml) and evaluation of the thermal contribution to water purification. Solar Energy, 141, 1-10.

Voelker, B.M., Morel, F.M.M., Sulzberger, B., 1997. Iron redox cycling in surface waters: Effects of humic substances and light. Environmental Science and Technology, 31, 1004-1011.

Wang, H-Y.L., O'Doherty, G.A., 2012. Modulators of Na/K-ATPase: a patent review. Expert Opinion on Therapeutic Patents, 22, 587-605.

Wang, W., Huang, G., Yu, J.C., Wong, P.K., 2015. Advances in photocatalytic disinfection of bacteria: Development of photocatalysts and mechanisms. Journal of Environmental Sciences, 34, 232-247.

Waterborg, J.H., 2002. The Lowry Method for protein quantitation. In: Walker, J.M., (Eds.), The Protein Protocols Handbook, 2nd Edition, 7-9, Humana Press Inc., Totowa, New Jersey, U.S.A.

Wegelin, M., Canonica, S., Mechsner, K., Fleischmann, T., Pesaro, F., Metzler, A., 1994. Solar water disinfection: Scope of the process and analysis of radiation experiments. Journal of Water Supply: Research and Technology – AQUA, 43, 3, 154-169.

Wegelin, M., Sommer, B., 1998. Solar water disinfection (SODIS)-destined for worldwide use? Waterlines, 16, 30-32.

WHO, 1999. The World Health Report: Making A Difference. World Health Organization, Geneva, Switzerland.

WHO, 2012. 3.4. Test for bacterial endotoxins. https://www.who.int/medicines/publications/pharmacopoeia/Bacterial-endotoxins_QAS11-452_FINAL_July12.pdf. Date accessed May 2018.

Wilson, M., McNab, R., Henderson, B., 2002. Bacterial Disease Mechanisms - An Introduction to Cellular Microbiology. Cambridge University Press, New York, U.S.A.

Wood, J.M., 2015. Bacteria responses to osmotic challenges. The Journal of General Physiology, 145, 5, 381-388.

Yalcin, Y., Kılıc, M., Cinar, Z., 2010. Fe^{+3}-doped TiO_2: A combined experimental and computational approach to the evaluation of visible light activity. Applied Catalysis B: Environmental, 99, 469-477.

Yin, E.T., Galanos, C., Kinsky, S., Bradshaw, R.A., Wessler, S., Lüderitz, O., Sarmiento, M.E., 1972. Pictogram-sensitive assay for endotoxin: Gelation of *Limulus polyphemus* blood cell lysate induced by purified lipopolysaccharides and lipid A from Gram-negative bacteria. Biochimica et Biophysica Acta, 261, 284-289.

Yu, J.C., Ho, W., Lin, J., Yip, H., Wong, P.K., 2003. Photocatalytic activity, antibacterial effect, and photoinduced hydrophilicity of TiO_2 films coated on a stainless steel substrate. Environmental Science and Technology, 37, 2296-2301.

Yu, J.C., Ho, W., Yu, J., Yip, H., Wang, P.K., Zhao, J., 2005. Efficient visible-light-induced photocatalytic disinfection on sulfur-doped nanocrystalline titania. Environmental Science and Technology, 39, 1175-1179.

Zafiriou, O.C., 1974. Sources and reactions of hydroxyl and daughter radicals in seawater. Journal of Geophysical Research, 79, 30, 4491-4497.

Zafiriou, O.C., Trye, M.B., 1979a. Nitrite photolysis in seawater by sunlight. Marine Chemistry, 8, 9-32.

Zafiriou, O.C., Trye, M.B., 1979b. Nitrate photolysis in seawater by sunlight. Marine Chemistry, 8, 33-42.

Zafiriou, O.C., Joussot-Dubien, J., Zepp, R.G., Zika, R.G., 1984. Photochemistry of natural waters. Environmental Science and Technology, 18, 12, 358A-371A.

Zepp, R.G., Wolfe, N.L., Gordon, J.A., Fincher, R.C., 1976. Light-induced transformations of methoxychlor in aquatic systems. Journal of Agricultural and Food Chemistry, 24, 727.

Zepp, R.G., Wolfe, N.L., Baughman, G.L., Hollins, R.C., 1977. Singlet oxygen in natural waters, Nature, 267, 421.

Zepp, R.G., Schlotzhauer, P.F., Sink, R.M., 1985. Photosensitized transformations involving electronic energy transfer in natural waters: Role of humic substances. Environmental Science and Technology, 19, 1, 74-81.

Zhang, J., Wang, X., Suo, X., Liu, X., Liu, B., Yuan, M., Wang, G., Liang, C., Shi, H., 2019. Cellular response of *Escherichia coli* to photocatalysis: Flagellar assembly variation and beyond. ACS Nano, 13, 2004-2014.

APPENDIX A: COMPOSITION OF WATER MATRIX SOLUTION

Table A.1. Composition of WM solution.

Common anions and cations	Concentration, mg/L
Anions*	
Cl^-	88.3
NO_3^-	6.11
SO_4^{2-}	59.5
$H_2PO_4^-$	3.23
Cations**	
Na^+	12.3
K^+	4.26
Ca^{2+}	61.0
Mg^{2+}	9.05

Reference methodology: *Ion chromatography (IC), **Flame atomic absorption spectroscopy (FAAS).

APPENDIX B: SPECTROSCOPIC CHARACTERIZATION OF 100 kDa HUMIC ACID SOLUTION

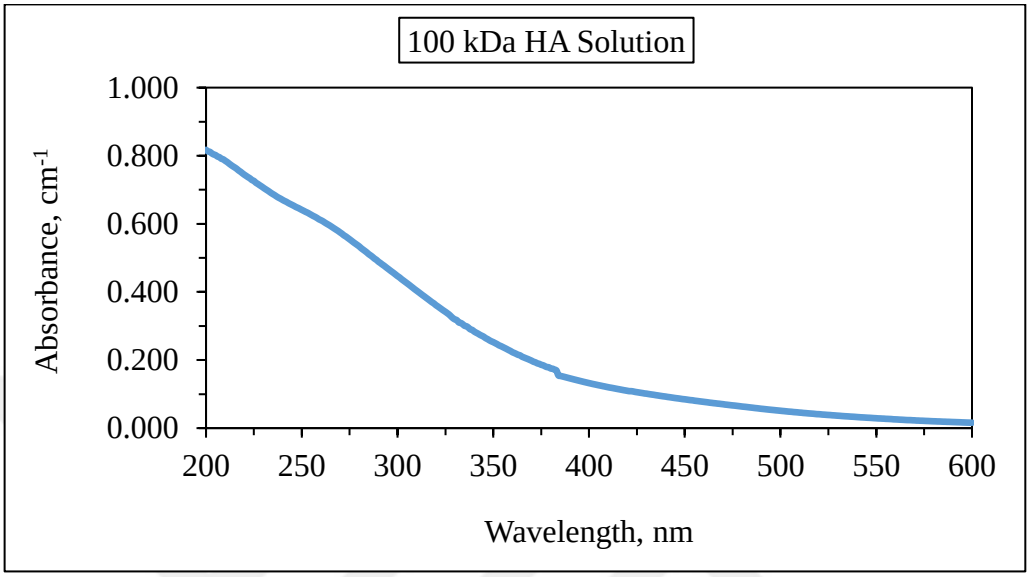

Figure B.1. UV-vis absorption spectra of 100 kDa HA solution.

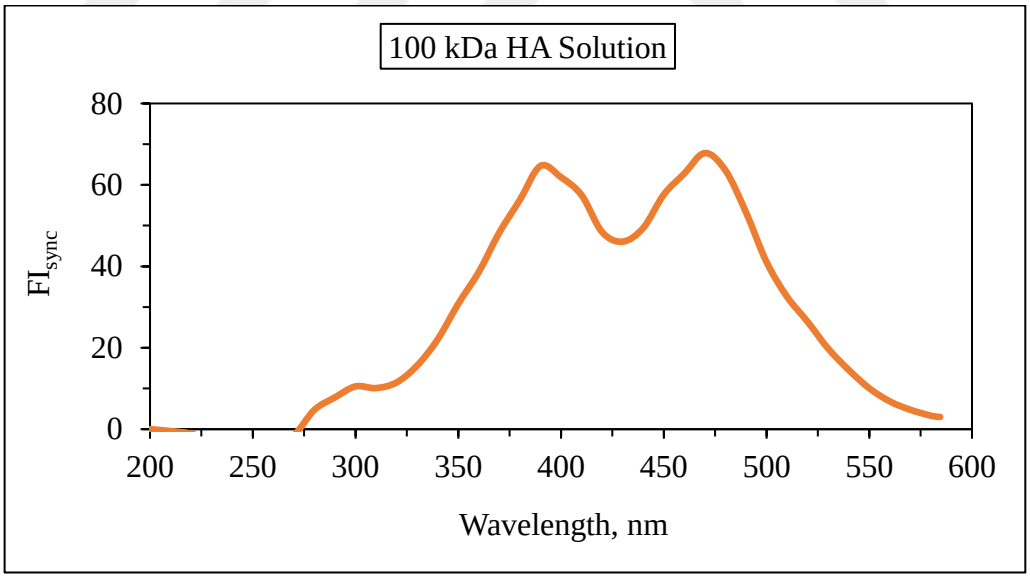

Figure B.2. Synchronous scan fluorescence spectra of 100 kDa HA solution.

Table B.1. Specified and specific UV-vis and fluorescence spectroscopic properties and NPOC of 100 kDa HA solution.

	UV-vis Spectroscopic Parameters, cm^{-1}				NPOC, mg/L	$SUVA_{254}$, L/m mg	$FI_{sync470}$	$SFI_{sync470}$	FI
	$Color_{436}$	UV_{365}	UV_{280}	UV_{254}					
100 kDa HA Solution	0.0960	0.2100	0.5337	0.6295	4.96	12.7	67.8	13.7	1.03

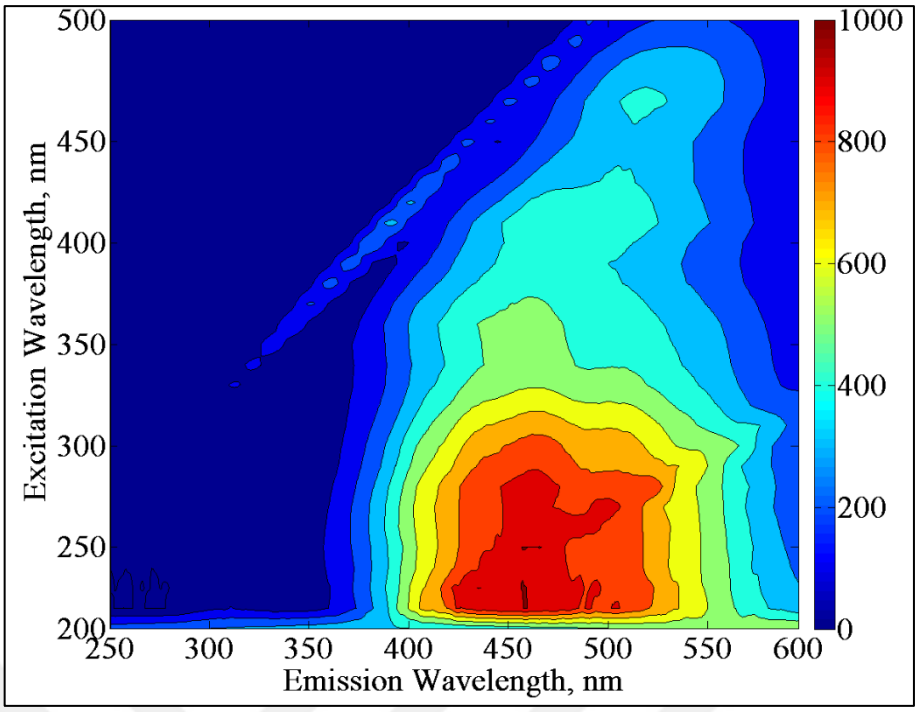

Figure B.3. EEM fluorescence contour plot of 100 kDa HA solution.

APPENDIX C: CHARACTERIZATION OF PHOTOCATALYST SPECIMENS

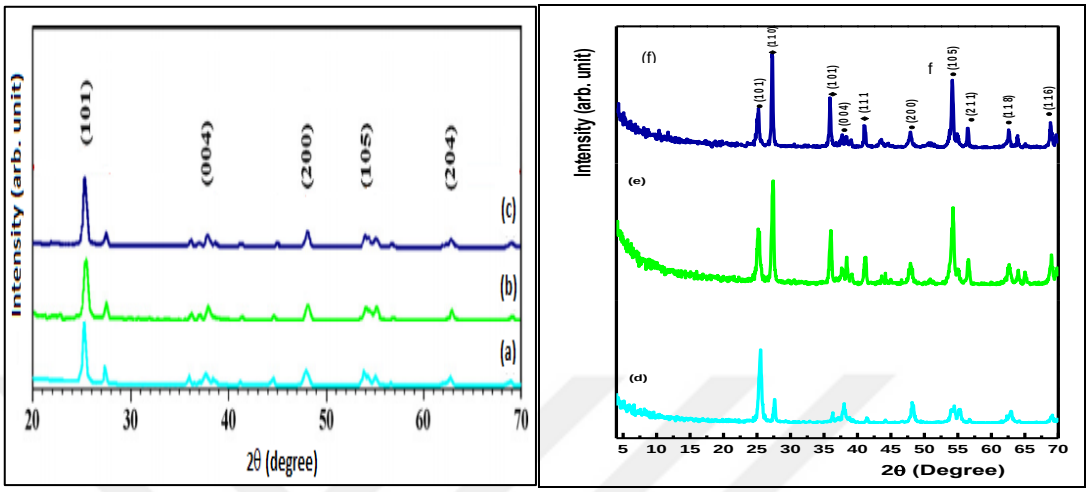

Figure C.1. X-Ray Diffraction (XRD) diffractograms of undoped and Fe-doped photocatalyst specimens: a. TiO_2, b. 0.25% Fe-TiO_2, c. 0.50% Fe-TiO_2 (Yalcin et al., 2010), d. SynTiO_2, e. 0.25% Fe-SynTiO_2, f. 0.50% Fe-SynTiO_2 (Turkten and Cinar, 2019).

Table C.1. Crystallite particle sizes, absorption wavelengths and band-gap energies (E_{bg}) of undoped and Fe-doped TiO_2 specimens.

Photocatalysts	Crystallite Particle Size, nm	E_{bg}, eV	Wavelength, nm	References
TiO_2	22.3	3.18	390	Turkten et al., 2019
SynTiO_2	33.1	2.91	410	Turkten et al., 2019
0.25% Fe-TiO_2	16.4	2.55	486	Yalcin et al., 2010
0.50% Fe-TiO_2	17.9	2.48	500	Yalcin et al., 2010
0.25% Fe-SynTiO_2	20.7	2.82	440	Turkten, 2016
0.50% Fe-SynTiO_2	23.7	2.67	466	Turkten and Cinar, 2019

Table C.2. BET surface areas of photocatalyst specimens.

Photocatalysts	BET surface area, m^2/g	References
TiO_2	57.6	Birben et al., 2015
SynTiO_2	50.3	Turkten et al., 2019
0.25% Fe-TiO_2	33.0	Birben et al., 2017
0.25% Fe-SynTiO_2	55.4	Turkten, 2016
0.50% Fe-SynTiO_2	34.0	Turkten and Cinar, 2019

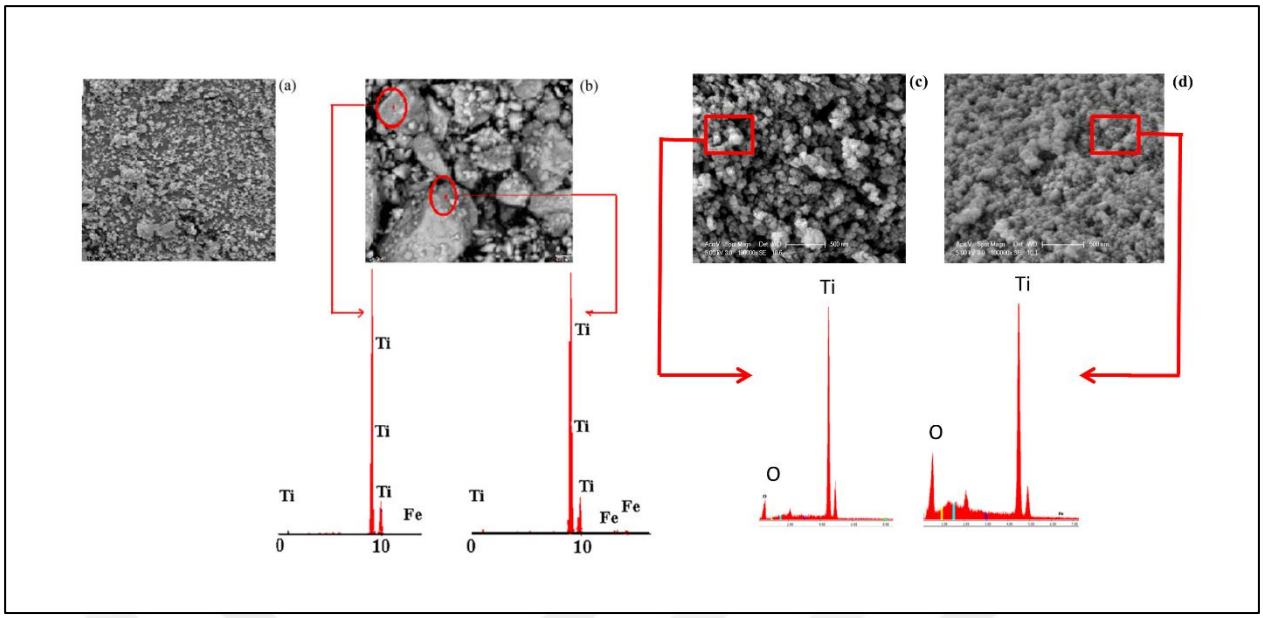

Figure C.2. SEM micrographs and Energy-Dispersive X-Ray (EDX) spectra of undoped and Fe-doped photocatalyst specimens:

a. TiO_2, b. 0.25% Fe-TiO_2 (Yalcin et al., 2010);

c. SynTiO_2, d. 0.50% Fe-SynTiO_2 (Turkten and Cinar, 2019).

APPENDIX D: CALIBRATION CURVE OF BOVINE SERUM ALBUMIN STANDARD

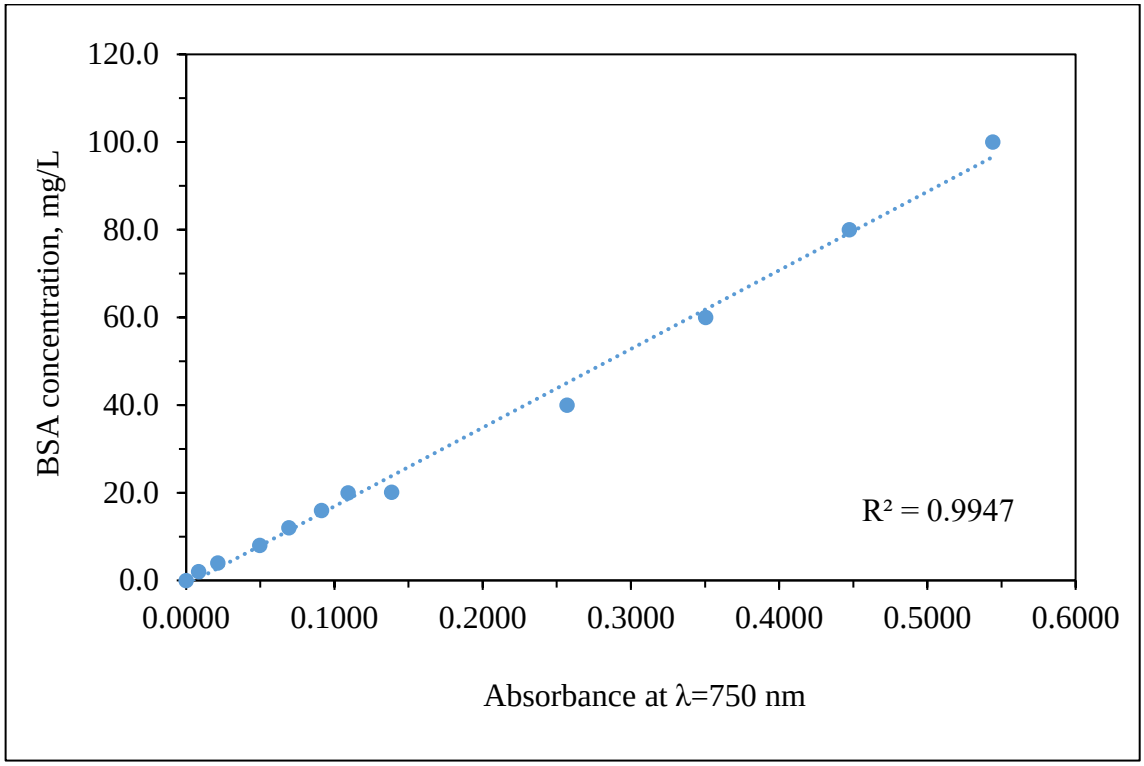

Figure D.1. Calibration curve of bovine serum albumin **(**BSA) standard.

$$y = 179.5x - 1.043$$

Where,

y = Concentration of total protein in solution, mg/L

x = Measured absorbance of the solution at λ=750 nm

APPENDIX E: CALIBRATION CURVE OF GLUCOSE STANDARD

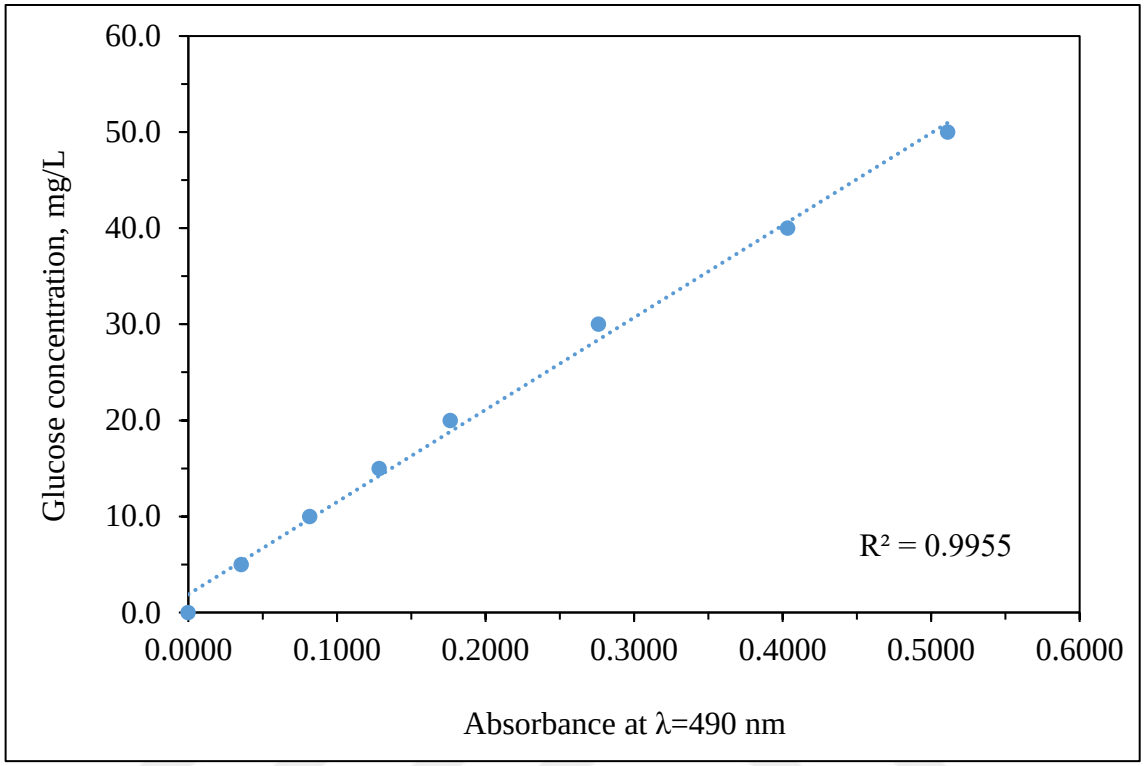

Figure E.1. Calibration curve of glucose standard.

$$y = 96.02x + 1.889$$

Where,

y = Concentration of total carbohydrate in solution, mg/L

x = Measured absorbance of the solution at λ=490 nm